Studies on Natural and Unnatural HIF Prolyl Hydroxylase Modulators



A THESIS SUBMITTED TO THE BOARD OF THE MATHEMATICAL, PHYSICAL AND LIFE SCIENCES DIVISION AT THE UNIVERSITY OF OXFORD IN PARTIAL FULFILMENT OF THE REQUIREMENTS FOR THE DEGREE OF DOCTOR OF PHILOSOPHY

Nadia Saffoon

Wadham College, Oxford

January 2025

To my daughter

Zunayra Zaheen

Acknowledgement

This doctoral journey has been one of the most transformative chapters of my life, and it would not have been possible without the support and encouragement of many individuals and institutions. First and foremost, I am profoundly grateful to my supervisor, Prof. Christopher Schofield, for his invaluable guidance, unwavering patience, and insightful feedback. His mentorship has been the cornerstone of this research, and I have learned immensely from his dedication to academic excellence. I am equally thankful to my co-supervisor, Prof. James McCullagh, for his expertise, encouragement, and thoughtful insights. His collaborative approach and constructive suggestions have significantly shaped the direction and depth of this thesis. I also wish to extend my gratitude to Dr. James Holt-Martyn for his invaluable support, and collaborative spirit, which have enriched my research journey. I am deeply thankful to Dr. Tobias John, Dr. John Walsby-Tickl, Dr. Ingvild Comfort Hvinden, and Elisabete Pires for their generosity in sharing knowledge and expertise, which has profoundly enhanced my understanding and growth throughout this journey. My heartfelt thanks go to my colleagues and friends from both Schofield and McCullagh groups at the University of Oxford who have been a constant source of support and camaraderie. The stimulating discussions, shared challenges, and memorable moments have made this journey more rewarding. I am deeply indebted to the Government of Bangladesh and Wadham College whose financial support made this research possible. The resources and opportunities provided by the Department of Chemistry have been indispensable in completing my work. I owe my deepest gratitude to my family for their unconditional love, encouragement, and belief in me, even during the most challenging moments. To my husband, Sahadat, his endless patience, support, and understanding have been my anchor throughout this journey. To my parents, especially my mother, Salma Alam, thank you for instilling in me the value of education and perseverance. Lastly, to my children, Zunayra & Anzar, their presence has been a source of boundless joy and motivation. This achievement is as much theirs as it is mine. This thesis is a testament to the collective effort of all those who have supported and inspired me, and I dedicate it to you all with gratitude and respect.

Declaration of Authorship

I hereby certify that this thesis is written, and the work is carried out by myself unless stated otherwise. Any other sources used in this thesis have been acknowledged properly.

Novel PHD inhibitors and enhancer molecules used in the work described in Chapters 2 & 4 were designed and synthesised by Dr. James Holt-Martyn. In-vivo experiments in chapter 2 were carried out by Dr. Hannah Lawson. The selectivity studies and RapidFire assay results in Chapters 2 & 4 were the results of assays and analysis by Dr Anthony Tumber.

The ICP-MS analyses described in Chapter 3 were conducted by Phil Holdship.

Nadia Saffoon

Oxford, January 2025

Abstract

This thesis describes studies on the hypoxia-inducible factor (HIF) mediated response to limited O_2 availability, using human cells. In particular, modulation of the activity of the HIF prolyl hydroxylases (PHDs) was studied using various treatments, including small molecules and food extracts. These methods include metabolomic analyses by Ion chromatography with mass spectrometry (IC-MS). The overall results provide new insight into the effects of hypoxia and hypoxia mimics on cells and help to open new avenues for modulation of the hypoxia response, both by promoting stabilisation and degradation of HIF-α.

Extended Abstract

The hypoxia-inducible factor (HIF) prolyl hydroxylases (PHDs) are Fe (II) and 2-oxoglutarate (2-OG)-dependent oxygenases. HIF-α isoforms are hydroxylated due to PHD catalysis, a post-translational modification that signals for their degradation via ubiquitination and subsequent proteasome mediated hydrolysis. Transcriptionally active α,ß-HIF promotes expression of the erythropoietin (*EPO*) gene and other genes that work to ameliorate the effects of hypoxia. PHD inhibitors are used for the treatment of anaemia by promoting *EPO* expression. The work described in this DPhil project focused on investigating novel HIF modulators, including PHD inhibitors, a PHD enhancer, proline/proline analogues and natural product extracts (*Spinacia Oleracea* leaf extracts), investigating their effects on HIF-1α levels. The work also involved semi-targeted metabolomics studies on HEK 293T cells treated with hypoxia, the hypoxia mimicking agent $CoCl_2$, and clinically used PHD inhibitors such as Roxadustat and Molidustat, comparing these conditions with normoxia. Metabolic changes, including those relating to glycolysis, were investigated – in each case measuring the impacts on HIF-1α stabilization.

Chapter 1 gives an overview of HIF and how it is regulated by the PHDs and factor-inhibiting hypoxia-inducible factor (FIH)**.** The physiological importance of HIF stabilization via clinically used PHD inhibitors and their applications, especially for the treatment of anaemia, are discussed. This chapter also briefly describes different natural diets/ food sources which showed potential for the treatment of anaemia. The historical role of $CoCl_2$ in the treatment of anaemia and the use of proline analogues as PHD inhibitors are discussed. The roles of HIF inhibition / HIF destabilization in cancer are summarized. An overview of metabolomics is

given, including the tools/techniques used to analyses changes in metabolites.

Chapter 2 briefly describes the discovery and development of a novel PHD inhibitor IOX5 from a 4-hydroxy-pyrimidine series and its prodrug form. Studies evaluating the activities of these PHD inhibitors in cells reveal their potent HIF-1α stabilization capability compared to clinically available PHD inhibitors (Roxadustat, Molidustat and Daprodustat). Cytotoxicity assays conducted on two different cell lines (HEPG2 and HEK 293T cell line) reveal IOX5 as a selective PHD inhibitor – IOX5 did not impact cell viability at 500 µM. IOX5 caused upregulation of some (*HIF-1α*, and *VEGF*) HIF target genes, but in the tested cells it did not significantly impact *EPO* or *CA9* gene expression (like Roxadustat). In-vivo experiments on mice revealed that IOX5 produces a significant increase in the red blood cell count, haemoglobin levels, and Hematocrit (HCT) levels.

Chapter 3 describes studies testing the hypothesis that a natural diet might be used for the treatment of anaemia via Co (II) or natural product mediated PHD inhibition. When incubated for 24 hours, raw spinach leaf extracts (750 µg /ml) show evidence of HIF-1α accumulation in cells. Although when compared to the use of pure $CoCl_2$, the signal was weak, the results suggest that diet therapy is a possibility for PHD inhibition/HIF-α upregulation.

Chapter 3 describes cell-based assays to test the ability of proline-related amino acids (L-4-thiazolidine carboxylic acid, L-proline, L-proline methyl ester hydrochloride, L-azetidine-2-carboxylic acid, 4-hydroxy proline, and deuterated proline) to stabilize HIF-α. Except for 4-hydroxy proline, proline and its analogues showed evidence for stabilization of HIF-1α. Further studies showed that L-4-thiazolidine carboxylic acid did not have a detrimental impact on cell viability at 500 µM. Upon evaluating the impact of L-4-thiazolidine carboxylic acid on HIF target genes, L-4-thiazolidine carboxylic acid showed a similar outcome to those for IOX5

and Roxadustat, that is significant upregulation of *HIF-1α and VEGF genes.* However, again like IOX5 and Roxadustat, L-4-thiazolidine carboxylic acid did not show any significant impact on the expression of the *EPO* and *CA9* genes.

Chapter 4 describes studies on a small molecule identified as a PHD enhancer in biochemical studies. The enhancer was evaluated in different cellular conditions. Under normoxic conditions, the enhancer apparently destabilizes HIF-1α, in the presence of Roxadustat**,** in HEK 293T cells and in 2OG depleted cell line (LN-18). Under hypoxia, the enhancer apparently destabilizes HIF-1α in HEK 293T cell line. The enhancer also caused apparent degradation of HIF-1α in the triple-negative breast cancer (TNBC) cell line in the presence of a chemotherapeutic agent.

Chapter 5 describes metabolomics studies analysing consequences after treatment of HEK 293T cells with hypoxia (1% O_2), $CoCl_2$, and selective PHD inhibitors (Roxadustat & Molidustat). A semi targeted metabolomics method was used. After comparing the five semi-targeted metabolomics analyses (1% O_2, 150 µM of $CoCl_2$, 20 & 100 µM of Roxadustat and 100 µM of Molidustat), changes in metabolite abundances were identified indicating all these five experimental conditions lead to common effects on metabolism. The results imply that Roxadustat or Molidustat treatment causes fewer profound changes compared to hypoxia (1% O_2) or $CoCl_2$. Pathway analysis supported this statement, with fewer pathways altered after Roxadustat & Molidustat treatment compared to 1% O_2 or $CoCl_2$.

Genes involved in the glycolysis pathway including glucose transporter 1 (*GLUT1)*, hexokinase (*HK 2)*, 3-phosphoinositide-dependent kinase 1 (*PDK1)*, Enolase 1 (*ENO 1)*, *and* lactate dehydrogenase A *(LDHA)* were significantly upregulated with 1% O_2 treatment, however, for

$CoCl_2$ and the selective PHD inhibitors a relatively high dose (100 & 200μM) was required to influence glycolysis. These results were verified using an orthogonal experimental approach. A Seahorse metabolic analyser was used to estimate the rate of glycolysis in live cells after the same treatments were applied.

Together these results provide new insight into the effects of hypoxia and hypoxia mimics on cells and help to open new avenues for modulation of the hypoxia response, both by promoting stabilization and degradation of HIFα.

Contents

Chapter: 1 1

Introduction 1

1. Introduction 2

1.2 The Hypoxia-inducible factor (HIF) 4

1.3 2-Oxoglutarate (2-OG) dependent oxygenase 6

1.3.1 HIF Prolyl Hydroxylases (PHDs) 7

1.3.1.1 Non-HIF targets of PHDs 8

1.4 PHD inhibitors can stabilize HIF-α 9

1.5 PHD inhibitors in clinical use 10

1.6 The therapeutic application of PHD inhibitors 12

1.6.1 Anaemia 12

1.6.2 Ischemic Disease 12

1.6.3 Inflammation 13

1.6.4 Wound healing 14

1.7 Natural / diet derived PHD inhibitors 14

1.7.1 Role of $CoCl_2$ in the treatment of anaemia 15

1.8 Effects of proline and its analogues on the activity of PHD and the Regulation of HIF signalling 16

Along with metal ions [118,119] and iron chelators [120,121], proline analogues, when

incorporated into HIF-1α derived peptides also have been stated to inhibit PHD activity [122-124]. 16

1.9 PHD enhancers 17

1.10 Metabolomics 17

1.10.1 Metabolomics Data 19

1.11 Ion-chromatography coupled with mass spectrometry (IC-MS) 19

1.12 Aims of the work described in this thesis 20

1.13 References 22

Chapter 2 45

Studies on the Novel PHD inhibitor IOX5 45

2.1. Discovery and development of IOX5 (5) 46

2.2 Cellular Investigations of IOX5 **(5)** 49

2.2.1 Human embryonic kidney (HEK 293T) cells treated with IOX5 for different incubation times 50

2.2.2 Human embryonic kidney (HEK 293T) cells treated with different concentrations of IOX5 52

2.2.3 Other clinically available PHD inhibitors and their ability to stabilize HIF-1α 54

2.3 Cell Viability Assays 56

2.4 Reverse transcription-quantitative polymerase chain reaction (RT-qPCR) 59

2.5 In-vivo mouse model studies 62

2.6 A prodrug (**6**) form of IOX5 (**5**) 66

2.6.1 Discovery and development of a Prodrug form (**6**) of the novel PHD inhibitor IOX5 66

2.6.2 Cellular Investigation of Prodrug **6** 66

2.7 Summary and Conclusions 70

2.8 Contributions of others 71

2.9 Materials and Methods 72

2.9.1 Chemicals 72

2.9.2 Cell lines used 72

2.9.3 Cell culture stock solutions 72

2.9.4 PHD inhibitors used for the experiments 73

2.9.5 Cell culture 73

2.9.6 Protein extraction and analysis 73

2.9.7 Reverse transcription-quantitative polymerase chain reaction (RT-qPCR) 74

2.9.8 Cell viability assays 75

2.9.9 Immunoblotting and SDS-PAGE assays 76

2.10 References 78

Chapter 3 84

Exploring the possibility of using a natural diet for PHD inhibition 84

3.1 $CoCl_2$ as a HIF stabilizer 85

3.2 Spinach- a natural diet as a source of CO(II) 86

3.3 Preparation of natural spinach leaf extraction and measurement of cobalt concentration 87

3.4 Investigating the effects of natural dietary components (*Spinacia Oleracea* leaf extracts) on HIF-1α levels 89

3.5 Effects of proline and its analogues on HIF-1α levels 91

3.5.1 Investigating Inhibition of prolyl hydroxylase domain (PHD) enzymes / HIF-1α upregulation by substrate analogue peptides 91

3.5.2 Proline mimics as PHD inhibitors 91

3.5.3 Cellular Investigation of proline-derived amino acids 93

3.5.4 Cell viability assays with L-4-thiazolidine carboxylic acid 95

3.5.5 Reverse transcription-quantitative polymerase chain reaction (RT-qPCR) effects of analysis of the L-4-thiazolidine carboxylic acid 97

3.6 Summary 99

3.7 Contributions of others 101

3.8 Materials and Methods 102

3.8.1 Chemicals 102

3.8.2 Cell line 102

3.8.3 Cell culture stock solutions 102

3.8.4 Cell culture and Protein extraction and analysis 102

3.8.5 PHD inhibitors used for the experiments 102

3.8.6 Metabolite extraction of Spinacia oleracea 102

3.8.6.1 Collection and identification of plant materials 102

3.8.6.2. Drying and grinding of S. Oleracea leaves 103

3.8.6.3 Extraction protocol 103

3.8.7 Analysis Interpretation of cobalt measurement from the *S. Oleracea* leaf extracts 104

3.8.8. Immunoblotting 105

3.8.9 Reverse transcription-quantitative polymerase chain reaction (RT-qPCR) 105

3.8.10 Cell viability assay 106

3.9 References 107

Chapter 4 113

Identification of a Novel Small Molecule as a PHD enhancer 113

4.1.1 Introduction 114

4.2 Prolyl hydroxylases (PHDs) and Hypoxia Inducible Factor (HIF): a potential target for cancer treatment 116

4.2.2.HIF-2α inhibitor in the treatment of kidney cancer 117

4.2.3 Potential enzyme enhancers 117

4.3 Discovery and development of the novel PHD enhancer **7** 118

4.4 Cellular investigations of the PHD enhancer **7** 120

4.4.1 Hypoxia and hydroxylation of HIF-1α 120

4.4.2 Mammalian cells accumulate HIF-1α in a hypoxic environment 121

4.4.3 Effects of PHD enhancer **7** in a 1% O_2 environment in HEK 293T cells 123

4.4.3.1 Different concentrations of the PHD enhancer **7** in a hypoxic environment 125

4.4.4 Studies on the PHD enhancer **7** in combination with the PHD inhibitor Roxadustat (**1**) 127

4.4.5 Effect of the PHD enhancer **7** on a 2-OG depleted cell line 131

4.4.6 Triple negative breast cancer (TNBC) cell line studies with **7** 133

4.4.6.1 Hypoxia in triple negative breast cancer (TNBC) cell line 133

4.4.6.2 The cellular investigations on TNBC cell line in combination with PHD enhancer **7** 134

4.5 Summary and Limitations of the Results 135

4.5.1 Contributions of others to the work described in this chapter 137

4.6 Methods and Materials 138

4.6.1 Chemicals 138

4.6.2 Cell line 138

4.6.5 Cell culture 139

4.6.6 Protein extraction and analysis 139

4.6.7 Immunoblotting in Normoxia 139

4.6.8 Immunoblotting for Hypoxia Experiment 139

4.6.9 RapidFire Assay Protocol 141

4.7 References 142

Chapter 5 150

Metabolomics Studies on Natural and Unnatural HIF Prolyl Hydroxylase Modulators 150

5.1 Metabolomics 151

5.2 Untargeted pathway analysis using Mummichog 154

5.3 Ion chromatography-mass spectrometry (IC-MS) 155

5.4 Metabolic adaptation in cellular hypoxia 156

5.4.1 Glycolysis in hypoxia 156

5.4.2 Effects of HIF-1α stabilization on glycolytic pathway 159

5.5 Research objectives 160

5.6 HIF-1α stability in human kidney cells and its metabolomic consequences 161

5.7 Metabolic changes in human kidney cells exposed to chronic hypobaric hypoxia (1% O_2) 165

5.7.1 Hypoxia (1% O_2) stabilizes HIF-1α 165

5.7.2 Metabolomics data quality 166

5.7.3 Effects of hypoxia on human HEK293T cell metabolites 168

5.7.3.1. Metabolic changes under hypoxia (1% O_2) 170

5.7.3.1.2 Glycolysis relevant changes due to hypoxia (1% O_2) 172

5.7.3.2. Interpretation of univariate statistical analysis 174

5.7.4 Patterns associated with altered metabolite profiles in hypoxia 174

5.7.5 Untargeted metabolic pathway analysis comparing hypoxic and normoxic HEK 293T cells 178

5.7.5.1. Data processing and analysis of pathway analysis of 1% O_2 experiment 179

5.7.5.1.1 Mummichog Pathway Analysis 179

5.7.5.1.2 Mummichog Pathway Analysis Results 179

5.7.6. Summary of semi-targeted metabolomics results comparing HEK293T cells in normoxia and hypobaric hypoxia. 184

5.8 Metabolic changes in HEK 293T kidney cells associated with $CoCl_2$(150µM) 186

5.8.1 $CoCl_2$ (100, 150 & 200 µM) stabilizes HIF-1α 186

5.8.2 Metabolomics data quality 187

5.8.3 Effect of 150µM of $CoCl_2$ on human metabolites in HEK 293T cells 188

5.8.3.1 Metabolic changes associated with $CoCl_2$ treatment 190

5.8.3.1.2 Glycolysis relevant changes due to $CoCl_2$ (150µM) treatment 192

5.8.3.2 Interpretation of univariate statistical analysis 195

5.8.4 Patterns associated with altered metabolite profiles in $CoCl_2$ 195

5.8.5 Untargeted metabolic pathway analysis of hypoxic HEK 293T cells. 199

5.8.5 1 Data processing and analysis 199

5.8.5.2 Mummichog Pathway Analysis Results 199

5.8.6 Summary of semi-targeted metabolomics results comparing HEK293T cells in $CoCl_2$ and control 202

5.9 Metabolic changes in human kidney cells associated with 20μM of Roxadustat treatment 204

5.9.1 Roxadustat (20, 100 & 200μM) stabilizes HIF-1α 204

5.9.2 Metabolomics data quality 205

5.9.3 Effect of inhibitor 20μM of Roxadustat on human kidney cell metabolites 206

5.9.3.1. Metabolic changes associated with 20μM Roxadustat treatment 208

5.9.3.1.2 Glycolysis relevant changes due to Roxadustat (20μM) treatment 210

5.9.3.2 Interpretation of univariate statistical analysis 212

5.9.4 Patterns associated with altered metabolite profiles in Roxadustat (20 μM) treated HEK 293T cells 213

5.9.5 Untargeted metabolic pathway analysis of HEK 293T cells treated with 20μM of Roxadustat 217

5.9.5.1 Data processing and analysis 217

5.9.5.2 Mummichog Pathway Analysis Results 217

5.9.6 Summary of semi-targeted metabolomics results comparing HEK293T cells in Roxadustat (20 μM) and control. 220

5.10 Metabolic changes in human kidney cells associated with 100 μM of Roxadustat 222

5.10.1 Metabolomics data quality 222

5.10.2. Effect of 100μM Roxadustat on human kidney cell metabolites 223

5.10.2.1 Metabolic changes associated with 100μM of Roxadustat 225

5.10.2.1.1 Glycolysis relevant changes due to Roxadustat (100µM) treatment 225

5.10.2. 2 Interpretation of univariate statistical analysis 228

5.10.3. Patterns associated with altered metabolite profiles in Roxadustat (100 µM) treated HEK 293T cells 228

5.10.4 Untargeted metabolic pathway analysis of HEK 293T cells treated with 100 µM Roxadustat 231

5.10.4.1 Data processing and analysis 231

5.10.4.2 Mummichog Pathway Analysis Results 232

5.10.5. Summary of semi-targeted metabolomics results comparing HEK293T cells in Roxadustat (100 µM) and control 234

5.11 Metabolic changes in human kidney cells associated with clinical Molidustat (100 µM) 237

5.11.1 Molidustat (20, 100 & 200µM) stabilizes HIF-1α 237

5.11.2 Metabolomics data quality 237

5.11.3 Effect of selective PHD inhibitor 100µM of Molidustat on human kidney cell's metabolites 239

5.11.3.1. Metabolic changes associated with clinical PHD inhibitor (100µM of Molidustat) 241

5.11.3.1.2 Glycolysis relevant changes due to Molidustat (100µM) treatment 243

5.11.3.2 Interpretation of univariant analysis 245

5.11.4 Patterns associated with altered metabolite profiles in Molidustat (100 µM) treated

HEK 293T cells 246

5.11.5 Untargeted metabolic pathway analysis of HEK 293T cells treated with 100 µM Molidustat 249

5.11.5.1 Data processing and analysis 249

5.11.5.2 Mummichog Pathway Analysis Results 250

5.11.6 Summary of semi-targeted metabolomics results comparing HEK293T cells in Molidustat (100 µM) and control 253

5.12 Interpretation of results: Hypoxia / hypoxia mimics show consistent effects on metabolism with highly selective PHD inhibitors showing distinct and overlapping effects 254

5.12.1 Significantly altered common metabolites 256

5.13 Reverse transcription-quantitative polymerase chain reaction (RT-qPCR) analysis of glycolytic gene expression 258

5.13.1 Results 260

5.13.2 Interpretation of Results 262

5.14 The Effect of $CoCl_2$, Roxadustat and Molidustat on the rate of glycolysis in live cells. 263

5.14.1 Seahorse Glycolytic Rate Assay 263

5.14.2 GlycoPER results 264

5.14.2.1 Interpretation of results 265

5.15 Chapter summary and conclusions 265

5.16 Methods and Materials 270

5.16.1 Chemicals 270

5.16.1.1 Chemicals for sample and hypoxia related processing and analysis 270

516.1.2 Chemicals for cell culture and hypoxia cell culture related solutions 270

5.16.3 Cell line, Cell culture stock solutions & PHD inhibitors 270

5.16.3.1 Cell culture and hypoxia related cell culture, thawing of cell aliquots, freezing of cell aliquots & passaging and splitting cells 270

5.16.4 Immunoblotting and Immunoblotting for hypoxia experiment 271

5.16.5 Treatment with different treatment groups 271

5.16.6. Treatment with 1% O_2 for the hypoxia immunoblotting and metabolomics study 271

5.16.7 Ion Chromatography Mass Spectrometry (IC-MS) 271

5.16.8 Plating for metabolomics and glycolytic rate assay experiment 272

5.16.9 Harvesting of metabolomics samples 273

5.16.10 Metabolomics cell sample preparation 273

5.16.11 Data processing and statistical analysis 274

5.16.12 Compound identification 275

5.16.13 Principal Component Analysis Plot and Partial Least Squares Discriminant Analysis 277

5.16.14 Volcano plot 277

5.16.15 False Discovery Rate (FDR) 278

5.16.16 Untargeted mummichog pathway analysis of IC-MS data 278

5.16.17 Reverse transcription-quantitative polymerase chain reaction (RT-qPCR) 279

5.16.18 Treatment with 1% O_2, $CoCl_2$ & PHD inhibitors for Seahorse glycolytic rate assays 280

5.17 References 282

Chapter 6 299

Conclusions and further work 299

6.1. Conclusions 300

6.2 References 311

7. Appendix 316

List of Abbreviations

2-DG……2-Deoxy-D-glucose

2D-LC……Two-dimensional liquid chromatography

2-HG…… 2-Hydroxyglutarate

2-OG…….2-Oxoglutarate

ADP……..Adenosine diphosphate

ALDA……Aldolase

ANOVA……Analysis of Variance

ARNT…….Aryl hydrocarbon receptor nuclear translocator

ATO……Atovaquone

ATP…… Adenosine triphosphate

BCSCs……Breast cancer stem cells

BNIP3……Bcl-2 interacting protein 3

CA9……Carbonic anhydrase 9

CBP……. CREB binding protein

cDNA……Complementary deoxyribonucleic acid

CE……Capillary electrophoresis

CKD……. Chronic kidney disease

CODD……C-Terminal oxygen-dependent degradation domain

CTAD….C-Terminal transactivation domain

D-2-HG……..D-2-Hydroxyglutarate

Da……Daltons

DMOG……Dimethyloxalylglycine

DNA……..Deoxyribonucleic acid

EASE……. Expression analysis systemic explorer

ECAR……..Extracellular acidification rate

EGCG……Epigallocatechin gallate

EGLN1……. Egl-9 Family Hypoxia Inducible Factor 1

EHMN……. Edinburgh Human Metabolic Network

ENOL……Enolase

EPO……. Erythropoietin

ETC……Electron transport chain

FBS……Fetal bovine serum

FC……..Fold change

FIH……Factor inhibiting HIF

GAPDH……Glyceraldehyde 3-phosphate dehydrogenase

GC-MS……Gas chromatography coupled with mass spectrometry

GDP……..Guanosine diphosphate

GLUT1……Glucose transporter 1

GlycoPER …. Glycolytic proton efflux rate

GSH……..Glutathione

HCA……. Hierarchical clustering analysis

HCT……Hematocrit

HEK 293T…Human embryonic kidney

HepG2……. Human hepatoblastoma

HER2……..Human epidermal growth factor receptor 2

HGB……Hemoglobin

HIF…….Hypoxia-inducible factor

HILIC……. Hydrophilic interaction liquid chromatography

HILIC-MS…Hydrophilic interaction chromatography–mass spectrometry

HK 2……Hexokinase 2

HMDB……Human Metabolome Database

HPLC……. High-performance liquid chromatography

HRE……. Hypoxia-responsive element

HRP……Horseradish peroxidase

IC-MS……Ion chromatography with mass spectrometry

ICP-MS……Inductively coupled plasma mass spectrometry

IDH……. Isocitrate dehydrogenase

IEC……..Ion-exchange chromatography

IP-MS……. Reversed phase chromatography–mass spectrometry using ion-pairing agents

KEGG……..Kyoto Encyclopedia of Genes and Genomes

LC-MS……..Liquid chromatography coupled to mass spectrometry

LDHA……. Lactate dehydrogenase A

LN-18……Human Brain Glioblastoma Cells

MCC……Multiple comparison correction

MS……Mass spectrometry

mTOR……Mammalian target of rapamycin

MTS……(3-(4,5-dimethylthiazol-2-yl)-5-(3-carboxymethoxyphenyl)-2-(4-sulfophenyl)-2H-tetrazolium)

NAD……Nicotinamide adenosine dinucleotide

NMR……. Nuclear magnetic resonance

NODD…...N-terminal oxygen-dependent degradation domain

NOG……N-Oxalylglycine

OCR……Oxygen consumption rate

ODD……Oxygen-dependent degradation domain

PAS……..Per-ARNT-Sim

PCA……Principal Component Analysis

PCR……Polymerase chain reaction

PDH……..Pyruvate dehydrogenase

PDK1……..Pyruvate dehydrogenase kinase1

PER……Proton Efflux Rate

PFKL……. Phosphofructokinase, liver type

PGK1……Phosphoglycerate kinase-1

PHD……. Prolyl hydroxylase domain

PLS-DA…. Partial Least Squares Discriminant Analysis

pVHL……Von hippel-lindau

RBC……Red blood cell count

rhEPO……Recombinant human erythropoietin

RNA……Ribonucleic acid

Rot/AA…Rotenone and Antimycin A

RT-qPCR…. Reverse transcription-quantitative polymerase chain reaction

SAR……Structure activity relationship

SCFAs…….Short-chain fatty acids

TAD……Transactivation domains,

TCA……Tricarboxylic acid cycle

TNBC……Triple-negative breast cancers

UTB……Urea, Tris, and β-mercaptoethanol

VEGF……..Vascular Endothelial Growth Factor

VIP……..Variable importance in projection

α-KG……..α- ketoglutarate

Chapter: 1

Introduction

1. Introduction

Most, if not all, organisms existing in an aerobic environment use atmospheric dioxygen (O_2), as an important energy source. Consequently, they have evolved mechanisms to adapt when O_2 supply levels become limiting, a condition sometimes referred to as hypoxia. Normoxia is defined as normal O_2 concentration in blood and tissues. It is important to note that concentrations of O_2 in cells and tissues can vary, including under-stressed and diseased situations. Many tumours (or regions of tumours) are hypoxic, with reported O_2levels in tumors ranging from 0.3% to 4.2%; in cell culture the atmospheric O_2 levels causing hypoxia considered to range from 4-1% to 0.1% O_2[1]. The mechanisms for delivering and maintaining an adequate O_2 supply to tissues and cells appear to have become more complex during the course of eukaryotic, and in particular, animal evolution with the cardiovascular system of higher animals helping to deliver O_2 efficiently to tissues. At the cellular level, many studies support the proposal that in animals the hypoxia-inducible factor (HIF) system plays a key role in the response to hypoxia[2,3].

The HIFs are α,ß-heterodimeric transcription factors, with levels of HIF-α, but not HIF-ß, being tightly regulated by the availability of O_2. The HIF-α prolyl hydroxylase domain (PHD) oxygenases (human PHD 1, 2, and 3) [4-9] are oxygen-dependent prolyl C4 prolyl hydroxylases that act on HIF-α, but not on HIF-ß proteins. PHD2 and, in particular PHD3, are upregulated in hypoxia in a HIF dependent manner [10]. Under normoxic conditions, i.e. in the presence of enough O_2 for normal cellular functions, the PHD enzymes catalyse efficient prolyl hydroxylation of HIF-α at specific proline-residues (Pro402 and Pro564) in HIF-α subunits [8-

11]. These hydroxylations take place in two HIF-α oxygen-dependent degradation domains[6, 12]: the C-terminal and N-terminal oxygen-dependent degradation domains (CODD and NODD respectively) of HIF-α isoforms, of which there are three in humans (HIF1-3α). The hydroxylated HIF-α isoforms are recognized by the von Hippel-Lindau (pVHL) ubiquitin E3 ligase complex and undergoes efficient ubiquitination-dependent degradation by proteasomes [7].

A second type of oxygenase enzyme, termed factor inhibiting HIF (FIH) also hydroxylates HIF-1/2α proteins, but in their C-terminal transactivation domain (CTAD), where it catalyses an asparaginyl hydroxylation. This post-translational modification regulates the transcriptional of HIF-α by hindering binding between HIF-α and the transcriptional co-activator proteins CBP and p30, which are histone acetyl transferases [13-17].

Under hypoxic conditions, the capacity of the PHDs to hydroxylate HIF-α activity is reduced, resulting in the accumulation of HIF-α. The stabilized HIF-α then can translocate to the nucleus and form HIF-α, β heterodimeric complexes [4, 5, 7-0]. These HIF-α, β heterodimeric complexes bind with hypoxia-responsive element (HRE) sequences and promote activation of HIF-α target genes, which helps enable adaptation to hypoxia. HIF target genes include those encoding for erythropoietin (EPO), which promotes red blood cell formation, and vascular endothelial growth factor, which promotes blood vessel formation [18].

HIF and its roles in angiogenesis, erythropoiesis, and glycolysis have made it an important pharmacological target in various disease situations, including anaemia, ischemic stroke, and myocardial infarction [12, 18]. HIF-1α mutations are linked to kidney cancer and many cancer

cells are subject to hypoxia, meaning HIF modulation is also an important current target for cancer.

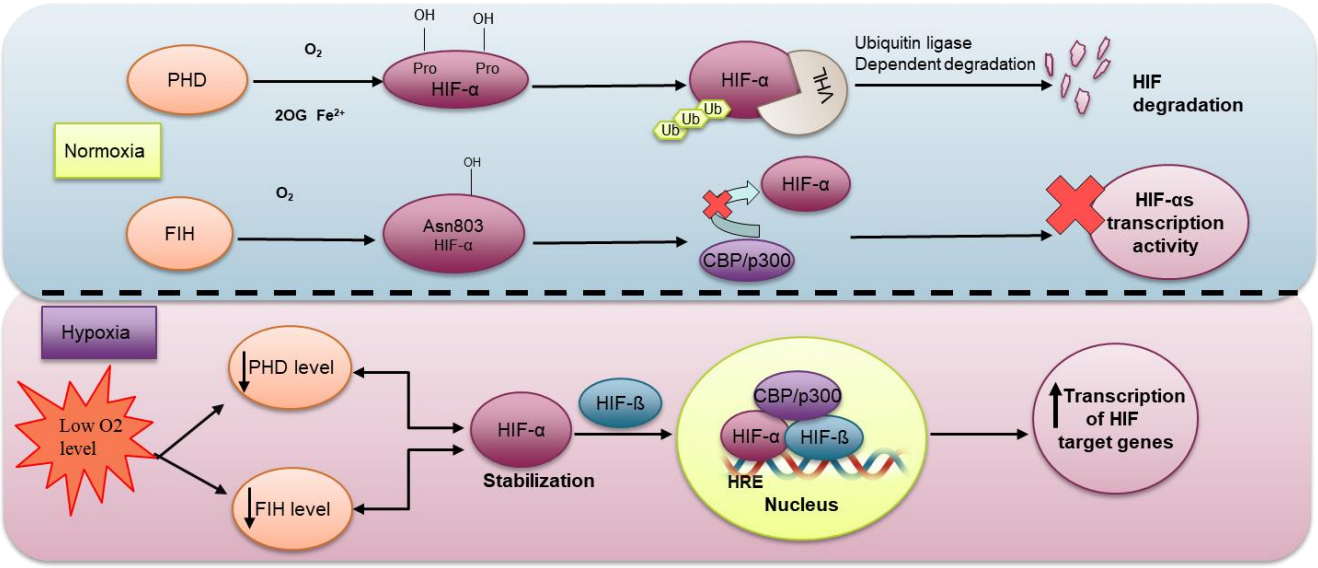


Figure 1.1.1: Flow chart of HIF-α and its regulation by the PHDs and FIH.

1.2 The Hypoxia-inducible factor (HIF)

HIF is an α,ß-heterodimer dimeric transcription factor. There are three human HIF-α isoforms: HIF-1 α, HIF-2 α, and HIF-3α [19]. The work described here primarily focuses on HIF-1 α because HIF-1α plays a crucial role in regulating acute responses to hypoxia, including in cancer cells. Amongst others, HIF-1α is important in regulating genes encoding for proteins involved in glycolysis, angiogenesis, and erythropoiesis[19]. The other two HIFα isoforms,

particularly HIF-2α and, to a lesser extent, HIF-3α, also have important roles. HIF-2α is particularly important in the regulation of the *EPO* gene and hence erythropoiesis and also has roles in the regulation of lipid metabolism [20-22]. HIF-2α plays an important part in adaptation to long-term hypoxia and HIF-2α is expressed mainly in the kidney, liver, and endothelium tissues [23,24]. Amongst the HIF isomers, HIF-3α is the least well-characterized. HIF-3α variants, like IPAS and HIF-3α4, are reported to act as negative regulators of HIF signaling, though a recent study shows that the HIF-3α variant can also act as a transcriptional activator [25-27].

MY work focused on HIF-1α study in part due its role in cancer, in part due to its ubiquitous expression and its role as a master regulator of cellular metabolism, and in part because, it has been extensively studied in HEK 293T cells, where it is generally expressed at a higher level than HIF-2α [28].

Both HIF-1α and β subunits have a basic helix-loop-helix motif and a Per-ARNT-Sim (PAS) domain [19, 29,30]. The basic helix-loop-helix domain is involved in DNA / HRE binding and is important for dimerization with HIF-1β [4, 5, 7-9, 12-17, 31-34]. The PAS domain also facilitates heterodimerization [35]. HIF-1α contains C- and N- terminal transactivation domains (TADs), which regulate transcriptional activity [29, 36-38]. Transcriptional co-activators like CREB binding protein (CBP) and p300 are histone acetyl transferases that interact with the C-TAD of HIF-α [16, 35]. HIF-1β is identical to the aryl hydrocarbon receptor nuclear translocator (ARNT) therefore it is also sometimes called ARNT [19] and there are two types of HIF-1β : ARNT2 and ARNT3 [39].

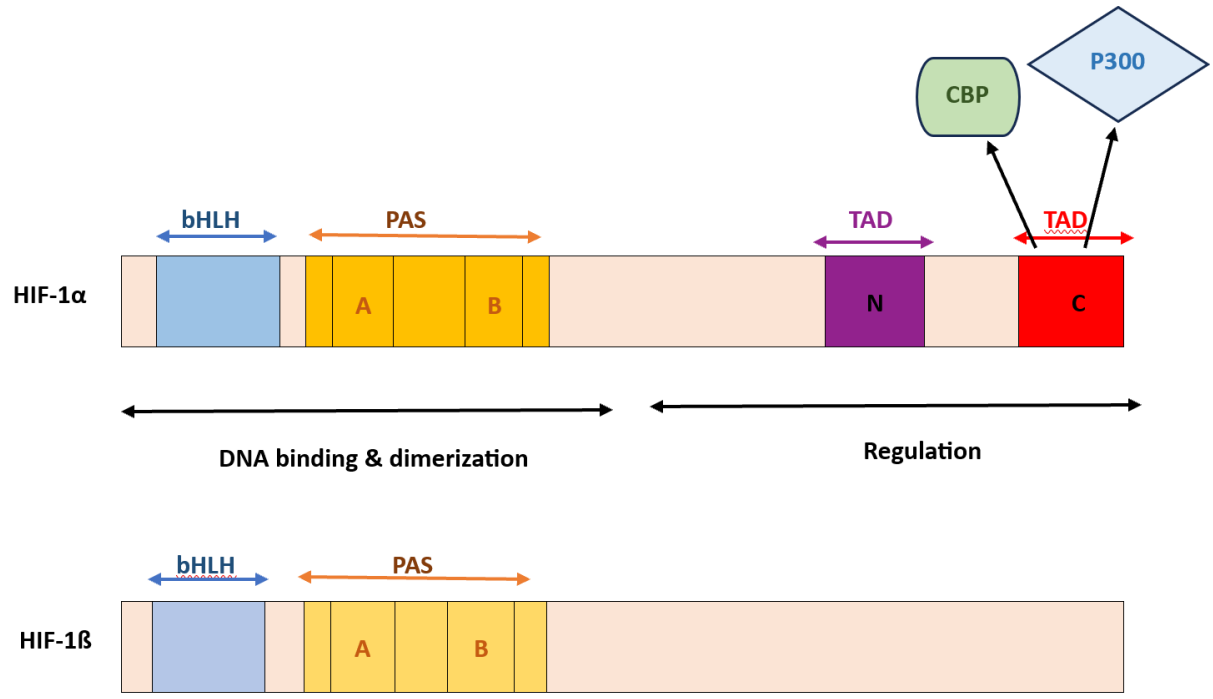


Figure 1.2.1: Domain architectures of HIF-1α and HIF-1β [25].

1.3 2-Oxoglutarate (2-OG) dependent oxygenase

2-Oxoglutarate (2-OG) dependent oxygenases (2-OGDDs) are an enzyme superfamily which most commonly catalyse hydroxylation and demethylation reactions, though in plants and microbes they catalyse a much wider range of reactions [40]. There are approximately seventy human 2OGDDs, which amongst other things have roles in the regulation of transcription, collagen by synthesis, lipid metabolism, and the hypoxic response. Although biochemical functions have been assigned to many human 2-OGDDs, the physiological functions a poorly understood. 2-OGDDs involved in the regulation of the chromatin machinery include the ten-eleven translocation TET enzymes,—human TET1, TET2, and TET3 - which are involved in oxidation of 5-methyl cytosine and its demethylation in DNA, through oxidation of 5-

methylcytosine to give 5-hydroxymethylcytosine and subsequent oxidation products [41]. The Jumonji C (JmjC) domain-containing histone 2OG dependent demethylases modify histones, in some cases in a manner reported to impact on chromatin structure and regulation of transcription by demethylating lysine- and arginine-residues on histone proteins [42,43]. Human members of the AlkB family of 2OGDDs, including ALKBH2 and ALKBH3, are involved in DNA damage repair via catalysing oxidative demethylations to repair alkylated nucleic acids [44]. The first 2-OG dependent oxygenases to be identified were the collagen prolyl and lysyl hydroxylases which catalyse post-translational modifications of collagen which are vital in extracellular matrix formation [46.47]. As described above and in more detail below, the HIF prolyl hydroxylases (PHDs) [47] and factors inhibiting HIF (FIH) [48], play key roles in regulating the hypoxic response.

1.3.1 HIF Prolyl Hydroxylases (PHDs)

The PHD enzymes are members of the non-heme ferrous iron dependent dioxygenase superfamily [12]. Catalysis by the PHDs depends on the presence of the cofactor Fe (II) and the co-substrates O_2, and 2-oxoglutarate (2-OG) [49]. There are three human isoforms, PHD1, PHD2, and PHD3, which are also known as EGLN2, EGLN1, and EGLN3, respectively [50]. There is another potential (as yet unvalidated) PHD isoform that has been recently characterized, named PH4/EGLN4/P4H-TM, which is structurally distinct from PHD1-3 [51].

PHD1 is mostly present in the brain, kidney, heart, and liver, whereas PHD2 (the most conserved of the PHDs in animals) is apparently present in almost every human tissue, whereas PHD3 and P4H-TM are reported to be mostly expressed in heart tissues [50,51].

PHD1 and PHD2 have 407 and 426 amino-acid residues respectively; on the other hand, PHD3 is shorter with 239 residues [4,5]. The PHDs have a conserved hydroxylase domain in their *C*-terminal region which is ~55% of the overall sequence of PHD2, whereas, the N-terminal regions are more diverse[4].

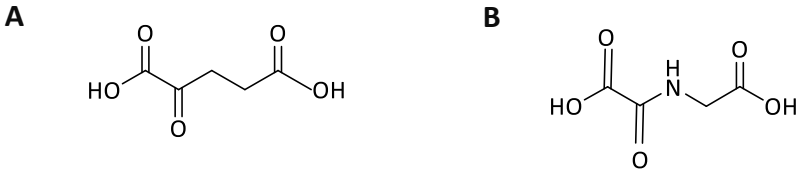
There is some evidence for the selectivity of the PHDs in the hydroxylation of HIFα protein isoforms, as well as evidence for different selectivity of the PHDs for different ODDs, with PHD3 preferentially acting on CODDs rather than NODDs, though these differences in selectivity are difficult to quantify in cells. PHD2 is proposed to be more active on HIF-1α compared to HIF-2α, whereas PHD1 and PHD3 are proposed to more effectively modify HIF-2α [52-54].

1.3.1.1 Non-HIF targets of PHDs

In addition to HIFα isoforms, multiple other human/animal substrates for the PHDs have been reported. Further PHD homologues in simple eukaryotes and bacteria have non-HIFα substrates, including elongation factor thermally unstable in bacteria.[55] In studies on human cells, important proteins such as tumor-suppressor protein p53, transcription factor Forkhead Box O3 (FOXO3a), epidermal growth factor receptor (EGFR), and nuclear factor-kappa B (NF-κB) are reported to be hydroxylated by PHDs [56] and the PHDs are reported to have HIF-independent effects on cell proliferation[56-58]. NF-κB has an important role in regulating inflammation and immune responses. The PHDs are reported to modulate the NF-κB pathway by hydroxylation of the inhibitor of NF-κB kinase subunit β (IKKβ), a reaction linking oxygen sensing to inflammation[59]. It is, however, important to state a study using

purified PHDs and substrates did not support any on the contemporary reported non HIFα PHD substrates[60].

1.4 PHD inhibitors can stabilize HIF-α



2-OG NOG

Figure 1.4.1: Structures of (A) 2-oxoglutarate (2-OG) and (B) N-oxalylglcyine (NOG), a broad spectrum 2OG oxygenase inhibitor [56]

Various small molecules and metal ions are linked to modulation of the hypoxic response, perhaps most notably Co (II) ions which have been used for the treatment of anaemia and which upregulate HIF-α isoforms (see below). Studies have also shown that naturally occurring organic compounds can cause HIF-α stabilization [12, 59, 61]. The PHDs need Fe(II) for their hydroxylase activity; various studies have shown that cobalt (II), copper (II), and nickel (II) ions can act as Fe(II) antagonists for the PHDs [62-64]. Furthermore, different iron chelators, such as deferoxamine mesylate, 3,4-dihydroxybenzoic acid, 1,10-phenanthroline, and quercetin, have also shown the capacity to upregulate HIF-α in cells. HIF-α upregulation and activation by these compounds is likely, at least in through restriction of the activities of the PHDs and FIH [2, 12, 59, 61].

Early research on developing selective PHD inhibitors began with the synthesis of 2-OG

analogues. N-Oxalylglycine (NOG) was the first 2-OG mimic to show activity against the PHDs in cells, where it was used in its dimethyloxalylglycine (DMOG) prodrug form [61]. Most, but not all, of the subsequently reported PHD inhibitors are 2-OG competitors, though some compete with HIF-α and some with both 2OG and HIF-α **(Figure 1.4)**[2].

1.5 PHD inhibitors in clinical use

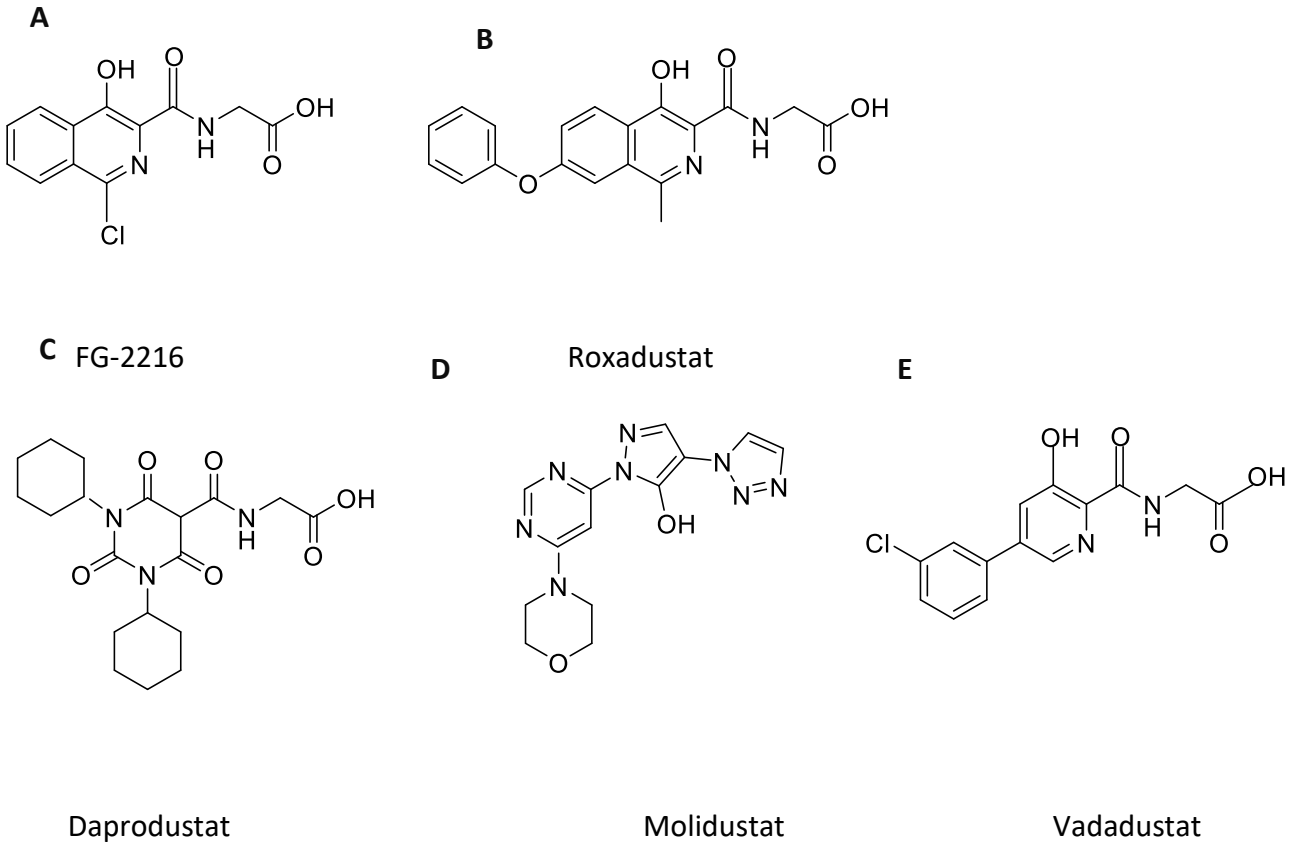


Figure 1.5.1: Structures of selected clinically used PHD inhibitors: (A) FG-2216, (B) Roxadustat (C)Daprodustat (D) Molidustat & (E) Vadadustat.

All the current clinically PHD inhibitors are 2OG competitors and bind at the PHD active side; they also contain at least one heterocyclic ring and bind in a manner that blocks HIF-α from binding with the active site (though HIF-α may bind away from the immediate active site region). These PHD inhibitors are used for the treatment of anaemia associated with chronic kidney disease (CKD). The clinically used PHD inhibitors have 3 common characteristics: (1) They all form a bidentate bond with the active site iron atom, (2) They all make interactions with the side chain of Arg383 (using the human PHD2 numbering system) (which forms a salt bridge with the 2OG C5 carboxylic acid), and (3) they all have a hydrogen bond acceptor for interaction with the phenolic hydroxyl group of Tyr303 (using the human PHD2 numbering system) [12, 5, 65-68].

FG-2216 was the first PHD inhibitor to be developed for clinical use (by Fibrogen) for the treatment of anaemia (**Figure 1.5.1 A**)[68]. However, due to adverse effects, FG-2216 was withdrawn from clinical development and was replaced with a structurally related compound, named FG-4592/ Roxadustat, which is now approved for clinical use for treatment of anaemia in chronic kidney disease (CKD) (**Figure 1.5.1 B**) [69].

Clinical PHD inhibitors that have passed through Phase III clinical trials are that is Daprodustat **(Figure 1.5.1 C)**, Molidustat **(Figure 1.5.1 D),** Vadadustat **(Figure 1.5.1 E)**, and Enarodustat [2, 69,70]. Moreover, Desidustat (ZYAN1) has been approved for the treatment of anaemia related to CKD in India and in the USA for the treatment of anaemia who have been under dialysis for at least four months [71]. JNJ-429045343 has also been reported to be under preclinical trials as a PHD inhibitor [70, 72].

1.6 The therapeutic application of PHD inhibitors

1.6.1 Anaemia

Multiple in vitro and in vivo studies provide evidence that the PHDs play roles in the regulation of erythropoiesis. One important example is the observation that PHD2 mutations are linked to higher blood haemoglobin levels [73]. These related observations have promoted interest in the use of PHD inhibitors for the treatment of various types of anaemia [74].

Often used treatments for anaemia include iron repletion and recombinant human EPO (rhEPO). However, the high price of rhEPO, the need for intravenous application, and treatment-related side effects mean rhEPO is an imperfect, though very useful, medicine. PHD inhibitors have potential benefits compared to current treatment options for anaemia, because they have the potential to be cheap and orally administered. As mentioned before PHD inhibitors can promote EPO production in the kidneys and liver via upregulation of HIF-α levels [75-77].

1.6.2 Ischemic Disease

HIF plays an important role in ischemic disease, which results from an impaired blood, and consequently O_2, supply [78]. As PHD inhibitors promote HIF accumulation and VEGF is a HIF target gene, they have the potential to protect against ischaemic diseases [58]. In addition to regulating VEGF, HIF is linked to ischemia via at least three different pathways. Firstly, HIF target genes are involved in the ischemic preconditioning process [79]; secondly, the HIF

pathway initiates metabolomic changes during hypoxia [80], and, lastly, ischemic preconditioning improves interleukin-10 transcription, which results in a reduction in the extent of myocardial infarction [81]. Different studies showed that direct inhibition of PHDs is associated with neuronal protection, and brain repair after stroke [82-85]. Several studies have been conducted to investigate the effects of PHD inhibitors on ischaemic animal models with positive results being observed [58].

1.6.3 Inflammation

Inflammation is associated with multiple diseases [65]. Inflamed tissues can induce hypoxia, and stimulate increased pro-inflammatory cytokines, which appear to collectively activate the HIF system [77, 86, 87]. Stabilisation of HIF-α has several impacts on inflammatory cells, including repairing tissues by decreasing cellular apoptosis and differentiation, as well as impacting the generation of cytokines [2,87]. Although the details are complex and more work is required, the overall evidence suggests that treatment with PHD inhibitors will have a positive impact on inflammation. Thus, treatment of a colitis mouse model with the PHD inhibitor FG-4497, increased the healing rate and reduced the inflammatory response [88]. Another study showed that treatment of acute lung injury mice models with FG-4497 reduces inflammatory infiltration and enhances the survival rate [89]. HIF-2α has also been reported to enable protective responses, such as an increased vascular barrier, in the lung [90].

1.6.4 Wound healing

Stabilization of HIF-1α by PHD inhibition is associated with improved tissue wound healing. HIF-1α target genes can influence inflammation, angiogenesis, and vasculogenesis, therefore stabilization of HIF-1α has the potential to help with wound healing. Studies have shown that when diabetic mice models were treated with PHD inhibitors there was an improved wound healing rate [91-95].

1.7 Natural / diet derived PHD inhibitors

The current clinically approved PHD inhibitors all come with side effects, such as liver failure and hypertension. Whether these side effects are due to on-target (i.e. PHD inhibition) or off target (e.g. inhibition of other human 2OG oxygenases) effects is presently unclear [96]. Iron supplementation remains a foundation of anaemia management and iron overload diseases are treated with synthetic metal-chelators.[97] The use of natural diets for PHD inhibition / HIF upregulation is an innovative and potentially sustainable method of treatment that has not been widely explored.

For most people, exposure to hypobaric hypoxia (at altitude, for example) or ingestion of moderate amounts of iron-chelators is not chronically toxic. Natural sources have long been used as medicinal treatments and starting points for drug discovery [98-100]. Use of natural food or plant-based diets rich in phytochemicals, such as flavonoids and other polyphenols, has the potential to act like an iron chelator and might be used for the treatment of anaemia[101-105]. Flavonoids are polyphenolic compounds found in foods, including tea, red

wine, citrus food, leafy vegetables & food, soy food, berries, dark chocolate, fruit, and nuts; are reported to help the body's natural mechanisms for treating anaemia [106]. Many phytochemicals can bind with iron, a property that may be useful not only for PHD inhibition, but also for other enzymes and globins, hence, caution is needed when using them, at least in high doses[101]. Further, natural medicines or remedies when used as extracts or in powdered form often have poorly defined components. A second complexity is that the desired effect may be due to a mixture of components.

Researchers have therefore been interested in exploring natural products/diets for PHD inhibition. Reported natural prolyl hydroxylase (PHD) inhibitors include compounds, including curcumin [107], quercetin [108], and epigallocatechin gallate (EGCG)[109]. These inhibitors work by reducing PHD activity; they can theoretically upregulate HIF-a consequently leading to downstream effects such as angiogenesis, erythropoiesis, and metabolic adaptation. More research on the mechanisms of action of these natural inhibitors may lead to them being a therapeutic option.

1.7.1 Role of $CoCl_2$ in the treatment of anaemia

Cobalt chloride was used since the 1930s for treating anaemia associated with chronic renal disease in humans [110]. Due to side effects, including gastro-intestinal disturbances, cardiomyopathy, nerve deafness, and thyroid dysfunction cobalt chloride was subsequently withdrawn from the market [110-115]. Treatment of cells with cobalt chloride stabilizes HIF-α, so upregulating erythropoietin (EPO) production. Athletes seek unjustified ways to stimulate EPO production and there has consequently been misuse of cobalt, as has been the

case for EPO itself and more recently PHD inhibitors [116]. In 2017, cobalt compounds, which are proposed to act via PHD inhibition, were added to the World Anti-Doping Agency's prohibited list of doping substances [117]. **Chapter 3** describes studies investigating the potential for diet / natural product-based therapies for anaemia via cobalt/natural product-mediated PHD inhibition.

1.8 Effects of proline and its analogues on the activity of PHD and the Regulation of HIF signalling

Along with metal ions [118,119] and iron chelators [120,121], proline analogues, when incorporated into HIF-1α derived peptides also have been stated to inhibit PHD activity [122-124].

Metal ions, such as Co(II) ions, inhibit by occupying the iron-binding site of the PHDs [4], whereas metal-ion chelators sequester iron from the PHDs [66, 125]. Unlike metal ion and iron chelators, proline analogue containing peptides have the potential to specifically inhibit PHD enzymes due to their HIF like structures [9, 123, 124]. To date, all the proline analogues reported as PHD inhibitors acting against the isolated enzymes are peptides – these are unlikely to be useful in cells or in vivo contexts. Chapter 3 of this thesis describes studies on simple proline derivatives such as thioproline, azitidine, L-proline as PHD inhibitors. Deuterated proline was also evaluated for its effect on PHD catalysis.

1.9 PHD enhancers

Hypoxia plays a critical role in the growth and progression of cancer. Hypoxia is a hallmark of solid tumours and one which can indicate that treatment of such tumours will be challenging. HIF-1α is one of the factors that is responsible for tumour cell adaptation and survival, even sometimes aggravating tumour progression [126-128]. In kidney tumours, mutations to the von Hippel Lindau protein cause stabilisation of HIF-2α and a drug (Belzutifan) suppressing HIF-2α activity has been developed to treat such (von Hippel Lindau disease)[129, 130]. HIF-1α is also proposed to help cancer cells for being targeted by cytotoxic T-lymphocytes [131, 132]. The presence of HIF-1α can cause resistance to chemo/radiotherapy, and over-expression of HIF can cause poor prognosis of cancers [133-135]. Therefore, either inhibiting HIF mediated transcription or enhancing PHD activity are promising strategies for novel cancer therapies. **Chapter 4** describes studies on potential PHD enhancers.

1.10 Metabolomics

Metabolomics is the youngest of the main 'omics' techniques which have revolutionized approaches used to understanding cellular chemistry in the 21st century. Metabolomics provides a comprehensive analysis of metabolites and their abundance changes in cells, tissues, biofluids and other tissues from living organisms [136]. Metabolomics most commonly involves the use of liquid chromatography coupled with mass spectrometry (LC-MS) to analyse the thousands of small metabolites (molecular weight ≤1500 Da), which function as intermediates or end products in the catabolic and anabolic reactions that sustain

life in biological systems [137].

Metabolomics offers a semi-quantitative approach for investigating metabolic states under different experimental conditions [136], including functional analysis of biological pathways. There are two types of metabolomics analysis [128]. One involves targeted approaches which analyse, or look for, a known group of metabolites to answer a defined biological question [129, 130]. A second approach involves untargeted analysis which measures as many metabolites as possible without distinction in a biological sample [129, 131-135]; untargeted analysis provides a way to explore metabolic changes, using statistical analysis of the data, which is hypothesis-generating [126, 136]. Metabolomics methods can be used to analyse various biological sample types, including urine, plasma, faeces, tissue, and mammalian cells treated with drugs [138]. Progress in mass spectrometry (MS) metabolomics technology has led to relatively high-throughput workflows to investigate specific metabolites and/or obtain a comprehensive profiling of metabolites within a biological matrix [139-150].

A semi-targeted analysis employing both targeted and untargeted analysis allows the identification and comparison of metabolites based on known standards and, simultaneously, analyses unknown features present in the same biological system.

Chapter 5 describes a semi targeted analysis of HEK 293T cells treated with different types of PHD inhibitors: (1) the clinically used PHD inhibitor Roxadustat, (2) the clinically used PHD inhibitor Molidustat; (3) the hypoxia mimic agent, $CoCl_2$ and, (4) hypoxia (1% O_2).

1.10.1 Metabolomics Data

Apart from the choice of analysis (targeted/untargeted/semi-targeted), the selection of instrumentation to analyse the samples plays an important role in the datasets generated in metabolomics experiments. MS is the commonly used method to generate metabolomics data. 'Hyphenated' MS techniques such as gas chromatography coupled with mass spectrometry (GC-MS), liquid chromatography coupled with mass spectrometry (LC-MS), reversed phase chromatography–mass spectrometry using ion-pairing agents (IP-MS), and hydrophilic interaction chromatography–mass spectrometry (HILIC-MS) are common hyphenated chromatographic-mass spectrometry techniques, which can provide high selectivity and quantitation capabilities [151-156]. First, compounds are separated, then they are subjected to different types of MS, which detects compounds based on their mass-to-charge ratio (*m/z*) [139]. Apart from MS, nuclear magnetic resonance (NMR) spectroscopy is also used for metabolomic analysis [157]. Once the MS has detected metabolites in a sample, the data are pre-processed and normalized [158]. As described above, metabolomic analyses can then be performed either in a targeted manner (where the researcher analyses (a) specific metabolite(s) or in an untargeted manner (where unknown compounds are identified based on available metabolomics databases) [159, 160].

1.11 Ion-chromatography coupled with mass spectrometry (IC-MS)

Traditional techniques such as GC-MS, LC-MS, IP-MS, and HILIC-MS are usually used for the analysis of highly polar and ionic compounds, but these methods often face limitations when

it comes to analysing ionic and ionizable analytes [148-152]. For example, GC-MS can analyse volatile molecules, but for polar and ionic molecules, derivatisation is required before GC-MS analysis reducing its analytical capability [156, 161-164]. IP-MS and HILIC-MS can analyse non-volatile and highly polar compounds without derivatisation, but like the GC-MS method, these methods also have limitations in analysing ionic and ionizable analytes [164]. Ion-exchange chromatography (IEC) coupled with mass spectrometry (IC-MS) provides a relatively new hyphenated mass spectrometry technique for metabolomics that is well-suited to the analysis of ionizable compounds from complex biological samples, making it an effective alternative to some of the traditional methods commonly used, providing enhanced sensitivity, selectivity and robustness, particularly for metabolites found in primary metabolism [165,166].

1.12 Aims of the work described in this thesis

The research described in this thesis focused on: (i) investigating a novel and selective PHD inhibitor / HIF modulator named IOX5, (ii) investigating the use of a natural mixture (*Spinacia Oleracea* leaf extracts) and proline analogues as potential PHD inhibitors; (iii) cellular studies on a PHD enhancer; and (iv) metabolomics studies on HEK293T cells to compare and contrast metabolic changes in cells treated with hypoxia (1% O_2), $CoCl_2$ (a hypoxia mimicking agent), and the clinical PHD inhibitors Roxadustat and Molidustat.

The individual aims of the work described in the thesis are as follows with the relevant chapter in parentheses:

1. Cell studies using a novel selective PHD inhibitor (IOX5) (Chapter 2)

2. Evaluation of natural extracts (*Spinacia Oleracea* leaf extracts) for PHD inhibition (Chapter 3)
3. Evaluation of different proline analogues as PHD inhibitors and investigations on mammalian cells treated with those proline analogs (Chapter 3)
4. Cellular investigations of a novel PHD enhancer (Chapter 4)
5. Semi-targeted metabolomics analysis of HEK 293T cells treated with (i) hypoxia (1% O_2), (ii) a hypoxia mimicking agent ($CoCl_2$), (iii) with different concentrations of the clinically used PHD inhibitor Roxadustat, and (iv) with different concentrations the clinically used PHD inhibitor Molidustat (Chapter 5)
6. Comparison of the metabolomics results between the experimental groups defined in (5). (Chapter 5)
7. Investigations into the impact on glycolysis in HEK 293T cells treated with the experimental groups defined in chapter 5 (except natural hypoxia). Chapter 5)
8. Pathway analysis of the experimental groups defined in chapter 5 to compare altered metabolic pathways. (Chapter 5)

1.13 References

1. McKeown SR. Defining normoxia, physoxia and hypoxia in tumours-implications for treatment response. Br J Radiol. 2014 Mar;87(1035):20130676. doi: 10.1259/bjr.20130676. PMID: 24588669; PMCID: PMC4064601.
2. Hirota, K., *HIF-α prolyl hydroxylase inhibitors and their implications for biomedicine: a comprehensive review.* Biomedicines, 2021. 9(5): p. 468. DOI: 10.3390/biomedicines9050468
3. Cavadas, M.A., L.K. Nguyen, and A. Cheong, *Hypoxia-inducible factor (HIF) network: insights from mathematical models.* J. Cell Commun. Signal., 2013. 11: p. 1-16. DOI: 10.1186/1478-811X-11-42
4. Epstein, A.C., et al., C. *elegans EGL-9 and mammalian homologs define a family of dioxygenases that regulate HIF by prolyl hydroxylation*. Cell, 2001. 107(1): p. 43-54. DOI: 10.1016/s0092-8674(01)00507-4
5. Bruick, R.K. and S.L. McKnight, *A conserved family of prolyl-4-hydroxylases that modify HIF.* Science, 2001. 294(5545): p. 1337-1340. DOI: 10.1126/science.1066373
6. Masson, N., et al., *Independent function of two destruction domains in hypoxia-inducible factor-α chains activated by prolyl hydroxylation*. The EMBO journal, 2001. DOI: 10.1093/emboj/20.18.5197
7. Maxwell, P.H., et al., *The tumour suppressor protein VHL targets hypoxia-inducible factors for oxygen-dependent proteolysis*. Nature, 1999. 399(6733): p. 271-275. DOI: 10.1038/20459

8. Ivan, M., et al., *HIFα targeted for VHL-mediated destruction by proline hydroxylation: implications for O2 sensing*. Science, 2001. 292(5516): p. 464-468. DOI: 10.1126/science.1059817
9. Jaakkola, P., et al., *Targeting of HIF-α to the von Hippel-Lindau ubiquitylation complex by O2-regulated prolyl hydroxylation*. Science, 2001. 292(5516): p. 468-472. DOI: 10.1126/science.1059796
10. Ivanov, S., et al., *Expression of hypoxia-inducible cell-surface transmembrane carbonic anhydrases in human cancer*. Am. J. Pathol , 2001. 158(3): p. 905-919. DOI: 10.1016/S0002-9440(10)64038-2
11. Yu, F., et al., *HIF-1α binding to VHL is regulated by stimulus-sensitive proline hydroxylation*. Proc. Natl. Acad. Sci., 2001. 98(17): p. 9630-9635. DOI: 10.1073/pnas.181341498
12. Schofield, C.J. and P.J. Ratcliffe, *Oxygen sensing by HIF hydroxylases.* Nat. Rev. Mol. Cell Biol. , 2004. 5(5): p. 343-354. DOI: 10.1038/nrm1366
13. Dames, S.A., et al., *Structural basis for Hif-1α/CBP recognition in the cellular hypoxic response.*Proc. Natl. Acad. Sci., 2002. 99(8): p. 5271-5276. DOI: 10.1073/pnas.082121399
14. Freedman, S.J., et al., *Structural basis for recruitment of CBP/p300 by hypoxia-inducible factor-1α.*Proc. Natl. Acad. Sci., 2002. 99(8): p. 5367-5372. DOI: 10.1073/pnas.082117899
15. Hewitson, K.S., et al., *Hypoxia-inducible factor (HIF) asparagine hydroxylase is identical*

to factor inhibiting HIF (FIH) and is related to the cupin structural family. J. Biol. Chem. , 2002. 277(29): p. 26351-26355. DOI: 10.1074/jbc.C200273200

16. Lando, D., et al., *Asparagine hydroxylation of the HIF transactivation domain: a hypoxic switch*. Science, 2002. 295(5556): p. 858-861. DOI: 10.1126/science.1068592
17. McNEILL, L.A., et al., *Hypoxia-inducible factor asparaginyl hydroxylase (FIH-1) catalyses hydroxylation at the β-carbon of asparagine-803.* Biochemical Journal, 2002. 367(3): p. 571-575. DOI: 10.1042/BJ20021162
18. Semenza, G.L., *Defining the role of hypoxia-inducible factor 1 in cancer biology and therapeutics*. Oncogene, 2010. 29(5): p. 625-634. DOI: 10.1038/onc.2009.441
19. Semenza, G. L. (2003). Targeting HIF-1 for cancer therapy. *Nature Reviews Cancer*, 3(10), 721–732. https://doi.org/10.1038/nrc1187
20. Wu, M. F., Zhang, G. D., & Liu, T. T. (2022). Hif-2α regulates lipid metabolism in alcoholic fatty liver disease through mitophagy. *Cell Bioscience*, 12, 198. https://doi.org/10.1186/s13578-022-00889-1
21. Luo, M., Li, T., & Sang, H. (2023). The role of hypoxia-inducible factor 1α in hepatic lipid metabolism. *Journal of Molecular Medicine (Berlin)*, 101(5), 487–500. https://doi.org/10.1007/s00109-023-02308-5
22. Shi, Y., & Gilkes, D. M. (2025). HIF-1 and HIF-2 in cancer: structure, regulation, and therapeutic prospects. *Cellular and Molecular Life Sciences*, 82, 44. https://doi.org/10.1007/s00018-024-05537-0
23. Semenza, G. L. (2012). Hypoxia-inducible factors in physiology and medicine. *Cell*,

148(3), 399–408. https://doi.org/10.1016/j.cell.2012.01.021

24. Makino, Y., Cao, R., Svensson, K., Bertilsson, G., Asman, M., Tanaka, H., ... & Poellinger, L. (2001). Inhibitory PAS domain protein is a negative regulator of hypoxia-inducible gene expression. *Nature*, 414(6863), 550–554. https://doi.org/10.1038/35107085
25. Zhang, P., Yao, Q., Lu, L., Li, Y., Chen, P. J., & Duan, C. (2014). Hypoxia-inducible factor 3 is an oxygen-dependent transcription activator and regulates a distinct transcriptional response to hypoxia. *Cell Reports*, 6(6), 1110–1121. https://doi.org/10.1016/j.celrep.2014.02.013
26. Lisy, K., & Peet, D. (2008). Turn me on: regulating HIF transcriptional activity. *Cell Death & Differentiation*, 15(4), 642–649. https://doi.org/10.1038/sj.cdd.4402315
27. Tolonen, J. P., Heikkilä, M., Malinen, M., Lee, H. M., Palvimo, J. J., Wei, G. H., & Myllyharju, J. (2020). A long hypoxia-inducible factor 3 isoform 2 is a transcription activator that regulates erythropoietin. *Cellular and Molecular Life Sciences*, 77(18), 3627–3642. https://doi.org/10.1007/s00018-019-03387-9
28. Wang V, Davis DA, Haque M, Huang LE, Yarchoan R. Differential gene up-regulation by hypoxia-inducible factor-1α and hypoxia-inducible factor-2α in HEK293T cells. Cancer research. 2005 Apr 15;65(8):3299-306.
29. Wang, G.L., et al., *Hypoxia-inducible factor 1 is a basic-helix-loop-helix-PAS heterodimer regulated by cellular O2 tension*.Proc. Natl. Acad. Sci., 1995. 92(12): p. 5510-5514. DOI: 10.1073/pnas.92.12.5510
30. Yang, J., et al., *Functions of the Per/ARNT/Sim domains of the hypoxia-inducible*

factor.J. Biol. Chem. , 2005. 280(43): p. 36047-36054. DOI: 10.1074/jbc.M501755200

31. Chapman-Smith, A., J.K. Lutwyche, and M.L. Whitelaw, *Contribution of the Per/Arnt/Sim (PAS) domains to DNA binding by the basic helix-loop-helix PAS transcriptional regulators*.J. Biol. Chem. , 2004. 279(7): p. 5353-5362. DOI: 10.1074/jbc.M310041200
32. Kaelin, W.G. and P.J. Ratcliffe, *Oxygen sensing by metazoans: the central role of the HIF hydroxylase pathway.*Molecular cell. , 2008. 30(4): p. 393-402. DOI: 10.1016/j.molcel.2008.04.009
33. Abboud, M.I., et al., *2-Oxoglutarate regulates binding of hydroxylated hypoxia-inducible factor to prolyl hydroxylase domain 2*.ChemComm. , 2018. 54(25): p. 3130-3133. DOI: 10.1039/c8cc00387d
34. Wenger, R.H., D.P. Stiehl, and G. Camenisch, *Integration of oxygen signaling at the consensus HRE.* Science's STKE, 2005. 2005(306): p. re12-re12. DOI: 10.1126/stke.3062005re12
35. Chowdhury, R., A. Hardy, and C.J. Schofield, *The human oxygen sensing machinery and its manipulation.* Chem. Soc. Rev., 2008. 37(7): p. 1308-1319. DOI: 10.1039/b701676j
36. Ziello, J.E., I.S. Jovin, and Y. Huang, *Hypoxia-Inducible Factor (HIF)-1 regulatory pathway and its potential for therapeutic intervention in malignancy and ischemia*.Yale J. Biol. Med. , 2007. 80(2): p. 51.
37. Zhulin, I.B., B.L. Taylor, and R. Dixon, *PAS domain S-boxes in Archaea, Bacteria and sensors for oxygen and redox.*Trends Biochem Sci. , 1997. 22(9): p. 331-333.

DOI: 10.1016/s0968-0004(97)01110-9

38. Ponting, C.P. and L. Aravind, *PAS: a multifunctional domain family comes to light.* Curr. Biol. , 1997. 7(11): p. R674-R677. DOI: 10.1016/s0960-9822(06)00352-6
39. Yang, C., et al., *Analysis of hypoxia-induced metabolic reprogramming.* Methods Enzymol. , 2014. 542: p. 425-455. DOI: 10.1016/B978-0-12-416618-9.00022-4
40. Fletcher, S. C., & Coleman, M. L. (2020). Human 2-oxoglutarate-dependent oxygenases: nutrient sensors, stress responders, and disease mediators. *Biochemical Society Transactions*, 48(5), 1843–1858. https://doi.org/10.1042/BST20190333
41. Zhang, X., Zhang, Y., & Wang, C. (2023). TET (Ten-eleven translocation) family proteins: structure, biological functions and applications. Signal Transduction and Targeted Therapy, 8, 297. https://doi.org/10.1038/s41392-023-01537-x
42. Tsukada, Y., Fang, J., Erdjument-Bromage, H., et al. (2006). Histone demethylation by a family of JmjC domain-containing proteins. *Nature*, 439(7078), 811–816. https://doi.org/10.1038/nature04433
43. Walport, L.J., R.J. Hopkinson, R. Chowdhury, R. Schiller, W. Ge, A. Kawamura, and C.J. Schofield, Arginine demethylation is catalysed by a subset of JmjC histone lysine demethylases. *Nat Commun.*, 2016. 7(1): p. 11974. DOI: 10.1038/ncomms11974
44. Falnes, P. Ø., Johansen, R. F., & Seeberg, E. (2002). AlkB-mediated oxidative demethylation reverses DNA damage in Escherichia coli. *Nature*, 419(6903), 178–182. https://doi.org/10.1038/nature00931
45. Longbotham, J. E., Levy, C., Johannissen, L. O., Tarhonskaya, H., Jiang, S., Loenarz, C.,

& Scrutton, N. S. (2015). Structure and Mechanism of a Viral Collagen Prolyl Hydroxylase. *Biochemistry*, 54(39), 6093–6105. https://doi.org/10.1021/acs.biochem.5b00789

46. Myllyharju, J. (2003). Prolyl 4-hydroxylases, the key enzymes of collagen biosynthesis. *Matrix Biology*, 22(1), 15–24. https://doi.org/10.1016/S0945-053X(03)00006-4
47. Schofield, C. J., & Ratcliffe, P. J. (2004). Oxygen sensing by HIF hydroxylases. *Nature Reviews Molecular Cell Biology*, 5(5), 343–354. https://doi.org/10.1038/nrm1366
48. Hewitson, K. S., et al. (2002). Hypoxia-inducible factor (HIF) asparagine hydroxylase is identical to factor inhibiting HIF (FIH) and is related to the cupin structural family. *Journal of Biological Chemistry*, 277(29), 26351–26355. https://doi.org/10.1074/jbc.C200273200
49. Hogenesch, J.B., et al., *The basic-helix–loop–helix-PAS orphan MOP3 forms transcriptionally active complexes with circadian and hypoxia factors*.Proc. Natl. Acad. Sci., 1998. 95(10): p. 5474-5479. DOI: 10.1073/pnas.95.10.5474
50. Hirsila, M., et al., *Characterization of the human prolyl 4-hydroxylases that modify the hypoxia-inducible factor.*J. Biol. Chem. , 2003. 278(33): p. 30772-30780. DOI: 10.1074/jbc.M304982200
51. Lieb, M.E., et al., *Mammalian EGLN genes have distinct patterns of mRNA expression and regulation*. Biochem. Cell Biol. , 2002. 80(4): p. 421-426. DOI: 10.1139/o02-115
52. Byts, N., et al., *Inactivation of mouse transmembrane prolyl 4-hydroxylase increases blood brain barrier permeability and ischemia-induced cerebral neuroinflammation*.J.

Biol. Chem. , 2022. 298(3). DOI: 10.1016/j.jbc.2022.101721

53. Appelhoff, R.J., et al., *Differential function of the prolyl hydroxylases PHD1, PHD2, and PHD3 in the regulation of hypoxia-inducible factor*.J. Biol. Chem. , 2004. 279(37): p. 38458-38465. DOI: 10.1074/jbc.M406026200
54. Metzen, E., et al., *Regulation of the prolyl hydroxylase domain protein 2 (phd2/egln-1) gene: identification of a functional hypoxia-responsive element*.Biochem. J. , 2005. 387(3): p. 711-717. DOI: 10.1042/BJ20041736
55. Fiorini G, Schofield CJ. Biochemistry of the hypoxia-inducible factor hydroxylases. Current Opinion in Chemical Biology. 2024 Apr 1;79:102428.
56. Watts, E. R., & Walmsley, S. R. (2019). Inflammation and hypoxia: HIF and PHD isoform selectivity. *Trends in Molecular Medicine*, 25(1), 33–46. https://doi.org/10.1016/j.molmed.2018.10.006
57. Strowitzki, M. J., Cummins, E. P., & Taylor, C. T. (2019). Protein Hydroxylation by Hypoxia-Inducible Factor (HIF) Hydroxylases: Unique or Ubiquitous? *Cells*, 8(5), 384. https://doi.org/10.3390/cells8050384
58. Cummins, E. P., Berra, E., Comerford, K. M., Ginouves, A., Fitzgerald, K. T., Seeballuck, F., ... & Taylor, C. T. (2006). Prolyl hydroxylase-1 negatively regulates IκB kinase-β, giving insight into hypoxia-induced NFκB activity. *Proceedings of the National Academy of Sciences*, 103(48), 18154–18159. https://doi.org/10.1073/pnas.0602235103
59. Pescador, N., et al., *Identification of a functional hypoxia-responsive element that*

regulates the expression of the egl nine homologue 3 (egln3/phd3) gene.Biochem. J . , 2005. 390(1): p. 189-197. DOI: 10.1042/BJ20042121

60. Cockman ME, Lippl K, Tian YM, Pegg HB, Figg WD, Abboud MI, Heilig R, Fischer R, Myllyharju J, Schofield CJ, Ratcliffe PJ. Lack of activity of recombinant HIF prolyl hydroxylases (PHDs) on reported non-HIF substrates. Elife. 2019 Sep 10;8:e46490. DOI: 10.7554/eLife.46490
61. Chan, M.C., et al., *Pharmacological targeting of the HIF hydroxylases–a new field in medicine development*.Mol. Asp. Med. , 2016. 47: p. 54-75. DOI: 10.1016/j.mam.2016.01.001
62. Wilkins, S.E., et al., *Targeting protein–protein interactions in the HIF system.* ChemMedChem, 2016. 11(8): p. 773-786. DOI: 10.1002/cmdc.201600012
63. Joharapurkar, A.A., et al., *Prolyl hydroxylase inhibitors: a breakthrough in the therapy of anemia associated with chronic diseases*.J. Med. Chem.2018. 61(16): p. 6964-6982. DOI: 10.1021/acs.jmedchem.7b01686
64. Goldberg, M.A., et al., *The regulated expression of erythropoietin by two human hepatoma cell lines.*Proc. Natl. Acad. Sci., 1987. 84(22): p. 7972-7976. DOI: 10.1073/pnas.84.22.7972
65. Goldberg, M.A., S.P. Dunning, and H.F. Bunn, *Regulation of the erythropoietin gene: evidence that the oxygen sensor is a heme protein.* Science, 1988. 242(4884): p. 1412-1415. DOI: 10.1126/science.2849206
66. Goldwasser, E., et al., *Studies on erythropoiesis: V. The effect of cobalt on the*

production of erythropoietin. Blood, 1958. 13(1): p. 55-60.

67. Chan, M.C., et al., *Potent and selective triazole-based inhibitors of the hypoxia-inducible factor prolyl-hydroxylases with activity in the murine brain*. PLoS One, 2015. 10(7): p. e0132004. DOI: 10.1371/journal.pone.0132004
68. McDonough, M.A., et al., *Cellular oxygen sensing: Crystal structure of hypoxia-inducible factor prolyl hydroxylase (PHD2)*.Proc. , 2006. 103(26): p. 9814-9819. DOI: 10.1073/pnas.0601283103
69. Chowdhury, R., et al., *Structural basis for binding of hypoxia-inducible factor to the oxygen-sensing prolyl hydroxylases.* Structure, 2009. 17(7): p. 981-989. DOI: 10.1016/j.str.2009.06.002
70. Chowdhury, R., et al., *Selective small molecule probes for the hypoxia inducible factor (HIF) prolyl hydroxylases.*ACS Chem. Biol. , 2013. 8(7): p. 1488-1496. DOI: 10.1021/cb400088q
71. Yeh, T.-L., et al., *Molecular and cellular mechanisms of HIF prolyl hydroxylase inhibitors in clinical trials.* Chemical science, 2017. 8(11): p. 7651-7668. DOI: 10.1039/c7sc02103h
72. Yap, D.Y., et al., *Recommendations by the Asian Pacific society of nephrology (APSN) on the appropriate use of HIF-PH inhibitors*. Nephrology, 2021. 26(2): p. 105-118. DOI: 10.1111/nep.13835
73. Joharapurkar A, Pandya V, Patel H, Jain M, Desai R. *Desidustat: a novel PHD inhibitor for the treatment of CKD-induced anemia.* Front. Nephrol. 2024 Oct

22;4:1459425. DOI: 10.3389/fneph.2024.1459425

74. Barrett, T.D., et al., *Prolyl hydroxylase inhibition corrects functional iron deficiency and inflammation-induced anaemia in rats*.Br. J. Pharmacol. , 2015. 172(16): p. 4078-4088. DOI: 10.1111/bph.13188
75. Percy, M.J., et al., *A gain-of-function mutation in the HIF2A gene in familial erythrocytosis*.N Engl J Med. , 2008. 358 2: p. 162-8. DOI: 10.1056/NEJMoa073123
76. Rabinowitz, M.H., et al., *Inhibitors of HIF prolyl hydroxylases*, inAnnu. Rep. Med. Chem . 2010, Elsevier. p. 123-139. DOI: 10.1021/jm400386j
77. Yan, L., V.J. Colandrea, and J.J. Hale, *Prolyl hydroxylase domain-containing protein inhibitors as stabilizers of hypoxia-inducible factor: small molecule-based therapeutics for anemia.*Expert Opin. Ther. Pat. , 2010. 20(9): p. 1219-1245. DOI: 10.1517/13543776.2010.510836
78. Muchnik, E. and J. Kaplan, *HIF prolyl hydroxylase inhibitors for anemia.*Expert Opin Investig Drugs. , 2011. 20(5): p. 645-656. DOI: 10.1517/13543784.2011.566861
79. Kim, S.Y. and E.G. Yang, *Recent advances in developing inhibitors for hypoxia-inducible factor prolyl hydroxylases and their therapeutic implications*. Molecules, 2015. 20(11): p. 20551-20568. DOI: 10.3390/molecules201119717
80. Hausenloy, D.J. and D.M. Yellon, *Myocardial ischemia-reperfusion injury: a neglected therapeutic target.*J. Clin. Investig. , 2013. 123(1): p. 92-100. DOI: 10.1172/JCI62874
81. Eckle, T., et al., *Hypoxia-inducible factor-1 is central to cardioprotection: a new paradigm for ischemic preconditioning*. Circulation, 2008. 118(2): p. 166-175.

DOI: 10.1161/CIRCULATIONAHA.107.758516

82. Eckle, T., et al., *Adora2b-elicited Per2 stabilization promotes a HIF-dependent metabolic switch crucial for myocardial adaptation to ischemia*. Nature medicine, 2012. 18(5): p. 774-782. DOI: 10.1038/nm.2728
83. Cai, Z., et al., *Hypoxia-inducible factor 1 is required for remote ischemic preconditioning of the heart*.Proc. Natl. Acad. Sci., 2013. 110(43): p. 17462-17467. DOI: 10.1073/pnas.1317158110
84. Karuppagounder, S.S. and R.R. Ratan, *Hypoxia-inducible factor prolyl hydroxylase inhibition: robust new target or another big bust for stroke therapeutics?*J Cereb Blood Flow Metab. , 2012. 32(7): p. 1347-1361. DOI: 10.1038/jcbfm.2012.28
85. Siddiq, A., et al., *Hypoxia-inducible factor prolyl 4-hydroxylase inhibition: a target for neuroprotection in the central nervous system*.J. Biol. Chem. , 2005. 280(50): p. 41732-41743. DOI: 10.1074/jbc.M504963200
86. Baranova, O., et al., *Neuron-specific inactivation of the hypoxia inducible factor 1α increases brain injury in a mouse model of transient focal cerebral ischemia.*J. Neurosci. , 2007. 27(23): p. 6320-6332. DOI: 10.1523/JNEUROSCI.0449-07.2007
87. Nagel, S., et al., *Neuroprotection by dimethyloxalylglycine following permanent and transient focal cerebral ischemia in rats.*J Cereb Blood Flow Metab. , 2011. 31(1): p. 132-143. DOI: 10.1038/jcbfm.2010.60
88. Eltzschig, H.K. and P. Carmeliet, *Hypoxia and inflammation.*N Engl J Med. , 2011.

364(7): p. 656-665. DOI: 10.1056/NEJMra0910283

89. Dang, E.V., et al., *Control of TH17/Treg balance by hypoxia-inducible factor 1.* Cell, 2011. 146(5): p. 772-784. DOI: 10.1016/j.cell.2011.07.033
90. Keely, S., et al., *Contribution of epithelial innate immunity to systemic protection afforded by prolyl hydroxylase inhibition in murine colitis*.Mucosal Immunol. , 2014. 7(1): p. 114-123. DOI: 10.1038/mi.2013.29
91. Gong, H., et al., *HIF2α signaling inhibits adherens junctional disruption in acute lung injury*.J. Clin. Investig. , 2015. 125(2): p. 652-664. DOI: 10.1172/JCI77701
92. Choi, H., et al., *Rapid degradation of hypoxia-inducible factor-1α by KRH102053, a new activator of prolyl hydroxylase* 2.Br. J. Pharmacol. , 2008. 154(1): p. 114-125. DOI: 10.1038/bjp.2008.70
93. Botusan, I.R., et al., *Stabilization of HIF-1α is critical to improve wound healing in diabetic mice.*Proc. Natl. Acad. Sci., 2008. 105(49): p. 19426-19431. DOI: 10.1073/pnas.0805230105
94. Kalucka, J., et al., *Loss of epithelial hypoxia-inducible factor prolyl hydroxylase 2 accelerates skin wound healing in mice*.Mol Cell Biol. , 2013. 33(17): p. 3426-3438. DOI: 10.1128/MCB.00609-13
95. Thangarajah, H., et al., *HIF-1α dysfunction in diabetes.* Cell cycle, 2010. 9(1): p. 75-79. DOI: 10.4161/cc.9.1.10371
96. Zhang, X., N. Alshakhshir, and L. Zhao, *Glycolytic metabolism, brain resilience, and Alzheimer's disease.*Front. Neurosci. , 2021. 15: p. 476.

DOI: 10.3389/fnins.2021.662242

97. . Brittenham GM. Iron chelators and iron toxicity. Alcohol. 2003 Jun 1;30(2):151-8. https://doi.org/10.1016/S0741-8329(03)00101-0

98. Myllyharju, J., *Prolyl 4-hydroxylases, master regulators of the hypoxia response*.Acta Physiol. , 2013. 208(2): p. 148-165. DOI: 10.1111/apha.12096

99. Del Vecchio, L. and F. Locatelli, *Roxadustat in the treatment of anaemia in chronic kidney disease.*Expert Opin. Investig. Drugs . , 2018. 27(1): p. 125-133. DOI: 10.1080/13543784.2018.1417386

100. Fu, T., et al., *VARIDT 2.0: structural variability of drug transporter.*Nucleic Acids Res. , 2022. 50(D1): p. D1417-D1431. DOI: 10.1093/nar/gkab1013

101. Fu, T., et al., *Exploring the binding mechanism of metabotropic glutamate receptor 5 negative allosteric modulators in clinical trials by molecular dynamics simulations*.ACS Chem. Neurosci. , 2018. 9(6): p. 1492-1502. DOI: 10.1021/acschemneuro.8b00059

102. Goddard, T.D., C.C. Huang, and T.E. Ferrin, *Software extensions to UCSF chimera for interactive visualization of large molecular assemblies*. Structure, 2005. 13(3): p. 473-482. DOI: 10.1016/j.str.2005.01.006

103. Hatcher, H.C., et al., *Synthetic and natural iron chelators: therapeutic potential and clinical use*.Future Med. Chem. , 2009. 1(9): p. 1643-1670. DOI: 10.4155/fmc.09.121

104. Kell, D.B., *Iron behaving badly: inappropriate iron chelation as a major*

contributor to the aetiology of vascular and other progressive inflammatory and degenerative diseases.BMC Med Genomics. , 2009. 2: p. 1-79. DOI: 10.1186/1755-8794-2-2

105. Morel, I., et al., *Antioxidant and iron-chelating activities of the flavonoids catechin, quercetin and diosmetin on iron-loaded rat hepatocyte cultures.* Biochem. Pharmacol.1993. 45(1): p. 13-19. DOI: 10.1016/0006-2952(93)90371-3

106. Hider, R.C., Z.D. Liu, and H.H. Khodr, *Metal chelation of polyphenols*, in *Methods in enzymology*. 2001, Elsevier. p. 190-203. DOI: 10.1016/s0076-6879(01)35243-6

107. Hatcher, H., et al., *Curcumin: from ancient medicine to current clinical trials.*Cell. Mol. Life Sci. , 2008. 65: p. 1631-1652. DOI: 10.1007/s00018-008-7452-4

108. Rao, Y.K., et al., *Antioxidant and cytotoxic activities of naturally occurring phenolic and related compounds: a comparative study*.Food Chem Toxicol. , 2007. 45(9): p. 1770-1776. DOI: 10.1016/j.fct.2007.03.012

109. Bahrami, A., et al., *Effects of curcumin on hypoxia-inducible factor as a new therapeutic target*.Pharmacol. Res. , 2018. 137: p. 159-169. DOI: 10.1016/j.phrs.2018.10.009

110. Jeon, H., et al., *Quercetin activates an angiogenic pathway HIF-1-VEGF by inhibiting HIF-prolyl hydroxylase: A structural analysis of quercetin for inhibiting HIF-prolyl hydroxylase.*Mol. Pharmacol. , 2007. DOI: 10.1124/mol.107.034041

111. Weinreb, O., et al., *Neuroprotective molecular mechanisms of (−)-epigallocatechin-3-gallate: a reflective outcome of its antioxidant, iron chelating and*

*neuritogenic properties.*Genes nutr , 2009. 4: p. 283-296. DOI: 10.1007/s12263-009-0143-4

112. Bowie, E. and P. Hurley, *Cobalt chloride in the treatment of refractory anaemia in patients undergoing long-term haemodialysis*.Aust N Z J Med. , 1975. 5(4): p. 306-313. DOI: 10.1111/j.1445-5994.1975.tb03263.x

113. Gardner, F.H., *The use of cobaltous chloride in the anemia associated with chronic renal disease*.J Lab Clin Med. , 1953. 41(1): p. 56-64.

114. Kesteloot, H., et al., *An enquiry into the role of cobalt in the heart disease of chronic beer drinkers*. Circulation, 1968. 37(5): p. 854-864. DOI: 10.1161/01.cir.37.5.854

115. Little, J.A. and R. Sunico, *Cobalt-induced goiter with cardiomegaly and congestive failure.*J. Pediatr. , 1958. 52(3): p. 284-288. DOI: 10.1016/s0022-3476(58)80117-1

116. Morin, Y. and P. Daniel, *Quebec beer-drinkers' cardiomyopathy: etiological considerations.*Can. Med. Assoc. J. , 1967. 97(15): p. 926.

117. Kriss, J.P., W.H. Carnes, and R.T. Gross, *Hypothyroidism and thyroid hyperplasia in patients treated with cobalt.* Journal of the American Medical Association, 1955. 157(2): p. 117-121. DOI: 10.1001/jama.1955.02950190017004

118. Ebert, B. and W. Jelkmann, *Intolerability of cobalt salt as erythropoietic agent.*Drug test anal. , 2014. 6(3): p. 185-189. DOI: 10.1002/dta.1528

119. Skalny, A.V., et al., *Cobalt in athletes: hypoxia and doping-new*

crossroads.J. Appl. Biomed. , 2019. 17(1): p. 28-28. DOI: 10.32725/jab.2018.003

120. Davidson, T.L., et al., *Soluble nickel inhibits HIF-prolyl-hydroxylases creating persistent hypoxic signaling in A549 cells.* Molecular Carcinogenesis: Published in cooperation with the University of Texas MD Anderson Cancer Center, 2006. 45(7): p. 479-489. DOI: 10.1002/mc.20176

121. Jones, S., A. Novak, and J. Elliott, *The role of HIF in cobalt-induced ischemic tolerance.* Neuroscience, 2013. 252: p. 420-430. DOI: 10.1016/j.neuroscience.2013.07.060

122. Wu, Y., et al., *Neuroprotection of deferoxamine on rotenone-induced injury via accumulation of HIF-1α and induction of autophagy in SH-SY5Y cells*.Neurochem. Int. , 2010. 57(3): p. 198-205. DOI: 10.1016/j.neuint.2010.05.008

123. Mecinović, J., et al., *2-Oxoglutarate analogue inhibitors of prolyl hydroxylase domain 2.*Bioorg. Med. Chem. Lett. , 2009. 19(21): p. 6192-6195. DOI: 10.1016/j.bmcl.2009.09.005Prockop, D.J. and K.I. Kivirikko, *Effect of polymer size on the inhibition of protocollagen proline hydroxylase by polyproline II*.Bioinorg. Chem. , 1969. 244(18): p. 4838-4842.

124. Gorres, K.L., et al., *Conformational preferences of substrates for human prolyl 4-hydroxylase*. Biochemistry, 2008. 47(36): p. 9447-9455. DOI: 10.1021/bi8009373

125. Li, D., et al., *Many amino acid substitutions in a hypoxia-inducible transcription factor (HIF)-1α-like peptide cause only minor changes in its hydroxylation by the HIF prolyl 4-hydroxylases: substitution of 3, 4-dehydroproline or azetidine-2-carboxylic*

acid for the proline leads to a high rate of uncoupled 2-oxoglutarate decarboxylation.J. biol. chem. , 2004. 279(53): p. 55051-55059. DOI: 10.1074/jbc.M410287200

126. McDonough, M.A., et al., *Selective inhibition of factor inhibiting hypoxia-inducible factor.*J. Am. Chem. Soc. , 2005. 127(21): p. 7680-7681. DOI: 10.1021/ja050841b

127. Soni, S. and Y.S. Padwad, *HIF-1 in cancer therapy: two decade long story of a transcription factor.*Acta Oncol. , 2017. 56(4): p. 503-515. DOI: 10.1080/0284186X.2017.1301680

128. Kumar, V. and D.I. Gabrilovich, *Hypoxia-inducible factors in regulation of immune responses in tumour microenvironment*. Immunology, 2014. 143(4): p. 512-519. DOI: 10.1111/imm.12380

129. Akanji, M.A., D. Rotimi, and O.S. Adeyemi, *Hypoxia-inducible factors as an alternative source of treatment strategy for cancer.*Oxid Med Cell Longev. , 2019. 2019. DOI: 10.1155/2019/8547846

130. Curry, L. and M. Soleimani, *Belzutifan: a novel therapeutic for the management of von Hippel–Lindau disease and beyond.* Future Oncology, 2024(0). DOI: 10.2217/fon-2023-0679

131. Stransky, L.A., et al., *Sensitivity of VHL mutant kidney cancers to HIF2 inhibitors does not require an intact p53 pathway*.Proc. Natl. Acad. Sci., 2022. 119(14): p. e2120403119. DOI: 10.1073/pnas.2120403119

132. Chouaib, S., et al., *Hypoxic stress: obstacles and opportunities for innovative*

immunotherapy of cancer. Oncogene, 2017. 36(4): p. 439-445. DOI: 10.1038/onc.2016.225

133. Lee, C.H., J. Cho, and K. Lee, *Tumour regression via integrative regulation of neurological, inflammatory, and hypoxic tumour microenvironment*.Biomol. Ther. , 2020. 28(2): p. 119. DOI: 10.4062/biomolther.2019.135

134. Liu, L., et al., *Hypoxia-inducible factor-1α contributes to hypoxia-induced chemoresistance in gastric cancer.*Cancer Sci. , 2008. 99(1): p. 121-128. DOI: 10.1111/j.1349-7006.2007.00643.x

135. Iijima, M., et al., *Development of single nanometer-sized ultrafine oxygen bubbles to overcome the hypoxia-induced resistance to radiation therapy via the suppression of hypoxia-inducible factor-1α*.Int. J. Oncol. , 2018. 52(3): p. 679-686. DOI: 10.3892/ijo.2018.4248

136. Ma, Z., et al. *Targeting hypoxia-inducible factor-1, for cancer treatment: Recent advances in developing small-molecule inhibitors from natural compounds.* In Seminars in cancer biology. 2022. Elsevier. DOI: 10.1016/j.semcancer.2020.09.011

137. Clish, C.B., *Metabolomics: an emerging but powerful tool for precision medicine*.Mol. Case Stud. , 2015. 1(1): p. a000588. DOI: 10.1101/mcs.a000588

138. Fiehn, O., *Metabolomics–the link between genotypes and phenotypes.*Plant Mol. Biol. , 2002. 48: p. 155-171. DOI:10.1023/A:1013713905833

139. Lamichhane, S., et al., *Strategy for nuclear-magnetic-resonance-based metabolomics of human feces*.Anal. Chem. , 2015. 87(12): p. 5930-5937.

DOI: 10.1021/acs.analchem.5b00977

140. Chen, L., et al., *Metabolite discovery through global annotation of untargeted metabolomics data.*Nat. Methods. , 2021. 18(11): p. 1377-1385. DOI: 10.1038/s41592-021-01303-3

141. Perakakis, N., K. Stefanakis, and C.S. Mantzoros, *The role of omics in the pathophysiology, diagnosis and treatment of non-alcoholic fatty liver disease*. Metabolism, 2020. 111: p. 154320. DOI: 10.1016/j.metabol.2020.154320

142. Guo, Q., et al., *High-throughput non-targeted metabolomics study of the effects of perfluorooctane sulfonate (PFOS) on the metabolic characteristics of A. thaliana leaves.*Sci Total Environ. , 2020. 710: p. 135542. DOI: 10.1016/j.scitotenv.2019.135542

143. Dührkop, K., et al., *Systematic classification of unknown metabolites using high-resolution fragmentation mass spectra*.Nat. Biotechnol. , 2021. 39(4): p. 462-471. DOI: 10.1038/s41587-020-0740-8

144. Han, S., et al., *A metabolomics pipeline for the mechanistic interrogation of the gut microbiome.* Nature, 2021. 595(7867): p. 415-420. DOI: 10.1038/s41586-021-03707-9

145. Harju, K., et al., *Simultaneous metabolomics analysis of atrial tissue, pericardial fluid and blood reveal novel metabolite signatures of the pathophysiology and biomarkers related to permanent atrial fibrillation*.Eur. Heart J. , 2022. 43(Supplement_2): p. ehac544. 503. DOI:10.1093/eurheartj/ehac544.503

146. Carter, B.Z., et al., *Inhibition of anti-apoptotic Mcl-1 exerts anti-leukemia activity through modulation of leukemia-stromal interactions and metabolic functions in AML. Blood*, 2019. 134: p. 3727. DOI:10.1182/blood-2019-124453

147. Yackoubov, D., et al., *Transcriptional and metabolic profiling of nicotinamide-enhanced natural killer (NAM-NK) cells (GDA-201)*. Blood, 2021. 138(Supplement 1): p. 4791-4791. DOI:10.1016/S2666-6367(22)00427-4

148. Niu, L., et al., *Noninvasive proteomic biomarkers for alcohol-related liver disease.*Nat. Med. , 2022. 28(6): p. 1277-1287. DOI:10.1038/s41591-022-01850-y

149. Hinshaw, D.C., et al., *Hedgehog signaling regulates metabolism and polarization of mammary tumor-associated macrophages*.Cancer Res. , 2021. 81(21): p. 5425-5437. DOI: 10.1158/0008-5472.CAN-20-1723

150. Forte, D., et al., *Circulating extracellular vesicles from acute myeloid leukemia patients drive distinct metabolic profile of leukemic cells and reveal crucial lipidomic biomarkers.* Blood, 2021. 138: p. 3471. DOI:10.1182/blood-2021-150339

151. Mallick, H., et al., *Predictive metabolomic profiling of microbial communities using amplicon or metagenomic sequences*.Nat. Commun. , 2019. 10(1): p. 3136. DOI: 10.1038/s41467-019-10927-1

152. Ren, J.-L., et al., *Advances in mass spectrometry-based metabolomics for investigation of metabolites.*RSC Adv. , 2018. 8(40): p. 22335-22350.

153. Tang, D.Q., et al., *HILIC-MS for metabolomics: An attractive and complementary approach to RPLC-MS.Mass Spectrom*. Rev. , 2016. 35(5): p. 574-600.

DOI: 10.1002/mas.21445

154. Nguyen, H.P. and K.A. Schug, *The advantages of ESI-MS detection in conjunction with HILIC mode separations: Fundamentals and applications*.J. Sep. Sci. , 2008. 31(9): p. 1465-1480. DOI: 10.1002/jssc.200700630

155. Sadi, B.B., A.P. Vonderheide, and J.A. Caruso, *Analysis of phosphorus herbicides by ion-pairing reversed-phase liquid chromatography coupled to inductively coupled plasma mass spectrometry with octapole reaction cell*.J. Chromatogr. A. , 2004. 1050(1): p. 95-101.

156. Qian, T., Z. Cai, and M. Yang, *Determination of adenosine nucleotides in cultured cells by ion-pairing liquid chromatography–electrospray ionization mass spectrometry*.Anal. Biochem. , 2004. 325(1): p. 77-84. DOI: 10.1016/j.ab.2003.10.028

157. Ma, J., et al., *Determination of organophosphorus pesticides in underground water by SPE-GC-MS*.J. Chromatogr. Sci., 2009. 47(2): p. 110-115. DOI: 10.1093/chromsci/47.2.110

158. Soininen, P., et al., *Quantitative serum nuclear magnetic resonance metabolomics in cardiovascular epidemiology and genetics*.Circ. Cardiovasc. Genet., 2015. 8(1): p. 192-206. DOI: 10.1161/CIRCGENETICS.114.000216

159. Chen, Y., E.-M. Li, and L.-Y. Xu, *Guide to metabolomics analysis: a bioinformatics workflow.* Metabolites, 2022. 12(4): p. 357. DOI: 10.3390/metabo12040357

160. Wishart, D.S., et al., *HMDB 4.0: the human metabolome database for 2018.*Nucleic Acids Res , 2018. 46(D1): p. D608-D617. DOI: 10.1093/nar/gkx1089

161. Keen, B., et al., *Metabolomics in clinical and forensic toxicology, sports anti-doping and veterinary residues*. Drug testing and analysis, 2022. 14(5): p. 794-807. DOI: 10.1002/dta.3245

162. Peña, F., et al., *Analysis of phenylurea herbicides from plants by GC/MS.* Talanta, 2002. 56(4): p. 727-734. DOI: 10.1016/s0039-9140(01)00616-6

163. Koek, M.M., et al., *Quantitative metabolomics based on gas chromatography mass spectrometry: status and perspectives*. Metabolomics, 2011. 7: p. 307-328. DOI: 10.1007/s11306-010-0254-3

164. Pasikanti, K.K., P. Ho, and E. Chan, *Gas chromatography/mass spectrometry in metabolic profiling of biological fluids.*J. Chromatogr. B. , 2008. 871(2): p. 202-211. DOI: 10.1016/j.jchromb.2008.04.033

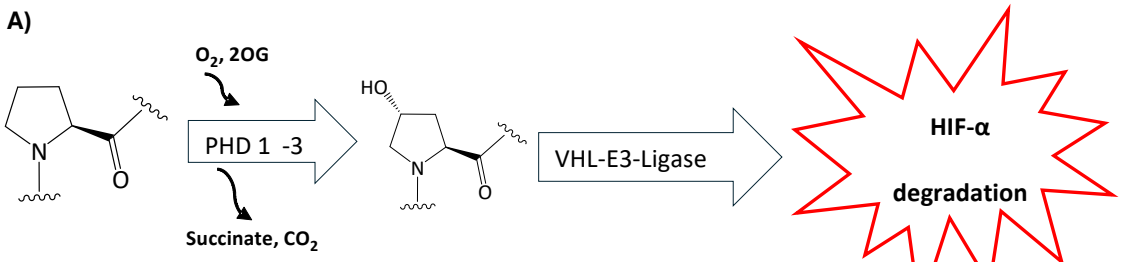
165. Johnson, C.H. and F.J. Gonzalez, *Challenges and opportunities of metabolomics.* J. Cell. Physiol. , 2012. 227(8): p. 2975-2981. DOI: 10.1002/jcp.24002

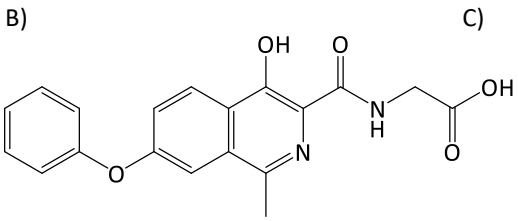
166. Ngere, J.B., et al., *Ion-exchange chromatography coupled to mass spectrometry in life science, environmental, and medical research*. Anal. Chem., 2023. 95(1): p. 152-166. DOI: 10.1021/acs.analchem.2c04298

Chapter 2

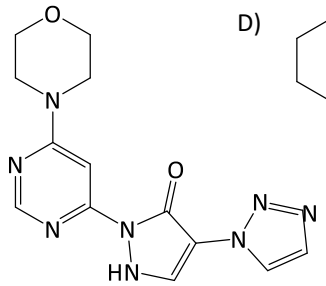
Studies on the Novel PHD inhibitor IOX5

2.1. Discovery and development of IOX5 (5)

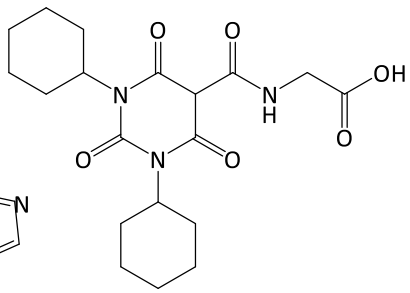




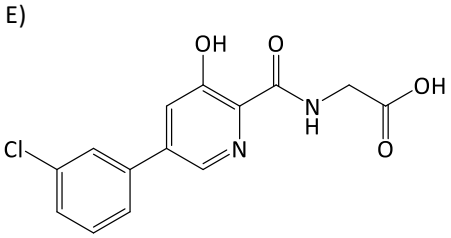
Roxadustat (**1**)



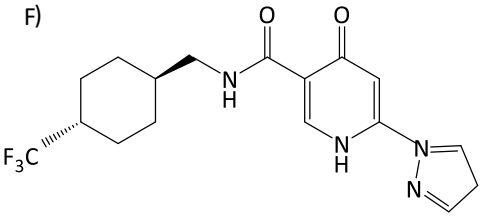
Molidustat (**2**)



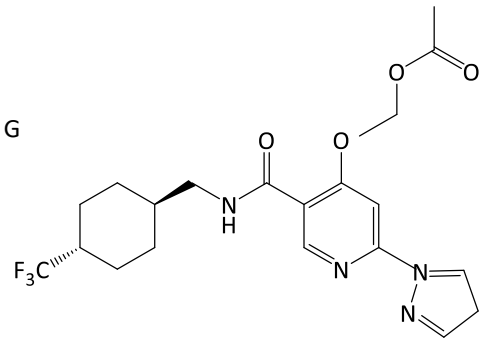
Daprodustat(**3**)



Vadadustat (**4**)



IOX5 (**5**)



Prodrug if IOX5 (**6**)

Figure 2.1.1: Examples of clinically used and novel PHD inhibitors. A) Prolyl-hydroxylases 1-3 (PHDs) are 2-oxoglutarate (2OG) and Fe^{II}-dependent oxygenases. In the HIF system, the PHDs act in an O_2 sensing capacity; they catalysed Prolyl hydroxylation of HIFα. The PHDs (1-

3) catalyse *trans*-4-prolyl hydroxylation of proline-residues of the HIF1-3α N- and C-terminal oxygen degradation domains (NODD and CODD), reactions linked to the change of dioxygen and 2OG to succinate and carbon dioxide[1-4]. The hydroxylated HIF is recognised by the von Hippel–Lindau (VHL) E3 ubiquitin ligase. This binding enables ubiquitination and proteasomal degradation of HIF-α under normoxic conditions [5]. **B)** Roxadustat (FG-4592, (**1**), **C)** Daprodustat (GSK1278863, (**2**), **D)** Molidustat (BAY 85-3924, (**3**) and **E)** Vadadustat (**4**). Structures of PHD inhibitors discussed in this chapter: **F)** the novel PHD inhibitor from the 4-hydroxypyridine series, **IOX5** (**5**) and, **G)** its prodrug (**6**). Note IOX5 (**5**) and its prodrug form (**6**) have the *trans*-stereochemistry on the cyclohexyl ring.

Most PHD inhibitors act by binding to the ferrous ion [Fe (II)] and they compete for binding with the 2-oxoglutarate (2OG) co-substrate (**Figure 2.1.1 A**); they compete to differing extents with binding by HIF-α isoforms [1-3]. At present, none of the existing clinically used PHD inhibitors have been shown to manifest complete selectivity over other human 2OG oxygenases e.g; **1-4** (**Figure 2.1.1 B, C, D & E**)[1]. Recently, structure activity relationship (SAR) studies have been carried out on a series of 4-hydroxypyridine containing PHD inhibitors, which were prepared by Dr. James Holt-Martyn (**5** & **6**) (**Figure 2.1.1 F & G**).

Most of the clinically used PHD inhibitors (such as Daprodustat, Roxadustat and Molidustat) employ a pharmacological mode of action relying on 2OG competition, however, this can come with potential off target effects such as inhibition of other 2OG-dependent oxygenases or 2OG using enzymes (**Table 2.2.1**); it is thus important to develop a highly selective PHD inhibitor[6].

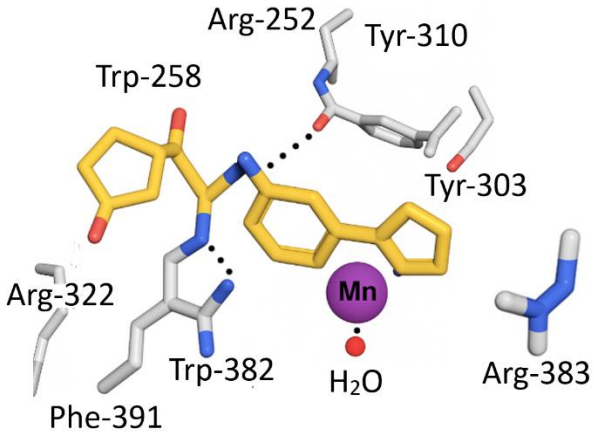


Figure 2.1.2: Prediction of the potential binding mode of IOX5 to PHD2(PDB: 6ST3). Note Mn in the crystal structures substitutes for catalytically active Fe(II) [6,7].

Crystallographic analysis identified a PHD-specific hydrophobic pocket near the PHD2 active site entrance and suggested that binding to this hydrophobic pocket may lead to selective PHD inhibition[7]. Docking studies analysing the potential IOX5 binding mode suggested that it will coordinate the PHD2 active site iron in a bidentate manner via chelation of its pyridone and pyrazole groups. The pyridone group of IOX5 was also predicted to form a hydrogen bond with Tyr-310 and Arg-252 and the 4-trifluoromethyl group linked to the cyclohexyl group is predicted to bind in the PHD-specific hydrophobic pocket at the entrance of the active site[7]. The key aim of my work was to identify and evaluate novel potent PHD inhibitors, including IOX5, aiming to identify compounds with high selectivity for the PHDs over other human 2OG oxygenases, so potentially enable improved medicines compared to the available clinically trialled PHD inhibitors.

2.2 Cellular Investigations of IOX5 **(5)**

Cellular investigations were carried out to evaluate the cell activity of IOX5 (**5**), which was shown to have high selectivity for the PHDs over other human 2OG oxygenases (**Table 2.2.1**), compared to the available clinically trialled/used PHD inhibitors.

Table 2.2.1: Selectivity of Roxadustat (1), Daprodustat (2), Molidustat (3), and IOX5 (5) against isolated recombinant human 2OG dependent oxygenases [8-11]**.** The Table is Modified from Lawson et al. and Yeh et al, which describe the methods used[1,6]. (FIH): Factor Inhibiting HIF, (JMJD3): Jumonji domain containing-3, (KDM4A): lysine-specific demethylase 4A, (KDM5B): lysine-specific demethylase 5B, (KDM6B): lysine-specific demethylase 6B. Rapid fire assays for IOX5 were carried out by Dr. A Tumber[1, 12,13].

	IC_{50} (μM)						
Inhibitor	**PHD2**	**JMJD6**	**FIH**	**KDM4A**	**KDM5B**	**KDM6B**	**OGFOD1**
Daprodustat	0.18	4.80	22	>100	>100	>100	1.73
Molidustat	1.32	1.52	66	>100	>100	35	1.34
Roxadustat	2.76	18.01	>100	>100	>100	>100	0.86
IOX5	0.19	>100	>100	>100	>100	>100	>50

The main aim of my work was to develop a robust cellular assay to characterize the activity of **5** in detail. The HEK293T cell line was considered to match the desired profile; as it is a kidney derived cell line that has physiological relevance related to EPO production [13,14] and is thus relevant to chronic kidney disease anaemia. Moreover, HEK 293T cells can grow fast and are easy to maintain. Before cellular investigations on **5**, to study whether stabilizes HIF-1α, different concentrations (1, 5, 10 & 20μM) of Roxadustat **(1)** were evaluated; use of 20 μM of **1** showed consistent HIF-1α accumulation therefore 20 μM of **1** was taken as the positive control for use in future cell work **Figure 2.2.1.** At the beginning of the cellular investigation, Roxadustat was selected as the positive control because it is the first orally active, clinically approved PHD inhibitor (approved in China, Japan, and the EMA in 2021) with

well-characterized effects on HIF stabilization and downstream gene expression. Its widespread use in both clinical trials and mechanistic studies makes it a reliable benchmark for validating PHD inhibition. Daprodustat and Molidustat, which were conditionally approved earlier, received FDA approval later in 2023[15,16]. Moreover, during the selection of a positive control, Roxadustat demonstrated more consistent and well-characterized HIF stabilization compared to Daprodustat and Molidustat **(Figure 2.2.3.1 and Figure 2.2.3.1)**.

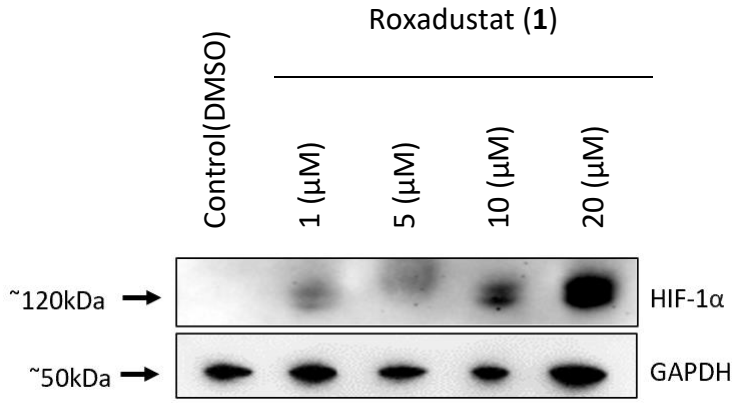


Figure 2.2.1: Stabilization of HIF-1α through cellular inhibition of HIF prolyl hydroxylation by clinical PHD inhibitor, Roxadustat (1). Immunoblot analysis of the protein expression of HIF-1α in HEK 293T cells treated with **Roxadustat (1)** (20, 10, 5 & 1 μM) for 18 hours in normoxia. Representative data from repeats are shown.

2.2.1 Human embryonic kidney (HEK 293T) cells treated with IOX5 for different incubation times

Yeh et al. showed Roxadustat (**1**) stabilizes HIF-1α in HeLa and Hep3b cell lines after 6h treatment, therefore, the effect of **5** treatment in HEK 293T cells was initially studied after 6-hour treatment. Western blot analysis showed that when HEK 293T cells were treated for 6h

with 100 µM of **5**, HIF-1α stabilization was observed; however, there was no HIF-1α stabilization observed at 50 µM of **5 (Figure 2.2.1.1 A)**. Cells treated with <1% DMSO were used as a negative control (showing no sign of HIF-1α stabilisation) and **1** was used as a positive control (showing HIF-1α stabilisation).

The amount of HIF-1α accumulated due to treatment of **5** was quantified using 'Image J software'. A graphical presentation was used to display the amount of HIF-1α expression compared to the control, which was given a value of 1. Quantification analysis showed that, compared to the control, **5** (100 µM) and 20 µM of **1** significantly increased HIF-1α levels in a dose-dependent manner (**Figure2.2.1.2 B**).

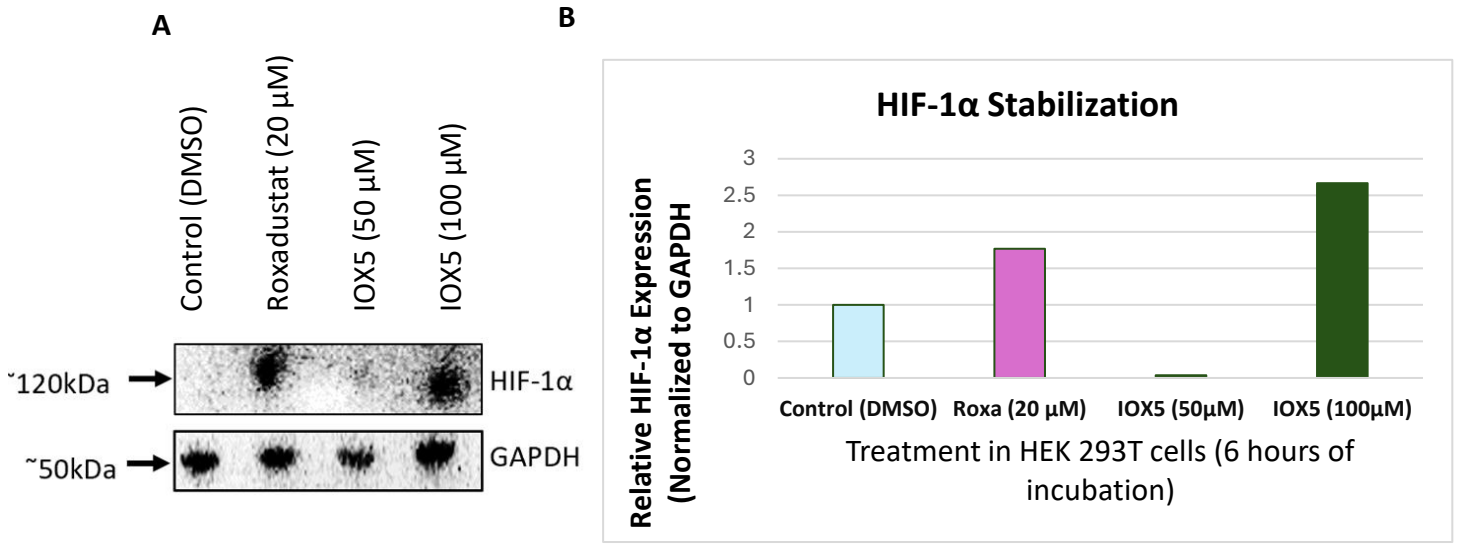


Figure 2.2.1.1: Stabilization of HIF-1α through cellular inhibition of HIF prolyl hydroxylation by 5. (A) Immunoblot analysis of HIF-1α in HEK 293T cells treated with **5** (100 & 50 µM) and **1** (20 µM) for 6 hours in normoxia. **(B)** Quantification of HIF-1α after treatment for 6 hours.

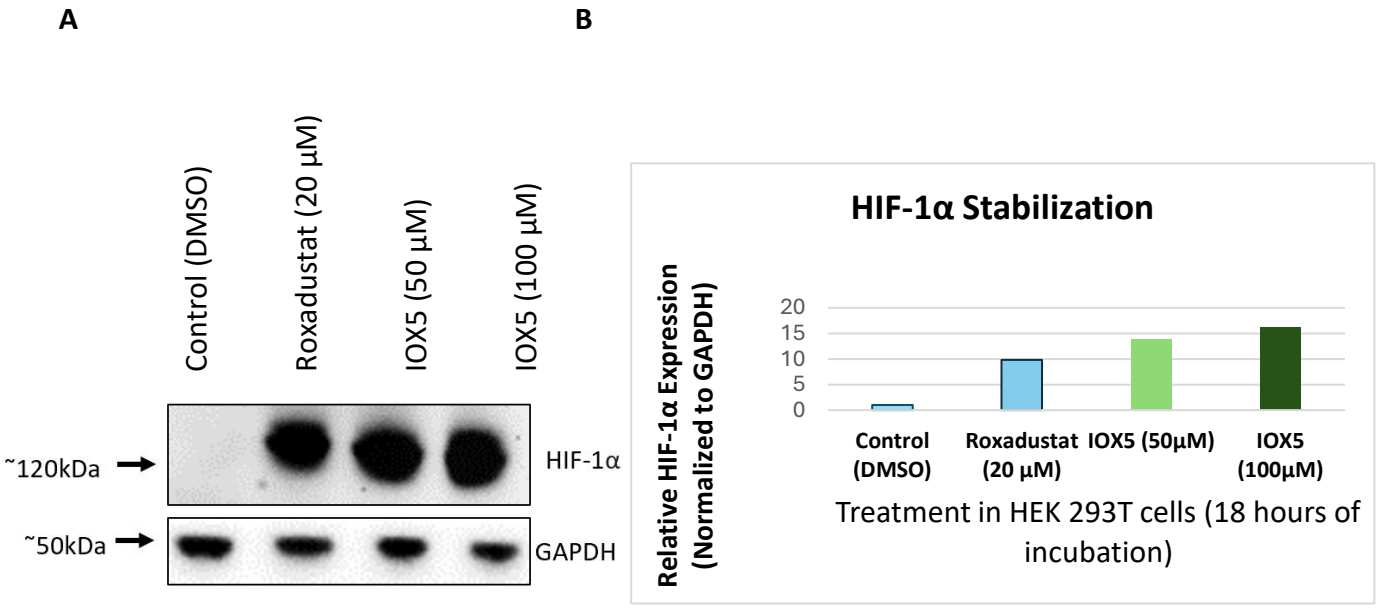


Figure 2.2.1.2: Stabilization of HIF-1α through cellular inhibition of HIF prolyl hydroxylation by 5. (A) Immunoblot analysis of the protein expression of HIF-1α in HEK 293T cells treated with **5** (100 & 50 µM) and **1** (20 µM) for 18 hours in normoxia. **(B)** Quantification of HIF-1α levels normalized to GAPDH after treatment for 18 hours in normoxia.

As at 50 µM, **5** did not show any signal for HIF-1α it was proposed that increasing the incubation time may lead to HIF-1α accumulation. Indeed, after 18 h treatment with 50 & 100 µM (single dose) **5**, HIF-1α was observed to accumulate (**Figure2.2.1.2 A & FigureA.7.1 A)**. Quantification analysis showed that, compared to the control, **5** (50 and 100 µM) and 20 µM of **1** significantly increased HIF-1α levels in a dose-dependent manner (**Figure2.2.1.2 & FigureA.7.1 B**).

2.2.2 Human embryonic kidney (HEK 293T) cells treated with different concentrations of IOX5

It was then investigated whether a lower concentration of **5** is capable of stabilizing HIF-1α in HEK 293T cells. Different concentrations (20, 10, 5, 1, and 0.5 µM) of **5** were tested. **Figure**

2.2.2.1 & Figure A.7.2 shows that when incubated for 18hs at 10 & 20 µM, **5** can stabilize HIF-1α. Quantification analysis showed that, compared to the control, **5** (10 and 20 µM)and 20 µM of **1** significantly increased HIF-1α levels in a dose-dependent manner (**Figure 2.2.2.1 B**).

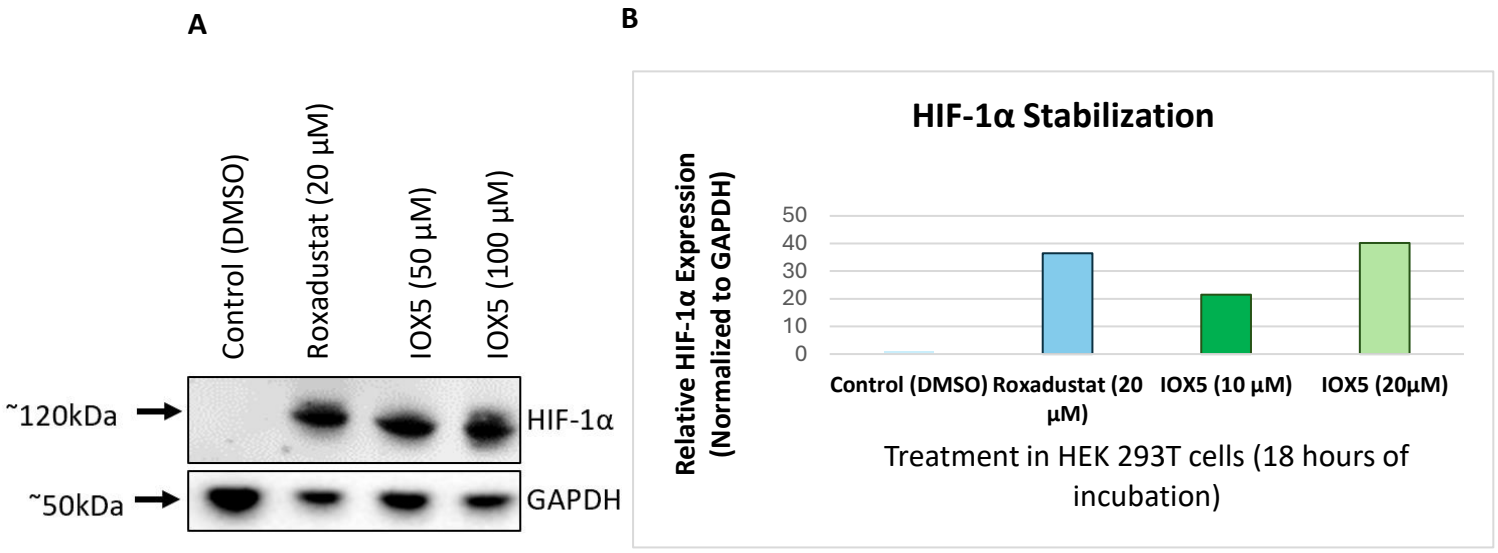


Figure 2.2.2.1: Stabilization of HIF-1α through cellular inhibition of HIF prolyl hydroxylation by different concentrations of 5. (A) Immunoblot analysis of the protein expression of HIF-1α in HEK 293T cells treated with **5** (10 & 20 µM) and **1** (20 µM) for 18 hours in normoxia. (B) Quantification of HIF-1α levels normalized to GAPDH after treatment for 18 hours in normoxia.

Further immunoblotting results with 5, 1, 0.5 µM of **5** showed that **5** induces HIF-1α accumulation at 0.5 µM when incubated for 18 h **(Figure A.7.2)**. To confirm the efficacy of **5** at lower concentrations repeat immunoblotting experiments were conducted - the results confirmed that **5** can induce HIF-1α accumulation at 0.5 µM with 18 h incubation **(Figure 2.2.2.2 & Figure A. 7.3)**.

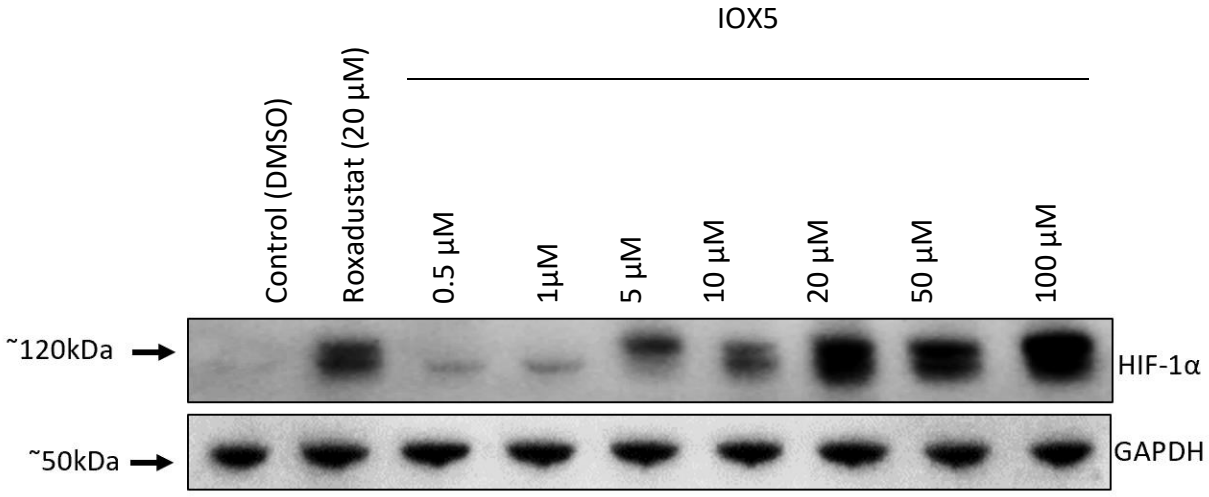


Figure 2.2.2.2: Stabilization of HIF-1 α through cellular inhibition of HIF prolyl hydroxylation by different concentrations of 5. Immunoblot analysis of the protein expression of HIF-1α in HEK 293T cells treated with **5** (100, 50, 20, 10, 5, 1 & 0.5 µM) and **1** (20 µM) for 18 hours in normoxia.

The differences in activity observed between 6 and 18h incubation suggest that non-optimal cell penetration may explain the differences in HIF stabilization observed at different time points. Other possible explanations include a requirement for metabolism to be a more active compound, though subsequent experiments supported the non-optimal cell-penetration proposal (see below).

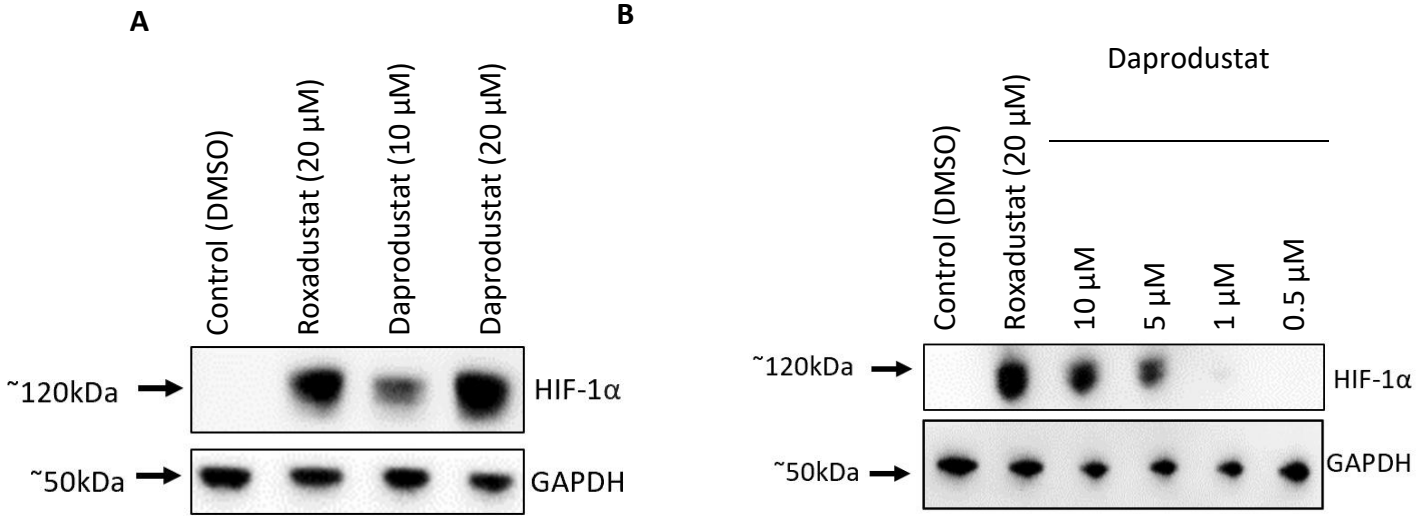
2.2.3 Other clinically available PHD inhibitors and their ability to stabilize HIF-1α

Roxadustat **(1)** was the first PHD inhibitor to be approved for the treatment of anaemia associated with CKD [17,18]. Daprodustat **(2)** was the first PHD inhibitor approved by the FDA

[15]. Molidustat (**3**) is a clinically used PHD inhibitor in countries including China and Japan [16].

Studies on **1** were carried out as described in **Section 2.2** (**Figure 2.2.1)**, similarly, to evaluate the other available clinical PHD inhibitors (Daprodustat (**2**) & Molidustat (**3**)) and their ability to stabilize HIF-1α in comparison with **5** studies were carried out. Different concentrations, i.e. 20, 10, 5, 1, and 0.5 µM of **2** and **3,** were tested for their effects on HEK 293T cells (**Figure 2.2.3.1)**.

Western blotting experiments showed that **1**& **3** did not observably stabilize HIF-1α below 10 µM **(Figure 2.2.1**. & **2.2.3.1 C)**, and **2** did not show any HIF-1α stabilization below 5 µM with 18 h treatment **(Figure 2.2.3.1 A & B)**. Thus, at least under the tested conditions, including 18 h treatment, **5** can induce HIF-1α stabilization at equal or lower concentrations than the clinically used inhibitors (**1**-**3**).



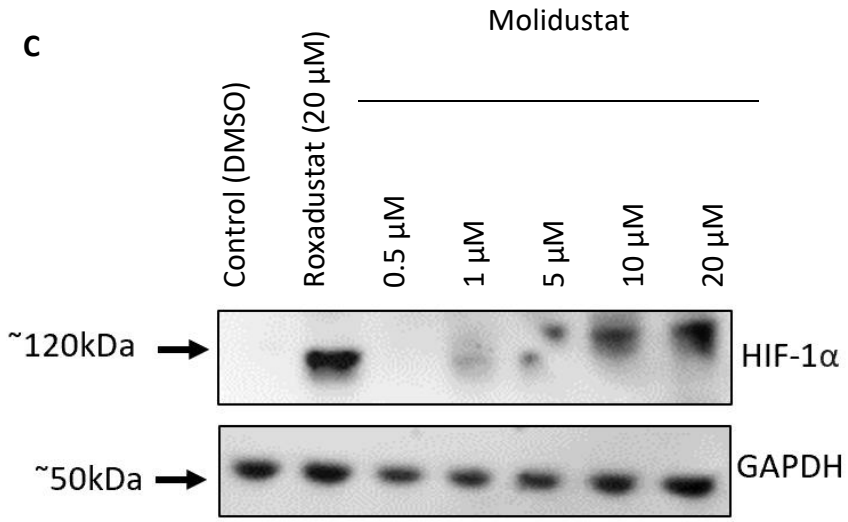


Figure 2.2.3.1: Stabilization of HIF-1α through cellular inhibition of HIF prolyl hydroxylation by the clinically used PHD inhibitors Daprodustat (2) and Molidustat (3). Immunoblot analysis of the protein expression of HIF-1α in HEK 293T cells treated with **(A & B) 2** (20, 10, 5 & 1 µM) and **C) 3** (20,10,5, 1 and 0.5 µM) for 18 hours in normoxia.

2.3 Cell Viability Assays

The cytotoxic effects of **5** were assessed via cell viability assays, using two cell lines, that is human hepatoblastoma (HepG2) and HEK 293T cells.

Along with HEK 293T cells, HepG2 cells were incorporated in the cytotoxicity assay HepG2 cells to evaluate liver-specific cytotoxicity, as HepG2 cells preserve the key metabolic functions relevant to drug detoxification[19]. HepG2 cells are widely used in toxicity screening which increases the translational applicability of the data[20]. Comparing HEK 293T and HepG2 cell lines allowed an assessment of compound toxicity across kidney and liver-derived human cells.

HepG2 and HEK 293T cells were then treated with **5** and **1** at six different concentrations (10,

20, 50, 300 & 500 µM) for 6 and 24 h, respectively. To determine the cell viability a one-step colorimetric MTS (3-(4,5-dimethylthiazol-2-yl)-5-(3-carboxymethoxyphenyl)-2-(4-sulfophenyl)-2H-tetrazolium) assay was performed. During the MTS assay the absorbance was measured at 490 nm, a wavelength which positively correlates with the number of viable cells present in each well [21]. In HepG2 cells both the **5** and **1** treatment groups showed an overall dose dependent decrease in cell viability compared to the control samples (p-value < 0.05, one-way ANOVA with Dunnett's test) after 6 hours of incubation. Moreover, when comparing treatment groups, both **5** and **1**, they showed similar effects on cell viability after 6 h treatment (**Figure 2.3.1**). The number of live cells in the control group was defined as 100%. With HepG2 cells, (**Figure 2.3.1**), even at high concentrations of **5** (300 & 500 µM), ˜80% of cells were viable after 6 h treatment, which indicates that even at higher concentrations **5** does not cause substantial cell damage.

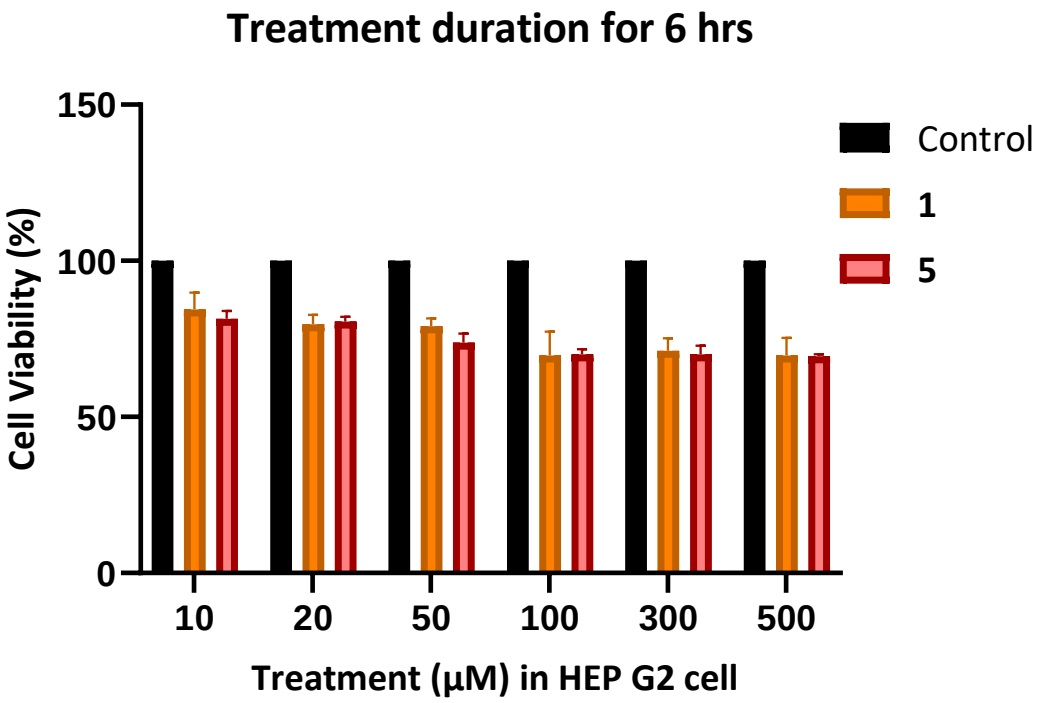


Figure 2.3.1: HepG2 cell viability studies with different concentrations of 5 and 1 (positive control) treatments. 10,000 cells were seeded in a 96-well plate. After the cells were attached (24 h), they were treated with different concentrations of **5** or **1** for 6 hours. After the 2.6.6treatment, viable cells were estimated using CellTiter 96 AQueous one solution reagent (Promega, G358C). (n=3, technical repeats).

As with HepG2 cells, with HEK 293T cells both the **5** and **1** treatment groups showed an overall dose dependent decrease in the number of cell viability compared to the control samples (p-value < 0.05, one-way ANOVA with Dunnett's test) after 24 hours of incubation.

Interestingly, when HEK 293T cells were treated with **5** for 24 hours, higher cell viability was observed compared to the control, except at higher concentrations of **5** (300 & 500 µM) (**Figure 2.3.2)**. At the lowest tested concentration of **5** (10 µM) the cell viabilities of **5** and **1** were similar; however, at 20, 50, and 100 µM, compared to **1**, **5** showed an increase in cell viability **(Figure 2.3.2)** after 24 hours treatment. As treatment of HEK 293T cells with **(Figure 2.3.2) 5** at concentrations such as 300 & 500 µM showed ˜70% cell viability after 24 hours of treatment, it seems that even at high concentrations, **5** does not cause substantial cell damage.

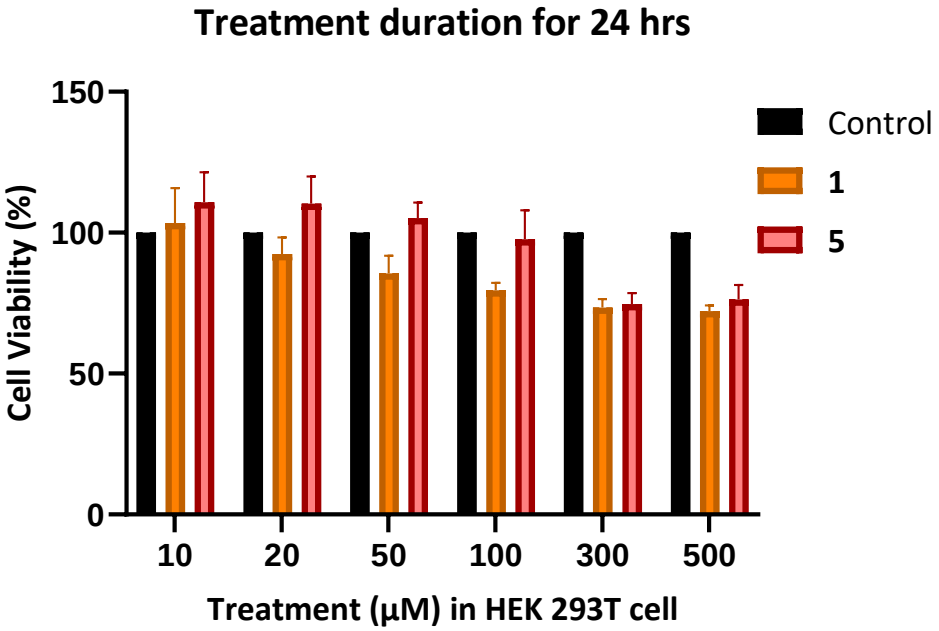


Figure 2.3.2: HEK293T cell viability with different concentrations of 5 and 1 (positive control) treatments. 10,000 cells were seeded in a 96-well plate. After the cells were attached (24 h), the cells were treated with different concentrations of **5** and **1** for 24 hours. After the drug treatment, viable cells were estimated using CellTiter 96 AQueous One Solution Reagent (Promega, G358C). (n=3, technical repeats).

2.4 Reverse transcription-quantitative polymerase chain reaction (RT-qPCR)

Investigations were carried out using the reverse transcription-quantitative polymerase chain reaction (RT-qPCR) technique to test whether **5** has any influence on HIF target gene expression in HEK 293T cells (**Figure 2.4.1: A, B, C, and D**). The expression levels of the following genes were measured: *HIF1α, EPO, VEGF*, and *CA9*, all of which have been validated as being regulated by HIF-1α can bind to the hypoxia-response elements (HREs) [22-24].

HEK293T cells were treated with 20 µM of **5** (group 1), 20 µM of **1** (group 2), and 0.9%$_{v/v}$ of

DMSO (control group) for 18 hours. Even though **5** stabilized HIF-1α at 0.5μM, for RT-qPCR, studies 20 μM was chosen as the dose for **1** and **5** because, throughout the cellular investigations, 20μM of **1** was used as the positive control.

Among all the genes examined by RT-qPCR assay, the *HIF-1α* and *VEGF* genes showed significant upregulation in both the treatment groups (**Figure 2.4.1 A and B**). When treated with **5**, the HIF*1α*, and *VEGF* genes showed substantial upregulation, i.e. by ~7.5 fold (p-value < 0.001) and ~2 fold (p-value < 0.001), compared to the control respectively (**Figure 2.4.1**); *EPO* and *CA9* gene expression was not significantly changed compared to the control (**Figure 2.4.1 C and D**). When cells were treated with **1,** the HIF-*1α*, and *VEGF* genes showed upregulation by ~6 fold (p-value was < 0.001), ~3 fold and ~1.5 fold (p-value < 0.05) compared to the control, respectively (**Fig. 2.4.1 A and B)**, while *EPO* and *CA9* expression was not changed compared to the control (**Fig. 2.4.1 C and D**).

The lack of substantial *EPO* and *CA9* gene expression may be due to insufficient HIF-2α in the tested cells, insufficient compound concentration or suboptimal exposure time. Testing higher concentrations or optimizing treatment duration could potentially enhance the expression of specific HIF target genes. Another variability is FIH activity which can suppress HIF target gene in a context dependent manner [25]. Indeed*, EPO* gene expression is known to be cell-type specific and often not robustly induced in vitro, even under hypoxic conditions or HIF stabilization, due to its strict tissue-specific regulation (primarily in kidney and liver cells in vivo)[26-30].

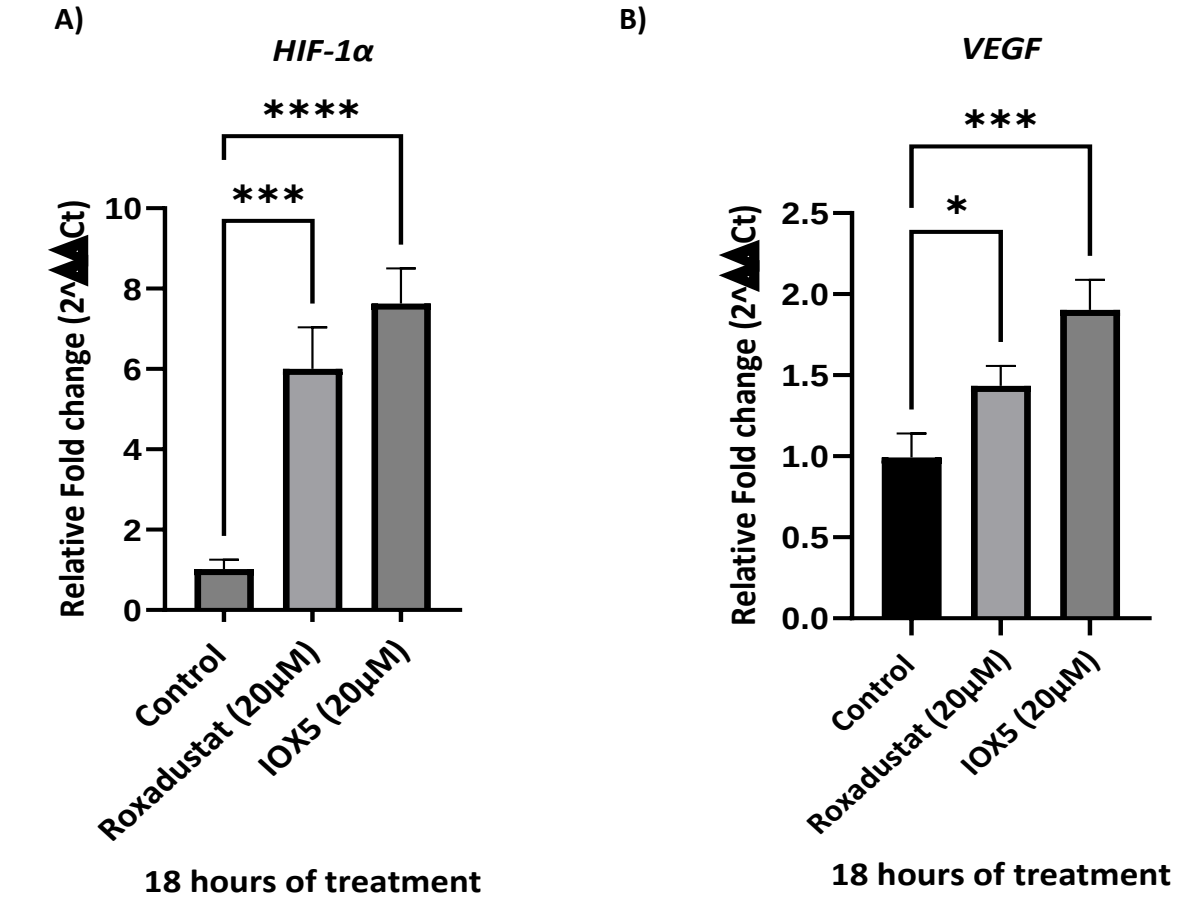

A)
HIF-1α
****
***
Relative Fold change (2^ΔΔCt)
10
8
6
4
2
0
Control
Roxadustat (20μM)
IOX5 (20μM)
18 hours of treatment
B)
VEGF
***
*
Relative Fold change (2^ΔΔCt)
2.5
2.0
1.5
1.0
0.5
0.0
Control
Roxadustat (20μM)
IOX5 (20μM)
18 hours of treatment
C)
EPO
ns
ns
Relative Fold change (2^ΔΔCt)
5
4
3
2
1
0
Control
Roxadustat (20μM)
IOX5 (20μM)
18 hours of treatment
D)
CA9
ns
ns
Relative Fold change (2^ΔΔCt)
1.5
1.0
0.5
0.0
Control
Roxadustat (20μM)
IOX5 (20μM)
18 hours of treatment

Figure 2.4.1: Effects of HIF PHD inhibitors (5 & 1) on hypoxia related gene expression. Expression of hypoxia genes, *HIF-1α*, *VEGF*, EPO, and CA9 after treatment with 20 µM PHD inhibitors in normoxia for 18 hours were normalised to *β-actin* levels. Significant upregulation of, *HIF-1α* and *VEGF* was seen with **5** and **1**. *EPO*, and *CA9* levels were not changed by any of the HIF PHD inhibitors. Each data point represented the mean and standard deviation of the relative fold change with respect to a 1% DMSO-treated sample normalised to reference gene *β-actin* level. Statistical significance was indicated as * = p-value < 0.05 and ** = p-value < 0.01, *** = p-value < 0.001 and **** = p-value < 0.0001, calculated with a Tukey's test. N represents the number of biological replicates, where N=3 biological replicates.

2.5 In-vivo mouse model studies

Following the in-vitro cell-based experiments with **5**, the next step was to take **5** into an in-vivo context using mouse model studies. The initial aim of the in vivo mouse study was to carry out early-stage work to assess the potential of **5** as a therapeutic agent for the treatment of anemia. The RBC count, hemoglobin levels, and hematocrit percentage in-vivo studies were used to assess the capacity of **5** capacity to stimulate erythropoiesis. Dr. Hannah Lawson (Institute of Cancer Research) conducted the in-vivo experiments [6] and chose Daprodustat(**2**) as the control, in part because of interest in the latter for treatment of cancer[6]. Roxadustat, which is used for anaemia treatment, was used as a control during the initial cellular experiments as it was one of the first well-characterized PHD inhibitors with robust in vitro data and availability at the time. However, by the time the work had progressed to in vivo studies, Daprodustat, which is more active than Roxadustat, had received FDA approval[31], providing a clinically validated and standardized reference compound for comparison. The choice of Daprdustat was thus based on scientific and translational relevance.

While using different control compounds (Roxadustat for cellular studies and Daprodustat for

physiologically relevant whole-animal model) can pose interpretation challenges, both serve as class-representative PHD inhibitors. Their use allowed benchmarking of IOX5 against two clinically relevant standards in different contexts.

For the in vivo experiments, the mice were divided into three groups (n = 5, for each group). Group 1 mice were treated with 30mg/kg of **2**; Group 2 mice were treated with 15mg/kg of **5**; and Group 3 mice were treated with 30mg/kg of **5**. All mice were intraperitoneally injected at a twice daily dose according to their groups. Samples were collected for analysis before treatment and on the 4th and 8th days after treatment.

Group 1 mice, after treatment with **2**, did not show any significant difference in red blood cell (RBC) count, haemoglobin (HGB) levels, or hematocrit (HCT) levels after 4th and 8th days of treatment compared to the pre-treatment condition in a mouse model **(Figure 2.5 A, B & C)**. Group 2 mice, after 8th day of treatment showed a significant increase in the RBC count compared to both the pre-treatment condition and 4th day of treatment in the mouse model **(Figure 2.5 A, B & C)**. However, there was not any significant difference between precondition and 4th day treatment in the group 2 mouse model.

Group 2 mice, after treatment with **5** also did not show any significant difference in HGB and HCT levels after the 4th and 8th days of treatment compared to the pre-treatment condition in a mouse model. However, when the dose of **5** was increased, to 30mg/kg of **5** (Group 3 mice), after the 4th day there was a significant increase in all the treatment parameters except for the RBC count compared to the pre-treatment condition in mouse model **(Figure 2.5 A, B & C)**. Interestingly, on treatment with 30mg/kg of **5,** after the 8th day, a significantly increased RBC count, and HGB / HCT levels compared to the pre-treatment condition in the mouse

model were observed **(Figure 2.5 A, B & C).**

Both Group 2 and Group 3 showed similar levels of effects when analysing the RBC count, suggesting that to achieve an effect on RBC count, a lower dose of **5** than used in Group 3 should be sufficient (**Figure 2.5 A**). The doses of all groups were well tolerated as none of the groups showed any sign of adverse effects after treatment.

During the cellular investigations, the ability of **5** to stabilize HIF-1α at concentrations as low as 0.5 μM demonstrated its ability to efficiently upregulate HIF activity at the cellular level. The in vivo results show that cellular activity translates into physiologically relevant effects, with 4 and 8-day treatments with **5** leading to significant increases in the RBC count, as well as hemoglobin and hematocrit levels compared to the pre-treatment baseline. These in-vivo study results are consistent with the PHD inhibition mediated upregulation of HIF-1α and likely HIF-2α causing upregulation erythropoietin and promotion of erythropoiesis. A recently published study supports this, by showing that IOX5 stabilizes HIF-1α in AML cell lines, resulting in metabolic reprogramming and apoptosis, highlighting the ability of **5** to impact on the HIF system [6]. The concordance between the in vitro and in vivo findings highlights **5** potential as a selective PHD inhibitor that through targeted HIF-α stabilization ican promote desired hematological responses.

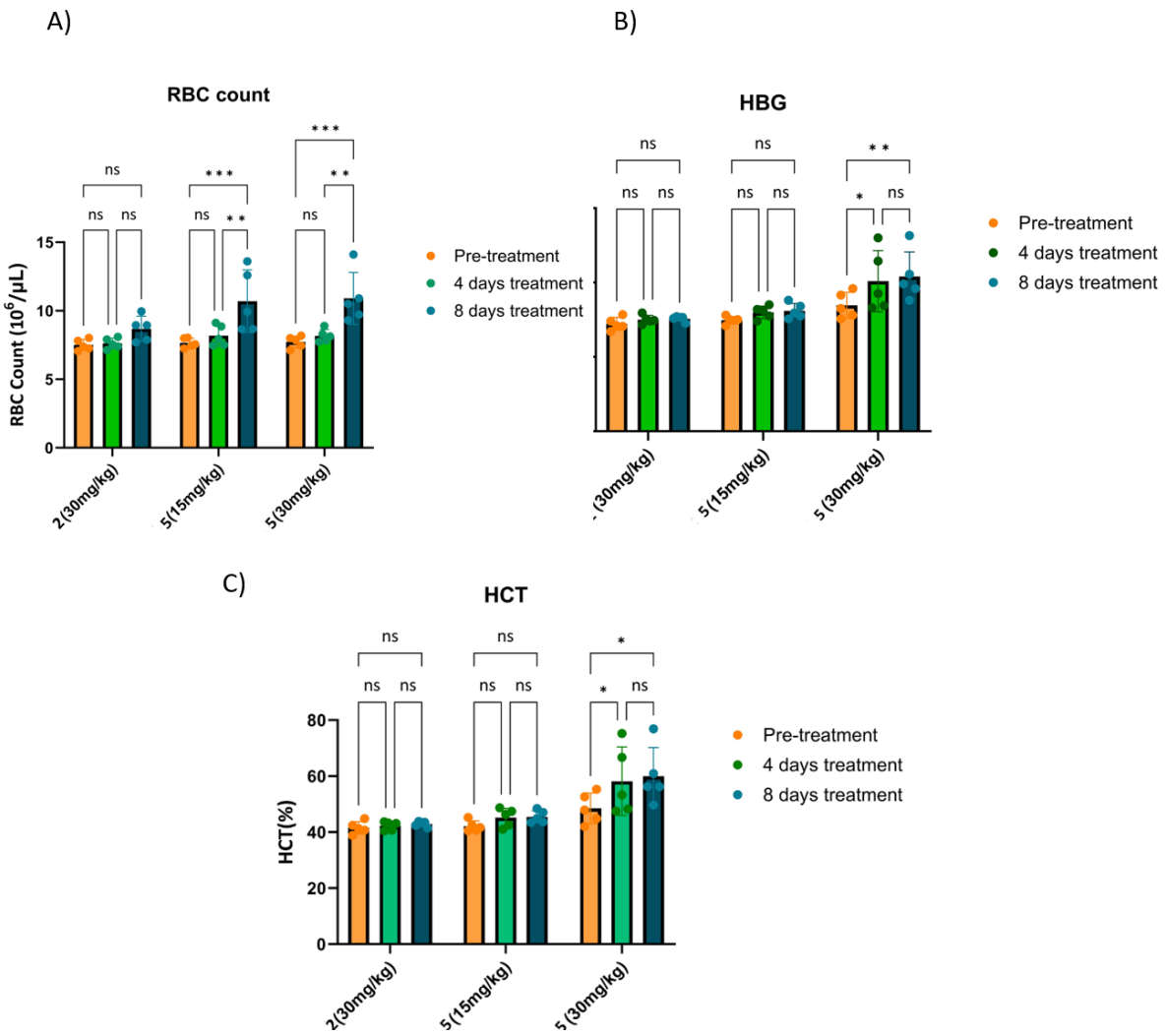


Figure 2.5: (A) Mouse red blood count (RBC), (B) Mouse haemoglobin (HBG), (C) percentage of mouse haematocrit (HCT). Normal mice (n=5) were administered twice daily of i.p dose, **2** or **5** at the doses indicated.

2.6 A prodrug (**6**) form of IOX5 (**5**)

2.6.1 Discovery and development of a Prodrug form (**6**) of the novel PHD inhibitor IOX5

Dr. James Holt-Martyn developed a prodrug of **5**, i.e. **6,** aiming to improve **5**'s cellular efficacy, (**Figure 2.2.1.1**). It was proposed that in cells, the prodrug group would be cleaved by esterases releasing **5** with acetic acid and formaldehyde as byproducts (**Figures 2.6.1.1**). Blocking the OH group of **5** resulted in a complete loss of inhibition of isolated PHD2 (IC_{50} >100 µM, Figure **2.6.1.1**)

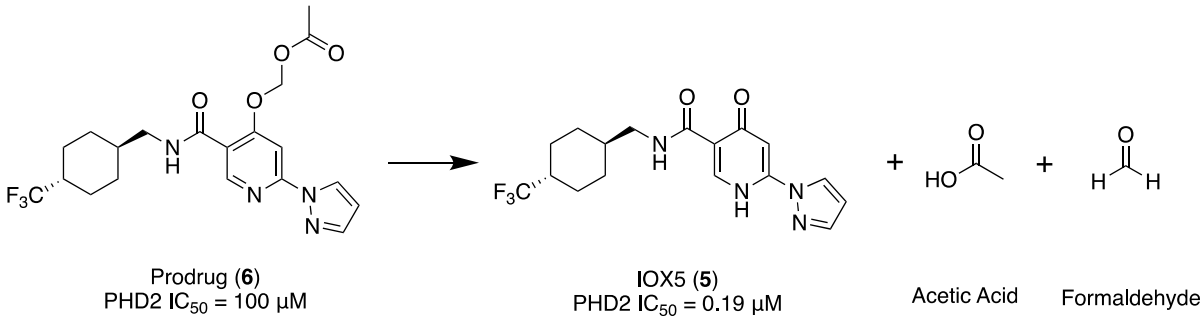


Figure 2.6.1.1: Pro-drugging the hydroxyl group of the 4-hydroxypyridine series.

2.6.2 Cellular Investigation of Prodrug **6**

Western blot analysis showed that when HEK 293T cells were treated for 6h with the prodrug form of **5**, i.e. **6,** HIF-1α stabilization was observed at 50 µM (**Figure 2.6.2.1 A**) but 50 µM of **5** did not stabilize HIF-1α after 6hrs of treatment.

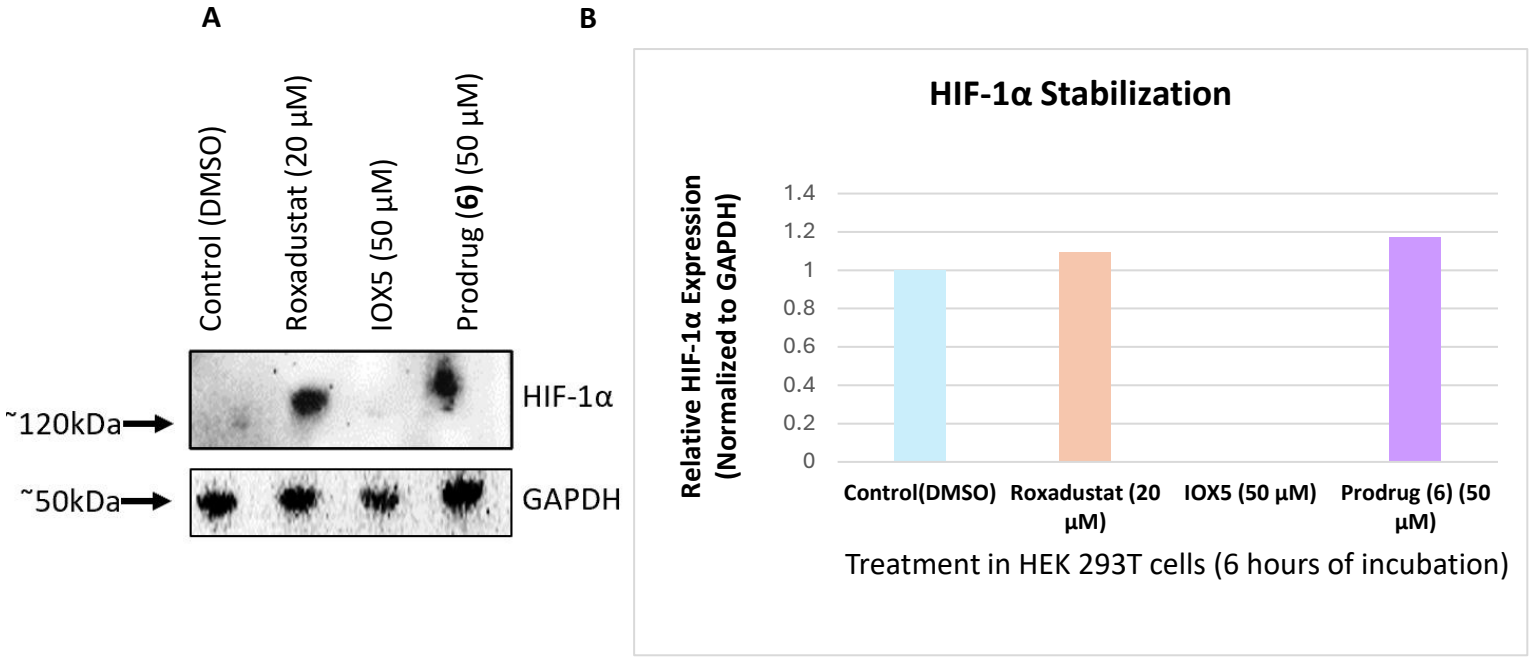


Figure 2.6.2.1: Stabilization of HIF-1α through cellular inhibition of HIF prolyl hydroxylation by 6 (a prodrug of 5). (A) Immunoblot analysis of the protein expression of HIF-1α in HEK 293T cells treated with **5** (50 µM) & **6** (50 µM) and **1** (20 µM) for 6 hours in normoxia. (B) Quantification of HIF-1α levels normalized to GAPDH after treatment for 6 hours in normoxia.

Quantification analysis showed that, compared to the control, **6** (50 µM) significantly increased HIF-1α levels (**Figure 2.6.2.1 B**).

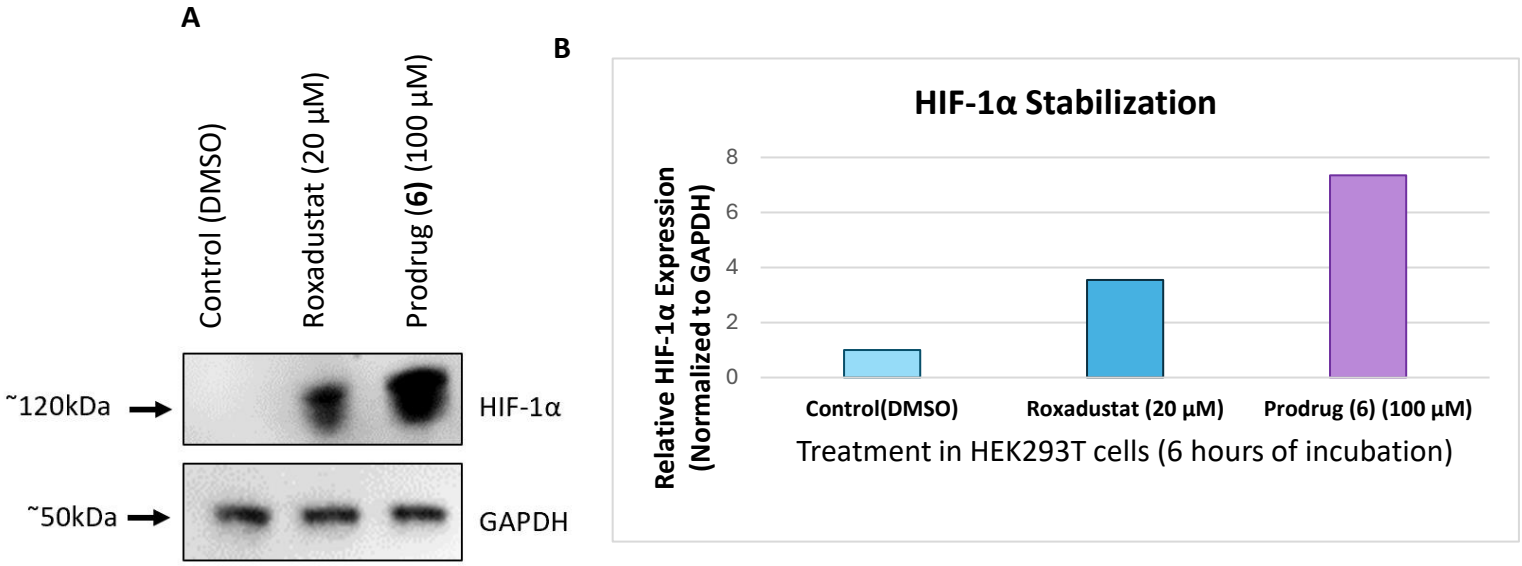


Figure 2.6.2.2: Stabilization of HIF-1α through cellular inhibition of HIF prolyl hydroxylation by 6. (A) Immunoblot analysis of the protein expression of HIF-1α in HEK 293T cells treated with **6** (100 µM) and **1** (20 µM) for 6 hours in normoxia. (B) Quantification of HIF-1α after treatment for 6 hours of treatment.

Western blot analysis showed that when HEK 293T cells were treated for 6h with **6,** HIF-1α stabilization was observed at 100 µM (**Figure 2.6.2.2 A**). Quantification analysis showed that, compared to the control, 6 (100 µM) significantly increased HIF-1α levels (**Figure 2.6.2.2 B**).

Figure A.7.4 shows **6** can stabilize HIF-1α at 50, 20, 10, and 5µM after 6 hours of incubation.

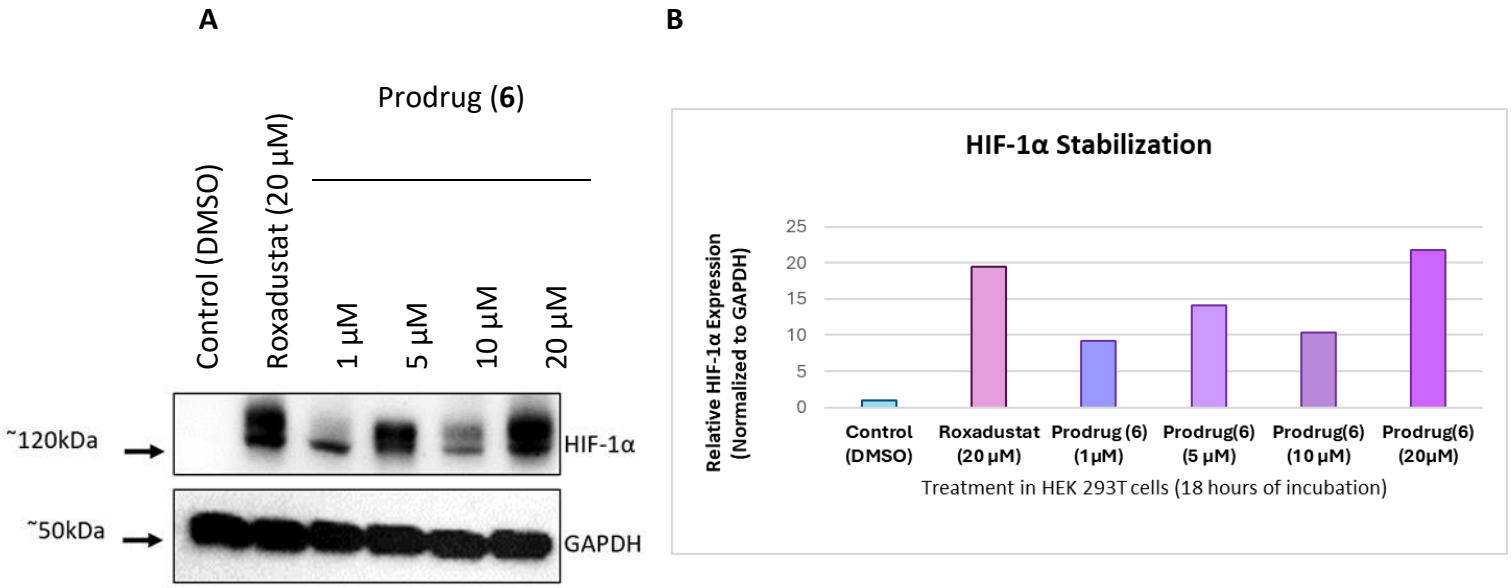


Figure 2.6.2.3: Stabilization of HIF-1α through cellular inhibition of HIF prolyl hydroxylation by 6. (A) Immunoblot analysis of the protein expression of HIF-1α in HEK 293T cells treated with **6** (20, 10, 5 & 1 µM) and **1** (20 µM) for 18 hours in normoxia. (B) Quantification of HIF-1α after treatment for 18 hours of treatment.

Figure 2.6.2.3 A shows **6** can stabilize HIF-1α at 50, 20, 10, 5 and 1µM after 18 hours of incubation. Quantification analysis showed that, compared to the control, **6** (20,10, 5 & 1µM) significantly increased HIF-1α levels **(Figure 2.6.2.3 B**).

Treatment with **6** was further explored using lower concentrations of **6**, i.e. 1 and 0.5 µM,

with 18 h of incubation (**Figure 2.6.2.4 A).** Western blot results showed that, when incubated for 18h, **6** can also upregulate HIF-1α at 0.5 μM compared to **1**.

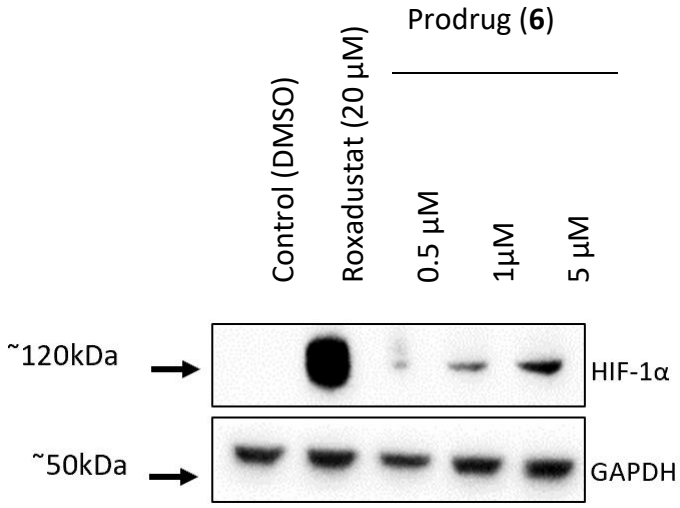


Figure 2.6.2.4: Stabilization of HIF-1α through cellular inhibition of HIF prolyl hydroxylation by 6. Immunoblot analysis of the protein expression of HIF-1α in HEK 293T cells treated with 6 (5, 1 & 0.5 μM) and **1** (20 μM) for 18 hours in normoxia.

In summary, the results indicate that **6** is more active than **5**, possibly due to better cell permeation. When incubated for 18h, **6** can stabilize HIF-1α at 1 μM. Note that 10 μM of **6** showed a relatively weak effect on suppression of HIF-1α compared to the **1** at 20 μM results (**2.6.2.3 (A)**), an observation requiring further investigation.

2.7 Summary and Conclusions

This chapter describes cellular studies focusing on a novel selective PHD inhibitor **5** and its prodrug **6,** both members of the 4-hydroxy-pyridine series of PHD inhibitrors. **5** was able to stabilize HIF-1α at 100 µM but not at 50 µM when incubated for 6h, possibly due to its zwitterionic properties causing poor cell permeability. However, when cells were treated with **5** for 18 hours, activity was observed even at 0.5 µM. As apparent in **Figures 2.2.1 & 2.2.3.1**, the clinically available PHD inhibitors did not apparently stabilize HIF-1α below 5 µM after 18 h treatment. Like **1**, **5** promoted expressions of HIF-1α target genes, i.e. *HIF1α* and *VEGF*. Also, like **1**, **5** did not show any significant impact on *EPO* and *CA9* gene expression. The effects of **5** on cell viability were evaluated using HEPG2 and HEK 293T cells. The results show no impact at 500 µM. Thus, **5** can be considered a promising PHD inhibitor.

Results of in-vivo experiments revealed that **5** can produce an increase in RBC count, HBG, and HCT levels comparable to the clinically used PHD inhibitor **2**. Interestingly, in-vivo experiments showed that both (low & high dose) treatment groups of **5** (15mg/kg and 30 mg/kg) showed higher ability to increase RBC compared to **2** (30mg/kg). All experimental groups did not show any adverse effects.

Studies on a pro-drug version of of **5** were conducted with the aim of improving cell permeability **Figure 2.6.1.1.** Cellular investigations showed that **6** was able to cause accumulation of HIF-1α at 0.5 µM **Figure 2.6.2.6.**

A possible explanation for double bands observed in some of the western blots for HIF-1α can be, HIF-1α, when it undergoes post-translational modifications, especially phosphorylation or hydroxylation, which may sometimes slightly change the molecular weight of HIF-1α and increase the protein's negative charge. These changes may affect how HIF-1α migrates on an SDS-PAGE gel [32-34].

In summary, the novel PHD pharmacophores defined here (**5** & **6**), demonstrated significant selectivity over all tested other human 2OG oxygenases, something that not clinically used PHD inhibitor has yet achieved (**Table 2.2.1**). **5** and **6** show better cellular efficacy compared to the clinically used / clinical candidates (**1-4**). Future work will be aimed at completing In-vivo experiments. More cellular investigations will be done to extend the cellular profiling of **6**.

2.8 Contributions of others

PHD inhibitors were designed and synthesised by Dr. James Holt-Martyn. Dr. Hannah Lawson (Institute of Cancer Research) conducted the in-vivo experiments. Dr Anthony Tumber conducted selectivity studies.

2.9 Materials and Methods

2.9.1 Chemicals

Methanol (≥ 99.9%, HPLC grade), acetonitrile (≥99.9%, for HPLC) and isopropanol (≥99.9%, for HPLC) were from Merck (Darmstadt, Germany). Unless otherwise specified, all methanol, acetonitrile and isopropanol samples were of HPLC grade purity. MTS kits were from Promega, USA. The primary antibody used, Purified Mouse Anti-Human HIF-1α [Catalog Number 610959] was from Thermo Fisher Scientific, (Waltham, MA, USA). The secondary antibody used, Rabbit Anti-Mouse IgG (D3V2A) mAb (HRP Conjugate) [Catalog Number 58802], was from (Cell Signaling Technology, Inc., Danvers, Massachusetts, USA). The RNeasy Plus Micro kit used for RNA extraction was from Qiagen (Manchester, UK). For cDNA synthesis, the qPCRBIO cDNA Synthesis Kit was used (PCR Biosystems Ltd, London, UK). The SYBR® Green master mix was from Life Technologies (San Diego, USA).

2.9.2 Cell lines used

Human Embryonic Kidney 293T cells were from the ATCC® (cat no. CRL-3216). HEPG2 (Glioblastoma cell line) was obtained from ATCC® (CRL-2610).

2.9.3 Cell culture stock solutions

Stock solutions of all inhibitors (IOX5, Roxadustat, Daprodustat and Molidustat) were dissolved in DMSO. DMSO was sterilised before any experiments using a 0.45 µM syringe filter.

2.9.4 PHD inhibitors used for the experiments

The used clinical PHD inhibitors were Roxadustat, Daprodustat and Molidustat obtained from MedChemExpress (Sollentuna, Sweden).

2.9.5 Cell culture

All cells were grown in Dulbecco's modified Eagle's medium (high glucose, pyruvate, no glutamine, Gibco) supplemented with 10% of fetal bovine serum (FBS), and 1% GlutaMAX in a 37°C incubator at 5% atmospheric CO_2. Cell confluency was measured microscopically (Motic AE31E trinocular microscope, Hong Kong).

2.9.6 Protein extraction and analysis

1.2×10^6 cells were seeded in a T75 flasks. Cells were washed with ice-cold PBS (Sigma, D8537) twice after treatment period was over. protein extraction was done using 1x RIPA buffer [Sigma, R0278] buffer, and a protease inhibitor [cOmplete™, Mini, EDTA-free Protease Inhibitor Cocktail, Roche]). With the help of a plastic scraper the adherent cells were scraped, and the cells were transferred into a microcentrifuge tube. The microcentrifuge tubes were kept on ice during the entire experiment. If the experiment carried on then the cell suspensions were kept on ice for 45 mins otherwise store at -20°C. After 45 mins the cells were sonicated for 3 cycles of 10 seconds pulse with 5 seconds intervals. Next the cells were centrifuge at 16,000 g, for 15 mins, at 4°C tempareture. The cell supernatant was collected and leveled accordingly and later following the manufacturer's directions, BCA protein assay kit was used for protein concentrations were determined.

2.9.7 Reverse transcription-quantitative polymerase chain reaction (RT-qPCR)

HEK 293T cells were seeded at a density of 1.2X106 cells into 6cm dishes. The treatment groups were carried out with biological triplicates. The next day, the cells were treated with 20µM of **5** or **1**. The control group was treated with DMSO [0.9% (v/v) final concentration]. The cells were treated for 18 hours and then harvested. During harvesting the cells were washed twice with ice cold PBS. For the RNA extraction, the RNeasy plus micro kit was used. Cells were disrupted by adding 350µl of RLT buffer and 350µl of 70% DEPC treated ethanol, then transferred into a RNeasy spin column. The RNeasy spin columns were centrifuged for 1 minute at 8000 g. The flow through was discarded; the RNA pellets were treated with RW1, DNase I master mix (10µl of DNase I and 70µl RDD buffer), and RPE buffer following the protocol. At the end of the process, 30-50 µl of the RNA pellet solution was eluted using nuclease-free water. The RNA concentration was measured using a NanoDropTM one/oneC microvolume UV-Vis spectrophotometer. (260/280 and 260/230 absorbances were used to quantify RNA). The next step was cDNA synthesis. The concentrated RNA extract (2 µl) was mixed with 18 µl of cDNA master mix, following the protocol. Amplification of 20 µl of cDNA template per reaction was done using the CFX96 touch real-time PCR detection system. The thermocycle process had 3 steps: An initial activation step, at 42°C for 30 minutes. After 40 cycles of a 2-step cycling process consisting of 85°C for 10 minutes and 4°C ∞. The primers related to hypoxia gene expressions such as *Hif1α*, *Bnip3*, *VEGF*, *and EPO* used for RT-qPCR analysis are given in **Table 2.9.7**. β-Actin was used here to normalize the level of mRNA. The ΔCt method was used for the quantification of expression of mRNA. The Bio-Rad CFX maestro system was used for quantification.

Table 2.9.7: List of primers used for RT-qPCR studies and their forward (FW)/reverse (RV) sequences

The primers used for RT-qPCR are given below.

HIF-1α	RV TAT CGA GGC TGT GTC GAC TG FW TCA AGT CAG CAA CGT GGA AG
VEGF	RV ACA GGA CGG CTT GAA GAT A FW TTA CTG CTG TAC CTC CAC
EPO	RV ACC CGA AGC AGT GAA GTG A FW AAT GGA GGT GGA AGA ACA GG
BNIP3	RV GAG GTT GTC AGA CGC CTT CC FW CCA CCC TCA GCA TGA GGA AC
ß-Actin	RV CAT GGA TGC CAC AGG ATT CCA TAC FW TGC CCT AGA CTT CGA GCA AGA

2.9.8 Cell viability assays

2.9.5.1 Treatment with **5** and **1**: Cell viability assay in 96-well plate

A colorimetric method using[3-(4,5-dimethylthiazol-2-yl)-5-(3-carboxymethoxyphenyl)-2-(4-sulfophenyl)-2H-tetrazolium, inner salt; MTS] was used for quantification of cell viability [27, 28]. First, 100 µL of fresh DMEM media containing HepG2 or HEK 293T cells (0.01 cells/ ml) were plated and kept for 24 hours for incubation. After 24 hours, the cells were treated with different concentrations of IOX5 (group 1) or Roxadustat (group 2); a control group was

treated with 0.09% (v/v) of DMSO. The inhibitor concentrations used were 10, 20, 50, 100, 300 and 500 µM. Stock solutions of both IOX5 and Roxadustat were prepared in DMSO; all the treated cells, including controls, had a final DMSO concentration of 0.09% (v/v). The incubation time of treatment was 6 and 24 hours for HepG2 and HEK 293T cells, respectively. The MTS reagents were thawed at room temperature; 10µL of MTS dye was added into each well including control wells, the 96 well plates were incubated in a 37°c and 5% atmospheric CO_2 incubator for 3 hours, and then the absorbance was recorded at 490nm using the ClarioStar plate reader.

2.9.9 Immunoblotting and SDS-PAGE assays

2.9.9.1 SDS-Page

Pre-cast NuPAGE 4-12% Bis-Tris Protein Gels (Life Tech) were used for polyacrylamide gel electrophoresis. All samples were loaded into the pre-cast NuPAGE 4-12% Bis-Tris Protein Gels. The gels were run (Mini Gel Tank, Life Technologies) in 1x Tris/glycine/SDS running buffer (20x NuPAGE MES SDS Running Buffer, Life tech) and the conditions were: 180 V., 45 min. 5µl of protein ladder marker (Page Ruler Prestained Protein Ladder, Thermo Scientific) was used to compare protein sizes.

2.9.9.2 Western Blot

1x transfer buffer solution (20x NuPAGE Transfer Buffer, Invitrogen) was used to transfer the gel which contains the resolved proteins onto a nitrocellulose membrane (Amersham Protran Premium 0.2 NC 300mm, GE Healthcare) . A Mini Protean Tetra Cell, Bio-Rad was used for the gel transfer. The conditions for gel transfer were: 100 volts and 60 mins. For blocking the

membranes 5% milk powder in 1x PBS-T was used. Membrane blocking was done for 30 mins. Membranes were incubated overnight with primary antibodies (in 1: 1000 dilutions) at 4 °C. Primary antibodies solutions were prepared in 1% milk powder in 1x PBS-T buffer. After overnight incubation the membranes were washed with 1x PBS-T for 10-min. This process was repeated for three times and then incubated with a horseradish peroxidise (HRP) conjugated secondary antibody (in 1:5000 dilutions) for 1 hour at Room temperature. The secondary antibody prepared solution was prepared with 1% milk powder in 1x PBS-T. The blots were then washed with 1xPBS-T for 10-mins. This process was repeated three times. Protein levels were measured using the GE Healthcare Amersham™ ECL™ Prime Western Blotting Detection Reagent (RPN2236) was added to the blot and protein levels were measured using a Bio-Rad Universal Hood iii. Values were normalized to glyceraldehyde 3-phosphate dehydrogenase (GAPDH).

2.10 References

1. Yeh, T.-L., et al., *Molecular and cellular mechanisms of HIF prolyl hydroxylase inhibitors in clinical trials*.Chem. Sci. , 2017. 8(11): p. 7651-7668. DOI: 10.1039/c7sc02103h

2. Abboud, M.I., et al., *2-Oxoglutarate regulates binding of hydroxylated hypoxia-inducible factor to prolyl hydroxylase domain 2*. Chem. Commun., 2018. 54(25): p. 3130-3133. DOI: 10.1039/c8cc00387d

3. Holt-Martyn, J.P., et al., *Studies on spiro [4.5] decanone prolyl hydroxylase domain inhibitors*. MedChemComm, 2019. 10(4): p. 500-504.

4. Figg Jr, W.D., M.A. McDonough, R. Chowdhury, Y. Nakashima, Z. Zhang, J.P. Holt-Martyn, A. Krajnc, and C.J. Schofield, *Structural basis of prolyl hydroxylase domain inhibition by molidustat. ChemMedChem*, 2021. **16(13)**: p. 2082–2088. DOI: 10.1002/cmdc.202100239

5.Maxwell, P.H., M.S. Wiesener, G.W. Chang, S.C. Clifford, E.C. Vaux, M.E. Cockman, C.W. Pugh, E.R. Maher, and P.J. Ratcliffe, *The tumour suppressor protein VHL targets hypoxia-inducible factors for oxygen-dependent proteolysis. Nature*, 1999. **399(6733)**: p. 271–275. DOI: 10.1038/20459

6.Lawson, H., J.P. Holt-Martyn, V. Dembitz, Y. Kabayama, L.M. Wang, A. Bellani, S. Atwal, N. Saffoon, J. Durko, L.N. van de Lagemaat, and A.L. De Pace, *The selective prolyl hydroxylase inhibitor IOX5 stabilizes HIF-1α and compromises development and progression of acute myeloid leukemia. Nat. Cancer*, 2024. **5**: p. 1–22. DOI: 10.1038/s43018-024-00761-w

7.Holt-Martyn, J.P., R. Chowdhury, A. Tumber, T.L. Yeh, M.I. Abboud, K. Lippl, C.T. Lohans, G.W. Langley, W. Figg Jr, M.A. McDonough, and C.W. Pugh, *Structure-activity relationship and crystallographic studies on 4-hydroxypyrimidine HIF prolyl hydroxylase domain inhibitors. ChemMedChem*, 2020. **15(3)**: p. 270–273. DOI: 10.1002/cmdc.201900687

8. Chan, M.C., et al., *Potent and selective triazole-based inhibitors of the hypoxia-inducible factor prolyl-hydroxylases with activity in the murine brain*. PLoS One, 2015. 10(7): p. e0132004. DOI: 10.1371/journal.pone.0132004

9. Chowdhury, R., et al., *Selective small molecule probes for the hypoxia inducible factor (HIF) prolyl hydroxylases*. ACS Chem. Biol., 2013. 8(7): p. 1488-1496. DOI: 10.1021/cb400088q

10. Horita, S., et al., *Structure of the ribosomal oxygenase OGFOD1 provides insights into the regio-and stereoselectivity of prolyl hydroxylases*. Structure, 2015. 23(4): p. 639-652. DOI: 10.1016/j.str.2015.01.014

11.Rose, N.R., et al., *Plant growth regulator daminozide is a selective inhibitor of human KDM2/7 histone demethylases*.J. Med. Chem. , 2012. 55(14): p. 6639-6643. DOI: 10.1021/jm300677j

12. Holt-Martyn, J., *Novel and selective small molecule inhibitors and activators for the prolyl hydroxylase domain enzyme*. 2018, University of Oxford.

13. Schoener, B. and J. Borger, *Erythropoietin stimulating agents.* 2019.

14. Jelkmann, W., *Erythropoietin.* Sports Endocrinology, 2016. 47: p. 115-127. DOI: 10.1159/000445174

15. Mullard, A., *FDA approves first hypoxia-inducible factor prolyl hydroxylase inhibitor*. Nat. Rev. Drug Discov., 2023. 22(3): p. 173-173. DOI: 10.1038/d41573-023-00028-6

16. Locatelli, F., L. Del Vecchio, and S. Elliott, *The anaemia treatment journey of CKD patients: from epoetins to hypoxia-inducible factor-prolyl hydroxylase inhibitors*.Clin. Kidney J. , 2023. 16(10): p. 1563-1579. DOI: 10.1093/ckj/sfad105

17. Dhillon, S., *Roxadustat: first global approval.* Drugs, 2019. 79: p. 563-572. DOI: 10.1007/s40265-019-01077-1

18. Provenzano, R., et al., *Oral hypoxia–inducible factor prolyl hydroxylase inhibitor roxadustat (FG-4592) for the treatment of anemia in patients with CKD*.Clin J Am Soc Nephrol , 2016. 11(6): p. 982-991. DOI: 10.2215/CJN.06890615

19. Wilkening, S., F. Stahl, and A. Bader, *Comparison of primary human hepatocytes and hepatoma cell line HepG2 with regard to their biotransformation properties. Drug Metab. Dispos.*, 2003. **31(8)**: p. 1035–1042. DOI: 10.1124/dmd.31.8.1035

20. Knasmüller, S., W. Parzefall, R. Sanyal, S. Ecker, C. Schwab, M. Uhl, V. Mersch-Sundermann, G. Williamson, G. Hietsch, T. Langer, and F. Darroudi, *Use of metabolically competent human hepatoma cells for the detection of mutagens and antimutagens. Mutat. Res.*, 1998. **402(1–2)**: p. 185–202. DOI: 10.1016/S0027-5107(97)00294-1

21. Malich, G., B. Markovic, and C. Winder, *The sensitivity and specificity of the MTS tetrazolium assay for detecting the in vitro cytotoxicity of 20 chemicals using human cell lines*. Toxicology, 1997. 124(3): p. 179-192. DOI: 10.1016/s0300-483x(97)00151-0

22. Wanner, R.M., et al., *Epolones induce erythropoietin expression via hypoxia-inducible factor-1α activation*. Blood, Am. J. Hematol. , 2000. 96(4): p. 1558-1565. DOI: https://doi.org/10.1182/blood.V96.4.1558

23. Ahluwalia, A. and A. S Tarnawski, *Critical role of hypoxia sensor-HIF-1α in VEGF gene activation. Implications for angiogenesis and tissue injury healing*.Curr. Med. Chem. , 2012. 19(1): p. 90-97. DOI: 10.2174/092986712803413944

24. Wykoff, C.C., et al., *Hypoxia-inducible expression of tumor-associated carbonic anhydrases.* Cancer research, 2000. 60(24): p. 7075-7083. DOI: 10.1016/S0002-9440(10)64048-5

25. Chan, M.C., Ilott, N.E., Schödel, J., Sims, D., Tumber, A., Lippl, K., Mole, D.R., Pugh, C.W., Ratcliffe, P.J., Ponting, C.P., Schofield, C.J., Tuning the transcriptional response to hypoxia by inhibiting hypoxia-inducible factor (HIF) prolyl and asparaginyl hydroxylases. *J Biol Chem.*, 2016. 291(39): p. 20661-20673. DOI: 10.1074/jbc.M116.749291

26. Maxwell, P.H., M.K. Osmond, C.W. Pugh, A. Heryet, L.G. Nicholls, C.C. Tan, B.G. Doe, D.J. Ferguson, M.H. Johnson, and P.J. Ratcliffe, *Identification of the renal erythropoietin-producing cells using transgenic mice. Kidney Int.*, 1993. **44(5)**: p. 1149–1162. DOI: 10.1038/ki.1993.363

27. Wang, G.L., and G.L. Semenza, *Characterization of hypoxia-inducible factor 1 and regulation of DNA binding activity by hypoxia. J. Biol. Chem.*, 1993. **268(29)**: p. 21513–21518. Link

28.Jelkmann, W., *Regulation of erythropoietin production. J. Physiol.*, 2011. **589(6)**: p. 1251–1258. DOI: 10.1113/jphysiol.2010.195057

29. Semenza, G.L., and G.L. Wang, *A nuclear factor induced by hypoxia via de novo protein synthesis binds to the human erythropoietin gene enhancer at a site required for transcriptional activation. Mol. Cell. Biol.*, 1992. **12(12)**: p. 5447–5454. DOI: 10.1128/mcb.12.12.5447-5454.1992

30. Pan, X., N. Suzuki, I. Hirano, S. Yamazaki, N. Minegishi, and M. Yamamoto, *Isolation and characterization of renal erythropoietin-producing cells from genetically produced anemia mice. PLoS ONE*, 2011. **6(10)**: e25839. DOI: 10.1371/journal.pone.0025839

31. Chan, M.C., Ilott, N.E., Schödel, J., Sims, D., Tumber, A., Lippl, K., Mole, D.R., Pugh, C.W., Ratcliffe, P.J., Ponting, C.P., Schofield, C.J., Tuning the transcriptional response to hypoxia by inhibiting hypoxia-inducible factor (HIF) prolyl and asparaginyl hydroxylases. *J Biol Chem.*, 2016. 291(39): p. 20661-20673.https://doi.org/10.1074/jbc.M116.731901

32.Richard, D.E., E. Berra, E. Gothié, D. Roux, and J. Pouysségur, p42/p44 mitogen-activated protein kinases phosphorylate hypoxia-inducible factor 1α (HIF-1α) and enhance the transcriptional activity of HIF-1. *J Biol Chem.*, 1999. 274(46): p. 32631–32637. https://doi.org/10.1074/jbc.274.46.32631

33. Contenti, J., Y. Guo, M. Larcher, L. Mirabal-Ortega, M. Rouleau, M. Irondelle, V. Tiroille, A. Mazzu, V. Duranton-Tanneur, F. Pedeutour, and I. Ben-Sahra, HIF-1 inactivation empowers HIF-2 to drive hypoxia adaptation in aggressive forms of medulloblastoma. *Cell Death Discov.*, 2024. 10(1): p. 338. https://doi.org/10.1038/s41420-024-01891-9

34. Pagé, E.L., G.A. Robitaille, J. Pouysségur, and D.E. Richard, Induction of hypoxia-inducible factor-1α by transcriptional and translational mechanisms. *J Biol Chem.*, 2002. 277(50): p.

48403–48409. https://doi.org/10.1074/jbc.M208237200

Chapter 3

Exploring the possibility of using a natural diet for PHD inhibition

3.1 $CoCl_2$ as a HIF stabilizer

Chapters 2 and 4 describe work focusing on the evaluation of new and improved HIF modulators, involving synthetic PHD inhibitors and PHD enhancers. By contrast, the work described in this chapter focused on the potential therapeutic use of naturally occurring materials to modulate HIF levels. Although exposure to hypoxia has multiple potential effects on animal biology, there is strong evidence that at least to some extent, moderate hypoxia (10-16% O_2) itself is relatively non-toxic; indeed, for example, hypoxia is extensively used by athletes in training and living at altitude is possible [1-4]. Further, simple naturally occurring 2OG analogues such as the naturally occurring molecule N-oxalylglycine (NOG) (**Figure 3.1.1 A**) can induce the hypoxic response, without, at least, apparent short-term toxicity [5-8].

A **B**



2-oxoglutrate (2OG) N-oxalylglycine (NOG)

Figure 3.1.1: Chemical structures of 2-oxoglutrate (2OG) (A) and (B)the 2OG analogue N-oxalylglycine (NOG).

Hence, there is potential scope for the use of natural product/diet therapies to induce the hypoxic response. Cobalt chloride ($CoCl_2$) is a vital trace element and in the past, $CoCl_2$ was used therapeutically to treat anaemia in CKD patients [9]. However, due to the side effects of $CoCl_2$, such as cardiomyopathy and thyroid dysfunction, $CoCl_2$ was subsequently withdrawn from treatment [10]. Cobalt chloride can enhance erythropoiesis and is used in research work

as an upregulator of HIF-α [11] and as a hypoxia-mimetic[3]. In 2017, cobalt compounds, proposed to act via PHD enzyme inhibition, were added to the World Anti-Doping Agency's prohibited list of doping substances because they upregulate EPO production [4, 12-14].

The work described in this chapter aimed to carry out preliminary studies to investigate diet / natural product therapies for the treatment of anaemia via cobalt or natural product mediated PHD inhibition.

3.2 Spinach- a natural diet as a source of CO(II)

Initially, a search for a natural source of cobalt ions was carried out, focusing on identifying one that was easily available and that is already consumed by many people on a daily basis. A search to identify foods rich in cobalt ions led to research papers suggesting leafy green vegetables such as lettuce, cabbage, and spinach that are relatively rich in cobalt ions see **Table 3.2.1** [15]. As shown by Saulea et al [16] (**Table 3.2.1**), Among the studied leafy green vegetables consumed by humans spinach contains the highest amount of cobalt, thus studies on whether extracts from *Spinacia oleracea* leaves, (**Table 3.2.1**) could stabilize HIF-1α using HEK 293T cells were carried out.

Table 3.2.1: Analysis of cobalt in food samples as described by Saulea et al [16].

No.	Sample	Co found (ng/g)	Co found (ng/L)
1	**Spinach leaves**	**7370**	
2	Lettuce leaves	1950	
3	Cabbage leaves (TR)	380	
4	Cabbage leaves (DB)	560	
5	Parsnip root	1280	
6	Celery root	850	
7	Garlic root	200	
8	White onion root	1700	
9	Red onion	600	
10	Orange	910	
11	Tangerine	920	
12	Red grapefruit	1930	
13	Apple	640	
14	Pear	4580	
15	Flour	960	
16	Cinnamon	2800	
17	Coffee (Elita red)	9600	
18	Coffee (Elita green)	4600	
19	Coffee (Jacobs red)	5900	
20	Chicken liver 1	1420	
21	Chicken liver 2	1200	
22	Powder milk	200	
23	Milk		<100
24	Beer (Ciuc brand)		100
25	Beer (Bucegi brand)		200

3.3 Preparation of natural spinach leaf extraction and measurement of cobalt concentration

The spinach leaf extraction process used is described in **Methods and Materials (section**

3.8.6). To measure the cobalt ion concentration in the natural spinach extracts, samples were analyzed by the Department of Earth Sciences of the University of Oxford. Dr Phil Holdship (a research fellow in trace element analysis) kindly analyzed the samples. Inductively coupled plasma mass spectrometry (ICP-MS) was used to measure cobalt concentrations from the samples. Thus, 0.5g of the natural spinach leaf extract was dissolved in 5 mL of deionized water and sent for analysis. The Department of Earth Science measured the samples in triplicate. After analysis, the amount of cobalt found ranged from 219.049 to 264.319 ng/g of spinach leaf extract. Note that the amount of cobalt present in prepared spinach extraction was lower (minimally by a factor of 28) compared to that reported by Saulea et al (7370ng/g) [16]. **Table 3.3.1** shows the amount of cobalt or cobalt measurements in the prepared spinach leaf extracts. The methods and materials section (**Table 3.8.7.1)** describes the analytical methods used for the interpretation of the ICP-MS analysis. It should be noted that the form of the cobalt is not defined – it could be free cobalt, cobalt complexed in the form of vitamin B12., or another form.

Table 3.3.1 Cobalt measurements in the spinach leaf extracts from ICP-MS analysis.

	Co-1 59 Helium KED (ppb)	Rh 103 (IS) Helium KED
	ng/g	IS
Blank	0.147	IS
Spinach extraction x2 diluted (1)	264.319	IS
Spinach extraction x2 diluted (2)	258.656	IS
Spinach extraction x2 diluted (3)	219.049	IS
Reference	212.725	IS

3.4 Investigating the effects of natural dietary components (*Spinacia Oleracea* leaf extracts) on HIF-1α levels

Investigations were carried out with HEK 293T cells to evaluate whether the natural spinach leaf extracts stabilize HIF-1α in cells, comparing the results with those for pure commercial $CoCl_2$. Thus, HEK 293T cells were exposed to natural spinach leaf extracts for 6 h and 24 h. The initial aim of these experiments was to investigate the incubation time required for the natural spinach leaf extraction treatment to stabilize HIF. Second, the studies aimed to investigate the amount of natural spinach leaf extracts required to observe HIF-1α stabilization.

Western blot analyses showed that when HEK 293T cells were incubated for 6 hrs with 750 µg/ml of natural spinach extracts, no evidence for HIF-1α upregulation was observed (**Figure 3.4.1 A & Figure A. 7.5**). By contrast when cells were treated for 24h with 750 µg /ml of the spinach extracts there was clear evidence for HIF-1α stabilization (**Figure 3.4.1 C &Figure A. 7.5**). Quantification analysis showed that, compared to the control, 150 µM of $CoCl_2$ and 750 µg / ml of natural spinach leaf extracts significantly increased HIF-1α levels when treated for 24 hours (**Figure 3.4.1 B,D & Figure A.7.5**).

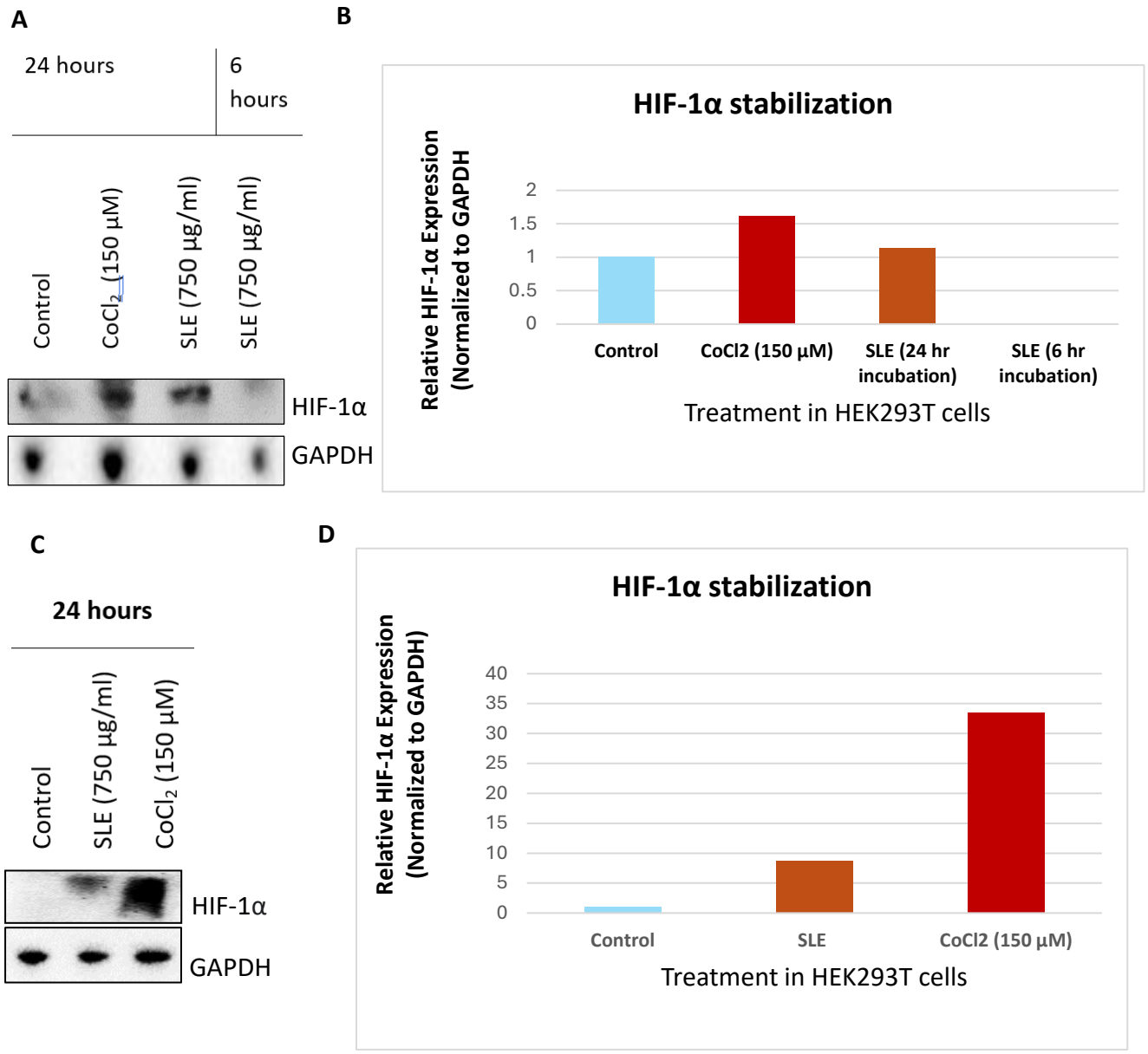


Figure 3.4.1: Stabilization of HIF-1α through cellular inhibition of HIF prolyl hydroxylation by spinach (*Spinacia Oleracea*) leaf extracts (SLE). (A) Immunoblot analysis of HIF-1α in HEK 293T cells treated with spinach (*Spinacia Oleracea*) leaf extracts (SLE) (750 µg/ml)) or $CoCl_2$ (150 µM) for 6 or 24 hours in normoxia. (C) Immunoblot analysis of HIF-1α in HEK 293T cells treated with spinach (*Spinacia Oleracea*) leaf extraction (SLE) (750 µg/ml)) and $CoCl_2$ (150 µM) for 24 hours in normoxia. SLE = spinach (*Spinacia Oleracea*) leaf extracts. (B&D) Quantification of HIF-1α after treatment for 6 and 24 hours.

Although there are variations, these assays clearly reveal the potential for spinach leaf extracts to upregulate HIF-1α levels in cells. The differences between 6 and 24h incubation

times suggest that the incubation time is a factor in terms of the extent to which natural spinach extract causes HIF-1α upregulation.

3.5 Effects of proline and its analogues on HIF-1α levels

3.5.1 Investigating Inhibition of prolyl hydroxylase domain (PHD) enzymes / HIF-1α upregulation by substrate analogue peptides

As described before, the PHDs catalyse hydroxylation of HIF-1α promoting proteasomal degradation of HIF-α [17, 18]. Several studies have shown that synthetic peptides that have HIF-1α 556–575 residues with modification at the proline residue can act as proline analogues, including inhibiting PHD2 activity [19-21]. Ma et al. have reported that synthetic peptides which contain a proline analogue at the normally hydroxylated position inhibit PHD3 [22]. Ahn et al. also synthesized a series of peptides that can reduce the interaction between HIF-1α and VHL–Elongin B–Elongin C (VBC) [23].

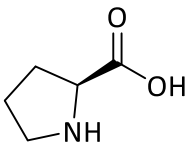
3.5.2 Proline mimics as PHD inhibitors

Studies have shown thiazoles and related compounds can act as proline analogues; e.g. Tegley et al., discovered structurally related novel hydroxy thiazole ring containing molecules that act as PHD inhibitors [24]. Kwon et al. have reported on five proline mimics that within a peptide inhibit the PHDs [21], 4-hydroxyproline and L-4-thiazolidine carboxylic acid being two examples.

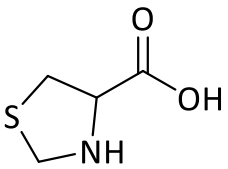
This chapter describes studies using L-4-thiazolidine carboxylic acid, L-proline, L-proline methyl ester hydrochloride, L-azetidine-2-carboxylic acid, trans-4-hydroxy-L-proline, and deuterated proline on mammalian (HEK 293T) cells aiming to investigate potential HIF-1α

upregulation/PHD inhibition. The deuterated proline was "D_7" labelled, i.e. all the C-H bonds were replaced with C-^{2}H bonds.

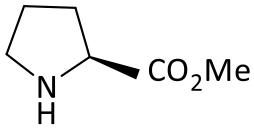
It was envisaged that the proline mimics might be incorporated via the translation machinery into HIF-α isoforms in a manner that would inhibit PHD catalysis so upregulating HIF-α levels. Note that proline methyl ester[25] can undergo hydrolysis to give proline and methanol, the latter of which can be oxidized to give formaldehyde which can react with cysteine to give thioproline [26-29]. Methanol was also tested as its metabolism produces formaldehyde and formate[30], which can interrupt oxidative metabolism [31]or initiate ROS generation[32-33]factors known to indirectly affect HIF stability.



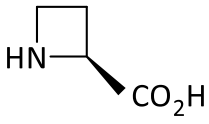
L-proline



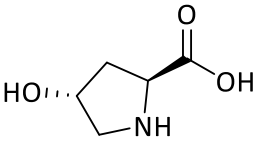
Thiazolidine-4-carboxylic acid



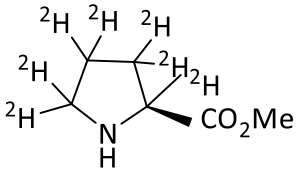
L-proline methyl ester



L-azetidine carboxylic acid



Trans-4-hydroxy-L-proline



D7 proline

Figure 3.5.2.1: Structures of proline and the proline analogues used in this work.

3.5.3 Cellular Investigation of proline-derived amino acids

Cellular investigations were carried out using HEK 293T cells to evaluate whether the proline analogues can stabilize HIF-1α. HEK 293T cells with 24h treatment. Western blot analyses showed that when incubated for 24 hrs with 100 μM of L-proline, L-proline methyl ester hydrochloride, L-4-thiazolidine carboxylic acid, or L-azetidine-2-carboxylic acid there was clear evidence for HIF-1α upregulation, although L-azetidine-2-carboxylic acid only showed a weak HIF-1α signal (**Figure 3.5.3.1 A,&D and Figure A.7.6**). Next, 4-hydroxy proline, methanol and deuterated proline were also investigated for their HIF-1α stabilizing capacity. The treatment of cells with 4-hydroxy proline did not lead to stabilization of HIF-1α protein (**Figure 3.5.3.1.C and Figure A.7.6 C,E**).

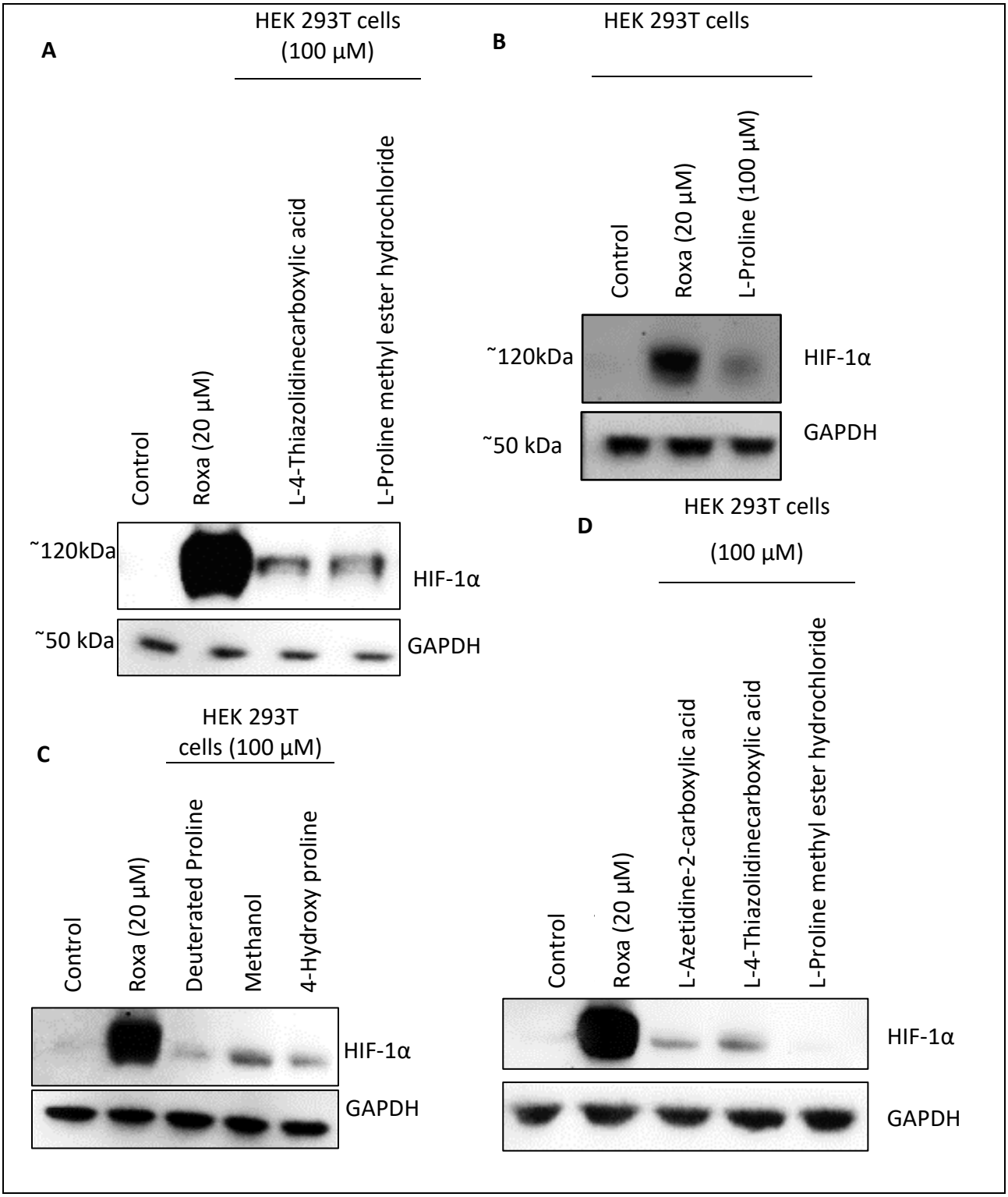


Figure 3.5.3.1. Stabilization of HIF-1α through cellular inhibition of HIF prolyl hydroxylation by different proline-derived amino acids. (A) Immunoblot analysis of HIF-1α in HEK 293T cells

treated with L-proline methyl ester hydrochloride or L-4-thiazolidine carboxylic acid (100 µM) for 24 hours in normoxia. (B) Immunoblot analysis of HIF-1α in HEK 293T cells treated with L-proline (100 µM) for 24 hours in normoxia. (C) Immunoblot analysis of HIF-1α in HEK 293T cells treated with 4-hydroxy proline, methanol or deuterated proline (100 µM) for 24 hours in normoxia. The deuterated proline is labelled "D_7" which means all the C-H bonds were replaced with C-^{2}H bonds. (D) Immunoblot analysis of HIF-1α in HEK 293T cells treated with L-proline methyl ester hydrochloride, L-4-thiazolidine carboxylic acid, L-proline or L-azetidine-2-carboxylic acid (100 µM) for 24 hours in normoxia.

The results with proline are interesting and non-trivial to interpret. The apparent low levels of HIF-1α upregulation in some cases, including by L-proline itself and its deuterated form, were unexpected and seem unlikely to be due to PHD inhibition. Further, work is required but it may reflect a more general effect on metabolism since proline, glutamine, glutamate, and 2-OG are closely related in metabolism. During the cellular investigations, the western blot analyses showed that L-4-thiazolidine carboxylic acid was able to consistently stabilize HIF compared to the other proline-derived amino acids. Therefore, L-4-thiazolidine carboxylic acid was selected for further experiments.

3.5.4 Cell viability assays with L-4-thiazolidine carboxylic acid

The cytotoxic effects of L-4-thiazolidine carboxylic acid were assessed via cell viability assay on the HEK 293T cell line. HEK 293T cells were treated with L-4-thiazolidine carboxylic acid and L-proline; MQ water-treated cells were used as a control. Six different concentrations (10, 20, 50, 100, 300 & 500 µM) of L-4-thiazolidine carboxylic acid and L-proline were used with 48-hour treatment. To investigate cell viability a one-step colorimetric assay employing MTS (3-(4,5-dimethylthiazol-2-yl)-5-(3-carboxymethoxyphenyl)-2-(4-sulfophenyl)-2H-tetrazolium) was performed [34]. The absorbance at 490 nm is reported to positively correlate with the number of viable cells present in each well [35]. The treated groups either with L-4-

thiazolidine carboxylic acid or L-proline showed a dose-dependent decrease in the number of viable cells present (**Figure 3.5.4.1**). For the calculation of viability, the number of live cells in the control group was defined as 100%. With L-proline treated HEK 293T cells (**Figure 3.5.4.1**) at a higher concentration (500 µM) ˜64% of cells were viable. With L-4-thiazolidine carboxylic acid at higher concentration (500 µM) ˜51% of cells were viable, again indicating it is tolerated by cells, but perhaps not as well as L-proline.

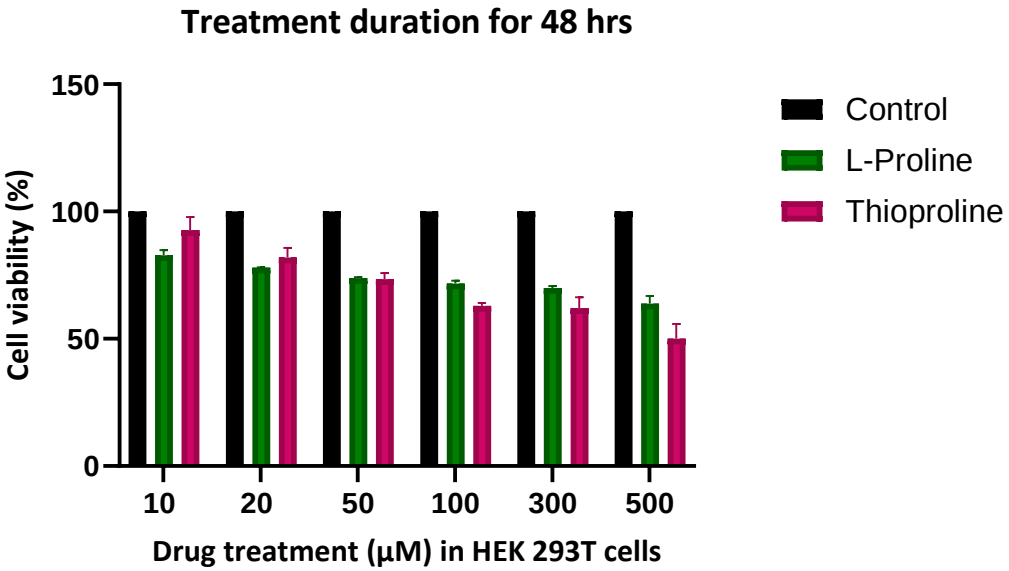


Figure 3.5.4.1: Cell viability (HEK 293T cells) studies with different concentrations of L-4-thiazolidine carboxylic acid or L-proline. 0.01X 106 cells were seeded in a 96-well plate. After the cells were attached, they were treated with different concentrations of L-4-thiazolidine carboxylic acid or L-proline for 48 hours. After the drug treatment, the viable cells were estimated using CellTiter 96 AQueous One Solution Reagent (Promega, G358C). (n=3, biological replicates).

3.5.5 Reverse transcription-quantitative polymerase chain reaction (RT-qPCR) effects of analysis of the L-4-thiazolidine carboxylic acid

It was of interest to evaluate the effects of L-4-thiazolidine carboxylic acid on expression related to HIF. Using RT-qPCR, the expression levels of selected hypoxia responsive genes, that is *HIF-1α*, *EPO*, *VEGF*, and *CA9,* were analysed in HEK 293T cells (**Fig. 3.5.5.1 A, B, C, and D**) as described in **Section 2.4.** HEK293T cells were treated with 100 µM of L-4-thiazolidine carboxylic acid for 24 hours and the RT-qPCR results were compared with those for the control (MQ water treated cells).

Amongst the hypoxia responsive genes examined by RT-qPCR, those for *HIF1α* and *VEGF* genes showed the most substantial upregulation in the 100 µM of L-4-thiazolidine carboxylic acid treated group (**Fig. 3.5.5.1A and B**). When treated with L-4-thiazolidine carboxylic acid, the *HIF1α* and *VEGF* genes showed evidence for modest upregulation, i.e. ~1.3-fold and ~1.4-fold respectively compared to the control (**Fig. 3.5.5.1 A and B**); *EPO* and *CA9* expression levels were not significantly changed compared to the control (**Fig. 3.5.5.1 C and D**).

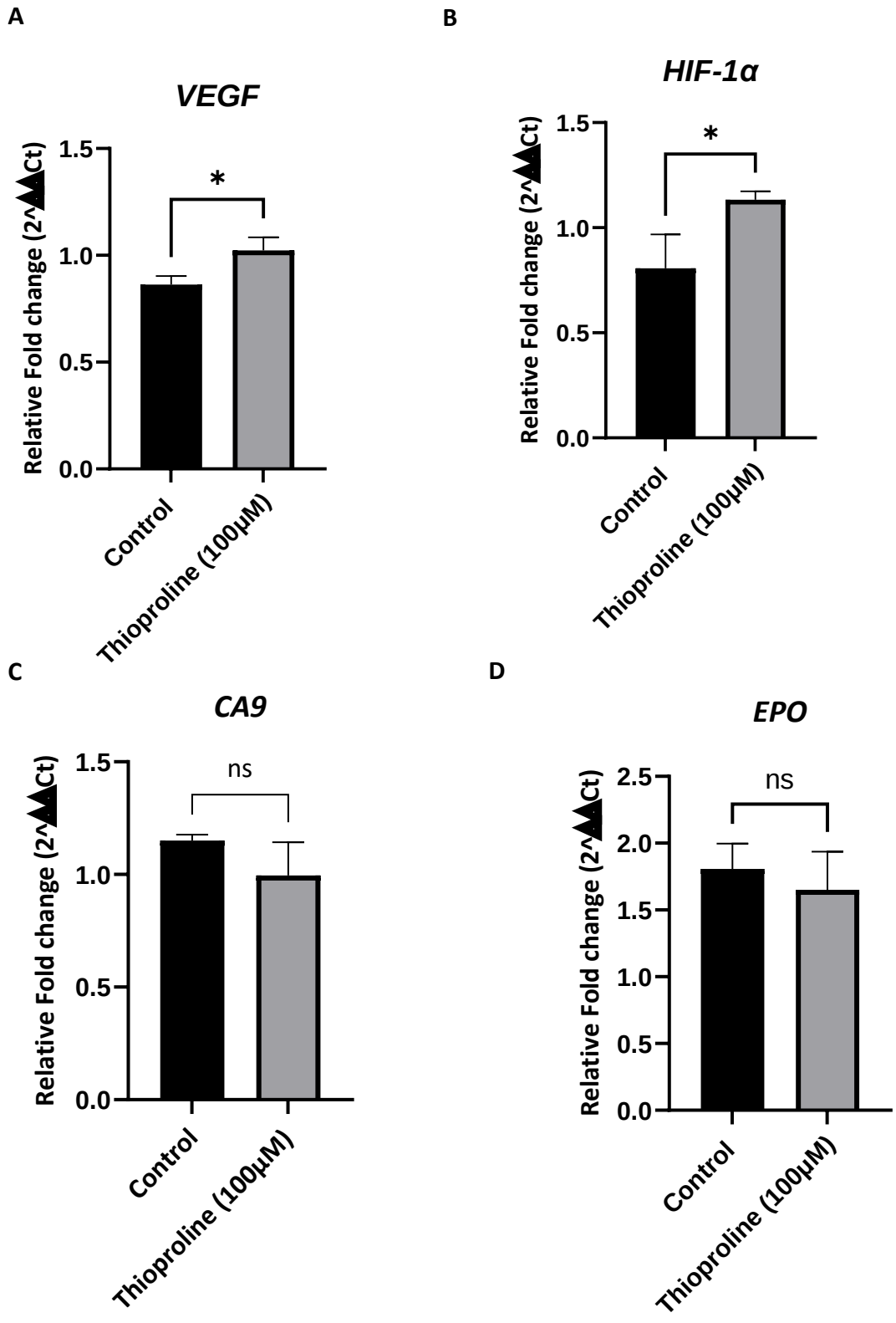


Figure 3.5.5.1: Effects of L-4-thiazolidine carboxylic acid on hypoxia gene expression. The

expression levels of selected hypoxia genes, *HIF1α*, *VEGF, EPO*, and *CA9* were analysed after treatment with 100 µM of L-4-thiazolidine carboxylic acid in normoxia for 24 hours, observations were normalized to *β-actin* levels. Upregulation of *HIF1α,* and *VEGF* expression was seen with L-4-thiazolidine carboxylic acid**.** *EPO* and *CA9* levels were not significantly changed by L-4-thiazolidine carboxylic acid treatment**.** Each data point represents the mean and standard deviation of the relative fold change concerning control (MQ treated cells) normalized to reference gene *β-actin* level. Statistical significance was indicated as *P < 0.05 (Two-way ANOVA, Tukey's *post-hoc* analysis).

3.6 Summary

Spinach leaf extracts were made and tested for their effect on HIF-1α upregulation in a relevant cellular setting. The spinach leaf extracts showed the ability to stabilize HIF-1α at 750 µg /ml when incubated for 24 hours but not when incubated for 6 hours. These observations suggest that incubation time is an important factor in HIF-1α accumulation when treated with spinach extracts. However, compared to treatment with pure chemical $CoCl_2$, the HIF-1α accumulation signal was weak when treated with spinach extracts. The results at least suggest that diet therapy is a promising avenue for PHD inhibition. The results with spinach extracts suggest that it is of interest to revisit other natural PHD inhibitors, including N-oxalylglycine which is present in many plants [8]. Future work will be aimed at completing more cellular investigations to complete the cellular profiles of the effects of spinach and other plant extracts with respect to HIF-α upregulation. This investigation together with in vivo studies will be useful to calculate how much spinach would be required to eat to influence HIF/EPO levels.

The work described in this chapter also evaluated different proline-related amino acids, that is L-4-thiazolidine carboxylic acid, L-proline, L-proline methyl ester hydrochloride, L-azetidine-

2-carboxylic acid, 4-hydroxy proline, and deuterated proline on mammalian (HEK 293T) with respect to their effects on HIF-1α levels. Except for 4-hydroxy proline, all the compounds increased HIF-1α levels as analysed by western blotting, though L-azetidine-2-carboxylic acid showed a relatively weak signal for HIF-1α accumulation. The effects of L-4-thiazolidine carboxylic acid on viability were evaluated using the HEK 293T cell line and it did not show a detrimental impact on cell viability at relatively high concentrations (500 μM).

The effect of L-4-thiazolidine carboxylic acid on HIF-1α target gene expression was also evaluated. When treated with L-4-thiazolidine carboxylic acid, certain HIF-1α genes, e.g. *VEGF* showed evidence for upregulation, as did the gene for *HIF-1α* itself. Treatment with L-4-thiazolidine carboxylic acid did not show any significant impact on *EPO* and *CA9* genes, consistent with the observations with inhibitors as described in Chapter 2.

At this stage, the reasons for the apparent effects of the proline analogues, including L-4-thiazolidine carboxylic acid, on HIF-1α levels and HIF target genes are unclear and require further investigation. It is possible that the proline analogue is imported into HIF-1α at the proline positions that undergo hydroxylation, so inhibiting HIF-1α degradation. But other explanations seem more likely. It is also notable that formaldehyde and formaldehyde precursors (L-proline methyl ester and L-4-thiazolidine carboxylic acid) cause HIF-1α upregulation. In this regard the observation that L-proline methyl ester causes HIF-1α upregulation is of interest. Note however, that the methyl ester is likely hydrolysed to give methanol and formaldehyde, the latter of which can react with cysteine to form L-4-thiazolidine carboxylic acid. Effects on proline/amino acid metabolism cannot be ruled out[25-29], and it is notable that proline, glutamine, glutamate, and 2-OG are closely related

in metabolism[36].

Future work will be aimed at completing more cellular investigations to complete cellular profiles with different concentrations. In particular, further cellular investigations on deuterated proline are of interest due to the possibility that its incorporation into HIF-1α may slow PHD catalysis due to an isotope effect or due to the possibility of perturbation in proline metabolism.

3.7 Contributions of others

Phil Holdship (Research Fellow in Trace Element Analysis) conducted the ICP-MS analyses.

3.8 Materials and Methods

3.8.1 Chemicals

These were described in Section 2.9.1

3.8.2 Cell line

Human Embryonic Kidney 293T cells were from the ATCC® (cat no. CRL-3216).

3.8.3 Cell culture stock solutions

Stock solutions of proline-derived amino acids (L-4-thiazolidine carboxylic acid, L-proline methyl ester hydrochloride, L-azetidine-2-carboxylic acid, 4-hydroxy proline, and deuterated proline) were made up in MQ purified water.

3.8.4 Cell culture and Protein extraction and analysis

These were described in Section 2.9.5 and 2.9.6.

3.8.5 PHD inhibitors used for the experiments

The used clinical PHD inhibitor Roxadustat was obtained from MedChemExpress (Sollentuna, Sweden).

3.8.6 Metabolite extraction of Spinacia oleracea

3.8.6.1 Collection and identification of plant materials

The leaves of *S. oleracea* were collected from a local grocery store Oxford in the United Kingdom. The plant parts were ground into a coarse powder with the help of a grinder. The

powder was stored in an airtight container and kept in a cool, dark, and dry place until further analysis commenced.

3.8.6.2. Drying and grinding of S. Oleracea leaves

Unwanted materials such as dirt or other plant parts were removed from the collected spinach leaves. The leaves were washed, and air dried at room temperature for seven days. the dried leaves of *S. oleracea* were crushed and all the dried leaves were ground into a fine powder with the help of a grinder machine (define this).

3.8.6.3 Extraction protocol

Extraction:

- Solvent selection: HPLC grade 80% (v/l) methanol was chosen as the solvent.
- Weighing: 100g of a fine *S. oleracea* powder weighed accurately.
- Addition of solvent: Add enough 80% (v/l) methanol (HPLC grade) to the fine *S. oleracea* powder and soak for several days in a closed glass container (into a flask) to ensure complete extraction.
- Shaking: The flask was kept on a shaker to shake vigorously.

Filtration:

- Whatman filter paper: The mixture was then filtered through Whatman filter paper and additional leaf debris was removed.
- Collect filtrate: the filtered extract was collected in a clean container.

Rotary evaporation:

- Installation: Rotary evaporation was used and therefore a round-bottomed flask was set up with a condenser, and a vacuum pump.
- Temperature: The temperature of the water bath of the Rotary evaporator was set to keep under the boiling point of methanol.
- Crude extraction: the vacuum pressure was applied step by step to ease methanol evaporation and during methanol evaporation, the round bottom flask was kept on rotating slowly.
- Collection: The concentrated crude extraction was collected in the flask. Slowly rotate the flask while the methanol evaporates, collecting the concentrated extract in the flask.

Storage:

- Dry extract: When almost all the methanol was evaporated, the concentrated extract was collected in an airtight container.

Storage: The crude extract was stored at -20 or -80 °C for later use.

3.8.7 Analysis Interpretation of cobalt measurement from the *S. Oleracea* leaf extracts

Table 3.8.7.1: Analytical interpretation of cobalt measurement from the *S. Oleracea* leaf extracts by ICP-MS analyses.

Analysis Interpretation	
Instrument	Perkin Elmer NexION 350D ICP-MS
Analysis Technique	Calibrations were obtained using external calibration analysis (a series of standards of known trace element concentrations were prepared to form a linear for calibration)
Calibration standard	Dilutions from a 10ppm multi transition element standard (Merck Certipur)
Quality check	An external standard was diluted and measured from a custom bought QMx multi-element solution
Internal Standard	All blanks, standards, and samples were also spiked with 1ng/g Rh so that any general instrument drift could be normalized
Diluent	Dilutions were made using a 2% HNO_3 solution, prepared using in-house distilled nitric acid and 18.2 megohm (MΩ) deionized DI water
Data evaluation	All data results are reported as elemental concentrations.
ng/g	Nanograms trace element per gram of sample material

3.8.8. Immunoblotting

These were as described in Section 2.9.9.

3.8.9 Reverse transcription-quantitative polymerase chain reaction (RT-qPCR)

This was as described in Section 2.9.7

Table 3.8.9.1: List of primers used for RT-qPCR studies and their forward (FW)/reverse (RV) sequences

The primers used for RT-qPCR are given below.

HIF-1α	RV TAT CGA GGC TGT GTC GAC TG FW TCA AGT CAG CAA CGT GGA AG
VEGF	RV ACA GGA CGG CTT GAA GAT A

	FW TTA CTG CTG TAC CTC CAC
EPO	RV ACC CGA AGC AGT GAA GTG A FW AAT GGA GGT GGA AGA ACA GG
ß-Actin	RV CAT GGA TGC CAC AGG ATT CCA TAC FW TGC CCT AGA CTT CGA GCA AGA
CA9	RV GGC CAA AAA CCA GGG CTA GG FW CAG CTG AAC TTC CGA GCG AC

3.8.10 Cell viability assay

3.8.10.1 Treatment with 14 and the PHD inhibitor, Roxadustat: Cell viability assay in a 96-well plate

This was described in section 2.9.8.

3.9 References

1. Navarrete-Opazo, A., and G.S. Mitchell, *Therapeutic potential of intermittent hypoxia: a matter of dose. Am. J. Physiol. Regul. Integr. Comp. Physiol.*, 2014. **307(10)**: p. R1181–R1197. DOI: 10.1152/ajpregu.00208.2014

2. Damgaard, V., J. Mariegaard, J.M. Lindhardsen, H. Ehrenreich, and K.W. Miskowiak, *Neuroprotective Effects of Moderate Hypoxia: A Systematic Review. Brain Sci.*, 2023. **13(12)**: p. 1648. DOI: 10.3390/brainsci13121648

3. Lippi, G., M. Franchini, and G. Guidi, *Cobalt chloride administration in athletes: a new perspective in blood doping?* Br. J. Sports Med., 2005. 39(11): p. 872-873. DOI: 10.1136/bjsm.2005.019232

4. Skalny, A.V., et al., *Cobalt in athletes: hypoxia and doping-new crossroads.* J. Appl. Biomed., 2019. 17(1): p. 28-28. DOI: 10.32725/jab.2018.003

5. Nagle, D.G. and Y.-D. Zhou, *Natural product-derived small molecule activators of hypoxia-inducible factor-1 (HIF-1).* Curr. Pharm. Des., 2006. 12(21): p. 2673-2688. DOI: 10.2174/138161206777698783

6. Dalgard, C.L., et al., *Endogenous 2-oxoacids differentially regulate expression of oxygen sensors.* Biochem. J., 2004. 380(2): p. 419-424. DOI: 10.1042/BJ20031647

7. Cunliffe, C.J., et al., *Novel inhibitors of prolyl 4-hydroxylase. 3. Inhibition by the substrate analog N-oxaloglycine and its derivatives.* J. Med. Chem., 1992. 35(14): p. 2652-2658. DOI: 10.1021/jm00092a016

8. Al-Qahtani, K., et al., *The broad spectrum 2-oxoglutarate oxygenase inhibitor N-oxalylglycine is present in rhubarb and spinach leaves.* Phytochemistry, 2015. 117: p. 456-461. DOI: 10.1016/j.phytochem.2015.06.028

9. Bowie, E. and P. Hurley, *Cobalt chloride in the treatment of refractory anaemia in patients undergoing long-term haemodialysis.* Aust N Z J Med., 1975. 5(4): p. 306-313. DOI: 10.1111/j.1445-5994.1975.tb03263.x

10. Manifold, I., M. Platts, and A. Kennedy, *Cobalt cardiomyopathy in a patient on maintenance haemodialysis.* Br. Med. J., 1978. 2(6152): p. 1609. DOI: 10.1136/bmj.2.6152.1609

11. Maxwell, P.H., et al., *The tumour suppressor protein VHL targets hypoxia-inducible factors for oxygen-dependent proteolysis.* Nature, 1999. 399(6733): p. 271-275. DOI: 10.1038/20459

12. Fraisl, P., J. Aragonés, and P. Carmeliet, *Inhibition of oxygen sensors as a therapeutic strategy for ischaemic and inflammatory disease.* Nat. Rev. Drug Discov. 2009. 8(2): p. 139-152. DOI: 10.1038/nrd2761

13. Yuan, Y., et al., *Cobalt inhibits the interaction between hypoxia-inducible factor-α and von Hippel-Lindau protein by direct binding to hypoxia-inducible factor-α.* J. Biol. Chem., 2003. 278(18): p. 15911-15916. DOI: 10.1074/jbc.M300463200

14. Matsuura, H., et al., *Inhibition of prolyl hydroxylase domain-containing protein downregulates vascular angiotensin II type 1 receptor.* Hypertension, 2011. 58(3): p. 386-393. DOI: 10.1161/HYPERTENSIONAHA.110.167106

15. Palit, S., A. Sharma, and G. Talukder, *Effects of cobalt on plants.* Bot. Rev. , 1994. 60: p. 149-181.

16. Saulea, M., et al., *Determination of cobalt in food samples.* Revista de Chimie, 2004. 55(5): p. 301-303.

17. Ivan, M., et al., *HIFα targeted for VHL-mediated destruction by proline hydroxylation: implications for O2 sensing.* Science, 2001. 292(5516): p. 464-468. DOI: 10.1126/science.1059817

18. Yu, F., et al., *HIF-1α binding to VHL is regulated by stimulus-sensitive proline hydroxylation.* Proc. Natl. Acad. Sci., 2001. 98(17): p. 9630-9635. DOI: 10.1073/pnas.181341498

19. Gorres, K.L., et al., *Conformational preferences of substrates for human prolyl 4-hydroxylase.* Biochemistry, 2008. 47(36): p. 9447-9455. DOI: 10.1021/bi8009373

20. Li, K., Y. Zheng, and X. Wang, *The potential relationship between HIF-1α and amino acid metabolism after hypoxic ischemia and dual effects on neurons.* Front. Neurosci. 2021. 15: p. 676553. DOI: 10.3389/fnins.2021.676553

21. Kwon, H.S., et al., *Inhibition of a prolyl hydroxylase domain (PHD) by substrate analog peptides.* Bioorg Med Chem Lett., 2011. 21(14): p. 4325-4328. DOI: 10.1016/j.bmcl.2011.05.050

22. Ma, X., et al., *Effect of proline analogues on activity of human prolyl hydroxylase and the regulation of HIF signal transduction pathway.* PLoS One, 2014. 9(4): p. e95692. DOI: 10.1371/journal.pone.0095692

23. Ahn, D.-R., et al., *HIF-1α Peptide Derivatives with modifications at the hydroxyproline residue as activators of HIF-1α.* Bioorg Med Chem Lett , 2009. 19(15): p. 4403-4405. DOI: 10.1016/j.bmcl.2009.05.083

24. Tegley, C.M., et al., *Discovery of novel hydroxy-thiazoles as HIF-α prolyl hydroxylase inhibitors: SAR, synthesis, and modeling evaluation.* Bioorg Med Chem Lett. , 2008. 18(14): p. 3925-3928. DOI: 10.1016/j.bmcl.2008.06.031

25. Williams, G., et al., *Formation and stability of the enolates of N-protonated proline methyl ester and proline zwitterion in aqueous solution: A nonenzymatic model for the first step in the racemization of proline catalyzed by proline racemase.* Biochemistry, 2003. 42(27): p. 8354-8361. DOI: 10.1021/bi0345992

26. Zhai, R., et al., *Evidence for conversion of methanol to formaldehyde in nonhuman primate brain.* Anal. Cell. Pathol. , 2016. 2016(1): p. 4598454. DOI: 10.1155/2016/4598454

27. Dorokhov, Y.L., et al., *Metabolic methanol: molecular pathways and physiological roles.* Physiological reviews, 2015. 95(2): p. 603-644. DOI: 10.1152/physrev.00034.2014

28. Weng, C., X. Peng, and Y. Han, *From methane to value-added bioproducts: microbial metabolism, enzymes, and metabolic engineering*, in *Advances in Applied Microbiology*. 2023, Elsevier. p. 119-146. DOI: 10.1016/bs.aambs.2023.07.004

29. Patterson, J.A., et al., *Thioproline formation as a driver of formaldehyde toxicity in Escherichia coli.* Biochem. J. , 2020. 477(9): p. 1745-1757.

30. Pietzke, M., J. Meiser, and A. Vazquez, *Formate metabolism in health and disease. Mol. Metab.*, 2020. **33**: p. 23–37. DOI: 10.1016/j.molmet.2019.05.012

31. Miller-Pinsler, L., A. Sharma, and P.G. Wells, *Enhanced NADPH oxidases and reactive oxygen species in the mechanism of methanol-initiated protein oxidation and embryopathies in vivo and in embryo culture. Arch. Toxicol.*, 2016. **90**: p. 717–730. DOI: 10.1007/s00204-015-1482-0

32. Morris, N.L., and S.M. Yeligar, *Role of HIF-1α in Alcohol-Mediated Multiple Organ Dysfunction. Biomolecules*, 2018. **8(4)**: p. 170. DOI: 10.3390/biom8040170

33. Jung, S.N., W.K. Yang, J. Kim, H.S. Kim, E.J. Kim, H. Yun, H. Park, S.S. Kim, W. Choe, I. Kang, and J. Ha, *Reactive oxygen species stabilize hypoxia-inducible factor-1 alpha protein and stimulate transcriptional activity via AMP-activated protein kinase in*

DU145 human prostate cancer cells. Carcinogenesis, 2008. **29(4)**: p. 713–721. DOI: 10.1093/carcin/bgn032

34. Cory, A.H., et al., *Use of an aqueous soluble tetrazolium/formazan assay for cell growth assays in culture.* Cancer Commun., 1991. 3(7): p. 207-212. DOI: 10.3727/095535491820873191

35. Malich, G., B. Markovic, and C. Winder, *The sensitivity and specificity of the MTS tetrazolium assay for detecting the in vitro cytotoxicity of 20 chemicals using human cell lines.* Toxicology, 1997. 124(3): p. 179-192. DOI: 10.1016/s0300-483x(97)00151-0

36. Phang, J.M., et al., *Proline metabolism and cancer: emerging links to glutamine and collagen.* Curr Opin Clin Nutr Metab Care, 2015. 18(1): p. 71-77. DOI: 10.1097/MCO.0000000000000121

Chapter 4

Identification of a Novel Small Molecule as a PHD enhancer

4.1.1 Introduction

In the presence of sufficient O_2 (normoxia), the PHDs catalyse hydroxylation of HIF-α at specific proline residues in the oxygen-dependent degradation domains (ODDs) of HIF- α isoforms, i.e., Pro-402 and Pro-564 in human HIF-1α [1-4]. The prolyl hydroxylated HIF-α proteins are recognized by the von Hippel–Lindau protein (pVHL), which is part of an E3 ubiquitin ligase complex, that promotes HIF-α degradation by proteasomes [1-4]. Under hypoxia, PHD activity on HIF-α and proteasomal degradation of HIF-α is slowed [5]. The levels of HIF-α consequently rise and it forms a heterodimeric complex with HIF-β which binds to hypoxia-responsive elements (HREs) and transcriptionally activates genes that work to ameliorate the effects of hypoxia [6]. Cell-based studies show the potential for hundreds of genes to be transcriptionally activated by HIF [7]. In addition to its role in the normal hypoxic response, enhancement of PHD activity or suppression of HIF-α may be beneficial to treat pathologies such as cancer (**Figure 4.1.1**).

Tumours can rapidly divide into entities that require an increased vascular supply compared to healthy tissues. However, tumour growth frequently surpasses the expansion rate of the vasculature, leading to a deficiency in the supply of nutrients and oxygen to the interior of the tumour area. Compared to normal cells, tumour cells can require an additional vascular supply [9, 10]. To address this need, tumour cells can promote blood vessel formation; however, this is often in the form of immature and irregular conformations of blood vessels within the tumour [6] [11]. This explains why solid tumours often have acute or chronic hypoxic regions [12, 13].

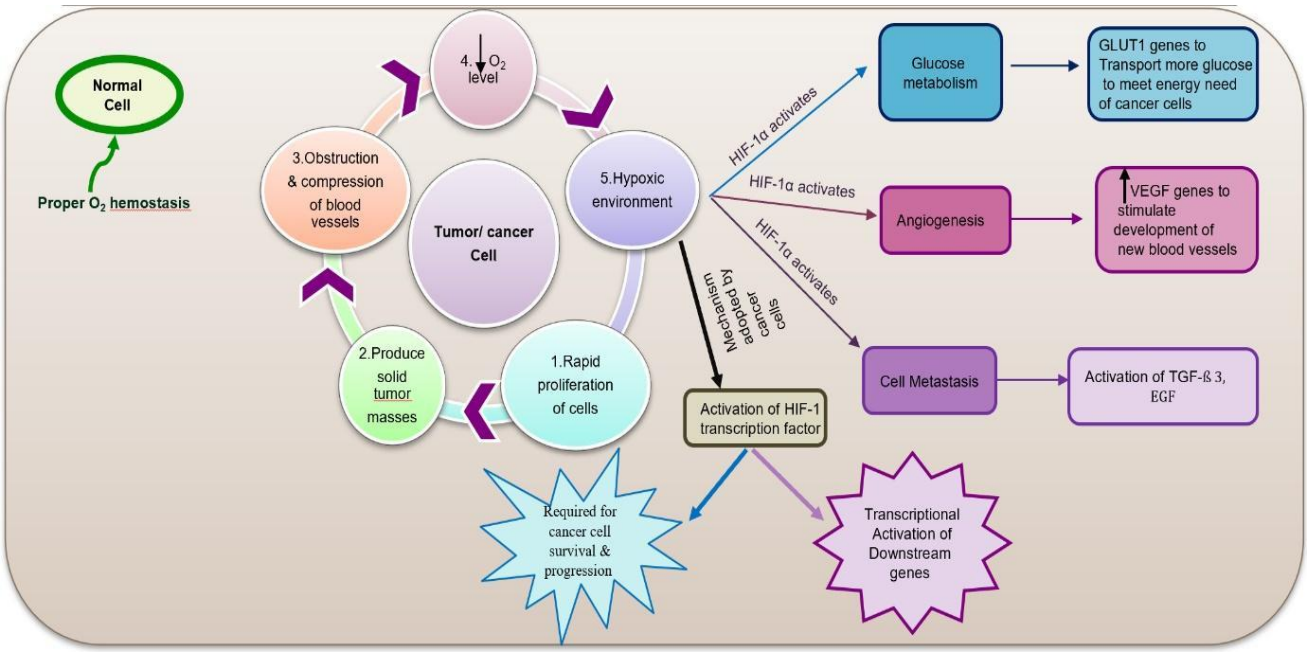


Figure 4.1.1: Summary of potential roles of the HIF system in cancer.[8]

In cancer pathology, there is evidence that HIF mediates the promotion of transcription of genes related to angiogenesis, proliferation, advanced disease stage, tumour progression and metastasis, treatment resistance, and poor diagnosis [14-16]. Following the pioneering work of HIF-α suppression for the treatment of kidney cancer by modulation of HIF-2α activity, ongoing studies are further investigating both the inhibition and promotion of HIF activity for anticancer drug discovery [17]. Both enhancing and inhibiting PHD activity are of interest, depending on the type of cancer. [8, 18].

Expression profiling of PHD isoforms in different cancer types has shown that PHD2 and PHD3 are relatively over-expressed in tumours of the lung, liver, and kidney [9, 19]. Among the human PHD isoforms (PHD 1-3), PHD2 has been most extensively studied [20]. Expression of

the PHD1 and PHD3 genes seems to be more limited than that of PHD2 [21].

Studies by Bordoli et al., using a hormone-dependent breast cancer mouse model (MCF7), and by Wottawa et al., using an invasive model of triple-negative breast cancers (TNBC) cell lines such as MDA-MB-231 cells, have shown that downregulation of PHD2 can delay tumour growth [9, 19, 22, 23]. Breast cancer stem cells (BCSCs) can develop secondary tumours, chemotherapy resistance, and recurrence after chemotherapy [24, 25]. Using TNBC cell lines such as MDA-MB-231, SUM-149, and SUM-159, Samanta et al. have shown that chemotherapy resistance occurs in a manner that is HIF activity-dependent, i.e. HIF is involved in multidrug resistance in cancer [25-27]. Samanta et al. suggested that combining a chemotherapeutic drug with a HIF inhibitor may help to overcome BCSC drug resistance [26]. The studies in this chapter describe work on a small molecule enhancer of PHD catalysis **(7)** and an in-vitro investigation of **7** on kidney, brain, and TNBC cell lines.

4.2 Prolyl hydroxylases (PHDs) and Hypoxia Inducible Factor (HIF): a potential target for cancer treatment

Several HIF inhibitors have been investigated for the treatment of cancer [28]. Direct HIF inhibitors and indirect HIF inhibitors are the two major categories of HIF inhibitors [28]. As the name suggests the 'direct inhibitors' act on HIF expression or function and 'indirect HIF inhibitors' exhibit action by regulating the upstream or downstream HIF pathways [29].

Several studies on HIF inhibitors have uncovered the close connection between HIF and tumour development, angiogenesis, and metastasis. Multiple HIF inhibitors including steroids and peptides have been developed; interestingly, some natural product derivatives that act

as HIF inhibitors are also reported [30].

4.2.2.HIF-2α inhibitor in the treatment of kidney cancer

VHL disease is a rare inherited condition that increases the risk of developing various tumours (cancerous and noncancerous), including kidney cancer (renal cell carcinoma) [2, 31]. Treatment for kidney cancer related to VHL disease typically requires repeated surgical intervention. Surgical options range from partial nephrectomy (for localized renal tumours) to radical nephrectomy (for larger or advanced renal tumours) [32]. Apart from that, targeted treatments such as mTOR inhibitors (everolimus, temsirolimus) [33] and VEGF Inhibitors (sunitinib, pazopanib) are used to inhibit tumour growth [34].

Belzutifan is an alternative to surgery that was approved by the FDA (in 2021) for the treatment of VHL patients with renal cell carcinoma, central nervous system hemangioblastomas (a type of noncancerous tumour), and pancreatic neuroendocrine tumours [35]. HIF-2α proteins can accumulate in VHL disease patient's cells, with consequent upregulation of numerous HIF-2α target genes which influence pathogenesis and promote tumour growth [37]. Belzutifan is a HIF-2α inhibitor [36].

4.2.3 Potential enzyme enhancers

A limited number of clinically used small molecule enzyme activity enhancers (the opposite of enzyme inhibitors) are available. They mainly bind to enzymes and increase their activity, however, only a few are well characterized [38, 39] KRH102053, KRH102140, and BBAP-1 are reported to be cell-active small molecule enhancers of PHD that decrease HIF-1α in cells [40-42]. However, their mechanisms of action are not well understood.

4.3 Discovery and development of the novel PHD enhancer **7**

The small molecule **7** was unexpectedly discovered to enhance PHD2 activity during SAR studies carried out on the 4-hydroxypyrimidine series of PHD inhibitors prepared by Dr. James Holt-Martyn. During the SAR studies a potential PHD inhibitor **8** was investigated where the hydroxyl group of **8** was replaced with a dimethyl amino group. Instead of inhibiting PHD2, **7** was observed to enhance PHD2 catalysed HIF-1α CODD prolyl hydroxylation (61%) compared to the DMSO control (**Figure 4.3.1 & Figure 4.3.2**) [43].

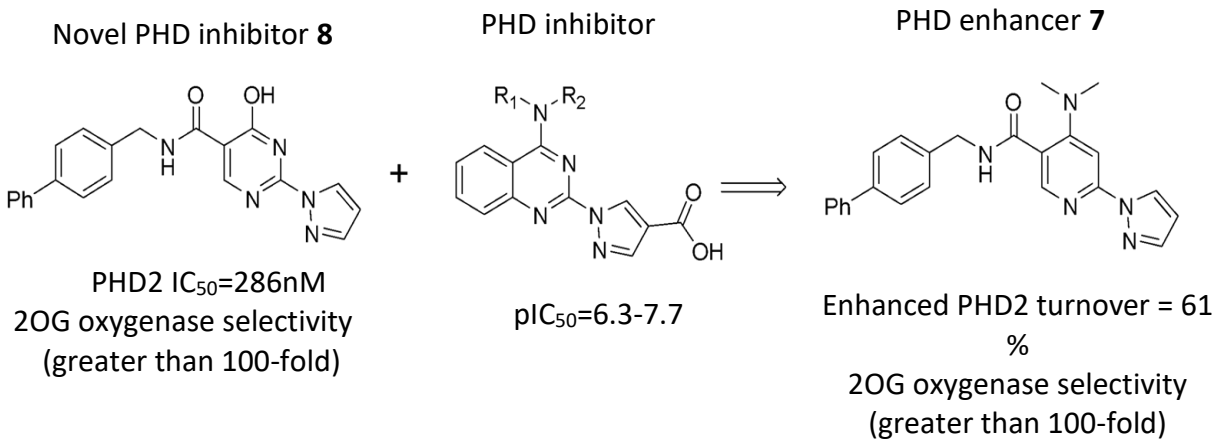


Figure 4.3.1: Discovery of enhancer 7. During SAR studies on the 4-hydroxypyrimidine series of PHD inhibitors, the hydroxyl group of **8** was substituted with a dimethyl amino group to give **7**. Instead of inhibiting PHD2, **7** increased the extent of HIF-1α CODD hydroxylation [43].

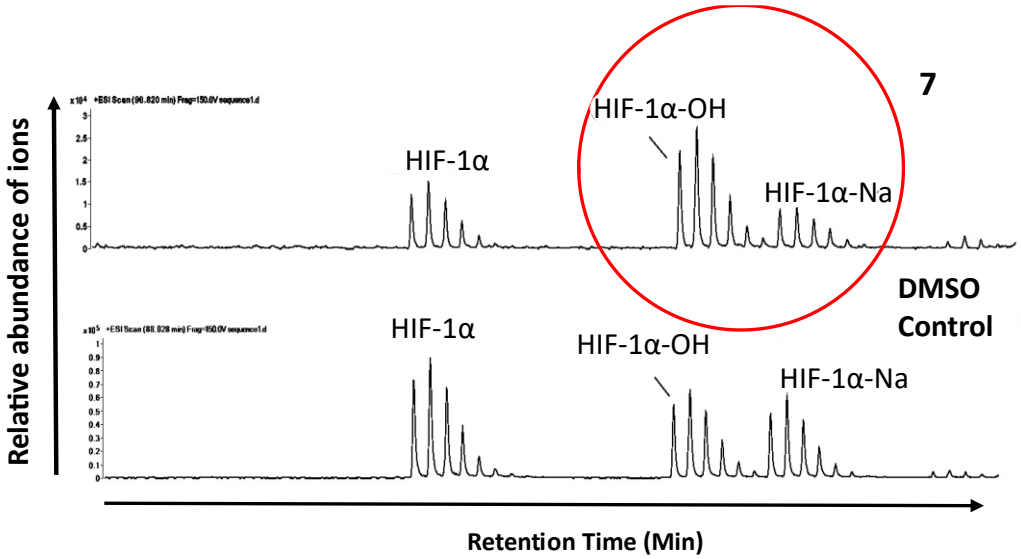


Figure 4.3.2: RapidFire MS spectra of PHD2 assay results showing hydroxylated HIF-1α CODD substrate and no hydroxylated CODD product in the (A) presence and (B) absence of 7. (A) Incubation with **7**: The ratio of HIF-1α: HIF-1α-OH is 1: 1.67.(B) Incubation with DMSO (control): the ratio of HIF-1α: HIF-1α-OH is 1: 0.86. Note (A) & (B) Shows a peak corresponding to the sodium adduct of HIF-1α CODD; the sodium adducts were not considered for the turnover calculations. [43]

7 showed an increase in hydroxylation of HIF-1α CODD compared to the control (DMSO) in the presence of PHD2 **(Figure 4.3.2)**. Repeat experiments were conducted with different batches of PHD2 and substrate, **7** reproducibly caused increased levels of HIF-1a CODD hydroxylation. The repeat assays consistently showed a 60% level of HIF-1α CODD turnover giving hydroxylated HIF-1α CODD compared to the control [43].

4.4 Cellular investigations of the PHD enhancer **7**

4.4.1 Hypoxia and hydroxylation of HIF-1α

The next step was to investigate the effect of **7** on HIF-1α in a cellular environment. Because the purpose of the experiments was to investigate the degradation of HIF-1α in the presence of **7**, the experiments could not be conducted in normoxic conditions as under normoxia HIF-1α is efficiently degraded. Cellular investigations were therefore conducted in a hypoxia chamber (1% O_2). The hypoxic environment was created by using the 'Whitley H35 Hypoxystation'. **Figure 4.4.1.1** shows the workflow of the hypoxia experiment and sample processing for immunoblotting experiments.

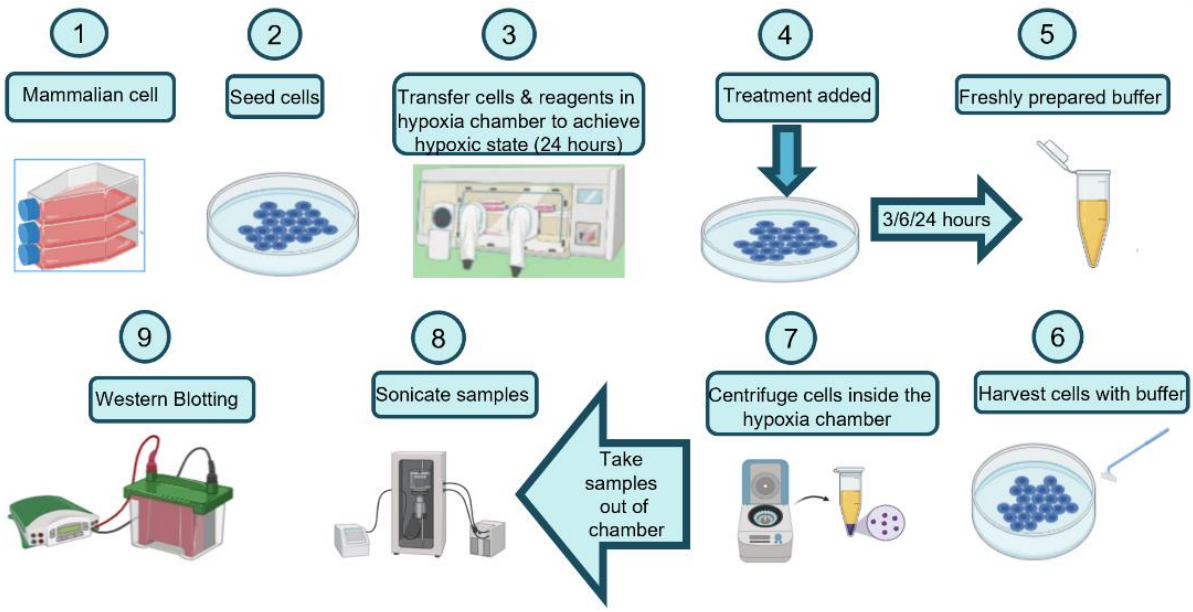


Figure 4.4.1.1: Workflow for hypoxia experiments on 7. All the hypoxia experiments were conducted inside a "Whitley H35 Hypoxystation" (steps 1-7). Steps 8-9 (outside the hypoxia station) show how the hypoxic samples were prepared for immunoblotting experiments.

HEK 293T cells were first seeded into a 6 cm petri dish, then transferred inside the "Whitley H35 Hypoxystation" and kept for 24 hours, to ensure that the mammalian cells were in a hypoxic state. As described in **Figure 4.4.1.1**, steps 3 to 7 (centrifugation) were conducted inside the hypoxia station. During each hypoxia experiment, all the relevant reagents needed for centrifuging and harvesting cells were also kept inside the hypoxia station.

4.4.2 Mammalian cells accumulate HIF-1α in a hypoxic environment

Initially, the time required for mammalian cells (HEK 293T cell) to reach a hypoxic state and stabilize HIF-1α under a hypoxic environment was investigated. Therefore, cells in hypoxia environment without any treatment and DMSO in hypoxic environment were evaluated first. Application of hypoxia (1% O_2) was observed to cause accumulation of HIF-1α in HEK 293T cells over 24 hours **(Figure 4.4.2.1 & Figure A. 7.7).** For control, <1% (v/v) of dimethyl sulfoxide (DMSO) (which is a widely used solvent for small molecules such as **7**) [46] was used in the hypoxia chamber. Note that in hypoxia it was observed that DMSO apparently promotes degradation of HIF-1α **(Figure 4.4.2.1 & Figure A. 7.7)**, as has been observed previously [43,47].

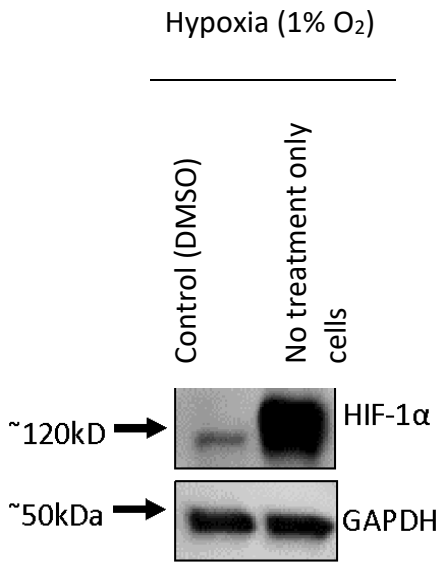


Figure 4.4.2.1: Hypoxia (1% O_2) leads to stabilization of HIF-1α protein in HEK 293T. Immunoblot image showing that under hypoxia (1% O_2) 24 hours, HEK 293T cells accumulate HIF-1α, note that DMSO also shows increases in HIF-1α level.

Figure 4.4.2.2 shows the accumulation of HIF-1α in HEK 293T cells under hypoxic conditions (1% O_2). DMSO was not observed to cause HIF-1α accumulation under normoxic conditions.

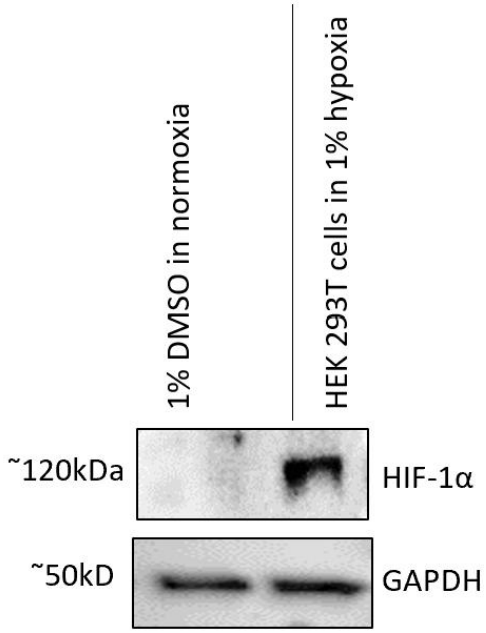


Figure 4.4.2.2: Hypoxia (1% O_2) leads to stabilization of HIF-1α protein in HEK 293T cells.

Immunoblot image showing that under hypoxic conditions (1% O_2) for 24 hours, HEK 293T cells accumulate HIF-1α. In normoxia no signal for HIF-1α is observed in the presence of DMSO.

4.4.3 Effects of PHD enhancer **7** in a 1% O_2 environment in HEK 293T cells

To explore whether the interaction of **7** with PHD2 is responsible for HIF-1α destabilization, the effects of **7** on HIF-1α were then tested in the HEK 293T cell line.In this study, the level of PHD2 was investigated primarily because of its central role in oxygen homeostasis and the availability of appropriate antibodies. PHD2 is the most important of the three human PHDs in regulating HIF-α stability under normoxic conditions[48]. Moreover, the distributions of PHD1 and PHD3 are more tissue-specific than that of PHD2 [49]. **Figure 4.4.3.1 A** shows that 100 µM of **7** was able to decrease HIF-1α levels under 1% O_2 when incubated for 24 hours in HEK 293T cells. PHD2 protein levels were observed to substantially increase in the presence of **7** (100 µM) and in hypoxic conditions (no treatment controls) in comparison to DMSO (**Figure 4.4.3.1 A)**. Quantification of the western blots was performed using 'Image J software'. Quantification analysis showed that, compared to the control, **7** (100 µM) significantly destabilize HIF-1α levels and hypoxic cells (1% O_2) without any treatment showed a significant accumulation of HIF-1α levels compared to the control (**Figure 4.4.3.1 B**).**Figure 4.4.3.1 C** shows evidence for increased PHD2 protein level after following treatment. Whether this is due to increased PHD2 production, PHD2 stabilization, a mixture of these, or some other factor is not known.

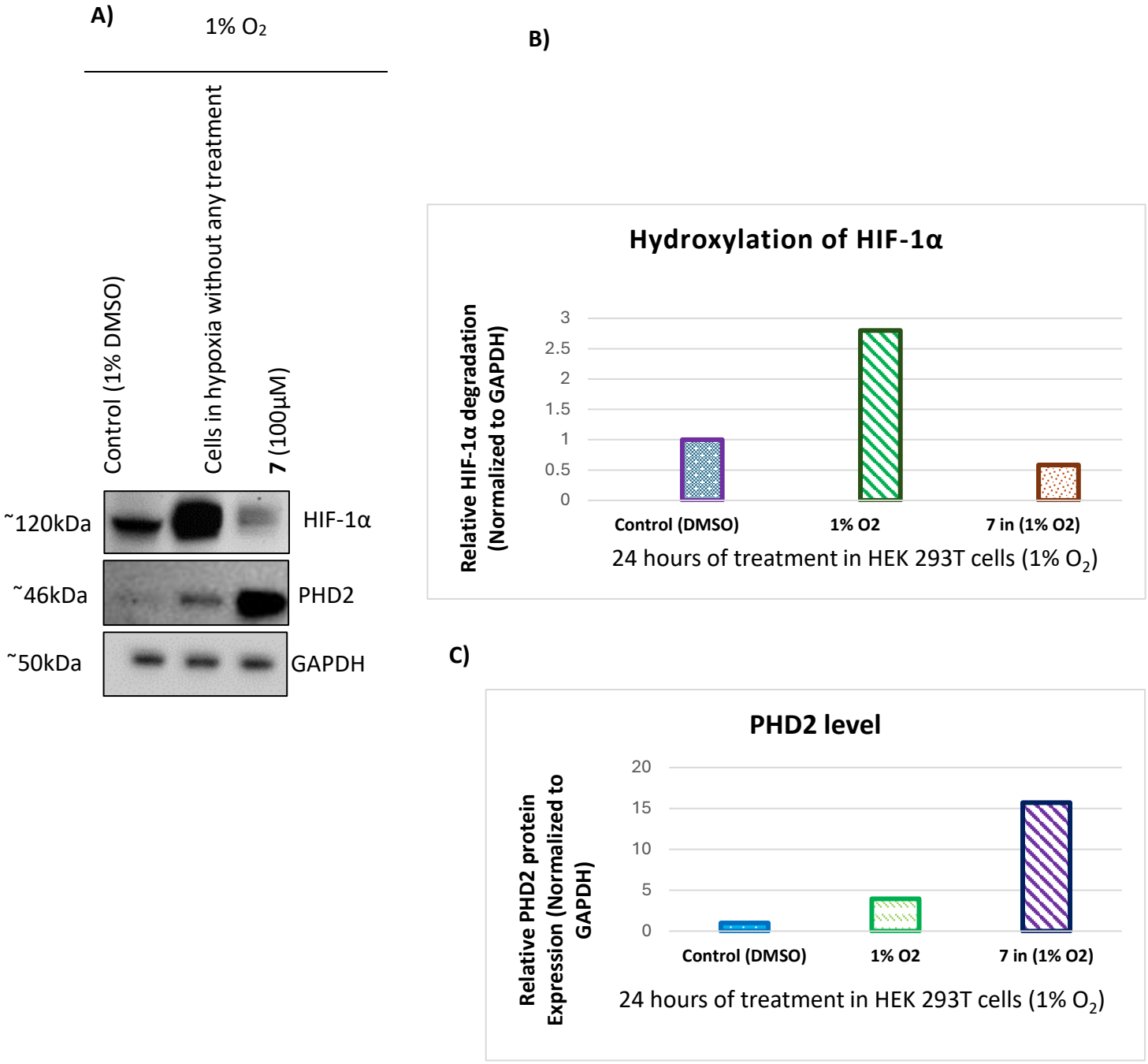


Figure 4.4.3.1: Inhibition of HIF-1α by 7 at 1% O_2. (A) Immunoblotting image showing degradation of HIF-1α in HEK 293T cells treated with 100 µM of **7** for 24 hours at 1% O_2.Control (1% DMSO) and cells without any treatment only in hypoxic enviroment (1% O_2) caused HIF-1α stabilization. (B) Quantification of HIF-1α degradation after 24-hour treatment with **7** using 'Image J software'. (C) Quantification of PHD2 enzyme expression after 24-hour treatment with **7** using 'Image J software'.

The goal of conducting cellular investigation of the PHD enzyme enhancer **7** was to obtain preliminary evidence for whether it can destabilize HIF-1α through enhanced PHD activity. The results from the western blot analysis showed a dose-dependent decrease in HIF-1α protein levels, suggesting that **7** may promote HIF-1α degradation. PHD2 protein levels were investigated to investigate a possible mechanism for enhancement involving upregulation of PHD2 production or stabilization of PHD2. Western blot analysis showed the presence of increased PHD2 protein levels in the presence of **7**, which can support the statement that **7** destabilize HIF-1α through enhanced PHD activity, which may be due to increased PHD2 production or stabilization of PHD2.

4.4.3.1 Different concentrations of the PHD enhancer **7** in a hypoxic environment

7 was then added to HEK293T cells at various concentrations (100,50 & 20 µM) at 1% O_2 to investigate whether the HIF-1α inhibition effects occur in hypoxia. The results showed that **7** was able to decrease HIF-1α levels at 20, 50, and 100 µM concentrations (**Figure 4.4.3.1.1 A & Figure A.7.8**). Quantification analysis showed that, compared to the control, **7** (20, 50, and 100 µM) significantly destabilized HIF-1α levels and hypoxic cells (1% O_2) without any treatment showed a significant accumulation of HIF-1α levels compared to the control (**Figure 4.4.1.1 B & Figure A. 7.8**). **Figure 4.4.3.1.1 C & Figure A.7.8** shows presence of PHD2 protein level during treatment. However, there was no clear evidence for increased PHD2 levels due to treatment with **7** under these conditions, though this cannot be ruled out.

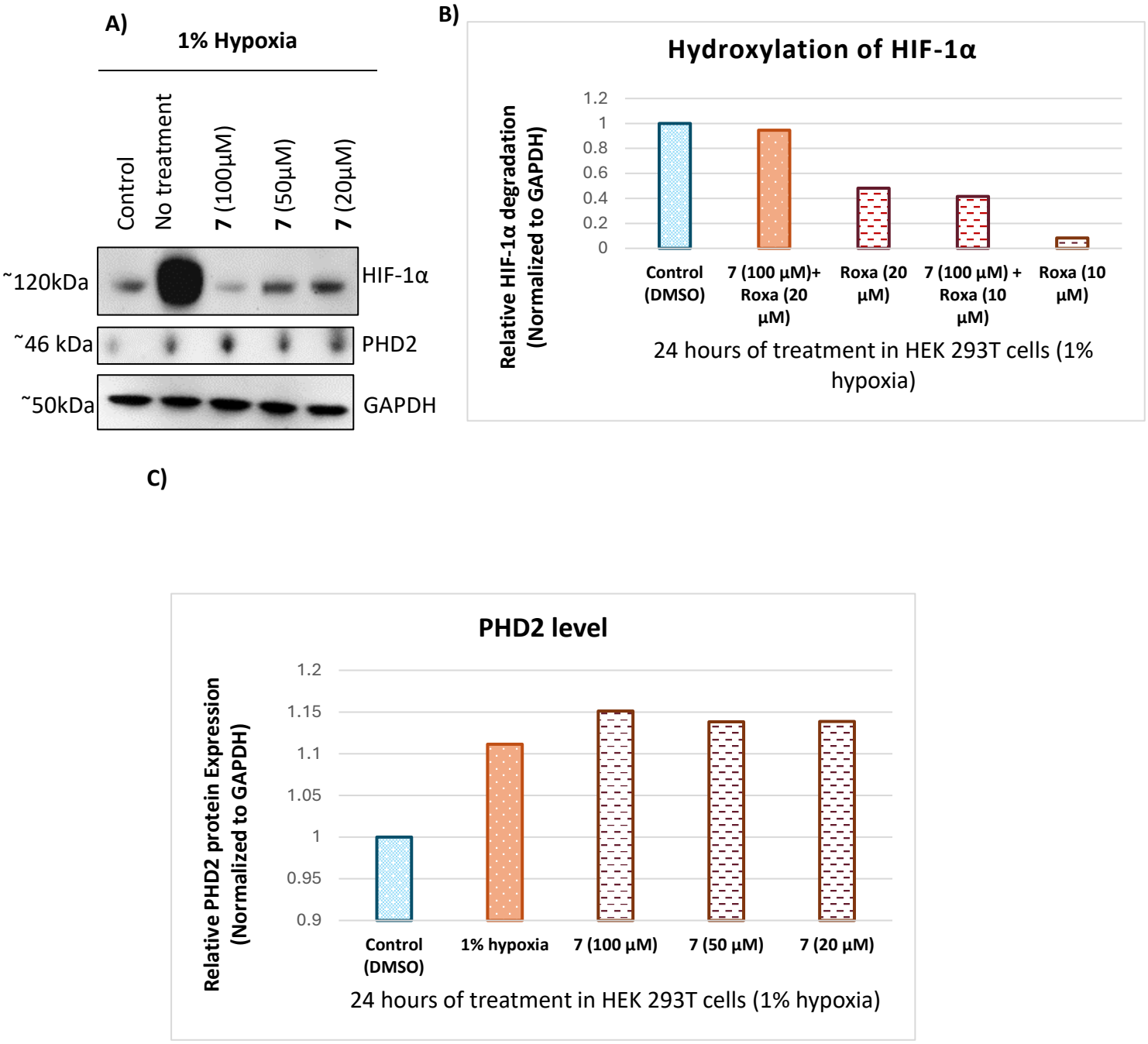


Figure 4.4.3.1.1: Effects of 7 on HIF-1α in 1% O_2. (A) Immunoblotting image showing evidence for degradation of HIF-1α in HEK 293T treated with 100, 50 and 20 µM of **7** for 24 hours at 1% O_2. Control (1% DMSO) and cells with no treatment showed high HIF-1α levels. (B) Quantification of HIF-1α degradation after 24 hours treatment of **7** using 'Image J software'. (C) Quantification of PHD2 enzyme expression after 24-hour treatment with **7** using 'Image J software'.

4.4.4 Studies on the PHD enhancer **7** in combination with the PHD inhibitor Roxadustat (**1**)

The effects of **7** and PHD inhibitors were then investigated under normoxic conditions in HEK 293T cells. **7** is a PHD enhancer, to test its HIF destabilizing capacity, the experimental condition should be hypoxic where HIF gets to stabilize naturally. Vice versa in normoxic condition HIF degrades naturally because PHD is active due to presence of O_2. Hence, in normoxia, HIF degradation is due to PHD activation or due to **7** will be questionable. Therefore during the normoxic experiments,**7** was tested in the presence of PHD inhibitor Roxadustat (**1**). Similar to the hypoxic experiments, treatment with **7** (100 µM) was able to downregulate HIF-1α levels in the presence of **1** (10 µM) (**Figure 4.4.4.1 A**) after 24 hours of treatment. Quantification analysis showed that, compared to the control, in 1% O_2, 100 µM of **7** in presence of **1** (10 µM) significantly reduced HIF-1α levels compared to the control (**Figure 4.4.4.1 B**). **Figure 4.4.4.1 C** shows presence of PHD2 protein during treatment. PHD2 levels were increased, in particular with the combination of 7 and Roxadustat.

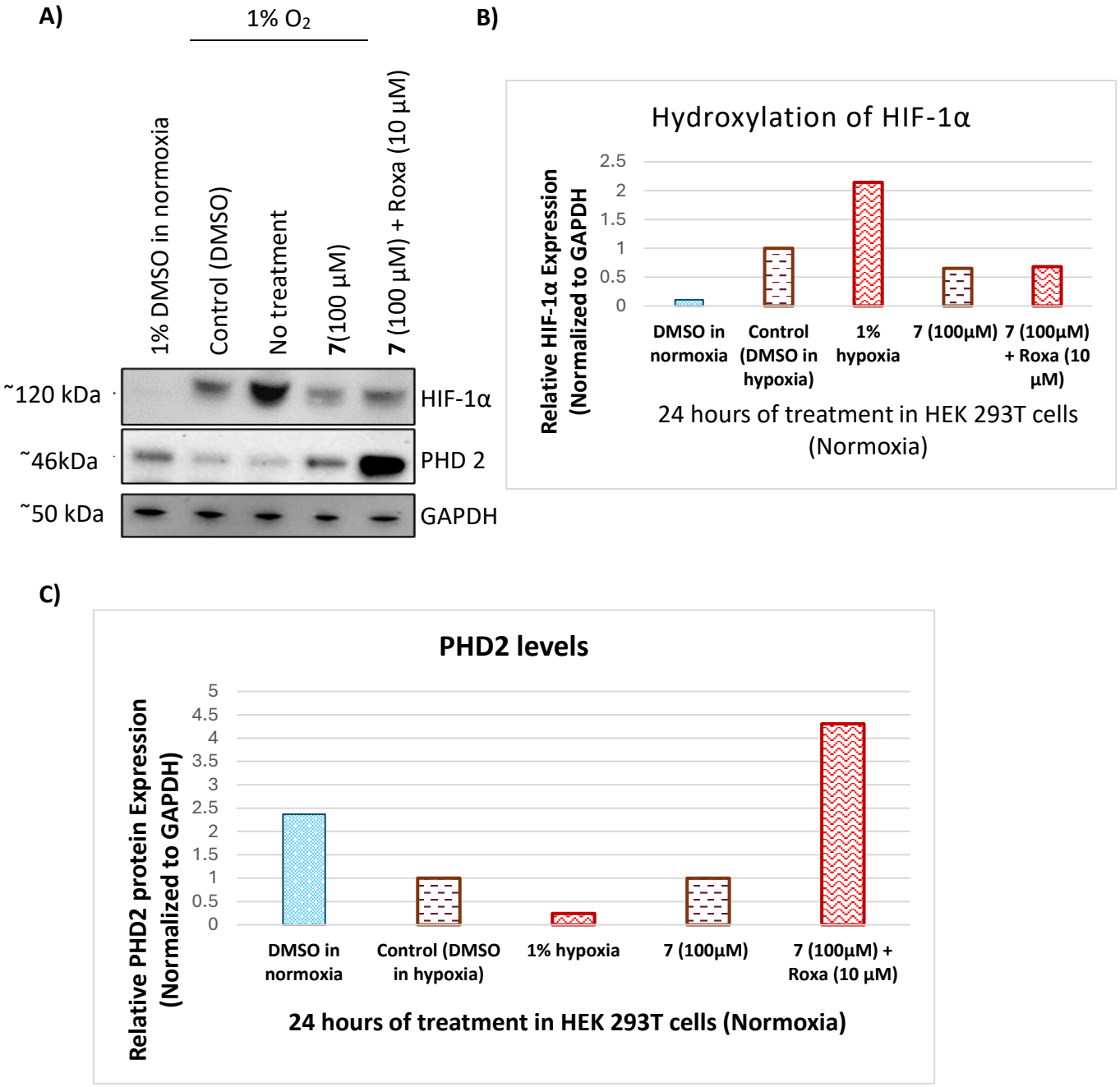
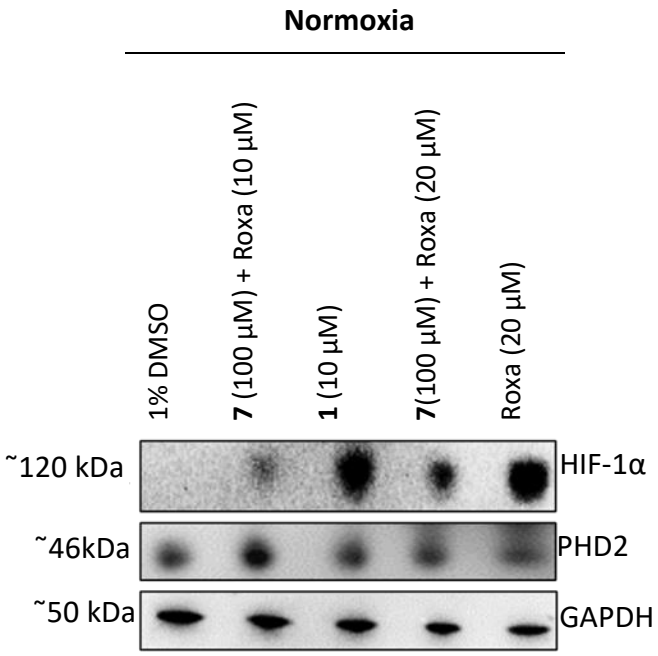


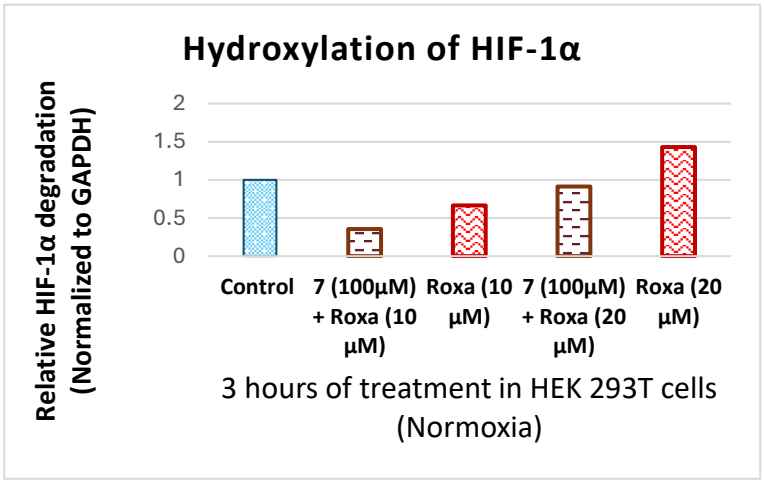
Figure 4.4.4.1: Effects on HIF-α by 7 in the presence of Roxadustat in HEK 293T cell line. (A) Immunoblots showing HIF-1α inhibition in HEK 293T cells when incubated for 24 hours with **7** (100µM) in the presence of Roxadustat (10 µM) in normoxia. DMSO under hypoxia and cells with no treatment caused HIF-1α stability. (B) Quantification of HIF-1α degradation after 24 hours treatment of **7** using 'Image J software'. (C) Quantification of PHD2 enzyme expression after 24-hour treatment with **7** in presence of Roxadustat using 'Image J software'.

7 was next evaluated in presence of higher concentration of **1** (20 µM) with two different incubation times (3 and 6 hours) under normoxia. Under all these conditions **7** in presence of **1** (10 µM) and **7** in presence of **1** (20 µM) were observed to cause HIF-1α degradation compared to **1** (10 µM) and **1** (20 µM) respectively (**Figure 4.4.4.2 A & D**). However, at 20 µM **7** showed evidence for only weak degradation of HIF-1α levels compared to the control.

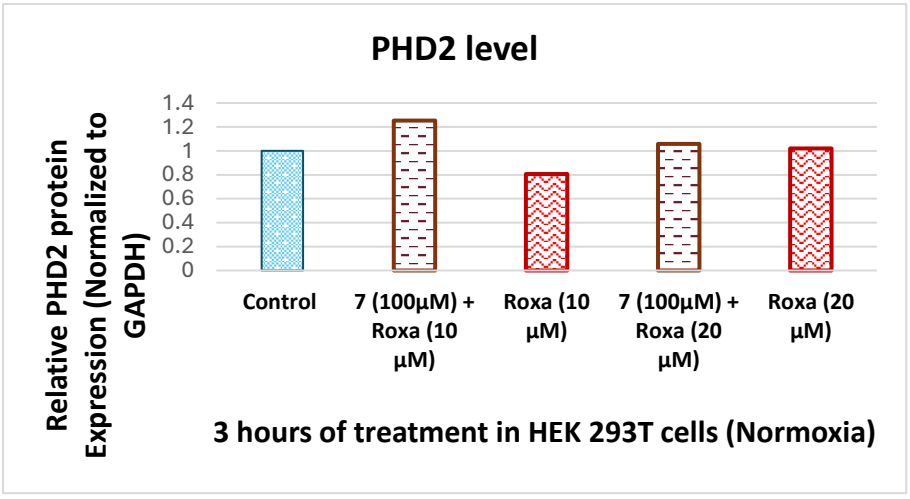
A)



B)



C)



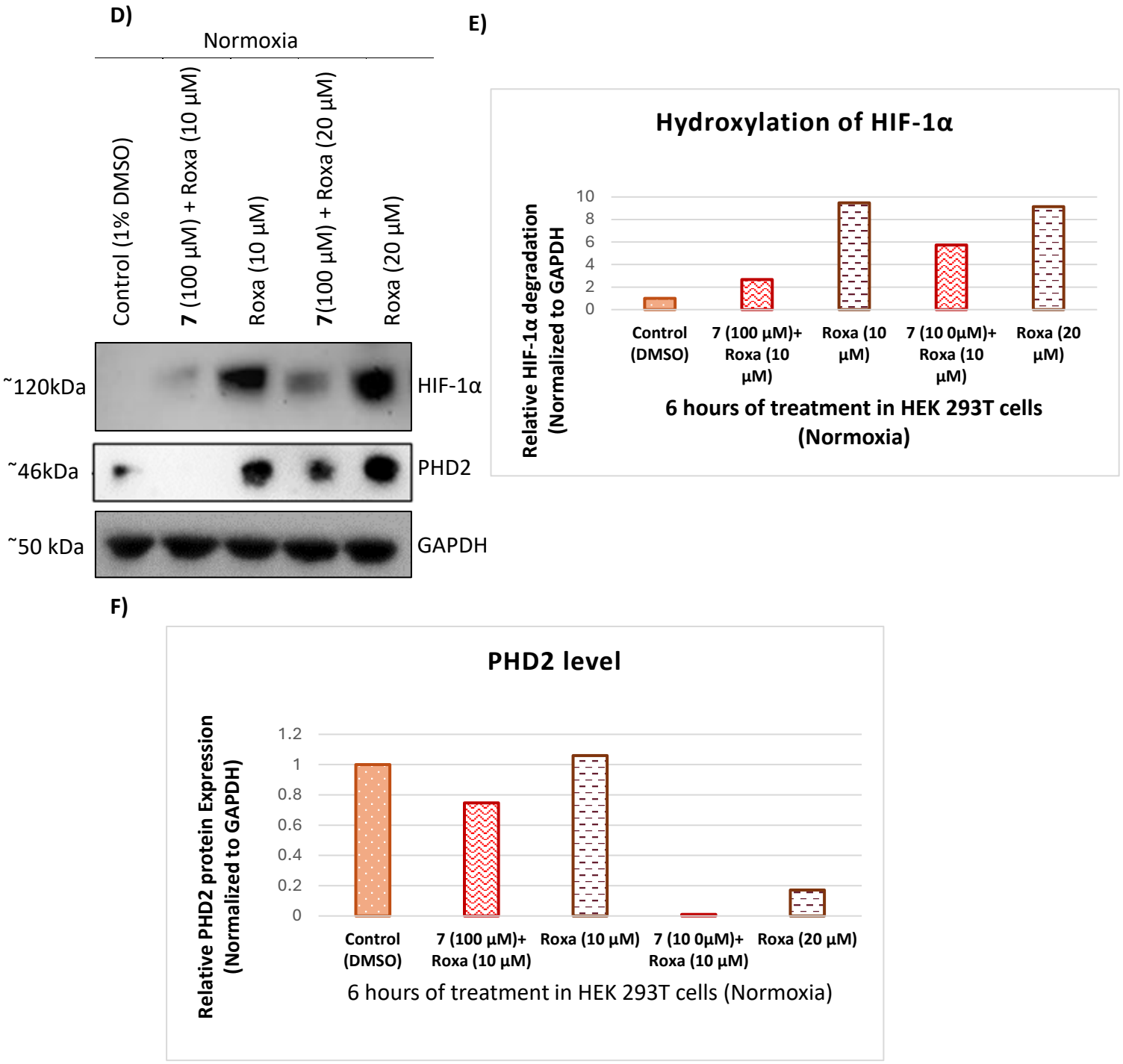


Figure 4.4.4.2: Effects on HIF-α by 7 in the presence of Roxadustat (1), in HEK 293T cell line with different incubation times. (A & E) Immunoblots showing HIF-1α inhibition in HEK 293T cells when incubated for 3& 6 hours with 7(100µM) in the presence of **1** (10 & 20 µM) in

normoxia. **(B & E)** Quantification of HIF-1α degradation after 3& 6 hours treatment with **7** (100 µM) in the presence of Roxadustat (**1)** (10 & 20 µM) using 'Image J software'. (**C &F**) Quantification of PHD2 enzyme expression after 3& 6 hours treatment with **7** using 'Image J software.

Quantification analysis showed that, compared to the control, **7** (100 µM) in presence of Roxadustat (**1)** (10 & 20 µM) significantly destabilize HIF-1α levels (**Figure 4.4.4.2 B & E**). **Figure 4.4.3.1 C & F** shows presence of PHD2 protein level during treatment.

4.4.5 Effect of the PHD enhancer **7** on a 2-OG depleted cell line

To further evaluate the HIF-1α reducing capacity of **7**, it was tested on a cellular system altered with respect to 2-OG metabolism [46]. LN-18 cells, which is a glioma cell line showed presence of an IDH-1 mutation [46,47,50]. This IDH-1 mutation may cause a reduction in 2OG levels, which is the reason for the enzyme to produce 2-hydroxyglutarate (2HG) instead and efficiently depletes the 2OG level within the cell[46-48]. Hvinden et al. showed that in IDH-1 mutants the level of 2-OG is reduced [46]. 2-OG is essential for prolyl hydroxylases (PHD) which promote HIF-1α degradation.

The effects of **7** on HIF-1α levels were thus evaluated in 2-OG depleted human brain glioblastoma cells (LN-18) under normoxia in the presence of **1**. Due to the lower levels of 2OG, **1** (a 2OG competitor) [51] should be a more potent inhibitor. **7** was found to reduce levels of HIF-1α stabilization in the presence of **1** (**Figure 4.4.5.1 A and Figure A.7.9**) after 24 hours of treatment. Protein levels of PHD2 were also measured. PHD2 protein levels increased noticeably in the presence of DMSO (control) in comparison to other treatment conditions. There was a slight increase in PHD2 protein levels in the presence of 100 µM of **7**

in combination with **1** (10 µM) treatment compared to **1** (10 µM)and PHD2 protein levels were almost similar for **7** (100 µM) and 100 µM of **7** in combination with **1** (20 µM) treatment (**Figure 4.4.5.1 A)**.

Quantification of the western blot analysis showed that there was a near to complete loss of HIF-1α levels when LN-18 cells were treated with 100 µM of **7** in the presence of **1** (10 µM) compared to the control (**Figure 4.4.5.1 B & and Figure A.7.9**).

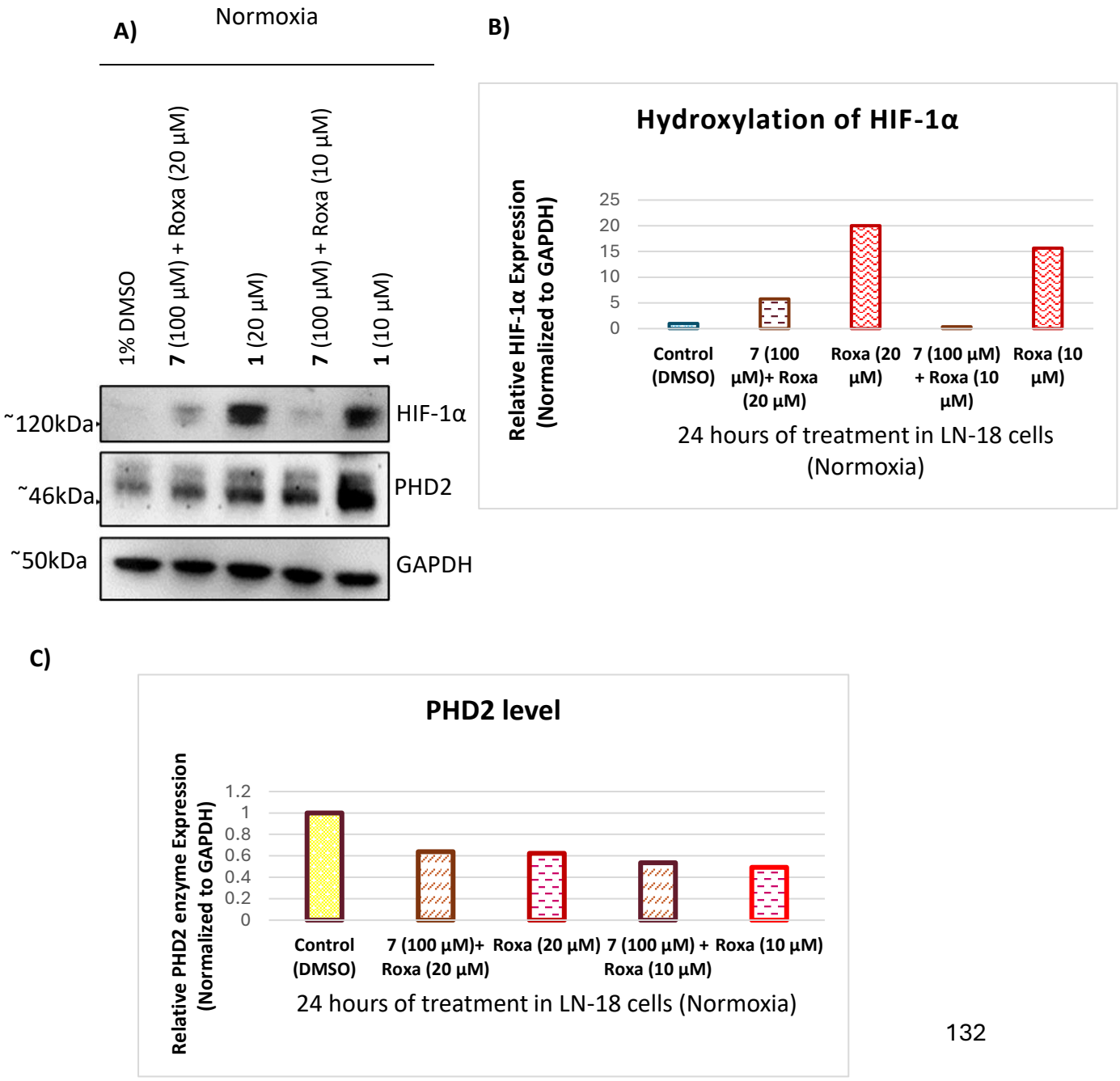


Figure 4.4.5.1: Reduction of HIF-1α by 7 in the presence of PHD inhibitor, 1. (**A**) Immunoblots showing HIF-1α levels in LN-18 cells when incubated for 24 hours with **7** (100μM) in the presence of **1** at 10 μM and 20 μM in normoxia. (**B**) Quantification of HIF-1α degradation (normalized to GAPDH) after 24 hours treatment of **7** 100μM in a presence of **1** at 10 μM and 20 μM in normoxia using 'Image J software'. (**C**) Quantification of PHD 2 level expression (normalized to GAPDH) after 24 hours treatment of **7** 100μM in a presence of **1** at 10 μM and 20 μM in normoxia using 'Image J software'.

4.4.6 Triple negative breast cancer (TNBC) cell line studies with **7**

4.4.6.1 Hypoxia in triple negative breast cancer (TNBC) cell line

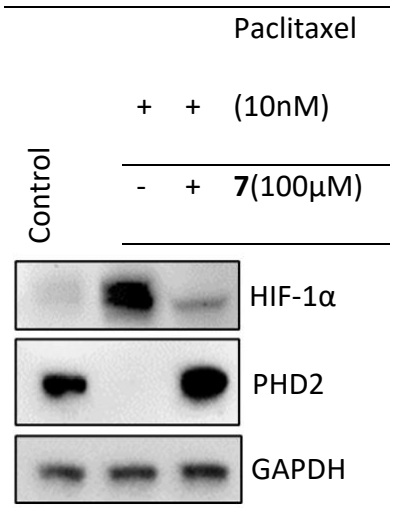
TNBC refers to breast cancer cells that do not have estrogen (ER) or progesterone (PR) receptors and which do not express or over-expressed human epidermal growth factor receptor 2 (HER2+) [52,53]. In TNBC all these criteria are "negative", hence they are called triple-negative breast cancer cells [52-55]. TNBCs have an increased percentage of breast cancer stem cells (BCSCs). [56-58] BCSCs have self-renewing properties, can play essential roles in tumour growth, and show chemotherapy resistance [59-61].

Paclitaxel and gemcitabine are used for the treatment of TNBCs [26, 62]. In 2014, Samanta et al. showed that paclitaxel or gemcitabine treatment can induce increased HIF activity; administration of HIF inhibitors along with chemotherapeutic agents was therefore proposed as a means of combat resistance to chemotherapy in TNBC and enable improved tumour treatment [26, 62].

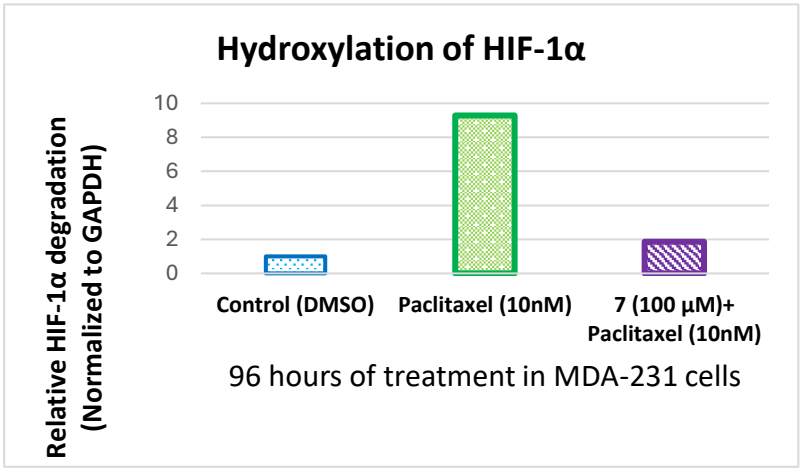
4.4.6.2 The cellular investigations on TNBC cell line in combination with PHD enhancer **7**

The effects of **7** on the TNBC cell line (MDA-MB-231) were evaluated. **7** was co-administered with a chemotherapeutic agent, paclitaxel (10nM) for 4 days. Immunoblot assays showed that treatment with 10nM of paclitaxel caused expression of HIF-1α; by contrast, treatment with **7** in combination with 10 nM paclitaxel led to reduced levels of HIF-1α (**Figure 4.4.6.2.1 A**). Quantification of the western blot showed that the combination of **7** and paclitaxel (10nM) significantly destabilize HIF-1α levels compared to 10 nM of paclitaxel alone (**Figure 4.4.6.2.1 B**). **Figure 4.4.6.2.1 c** shows presence of PHD2 protein level during treatment. PHD2 protein levels were observed to substantially increased in the presence of DMSO and 100 µM of **7** in combination with 10 nM paclitaxel and there was a complete loss of PHD2 protein levels after 10 nM paclitaxel treatment (**Figure 4.4.6.2.1 C).**

A)
(MDA-MB-231 cell line)



B)



C)

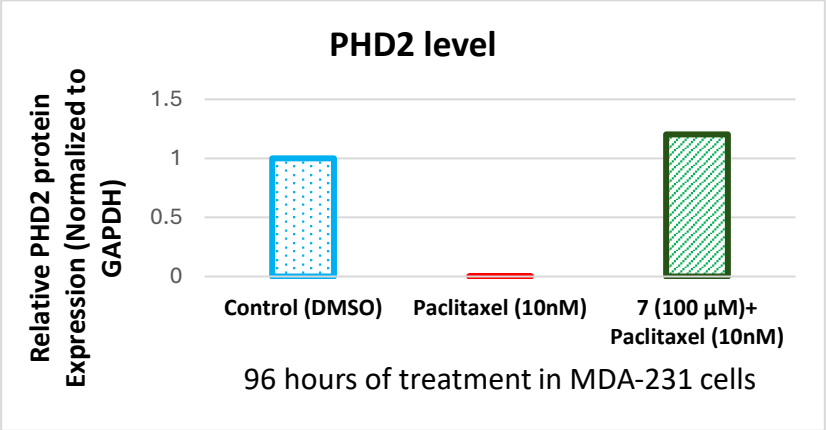


Figure 4.4.6.2.1: Paclitaxel-induced HIF-1α expression is reduced by compound 7. (**A**) Immunoblot assays show HIF-1α levels in MDA-MB-231 cells when incubated for 96 hours with **7** 100µM in the presence of paclitaxel (10nM). 10nM of paclitaxel induces HIF-1α expression in MDA-231 cells. (**B**) Quantification of HIF-1α degradation after 96 hours of treatment **7** (100µM) in the presence of paclitaxel (10nM) using 'Image J software'.
(**C**) Quantification of PHD 2 level expression (normalized to GAPDH) after 96 hours treatment of **7** (100µM) in the presence of paclitaxel (10nM) using 'Image J software'.

4.5 Summary and Limitations of the Results

This chapter describes studies conducted on the small molecule **7**, that promotes PHD2-catalysed HIF-1α progrlyl hydroxylation. **7** causes increased CODD hydroxylation with isolated PHD2. **7** was shown to cause a reduction of HIF-1α levels in HEK 293T cell line under hypoxic conditions. It also did so in the presence of **1** in HEK 293T cells and 2-OG depleted cell line (LN-18) under normoxia. **7** also caused a reduction of HIF-1α levels in the TNBC cell line in the presence of a chemotherapeutic agent. Considering the results- a dose-dependent decrease in HIF-1α protein levels, it can be suggested that **7** promote HIF-1α degradation.

Previous experiments [43] with **7** revealed that the HIF inhibitor effect also occurred in HEP3b

cells further demonstrating that this isn't a cellular specific effect.

One possible mechanism of HIF degradation, other than PHD enhancement, is through mitochondrial complex 1 inhibition. **7** along with the 4-hydroxypyrimidine starting points were tested for their impact on oxygen consumption rate (OCR) using the seahorse assay. Previous results [43] showed that in contrast with BAY 87-2243 (a mitochondrial complex 1 inhibitor, that is known to decrease HIF-1α levels in a manner dependent on VHL and PHD activity) [63-65], **7** apparently causes a weak reduction in OCR suggesting it has small if any effects on mitochondria. To investigate the potential role of mitochondria in the HIF degradation mechanism, **7** was tested in comparison to Bay-87 2243 and in mitochondria deficient cell lines [43]. **7** was able to decrease HIF-1α levels. By contrast, BAY 87-2243 apparently caused HIF-1α stabilization. These results from the mitochondria-deficient cell line indicate that the HIF-α reduction due to **7** is likely not mitochondria dependent (unlike the mitochondrial inhibitor BAY 87-2243).

PHD2 protein levels were also tested to explore the mechanism of **7**. Except for one or two conditions, PHD2 levels appeared to increase on treatment with **7**, supporting the hypothesis that **7** may destabilize HIF-1α through stabilization of PHD2 or upregulation of *PHD2* expression, or both of these. However, in certain western blots, an enhancement in PHD2 levels was absent. A possible explanation could be technical variability, such as antibody sensitivity or protein loading issues. Another explanation could be disrupted antibody recognition due to post-translational modifications. There is also probability that **7** enhances PHD activity indirectly, avoiding modifying total PHD2 protein levels, for instance, by modulating its cofactors. Additional studies such as enzyme activity assays, RT-qPCR for PHD2

mRNA, and co-factor analysis can be done to investigation whether this occurs via enhanced PHD2 production, PHD2 stabilization, or direct enhancement of its enzymatic function.

Given that **7** promotes the activity of isolated PHD2, it is possible that a similar direct mechanism operates in cells. Once this mechanism is defined with isolated PHD2, it should be possible to test whether this occurs in cells by PHD2 studies involving mutagenesis of **7**. Note the effects of **7** may be more than one mechanism, e.g. it cannot be ruled out that the apparent competition with **1** is in part due to competition with respect to cell uptake.

4.5.1 Contributions of others to the work described in this chapter

7 was designed and synthesised by Dr. James Holt-Martyn. Dr. A Tumber performed and analysed the biochemical and Rapid Fire MS assays.

4.6 Methods and Materials

4.6.1 Chemicals

The primary antibody used for western blot experiments was Purified Mouse Anti-Human HIF-1α [Catalog Number 610959], which was from Thermo Fisher Scientific, (Waltham, MA, USA) and PHD-2/Egln1 Antibody[Catalog Number 3293], which was from Cell Signaling Technology, (Danvers, MA, USA,). The secondary antibody used, Rabbit Anti-Mouse IgG (D3V2A) mAb (HRP Conjugate) [Catalog Number 58802], was from (Cell Signaling Technology, Inc., Danvers, Massachusetts, USA) and Mouse Anti-rabbit IgG mAb (HRP Conjugate) [Catalog Number 5127], which was from Cell Signaling Technology, (Danvers, MA, USA,).

4.6.2 Cell line

Human Embryonic Kidney 293T cells were from the ATCC® (cat no. CRL-3216) and Glioblastoma cell line LN-18 were from the ATCC® (cat no. CRL-2610). The MDA-MB-231 cell line was kindly gifted by Prof. Hagan Bayley's group (University of Oxford).

4.6.3 Cell Culture Stock Solutions

Stock solutions of all tested compounds (**7**, and Roxadustat) were made up in DMSO. DMSO was sterilised before any experiments using a 0.45 µM syringe filter.

4.6.4 PHD inhibitors used for the experiments

The used PHD inhibitor Roxadustat was obtained from MedChemExpress (Sollentuna, Sweden).

4.6.5 Cell culture

All cells except MDA-MB-231 cells were grown in Dulbecco's modified Eagle's medium (high glucose, pyruvate, no glutamine, Gibco) supplemented with 10% of fetal bovine serum (FBS), and 1% GlutaMAX in a 37°C incubator at 5% atmospheric CO_2. Cell confluency was measured microscopically (Motic AE31E trinocular microscope, Hong Kong). MDA-MB-231 cells were grown in RPMI-1640 media.

4.6.6 Protein extraction and analysis

This was described in **Section 2.9.6.**

4.6.7 Immunoblotting in Normoxia

The immunoblotting method followed the process described in **Chapter 2**, **section 2.9.9.** The dilution for PHD-2/Egln1 primary antibody was 1:1000 and dilution for Mouse Anti-rabbit IgG mAb (HRP Conjugate) secondary antibody was 1: 5000.

4.6.8 Immunoblotting for Hypoxia Experiment

4.6.8.1 Cell lysis for hypoxia experiment

For hypoxia experiments cells were seeded at a density of 1.2X106 cells into 6cm dishes and transferred into the Whitley H35 hypoxia station (Don Whitley Scientific Limited, West Yorkshire, UK) along with required reagents (PBS, and ethanol required for harvesting) for 24 hours to reach a hypoxic state. When the cells reached the desired hypoxic state, treatments e.g. 20, 50, and 100 µM of **7** and 1% DMSO were added. After treatment (3/6/ or 18 hours), on the day of harvesting, all the media were discarded from the plates, and the cells were

washed with 1 ml of PBS, then scraped and collected into an Eppendorf vial. With a mini centrifuge, the collected cells were centrifuged for ~ 10 seconds to get cell pellets. The supernatants were discarded, and the pellets were resuspended with 25µl of freshly prepared UTB buffer. Samples were kept on ice during the entire procedure.

4.6.8.2 Sonication

Cells were disrupted by sonication (20s on, 10 s off on ice, 20s on ice, 40% amplitude) using a Sonics Vibra-CellTM machine (SONICS & MATERIALS, INC, Newtown, USA). Samples then were centrifuged at 13,000 Xg for 10 mins at 4 degrees.

4.6.8.3 Preparing Urea-Tris-Bicine (UTB) lysis buffer

A stock solution was prepared using 9M urea and 75mM Tris-HCl. The pH was maintained at 7.5. when prepared the fresh UTB buffer, was in 1ml of the stock, 5µl of beta-mercaptoethanol was added and taken inside the hypoxia station.

4.6.8.4 Quantification

For quantification of protein, a nanodrop at protein 280 setting was used and quantification of the immunoblotting signal was performed with Image LabTM software from BIO-RAD.

4.6.8.5 SDS-Page

To perform the polyacrylamide gel electrophoresis all samples were loaded into a pre-cast NuPAGE 4-12% Bis-Tris Protein Gels (Life Tech). The gels were run in 1x Tris/glycine/SDS running buffer (20x NuPAGE MES SDS Running Buffer, Life tech) at 180 V for 45 min (Mini Gel Tank, Life Technologies). 5µl of protein ladder marker (Page Ruler Pre-Stained Protein Ladder, Thermo Scientific) was used to compare protein sizes.

4.6.9 RapidFire Assay Protocol

25µM of **7**, was tested at 37℃ with $PHD2_{181-426}$ and CODD substrate using the rapidfire assay. The enzyme assay monitors increased hydroxylation of the CODD substrate in comparison to the control (0.5% (v/v) DMSO) using 25 µM of **7**. A typical incubation time for $tPHD2_{181-426}$ and **7** was 15 minutes. Assay conditions: 384-well assay plate, 25 µl of reaction mix, assay buffer-20 µM ferrous iron sulfate, 200 µM L-ascorbic acid, 10 µM CODD peptide and 20 µM 2-OG. 25 µl of substrate was used to initiate a reaction, the typical incubation time for tPHD2181-426 and **7** was 15 minutes and 5 µl of 10% (v /v) formic acid was used for the termination of the reaction. Equipment used: RapidFire RF360 sampling robot (Agilent), Agilent 6530 quadrupole-time-of-flight (QTOF) mass spectrometer and RapidFire Integrator software (Agilent) [43]. Rapid Fire MS assay was performed by Dr. A Tumber.

4.7 References

1. Jaakkola, P., et al., *Targeting of HIF-α to the von Hippel-Lindau ubiquitylation complex by O2-regulated prolyl hydroxylation.* Science, 2001. 292(5516): p. 468-472. DOI: 10.1126/science.1059796

2. Ivan, M. and W.G. Kaelin Jr, *The von Hippel–Lindau tumor suppressor protein.* Curr Opin Genet Dev, 2001. 11(1): p. 27-34. DOI: 10.1038/nrc2502

3. Masson, N., et al., *Independent function of two destruction domains in hypoxia-inducible factor-α chains activated by prolyl hydroxylation.* The EMBO journal, 2001. DOI: 10.1093/emboj/20.18.5197

4. Yu, F., et al., *HIF-1α binding to VHL is regulated by stimulus-sensitive proline hydroxylation.* PNAS, 2001. 98(17): p. 9630-9635. DOI: 10.1073/pnas.181341498

5. Simon, M.C. and B. Keith, *The role of oxygen availability in embryonic development and stem cell function.* Nat Rev Mol Cell Biol, 2008. 9(4): p. 285-96. DOI: 10.1038/nrm2354

6. Semenza, G.L., *Hypoxia-inducible factor 1 (HIF-1) pathway.* Sci STKE, 2007. 2007(407): p. cm8. DOI: 10.1126/stke.4072007cm8

7. Liu, W., et al., *Targeted genes and interacting proteins of hypoxia inducible factor-1.* Int J Biochem Mol Biol, 2012. 3(2): p. 165-78.

8. Gaete, D., et al., *HIF-Prolyl Hydroxylase Domain Proteins (PHDs) in Cancer-Potential Targets for Anti-Tumor Therapy?* Cancers (Basel), 2021. 13(5). DOI: 10.3390/cancers13050988

9. Meneses, A.M. and B. Wielockx, *PHD2: from hypoxia regulation to disease progression.* Hypoxia, 2016: p. 53-67. DOI: 10.2147/HP.S53576

10. Casazza, A., et al., *Tumor stroma: a complexity dictated by the hypoxic tumor*

microenvironment. Oncogene, 2014. 33(14): p. 1743-1754. DOI: 10.1038/onc.2013.121

11. Hanahan, D. and R.A. Weinberg, *Hallmarks of cancer: the next generation.* cell, 2011. 144(5): p. 646-674. DOI: 10.1016/j.cell.2011.02.013

12. Gray, L.H., et al., *The concentration of oxygen dissolved in tissues at the time of irradiation as a factor in radiotherapy.* Br J Radiol, 1953. 26(312): p. 638-648. DOI: 10.1259/0007-1285-26-312-638

13. Thomlinson, R.H. and L.H. Gray, *The histological structure of some human lung cancers and the possible implications for radiotherapy.* Br J Radiol, 1955. 9(4): p. 539. DOI: doi: 10.1038/bjc.1955.55

14. Keith, B., R.S. Johnson, and M.C. Simon, *HIF1α and HIF2α: sibling rivalry in hypoxic tumour growth and progression.* Nat. Rev. Cancer, 2012. 12(1): p. 9-22. DOI: 10.1038/nrc3183

15. Semenza, G.L., *Evaluation of HIF-1 inhibitors as anticancer agents.* Drug Discov. Today, 2007. 12(19-20): p. 853-859. DOI: 10.1016/j.drudis.2007.08.006

16. Zhong, H., et al., *Overexpression of hypoxia-inducible factor 1α in common human cancers and their metastases.* Cancer Research, 1999. 59(22): p. 5830-5835.

17. Zhang, J. and Q. Zhang, *VHL and hypoxia signaling: beyond HIF in cancer.* Biomedicines, 2018. 6(1): p. 35. DOI: 10.3390/biomedicines6010035

18. Semenza, G.L. and G.L. Wang, *A nuclear factor induced by hypoxia via de novo protein synthesis binds to the human erythropoietin gene enhancer at a site required for transcriptional activation.* MCB, 1992.Dec 1. DOI: 10.1128/mcb.12.12.5447-5454.1992

19. Rhodes, D.R., et al., *Oncomine 3.0: genes, pathways, and networks in a collection of 18,000 cancer gene expression profiles.* Neoplasia, 2007. 9(2): p. 166-180. DOI: 10.1593/neo.07112

20. Epstein, A.C., et al., *C. elegans EGL-9 and mammalian homologs define a family of dioxygenases that regulate HIF by prolyl hydroxylation.* Cell, 2001. 107(1): p. 43-54. DOI: 10.1016/s0092-8674(01)00507-4

21. Appelhoff, R.J., et al., *Differential function of the prolyl hydroxylases PHD1, PHD2, and PHD3 in the regulation of hypoxia-inducible factor.* J. Biol. Chem., 2004. 279(37): p. 38458-38465. DOI: 10.1074/jbc.M406026200

22. Bordoli, M.R., et al., *Prolyl-4-hydroxylase PHD2-and hypoxia-inducible factor 2-dependent regulation of amphiregulin contributes to breast tumorigenesis.* Oncogene, 2011. 30(5): p. 548-560. DOI: 10.1038/onc.2010.433

23. Wottawa, M., et al., *Knockdown of prolyl-4-hydroxylase domain 2 inhibits tumor growth of human breast cancer MDA-MB-231 cells by affecting TGF-β1 processing.* Int J Cancer, 2013. 132(12): p. 2787-2798. DOI: 10.1002/ijc.27982

24. Oskarsson, T., E. Batlle, and J. Massagué, *Metastatic stem cells: sources, niches, and vital pathways.* Cell stem cell, 2014. 14(3): p. 306-321. DOI: 10.1016/j.stem.2014.02.002

25. Prabhakar, N.R. and G.L. Semenza, *Adaptive and maladaptive cardiorespiratory responses to continuous and intermittent hypoxia mediated by hypoxia-inducible factors 1 and 2.* Physiological Reviews, 2012. 92(3): p. 967-1003. DOI: 10.1152/physrev.00030.2011

26. Samanta, D., et al., *Hypoxia-inducible factors are required for chemotherapy resistance of breast cancer stem cells.* PNAS, 2014. 111(50): p. E5429-E5438. DOI: 10.1073/pnas.1421438111

27. Brigham, et al., *Comprehensive molecular portraits of human breast tumours.* Nature, 2012. 490(7418): p. 61-70. DOI: 10.1038/nature11412

28. Wigerup, C., S. Påhlman, and D. Bexell, *Therapeutic targeting of hypoxia and hypoxia-inducible factors in cancer.* Clin. Pharm. Therap., 2016. 164: p. 152-169. DOI: 10.1016/j.pharmthera.2016.04.009

29. Fallah, J. and B.I. Rini, *HIF inhibitors: status of current clinical development.* Curr. Oncol. Rep, 2019. 21: p. 1-10. DOI: 10.1007/s11912-019-0752-z

30. Ban, H.S., et al., *Hypoxia-inducible factor (HIF) inhibitors: a patent survey (2011-2015).* Expert Opin. Ther. Pat., 2016. 26(3): p. 309-322. DOI: 10.1517/13543776.2016.1146252

31. Maynard, M.A. and M. Ohh, *Von Hippel-Lindau tumor suppressor protein and hypoxia-inducible factor in kidney cancer.* Am. J. Nephrol, 2004. 24(1): p. 1-13. DOI: 10.1159/000075346

32. Jonasch, E., et al., *Belzutifan for renal cell carcinoma in von Hippel–Lindau disease.* N Engl J Med, 2021. 385(22): p. 2036-2046. DOI: 10.1056/NEJMoa2103425

33. Clark, P.E., *The role of VHL in clear-cell renal cell carcinoma and its relation to targeted therapy.* Kidney international, 2009. 76(9): p. 939-945. DOI: 10.1038/ki.2009.296

34. Mazumder, S., P.J. Higgins, and R. Samarakoon, *Downstream targets of VHL/HIF-α signaling in renal clear cell carcinoma progression: mechanisms and therapeutic relevance.* Cancers, 2023. 15(4): p. 1316. DOI: 10.3390/cancers15041316

35. Fallah, J., et al., *FDA approval summary: belzutifan for von Hippel-Lindau disease–associated tumors.* Clin Cancer Res, 2022. 28(22): p. 4843-4848. DOI: 10.1158/1078-0432.CCR-22-1054

36. Deeks, E.D., *Belzutifan: first approval.* Drugs, 2021. 81(16): p. 1921-1927. DOI: 10.1007/s40265-021-01606-x

37. Curry, L. and M. Soleimani, *Belzutifan: a novel therapeutic for the management of von Hippel–Lindau disease and beyond.* Future Oncology, 2024(0). DOI: 10.2217/fon-2023-0679

38. Lopina, O.D., *Enzyme inhibitors and activators*, in *Enzyme inhibitors and activators*. 2017, IntechOpen.

39. Zorn, J.A. and J.A. Wells, *Turning enzymes ON with small molecules.* Nat. Chem. Biol., 2010. 6(3): p. 179-188. DOI: 10.1038/nchembio.318

40. Choi, H., et al., *Rapid degradation of hypoxia-inducible factor-1α by KRH102053, a new activator of prolyl hydroxylase 2.* Br. J. Pharmacol., 2008. 154(1): p. 114-125. DOI: 10.1038/bjp.2008.70

41. Nepal, M., et al., *An activator of PHD2, KRH102140, decreases angiogenesis via inhibition of HIF-1α.* Cell Biochem. Funct., 2011. 29(2): p. 126-134. DOI: 10.1002/cbf.1732

42. Singh, M., et al., *Chemical activation of prolyl hydroxylase-2 by BBAP-1 down regulates hypoxia inducible factor-1α and fatty acid synthase for mammary gland chemoprevention.* RSC advances, 2018. 8(23): p. 12848-12860. DOI:10.1039/c8ra01239c

43. Holt-Martyn, J., *Novel and selective small molecule inhibitors and activators for the prolyl hydroxylase domain enzyme*. 2018, D.Phil thesis, University of Oxford.

44. Kuroda, K., et al., *Non-aqueous, zwitterionic solvent as an alternative for dimethyl sulfoxide in the life sciences.* Commun. Chem., 2020. 3(1): p. 163. DOI: 10.1038/s42004-020-00409-7

45. Yeh, T.-L., et al., *Molecular and cellular mechanisms of HIF prolyl hydroxylase inhibitors in clinical trials.* Chem. Sci., 2017. 8(11): p. 7651-7668. DOI: 10.1039/c7sc02103h

46. Hvinden IC, Cadoux-Hudson T, Schofield CJ, McCullagh JS. Metabolic adaptations in

cancers expressing isocitrate dehydrogenase mutations. Cell Rep. 2021 Dec 21;2(12). DOI: 10.1016/j.xcrm.2021.100469

47. Dang L, White DW, Gross S, Bennett BD, Bittinger MA, Driggers EM, Fantin VR, Jang HG, Jin S, Keenan MC, Marks KM. Cancer-associated IDH1 mutations produce 2-hydroxyglutarate. Nature. 2009 Dec 10;462(7274):739-44. DOI: 10.1038/nature08617

48.Berra, E., E. Benizri, A. Ginouves, V. Volmat, D. Roux, and J. Pouysségur, *HIF prolyl-hydroxylase 2 is the key oxygen sensor setting low steady-state levels of HIF-1α in normoxia. EMBO J.*, 2003. **22(16)**: p. 4082–4090. DOI: 10.1093/emboj/cdg392

49. Kunze, R., W. Zhou, R. Veltkamp, B. Wielockx, G. Breier, and H.H. Marti, *Neuron-specific prolyl-4-hydroxylase domain 2 knockout reduces brain injury after transient cerebral ischemia. Stroke*, 2012. **43(10)**: p. 2748–2756. DOI: 10.1161/STROKEAHA.112.660258

50. Liu S, Cadoux-Hudson T, Schofield CJ. Isocitrate dehydrogenase variants in cancer—Cellular consequences and therapeutic opportunities. Curr Opin Chem Biol. 2020 Aug 1;57:122-34. DOI: 10.1016/j.cbpa.2020.06.012

51. Su K, Li Z, Yu Y, Zhang X. The prolyl hydroxylase inhibitor roxadustat: Paradigm in drug discovery and prospects for clinical application beyond anemia. Drug Discov. Today. 2020 Jul 1;25(7):1262-9. doi: 10.1016/j.drudis.2020.04.017.

52. Sørlie, T., et al., *Gene expression patterns of breast carcinomas distinguish tumor subclasses with clinical implications.* PNAS, 2001. 98(19): p. 10869-10874. DOI: 10.1073/pnas.191367098

53. Sørlie, T., et al., *Repeated observation of breast tumor subtypes in independent gene expression data sets.* PNAS, 2003. 100(14): p. 8418-8423. DOI: 10.1073/pnas.0932692100

54. Sotiriou, C., et al., *Breast cancer classification and prognosis based on gene expression profiles from a population-based study.* PNAS, 2003. 100(18): p. 10393-10398. DOI: 10.1073/pnas.1732912100

55. Irvin Jr, W.J. and L.A. Carey, *What is triple-negative breast cancer?* Eur. J. Cancer, 2008. 44(18): p. 2799-2805. DOI: 10.1016/j.ejca.2008.09.034

56. Dai M, Zhang C, Ali A, Hong X, Tian J, Lo C, Fils-Aimé N, Burgos SA, Ali S, Lebrun JJ. CDK4 regulates cancer stemness and is a novel therapeutic target for triple-negative breast cancer. Sci. Rep. 2016 Oct 19;6(1):35383. DOI: 10.1038/srep35383

57. He L, Wick N, Germans SK, Peng Y. The role of breast cancer stem cells in chemoresistance and metastasis in triple-negative breast cancer. Cancers. 2021 Dec 9;13(24):6209. DOI: i: 10.3390/cancers13246209

58. Park SY, Choi JH, Nam JS. Targeting cancer stem cells in triple-negative breast cancer. Cancers. 2019 Jul 9;11(7):965. DOI: 10.3390/cancers11070965

59. Li, X., et al., *Intrinsic resistance of tumorigenic breast cancer cells to chemotherapy.* J. Clin Inest, 2008. 100(9): p. 672-679. DOI: 10.1093/jnci/djn123

60.Creighton, C.J., et al., *Residual breast cancers after conventional therapy display mesenchymal as well as tumor-initiating features.* PNAS, 2009. 106(33): p. 13820-13825.

61. Bhola, N.E., et al., *TGF-β inhibition enhances chemotherapy action against triple-negative breast cancer.* J. Clin Inest, 2013. 123(3): p. 1348-1358. DOI: 10.1073/pnas.0905718106

62. O'Reilly, E.A., et al., *The fate of chemoresistance in triple negative breast cancer (TNBC).* BBA clinical, 2015. 3: p. 257-275. DOI: 10.1016/j.bbacli.2015.03.003

63. Ellinghaus P, Heisler I, Unterschemmann K, Haerter M, Beck H, Greschat S, Ehrmann A,

Summer H, Flamme I, Oehme F, Thierauch K. BAY 87-2243, a highly potent and selective inhibitor of hypoxia-induced gene activation has antitumor activities by inhibition of mitochondrial complex I. Cancer Med. 2013 Oct;2(5):611-24. DOI: 10.1002/cam4.112

64. Helbig L, Koi L, Brüchner K, Gurtner K, Hess-Stumpp H, Unterschemmann K, Baumann M, Zips D, Yaromina A. BAY 87–2243, a novel inhibitor of hypoxia-induced gene activation, improves local tumor control after fractionated irradiation in a schedule-dependent manner in head and neck human xenografts. Radiat. Onco. 2014 Dec;9:1-0. DOI: 10.1186/1748-717X-9-207

65. Clark PE. The role of VHL in clear-cell renal cell carcinoma and its relation to targeted therapy. Kidney Int. 2009 Nov 1;76(9):939-45. DOI: 10.1038/ki.2009.296

Chapter 5

Metabolomics Studies on Natural and Unnatural HIF Prolyl Hydroxylase Modulators

PHD inhibitors such as Daprodustat, Roxadustat, and Molidustat are used clinically for the treatment of anaemia in chronic kidney disease (CKD) patients [1]. These PHD inhibitors have pro-erythropoietic effects and increase HIF levels by inhibiting the HIF prolyl hydroxylases. Extensive biological studies, however, suggest these drugs also likely have other effects related to HIF stabilization and the regulation of vital biological processes, including glucose metabolism, cell proliferation, apoptosis, and mitochondrial metabolism [2-9]. Metabolomic changes at the cellular level, caused by treatment with clinically used PHD inhibitors, have not previously been investigated in detail. The work described in this chapter reports on the development of a semi-targeted metabolomic workflow and its application to explore or investigate the metabolic consequences when HEK 293T cells are cultured in hypobaric hypoxia and with hypoxia mimicking agents, and/ or with clinically relevant selective PHD inhibitors.

5.1 Metabolomics

Metabolic intermediates and end products of cellular biochemistry are collectively referred to as metabolites and typically represent small molecules ranging in mass from 50 – 1500 Daltons (Da)[10]. The field of metabolomics concerns detailed and comprehensive analyses of metabolism, metabolic reactions, and their products in biological systems [11] often to investigate biological functions or identify biomarkers of altered biological conditions. Metabolomic analyses can be categorized into three different analytical approaches;

'targeted', 'semi-targeted', and 'untargeted' metabolomics which occupies complementary analytical space across the spectrum from broader to more targeted coverage [12, 13].

Targeted metabolomics aims to detect and analyse known metabolites or small groups of known metabolites, often using mass spectrometry (MS). However, other methods, such as Nuclear Magnetic Resonance (NMR) are also used. Targeted metabolomics methods tend to provide high sensitivity and quantitative accuracy compared to semi-targeted and untargeted methods, but targeted methods are limited to characterising a relatively small number of metabolites and are therefore hypothesis-led [14-16]. Untargeted metabolomics methods aim to identify as many metabolites as possible in a given biological sample and utilize high-resolution MS systems to provide high mass accuracy. The approach also often incorporates multiple chromatographic approaches [17, 18]. Untargeted metabolomics aims to provide an overview of the metabolome that is as broad as possible, under different experimental conditions; however, in doing so it sacrifices some sensitivity for particular metabolites and, although it relies on relative quantitation to show differences between experimental groups, it tends to provide lower quantitative accuracy compared to targeted methods.

Untargeted metabolomics methods can be coupled with database searches to enable putative metabolite identifications (e.g. using The Human Metabolome Database (HMDB), METLIN (Metabolite and Chemical Entity Database), and MS-DIAL (Mass Spectrometry – Data Independent Analysis;[19-23] However, the identification of many compound-features (unidentified peaks) is usually not the priority for untargeted studies. Dedicated software

platforms have been developed to process and analyse the large datasets produced in untargeted metabolomics. The development of integrated software has helped enable comprehensive metabolomic analyses. Such software includes XCMS [24], MS-DIAL [21], MetaboAnalyst [25], molecular-formula-oriented and peak detection techniques such as HERMES [26], and software to understand biochemical pathways such as MetPA (Metabolomics Pathway Analysis) [27], MetaboAnalyst [25] and KEGG (Kyoto Encyclopedia of Genes and Genomes) [28].

Coupled with the development of high-resolution accurate mass spectrometers, contemporary metabolomic studies offer improved analytical outcomes compared to traditional approaches [29-31] and in general, targeted and untargeted metabolomics methods provide complementary information. Untargeted metabolomics is hypothesis-generating (e.g. datasets can be explored to identify unanticipated changes associated with an experimental intervention). This contrasts with targeted metabolomics which is hypothesis-led (e.g. a-priori information about metabolic changes is required to select potential metabolite changes of interest to study).

Semi-targeted metabolomics aims to merge the benefits of both targeted and untargeted approaches; it expands the number of targeted metabolites significantly and applies more rigorous identification and quantification criteria than are generally found in untargeted metabolomics. Importantly semi-targeted studies provide some hypothesis-generating capabilities through their comprehensive identification and quantification (typically hundreds or thousands of metabolites) [32, 33].

5.2 Untargeted pathway analysis using Mummichog

One of the benefits of untargeted and semi-targeted metabolomics is that the broad overview can capture information about altered metabolism at a functional level – e.g. at the level of metabolic pathways. Metabolic pathway analysis involves the statistical analysis of metabolite abundance changes as well as the assignment of metabolite identities and their association with known metabolic pathways to infer system-level information about biological function. There are various methods available; one of these enables the assignment of unidentified mass spectral peaks directly to metabolic pathways without the need for formal identification of an individual peak on a peak basis. This method is therefore compatible with semi-targeted and untargeted datasets. Using an algorithm known as 'Mummichog', untargeted pathway analysis [34, 35] provides insights into metabolic responses at the level of metabolic pathways without the need to formally identify metabolites [36]. This method contrasts with conventional metabolomics pathway analysis tools which only work with identified metabolite information. Due to advancements in computational biology and bioinformatics, the mummichog algorithm has been validated using metabolic, immune response, and cellular signaling pathways [37].

5.3 Ion chromatography-mass spectrometry (IC-MS)

Ion-exchange chromatography (IC) is a well-established chromatographic method for the analysis of highly polar and ionic metabolites [38] [39]. IC is capable of separating analytes in their ionized form and is therefore capable of analysing highly polar and ionic metabolites. Such ionic compounds are also compatible with MS which requires analytes to be charged, however, the strong acids and bases typically used to elute compounds from IC stationary phases are not directly compatible with mass spectrometry ion sources due to their high ion-concentrations and corrosiveness [40]. Relatively recently IC-MS systems have been developed with a solution to this technical incompatibility challenge [41].

Online electrolytic suppressors (and in some cases chemical suppressors) are used to remove high ion-strength mobile phase components, during post chromatographic separation whilst maintaining chromatographic separation of analyses [42-45]. Unlike reversed-phase liquid chromatography (RPLC) or hydrophilic interaction liquid chromatography (HILIC), IC involves ionic interactions with the stationary phase and an increasing ionic strength gradient is often used to elute analytes over time. IC-MS has been applied in metabolomics experiments mostly for the analysis of highly polar and ionic anions. [46].

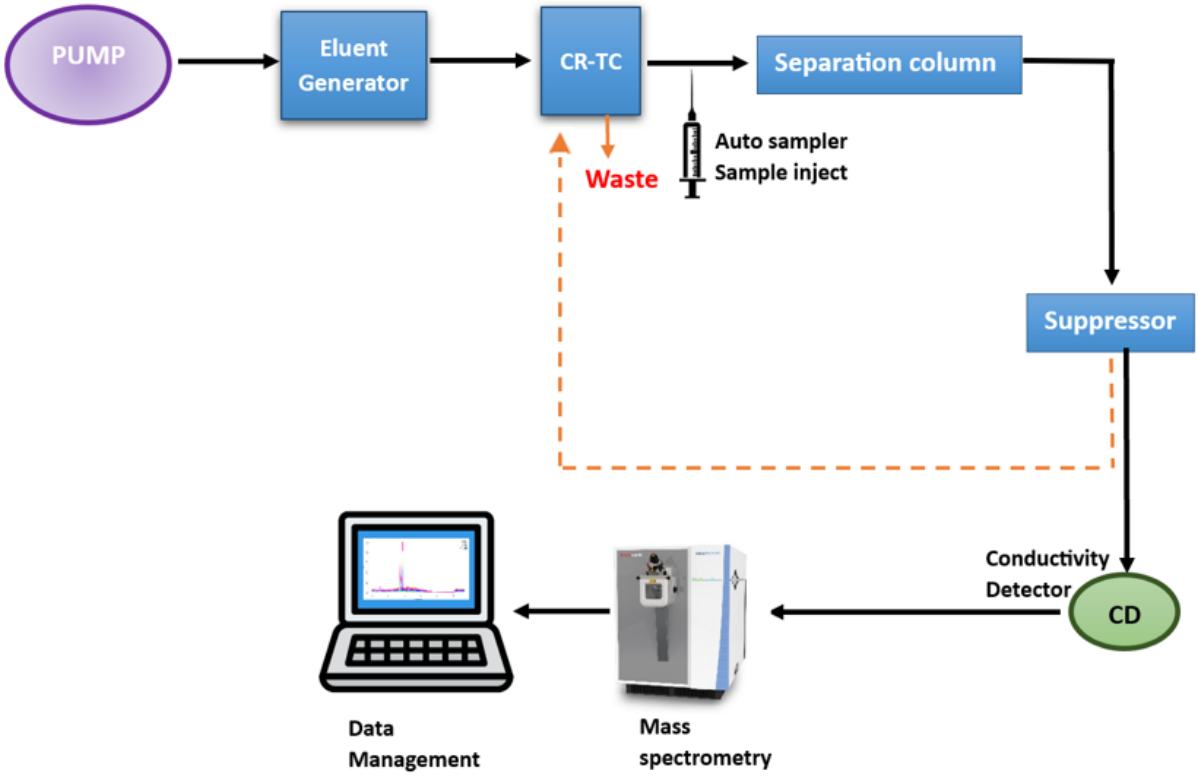


Figure 5.3.1: IC-MS workflow diagram.

5.4 Metabolic adaptation in cellular hypoxia

5.4.1 Glycolysis in hypoxia

The process by which one glucose molecule is anaerobically metabolized into two pyruvate molecules is known as glycolysis, which occurs in the cytoplasm of cells. In addition to pyruvate, glycolysis reduces nicotinamide adenosine dinucleotide (NAD) giving nicotinamide-adenine dinucleotide (NADH); a net gain of two adenosine triphosphate (ATP) molecules results. When there is an adequate amount of molecular oxygen present, the tricarboxylic

acid cycle (TCA) in mitochondria further metabolises the pyruvate produced. The TCA cycle then supplies electrons to the electron transport chain (ETC), which produces an additional ~36 molecules of ATP for every glucose molecule that enters the glycolytic pathway. In normal physiological conditions glycolysis, the TCA cycle, and the ETC work together to produce sufficient ATP to meet the requirements of cells, tissues, and whole organisms in order to preserve homeostasis [47, 48]. However, under hypoxia, eukaryotic cells typically switch towards a greater proportion of ATP production via glycolysis, which, although less efficient for ATP production per glucose molecule (compared to mitochondrial respiration), does not require O_2 (unlike mitochondrial respiration) and therefore ensures ATP production in the absence of O_2 [49].

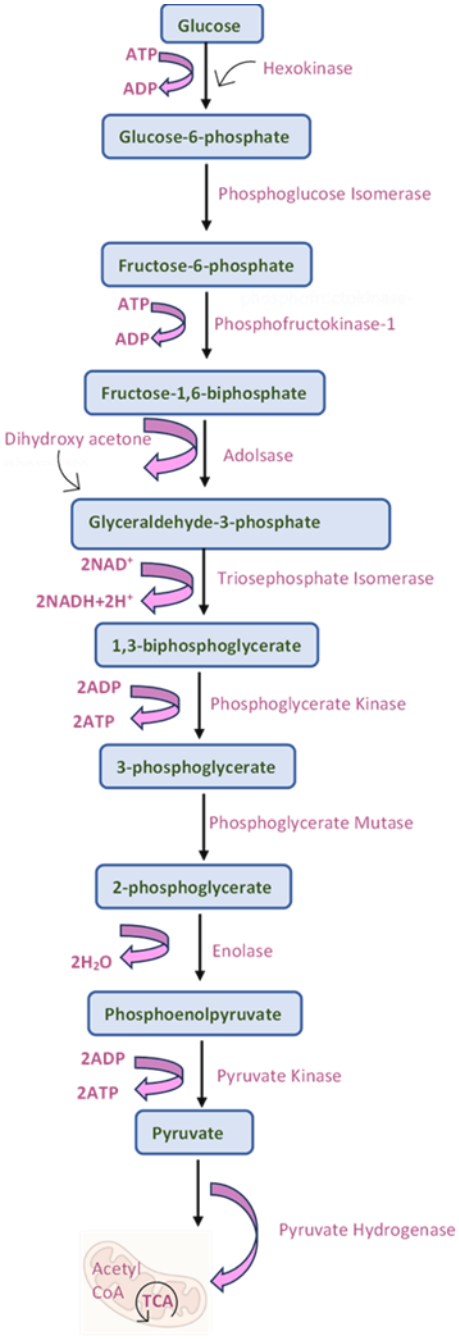


Figure 5.4.1: Schematic summary of the glycolytic pathway[48]. Glycolysis metabolises glucose into two molecules of pyruvate. The glycolysis pathway involves ten enzymes. Step 1: hexokinase, Step 2: Phosphoglucose Isomerase, Step 3: Phosphofructokinase, Step 4: Aldolase, Step 5: Triosephosphate isomerase, Step 6: Glyceraldehyde-3-phosphate Dehydrogenase, Step 7: Phosphoglycerate Kinase, Step 8: Phosphoglycerate Mutase, Step 9: Enolase and Step 10: Pyruvate Kinase.

Changes in glycolysis can support cell survival, cellular homeostasis, and maximize energy output [50]. Hypoxia can result in increased levels of metabolites including lactate, succinate, and fumarate [51]. ATP generation decreases in hypoxia, eventually reducing the ATP/AMP ratio[48]. Normally, in the TCA cycle pyruvate dehydrogenase (PDH) converts pyruvate to acetyl-CoA; in hypoxia when HIF-1α has activated the production of pyruvate dehydrogenase kinase 1 (PDK1) increases, an action which inhibits PDH, hindering the conversion of pyruvate to acetyl-CoA and therefore limiting TCA cycle action [52, 53]. HIF-1α also promotes transcription of lactate dehydrogenase A (LDHA), which reduces pyruvate to lactate (so directing metabolism away from the TCA cycle), concomitantly producing NAD^+, which is essential for glycolysis [54].Thus, PDK1 and LDHA collectively inhibit the formation of acetyl Co-A from pyruvate in the TCA cycle [47, 55].

5.4.2 Effects of HIF-1α stabilization on glycolytic pathway

It has been proposed that the upregulation of TCA cycle-related dicarboxylic acids, in particular succinate, fumarate, and 2-HG, can lead to inhibition of PHDs by competition with 2OG binding, leading to upregulation of HIFα isoforms [42, 43, 56]. Furthermore, the activation of HIF-1α in hypoxia leads to the transcriptional upregulation of various genes involved in glycolysis, angiogenesis, and cell survival [42]. To date, various mechanisms have been considered for how glycolysis is regulated in hypoxia, including factors whose actions are HIF pathway dependent [44]. HIF-1α dependent glucose metabolism minimizes dependence on oxygen-dependent energy generation [53]. This adaptation involves the activation of HIF-1α induced genes which encode for glucose transporters (e.g., *PDK1*, *GLUT1*,

and *GLUT 3*) and glycolytic enzymes [44, 45, 53, 57, 58]. HIF binds to a hypoxia-responsive element (HRE) sequence (5'-RCGTG-3') and mediates enhanced expression of HRE regulated genes encoding for glucose transporters and glycolytic enzymes [49], the latter including phosphofructokinase, liver type (*PFKL*), aldolase (*ALDA*), phosphoglycerate kinase-1 (*PGK1*), enolase (*ENOL*), and lactate dehydrogenase-A (*LDHA*).

HIF mediated expression promotes both flux and lactate production through glycolysis under hypoxic conditions [52, 59, 60]. Such circumstances can upregulate glucose transporters and increase glycolytic enzyme expression leading to increased production of pyruvate[59]. With the help of lactate dehydrogenase (LDH), the additional pyruvate then can promote the conversion of pyruvate to lactate [52, 59, 61].

HIF-1α mediated promotion of glycolysis can be achieved by treatment with PHD inhibitors (e.g., Roxadustat, Molidustat) [1], iron chelators (e.g. Deferoxamine mesylate), or with 2-OG analogues, e.g. NOG) [4, 62, 63]. Tojo et al. have reported that stabilization of HIF-1α through PHD inhibition causes enhanced glycolysis and protects alveolar epithelial cells from acute lung injury [64]. Ito to et al. showed that treatment of oxygen-glucose-deprived renal proximal tubule cells (a model of ischemia) with PHD inhibitors leads to increased glycogen storage and protection of the kidney from ischemia [65].

5.5 Research objectives

This chapter describes work investigating the effect of hypobaric hypoxia and hypoxia mimicking drugs on cellular metabolism. Studies were performed using HEK293T cells grown under five different experimental conditions, i.e. treatment with: (1) hypobaric hypoxia (1%

O_2), (2) 100 µM $CoCl_2$, (3), 20 µM Roxadustat, (4) 100 µM Roxadustat, and (5) 100 µM Molidustat. The cells were incubated under different conditions for 24 hours before quenching, harvesting, and metabolite extraction. The experiments were designed to investigate:

1. The effect of hypoxia and hypoxia mimicking drugs on the regulation of HIF-1α.
2. Explore physiological regulation of glycolysis in hypobaric hypoxia and cells treated with hypoxia-mimicking drugs.
3. Identify and compare cellular metabolic phenotypes associated with each experimental treatment/condition.

Perform functional (pathways) analysis at the metabolic level to investigate how metabolic pathways respond to altered hypobaric hypoxia and hypoxia-mimicking treatments.

5.6 HIF-1α stability in human kidney cells and its metabolomic consequences

As the semi targeted metabolomic studies aimed to investigate the metabolomic consequences of hypobaric hypoxia and hypoxia mimicking drugs on the regulation of HIF-1α, initially different concentration of drug treatment such as 1% O_2, 100, 150 & 300 µM of $CoCl_2$ and 20, 100 & 200 µM of Roxadustat and Molidustat were applied to HEK293T cells to show that they lead to upregulation of HIF-1α in HEK293T cells after 24 hours of treatment. Western blot analysis showed HIF-1α accumulation after the treatment (**Figure 5.7.1, 5.8.1, 5.9.1, & 5.11.1.1)** hence, these treatments were selected for subsequent experiments, that is 1% O_2,

150 µM of $CoCl_2$, 100µM of Roxadustat & Molidustat were used for semi-targeted metabolomics experiments, 100µM of $CoCl_2$, Roxadustat & Molidustat were used for Seahorse experiments and 1% O_2, 100 & 200 µM of $CoCl_2$, Roxadustat & Molidustat were used for RT-qPCR experiments.

To investigate the metabolic effects of HIF-1α stabilization under these different treatment conditions, the cell lysates were subsequently prepared for metabolomics analysis. Semi-targeted metabolic profiling experiments were performed using HEK2193T cell lysates for each condition. Semi-targeted anion-exchange chromatography-tandem mass spectrometry (IC-MS) was used for metabolomics analysis and metabolites were identified at Level 1 and Level 2 using authentic standards (see **Materials and Methods section: 5.16.12**)[66]. The compound identification and putative metabolite identification criteria are described in **Section 5.16.12.** A list of identified metabolites and identification criteria are provided in the appendix **(Table A.7.1. and A.7.2).** During all the metabolomics experiments, cells were grown in DMEM media. Each group had 10 replicates. The **Materials and Methods section (5.16.3.1, 5.16.5, 5.16.12, 5.16.16 and 5.16.17)** describes the process for cell planting and harvesting, sample preparation, and normalization for all the five experimental groups. After the samples were analysed by IC-MS, data were processed using the Progenesis QI software. Progenesis QI-generated datasets were analysed using either MetaboAnalyst 5.0 or 6.0 software [67]. A multivariate statistical analysis was performed using MetaboAnalyst 5.0 or 6.0 where the fold (FC) change value was 1.5 and the p-value cut-off was < 0.05 [67]. Metabolomics sample preparation, sample analysis, data analysis using Progenesis QI Software and data analysis

through MetaboAnalyst are described in the **Materials and Methods section (5.16.9, 5.16.10, and 5.16.12).** The normalization and scaling parameters help to minimize systematic bias identified by the heatmap and provide a normal or almost-normal sample distribution plot. The experimental plan and workflow used are shown in **Figures 5.6.1 & 5.6.2.**

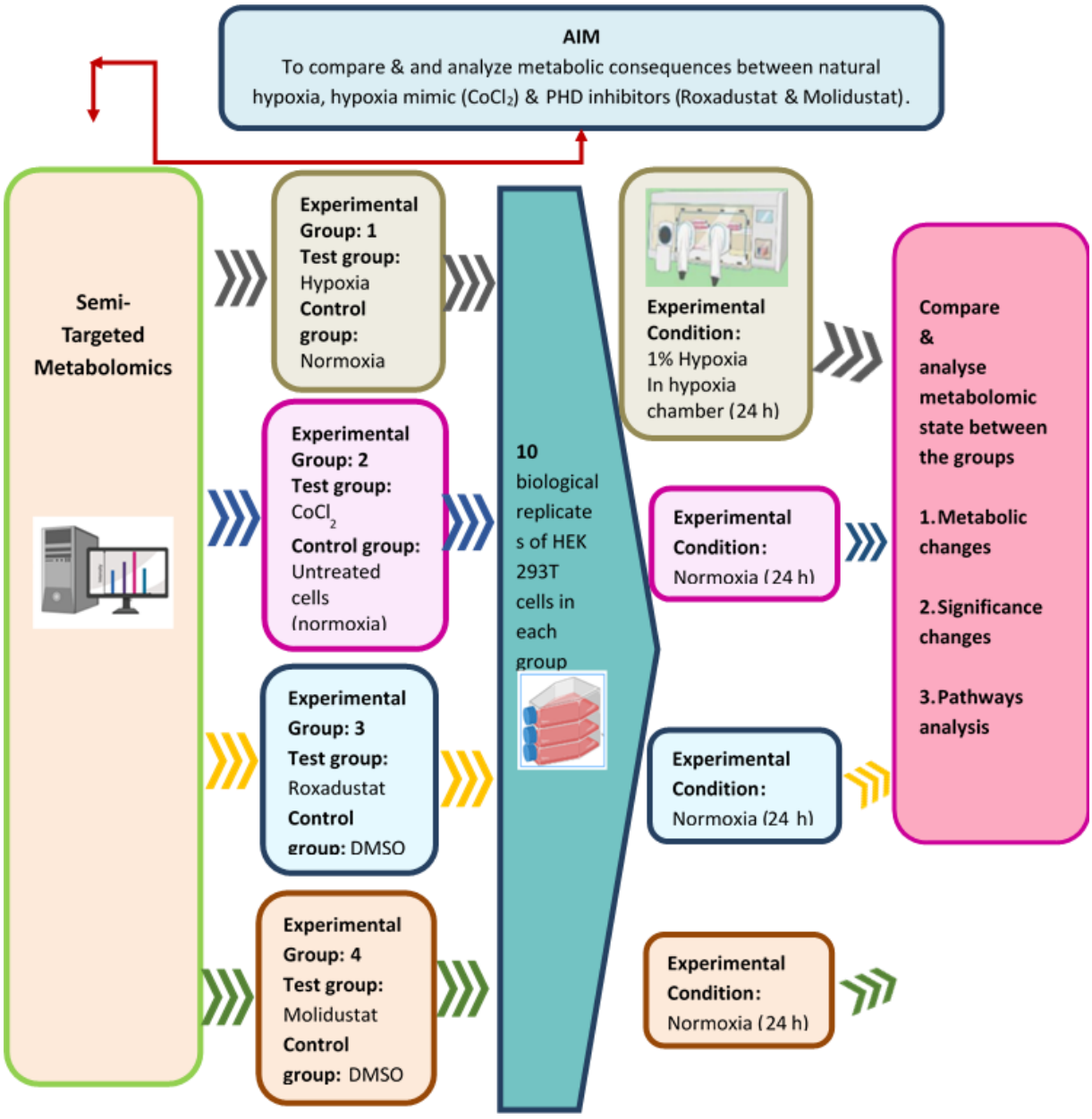


Figure 5.6.1: Experimental design for the metabolomics studies described in this thesis.

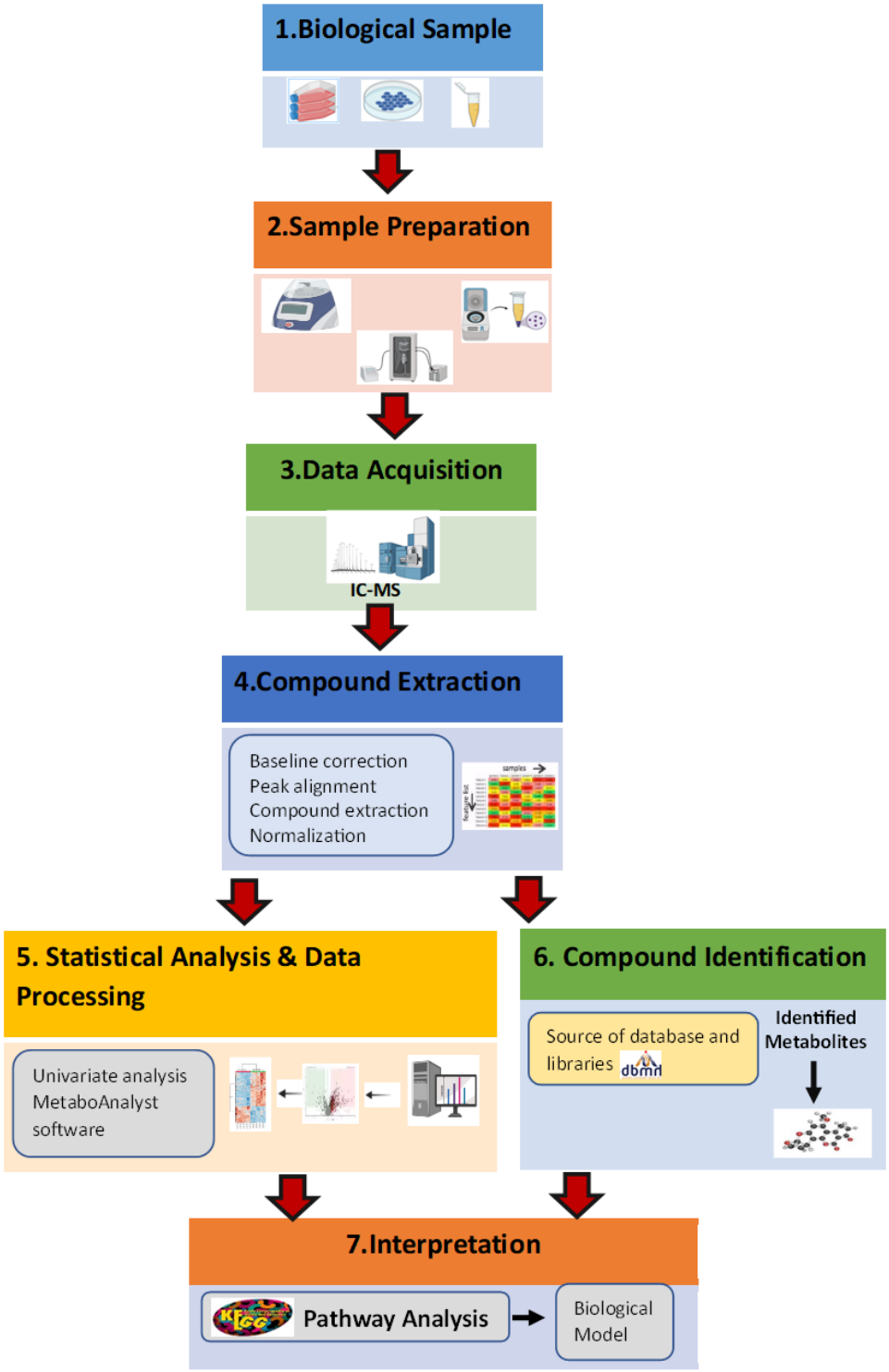


Figure 5.6.2: Experimental workflow for the metabolomics studies.

5.7 Metabolic changes in human kidney cells exposed to chronic hypobaric hypoxia (1% O_2)

5.7.1 Hypoxia (1% O_2) stabilizes HIF-1α

The levels of HIF-1α were measured in treated HEK 293T cell lysates using immunoblotting (see **Materials and Methods section 5.16.4** for details). **Figure 5.7.1** shows western blotting of HEK 293T cells lysates after treatment with 1% O_2, which leads to upregulation of HIF-1α after 24 hours of treatment.

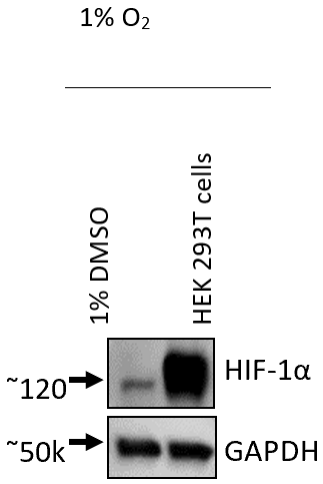


Figure 5.7.1: HIF-α stabilization after 24 h treatment of HEK 293T cells with 1% O_2.

To investigate the metabolic impact of hypobaric hypoxia, semi-targeted metabolomics was performed to compare HEK 293T cells grown in normoxia and 1% O_2. Cells were split into two groups. Cells were plated and treated with 1% O_2 for 24 hours in a hypoxic chamber; the control group was plated and grown in normoxia for 24 hours (**Figure 5.6.1)**. After cell

harvesting, metabolite extraction and preparation of samples followed by semi-targeted metabolomics, a total of 6,645 compound-features were measured and 182 metabolites were identified. The list of identified metabolites is provided in **Table A.7.3.**

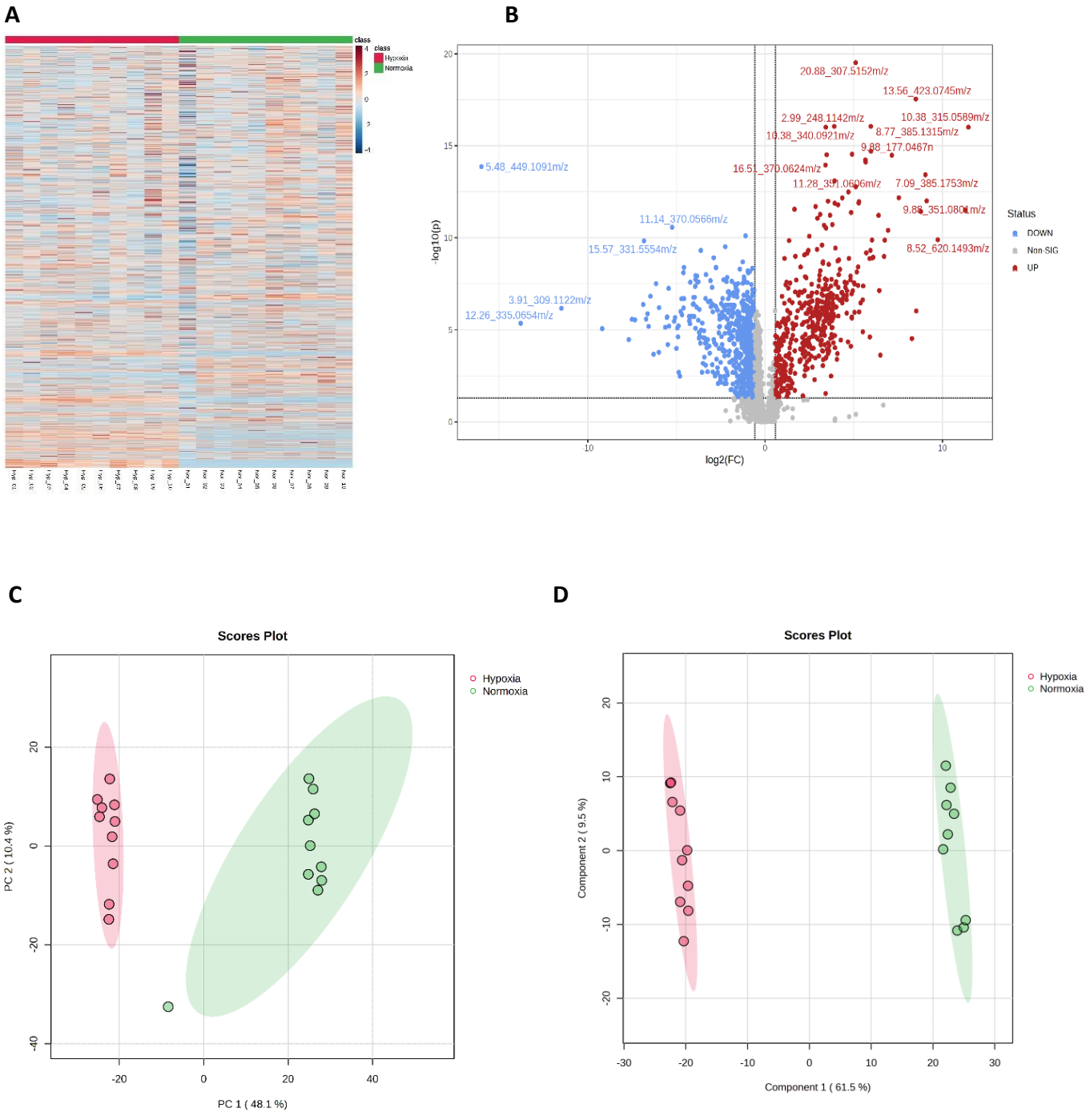
5.7.2 Metabolomics data quality

To evaluate the quality of the metabolomics dataset (which includes all the five experiments discussed in this chapter) and the impact of data processing parameters, quality control (QC) samples were included in the analytical sequence. Before investigating metabolic changes, the dataset was assessed for its overall quality and reproducibility. The following assessments were made: (1) whether sample outliers were present, (2) whether class bias was present (systematic differences between experimental groups), (3) whether there was evidence of any intensity drift across the analytical sequence (e.g. by comparing QC sample intensities across the sequence) and (4) the effect of data normalisation, transformation and scaling of the dataset to reduce any class bias and ensure the dataset was normally distributed. This was performed to satisfy the assumptions of various multivariate statistical tools used for subsequent data analysis (e.g. PCA analysis). All the expermental groups (control and treatment) have same number of repicates (n=10); however, outliers were discarded to avoid possible class biassness as apart of normalisation and scaling processes (as applied, e.g., in the data relevant to Figure 5.7.3.1.2, 5.8.3.1.1, 5.8.3.1.2, 5.10.2.1, 5.10.2.1.1 & 5.11.3.1). The normalisation and scaling processes are described in the **Materials and Methods section (Section 5.16.11)**.

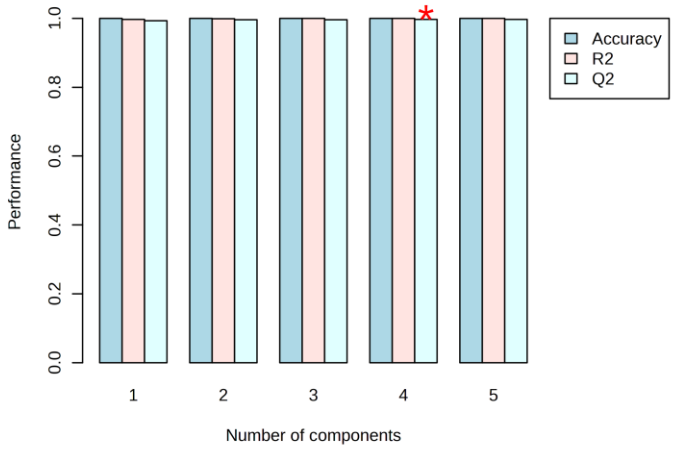
First, a heatmap of all compound features across all samples was extracted, along with a PCA

scores plot labeling the hypoxic and normoxic group separately **(Figure 5.7.3 A & C)**. In both representations of the dataset an outlier was apparent in the normoxia group (e.g. it was just outside the 95% confidence interval shaded in green on the PCA plot). This outlier was removed from subsequent data analyses. After assaying a number of data normalization approaches (**Figure A.7.10)**, the median normalization, log transformed, and pareto scaled methods showed a normal (or as close to normal) distribution for compound features and samples, therefore, the data was median normalized, log transformed, and pareto scaled **Figure 5.7.3.1 A**. No appreciable intensity drift was observed across QC samples **(Figure A.7.11 A & B).** These data together show no appreciable analytical or experimental biases suggesting its suitability for making biological interpretations.

5.7.3 Effects of hypoxia on human HEK293T cell metabolites



E



PLS-DA cross validation details:

Measure	1 comps	2 comps	3 comps	4 comps	5 comps
Accuracy	1.0	1.0	1.0	1.0	1.0
R2	0.99729	0.99894	0.9999	0.99999	1.0
Q2	0.99322	0.99592	0.99647	0.99655	0.99654

F

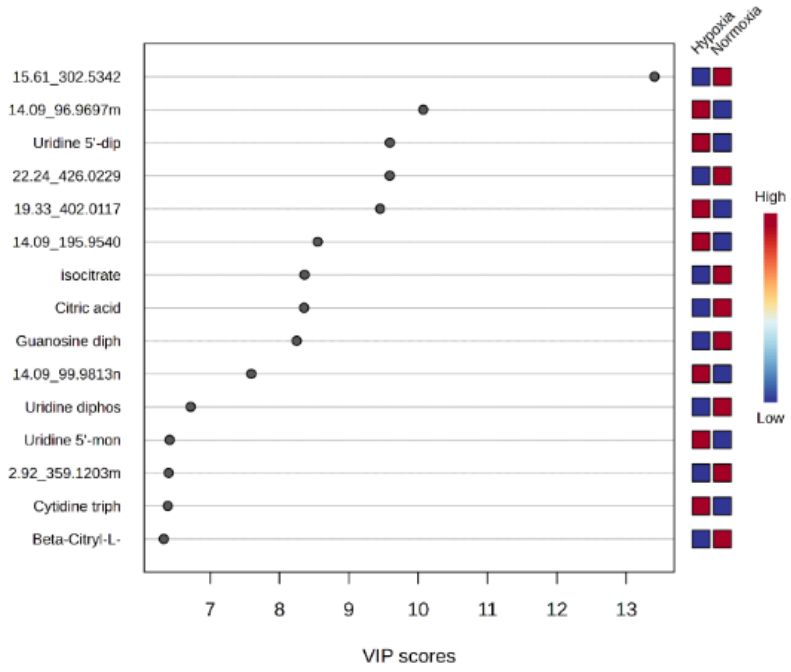


Figure 5.7.3.1: Analysis of hypoxia vs. normoxia group metabolomics. (a) Heatmap after normalization of IC-MS data for the hypoxic vs. normoxic group of HEK 293T cell metabolomics experiment. A red arrow indicates outliers in the normoxia group that were removed. N = 9 for the normoxia group and N=10 for the hypoxia group (unless an outlier was removed). (b) Volcano plot with a fold change (FC) threshold level of 1.5 and the FDR corrected p-value cut off < 0.05. Both FC and p values were log transformed. (c) PCA scores plot. (d) PLS-DA scores plot. (e) Measurement of the predictive accuracy of the model. (f) Top

15 important metabolites identified by VIP scores. The red & blue boxes show the relative concentrations of the corresponding metabolites in the hypoxia and normoxia groups.

5.7.3.1. Metabolic changes under hypoxia (1% O_2)

In order to explore the effects on metabolism when cells are grown in hypoxia compared to normoxia, t-tests were performed (with FDR correction for multiple testing) and fold-change analysis of all compound-features found across the hypoxic and normoxic group.

A volcano plot was generated using MetaboAnalyt 5.0 to visualize the results **(Figure 5.7.3.1B)**. The volcano plot analysis indicates that 1% O_2 in HEK 293T cells results in significant upregulation of a total of 503 identified metabolites and/or compound-features (significantly increased in abundance in hypoxia) and 630 downregulated identified metabolites and /or compound-features (significantly reduced in abundance in hypoxia) **Figure 5.7.3.1 B**). Among these, 64 were identified metabolites. A list of these significantly altered identified metabolites by volcano plot analysis is shown in **Table A 7.4.**

Figure 5.7.3.1.1 shows selected significantly altered metabolites identified by the volcano plot analysis. N-Carbamoyl-L-aspartic acid, fructose 1,6-bisphosphate, sedoheptulose 1-phosphate and aspartate were some high abundant metabolites identified in the hypoxia group compared to the control. NADH, isocitrate, beta-citryl L-glutamate and citric acid were some of the lower abundant metabolites identified in the hypoxia group compared to the control. Multivariant analysis (VIP plot and hierarchical cluster analysis (HCA)) identified patterns associated with these metabolites has been described later.

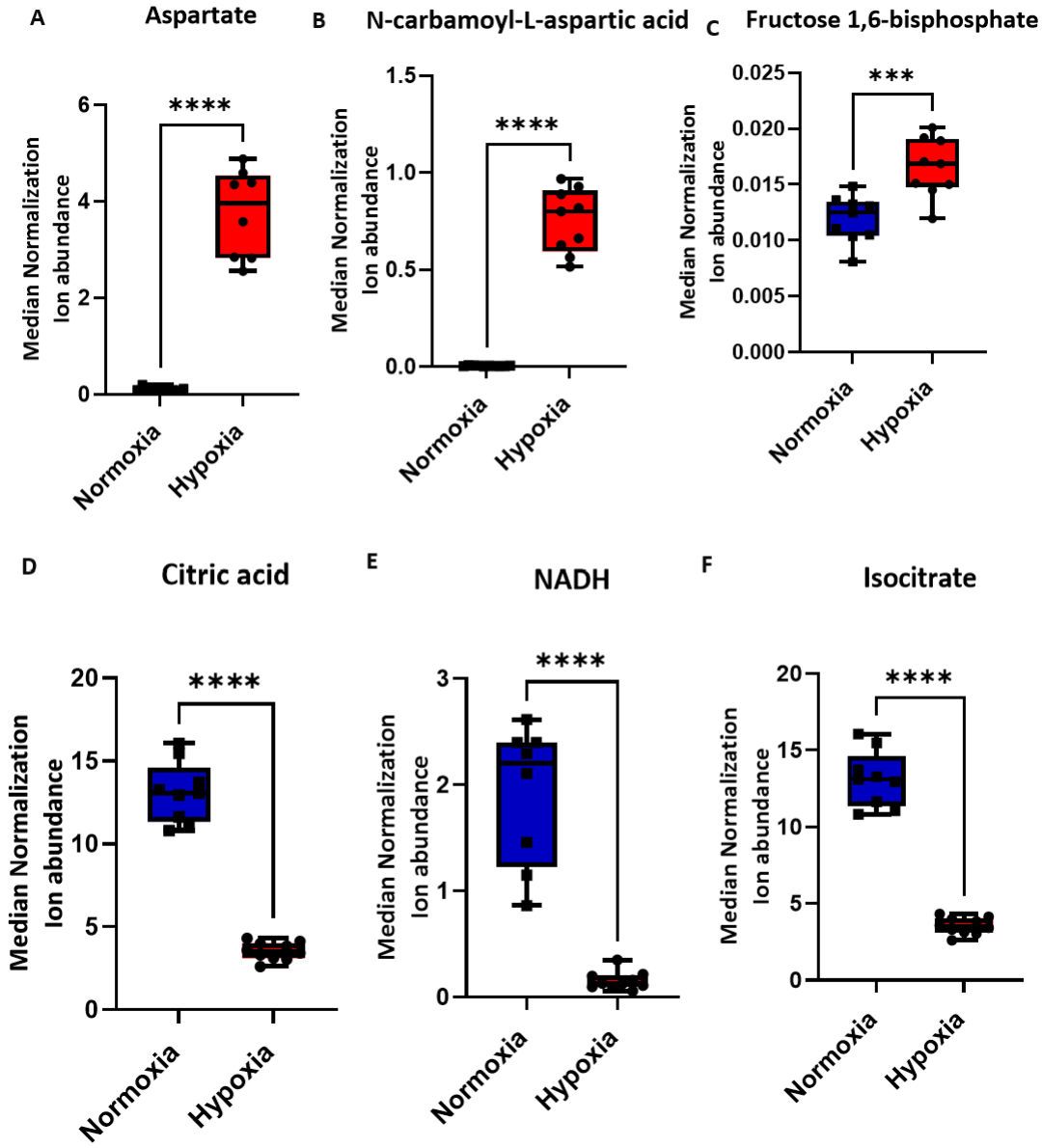


Figure 5.7.3.1.1: Selected significantly altered identified metabolites in HEK 293T cells treated with 1% O_2 and normoxia identified by volcano plot analysis. (A, B, and C) shows some of the higher abundance metabolites in HEK 293T cells when treated with 1% O_2. (D, E, and F) show some of the lower abundance metabolites in HEK 293T cells when treated with 1% O_2. The splitting line in the box represents the median value and the upper quantile of the box plot represents 75% of the data and the lower quantile represents 25% of the data. The p-value cutoff was <0.05. where * = p-value < 0.05 and ** = p-value < 0.01, *** = p-value < 0.001 and **** = p-value < 0.0001, calculated with a Tukey's test. N represents number of biological replicates, N= 8-10 for hypoxia and control group.

5.7.3.1.2 Glycolysis relevant changes due to hypoxia (1% O_2)

HIF-1α has been shown to promote glycolysis via transcriptionally up-regulating glycolytic enzymes and glucose transporters during hypoxia, (**Section 5.4.1)**, so stimulating increased flux through the glycolysis pathway [68]. This semi-targeted metabolomics analysis also explores glycolysis relevant changes in more detail in each dataset. The relative abundances of metabolites involved in the glycolytic pathways were compared between the hypoxic and normoxic conditions. Box plots for relevant metabolites are shown in **Figure 5.7.3.1.2.**

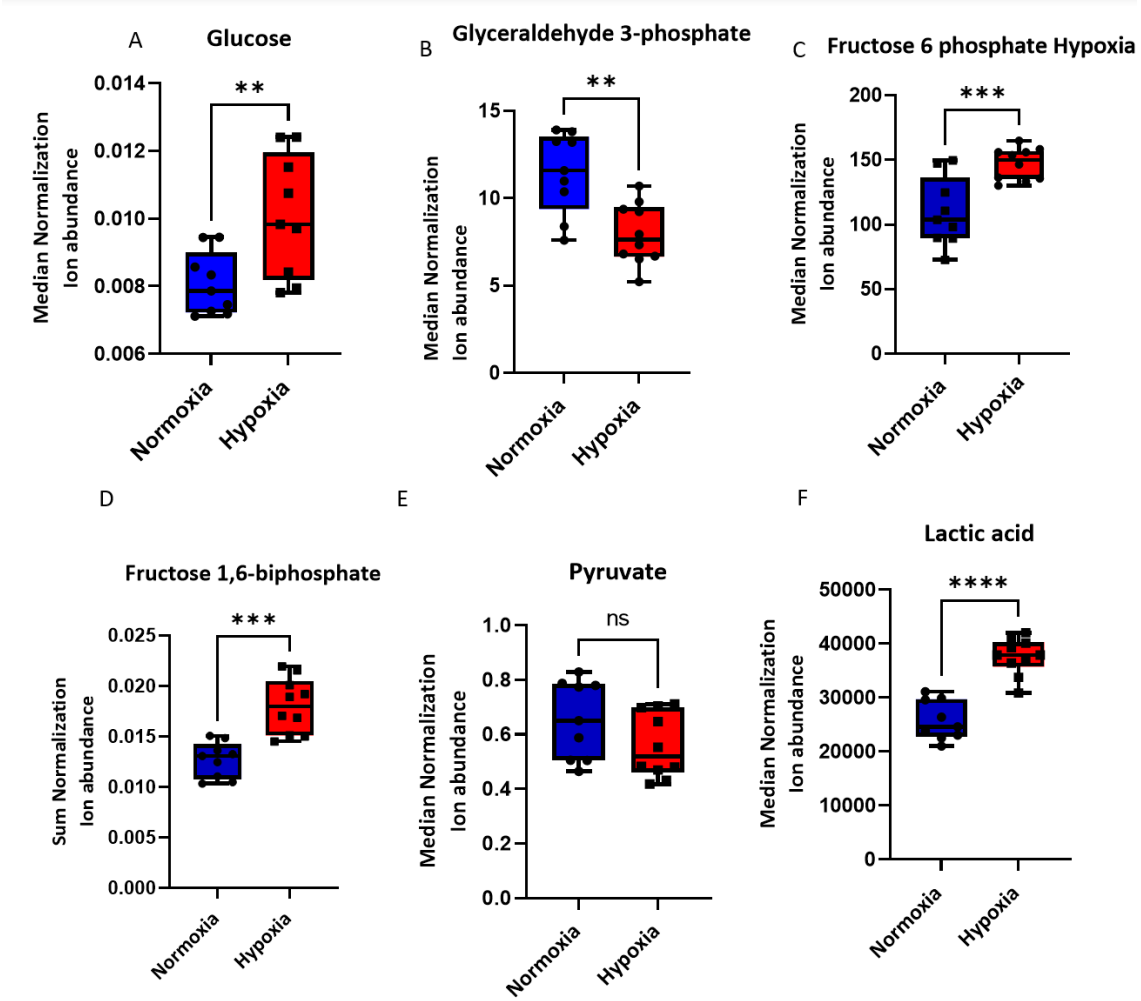


Figure 5.7.3.1.2: Box plot and whisker diagrams of metabolites involved in the glycolysis

comparing hypoxia and normoxia treated HEK 293T cells. A) Glucose, B) Glyceraldehyde 3-phosphate C) Fructose 6-phosphate D) Fructose 1,6-phosphate E) Pyruvate, and F) Lactic acid. The splitting line in the box represents the median value and the upper quantile of the box plot represents 75% of the data and the lower quantile represents 25% of the data. The p-value cutoff was <0.05. where * = p-value < 0.05 and ** = p-value < 0.01, *** = p-value < 0.001 and **** = p-value < 0.0001, calculated with a Tukey's test. N represents number of biological replicates, N= 9-10 for Roxadustat (100µM) and control group.

The key outcomes arising from comparing abundance changes of metabolites involved in the glycolysis pathway were:

1. All the glycolytic metabolites except pyruvate were significantly higher in abundance in the hypoxia treated HEK 293T cells group compared to the normoxia group.
2. The differences in pyruvate levels between the hypoxia and normoxia groups were not statistically significant (**Figure 5.7.3.1.2 E)**.

Table 5.7.3.1.1: Comparing fold changes in hypoxia and normoxia treated HEK 293T cell metabolites involved in the glycolysis pathway. (The p-value cutoff was <0.05. calculated with a Tukey's test.) (**Figure 5.7.3.1.2)**.

Metabolites	**Higher abundance**	**Fold Change**	**p-value**
Glucose	In hypoxia group	1.2	< 0.01
Glyceraldehyde 3-phosphate	In hypoxia group	1.3	< 0.01
Fructose 6-phosphate	In hypoxia group	1.5	< 0.001
Fructose 1,6-phosphate	In hypoxia group	1.6	< 0.001
Lactic acid	In hypoxia group	1.9	< 0.0001
Pyruvate	In normoxia group	Non-significant	-

5.7.3.2. Interpretation of univariate statistical analysis

The univariate analyses (statistical significance testing) outcomes showed that 1% O_2 leads to metabolomic changes compared to the normoxic group on HEK 293T cells. In particular, all the glycolytic metabolites, except pyruvate, were higher in abundance in the 1% O_2 treated group compared to the normoxia group **(Table 5.7.3.1.1)**. The glycolysis end product lactate was higher in abundance in the hypoxia group compared to the control therefore it can be stated that 1% O_2 treatment promotes glycolysis.

5.7.4 Patterns associated with altered metabolite profiles in hypoxia

Having established that extensive metabolite changes occurred in HEK293T cells treated with 1% O_2 lead to statistically significant changes in a range of identified metabolites including those found in glycolysis pathway, the metabolic phenotype was explored in more detail using multivariate data modelling. The PLS-DA scores plot showed a complete separation between the hypoxia and normoxia groups (first component/LV), (**Figure 5.7.3.1 D**). The separation in the scores plot suggested a metabolic difference between hypoxia and normoxia treated HEK 293T cells. Cross-validation of the model measured the accuracy where Q^2 and R^2 values inform how well the data is fitted to the model **(Figure 5.7.3.1 E). Figure 5.7.3.1 E** shows the results of the cross-validation with R^2 and Q^2 values for the first five components used to choose the ideal number of the components to be used in the PLS-DA model. Generally, the R^2 value should be above 0.7, and the Q^2 value should be close to R^2 value indicating that the data is a good fit for the model [75]. As the Q^2 score was within 0.20 of the R^2 score and the accuracy score was 1 for all five components,

this indicated a strong model of hypoxia compared to normoxia had been developed. **Figure 5.7.3.1 E** shows overall cross-validation results.

The variable importance in projection (VIP) is the score of individual features depending on their capability to create difference between groups; this score is the projection of its contribution to the PLS-DA model. A high VIP score indicates that specific metabolite have more influence in distinguishing between groups [76, 77]. The VIP score ranked a total of 8 identified metabolites and 7 compound features **Figure 5.7.3.1 D**. The eight identified metabolites were uridine 5'-diphosphate, uridine 5'-monophosphate, cytidine triphosphate, isocitrate, citric acid, guanosine diphosphate, uridine diphosphate and beta-citryl-L-glutamic acid [78]. These metabolites were predicted during volcano plot analyses (**Table A 7.4**).

The rest of the unassigned compound features did not provide any direct HMDB matches based on common adducts (M-H, M-2H, 2M-h, 3M-H and M-H_2O at 5 ppm accuracy). These are likely to be fragments of metabolites and/or other adduct forms.

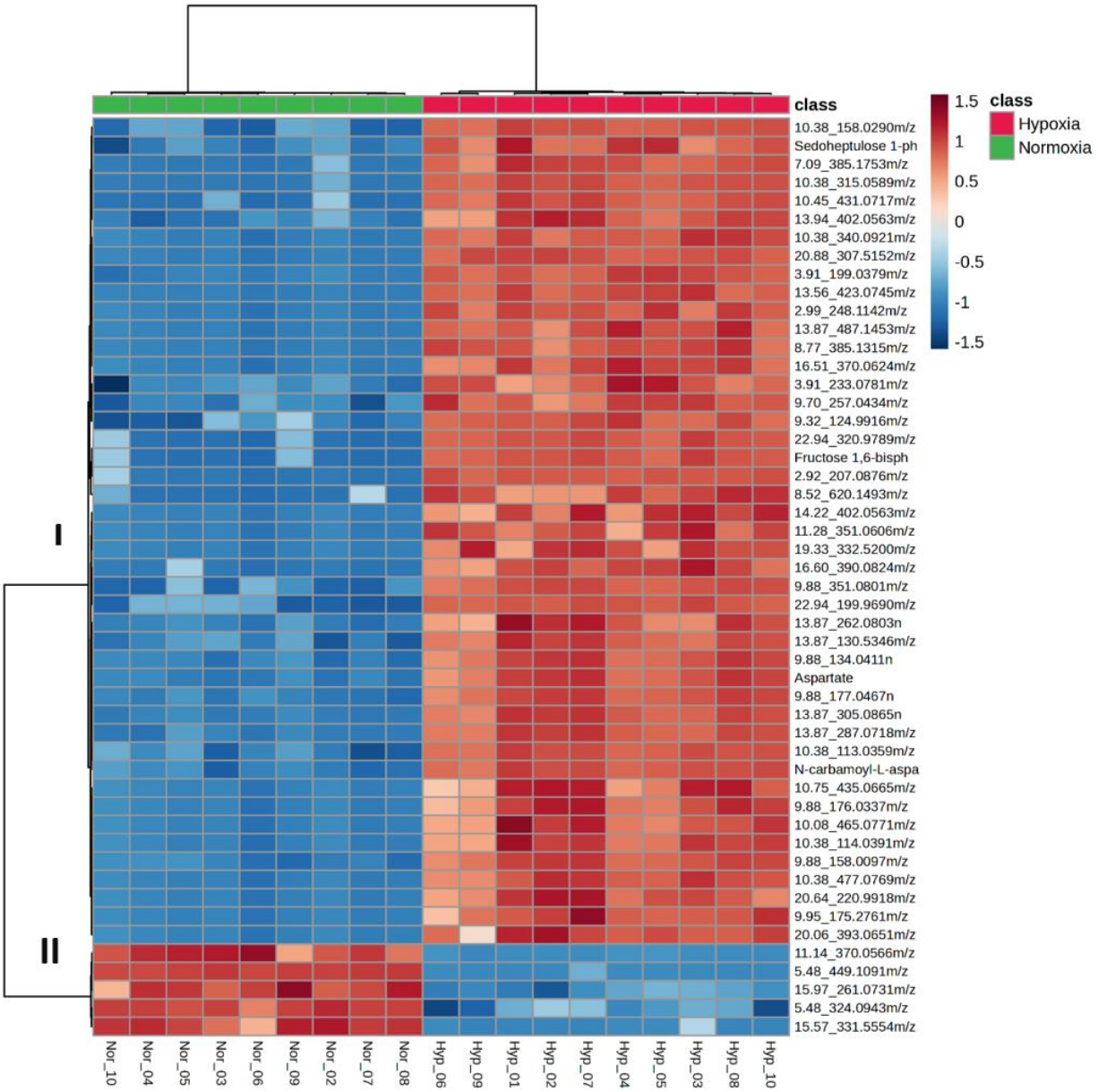


Figure 5.7.4.1: **Hierarchical cluster analysis (HCA) of hypoxia vs normoxia in HEK293T cell data collected by IC-MS analysis.** The HCA represents the top 50 significant features between the hypoxic and normoxic groups. Both features and samples were clustered. A dark blue colour indicates the lowest value and a bright red colour indicates the highest value. Light blue or red colours are used to specify middle values. Clusters of rows which show homogenous colours indicate similar values. Hierarchical clustering was used in combination with heat map analysis. The data were interquartile range filtered, median normalized, log transformation, and pareto scaled. N = 10 for hypoxia and normoxia HEK 293Tcell samples.

A hierarchically clustered heatmap was created showing the top 50 features/metabolites across the hypoxia and normoxia groups (**Figure 5.7.4.1**). Hierarchical cluster analysis helps to explore patterns and associations between different phenotypes by grouping samples with similar metabolic profiles, this can be helpful for identifying potential biomarkers or to explore the fundamental biological processes associated with a study. Hierarchical clustering helps to arrange features based on similarity or 'distance' between them. Hierarchical clustering can be used to identify clusters of rows with similar values, as these are demonstrated as areas of similar colour [79-81]. A hierarchical clustering heat map was created using MetaboAnalyst 5.0.

In the HCA, there were two main feature clusters (I) and (II). Both the main feature clusters (I) and (II), had elevated metabolite abundance in hypoxia relative to normoxia cells, the following identified metabolites were present in clusters (I): fructose 1,6-bisphosphate, and sedoheptulose 1-phosphate and in clusters (II): aspartate, and N-carbamoyl-L-aspartic acid **(Figure 5.7.3.1)**. A similar pattern of metabolite abundance was observed in the volcano plot analyses (**Table A 7.4**). The HCA map and volcano plot analyses showed a similar pattern of altered compound-features **(Figure 5.7.3.1 & 5.7.4.1)**. For instance, both the HCA map and volcano plot showed the following common compound-features: 20.88_307.5152m/z, 13.56_423.0745m/z, 2.99_248.1142m/z, 8.77_385.1315m/z, 10.38_340.0921m/z, 9.88_177.0467m/z, 16.51_370.0624m/z, 11.28_351.0606m/z, 7.09_385.1753m/z, 9.88_351.0801m/z and 8.52_620.1493m/z which were in elevated abundance and 15.57_331.5554m/z, 5.48_449.1091m/z, 11.14_370.0566m/z were in lower abundance in the

hypoxic group compared to control. However, the top 50 compound features did not provide any direct HMDB matches based on common adducts (M-H, M-2H, 2M-h, 3M-H and M-H_2O at 5 ppm accuracy). These are likely to be fragments of metabolites and/or other adduct forms.

5.7.5 Untargeted metabolic pathway analysis comparing hypoxic and normoxic HEK 293T cells

Untargeted and semi-targeted mass spectrometry-based metabolomics generates data on very large numbers of compound-features, whose changes in abundance are assumed to reflect functional changes in metabolism; a major challenge remains, however, in identifying the particular metabolites these measured compound-features represent [82, 83]. This means that although untargeted metabolomics is effective at demonstrating altered metabolic phenotypes, and even in identifying specific biomarkers at the compound-feature level, a bottleneck to the functional interpretation of metabolic changes remains. Pathway analysis is commonly used for functional interpretation of metabolomics data [84] [85] and uses already available knowledge about biological pathways to map metabolites onto an appropriate pathway [86]. Conventional pathway analysis addresses functional interpretation of results but is limited by the number of identified metabolites. Untargeted pathway analysis, on the other hand, is designed to translate information directly from compound-features profile changes to metabolic pathways (without the need for formal identification in-between), thus removing the bottleneck in functional interpretation of metabolomics

datasets. Untargeted pathway analysis maps *m/z* values directly to metabolic pathways by statistically fitting the data to an organisms-specific metabolic network. [37]. The work described here applies untargeted pathway analysis to support the biological interpretation of altered metabolism identified in hypoxia.

5.7.5.1. Data processing and analysis of pathway analysis of 1% O_2 experiment

During pathway analysis of the 1% O_2 experiment for pathway analysis the "functional analysis" methodology of MetaboAnalyst 6.0 was conducted [37].

5.7.5.1.1 Mummichog Pathway Analysis

MetaboAnalyst 6.0 software, was used for the application of mummichog to predict pathway activities from IC-MS peaks. To perform functional analysis with mummichog, *m/z* values and RT values are required. The mummichog algorithm also requires a p-value, with the default p-value being set at 0.05 [74]. In mummichog, a scatter plot is used to show pathway activities. The x-axis of the scatter plot represents the 'enrichment Factor', while the y-axis represents '-log10(P)' [74].

5.7.5.1.2 Mummichog Pathway Analysis Results

The mummichog analysis generated a table with ranked pathways, the number of metabolite matches (hits), and the expected number of hits per pathway (total hits) along with the statistical significance of the results calculated at a pathway level.

The mummichog analysis of 1% O_2 experiment ranked a total of 103 pathways with 15 predicted to be significantly altered based on the expression analysis systemic explorer (EASE) score adjusted p-value (< 0.05). **Table 5.7.5.1.2.1** shows the top 10 ranked pathways hierarchical by p-value (based on EASE score); the pathways are given in **Table A.7.5**. The mummichog analysis provides a list of KEGG metabolite codes (**Table A.7.5** shows the KEGG metabolite codes). **Figure 5.7.5.1.2.1** shows -log(p) versus enrichment factor plot for hypoxia vs normoxia pathway. This analysis relates pathway significance (e.g. how significant alterations are to the pathway as a single unit) with the enrichment (using hypergeometric testing to assess over-representation at the pathways level) [87].

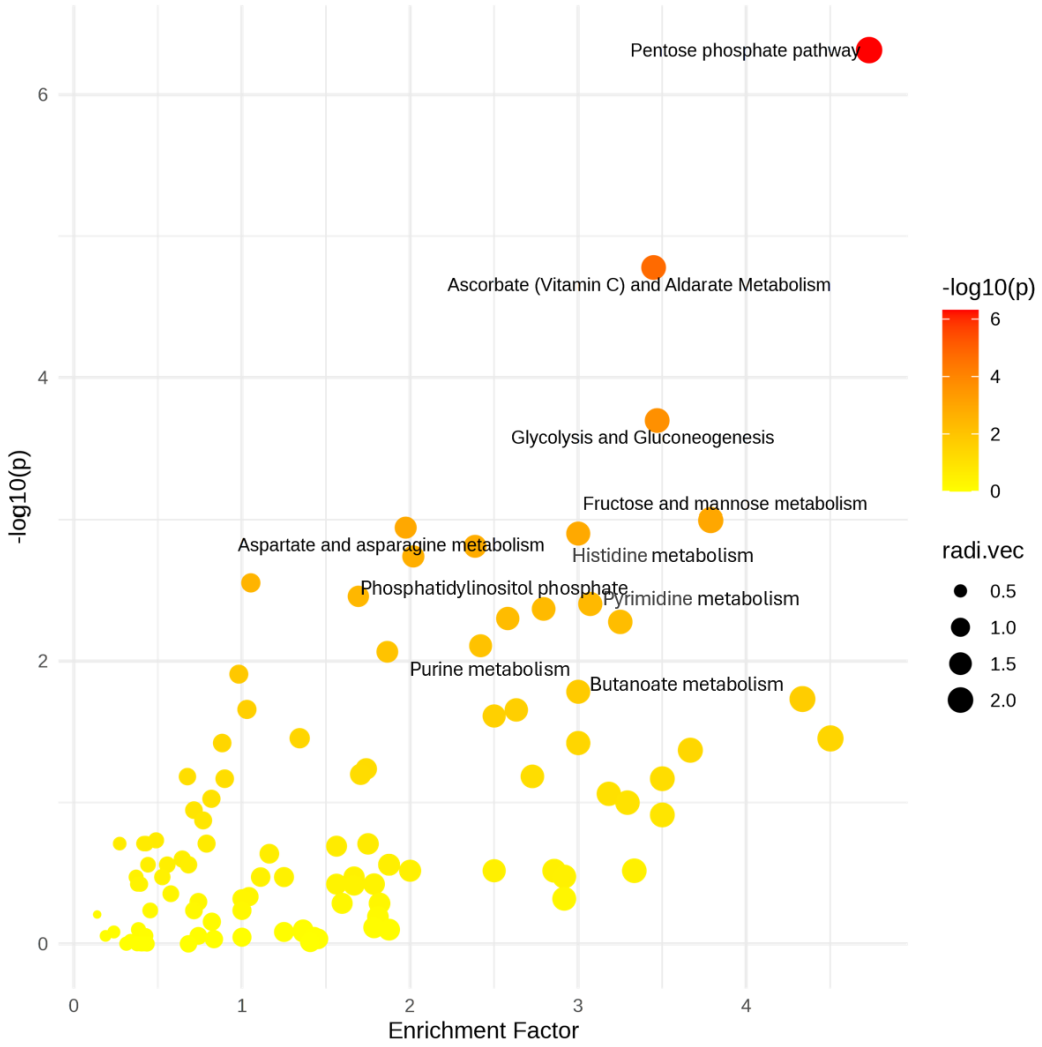


Figure 5.7.5.1.2.1: Summary of Hypoxia vs Normoxia Mummichog Pathway Analysis with HEK 293T cells. Circles represent matched pathways. The ratio of significant pathway hits and probable compound hits within a pathway is used to calculate the enrichment factor. The intensity of colour represents p-value, and the size of the circle represents the enrichment factor. Pathway analysis was conducted using the MetaboAnalyst 6.0 software.

Table 5.7.5.1.2.1: Top 10 significantly altered metabolic pathways ranked by mummichog analysis. The significance was calculated using the EASE score; the p-value cutoff was < 0.05.

Pathway Name	Pathway total	Hits total	Hits significant	P(EASE)
Pentose phosphate pathway	37	37	31	1.59E-05
Glycolysis and Gluconeogenesis	49	39	32	2.70E-05
Ascorbate (Vitamin C) and Aldarate Metabolism	29	20	18	0.000185
Aspartate and asparagine metabolism	114	54	39	0.000584
Fructose and mannose metabolism	33	29	23	0.001048
Histidine metabolism	33	20	17	0.001218
Pyrimidine metabolism	70	54	37	0.003858
Phosphatidylinositol phosphate metabolism	59	27	20	0.009139
Butanoate metabolism	34	22	16	0.02576
Purine metabolism	80	56	35	0.038113

Metabolic pathway analysis predicted a broad range of altered metabolic pathways, commensurate with the strong metabolic phenotype as was indicated by multivariate modeling and individual metabolite abundance changes observed from univariate statistical analysis. The top five pathways identified were the 'pentose phosphate pathway' (PPP), 'glycolysis/gluconeogenesis' (Glycolysis), ascorbate and aldarate, aspartate and asparagine, and fructose and mannose metabolism suggesting these were the most significantly perturbed pathways in HEK293T cells when exposed to hypoxia (**Figure 5.7.5.1.2.1**). Previously, researchers have reported metabolomics studies that show hypoxia significantly impacts glycolysis/ gluconeogenesis and the pentose phosphate pathway [70, 73]. Valdés et al. reported that hypoxia enriches the following pathways: 1. glycolysis or gluconeogenesis

pathway, 2. the fructose and mannose metabolism, 3. pentose phosphate pathway; and 4. alanine, aspartate, and glutamate metabolism [71]. None have done so using the IC-MS platform, however. The results reported here support this prior work and additionally reveal that histidine, pyrimidine, and purine metabolism are significantly impacted in hypoxia versus normoxia treatment of HEK293T cells (**Figure 5.7.5.1.2.1**). Gao et al., have reported that hypoxia can dysregulate several metabolic pathways via analysis of human plasma samples, including purine, histidine, and ascorbate metabolism [70]. Cohen et al. found that the glycine-serine-threonine, alanine-aspartate-glutamate, arginine pathways and ascorbate, and purine metabolism are altered in hypoxia [72]. The pyrimidine de novo synthesis pathway is linked with the use of oxygen and mitochondrial respiration. Under hypoxia, pyrimidine de novo synthesis plays a pioneer role in cell growth and reproduction [88-93]. Other significant pathways predicted to be altered were butanoate and phosphatidylinositol phosphate metabolism (**Table 5.7.5.1.2.1**).

The butanoate and propanoate pathways include short-chain fatty acid (SCFA) metabolism [94]. SCFAs include acetate, propionate, and butyrate, which when found in human body are usually supplied by the gut microbiome via fermentation of dietary fibers [69, 94]. However, HEK 293T cells used in this metabolomic study weren't cultured with bacteria hence altered butanoate metabolism may be due to hypoxia treatment. Butanoate and propanoate pathways also involve succinate and succinate semialdehyde alongside acetyl-CoA metabolism, which may contribute significantly to the cellular response, possibly by regulating the activity of HIF [94]. Under low oxygen conditions succinate levels can

increase and trigger adaptations to hypoxia, including increased glycolysis and angiogenesis [95].

5.7.6. Summary of semi-targeted metabolomics results comparing HEK293T cells in normoxia and hypobaric hypoxia.

To investigate the effect of hypoxia on the regulation of HIF-1α on HEK 293T cells a semi-targeted metabolomics method was applied. Before the metabolomics experiment, a western blot experiment was conducted on HEK 293T cells to ensure 1% O_2 stabilizes HIF-1α.

As a part of maintaining overall dataset quality and to ensure normalization of data, one outlier was removed from the dataset based on PCA & HCA analysis. PLS-DA cross-validation of the model was conducted to measure the accuracy of the model. The overall R^2 value was above 0.7, and the Q^2 value was close to R^2 value, and the accuracy score was 1 for all five components, indicating that the data is a good fit for the model.

Volcano plot analysis showed 1% O_2 can significantly upregulate and downregulate the number of metabolites in HEK 293T cells. Multivariate analyses were performed to find out any metabolic phenotype associated with 1% O_2. Multivariate models (PLS-DA and HCA) were used to identify features with patterns of interest. A similar pattern of altered metabolites was observed in volcano plot and VIP plot analyses. Volcano plot analysis predicted some metabolites, including uridine 5'-monophosphate, cytidine triphosphate, isocitrate, citric acid, guanosine diphosphate, uridine diphosphate and beta-citryl-L-glutamic acid (**Table A.7.4**) which were identified by VIP plot as well. Uridine 5'-diphosphate, uridine 5'-monophosphate, and cytidine triphosphate were higher in abundance and isocitrate, citric acid, guanosine diphosphate, and

beta-citryl-L-glutamic acid were lower in abundance in the hypoxia group than the control group, in volcano plot analysis. A similar pattern of altered metabolites was observed in the HCA map and volcano plot analyses. For example, fructose 1,6-bisphosphate, sedoheptulose 1-phosphate, aspartate, and N-carbamoyl-L-aspartic acid were higher in abundance in hypoxia group than control group by both volcano and HCA map analysis.

Glycolytic metabolites (glucose, glyceraldehyde 3-phosphate, fructose 6-phosphate, fructose 1,6-phosphate, and lactic acid), except pyruvate, were significantly higher in abundance in the hypoxia treated HEK 293T cells group compared to the normoxia (control) group. From the results it can be stated that hypoxia induces increased glycolytic flux as an adaptation to O_2 deficit.

MetaboAnalyst offers 'functional analysis' as a tool to execute untargeted pathway analysis. Here mummichog pathway analysis suggested that hypoxia can significantly alter several metabolic pathways including 'pentose phosphate pathway' (PPP), 'glycolysis/gluconeogenesis' (Glycolysis), ascorbate and aldarate, aspartate and asparagine, and fructose and mannose metabolism.

5.8 Metabolic changes in HEK 293T kidney cells associated with $CoCl_2$(150µM)

5.8.1 $CoCl_2$ (100, 150 & 200 µM) stabilizes HIF-1α

$CoCl_2$ treatment leads to upregulation of HIF-1α when HEK293T cells were treated for 24 hours. **Figure 5.8.1** shows, the accumulation of HIF-1α on HEK 293T cells after $CoCl_2$ (100, 150 & 200 µM) treatment.

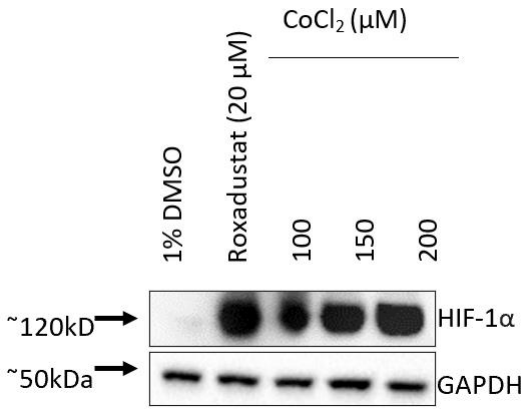


Figure 5.8.1: HIF-α stabilization after 24 h treatment of HEK 293T cells with 200, 150 & 100 µM $CoCl_2$. All treatments lead to upregulation of HIF-α. 150µM of $CoCl_2$ was used for semi-targeted metabolomics analysis, 100µM of $CoCl_2$ was used for Seahorse analysis, and 100 & 200 µM of $CoCl_2$ were used for reverse transcription-quantitative polymerase chain analysis (RT-qPCR) analysis.

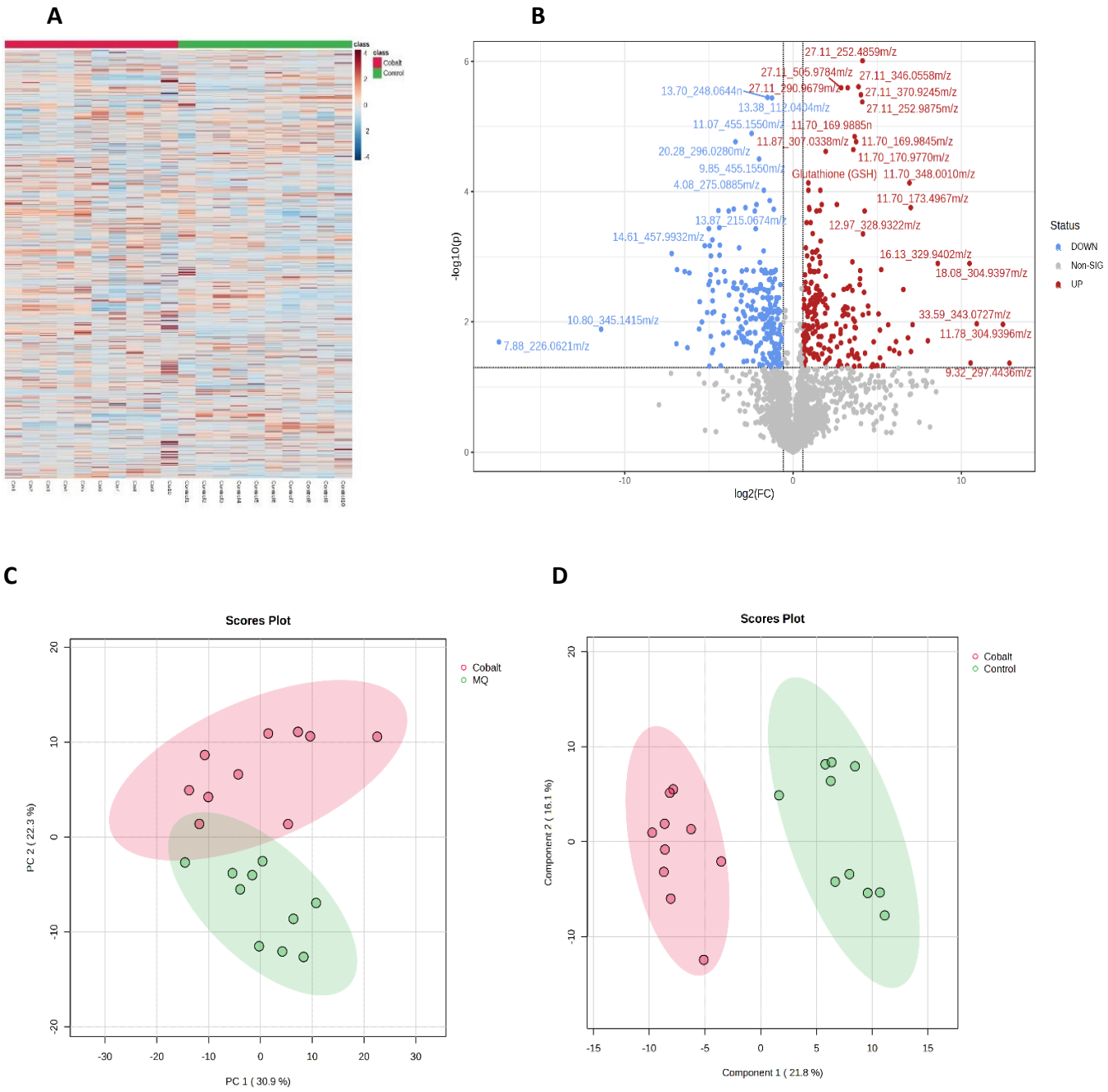
To assess the impact of $CoCl_2$ treatment on downstream metabolism (enabling a comparison with the effects of hypobaric hypoxia) semi-targeted metabolomics was performed comparing HEK 293T cells treated with 150 µM $CoCl_2$ comparing with untreated cells for 24 hours (n=10 per group). After cell harvesting, metabolite extraction and preparation of samples followed by semi-targeted metabolomics, a total of 5560 compound-features were measured and 176 metabolites were identified. The list of identified metabolites is provided in

Table A 7.6.

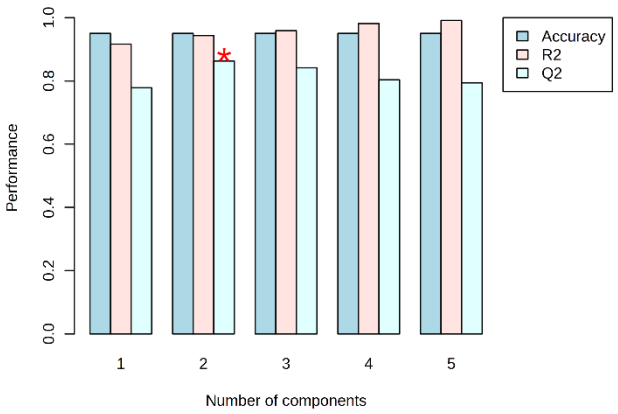
5.8.2 Metabolomics data quality

A heatmap of all compound-features across all samples was extracted **(Figure 5.8.3.1 A.)**, along with a PCA scores plot labelling the $CoCl_2$ treated and control group **(Figure 5.8.3.1 C).** Data normalisation and transformation and scaling were performed (**Figure A.7.11 & Figure A.7.12)**, no outlier removal or drift correction was performed. Sum normalized, and pareto scaling (**Figure A.7.12)** showed normal (or as close to normal) distributions of features and samples.

5.8.3 Effect of 150μM of $CoCl_2$ on human metabolites in HEK 293T cells



E



PLS-DA cross validation details:

Measure	1 comps	2 comps	3 comps	4 comps	5 comps
Accuracy	0.95	0.95	0.95	0.95	0.95
R2	0.91585	0.94319	0.95889	0.98135	0.99121
Q2	0.77835	0.86257	0.8418	0.80384	0.79339

F

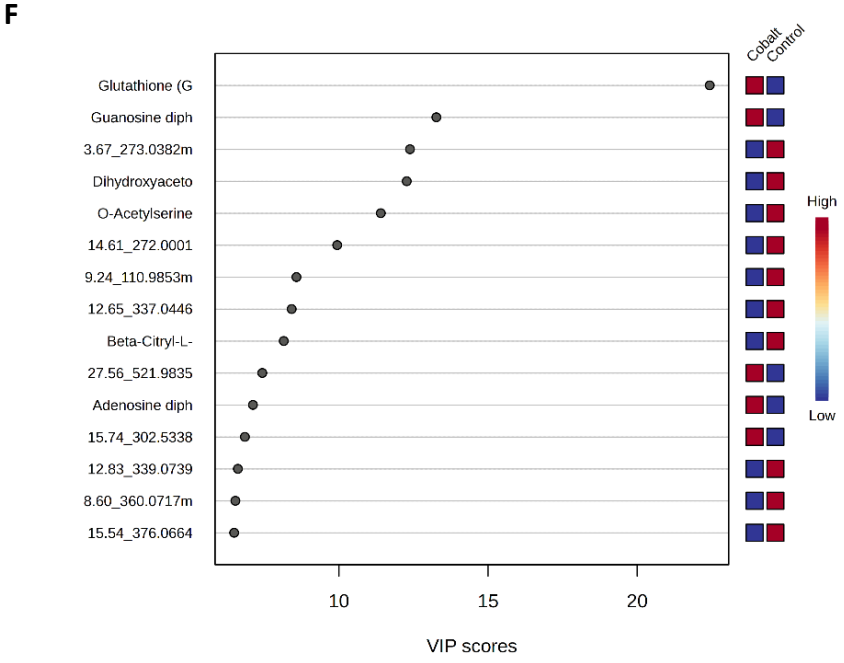


Figure 5.8.3.1: Analysis of hypoxia mimic agent $CoCl_2$ versus control group. (a) Heatmap after normalization of IC-MS data from hypoxia mimic agent $CoCl_2$ vs control group of HEK293T cell metabolomics experiment. N = biological replicates and N = 10 for $CoCl_2$ and control group. (b) Volcano plot with a fold change (FC) threshold level of 1.5 and the FDR corrected p value cut off < 0.05. Both FC and p values were log transformed. (c) PCA scores plot. (d) PLS-DA scores plot. (e) Measurement of the predictive accuracy of the model. (f) Top 15 important metabolites identified by VIP scores. The red & blue boxes show relative concentrations of the corresponding metabolites in the $CoCl_2$ and the control group.

5.8.3.1 Metabolic changes associated with $CoCl_2$ treatment

In order to explore which metabolites were altered in cells grown with $CoCl_2$ treatment compared to the control (untreated), t-tests were performed with FDR correction for multiple tresting and fold-change analysis of all compound-features found across the 150 µM of $CoCl_2$ and control groups. A volcano plot was generated using MetaboAnalyt 5.0 to visual the results **(Figure 5.8.3.1)**. The volcano plot analysis revealed that treating cells with 150 µM of $CoCl_2$ significantly upregulated a total of 257 identified metabolites and/ or compound-features (significantly increased in abundance in $CoCl_2$ group) and downregulated 267 identified metabolites and/ or compound-features (significantly reduced in abundance in $CoCl_2$ group) (**Figure 5.8.3.1 B**). Among them 21 of them were identified metabolites and a list of these significantly altered identified metabolites by volcano plot analysis is shown in **Table A 7.7.**

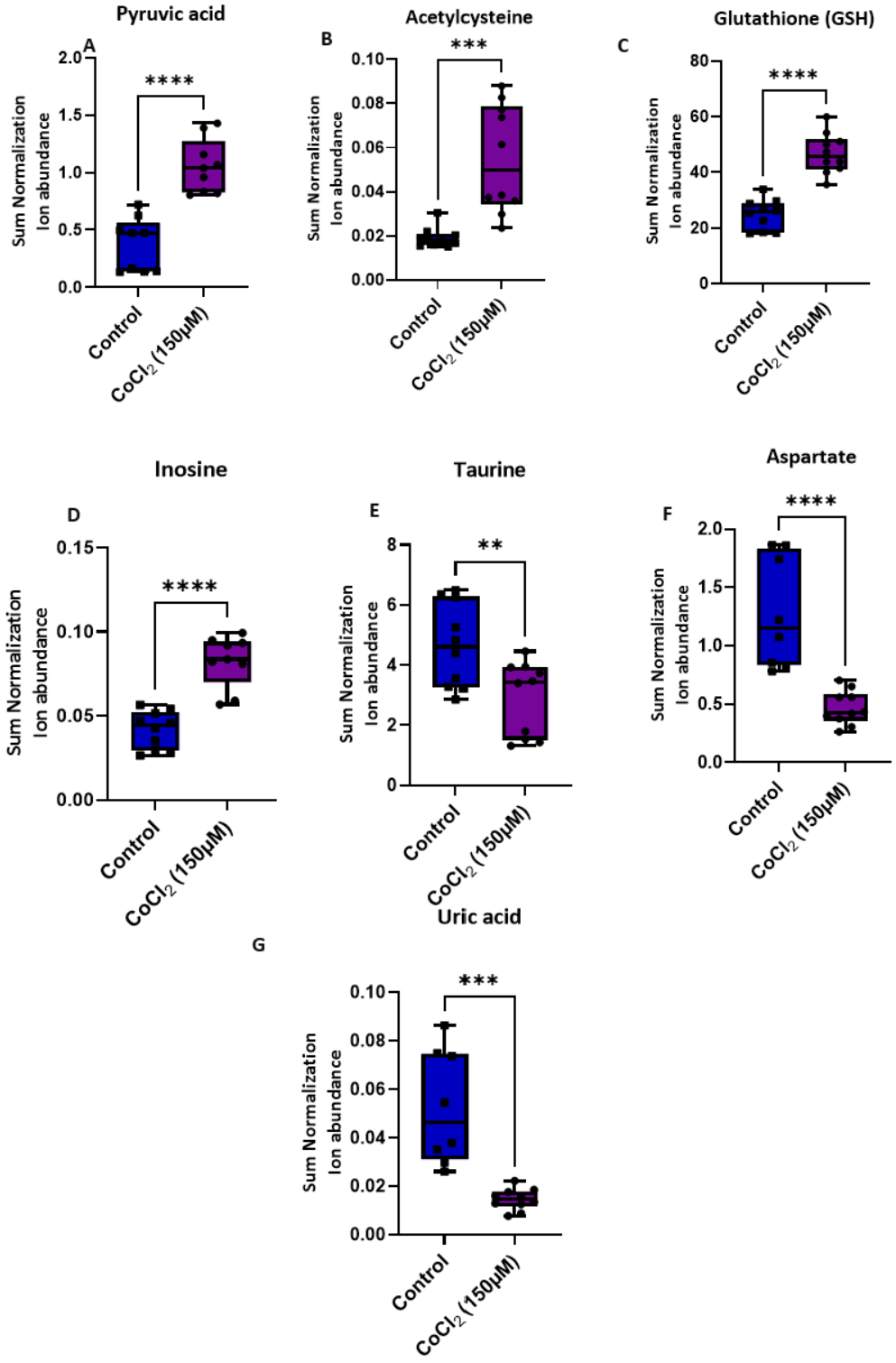


Figure 5.8.3.1.1: Significantly altered identified metabolite in HEK 293T cells identified by volcano plot analysis when treated with $CoCl_2$ (150μM) and control. (A, B, C, & D) showing

some of the higher abundance metabolites in HEK 293T cells when treated with $CoCl_2$ (150µM). (E, F and G) showing some of the lower abundance metabolites in HEK 293T cells when treated with $CoCl_2$ (150µM). The splitting line in the box represents the median value and the upper quantile of the box plot represents 75% of the data and the lower quantile represents 25% of the data. The p-value cutoff was <0.05. where * = p-value < 0.05 and ** = p-value < 0.01, *** = p-value < 0.001 and **** = p-value < 0.0001, calculated with a Tukey's test. N represents the number of biological replicates, N= 8-10 for $CoCl_2$ and control group.

Figure 5.8.3.1.1 shows some significantly altered identified metabolites by the volcano plot. Acetylcysteine, pyruvic acid, glutathione, and inosine were some of the higher abundance metabolites and taurine, aspartate, and uric acid were some of the lower abundance metabolites in the $CoCl_2$ (150µM) group compared to the control. Further multivariant analysis (VIP plot and HCA map) showed similar patterns as discussed below.

5.8.3.1.2 Glycolysis relevant changes due to $CoCl_2$ (150µM) treatment

In order to explore glycolysis relevant changes in more detail from the given dataset the relative abundances of metabolites involved in the glycolytic pathways were compared between the $CoCl_2$ treated and untreated (control) group. Box plots for relevant metabolites are shown in **Figure 5.8.3.1.2.**

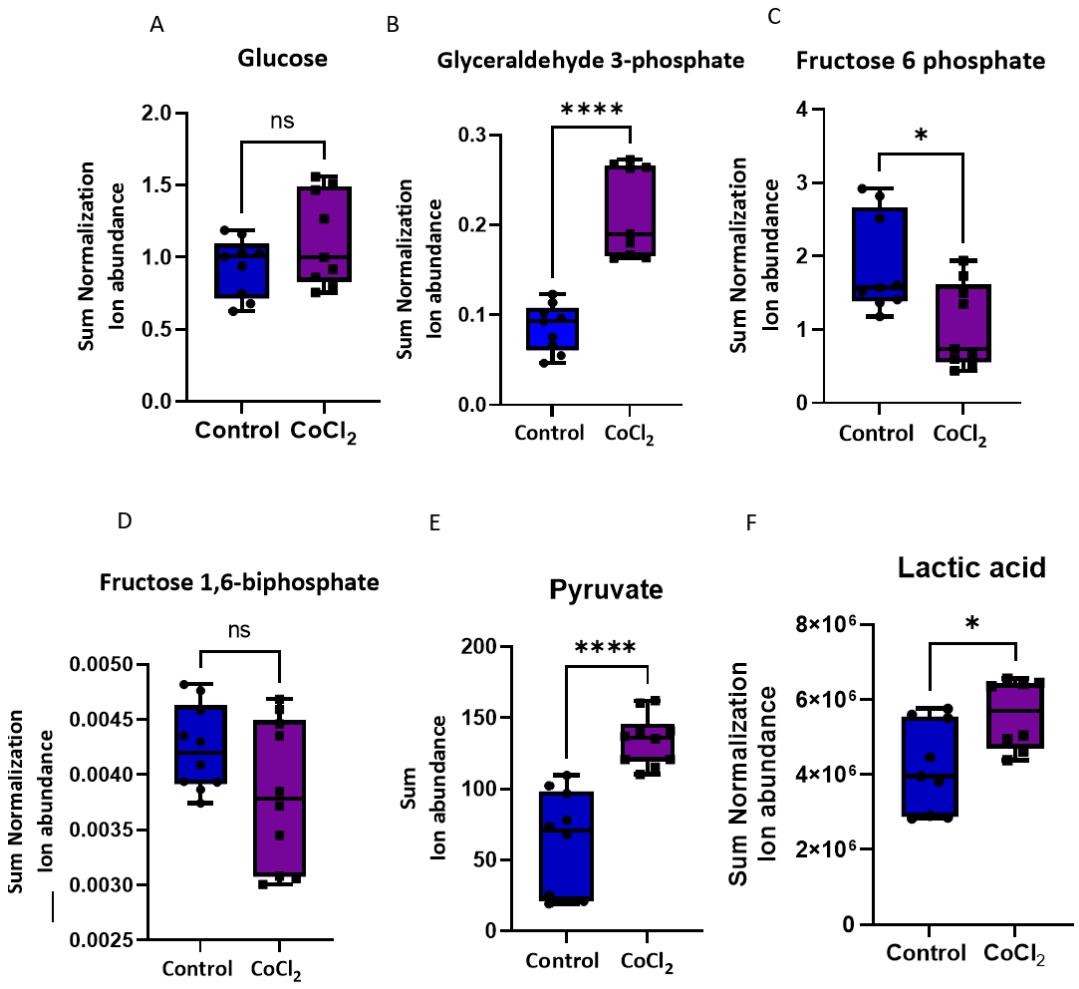


Figure 5.8.3.1.2: **Box plot and whisker diagrams of metabolites involved in the glycolysis pathway of $CoCl_2$, and control treated HEK 293T cells.** A) Glucose, B) Glyceraldehyde 3-phosphate C) Fructose 6-phosphate D) Fructose 1,6-phosphate E) Pyruvate, and F) Lactic acid. The splitting line in the box represents the median value and the upper quantile of the box plot represents 75% of the data and the lower quantile represents 25% of the data. The p value cutoff was <0.05. where * = p-value < 0.05 and ** = p-value < 0.01, *** = p-value < 0.001 and **** = p-value < 0.0001, calculated with a Tukey's test. N represents number of biological replicates, N=10 for $CoCl_2$ and the control group, and N=9 for the control group (for lactic acid).

The key outcomes arising from comparing abundance changes for metabolites involved in the glycolysis pathway were:

1. Glyceraldehyde 3-phosphate, pyruvate, and lactic acid were significantly higher in abundance in the $CoCl_2$ group than the control group (**Figure 5.8.3.1.2 B,E &F**).
2. Level of fructose 3-phosphate and fructose 1,6 biphosphate were lower in abundance in $CoCl_2$ treated cells compared to the control group (**Figure 5.8.3.1.2 C**).
3. However, the changes in glucose and fructose 1,6 biphosphate levels in the $CoCl_2$ treated cells compared to control group were non-significant (**Figure 5.8.3.1.2 A & D**).

Table 5.8.3.1: Comparing fold change of $CoCl_2$ and control treated HEK 293T cell's metabolites involved in the glycolysis pathway. (The p-value cutoff was <0.05. calculated with a Tukey's test.) (**Figure 5.9.3.1)**.

Metabolites	**Higher abundance**	**Fold Change**	**p-value**
Glyceraldehyde 3-phosphate	In $CoCl_2$ group	2.5	p-value< 0.0001
Pyruvate	In $CoCl_2$ group	2.6	p-value < 0.0001
Lactic acid	In $CoCl_2$ group	1.7	p-value < 0.05
fructose 3-phosphate	In control group	1.8	p-value < 0.05
Glucose	In control group	Non-significant	
fructose 1,6 biphosphate	In control group	Non-significant	

5.8.3.2 Interpretation of univariate statistical analysis

The univariate analyses (statistical significance testing) outcomes showed that $CoCl_2$ (150µM) treatment leads to metabolomic changes compared to the control group on HEK 293T cells. In particular, glycolytic metabolites (glyceraldehyde 3-phosphate, pyruvate, and lactic acid) were higher in abundance in the $CoCl_2$ (150µM) treated group compared to the control group. Overall, it can be stated that $CoCl_2$ (150µM) increases glycolysis.

5.8.4 Patterns associated with altered metabolite profiles in $CoCl_2$

Multivariate data modelling was used to inspect the metabolic phenotype associated with the univariate analysis observed changes. PLS-DA in the $CoCl_2$ (150 µM) and control experiment was performed using MetaboAnalyst 5.0 software [77]. The PLS-DA scores plot showed a complete separation between the $CoCl_2$ (150 µM) and control group (**Figure 5.8.3.1 D),** implying the metabolic differences between the $CoCl_2$ (150 µM) and control treated HEK 293T cells. Cross-validation was performed before evaluating metabolic changes **(Figure 5.8.3.1 E)**. As the Q^2 score was within 0.20 of the R^2 score and the accuracy score was 0.95 for all the five components, it can be proposed that the data is a good fit for the model. **Figure 5.8.3.1 E** shows the overall cross-validation results.

The VIP score plot ranked a total of 6 identified metabolites and 9 compound features **(Figure 5.8.3.1 F)**. Among them, glutathione (GSH) was ranked highest in the VIP plot analysis. Other metabolites ranked by the VIP plot which were significant to create differentiates between the experimental groups were guanosine diphosphate (GDP), adenosine diphosphate (ADP),

dihydroxyacetone phosphate, O-acetylserine and beta-citryl-L-glutamic acid **(Figure 5.8.3.1 F)**. Glutathione (GSH) and O-acetylserine were predicted by volcano plot as well. Glutathione (GSH) was high in abundance and O-acetylserine was low in abundance in $CoCl_2$ treated HEK 293T cells compared to the control **(Table A.7.7).** It has been suggested in the literature that glutathione (GSH) has a role in HIF-1α regulation; there is, therefore, a possible correlation between HIF-1α stabilization and elevated levels of glutathione [96, 97].

The unassigned compound features did not provide any direct HMDB matches based on common adducts (M-H, M-2H, 2M-h, 3M-H and M-H_2O at 5 ppm accuracy). These are likely to be fragments of metabolites and/or other adduct forms.

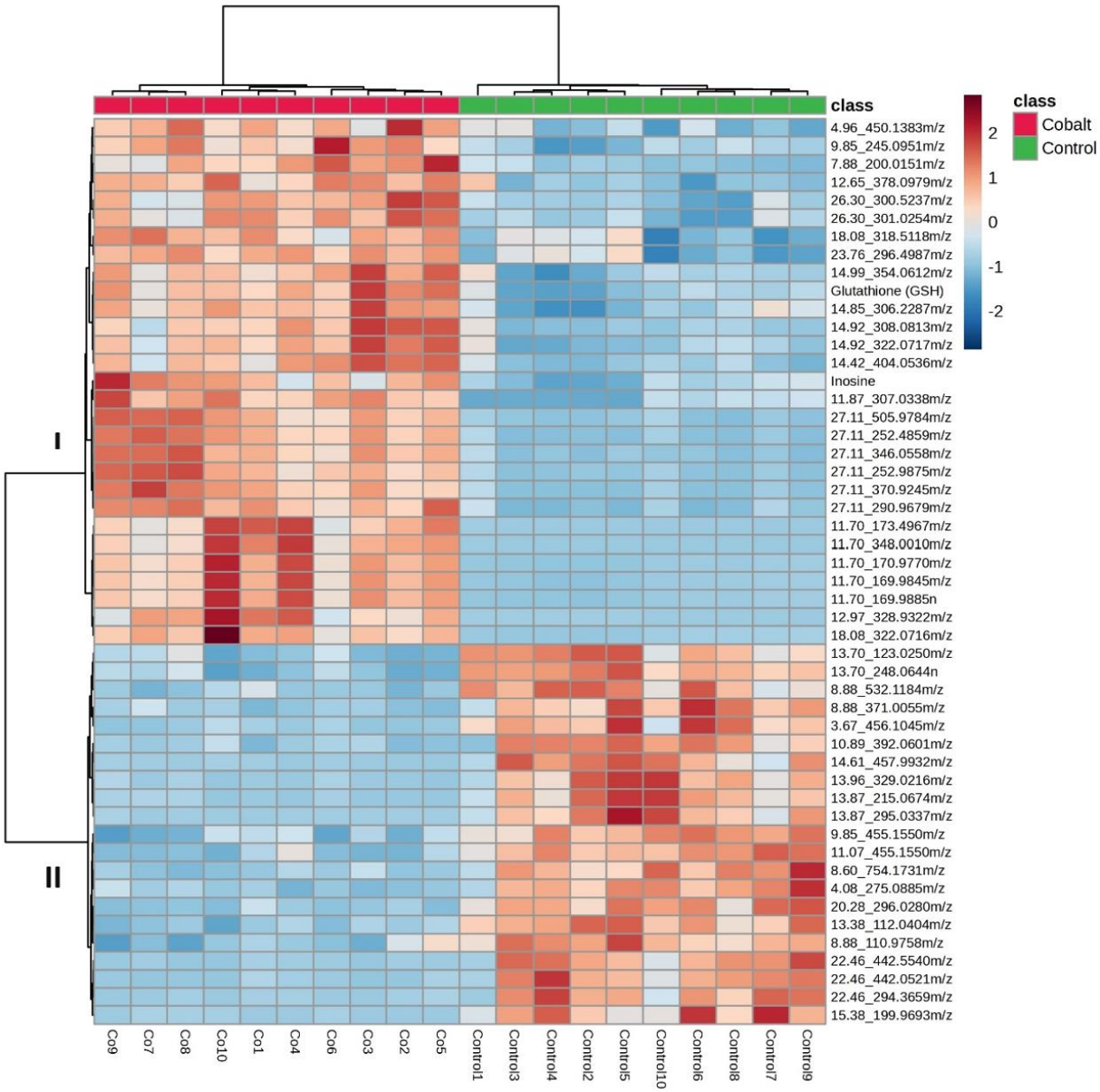


Figure 5.8.4.1: Hierarchical cluster analysis of $CoCl_2$ vs control in HEK293T cell data collected by IC-MS analysis. The HCA represents the top 50 significant features between the $CoCl_2$ vs control group. Both features and samples were clustered. The data was interquartile range filtered, sum normalized and pareto scaled. N = 10 for $CoCl_2$ and control HEK 293Tcell samples.

A hierarchical clustering heat map was created using MetaboAnalyst 5.0 analysis. Heat map analysis helped to show the graphical clustering of $CoCl_2$ compared to the control group (**Figure 5.8.4.1**). In the HCA, there were two main feature clusters (I) and (II). In the first main feature cluster (I), which had elevated metabolite abundance in $CoCl_2$ treated cells relative to control treated cells, the following identified metabolites were present: Glutathione (GSH) and inosine. As mentioned before, glutathione (GSH) was ranked first in VIP plot and was identified by both volcano and VIP plot analysis.

The HCA map and volcano plot analyses showed a similar pattern of impacts after $CoCl_2$ treatment **(Figure 5.8.3.1 & 5.8.4.1)**. For instance, compound-features such as 27.11_252.4859*m/z*, 27.11_505.9784*m/z*, 27.11_290.9679 *m/z*, 27.11_346.0558 *m/z*, 27.11_370.9245 *m/z*, 27.11_252.9875 *m/z*, 11.87_307.0338 *m/z*, , 11.70_169.9885n, 11.70_170.9770 *m/z*, 11.70_348.0010 *m/z*, and 12.97_328.9322 *m/z*, were higher in abundance in $CoCl_2$ treated HEK 293T cells group compared to the control, as identified by both HCA map and volcano plot analysis. Compound-features such as 13.70_248.0644n, 13.38_112.0404*m/z*, 11.07_455.1550*m/z*, 20.28_296.0280*m/z*, 9.85_455.1550*m/z*, 4.08_275.0885*m/z*, 13.87_215.0674*m/z*, 14.61_457.9932*m/z* were lower in abundance in $CoCl_2$ treated HEK 293T cells group compared to the control as identified by both HCA map and volcano plot analysis.

Compound feature, 27.11_346.0558 was putatively assigned 2'-deoxyguanosine 5'-monophosphate; compound features, 27.11_346.0558 had an isotope similarity (96%) as 2'-deoxyguanosine 5'-monophosphate with the ppm error being 0.234056846 for its formula. A

possible explanation for the RT value could be, 2'-deoxyguanosine 5'-monophosphate is a fragment of 2'-deoxyguanosine 5'-triphosphate. The retention time of 2'-deoxyguanosine 5'-triphosphate was confirmed using an authentic standard. The rest of the unassigned compound features did not provide any direct HMDB matches based on common adducts (M-H, M-2H, 2M-h, 3M-H and M-H_2O at 5 ppm accuracy). These could be fragments of metabolites and/or other adduct forms.

5.8.5 Untargeted metabolic pathway analysis of hypoxic HEK 293T cells.

Untargeted mummichog pathway analysis was conducted to assess metabolic changes at the pathway level when HEK 293T cells were treated with 150µM $CoCl_2$.

5.8.5 1 Data processing and analysis

During pathway analysis of 150µM of $CoCl_2$ experiment for pathway analysis the "functional analysis" methodology of MetaboAnalyst 6.0 was conducted [37].

5.8.5.2 Mummichog Pathway Analysis Results

The mummichog analysis ranked a total of 87 pathways with 12 of them predicted to be significantly altered based on the expression analysis systemic explorer (EASE) score adjusted p-value (< 0.05). **Table 5.8.5.2.1** shows the top 10 ranked pathways hierarchical by p-value (based on EASE score); and all pathways are given in **Table A.7.8**. The mummichog analysis

also provides a list of KEGG metabolite codes. **Table A.7.8** shows the KEGG metabolite codes.

Figure 5.8.5.2.1 shows -log(p) versus enrichment factor plot for the $CoCl_2$ (150 µM) vs control pathway analysis.

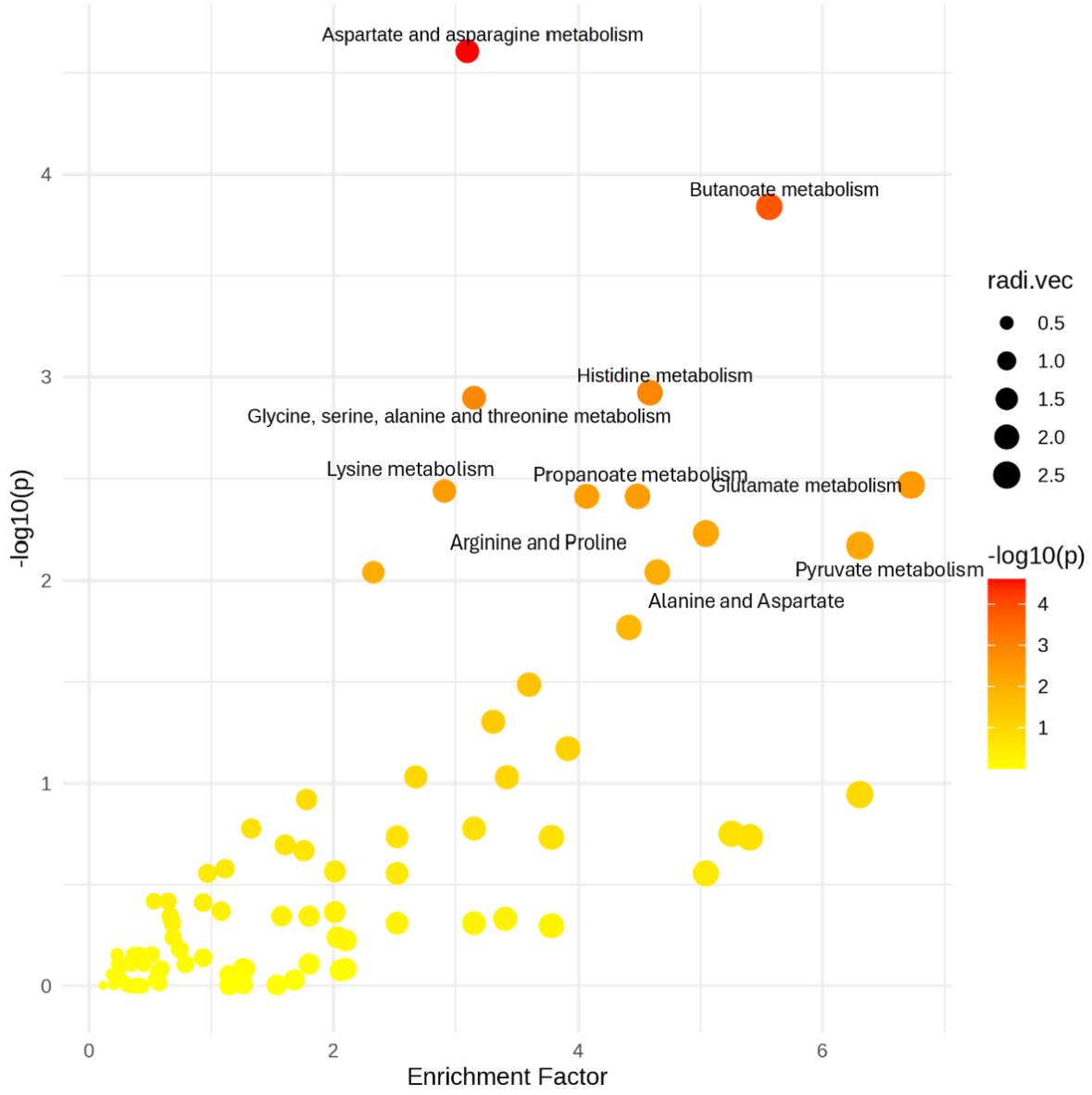


Figure 5.8.5.2.1: Summary of $CoCl_2$ vs control Mummichog Pathway Analysis with HEK 293T cells. Circles represent matched pathways. The ratio of significant pathway hits and probable compound hits within a pathway is used to calculate the enrichment factor. The intensity of colour represents the p-value, and the size of the circle represents the enrichment factor. Pathway analysis was conducted using the MetaboAnalyst 6.0 software.

Table 5.8.5.2.1: Top 10 significantly altered metabolic pathways ranked by mummichog analysis. The significance was calculated using the EASE score and the p-value cutoff was < 0.05.

Pathway Name	Pathway total	Hits total	Hits significant	P(EASE)
Aspartate and asparagine metabolism	114	54	28	7.53E-05
Butanoate metabolism	34	24	15	0.000645
Glycine, serine, alanine and threonine metabolism	88	47	22	0.003197
Histidine metabolism	33	20	12	0.004791
Arginine and Proline Metabolism	45	33	16	0.010408
Lysine metabolism	52	22	12	0.012067
Propanoate metabolism	31	17	10	0.014749
Glutamate metabolism	15	12	8	0.016639
Alanine and Aspartate Metabolism	30	23	12	0.017927
Pyruvate Metabolism	20	18	10	0.022959

The results from mummichog pathway analysis show:

1. Aspartate and asparagine metabolism, histidine metabolism and butanoate metabolism pathways were significantly altered with $CoCl_2$ vs control treatment. These pathways were also significantly altered with 1% O_2 vs normoxia treatment.
2. **Section 5.4.2 & 5.7.5.1.2** discussed how hypoxia/HIF-induced hypoxia impacts on the alanine, aspartate, and glutamate metabolism pathway, butanoate metabolism, pyruvate metabolism and the histidine metabolism pathway.

3. Other altered pathways after $CoCl_2$ vs control treatment were arginine and proline metabolism and lysine metabolism.

5.8.6 Summary of semi-targeted metabolomics results comparing HEK293T cells in $CoCl_2$ and control

To investigate the effect of $CoCl_2$ on the regulation of HIF-1α on HEK 293T cells a semi-targeted metabolomics method was applied. Western blot experiment on HEK 293T cells showed that $CoCl_2$ (150μM) stabilizes HIF-1α. PCA & HCA analysis did not show presence of any outliers within the dataset. To ensure dataset quality and to measure the accuracy of the model, a PLS-DA cross-validation of the model was conducted. The overall R^2 value was above 0.7 and the Q^2 value was close to R^2 value, and the accuracy score was 0.95 for all five components, indicating that the data is a good fit for the model. Volcano plot analysis showed that like 1% O_2, $CoCl_2$ treatment also significantly upregulates and downregulates specific metabolites in HEK 293T cells.

Multivariate analyses were performed to identify metabolic phenotypes associated with $CoCl_2$ treatment. Multivariate models (PLS-DA and HCA) were used to identify features with patterns of interest. A similar pattern of altered metabolites was observed between volcano plot and VIP plot analyses. Volcano plot analysis predicted some of the VIP metabolites such as glutathione, and O-acetylserine **(Table A.7.7).** A similar pattern of altered compound features was observed both in the heat map and volcano plot analyses. Among the identified metabolites, inosine was higher in abundance both in the volcano plot and HCA analyses.

Glycolysis related metabolites (glyceraldehyde 3-phosphate, pyruvate, and lactic acid) were significantly higher in abundance in the hypoxia treated HEK 293T cells group than in the normoxia (control) group. From the results, it can be stated that hypoxia induces glycolytic flux.

MetaboAnalyst offers 'functional analysis' as a tool to execute untargeted pathway analysis. Mummichog pathway analysis suggested that, like hypoxia, $CoCl_2$ treatment significantly alters several metabolic pathways**.** Interestingly, in addition to glycolysis, 1% O_2 treatment and $CoCl_2$ treatment have significant impact on common pathways, including 'aspartate and asparagine', 'histidine', and 'butanoate' metabolism.

5.9 Metabolic changes in human kidney cells associated with 20µM of Roxadustat treatment

5.9.1 Roxadustat (20, 100 & 200µM) stabilizes HIF-1α

Figure 5.9.1 shows western blotting of HEK 293T cells lysates after treatment with Roxadustat (20,100 & 200µM), which leads to upregulation of HIF-1α when treated for 24 hours.

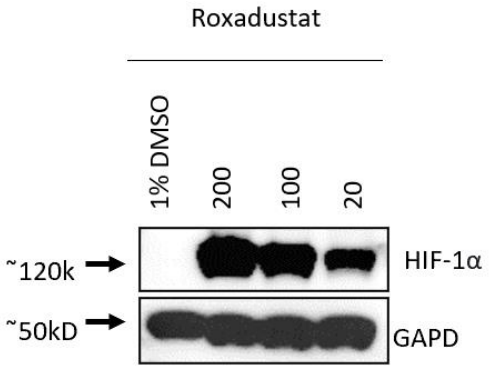


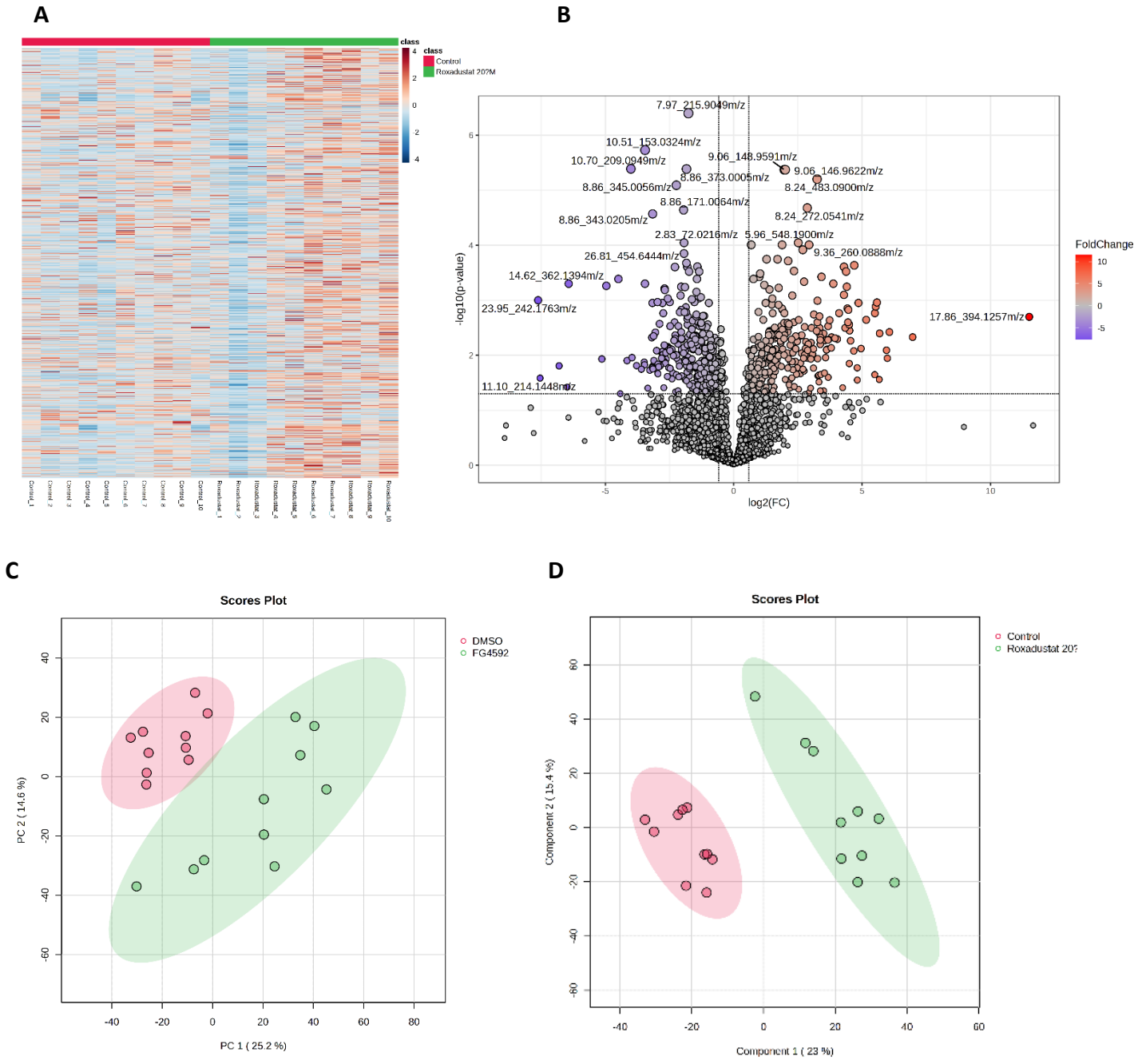
Figure 5.9.1: HIF-α stabilization after 24 h treatment of HEK 293T cells with Roxadustat (20, 100 & 200 µM). 20 & 100µM of Roxadustat was used for semi-targeted metabolomics analysis; 100µM Roxadustat was used for Seahorse analysis and 100 & 200 µM Roxadustat was used for reverse transcription-quantitative polymerase chain reaction (RT-qPCR) analysis.

After investigating the metabolomic impacts of 1%O_2 and $CoCl_2$, next, semi-targeted metabolomics was performed comparing HEK 293T cells treated with Roxadustat at 20 µM vs control (untreated) for 24 hours (n=10per group). After cell harvesting, metabolite extraction and preparation of samples followed by semi-targeted metabolomics, a total of 4425 compound-features were measured and 212 metabolites were identified. The list of identified metabolites is provided in **Table A.7.9.**

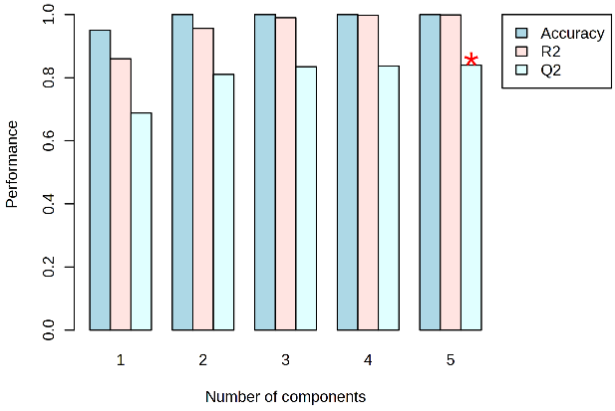
5.9.2 Metabolomics data quality

A heatmap of all compound-features across all samples was extracted **(Figure 5.9.3.1 A),** along with a PCA scores plot labelling the Roxadustat (20 µM) and control group separately **(Figure 5.9.3.1 C).** Data normalisation and transformation and scaling were performed (**Figure A.7.11 & Figure A.7.13)**, no outlier removal or drift correction was performed. Sum normalized, and auto data scaling (**Figure A.7.13)** showed normal (or as close to normal) distributions of features and samples.

5.9.3 Effect of inhibitor 20μM of Roxadustat on human kidney cell metabolites



E



PLS-DA cross validation details:

Measure	1 comps	2 comps	3 comps	4 comps	5 comps
Accuracy	0.95	1.0	1.0	1.0	1.0
R2	0.85981	0.9557	0.98997	0.99758	0.99937
Q2	0.68791	0.81061	0.835	0.837	0.83924

F

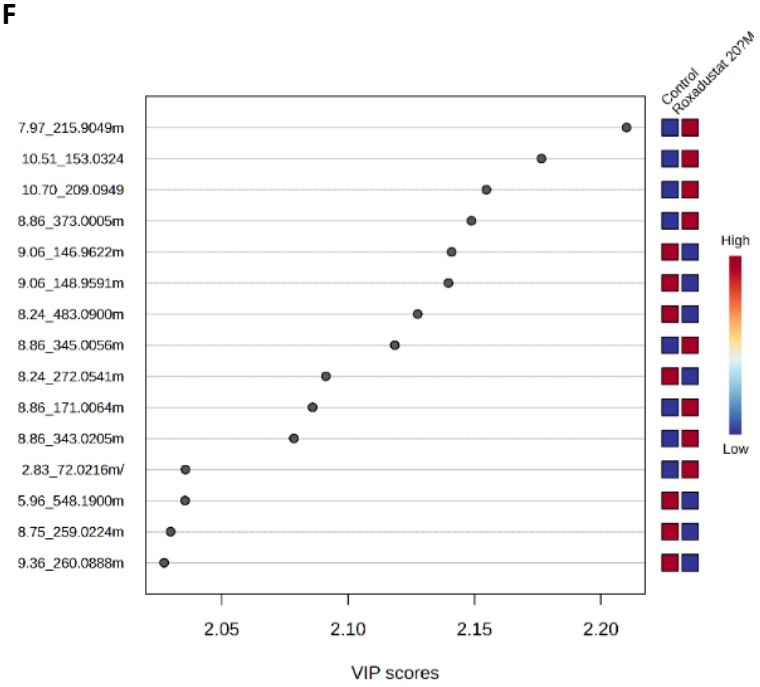


Figure 5.9.3.1: Analysis of Roxadustat (20 µM) treatment versus the control group. (a) Heatmap after normalization of IC-MS data from Roxadustat (20 µM) vs. a control group of HEK 293T cells metabolomics experiment. N = biological replicates and N = 10 for Roxadustat (20 µM) and control group. (b) Volcano plot with a fold change (FC) threshold level of 1.5 and the FDR corrected p value cut off < 0.05. Both FC and p values were log transformed. (c) PCA scores plot. (d) PLS-DA scores plot. (e) Measurement of the predictive accuracy of the model. (f) Top 15 important metabolites identified by VIP scores. The red & blue boxes show the relative concentrations of the corresponding metabolite in Roxadustat (20 µM) and control group.

5.9.3.1. Metabolic changes associated with 20µM Roxadustat treatment

In order to explore metabolites altered in cells treated with Roxadustat (20 µM) compared to control (untreated), t-tests were performed with FDR correction for multiple testing and fold-change analysis of all compound-features found across the Roxadustat (20 µM) and control group. A volcano plot was generated using MetaboAnalyt 6.0 to visual results **(Figure 5.9.3.1**). According to the volcano plot analysis, 20µM of Roxadustat treated HEK 293T cells significantly upregulated a total of 265 identified metabolites and/or compound-features (significantly increased in abundance in Roxadustat group) and downregulated 327 identified metabolites and/or compound-features (significantly reduced in abundance in Roxadustat group).

Among them, only 7 (Uridine triphosphate, Phosphocreatine, Phenylpyruvic acid, N-Acetylglutamate, Inositol 1,3,4-trisphosphate, 4-Acetylbutyrate, 3,3 Dimethyl glutarate, and 2,3-Diphosphoglyceric acid) of them were identified metabolites. A list of these significantly altered identified metabolites by volcano plot analysis is shown in **Table A 7.10.**

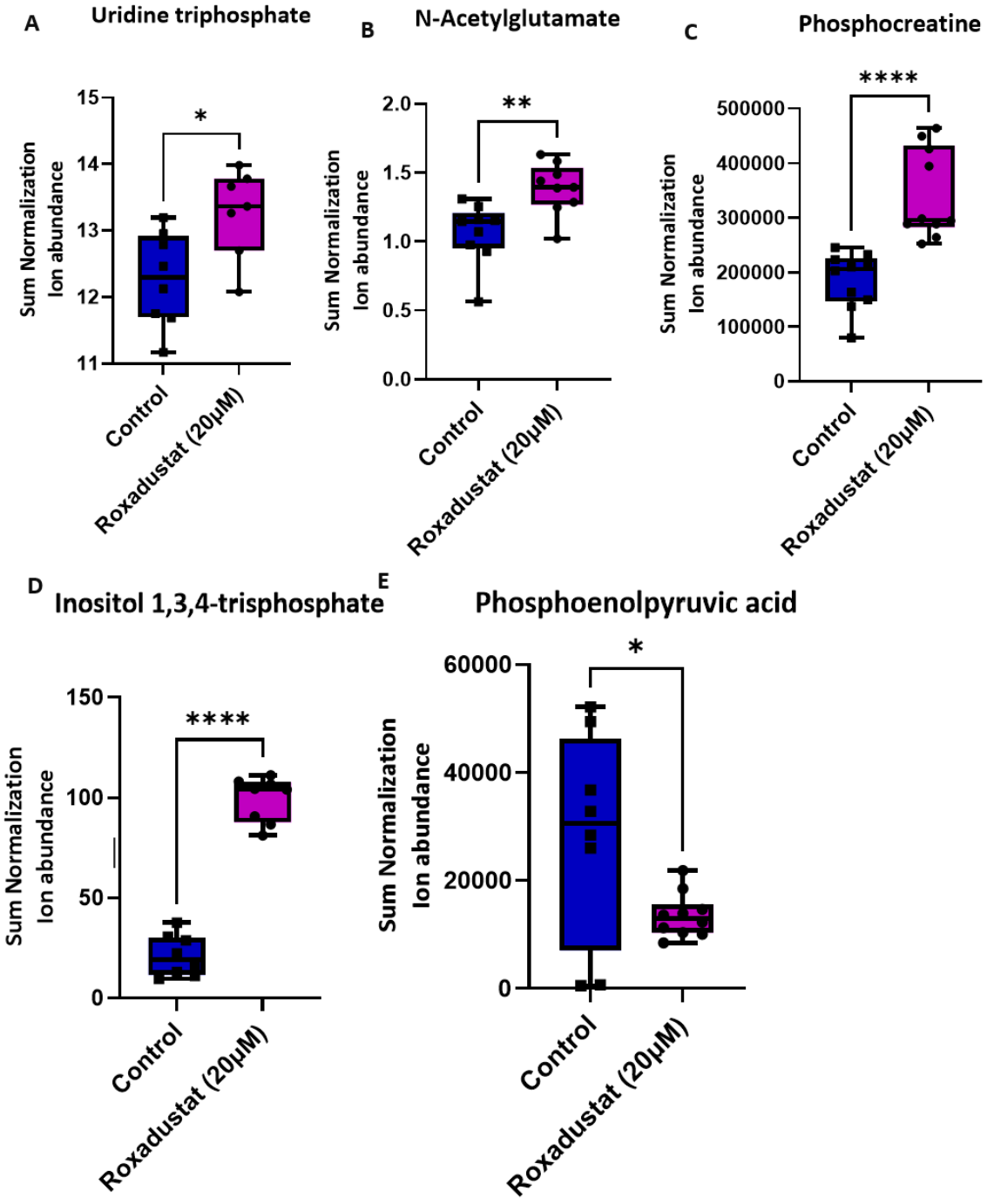


Figure 5.9.3.1.1.: Significantly altered identified metabolite in HEK 293T cells identified by volcano plot analysis when treated with Roxadustat (20µM). (A, B, C, and D) showing the higher abundance and **E)** lower abundance metabolites in HEK 293T cells when treated with Roxadustat (20µM). The splitting line in the box represents the median value and the upper

quantile of the box plot represents 75% of the data and the lower quantile represents 25% of the data. The p-value cutoff was <0.05. where * = p-value < 0.05 and ** = p-value < 0.01, *** = p-value < 0.001 and **** = p-value < 0.0001, calculated with a Tukey's test. N represents the number of biological replicates, N= 8-10 for Roxadustat (20µM) and control group.

Figure 5.9.3.1.1 shows the some of the upregulated metabolites identified by volcano plot analysis which were upregulated in the Roxadustat (20µM) group compared to control group.

5.9.3.1.2 Glycolysis relevant changes due to Roxadustat (20µM) treatment

In order to explore glycolysis relevant changes in more detail from the given dataset the relative abundances of metabolites involved in the glycolytic pathways were compared between the Roxadustat (20 µM) treated and untreated (control) group. Box plots for relevant metabolites are shown in **Figure 5.9.3.1.2.**

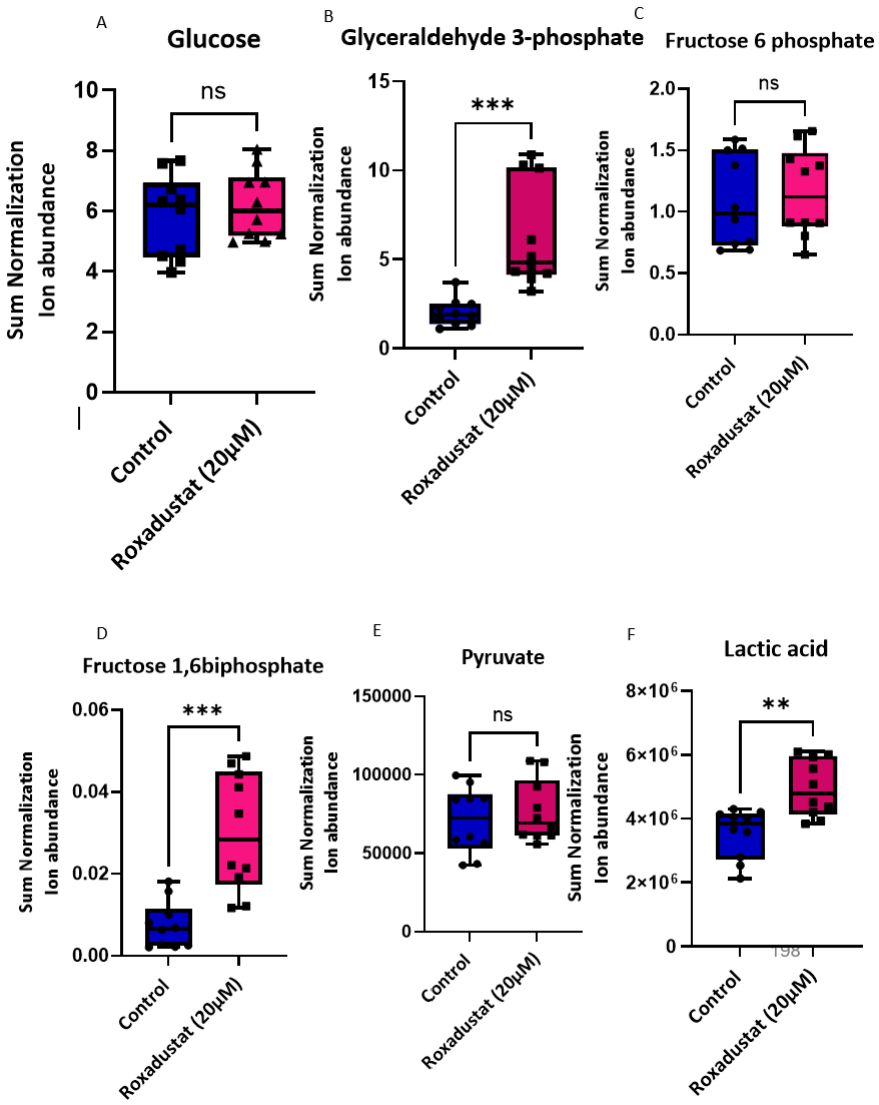


Figure 5.9.3.1.2: Box plot and whisker diagrams of metabolites involved in the glycolysis pathway of Roxadustat (20µM) and control treated HEK 293T cells. A) Glucose, B) Glyceraldehyde 3-phosphate C) Fructose 6-phosphate D) Fructose 1,6-phosphate E) Pyruvate, and F) Lactic acid. The splitting line in the box represents the median value and the upper quantile of the box plot represents 75% of the data and the lower quantile represents 25% of the data. The p-value cutoff was <0.05. where * = p-value < 0.05 and ** = p-value < 0.01, *** = p-value < 0.001 and **** = p-value < 0.0001, calculated with a Tukey's test. N represents a number of biological replicates, N= 10 for Roxadustat (20µM) and the control group.

The key outcomes arising from comparing abundance changes for metabolites involved in the glycolysis pathway were:

1. Glyceraldehyde 3-phosphate, fructose 1,6 biphosphate, and lactic acid were significantly more abundant in the Roxadustat (20µM) group than the control group (**Figure 5.9.3.1.2 B, D & F**).
2. The levels of glucose, fructose 6-phosphate, and pyruvate may be slightly higher in the Roxadustat (20µM) group compared to the control, but the changes were not significant **(Figure 5.9.3.1.2 A, C & E).**

Table 5.9.3.1.1: Fold changes in the Roxadustat (20µM) and control-treated HEK 293T cell metabolites involved in the glycolysis pathway. (The p-value cutoff was <0.05. calculated with a Tukey's test.) (**Figure 5.9.3.1.2)**.

Metabolites	Higher abundance	Fold Change	p-value
Glyceraldehyde 3-phosphate	In Roxadustat group	3.08	p-value < 0.001
fructose 1,6 biphosphate	In Roxadustat group	4.05	p-value < 0.001
lactic acid	In Roxadustat group	2.4	p-value < 0.01
Glucose	In Roxadustat group	Non-significant	
Fructose 6-phosphate	In Roxadustat group	Non-significant	
Pyruvate	In Roxadustat group	Non-significant	

5.9.3.2 Interpretation of univariate statistical analysis

The volcano plot analysis showed that when HEK 293T cells underwent Roxadustat (20µM) treatment some metabolites were higher in abundance compared to the control **(Table A.7.10)**. Glycolysis related glycolytic metabolites such as glyceraldehyde 3-phosphate,

fructose 1,6 biphosphate, and lactic acid were higher in abundance in the Roxadustat (20µM) treated group compared to the control group. Since lactate was higher in abundance in the Roxadustat (20µM) group compared to the control therefore it can be stated that Roxadustat (20µM) can increase glycolysis.

5.9.4 Patterns associated with altered metabolite profiles in Roxadustat (20 µM) treated HEK 293T cells

PLS-DA in the Roxadustat (20 µM) and control experiment was performed using MetaboAnalyst 6.0 software [77]. The PLS-DA scores plot showed a complete separation between the Roxadustat (20 µM) and control group **(Figure 5.9.3.1 D)**. The separation in the scores plot suggested a metabolic difference between Roxadustat (20 µM), and control treated HEK 293T cells. A validation of the model (Cross-validation) was performed before evaluating metabolic changes (Figure 5.9.3.1 E). Both the R2 and Q2 scores were above 0.80, and Q2 was within 0.20 of the R2 score and the accuracy score was between 0.95 to 1 for all the five components. This therefore provided a strong model to evaluate the changes in metabolism associated with Roxadustat (20µM) treatment. **Figure 5.9.3.1 F** shows the top 15 compound features, ranked by the VIP plot. The volcano plot and VIP score plot showed similar patterns, as all these 15 compound features were identified by the volcano plot as well (**Figure 5.9.3.1 B & F)**.

Compound feature 8.86_171.0064 (ranked by VIP score) was putatively assigned Glycerol 3-phosphate; compound feature 8.86_171.0064 had an isotope similarity (93%) as Glycerol 3-phosphate with the ppm error being 0.06 for its formula. Dimer and tetramer *m/z* values were

also identified at the same RT (8.86_343.0205 (2M-H) and 8.86_515.0335 (3M-H) to within 5ppm. The retention time was confirmed using an authentic standard and the compound-feature 8.86_171.0064 was assigned as the M-H adduct of glycerol-3-phosphate.

The rest of the unassigned compound features did not provide any direct HMDB matches based on common adducts (M-H, M-2H, 2M-h, 3M-H and M-H_2O at 5 ppm accuracy). These could be fragments of metabolites and/or other adduct forms.

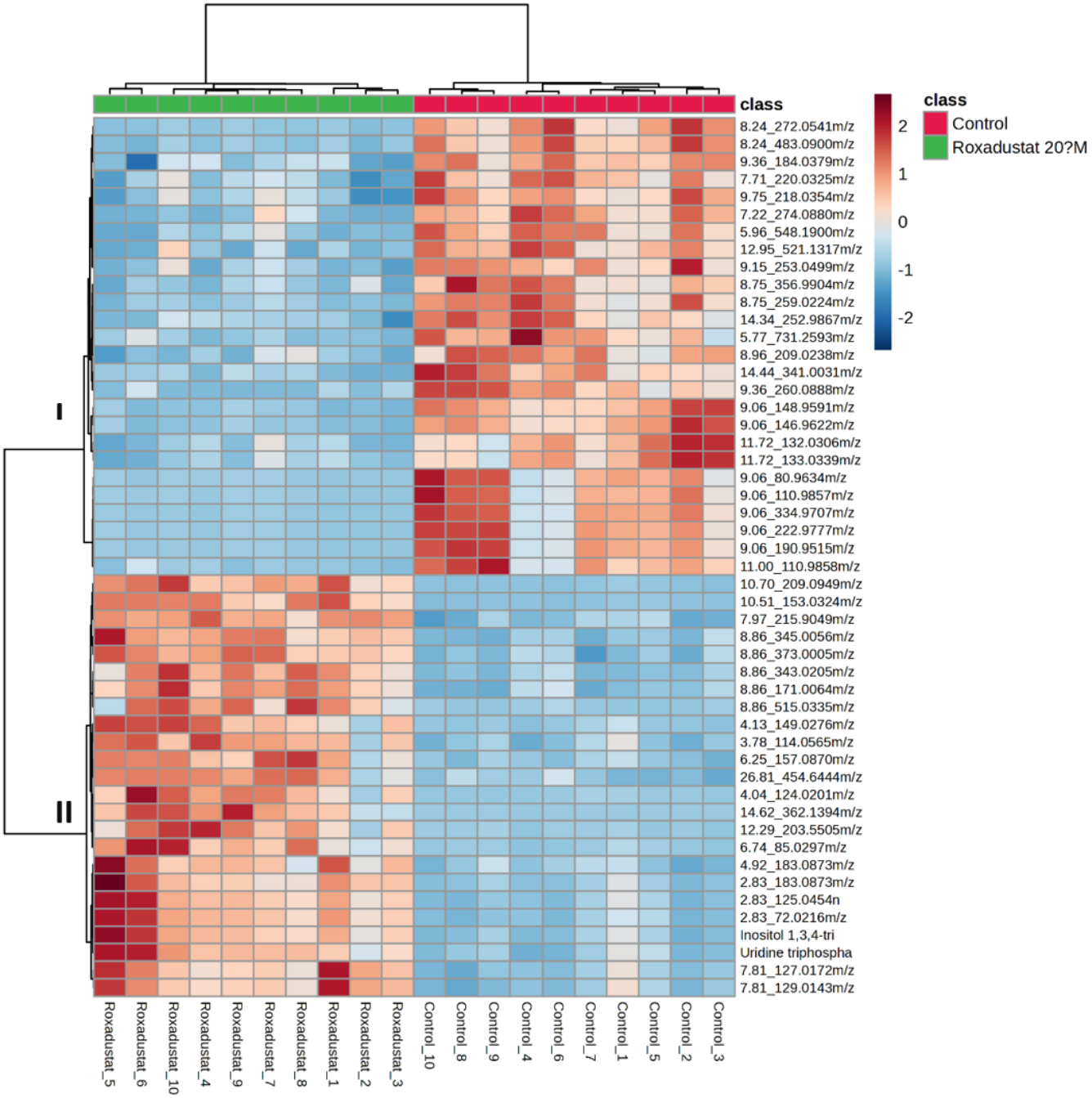


Figure 5.9.4.1: Hierarchical cluster analysis of Roxadustat (20µM) versus control in HEK293T cell data collected by IC-MS analysis. The HCA represents the top 50 significant features between the Roxadustat (20µM) vs the control group. Both features and samples were clustered. The data was interquartile range filtered, sum normalized, and auto scaled. N = 10 for Roxadustat (20µM) and control HEK 293Tcell samples.

A hierarchical clustering heat map was created using MetaboAnalyst 6.0. The HCA helped to show the graphical clustering of Roxadustat (20µM) and the control group (**Figure 5.9.4.1**). In the HCA, there were two main feature clusters (I) and (II). In the other main feature cluster (II), which had elevated metabolite abundance in Roxadustat (20µM) treated cells relative to control treated cells, the following identified metabolites were present: Inositol 1,3,4-trisphosphate and uridine triphosphate. A similar pattern of metabolite abundance was observed in volcano plot analyses (**Table A.7.10**) for example, uridine triphosphate, and inositol 1,3,4-trisphosphate were higher in abundance in the Roxadustat (20µM) group compared to the control according to the volcano plot analyses.

A similar pattern of altered compound features was observed between the HCA map and volcano plot analysis. Both the HCA map and volcano plot showed the following common compound-features: 9.06_146.9622*m/z*, 9.06_148.9591 *m/z*, 8.24_483.0900 *m/z*, 8.24_272.0541 *m/z*, 5.96_548.1900 *m/z* and 9.36_260.0888 *m/z* were higher in abundence and 7.97_215.9049 *m/z*, 10.51_153.0324 *m/z*, 10.70_209.0949 *m/z*, 8.86_373.0005 *m/z*, 8.86345.0056 *m/z*, 8.86_171.0064 *m/z*, 8.86_343.0205 *m/z*, 2.83_72.0216 *m/z*, 8.75_259.0224 *m/z* and 11.10_214.1448 *m/z* were lower in abundence in the Roxadustat (20µM) treated HEK 293T cells group compared to the control group.

The rest of the unassigned compound features did not provide any direct HMDB matches based on common adducts (M-H, M-2H, 2M-h, 3M-H and M-H_2O at 5 ppm accuracy). These could be fragments of metabolites and/or other adduct forms.

5.9.5 Untargeted metabolic pathway analysis of HEK 293T cells treated with 20µM of Roxadustat

Untargeted pathway analysis was conducted to assess metabolic changes at the pathway level when HEK 293T cells were treated with 20µM of Roxadustat.

5.9.5.1 Data processing and analysis

During pathway analysis of 20µM of Roxadustat experiment for pathway analysis the "Functional Analysis" methodology in MetaboAnalyst 6.0 was conducted [37].

5.9.5.2 Mummichog Pathway Analysis Results

The mummichog analysis ranked a total of 98 pathways with only 5 predicted to be significantly altered based on the expression analysis systemic explorer (EASE) score adjusted p-value (< 0.05).

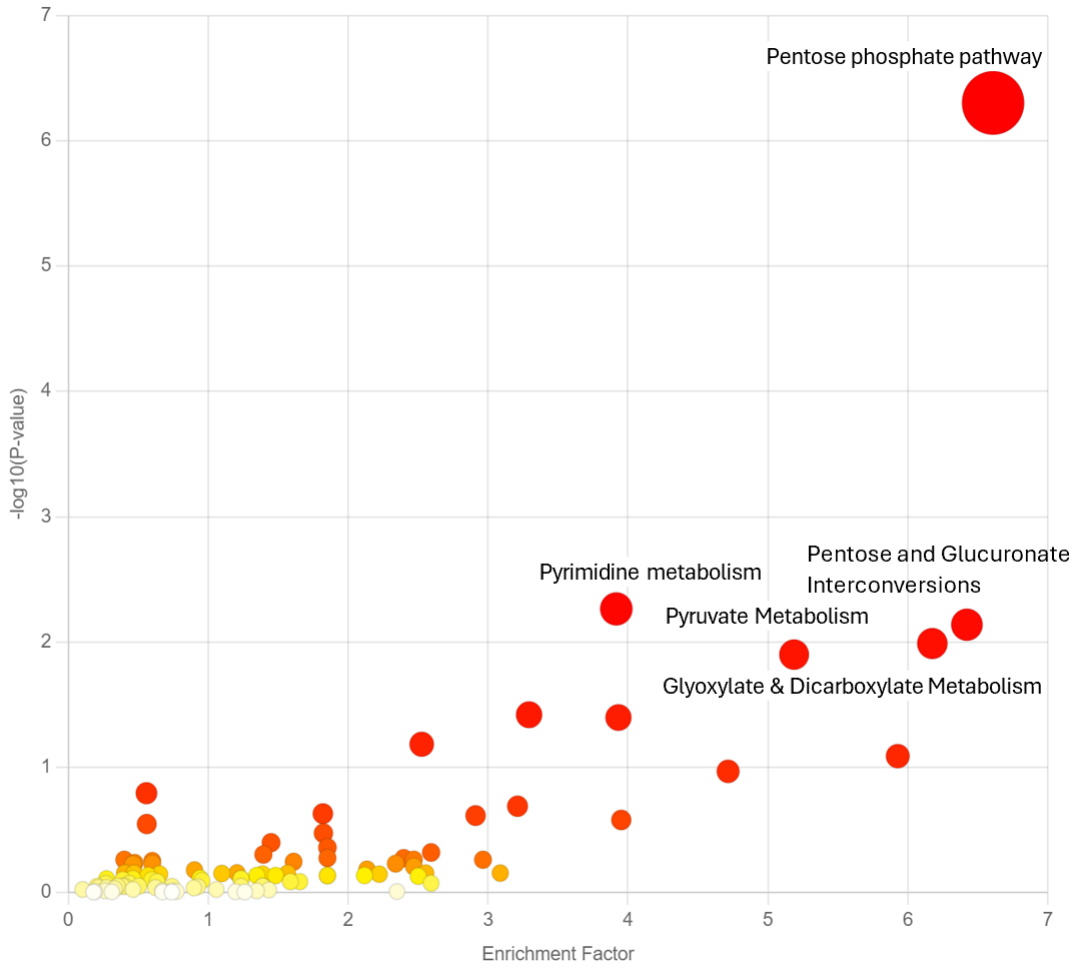


Figure 5.9.5.2.1: Summary of Roxadustat (20µM) vs control Mummichog Pathway Analysis with HEK 293T cells. The circles represent matched pathways. The ratio of significant pathway hits and probable compound hits within a pathway is used to calculate the enrichment factor. The intensity of colour represents its p-value and the size of the circle represents the enrichment factor. Pathway analysis was conducted using MetaboAnalyst 6.0 software.

Based on these results, it can be proposed that, compared to the other experimental groups (1% O_2 and 150 µM $CoCl_2$), 20µM Roxadustat had less impact on metabolism (**Figure 5.7.5.2.1, 5.8.5.2.1, & 5.9.5.2.1**). **Table 5.9.5.2.1** shows the 5 ranked pathways hierarchical by p-value (based on EASE score); all pathways are given in **Table A.7.11**.

Table A.7.11 shows the KEGG metabolite codes. **Figure 5.9.5.2.1** shows -log(p) versus enrichment factor plot for the Roxadustat (20µM) versus control experiment.

Table 5.10.4.2.1: All 5 significant metabolic pathways ranked by mummichog analysis. The significance was calculated using the EASE score and the p-value cutoff was < 0.05.

Pathway Name	Pathway total	Hits total	Hits significant	P(EASE)
Pentose phosphate pathway	**37**	**36**	**33**	**3.73E-06**
Pyrimidine metabolism	**70**	**52**	**37**	**0.011699**
Pentose and Glucuronate Interconversions	**15**	**15**	**13**	**0.030616**
Pyruvate Metabolism	**20**	**17**	**14**	**0.042995**
Glyoxylate and Dicarboxylate Metabolism	**12**	**11**	**10**	**0.050882**

Conclusions from the mummichog Pathway Analysis were:

1. Roxadustat (20µM) vs control treatment exerted significant impact on only 5 metabolic pathways (**Table 5.9.5.2.1).**
2. The pentose phosphate pathway, pyrimidine metabolism, and pyruvate metabolism were significantly altered with Roxadustat (20µM) vs control treatment. These pathways were also significantly altered in the other treatment groups (1% O_2 and 150 µM of $CoCl_2$) (**Figure 5.7.5.2.1, 5.8.5.2.1 & 5.9.5.2.1**).

5.9.6 Summary of semi-targeted metabolomics results comparing HEK293T cells in Roxadustat (20 µM) and control.

Western blot experiment on HEK 293T cells showed that Roxadustat (20µM) stabilizes HIF-1α. PCA & HCA analyses did not show the presence of any outlier within the dataset. To ensure dataset quality and to measure the accuracy of the model, a PLS-DA cross-validation of the model was conducted. The overall R2 value, which was above 0.7, and the Q2 value was close to R2 value, and the accuracy score was 1 for all components (except one) indicates that the data is a good fit for the model.

Volcano plot analysis showed that, unlike 1% O_2 and $CoCl_2$, Roxadustat at 20µM significantly altered only seven metabolites in HEK 293T cells. These metabolites were higher in abundance in the Roxadustat (20µM) group compared to the control.

Multivariate analyses were performed to investigate the metabolic phenotype associated with Roxadustat (20µM) treatment. After multivariate analysis, VIP plot and HCA map analyses also showed similar patterns with univariant analysis. Volcano plot analysis predicted all the 15 compound features which were later ranked by the VIP plot. Uridine triphosphate, and inositol 1,3,4-trisphosphate were higher in abundance in the Roxadustat (20µM) group both in volcano plot and HCA map analyses.

Glycolytic metabolites such as glyceraldehyde 3-phosphate, fructose 1,6 biphosphate, and lactic acid were significantly higher in abundance in Roxadustat (20µM) treated group compared to the control group. From the results, it can be stated that Roxadustat (20µM) can induce glycolytic flux.

20 µM Roxadustat treatment significantly altered only a few metabolomic pathways. Among them ‘pentose phosphate’, ‘pyrimidine’, and ‘pyruvate metabolism’ pathways were commonly altered in 1% O_2 or $CoCl_2$ experiments as well . Hence it can be concluded that Roxadustat (20µM) treatment did not lead to the same extensive metabolic changes as observed with 1% O_2 or $CoCl_2$.

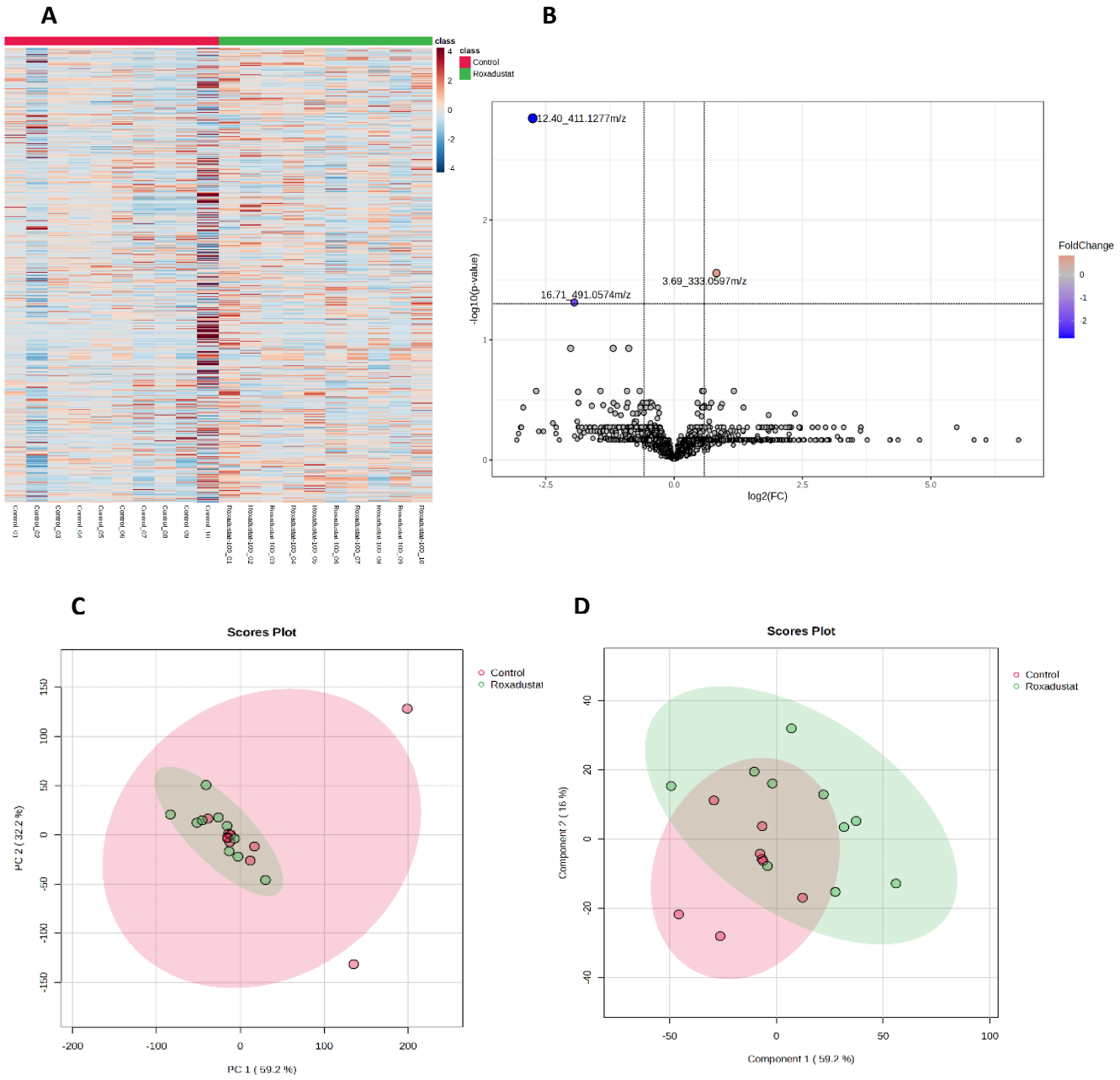
5.10 Metabolic changes in human kidney cells associated with 100 µM of Roxadustat

Treatment with 20 µM of Roxadustat did not lead to extensive metabolic changes (**Figure 5.9.3.1**) as was observed with 1% O_2 (**Figure 5.7.3.1**) or $CoCl_2$ (**Figure 5.8.3.1**) experiment. A semi-targeted metabolomics analysis was therefore performed comparing HEK 293T cells treated with a higher dose of Roxadustat (100 µM) (n=10 per group) vs control (untreated) (n=8 per group) for 24 hours. 100µM of Roxadustat stabilized HIF-1α when incubated for 24 hours (**Figure 5.9.1)**. After cell harvesting, metabolite extraction and preparation of samples followed by semi-targeted metabolomics, a total of 3643 compound-features were measured and 131 metabolites were identified **(Table A.7.12).**

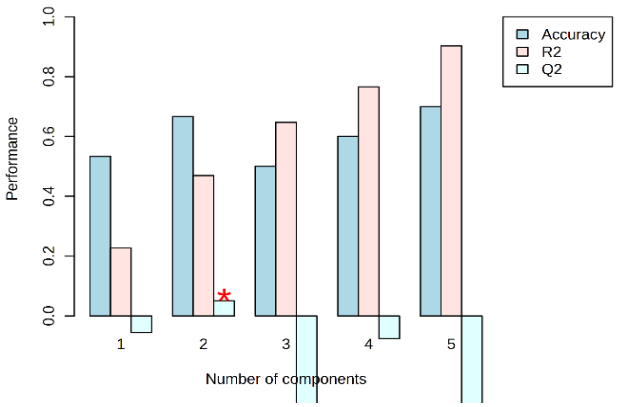
5.10.1 Metabolomics data quality

A heatmap of all compound-features across all samples was extracted **(Figure 5.10.2.1 A.)**, along with a PCA scores plot labelling the Roxadustat (100 µM) and control group separately **(Figure 5.10.2.1 C)**. Data normalisation and transformation and scaling were performed (**Figure A.7.11 & Figure A.7.14)**, no outlier removal or drift correction was performed. In both representations of the dataset, two outliers were apparent in the control group (e.g. this can be seen just outside the 95% confidence interval shaded in green on the PCA plot). This outlier was removed from subsequent data analyses. Sum normalized, and mean scaling **(Figure 5.10.2.1)** showed normal (or as close to normal) distributions of features and samples.

5.10.2. Effect of 100μM Roxadustat on human kidney cell metabolites



E



PLS-DA cross validation details:

Measure	1 comps	2 comps	3 comps	4 comps	5 comps
Accuracy	0.56667	0.71667	0.58333	0.6	0.6
R2	0.22913	0.47112	0.65962	0.76674	0.90486
Q2	-0.065657	0.017616	-0.13726	0.11264	-0.14577

F

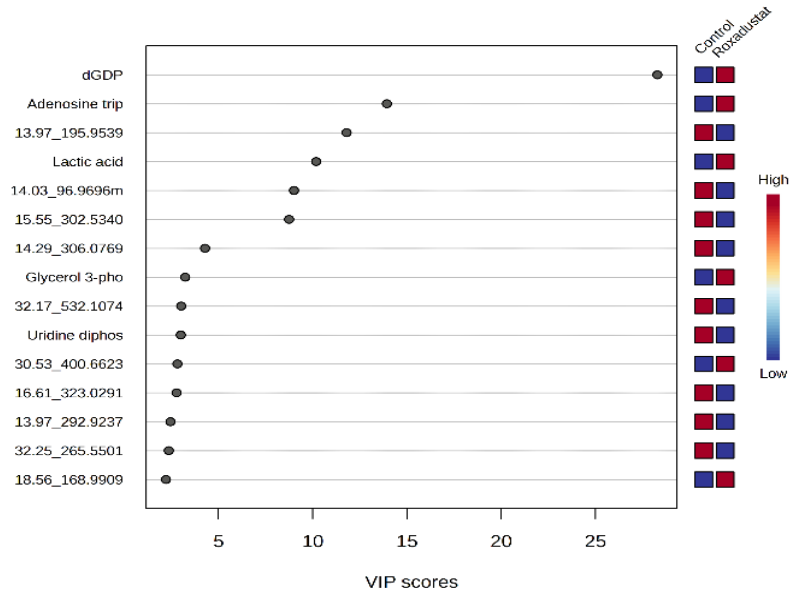


Figure 5.10.2.1: Analysis of clinical PHD inhibitor Roxadustat (100 µM) versus the control group. (a) Heatmap after normalization of IC-MS data from Roxadustat (100 µM) vs. a control group of HEK 293T cells metabolomics experiment. Red arrow indicating outliers in the control group, that were removed from the group. N = biological replicates and N = 8 for the control group and N=10 in Roxadustat (100 µM) group, unless an outlier was removed. (b) Volcano plot with a fold change (FC) threshold level of 1.5 and the FDR corrected p value cut off < 0.05. Both FC and p values were log transformed. (c) PCA scores plot. (d) PLS-DA scores plot. (e) Measurement of the predictive accuracy of the model. (f) Top 15 important metabolites identified by VIP scores. The red & blue boxes show the relative concentrations of the corresponding metabolite in Roxadustat (100 µM) and control group.

5.10.2.1 Metabolic changes associated with 100µM of Roxadustat

In order to explore which metabolites were altered in cells grown in the Roxadustat (100 µM) treatment compared to control (untreated), t-tests were performed with FDR correction for multiple testing and fold-change analysis of all compound-features found across the Roxadustat (100 µM) and control groups. A volcano plot was generated using MetaboAnalyst 6.0 to visual the results **(Figure 5.10.2.1 B**). According to the volcano plot analysis, 100µM of Roxadustat treated HEK 293T cells significantly altered only 3 compound features and among them, one was significantly upregulated and only two were significantly downregulated when treated with Roxadustat (100µM) group compared to the control (**Figure 5.10.2.1B**).

5.10.2.1.1 Glycolysis relevant changes due to Roxadustat (100µM) treatment

To explore glycolysis relevant changes in more detail the relative abundances of metabolites involved in the glycolytic pathways were compared between the Roxadustat (100 µM) treated and control group. Box plots for relevant metabolites are shown in **Figure 5.10.2.1.1.**

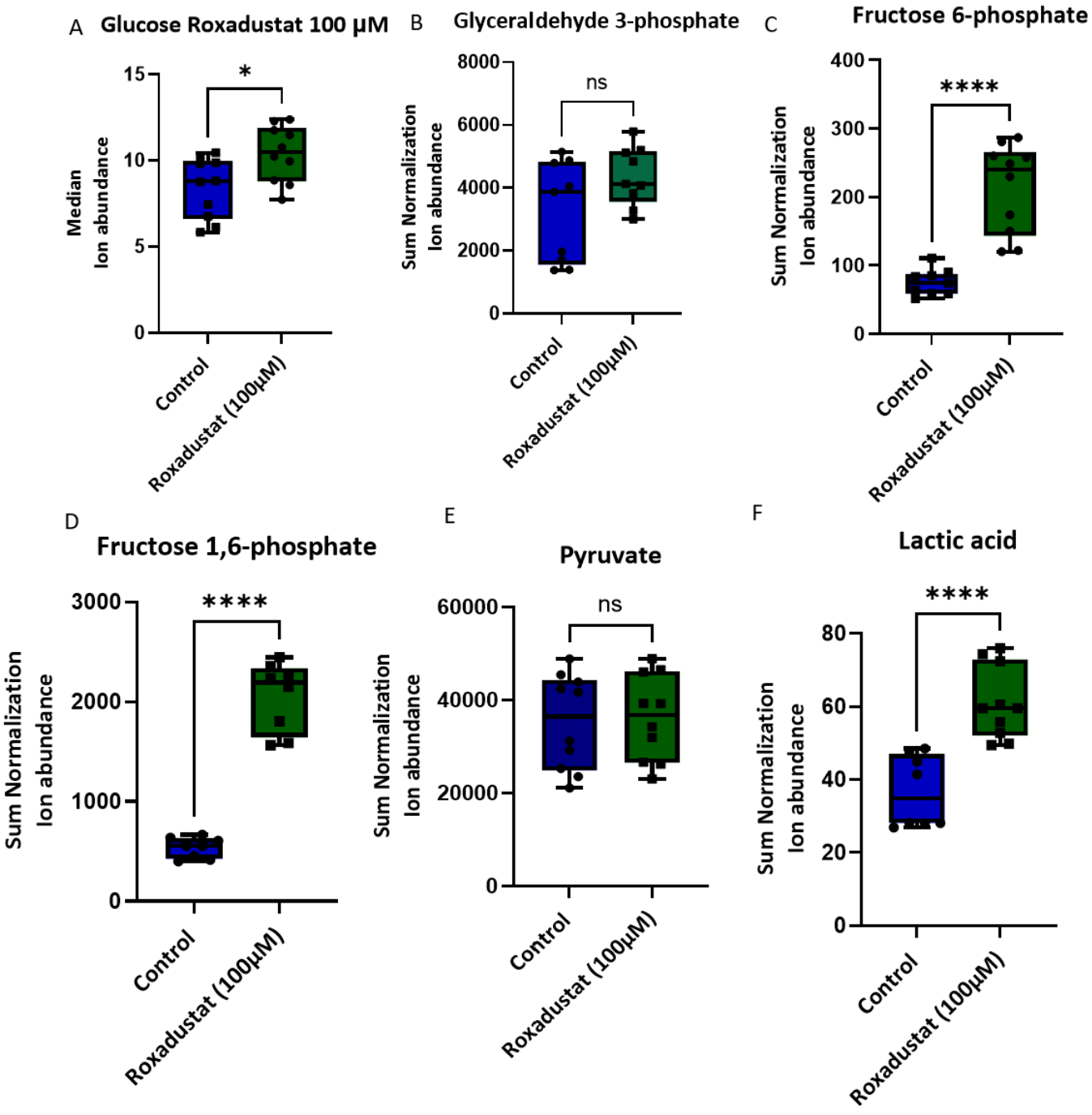


Figure 5.10.2.1.1: Box plot and whisker diagrams of metabolites involved in the glycolysis pathway of Roxadustat (100µM) and control treated HEK 293T cells. A) Glucose, B) Glyceraldehyde 3-phosphate C) Fructose 6-phosphate D) Fructose 1,6-phosphate E) Pyruvate, and F) Lactic acid. The splitting line in the box represents the median value and the upper

quantile of the box plot represents 75% of the data and the lower quantile represents 25% of the data. The p-value cutoff was <0.05. where * = p-value < 0.05 and ** = p-value < 0.01, *** = p-value < 0.001 and **** = p-value < 0.0001, calculated with a Tukey's test. N represents number of biological replicates, N= 8-9 for Roxadustat (100µM) and N= 9-10 for control group.

The key outcomes arising from comparing abundance changes for metabolites involved in the glycolysis pathway were:

1. Glucose, fructose 6-phosphate, fructose 1,6 biphosphate, and lactic acid were significantly more abundant in the Roxadustat (100µM) group than the control group (**Figure 5.10.2.1.1 A, C, D, & F**).
2. There was no significant difference in glyceraldehyde 3-phosphate and pyruvate levels between the Roxadustat (100µM) and the control group (**Figure 5.10.2.1.1 B & E)**

Table 5.10.2.1.1: Fold change of Roxadustat (100µM) and control treated HEK 293T cell's metabolites involved in the glycolysis pathway. (The p-value cutoff was <0.05. calculated with a Tukey's test.) (**Figure 5.10.2.1.1**).

Metabolites	Higher abundance	Fold Change	p-value
Glucose	In Roxadustat group	1.8	p-value < 0.001
Fructose 6-phosphate	In Roxadustat group	3.20	p-value < 0.0001
Fructose 1,6 biphosphate	In Roxadustat group	3.8	p-value < 0.0001
Lactic acid	In Roxadustat group	2.07	p-value < 0.0001
Glyceraldehyde 3-phosphate	In Roxadustat group	Non-significant	
Pyruvate	In Roxadustat group	Non-significant	

5.10.2. 2 Interpretation of univariate statistical analysis

The volcano plot analysis of Roxadustat 100µM showed a similar pattern to the 20µM Roxadustat treatment; it confirmed a similar effect on a limited number of metabolites compared to hypoxia or $CoCl_2$ treatments discussed earlier in the chapter. Glycolytic metabolites such as glucose, fructose 6-phosphate, fructose 1,6 biphosphate, and lactic acid were higher in abundance in the Roxadsutat (100µM) treated group compared to the control group. Thus, Roxadustat does appear to promote glycolysis. The univariate analyses outcomes show that Roxadustat (100µM) treatment leads to fewer metabolomic changes (compared to the control group) in HEK 293T cells, but that there are metabolomic consequences on HEK 293T cells.

5.10.3. Patterns associated with altered metabolite profiles in Roxadustat (100 µM) treated HEK 293T cells

PLS-DA in the Roxadustat (100 µM) and control experiment was performed using MetaboAnalyst 6.0 software [77]. The PLS-DA scores plot showed a substantial overlap between Roxadustat (100µM) and the control group indicating that there are metabolic similarities between the groups **(Figure 5.10.2.1 D)**. Cross-validation was carried out to measure the accuracy of the model, however, neither R2 nor Q2 scored above 0.70, and the accuracy score was below 1, see **Figure 5.10.2.1 E.** It is unclear why the models were poorer with 100 µM Roxadustat compared to 20 µM Roxadustat but may be due to the outlier issues and subsequently fewer number of replicates per experimental group.

The VIP score plot ranked a total of 5 identified metabolites and 10 compound features. The 5 metabolites were dGDP, adenosine triphosphate, lactic acid, glyceraldehyde 3-phosphate and uridine diphosphate. The ranked compound-features identified by VIP plot were compound features 18.56_168.9909 *m/z*, 30.53_400.6623 *m/z*, 13.97_195.9539 *m/z*, 15.55_302.5340 *m/z*, 13.97_292.9237 m/z, 14.03_96.9696 *m/z*, 14.29_306.0769 *m/z*, 16.61_323.0291 *m/z*, 32.17_532.1074 *m/z*, and 32.25_265.5501*m/z*. The unassigned compound features did not provide any direct HMDB matches based on common adducts (M-H, M-2H, 2M-h, 3M-H and M-H_2O at 5 ppm accuracy). These are likely to be fragments of metabolites and/or other adduct forms.

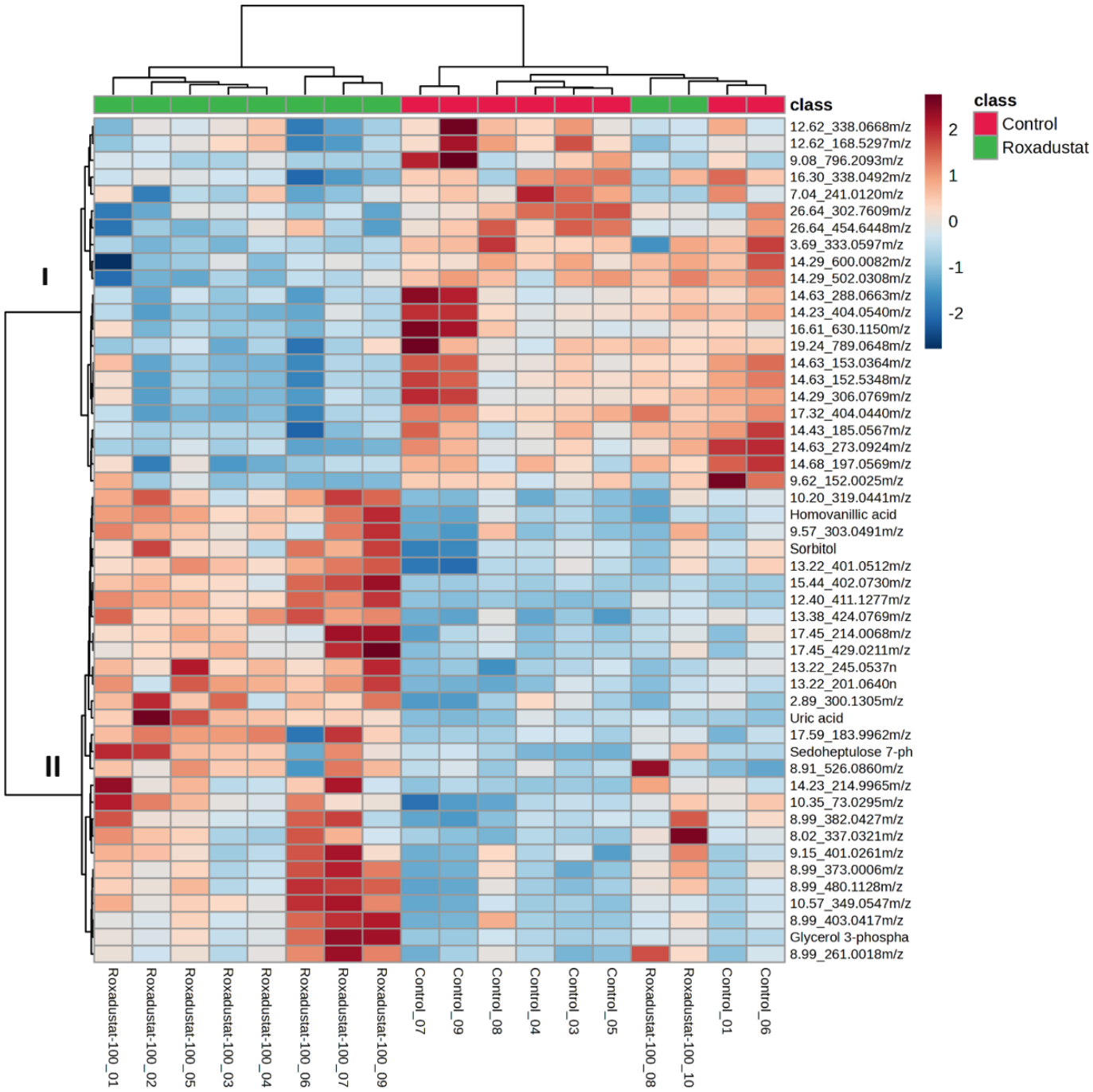


Figure 5.10.3.1: Hierarchical cluster analysis of Roxadustat (100µM) vs control in HEK293T cell data collected by IC-MS analysis. The HCA represents the top 50 significant features between the Roxadustat (100µM) vs the control group. Both features and samples were clustered. The data was interquartile range filtered, sum normalized and mean scaled. N = 10 for Roxadustat (100µM) and control HEK 293Tcell samples.

The HCA map was created by MetaboAnalyst 6.0. The map helped to show the graphical clustering of Roxadustat (100µM) and the control group (**Figure 5.10.3.1**). In the HCA, there were two main feature clusters (I) and (II). In the other main feature cluster (II), which had elevated metabolite abundance in Roxadustat (100µM) treated cells relative to control treated cells, the following identified metabolites were present: homovanillic acid, sorbitol, sedoheptulose 1,7-bisphosphate, and glycerol 3-phosphate **(Figure 5.10.3.1)**. A similar pattern of altered metabolites was observed between the HCA map and the volcano plot. Both the heat map and volcano plot identified common high abundance compound feature 12.40_411.1277*m/z*, and low abundance compound feature 3.69_333.0597 *m/z* in HEK 293T cells treated with Roxadustat (100µM) compared to the control.

The unassigned compound features did not provide any direct HMDB matches based on common adducts (M-H, M-2H, 2M-h, 3M-H and M-H_2O at 5 ppm accuracy). These could be fragments of metabolites and/or other adduct forms.

5.10.4 Untargeted metabolic pathway analysis of HEK 293T cells treated with 100 µM Roxadustat

Untargeted mummichog pathway analysis was conducted to assess metabolic changes at the pathway level when HEK 293T cells were treated with 100µM Roxadustat.

5.10.4.1 Data processing and analysis

During pathway analysis of the dataset for 100µM Roxadustat treatment the “functional analysis” methodology of MetaboAnalyst 6.0 was conducted [37]. Features were ranked by p-

value and the selected p-value selected by MetaboAnalyst 6.0 was < 0.25 (by default). The MetaboAnalyst 6.0 by default suggests the p-value cut-off was < 0.25 (when trying to run analysis at p-value <0.05 the MetaboAnalyst 6.0 did not generate any graphical representation of mummichog pathway analysis suggesting the significance threshold to run successful pathway analysis needed to be higher (presumably due to the small number of significantly altered metabolites already observed from the univariate analysis).

5.10.4.2 Mummichog Pathway Analysis Results

The mummichog analysis ranked a total of 69 pathways with 2 predicted to be significantly altered based on the expression analysis systemic explorer (EASE) score adjusted p-value (< 0.25). These results imply that compared to 1% O_2 or 150 µM of $CoCl_2$ treatment, 100µM of Roxadustat treatment has less impact on metabolic pathways (**Figure 5.7.5.2.1, 5.8.5.2.1 & 5.10.4.1**). **Table 5.10.4.1** shows the top 2 ranked pathways (based on EASE score). **Figure 5.10.4.1** shows -log(p) versus enrichment factor plot for the 100 µM Roxadustat vs control pathway analysis.

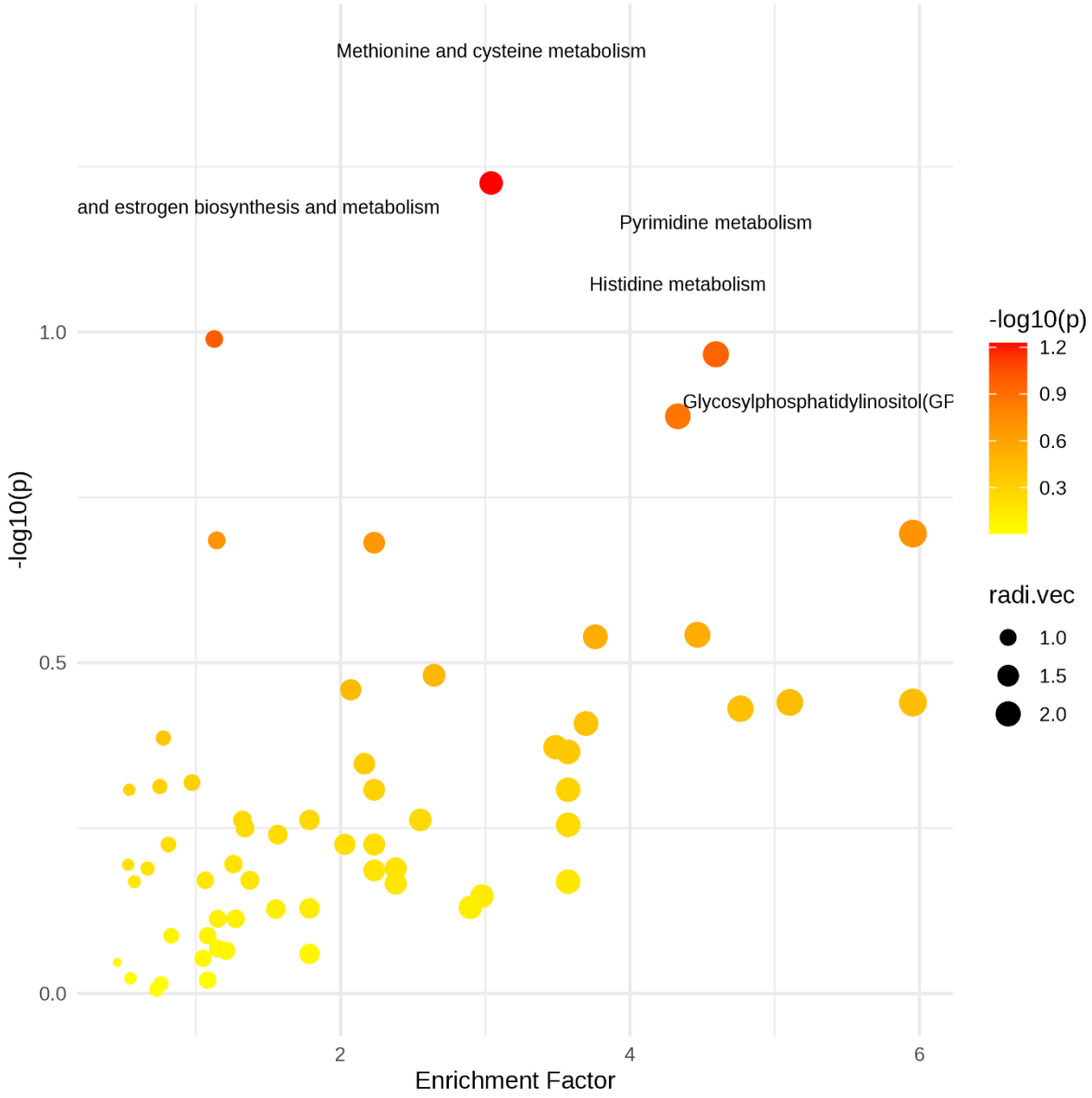


Figure 5.10.4.1: Summary of Roxadustat (100µM) vs control Mummichog Pathway Analysis with HEK 293T cells. The circles represent matched pathways. The ratio of significant pathway hits and probable compound hits within a pathway is used to calculate the enrichment factor. The intensity of colour represents p-value. Compared to the other treatment groups, 100µM Roxadustat treatment showed a lack of significance (no red circles). The size of the circle represents the enrichment factor. Pathway analysis was conducted using the MetaboAnalyst 6.0 software.

Table 5.10.4.1: Showing two significant metabolic pathways ranked by mummichog analysis. The significance was calculated using the EASE score and the p-value cutoff was < 0.25.

Pathway Name	Pathway Total	Hits total	Hits significant	P(EASE)
Methionine and cysteine metabolism	94	41	8	0.1285
Pyrimidine metabolism	70	54	9	0.19669

Compared to the other experiments (1% O_2 and $CoCl_2$), 100µM of Roxadustat vs control treatment exert significant impact only on 2 metabolomic pathway ('methionine and cysteine', and 'pyrimidine' metabolism pathway) using p-value cutoff was < 0.25 mentioned in **Table 5.10.4.1.** Pyrimidine metabolism was the common significantly altered pathway in the 1% O_2 and 100µM of Roxadustat groups, (**figure 5.7.5.2.1 & 5.10.4.1**). As seen in the pathway analysis similar to 20 µM Roxadustat, 100 µM of Roxadustat also does not have any extensive impact on biological metabolomic pathways. It can be said that a higher concentration of Roxadustat did not show any profound metabolomic effect at FDR-corrected p-value < 0.05.

5.10.5. Summary of semi-targeted metabolomics results comparing HEK293T cells in Roxadustat (100 µM) and control

Western blot experiment on HEK 293T cells showed that Roxadustat (100µM) stabilizes HIF-1α. To help maintain overall metabolomics dataset quality, two outliers were removed from the dataset based on PCA & HCA analysis. To ensure dataset quality and to measure the accuracy of the model, a PLS-DA cross-validation of the model was conducted. The R2 value for the

last two components was above 0.7 but the rest of them were below 0.7. The Q2 value was not that close to R2 value and the accuracy score range was 0.56 to 0.7. The reason for poor cross-validation may be because there were insufficient replicates in each group, something that can be addressed in future work. Nonetheless, the preliminary results are interesting.

Volcano plot analysis showed 100µM Roxadustat significantly altered only 3 compound features in HEK 293T cells.

Multivariate analyses were performed to investigate metabolic changes associated with Roxadustat (100µM) treatment. Multivariate models (PLS-DA and HCA) were used to identify patterns of interest. As volcano plot only identified 3 significantly altered compound features, there was not any association of similar pattern between the VIP plot and the volcano plot. Compound feature 12.40_411.1277 was higher in abundance and compound feature 3.69_333.0597 was lower in abundance in both volcano plot and HCA map analysis in HEK 293T cells treated with Roxadustat (100µM). The highly ranked metabolites by VIP plot were dGDP, adenosine triphosphate, lactic acid, and glyceraldehyde 3-phosphate. HCA map analysis showed homovanillic acid, sorbitol, sedoheptulose 1,7-bisphosphate, and glycerol 3-phosphate were higher in abundance in the Roxadustat (100µM) group compared to the control.

Glycolytic pathway related metabolites such as glucose, fructose 6-phosphate, fructose 1,6 biphosphate, and lactic acid were observed to be significantly higher in abundance in the Roxadustat (100µM) group.

100 µM Roxadustat treatment alters only two metabolomic pathways. Hence Roxadustat

treatment did not lead to the same widespread metabolic changes on biological pathways as observed for hypoxia or the other hypoxia mimics.

5.11 Metabolic changes in human kidney cells associated with clinical Molidustat (100 µM)

5.11.1 Molidustat (20, 100 & 200µM) stabilizes HIF-1α

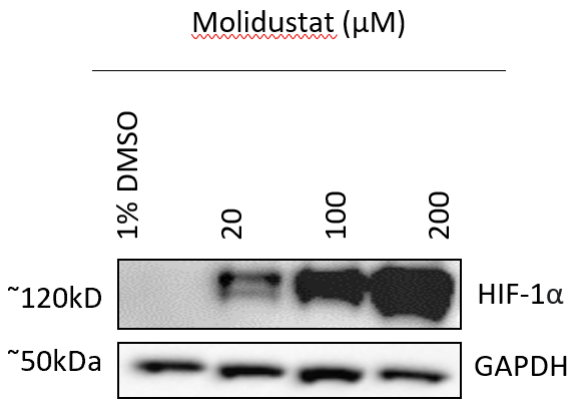


Figure 5.11.1.1: HIF-α stabilization after 24 h treatment of HEK 293T cells with Molidustat (20,100 & 200µM). 100µM Molidustat was used for semi-targeted metabolomics analysis, dose of 100µM Molidustat was used for Seahorse analysis and 100 & 200 µM of Molidustat was used for Reverse transcription-quantitative polymerase chain reaction (RT-qPCR) analysis.

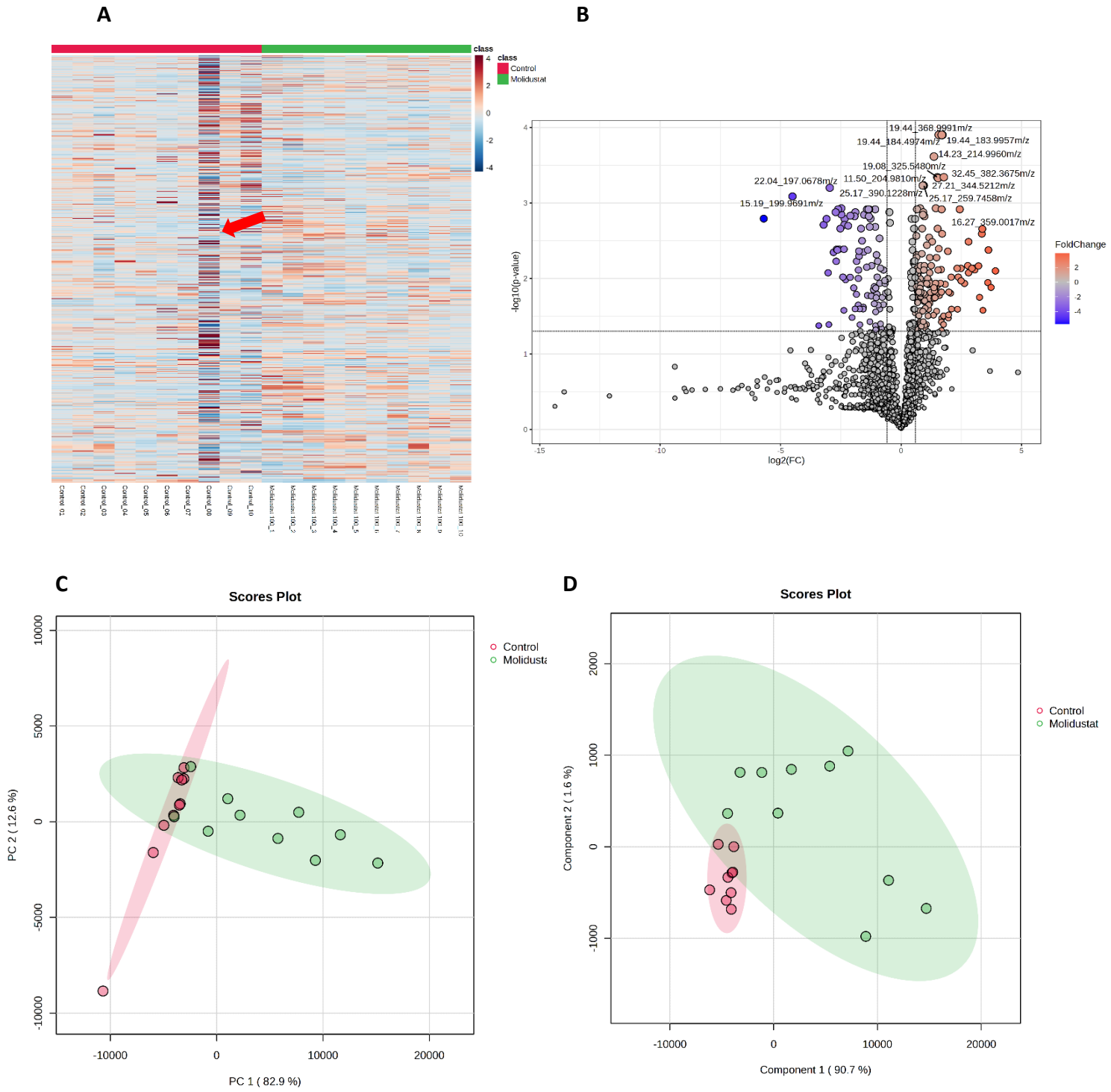
Figure 5.11.1.1 shows western blotting of HEK 293T cells lysates after treatment with Molidustat (20,100 & 200µM). Molidustat (20,100 & 200µM) treatment leads to upregulation of HIF-1α when HEK293T cells were treated for 24 hours **Figure 5.11.1.1.**

5.11.2 Metabolomics data quality

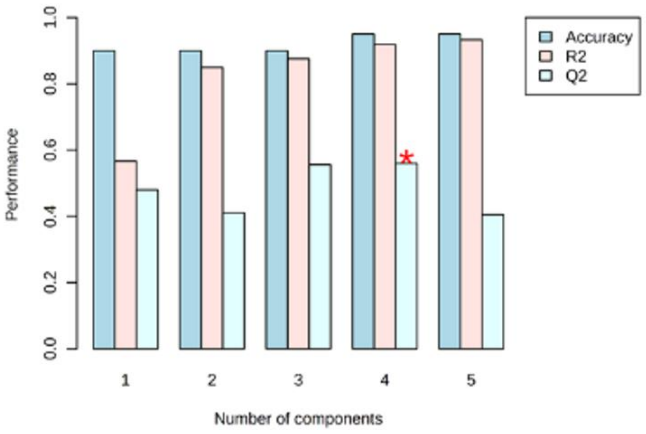
A heatmap of all compound-features across all samples was extracted **(Figure 5.11.3.1A.)**, along with a PCA scores plot labelling the Molidustat (100 µM) and control group separately **(Figure 5.11.3.1 C).** Data normalisation and transformation and scaling were performed

(**Figure A.7.11 & Figure A.7.15)**, no outlier removal or drift correction was performed. In both representations of the dataset two outliers were apparent in the control group (e.g. this can be seen just outside the 95% confidence interval shaded in green on the PCA plot). This outlier was removed from subsequent data analyses. Median normalized, and mean scaling **(Figure 5.11.3.1)** showed normal (or as close to normal) distributions of features and samples.

5.11.3 Effect of selective PHD inhibitor 100μM of Molidustat on human kidney cell's metabolites



E



PLS-DA cross validation details:

Measure	1 comps	2 comps	3 comps	4 comps	5 comps
Accuracy	0.9	0.9	0.9	0.95	0.95
R2	0.56646	0.84944	0.87594	0.91795	0.9332
Q2	0.47959	0.41107	0.55592	0.55904	0.40534

F

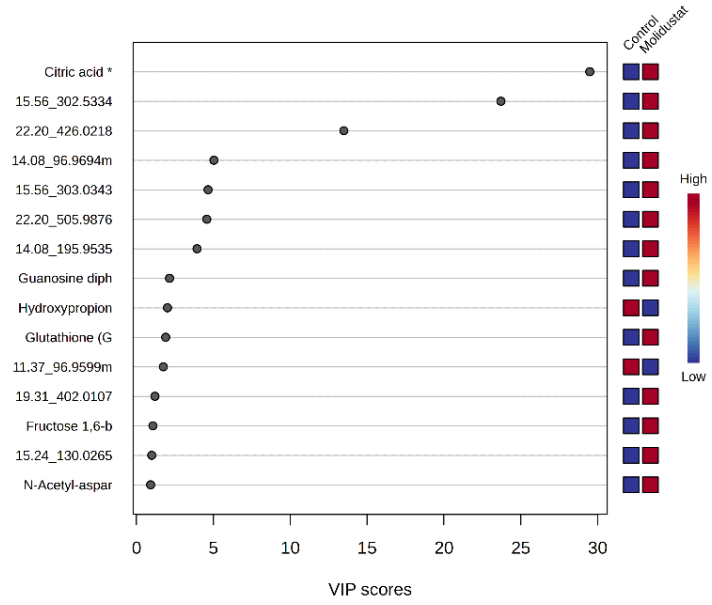


Figure 5.11.3.1: Analysis of clinical PHD inhibitor Molidustat (100 µM) vs. control group. (a) Heatmap after normalization of IC-MS data from Molidustat (100 µM) vs. control group of HEK 293T cells metabolomics experiment. Red arrow indicating outliers in the control group, that were removed from the group. N = biological replicates and N = 9 for the control group and N=10 in Molidustat (100 µM) group, unless an outlier was removed. (b Volcano plot with a fold change (FC) threshold level of 1.5 and the FDR corrected p value cut off < 0.05. Both FC and p values were log transformed. (c) PCA scores plot. (d) PLS-DA scores plot. (e) Measurement of the predictive accuracy of the model. (f) Top 15 important metabolites identified by VIP scores. The red & blue boxes show the relative concentrations of the corresponding metabolite in the Molidustat (100 µM) and the control group.

5.11.3.1. Metabolic changes associated with clinical PHD inhibitor (100µM of Molidustat)

In order to explore which metabolites were altered in cells grown in Molidustat (100 µM) treatment compared to the control (untreated), t-tests (with FDR correction for multiple tresting) and fold-change analysis of all compound-features found across the Molidustat (100 µM) and the control group were performed. A volcano plot was generated using MetaboAnalyst 6.0. According to the volcano plot analysis **(Figure 5.11.3.1B**), 100µM of Molidustat treated HEK 293T cells significantly upregulated 136 identified metabolites and/or compound-features (significantly increased in abundance in Molidustat group) and downregulated 183 metabolites and/or compound-features (significantly reduced in abundance in Molidustat group)**.** Among them 33 of them were identified metabolites and a list of these significantly altered identified metabolites by volcano plot analysis is shown in **Table A 7.14.**

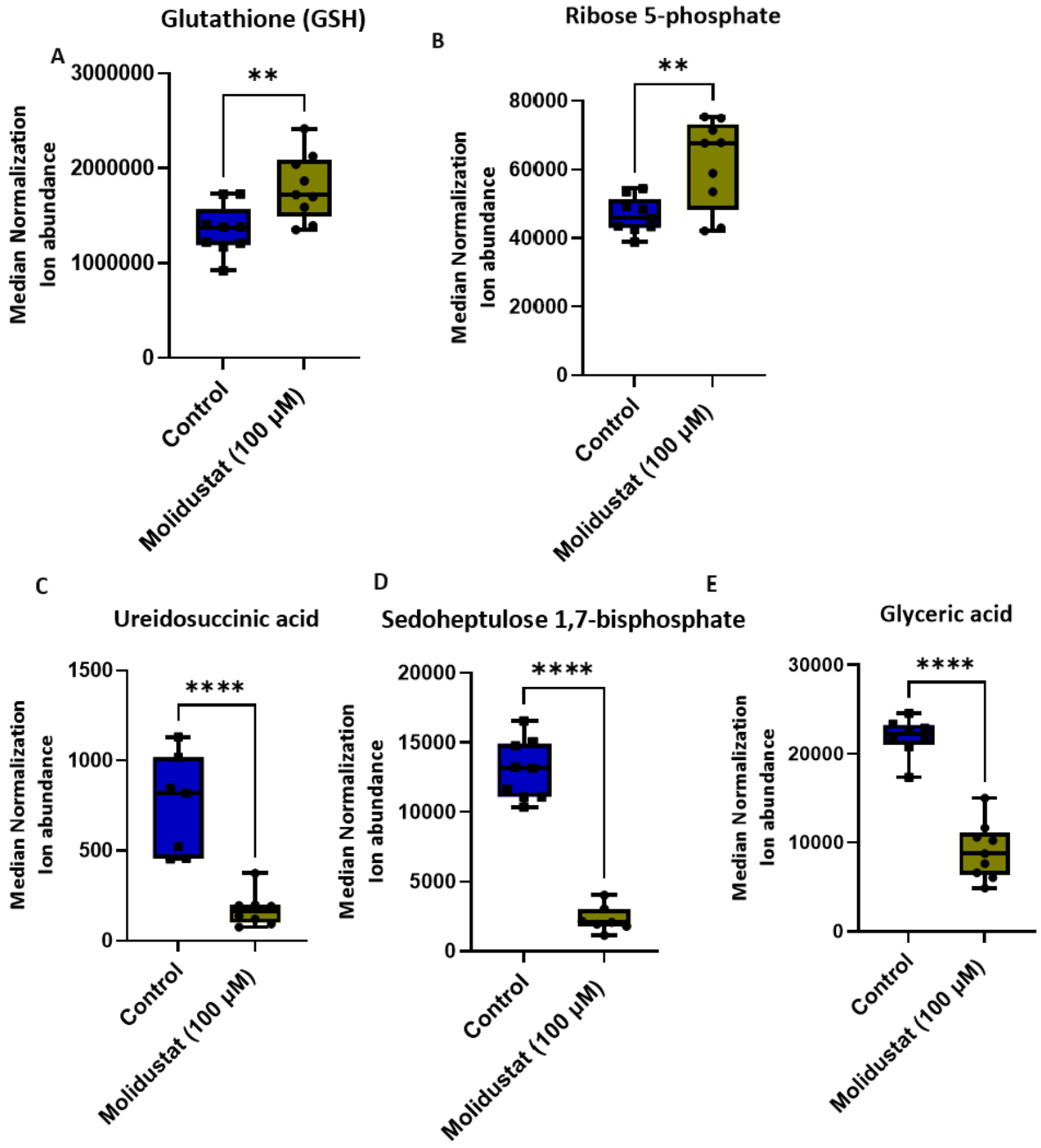


Figure 5.11.3.1.1: Significantly altered identified metabolite in HEK 293T cells identified by volcano plot analysis when treated with Molidustat (100µM) and control. (A, and B) showing the higher abundance metabolites in HEK 293T cells when treated with Molidustat (100µM). (C, D, & E) showing the lower abundance metabolites in HEK 293T cells when treated with Molidustat (100µM). The splitting line in the box represents the median value and the upper quantile of the box plot represents 75% of the data and the lower quantile represents 25% of the data. The p-value cutoff was <0.05. where * = p-value < 0.05 and ** = p-value < 0.01, ***

= p-value < 0.001 and **** = p-value < 0.0001, calculated with a Tukey's test. N represents the number of biological replicates, N= 8-10 for the Molidustat (100µM) and control group.

Figure 5.11.3.1.1 shows some significantly altered identified metabolites. Glutathione (GSH), and ribose 5 phosphate were some of the higher abundance metabolites and ureidosuccinic acid (N-carbamoyl-L-aspartic acid), sedoheptulose 1,7-bisphosphate and glyceric acid were some of the lower abundance metabolites in the Molidustat (100µM) group compared to the control group identified by the volcano plot.

5.11.3.1.2 Glycolysis relevant changes due to Molidustat (100µM) treatment

To explore glycolysis related changes in more detail the relative abundances of metabolites involved in the glycolytic pathways were compared between the Molidustat (100 µM) treated and untreated (control) group. Box plots for relevant metabolites are shown in **Figure 5.11.3.1.2.**

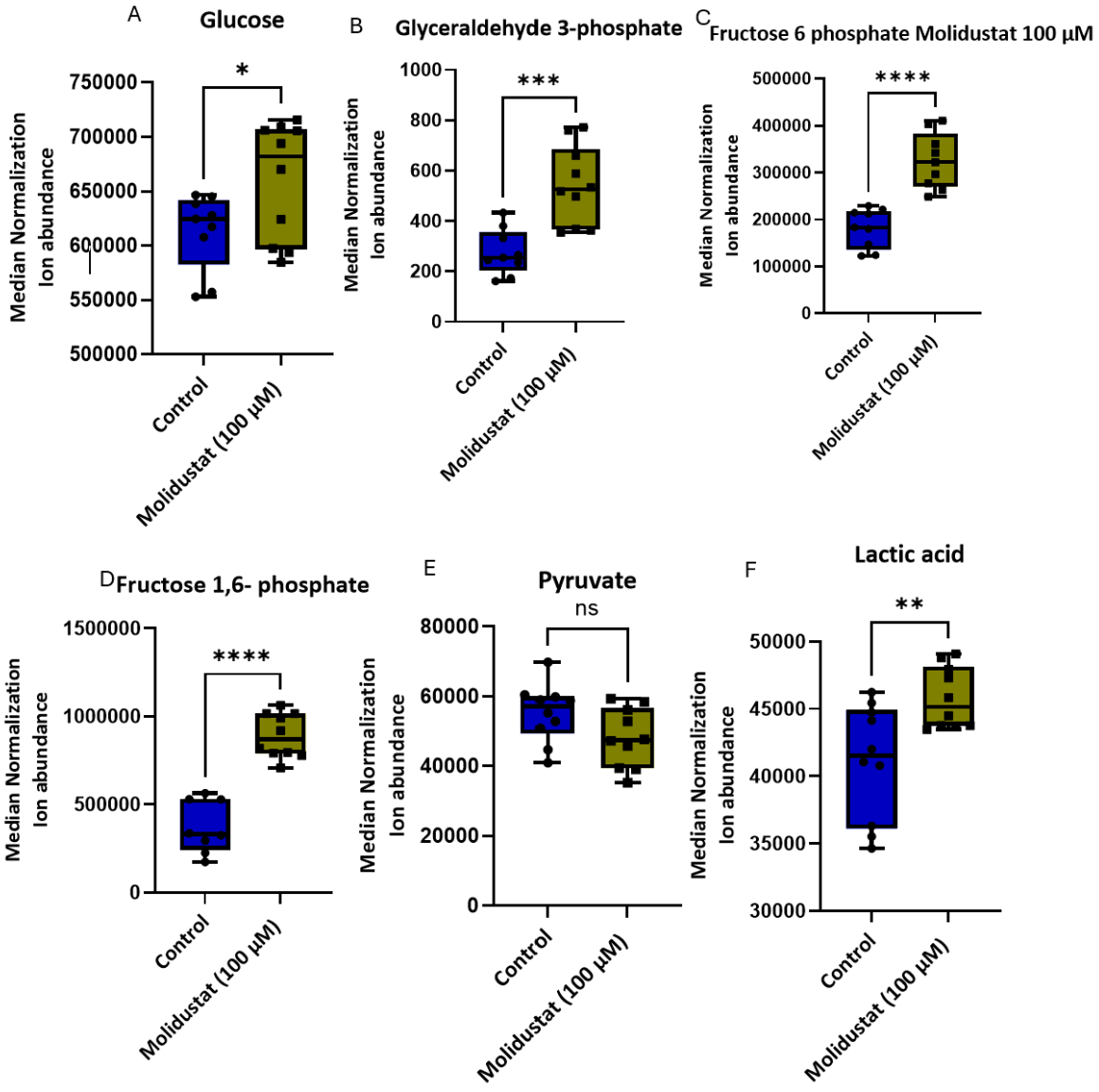


Figure 5.11.3.1.2: **Box plot and whisker diagrams of metabolites involved in glycolysis pathway of Molidustat (100µM) and control treated HEK 293T cells.** A) Glucose, B) Glyceraldehyde 3-phosphate C) Fructose 6-phosphate D) Fructose 1,6-phosphate E) Pyruvate, and F) Lactic acid. The splitting line in the box represents the median value and the upper quantile of the box plot represents 75% of the data and the lower quantile represents 25% of the data. The p-value cutoff was <0.05. where * = p-value < 0.05 and ** = p-value < 0.01, *** = p-value < 0.001 and **** = p-value < 0.0001, calculated with a Tukey's test. N represents a number of biological replicates, N= 8-9 for Molidustat (100µM) and N= 9-10 for the control

group.

The key outcomes arising from comparing abundance changes for metabolites involved in the glycolysis pathway were:

1. All the glycolytic metabolites except pyruvate were significantly more abundant in the Molidustat (100µM) group compared to the control group (**Figure 5.11.3.1.2**).
2. There was no significant difference in pyruvate levels between the Molidustat(100µM) and the control group (**Figure 5.11.3.1.2 E**).

Table 5.11.3.1.1: Fold change of Molidustat (100µM) and control treated HEK 293T cell's metabolites involved in the glycolysis pathway. (The p-value cutoff was <0.05. calculated with a Tukey's test.) (**Figure 5.11.3.1.2)**.

Metabolites	**Higher abundance**	**Fold Change**	**p-value**
Glucose	In Molidustat group	1.06	p-value < 0.05
Glyceraldehyde 3-phosphate	In Molidustat group	1.8	p-value < 0.001
Fructose 6-phosphate	In Molidustat group	2.2	p-value < 0.0001
Fructose 1,6-phosphate	In Molidustat group	3.0	p-value < 0.0001
Lactic acid	In Molidustat group	1.1	p-value < 0.01
Pyruvate	In Molidustat group	Non-significant	

5.11.3.2 Interpretation of univariant analysis

The volcano plot analysis showed that when HEK 293T cells underwent Molidustat (100µM) treatment some metabolites got higher in abundance and some metabolites to downregulate significantly compared to control **(Table A.7.14)**. When measured glycolysis related changes all the glycolytic metabolites except pyruvate were higher in abundance in the Molidustat

(100µM) treated group compared to the control group. Lactate was higher in abundance in the Molidustat (100 µM) group compared to control, Molidustat can increase glycolysis. As univariate analyses outcomes showed that Molidustat (100µM) treatment leads to metabolomic changes compared to the control group on HEK 293T cells, the results further support the proposal that selective PHD inhibitors have metabolomic consequences on HEK 293T cells.

5.11.4 Patterns associated with altered metabolite profiles in Molidustat (100 µM) treated HEK 293T cells

In the PLS-DA model scores plot of this experiment, there was some overlap between the Molidustat (100µM) and the control group which indicates that there are metabolic similarities between the experimental groups **(Figure 5.11.3.1D).** Cross-validation of the PLS-DA model was carried out. The R2 scores were above 0.8 except for component 1, and the Q2 value was not that close to R2 value except for component 1. The Q2 score was within 0.09, 0.43, 0.32, 0.36 and 0.52 of the R2 score for component 1, 2, 3, 4, and 5 respectively (**Figure 5.11.3.1E).**

The VIP score plot ranked a total of 6 identified metabolites and 9 compound features.

Metabolites ranked by the VIP plot which were significant to create differentiates between the experimental groups were citric acid, glutathione (GSH), fructose 1,6 biphosphate, hydroxypropionic acid, Guanosine diphosphate (GDP) and N-acetyl-aspartate (**Figure 5.11.3.1F)**.

A similar pattern of metabolite was observed in volcano plot analyses. According to the volcano plot glutathione (GSH), fructose 1,6 biphosphate and N-acetyl-aspartate were some of the highly abundance metabolites in the Molidustat (100µM) group compared to control (**Table A.7.14**). Glutathione (GSH) was also high in abundance in the $CoCl_2$ treated group.

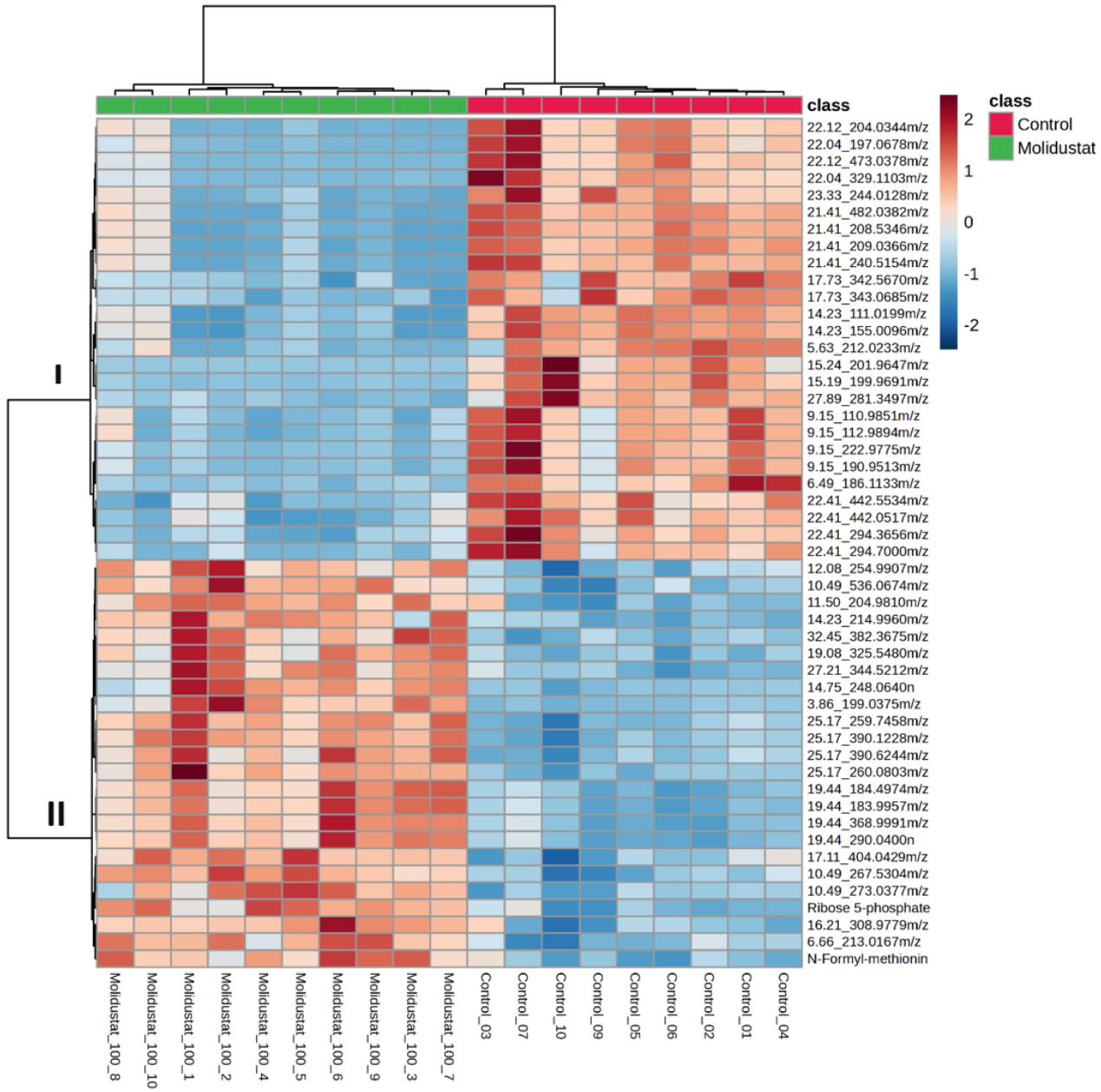


Figure 5.11.4.1.1: Hierarchical cluster analysis of Molidustat (100µM) vs control in HEK293T cell data collected by IC-MS analysis. The HCA represents the top 50 significant features between the Molidustat (100µM) and the control group. Both features and samples were clustered. The data was interquartile range filtered, median normalized, and mean scaled. N = 10 for Molidustat (100µM) and control HEK 293Tcell samples.

In the HCA, there were two main feature clusters (I) and (II). In the other main feature cluster (II), which had elevated metabolite abundance in Molidustat (100µM) treated cells relative to control treated cells, the following identified metabolites were present: N-Formyl-methionine and ribose 5 phosphate (**Figure 5.11.4.1.1)**. A similar pattern of altered metabolites was observed in both the HCA map (**Figure 5.11.4.1.1)** and volcano plot analysis (**Figure 5.11.3.1B)**. Ribose 5 phosphate which is identified by both volcano plot and HCA map was higher in abundance in the Molidustat (100µM) group compared to the control. All the compound features identified by the volcano plot were present in the 50 significant HCA map, except for 16.27_359.0017 *m/z* and 11.50_204.9810 *m/z*.

The unassigned compound features did not provide any direct HMDB matches based on common adducts (M-H, M-2H, 2M-h, 3M-H and M-H_2O at 5 ppm accuracy). These are likely to be fragments of metabolites and/or other adduct forms.

5.11.5 Untargeted metabolic pathway analysis of HEK 293T cells treated with 100 µM Molidustat

Untargeted mummichog pathway analysis was conducted to assess metabolic changes at the pathway level when HEK 293T cells were treated with 100µM Molidustat.

5.11.5.1 Data processing and analysis

During pathway analysis of 100µM of Molidustat experiment for pathway analysis the

"functional analysis" methodology of MetaboAnalyst 6.0 was conducted [37].

5.11.5.2 Mummichog Pathway Analysis Results

Mummichog analysis ranked a total of 95 pathways with only 5 predicted to be significantly altered based on the expression analysis systemic explorer (EASE) score adjusted p-value (< 0.05). Based on these results it can be proposed that when HEK293T cells were treated with 100µM of Molidustat, compared to 1% O_2 or 150 µM $CoCl_2$, Molidustat had a limited impact (**Figure 5.7.5.2.1, 5.8.5.2.1, 5.9.5.2.1, 5.10.5.2.1 & 5.11.5.2.1),** as was observed for Roxadustat. **Table 5.11.5.2.1** shows the 5 ranked pathways hierarchical by p-value (based on EASE score); all pathways are given in **Table A.7.15**. Mummichog analysis also provides a list of KEGG metabolite codes. **Table A.7.15** shows the KEGG metabolite codes. **Figure 5.11.5.2.1** shows -log(p) versus enrichment factor plot for the Molidustat (100µM) vs control pathway analysis.

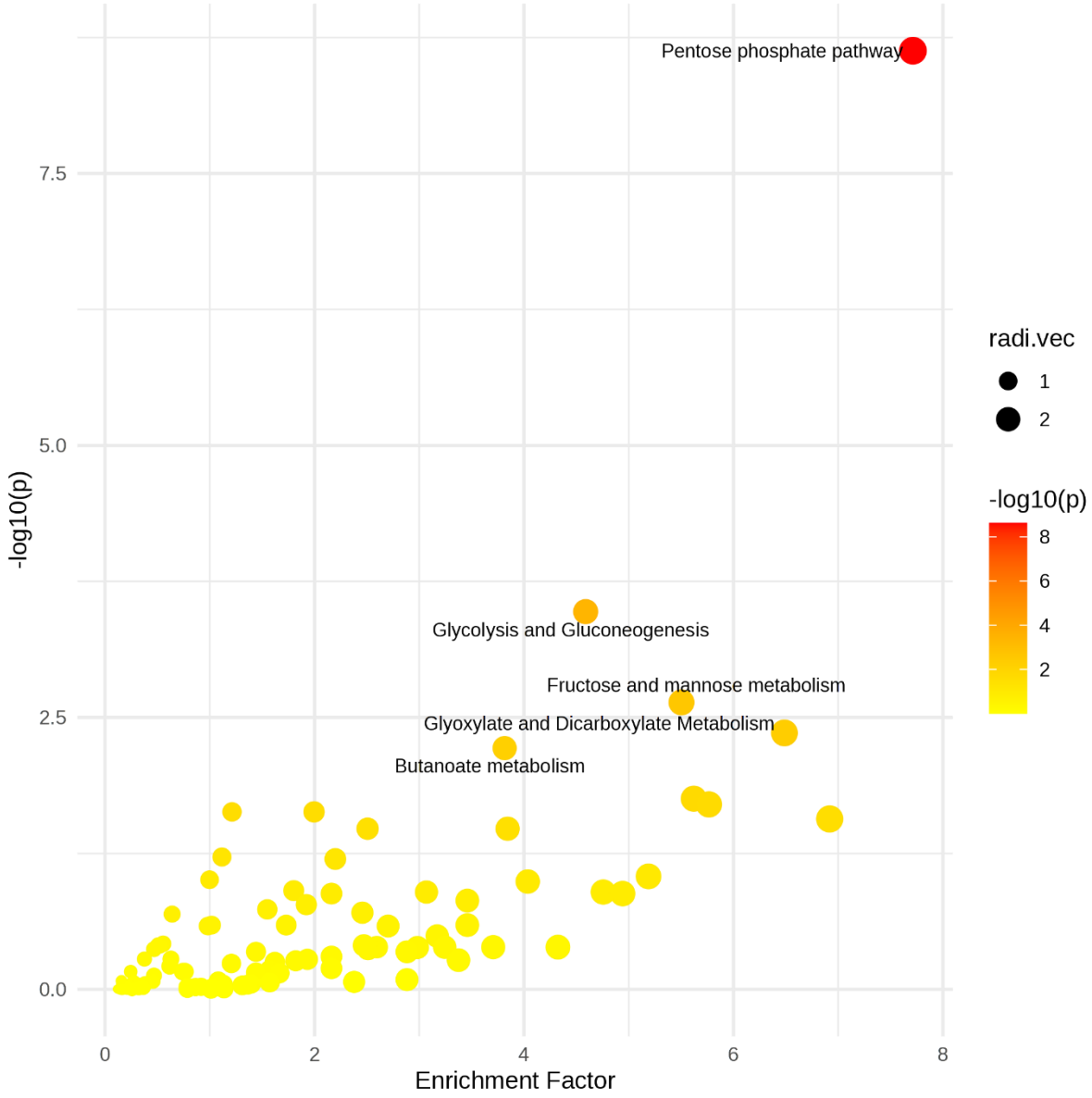


Figure 5.11.5.2.1: Summary of Molidustat (100µM) vs control Mummichog Pathway Analysis with HEK 293T cells. The circles represent matched pathways. The ratio of significant pathway hits and probable compound hits within a pathway is used to calculate the enrichment factor. The intensity of colour represents p-value. Compared to the other treatment groups (1% O_2 & 150 µM $CoCl_2$), 100µM Molidustat treatment showed a lack of significance (no red circles). The size of the circle represents the enrichment factor. Pathway

analysis was conducted using the MetaboAnalyst 6.0 software.

Table 5.11.5.2.1: The 5 significantly altered metabolic pathways with 100µM Molidustat ranked by mummichog analysis. The significance was calculated using the EASE score and the p-value cutoff was < 0.05.

Pathway Name	Pathway total	Hits total	Hits significant	P(EASE)
Pentose phosphate pathway	37	36	33	2.43E-08
Glycolysis and Gluconeogenesis	49	35	26	0.001123
Fructose and mannose metabolism	33	29	21	0.006976
Butanoate metabolism	34	20	15	0.020046
Glyoxylate and Dicarboxylate Metabolism	12	10	9	0.026587

The results show:

1. Compared to other experiments (1% O_2 & 150 µM $CoCl_2$) 100µM Molidustat was observed to exert significant impact only on 5 pathways (**Table 5.11.5.2.1).**
2. All these five significantly altered pathways (**Table 5.11.5.2.1)** were significantly altered in the other experimental groups (1% O_2, & 150 µM $CoCl_2$) as well (**Figures 5.7.5.2.1**, **5.8.5.2.1, 5.9.5.2.1** & **5.11.5.2.1).**

5.11.6 Summary of semi-targeted metabolomics results comparing HEK293T cells in Molidustat (100 µM) and control

Western blot experiment on HEK 293T cells show that Molidustat (100µM) stabilizes HIF-1α. As a part of maintaining overall dataset quality, two outliers were removed from the Molidustat (100µM) metabolomics dataset based on PCA & HCA analysis. To ensure dataset quality and to measure the accuracy of the model, a PLS-DA cross-validation of the model was conducted. The overall R2 value was above 0.7, except for one component, and the Q2 value was close to R2 value, and the accuracy score was near to 1, indicating that the data is a good fit for the model.

Volcano plot analysis showed Molidustat (100µM) can significantly upregulate and downregulate a number of metabolites in HEK 293T cells. A similar pattern of altered metabolites was observed in the volcano plot analyses and VIP plot. Volcano plot analysis predicted some VIP metabolites such as citric acid, guanosine, glutathione (GSH), fructose 1,6 biphosphate, and N-acetyl-aspartate (**Table A .7.14**). A similar pattern of altered compound features was observed between heat map and volcano plot analyses. Among the identified metabolites, ribose 5 phosphate was higher in abundance in both the volcano plot and HCA analyses.

All the glycolytic pathway related metabolites except pyruvate were significantly higher in abundance in the Molidustat (100µM) treated group compared to the control group. From the results, it can be stated that 1% O_2 induces increased glycolytic flux as an adaptation to O_2 deficit.

100 µM of Molidustat treatment was observed to alter only five metabolic pathways. Thus, it can be proposed that like Roxadustat, Molidustat treatment did not lead to as extensive metabolic changes as observed for 1% O_2 or $CoCl_2$ treatment.

5.12 Interpretation of results: Hypoxia / hypoxia mimics show consistent effects on metabolism with highly selective PHD inhibitors showing distinct and overlapping effects

Taken together the results from semitargeted metabolomics experiments comparing hypobaric hypoxia and hypoxia mimicking drugs with untreated controls show interesting outcomes. It is worth mentioning that pathways modelling has limitations, including that 1) the KEGG pathways are the division of an interconnected system (all relevant metabolic processes) into pre-defined individual pathways, where these start and stop are subjective and can lead to biases [84, 98, 99]. 2) The metabolites present in the KEGG database are biased towards functional pathways and don't model co-factors and signaling molecules well. 3) pathway analysis is based on a statistical approach and is therefore subject to implicit and mathematical biases (some pathways may be more likely to be overrepresented based on their composition) [98, 99]. 4) The data analysis method (Over-representation analysis (ORA)) has limitations, because the parameters which were selected to identify metabolites can introduce bias [84, 99] and 5) the KEGG pathway mostly relies on well-studied model organisms meaning it is restricted for interpreting complex regulatory interactions [98, 100].

Table 5.12.1: Significantly altered common pathways. (FDR-corrected p-value < 0.05 except for 100 µM of the Roxadustat group, where the p-value cutoff was < 0.25).

Significantly altered pathways					
Name of Pathway	**Natural hypoxia treatment (p-value <0.05)**	**$CoCl_2$ treatment (p-value <0.05)**	**20 µM of Roxadustat treatment (p-value <0.05)**	**100 µM of Roxadustat treatment (p-value <0.25)**	**100 µM of Molidustat treatment (p-value <0.05)**
Pentose phosphate pathway			✓		✓
Glycolysis & gluconeogenesis	✓				✓
Aspartate & asparagine metabolism	✓	✓			
Fructose and mannose metabolism	✓				✓
Histidine metabolism	✓	✓			
Pyrimidine metabolism	✓		✓	✓	
Butanoate metabolism	✓	✓			✓
Pyruvate metabolism		✓	✓		
Glyoxylate and dicarboxylate metabolism			✓		✓

Table 5.12.1 shows evidence for significantly altered common pathways, however, in case of selective inhibitors the effects seem to be concentration dependent. As shown in **Table 5.12.1**, the pentose phosphate pathway, butanoate metabolism, and pyrimidine pathway were predicted to be the most significantly altered in hypoxia, hypoxia mimics, and at least in Roxadustat or Molidustat group. The comparison is shown in Table **5.12.1**.

The 'glycolysis/gluconeogenesis pathway' and 'fructose and mannose metabolism' pathways both were significantly altered in natural hypoxia and Molidustat group. It seems natural hypoxia and hypoxia mimics also have a significant impact on 'aspartate and asparagine metabolism' and 'histidine metabolism', whereas 'pyruvate metabolism' pathway is

commonly impacted by $CoCl_2$ and Roxadustat (20 µM) treatment. From the comparison table (**Table 5.12.1**), it can be suggested that the selective PHD inhibitors can influence 'glyoxylate and dicarboxylate metabolism' pathway. All the pathway analysis results were considered significant with FDR-corrected p-values < 0.05, except for the 100 µM Roxadustat group, where the p-value cutoff was < 0.25.

When comparing all the untargeted metabolic pathway analyses, it seems that the hypoxia and hypoxia mimic group (150 µM $CoCl_2$) significantly altered a total of 15 and 12 metabolic pathways at FDR-corrected p-value < 0.05, respectively, whereas, 20 µM & 100 µM of Roxadustat and 100 µM of Molidustat significantly altered only 5, 2 & 5 metabolic pathways at the FDR-corrected p-value < 0.05, (expect for 100 µM of Roxadustat: FDR-corrected p-value < 0.25), respectively. It can be concluded that hypoxia/hypoxia mimics have more profound effects on metabolomic pathways than 20 µM & 100 µM Roxadustat or 100 µM of Molidustat. Previous work has shown the case for this is also the case for transcriptional studies [101].

5.12.1Significantly altered common metabolites

Table 5.12.1.1 shows evidence for significantly altered common metabolites. As shown in **Table 5.12.1.1**, glutathione (GSH), N-Acetylglutamate, phosphocreatine, phenylacetylglycine/phenaceturic acid, sorbitol and taurine were some common significantly altered metabolites in hypoxia, hypoxia mimics, and at least in Roxadustat (20µM) or Molidustat group. This table does not include Roxadustat (100µM), as volcano plot analysis showed that Roxadustat (100µM) treatment significantly altered only 3 compound features.

Table 5.12.1.1: Significantly altered common metabolites. (FDR-corrected p-value < 0.05

except for 100 µM of the Roxadustat group, where the p-value cutoff was < 0.25).

Significantly altered common metabolites				
Name of metabolites	**Natural hypoxia treatment (p-value <0.05)**	**$CoCl_2$ treatment (p-value <0.05)**	**20 µM of Roxadustat treatment (p-value <0.05)**	**100 µM of Molidustat treatment (p-value <0.25)**
Glutathione (GSH)		✓		✓
N-Acetylglutamate		✓	✓	
Phosphocreatine	✓		✓	
Phenylacetylglycine/Phenaceturic acid	✓	✓		
Sorbitol	✓			✓
Taurine	✓	✓		

N-Acetylglutamate was significantly altered in $CoCl_2$ and Roxadustat (20 µM) group. It seems hypoxia and hypoxia mimics also have a significant impact on phenylacetylglycine/phenaceturic acid and taurine metabolites, and phosphocreatine was commonly impacted by hypoxia and Roxadustat (20 µM) treatment. Glutathione (GSH) was significantly altered in $CoCl_2$ and Molidustat (100 µM) group and sorbitol was commonly impacted by hypoxia and Molidustat (100 µM) treatment. All the pathway analysis results were considered significant with FDR-corrected p-values < 0.05.

5.13 Reverse transcription-quantitative polymerase chain reaction (RT-qPCR) analysis of glycolytic gene expression

As described in **Section 5.4**, hypoxia or PHD inhibitor treatment can promote metabolic changes in glucose metabolism [48]. This reprogramming involves genes such as glucose transporter 1 (*GLUT1*), hexokinase 2 (*HK 2*), pyruvate dehydrogenase kinase 1 (*PDK1*), enolase 1 (*ENO 1*), lactate dehydrogenase A (*LDHA*) [72], which are all involved in the glycolytic pathway. Glucose transporters (*GLUT 1-14*) are glycoproteins that facilitate glucose cell uptake [102] and among them, *GLUT 1* and *3* have the maximum affinity for glucose [103, 104]. Hexokinase 2 (*HK 2*) helps to convert glucose into glucose 6-phosphate in the glycolysis pathway [105]. *ENO1* is a glycolytic enzyme vital for the glycolytic pathway. ENO1 acts as a catalyst which catalyses the formation of phosphoenolpyruvate from 2-phosphoglycerate[106]. Under hypoxia, HIF-1α promotes the expression of *PDK1* [52, 53] and *LDHA*. PDK1 blocks the conversion of pyruvates into acetyl Co-A hence hindering the TCA cycle function; LDHA catalyses the conversion of pyruvate into lactic acid [43, 107].

The experiments described here aimed to investigate the effects of glycolytic enzyme encoding genes on HEK293T cells treated with **1.** natural hypoxia (1% O_2), **2.** 100, 150 & 300 µM of $CoCl_2$, **3.** 20, 100, and 200 µM Roxadustat, and **4.** 20, 100, and 200 µM Molidustat. HEK 293T cells treated with <1% DMSO considered as the control. Three different dose concentrations within each experimental group concentration were analysed.

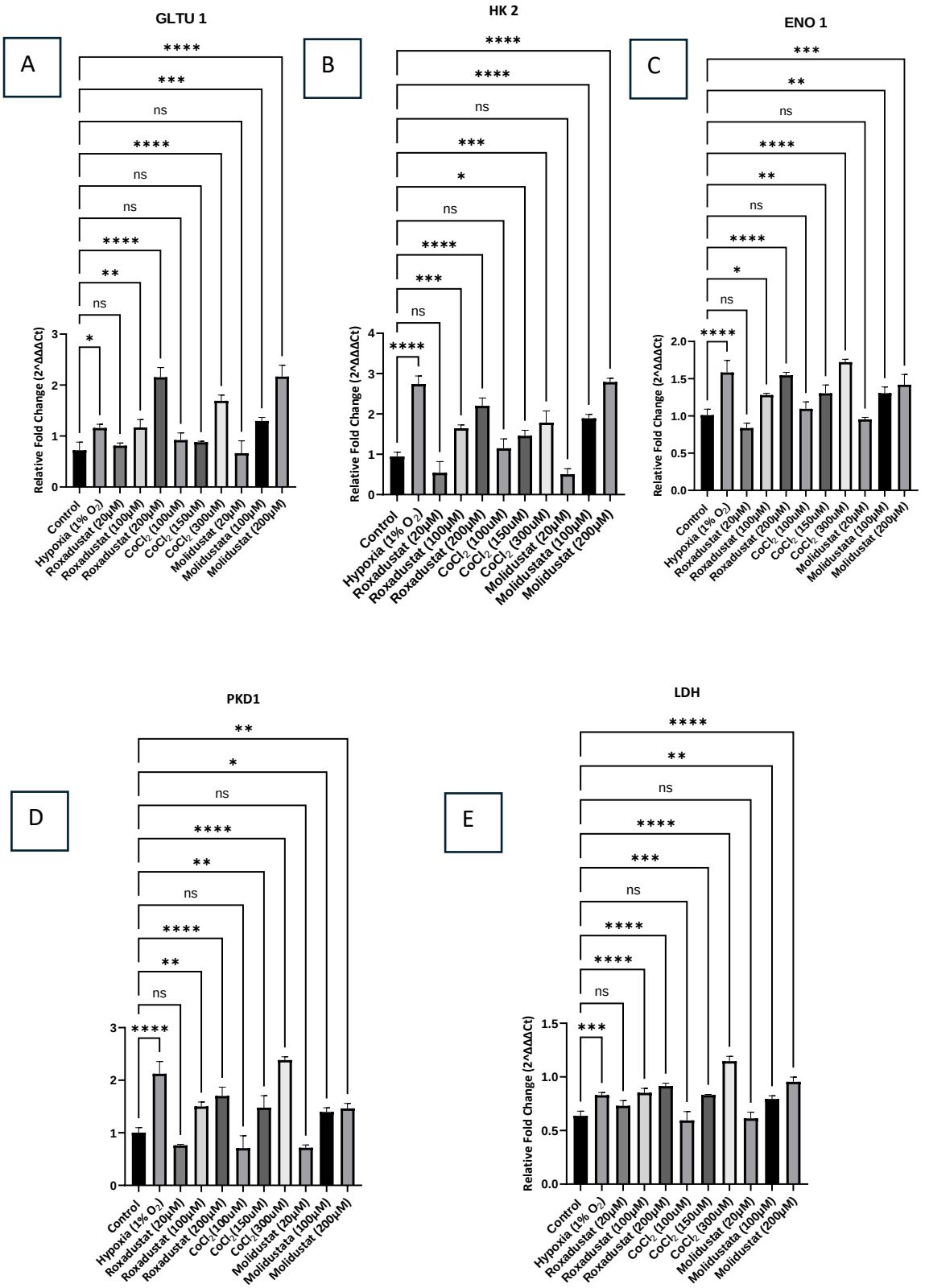

A
GLTU 1
Relative Fold Change (2^ΔΔΔCt)
B
HK 2
Relative Fold Change (2^ΔΔΔCt)
C
ENO 1
Relative Fold Change (2^ΔΔΔCt)
D
PKD1
Relative Fold Change (2^ΔΔΔCt)
E
LDH
Relative Fold Change (2^ΔΔΔCt)
Control
Hypoxia (1% O2)
Roxadustat (20μM)
Roxadustat (100μM)
Roxadustat (200μM)
CoCl2 (100uM)
CoCl2 (150uM)
CoCl2 (300uM)
Molidustat (20μM)
Molidustata (100μM)
Molidustat (200μM)

Figure 5.13.1: Effects of hypoxia (1% O_2), 100, 150 & 300 µM $CoCl_2$, and PHD inhibitors (20, 100, 200 µM Roxadustat and Molidustat) on glycolytic gene expression (GLUT1, HK2, ENO1, PKD1 and LDHA). Each data point represents the mean and standard deviation of the relative fold change concerning the control (<1% DMSO) treated sample normalized to reference gene β-actin level. Statistical significance: * = p-value < 0.05 and ** = p-value < 0.01, *** = p-value < 0.001 and **** = p-value < 0.0001, calculated with One-way ANOVA, multiple comparisons Dunnett test. N represents the number of biological replicates, N= 3 for all the experimental groups.

5.13.1 Results

The glycolytic genes *GLUT1, HK2, ENO1, PKD1*, and *LDHA* were significantly upregulated in the hypoxia (1% O_2) treated group compared to the control group in HEK 293T cells. The FC and p-value for *GLUT1, HK2, ENO1, PKD1*, and *LDHA* were FC= 1.6 (hypoxia /control) and p-value < 0.05, FC = 2.9 (hypoxia /control)and p-value < 0.0001, FC = 1.1 (hypoxia /control)and p-value < 0.0001, FC = 2.1 (hypoxia /control)and p-value < 0.0001, and FC = 1.3 (hypoxia /control)and p-value < 0.05, Dunnett test, respectively (**Figure 5.13.1 A, B, C, D & E**).

100 µM of $CoCl_2$ and 20 µM of Roxadustat and 20 µM Molidustat treatment did not show any significant difference in glycolytic pathway gene expression (*GLUT1, HK2, ENO1, PKD1* and *LDHA)* compared to the control group (**Figure 5.13.1 A, B, C, D & E**) when calculated with the One-way ANOVA, multiple comparisons Dunnett test.

The 150 µM $CoCl_2$ treatment caused significant upregulation of glycolytic genes, i.e, *HK2, ENO1, PKD1*and *LDHA, but not GLUT1,* compared to the control group in HEK 293T cells. The fold change (FC) and p-value for *HK2, ENO1, PKD1*, and *LDHA* were FC = 1.5 ($CoCl_2$ (150 µM) /control) and p-value < 0.05, FC = 1.3 ($CoCl_2$ (150 µM) /control) and p-value < 0.01, FC = 1.5 ($CoCl_2$ (150 µM) /control) and p-value < 0.01, FC = 1.3 ($CoCl_2$ (150 µM) /control) and p-value

< 0.001, when calculated with One-way ANOVA, multiple comparisons Dunnett test, respectively (**Figure 5.13.1 A, B, C, D & E**).

The highest concentration (300 µM) of $CoCl_2$ treatment significantly upregulated all the tested glycolytic genes, i.e. *GLUT1, HK2, ENO1, PKD1*, and *LDHA* in HEK 293T cells, compared to the control group (**Figure 5.13.1 A, B, C, D & E**). The fold change (FC) and p-value for *GLUT1, HK2, ENO1, PKD1* and *LDHA in* 300 µM of $CoCl_2$ group were FC = 2.3 ($CoCl_2$ (300 µM) /control) and p-value < 0.0001, FC = 1.9 ($CoCl_2$ (300 µM) /control)and p-value < 0.001, FC = 1.7 ($CoCl_2$ (300 µM) /control)and p-value < 0.0001, FC = 2.4 ($CoCl_2$ (300 µM) /control)and p-value < 0.0001, and FC = 1.8 ($CoCl_2$ (300 µM) /control)and p-value < 0.0001, Dunnett test, respectively (**Figure 5.13.1 A, B, C, D & E**).

The other treatment conditions, i.e. 100 & 200 µM Roxadustat & Molidustat significantly upregulated all the tested glycolytic genes, i.e, *GLUT1, HK2, ENO1, PKD1*, and *LDHA* compared to the control group in HEK 293T cells (**Figure 5.13.1 A, B, C, D & E**).

The FC and p-value for *GLUT1, HK2, ENO1, PKD1*, and *LDHA* in Roxadustat (100 µM) treated HEK 293T cells were FC = 1.6 (Roxadustat (100 µM) /control) and p-value < 0.01 FC = 1.7 (Roxadustat (100 µM) /control) and p-value < 0.001, FC = 1.3 (Roxadustat (100 µM) /control) and p-value < 0.05, FC = 1.5 (Roxadustat (100 µM) /control) and p-value < 0.001, and FC = 1.3 (Roxadustat (100 µM)/control) and p-value < 0.0001, Dunnett test, respectively (**Figure 5.13.1 A & E**).

The FC and p-value for *GLUT1, HK2, ENO1, PKD1* and *LDHA* in the Molidustat (100 µM) treated HEK 293T cells were FC = 1.8 (Molidustat (100 µM)/control) and p-value < 0.001, FC = 2

(Molidustat (100 µM) /control) and p-value < 0.0001, FC = 1.3 (Molidustat (100 µM) /control) and p-value < 0.01, FC = 1.4 (Molidustat (100 µM) /control) and p-value < 0.05, and FC = 1.3 (Molidustat (100 µM)/control) and p-value < 0.0001, Dunnett test, respectively (**Figure 5.13.1 A & E**).

The FC and p-value for *GLUT1, HK2, ENO1, PKD1* and *LDHA in* 200 µM in the Roxadustat treatment were FC = 3.0 (Roxadustat (200 µM) /control) and p-value < 0.0001, FC = 2.3 (Roxadustat (200 µM) /control)and p-value < 0.0001, FC = 1.5 (Roxadustat (200 µM) /control)and p-value < 0.0001, FC = 1.7 (Roxadustat (200 µM) /control)and p-value < 0.0001, and FC = 1.4 (Roxadustat (200 µM) /control)and p-value < 0.0001, Dunnett test, respectively (**Figure 5.13.1 A, B, C, D & E**).

The FC and p-value for *GLUT1, HK2, ENO1, PKD1* and *LDHA* in the 200 µM Molidustat treatment were FC = 3.0 (Molidustat (200 µM) /control) and p-value < 0.0001, FC = 2.9 (Molidustat (200 µM) /control)and p-value < 0.0001, FC = 1.4 (Molidustat (200 µM) /control)and p-value < 0.001, FC = 1.5 (Molidustat (200 µM)/control)and p-value < 0.001, and FC = 1.5 (Molidustat (200 µM)/control)and p-value < 0.0001, Dunnett test, respectively (**Figure 5.13.1 A, B, C, D & E**).

5.13.2 Interpretation of Results

In summary, all the evaluated glycolytic genes such as GLUT1, HK2, ENO1, PKD1, and LDHA were seen to be upregulated; it can therefore be stated that HEK 293T cells underwent hypoxia allowing increased glucose flux into the glycolytic pathway. The same enhanced expression was observed with 150 & 300 µM of $CoCl_2$ (except for *GLUT1* gene at 150 µM), and

100 & 200 µM of Roxadustat or Molidustat. At 100 µM of $CoCl_2$, and 20 µM of Roxadustat & Molidustat did not show any elevated glycolytic genes.

Therefore, it can be concluded that at higher concentrations Roxadustat and Molidustat can stimulate glycolysis.

5.14 The Effect of $CoCl_2$, Roxadustat and Molidustat on the rate of glycolysis in live cells.

After evaluating glycolytic gene expression, the effects of 150 µM of $CoCl_2$, Roxadustat (100 µM), or Molidustat (100 µM) treatment on the glycolytic rate of HEK 293T cells was investigated.

5.14.1 Seahorse Glycolytic Rate Assay

The Seahorse glycolytic rate assay measures the real-time extracellular acidification rate (ECAR). Mitochondrial activity produces CO_2, which promotes extracellular acidification of the surrounding media. Injection of Rotenone and Antimycin A (Rot/AA) enables inhibition of mitochondrial function, which helps to distinguish the mitochondrial-associated acidification. Subtracting this value from the total proton efflux rate gives the glycolytic proton efflux rate (PER). A second injection of 2-deoxy-D-glucose (2-DG) stops glycolytic acidification. The PER generated before 2-DG injection is PER produced by glycolysis [108, 109]. Seahorse XF DMEM medium where the concentration of glucose solution is 10mM was used to avoid media inducing high glucose effect (**method and materials 5.16.18.1**).

5.14.2 GlycoPER results

HEK 293T cells were treated with 150 µM $CoCl_2$, 100 µM Roxadustat, or 100 µM Molidustat, and 1% DMSO used as a control. The total PER was measured. All the experimental groups showed an increased proton flux rate i.e., enhanced extracellular medium acidification (**Figure 5.14.2.1).** GlycoPER analysis revealed that 100 µM of Roxadustat treated HEK 293T cells displayed the highest proton flux rate, amongst the treatments (**Figure 5.14.2.1**).

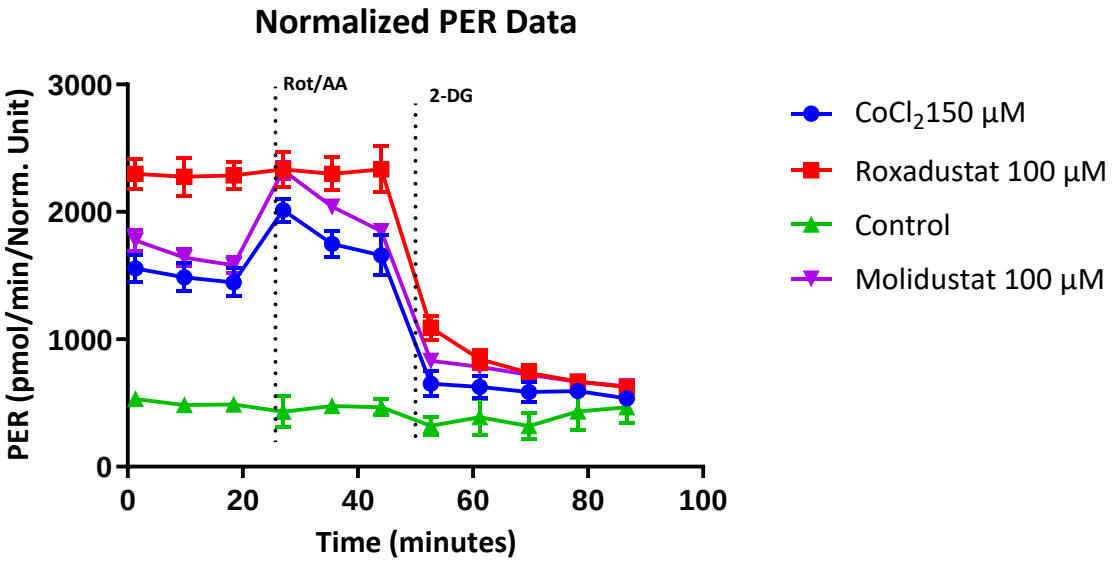


Figure 5.14.2.1: Time-course quantification of glycolytic proton efflux rate (glycoPER) in HEK293T cells treated with $CoCl_2$ (150 µM) or 100 µM of Roxadistat or Molidustat for 24 hours. N represents the number of biological replicates, N= 3 for all the experimental groups.

5.14.2.1 Interpretation of results

The Seahorse glycolytic rate assay results support the evidence that hypoxia or increasing HIF-1α levels promotes glycolysis. Roxadustat 100 µM at displayed the highest proton flux rate, followed by 100 µM of Molidustat and then 150 µM of $CoCl_2$ compared to controls. Experiments conducted previously (**Section 5.8.3.1, 5.9.3.1, 5.10.3.1& 5.11.3.1)** investigating effects of $CoCl_2$, Roxadustat, and Molidustat also support increased glycolysis. Therefore, it can be concluded that hypoxia / HIF-α stabilization increases the glycolytic rate in HEK 293T cells.

5.15 Chapter summary and conclusions

The work described in this chapter used semi-targeted metabolomics to investigate the metabolomic consequences of hypoxia (1% O_2), $CoCl_2$, and selective PHD inhibitors which are capable of inducing HIF-1α accumulation in HEK 293T cells **(Sections 5.7.1, 5.8.1, 5.9.1, and 5.11.1)**. The work also measured effects of the treatments on individual metabolites related to glycolysis **(Sections 5.7.3.1.2, 5.8.3.1.2, 5.9.3.1.2, 5.10.2.1.2 and 5.11.3.1.2)**, impacts on pathways **(Sections 5.7.4, 5.8.4, 5.9.4, 5.10.4, and 5.11.4)**, evaluated gene expression level related to glycolysis enzymes **(Section 5.13),** and measured glycolytic rates **(section 5.14)** when HEK293T cells treated with above-mentioned treatment groups.

Individual semi-targeted metabolomics analysis and interpretation of results were carried out for each experiment. Every experimental group showed commonly altered metabolites or

compound-features that appeared either in the volcano plot, and/or VIP score plot, and/or HCA analyses.

Comparing the semi targeted metabolomics analyses, there were some common metabolites, including guanosine, glutathione (GSH), beta-citryl-L-glutamic acid, citric acid, N-acetyl-aspartate and isocitrate, levels of which were ranked in at least one of the experimental group's VIP plots (**Figure 5.8.2.1, 5.9.2.1, 5.10.2.1, 5.11.2.1, & 5.12.2.1**).

The volcano plot analysis also revealed that hypoxia, hypoxia mimics, and Roxadustat at lower concentration (20 μM) treatments caused upregulation and downregulation of several compound features (**section 5.7.3.1, 5.8.3.1,** and **5.9.3.1**). Both Roxadustat and Molidustat at 100 μM showed fewer changes in compound features abundances compared to the other treatments. Notably, volcano plot analysis revealed that 100 μM of Roxadustat, upregulated only 2 and downregulated only 1 compound feature (**section 5.10.2.1**). These observations imply that PHD inhibitors, likely due to their selectivity, have fewer profound effects compared to hypoxia or the hypoxic mimicking agent ($CoCl_2$). Glutathione (GSH), N-Acetylglutamate, phosphocreatine, phenylacetylglycine/phenaceturic acid, sorbitol and taurine were some common significantly altered metabolites in hypoxia, hypoxia mimics, and at least in Roxadustat (20μM) or Molidustat group. Similar outcomes were observed in the pathway analysis studies.

Untargeted pathway analysis was performed to investigate alterations in metabolomic pathways resulting from hypoxia, hypoxia mimicking agent ($CoCl_2$), and selective PHD

inhibitor treatment. The pathway analysis results indicate that the hypoxia/hypoxia mimic has a more widespread effect compared to the selective PHD inhibitors. As mentioned in **Section 5.12,** there were common metabolic pathways that were influenced by the different treatments, implying some common impacts on HEK 293T cell metabolomic profile.

The impact of hypoxia, hypoxia mimic agent, and selective PHD inhibitors on glycolysis was measured. Not all, but most glycolysis related metabolites were significantly upregulated with all the treatments, with pyruvate being a notable exception. Lactic acid was significantly elevated abundance in all the treatment groups (**Figure 5.7.3.1.2, 5.8.3.1.2, 5.9.3.1.2, 5.10.2.1.2 and 5.11.3.1.2**)[60].

Hypoxia (1% O_2) caused significant changes in glycolysis gene expression levels, with *GLUT1*, *HK 2*, *PDK1*, *ENO 1*, *and LDHA* being significantly upregulated compared to the control. Low concentrations of other treatment groups, i.e. 100 & 150 µM $CoCl_2$, 20 µM Roxadustat, and 20 µM Molidustat did not show any significant difference in glycolysis gene expression levels **(Figure 5.13.1**). When the doses were increased (200 µM $CoCl_2$, 100 & 200 µM Roxadustat and Molidustat), significant upregulation in glycolysis gene expression levels was observed. With the Seahorse glycolytic rate experiments, the selective PHD inhibitors manifested the highest proton efflux, followed by $CoCl_2$ compared to the control. Interestingly, the same result was seen when measuring the influence on the glycolysis pathway, where lactic acid was high in abundance in all the treatment groups compared to the control. Hence it can be concluded that hypoxia increases the rate of glycolysis likely via HIF-1α stabilization. Although

further work could include titration experiments (not possible to date for cost/time reasons), the combined results clearly provide evidence that 'natural' hypoxia and, to a lesser extent $CoCl_2$, have more profound effects on cellular metabolism than the (at least partially) selective PHD inhibitors. In some regards this may be expected given a multitude of cellular processes involve O_2 and many are likely modulated by $CoCl_2$ ions. Thus, the results suggest that the characterization of HIF as the 'master' regulator of hypoxia may be an exaggeration. Perhaps more importantly, given that limited hypoxia does not normally appear to be dangerous, they raise the open question as to whether better mimics of natural hypoxia with broader effects than the current PHD selective inhibitors, might, at least for some situations, be safer from a therapeutic perspective. One of the limitations of this study is absence of metabolomics study of IOX5. IOX5 was intended to test initially during metabolomics study however, after the five-metabolomics study/ experimental conditions due to time constraints IOX5 couldn't evaluate at the same time.

Hypoxia or HIF stabilization can reshape cellular metabolism as reported by previous studies however, there isn't enough studies which specifically address metabolomic changes in HEK 293T cells using IC-MS–based semitargeted metabolomics. This study showed metabolic switch towards glycolysis and elevated lactate levels after the treatments, which are hallmark characteristics of hypoxia.

Previous reports also showed similar findings such as hypoxia induce HIF-1α activation promote metabolic switch towards glycolysis, along with shifts in TCA cycle intermediates[110], suppression of mitochondrial respiration[111,112]. treatment with $CoCl_2$,

also reported to led to a metabolic shift suppressing oxidative phosphorylation and promote glycolysis and disrupt redox balance [113,114].

Some studies on Roxadustat and Molidustat, showed glycolytic shift and lipid metabolism using renal or hepatic models [115-117]. This work used Pathway enrichment analysis showed that hypoxic stress can alter pentose phosphate pathway (PPP) and nucleotide metabolism along with other pathways. Alternation of these pathways reflects a pattern associated with cell survival technique under hypoxic stress [111,118].

Taken together, the findings from this study share similar metabolic signatures induce by hypoxia or HIF stabilization as reported by previous studies. Moreover, semi targeted IC-MS profiling of HEK 293T cells undergoes hypoxia or treatment with hypoxia mimic agent and clinical PHD inhibitors and the specific pathway-level consequences provides a novel contribution in this field. These findings not only confirm the impact of hypoxia on glycolysis and lactate production but also uncover unique cell specific adaptations under PHD inhibition.

5.16 Methods and Materials

5.16.1 Chemicals

5.16.1.1 Chemicals for sample and hypoxia related processing and analysis

Chemicals for sample and hypoxia related processing and analysis are described in **Sections 2.9.1.** Cobalt (II) chloride was from Merck (USA); the Seahorse XF Glycolytic Rate Assay Kit fqa rom Agilent (Agilent, USA).

516.1.2 Chemicals for cell culture and hypoxia cell culture related solutions

Media for glycolytic rate assays, i.e. XF DMEM medium, pH 7.4, XF 1.0 M glucose solution, XF 100 mM pyruvate solution, and XF 200 mM glutamine solution were from Agilent Technologies (USA). Other chemicals are as described in **Sections 2.9.5.**

5.16.3 Cell line, Cell culture stock solutions & PHD inhibitors

These are described in Sections 2.9.2., 2.9.3., 2.9.4.

5.16.3.1 Cell culture and hypoxia related cell culture, thawing of cell aliquots, freezing of cell aliquots & passaging and splitting cells

These are described in Sections 2.9.5. and 4.7.8.

5.16.4 Immunoblotting and Immunoblotting for hypoxia experiment

These are described in Sections 2.9.9. and 4.7.8.

5.16.5 Treatment with different treatment groups

5.16.5.1 Treatment with hypoxia mimic agent & PHD inhibitors for immunoblotting and metabolomics study

Cells were grown over 24 hours in 6 cm plates with a total media volume of 5 mL. 1 mL of the media was then discarded and 1 mL of fresh media containing 20 µM $CoCl_2$, 30 µM $CoCl_2$, or 60 µM $CoCl_2$ was added, giving final concentrations of 100 µM, 150 µM and 300 µM of $CoCl_2$, respectively. The control group in the medium contained 1 ml MQ water. In the case of PHD inhibitors, 1 mL of the media was discarded and 1 mL of fresh media containing 4 µM Roxadustat / Molidustat, 20 µM Roxadustat / Molidustat, or 40 µM Roxadustat / Molidustat was added, giving final concentrations of 20 µM, 100 µM and 200 µM respectively. DMSO was added in the control group with a final concentration of DMSO of 0.1% (v/v). After adding the treatments cells were incubated for 24 hours.

5.16.6. Treatment with 1% O_2 for the hypoxia immunoblotting and metabolomics study

Described in section 4.7.8.

5.16.7 Ion Chromatography Mass Spectrometry (IC-MS)

For all the analysis the volume for sample was 5 µL partial loop injection. Chromatographic

separations were operated using Dionex ICS-5000+ Capillary HPIC system. Dionex ICS-5000+ Capillary HPIC system was coupled the Q-Exactive HF. Q-Exactive HF is a hybrid quadrupole-Orbitrap mass spectrometer. The temperature for the sample manager was 4.0 °C and for column temperature it was 30 °C. Column flow was 0.250 m/min. The steps for the aqueous hydroxide ion gradient were used: 0.0 min, 5 mM; 1.0 min, 5 mM; 15.0 min, 60 mM; 25.0 min, 100 mM; 30.0 min, 100 mM; 30.1 min, 5 mM; 37.0 min, 5 mM. A regenerated trap column was used constantly to remove ionic contaminants from the eluent. The ion suppression was accomplished in external water mode with a flow rate of 0.5 ml/min. The mass spectrometer was equipped with a HESI II probe operated in the negative ion mode and parameters were: spray voltage –3.60 kV, capillary temperature 320 °C, heater temperature 350 °C and S-Lens RF level was set to 70.0%. Parameters for gas flow rates were: sheath gas flow rate; 60, auxiliary gas flow rate;20 and spare gas flow rate; 0. The method was run with full MS and data dependent (dd) MS/MS scan. The full MS scan parameters were; micro scans, 2; resolution, 7×10^4; AGC target, 1×10^6 ions; maximum IT, 120 ms and parameters for MS/MS scan were; resolution, 1.75 × 103; microscans, 2; AGC target, 1.0 × 105; and maximum IT, 250 ms [119].

5.16.8 Plating for metabolomics and glycolytic rate assay experiment

6 cm dishes and 24-well seahorse XF cell culture microplate was used for cell planting and harvesting for metabolomics analysis and Seahorse glycolytic rate assay experiments, respectively. For cell counting, 1 µL of trypan blue dye was mixed and resuspended with 1 µL of cells (1:1 ratio) in a 0.5 mL microtube, then transferred into a cell counting chamber; cell

counting was done using Countess™ II FL Automated Cell Counter. For metabolomics studies, HEK 293T cells were seeded at a density of 1.2X106 cells into 6cm dishes; for glycolytic rate assay experiment, HEK 293T cells were seeded at a density of $1X10^5$ cells into 24 well plates, then grown for 24 hours.

5.16.9 Harvesting of metabolomics samples

The harvesting of cells from 6 cm dishes was done in a randomized manner. Before harvesting inside a laminar flow hood, all cells were briefly inspected under a microscope to observe cell density and morphology. The media was discarded from the 6cm dish, which was then washed twice with 5 mL (approx.) of PBS followed by the addition of 5 mL (approx.) of liquid nitrogen to stop cellular processes. Once the liquid nitrogen had evaporated, 180 µL of 80% MeOH(aq) was added and with the help of a cell scraper, the metabolites were extracted. Then the denatured proteins were transferred into a 1.5 mL microtube and labelled accordingly. During the whole harvesting time, the 6cm dishes and 1.5 mL microtube were kept on ice. After harvesting the samples were stored at -80 °C, if not immediately used for metabolomics sample preparation.

5.16.10 Metabolomics cell sample preparation

During metabolomics sample preparation the samples were taken out of -80 °C and the samples were thawed on ice. Once the centrifuge was cooled down to 4 °C the samples/cells were spun down at 14,000 rpm for 25 minutes and the sample supernatant without disturbing the cell pellets was collected in a 1.5 mL tube. A NanoDrop One machine was used to measure

the DNA (dsDNA (ng/µL)) concentration. 2.0 µL of samples were taken to NanoDrop and 2.0 µL of 80% MeOH (aq) was used as blank.

Molecular weight cut-off filters (10 kilo Dalton (kDA)) was used for cell sample filtration. Before filtration,10 kDA cut-off filters were washed once with 500 µL H_2O by centrifuging using the same settings. After centrifugation, the residual water was discarded from the filter and a fresh tube was used to collect the filtered cell sample; the supernatant was transferred to the filter and centrifuged using the same settings.

After the filtration, samples were diluted according to the relative DNA concentration and transferred to total recovery vials for IC-MS (final volume: 80 or 100 µL).

The method used is described in Section 5.16.9 and 5.16.10, as developed by Dr J. Walsby-Tickle[109, 119].

5.16.11 Data processing and statistical analysis

5.16.11.1 Processing of IC-MS raw data by Progenesis QI: semi-targeted analysis

To analyse the raw data Progenesis QI Software from Nonlinear Dynamics/Waters™ (Waters USA) was used. The raw files of IC-MS data were uploaded to Progenesis QI. The specification used was type of instrument: 'high-resolution mass spectrometer'; data format: 'profile data'; ionisation polarity: negative; adducts: M-H, M-2H, 2M-h, 3M-H and M-H_2O. The software chooses a reference (the one that has the most similar alignment with the other runs). Progenesis QI accepts a run if ≥ 90% of the alignment is in accord with the reference**.** Based on retention time and *m/z* pairs Progenesis QI picks peaks, then identifies compounds. For compound identification, an in-house database was used, where maximum retention time

deviation, maximum precursor tolerance, and maximum fragment tolerance were set to 3.0 minutes, 5 ppm, and 12 ppm, respectively. The parameters considered during metabolite identification were retention time error, mass error, fragmentation score, isotope similarity, minimum coefficient of variation (CV), and maximum abundance. Progenesis QI provides a peak intensity table for compound ions.

5.16.11.2 MetaboAnalyst: data analysis

The work described in this chapter used MetaboAnalyst 5.0 & 6.0 software to analyze data from the raw spectra. For data filtering interquartile range (IQR) was used to remove near constant non-informative variables. MetaboAnalyst software generates a PCA scores plot which helps to define outliers. Samples falling outside of the 95% confidence interval were considered as outliers and have been removed.

To confirm the appropriate normalization of data, all the possible combinations of parameters (none, median, sum and quantile normalisation, none or log transformation, and none, auto- or pareto-scaling) were applied but the combination that provided a normal (or as close to normal) distributions of features and samples and a heatmap without outlier columns was selected.

5.16.12 Compound identification

5.16.12.1 'confident, 'putative' or 'not accepted 'identification criteria

For compound identification an in-house retention time database was used **(Table A.7.1).** During searching (IC-MS database) the parameters setup was following maximum retention

time deviation: 2.0 minutes, maximum precursor tolerance: 5 ppm and maximum fragment tolerance: 12 ppm. Retention time error, mass error, fragmentation score, isotope similarity, minimum coefficient of variation (CV) and maximum abundance these parameters were used throughout metabolite identification. In general Level 1& Level 2 authentic identification standards or parameters [66] were used to decide whether an identification was confident or putative metabolite. In case of Level 1 identification, IC-MS data has been collected for metabolites and then RT has been matched to an authentic standard (e.g. in our in-house database or when separate standards were purchased and run such as after a putative ID) or Levels 2 identification were done, where for example accurate mass and ms/ms data match but have not been confirmed by running an authentic standards. retention time and mass spectrum, accurate mass and tandem MS, accurate mass and isotope pattern were used to decide whether an identification was confident or putative metabolite. **Table 5.16.12.1** shows the parameter cut-offs applied during 'confident', 'putative' or 'not accepted identification'. The parameters used to decide whether an identification should be considered confident, putative, or not acceptable are specified in **Table 5.16.12.1.**

Table 5.16.12.1.: Confident, putative, and not accepted metabolites identification criteria

Instrument	**Identification criteria**	**Retention time error (minutes)**	**ppm Error**	**Isotope similarity (%)**	**Max. abundance**
IC-MS Acquired with QExactive	Confident (metabolite)	< 1.0	2.5	> 90	-
	Putative	> 1.5 min	> 3 ppm	< 90%	-
	Not acceptable	-	-	< 85	< 50

A step-by-step putative metabolite ID protocol using human metabolome database (HMDB) was used. (www.hmdb.ca/spectra/ms/search). Searching parameters were ionisation mode; negative, mass error; 5 ppm and adducts used: M-H, M-2H, 2M-h, 3M-H and M-H_2O .

5.16.13 Principal Component Analysis Plot and Partial Least Squares Discriminant Analysis

PCA plot is a graphical representation of data produced by Principal Component Analysis (PCA). In a PCA plot, each data point represents a sample, and similar samples based on their metabolite profiles, shown as clusters in the PCA plot. PCA plot allows identification of potential patterns in a dataset. It provides overall idea or general structure of a metabolomics data before conducting any further analysis [79,121,122].

A "Partial Least Squares Discriminant Analysis" (PLS-DA) plot, Unlike PCA plot is a visual presentation used in data analysis to show how well the experimental groups of samples are separated. Each data point in the plot represents a sample and the position of the data point specifies its classification in the group. PLS-DA plot allows identification of potential outliers [79,121].

5.16.14 Volcano plot

The volcano plot is a tool, that with the help of fold change and t-test values, identifies biologically significant metabolites in a conducted experiment. In the volcano plot the X-axis represents the log2 fold differences between experimental groups and the Y-axis represents -log10 p-value differences, which helps to point out biologically upregulated and

downregulation of metabolites within the experimental groups. The horizontal line in the plot is the threshold level of significance. Data points that are more away from the (0,0) in the graph, the more significant and large magnitudes features are on both sides [79].

5.16.15 False Discovery Rate (FDR)

FDR is a statistical method used in metabolomics to monitor the ratio of false positives of each significant result when performing multiple statistical tests concurrently. In MetaboAnalyst, FDR is generally used in combination with other techniques such as t-test, ANOVA. [79,123].

5.16.16 Untargeted mummichog pathway analysis of IC-MS data

Untargeted pathway analysis was only carried out with IC-MS data. The parameters were: mass error: 5.0 ppm, MS mode; negative and retention time in minutes.

5.16.16.1 Data processing and analysis of pathway analysis

During untargeted metabolic pathway analysis of the IC MS data from all the five experimental groups, the 'functional analysis' methodology of MetaboAnalyst 6.0 was used [44]. The data were processed using univariate analysis. For pathway analysis *m/z* values and retention time were used. The p values and t scores were calculated without multiple comparison correction (MCC). Features were ranked by p values; the selected p value cut off < 0.05 expect Roxadustat (100µM) pathway analysis the selected p value cut off was <0.25.

5.16.16.2 Univariate statistics and regression analyses

Statistical analyses were performed using Prism 10.0 (GraphPad, USA). For single binary comparisons, an unpaired parametric Student's t-test was used. For multiple comparisons, one-way ANOVA followed by Tukey's or Dunnett's multiple comparison tests were used. The Dunnett's test was used when a single group (control) was compared to a number of others (treated)). Tukey's tests were used when multiple comparisons were carried out, per recommendations by Prism. Simple linear regression was carried out without forcing the line through x = 0, y = 0.

5.16.17 Reverse transcription-quantitative polymerase chain reaction (RT-qPCR)

This is described in **Section 2.9.7.**

Table 5.16.17.1: Primers used for RT-qPCR studies with forward (FW)/reverse (RV) sequences.

GLUT1	RV CTT GTGCTC CTG AGA GAT CC FW TCA CTG TGC TCC TGG TTC TG
HK2	RV CTT ACA CGA GGT CAC ATA GC FW CCA GTT CAT TCA CAT CAT CAG
ENO1	RV GAT GAC ACG AGG CTC AC FW CGT ACC GCT TCC TTA GA
LDHA	RV ATA GCC CAG GAT GTG TAG CC FW TGG AGT GGA ATG AAT GTT GC

Actin	RV CAT GGA TGC CAC AGG ATT CCA TAC FW TGC CCT AGA CTT CGA GCA AGA

5.16.18 Treatment with 1% O_2, $CoCl_2$ & PHD inhibitors for Seahorse glycolytic rate assays

HEK 293T cells were seeded at a predetermined density in the Agilent Seahorse XF cell culture microplate using the appropriate cell culture growth medium, waiting for 24 hours for cells to attach. The cells were then treated with 150 µM $CoCl_2$, 100µM Roxadustat or Molidustat; and the control group was treated with DMSO (the final concentration 0.1% (v/v)). Four wells of the microplate were kept without cells as background correction wells.

The Hydrate sensor cartridge was prepared the day before assays and kept overnight in the non-CO_2 chamber of the Seahorse XF 37 °C.

5.16.18.1 Preparation of glycolytic rate assay medium

The assay medium was prepared on the day the assay was conducted, using Seahorse XF DMEM medium (Agilent), adjusting the pH to 7.4 with HEPES. 1 mM of pyruvate, 2 mM of glutamine, and 10 mM of glucose solution (Agilent) were added to the Seahorse XF DMEM media (at 37 °C).

5.16.18.2 Preparation of Seahorse XF Cell culture microplate

The Seahorse 24 well microplate was taken out of the 37 °C CO_2 chamber; the cell culture growth medium carefully was removed from 24 microplates, which were then washed with

Seahorse XF DMEM medium and incubated with assay medium at 37 °C in a non-CO2 incubator for 45-60 minutes prior to the assay. Before starting the experiment, the 24 microplate was washed again with fresh warm assay medium, and the final assay medium volume was 500µL.

5.16.18.3 Preparation of Seahorse stock compounds

Stock compounds were from Agilent (USA) and were freshly prepared daily. The Agilent Seahorse glycolytic rate assay kit contains two vials: one rotenone and antimycin A (Rot/AA) vial and one 2-deoxy-D-glucose (2-DG) vial/ stock solutions were prepared as in **Table 5.16.8.1.**

Table 5.16.18.1: Stock solutions.

Compound	**Volume of assay medium**	**Resulting stock concentration**	**Final Concentration**
Rot/AA	540 µL	50 µM	0.5 µM
2-DG	3000 µL	500 mM	50mM

5.16.18.4 Load sensor cartridge

The hydrated cartridge and cartridge lid were removed, and the compounds were loaded into the ports as required and placed inside the XFe24 analyzer for calibration; Seahorse XFe assays were then carried out.

5.17 References

1. Haase, V.H., *Hypoxia-inducible factor–prolyl hydroxylase inhibitors in the treatment of anemia of chronic kidney disease*. Kidney Int. Suppl., 2021. 11(1): p. 8-25. DOI: 10.1016/j.kisu.2020.12.002

2. Semenza, G.L., *Hypoxia-inducible factors in physiology and medicine*. Cell, 2012. 148(3): p. 399-408. DOI: 10.1016/j.cell.2012.01.021

3. Semenza, G.L., *Oxygen sensing, homeostasis, and disease*. N Engl J Med, 2011. 365(6): p. 537-547. DOI: 10.1056/NEJMra1011165

4. Wang, G.L. and G.L. Semenza, *General involvement of hypoxia-inducible factor 1 in transcriptional response to hypoxia*. PNAS, 1993. 90(9): p. 4304-4308. DOI: 10.1073/pnas.90.9.4304

5. Maxwell, P., C. Pugh, and P. Ratcliffe, *Inducible operation of the erythropoietin 3'enhancer in multiple cell lines: evidence for a widespread oxygen-sensing mechanism*. PNAS, 1993. 90(6): p. 2423-2427. DOI: 10.1073/pnas.90.6.2423

6. Firth, J., et al., *Oxygen-regulated control elements in the phosphoglycerate kinase 1 and lactate dehydrogenase A genes: similarities with the erythropoietin 3'enhancer*. PNAS, 1994. 91(14): p. 6496-6500. DOI: 10.1073/pnas.91.14.6496

7. Levy, A.P., et al., *Transcriptional Regulation of the Rat Vascular Endothelial Growth Factor Gene by Hypoxia*. J. Biol. Chem., 1995. 270(22): p. 13333-13340. DOI: 10.1074/jbc.270.22.13333

8. Watanabe, K., et al., *What's new in the molecular mechanisms of diabetic kidney disease: Recent advances*. Int. J. Mol. Sci., 2022. 24(1): p. 570. DOI: 10.3390/ijms24010570

9. Watanabe, K., et al., *Changes in Metabolomic Profiles Induced by Switching from an Erythropoiesis-Stimulating Agent to a Hypoxia-Inducible Factor Prolyl Hydroxylase Inhibitor in Hemodialysis Patients: A Pilot Study*. Int. J. Mol. Sci., 2023. 24(16): p. 12752. DOI: 10.3390/ijms241612752

10. Fiehn, O., *Metabolomics–the link between genotypes and phenotypes*. Plant Mol. Biol., 2002. 48: p. 155-171.

11. Tolstikov, V., *Metabolomics: bridging the gap between pharmaceutical development and population health*. Metabolites, 2016. 6(3): p. 20. DOI: 10.3390/metabo6030020

12. Patti, G.J., O. Yanes, and G. Siuzdak, *Metabolomics: the apogee of the omics trilogy*. Nat. Rev. Mol. Cell Biol., 2012. 13(4): p. 263-269. DOI: 10.1038/nrm3314

13. Johnson, C.H., J. Ivanisevic, and G. Siuzdak, *Metabolomics: beyond biomarkers and towards mechanisms*. Nat. Rev. Mol. Cell Biol., 2016. 17(7): p. 451-459. DOI: 10.1038/nrm.2016.25

14. Llufrio, E.M., K. Cho, and G.J. Patti, *Systems-level analysis of isotopic labeling in untargeted metabolomic data by X13CMS*. Nature protocols, 2019. 14(7): p. 1970-1990. DOI: 10.1038/s41596-019-0167-1

15. Roberts, L.D., et al., *Targeted metabolomics*. Current protocols in molecular biology, 2012. 98(1): p. 30.2. 1-30.2. 24. DOI: 10.1002/0471142727.mb3002s98

16. Ribbenstedt, A., H. Ziarrusta, and J.P. Benskin, *Development, characterization and comparisons of targeted and non-targeted metabolomics methods*. PLoS One, 2018. 13(11): p. e0207082. DOI: 10.1371/journal.pone.0207082

17. Han, S., et al., *A metabolomics pipeline for the mechanistic interrogation of the gut microbiome*. Nature, 2021. 595(7867): p. 415-420. DOI: 10.1038/s41586-021-03707-9

18. Alarcon-Barrera, J.C., et al., *Recent advances in metabolomics analysis for early drug development*. Drug Discov. Today, 2022. 27(6): p. 1763-1773. DOI: 10.1016/j.drudis.2022.02.018

19. Wishart, D.S., et al., *HMDB 5.0: the human metabolome database for 2022*. Nucleic Acids Res., 2022. 50(D1): p. D622-D631. DOI: 10.1093/nar/gkab1062

20. Smith, C.A., et al., *METLIN: a metabolite mass spectral database*. Ther. Drug Monit., 2005. 27(6): p. 747-751. DOI: 10.1097/01.ftd.0000179845.53213.39

21. Tsugawa, H., et al., *MS-DIAL: data-independent MS/MS deconvolution for comprehensive metabolome analysis*. Nature methods, 2015. 12(6): p. 523-526. DOI: 10.1038/nmeth.3393

22. Salek, R.M., et al., *The role of reporting standards for metabolite annotation and identification in metabolomic studies*. GigaScience, 2013. 2(1): p. 2047-217X-2-13. DOI: 10.1186/2047-217X-2-13

23. Wishart, D.S., et al., *HMDB: the human metabolome database*. Nucleic Acids Res., 2007. 35(suppl_1): p. D521-D526. DOI: 10.1093/nar/gkl923

24. Smith, C.A., et al., *XCMS: processing mass spectrometry data for metabolite profiling using nonlinear peak alignment, matching, and identification*. Analytical chemistry, 2006. 78(3): p. 779-787. DOI: 10.1021/ac051437y

25. Xia, J. and D.S. Wishart, *Web-based inference of biological patterns, functions and pathways from metabolomic data using MetaboAnalyst*. Nature protocols, 2011. 6(6): p. 743-760. DOI: 10.1038/nprot.2011.319

26. Giné, R., et al., *HERMES: a molecular-formula-oriented method to target the metabolome*. Nature Methods, 2021. 18(11): p. 1370-1376. DOI: 10.1038/s41592-021-01307-z

27. Xia, J. and D.S. Wishart, *MetPA: a web-based metabolomics tool for pathway analysis and visualization*. Bioinformatics, 2010. 26(18): p. 2342-2344. DOI: 10.1093/bioinformatics/btq418

28. Du, J., et al., *A decision analysis model for KEGG pathway analysis*. BMC bioinformatics, 2016. 17(1): p. 1-12. DOI: 10.1186/s12859-016-1285-1

29. Liu, N., et al., *Comparison of untargeted metabolomic profiling vs traditional metabolic screening to identify inborn errors of metabolism*. JAMA Network Open, 2021. 4(7): p. e2114155-e2114155. DOI: 10.1001/jamanetworkopen.2021.14155

30. Miller, M.J., et al., *Untargeted metabolomic analysis for the clinical screening of inborn errors of metabolism*. J. Inherit. Metab. Dis., 2015. 38: p. 1029-1039. DOI: 10.1007/s10545-015-9843-7

31. Schrimpe-Rutledge, A.C., et al., *Untargeted metabolomics strategies—challenges and emerging directions*. J Am Soc Mass Spectrom, 2016. 27(12): p. 1897-1905. DOI: 10.1007/s13361-016-1469-y

32. Che, N., et al., *Integrated semi-targeted metabolomics analysis reveals distinct metabolic dysregulation in pleural effusion caused by tuberculosis and malignancy*. Clinica Chimica Acta, 2018. 477: p. 81-88. DOI: 10.1016/j.cca.2017.12.003

33. Amer, B., R.R. Deshpande, and S.S. Bird, *Simultaneous quantitation and discovery (SQUAD) analysis: combining the best of targeted and untargeted mass spectrometry-based metabolomics*. Metabolites, 2023. 13(5): p. 648. DOI: 10.3390/metabo13050648

34. Karnovsky, A. and S. Li, *Pathway analysis for targeted and untargeted metabolomics. Computational methods and data analysis for metabolomics*, 2020: p. 387-400. DOI: 10.1007/978-1-0716-0239-3_19

35. Chong, J., et al., *MetaboAnalyst 4.0: towards more transparent and integrative metabolomics analysis*. Nucleic Acids Res., 2018. 46(W1): p. W486-W494. DOI: 10.1093/nar/gky310

36. Streiff, M., *Metabolic Pathway Activation: An Analysis of the Effects of Traffic Related Air Pollution and Physical Activity*. 2020. DOI: 10.1016/S2213-8587(23)00361-3

37. Li, S., et al., *Predicting network activity from high throughput metabolomics*. PLoS computational biology, 2013. 9(7): p. e1003123. DOI: 10.1371/journal.pcbi.1003123

38. Amin, M., L.W. Lim, and T. Takeuchi, D*etermination of common inorganic anions and cations by non-suppressed ion chromatography with column switching*. J. Chromatogr. A, 2008. 1182(2): p. 169-175. DOI: 10.1016/j.chroma.2008.01.007

39. Fan, J., et al., *Ion chromatography based urine amino acid profiling applied for diagnosis of gastric cancer*. Gastroenterology research and Practice, 2012. 2012. DOI: 10.1155/2012/474907

40. Sekiguchi, Y., et al., *Development of a comprehensive analytical method for phosphate metabolites in plants by ion chromatography coupled with tandem mass spectrometry*. J. Chromatogr. A, 2005. 1085(1): p. 131-136. DOI: 10.1016/j.chroma.2005.01.098

41. Ngere, J.B., et al., *Ion-exchange chromatography coupled to mass spectrometry in life science, environmental, and medical research*. Anal. Chem., 2023. 95(1): p. 152-166. DOI: 10.1021/acs.analchem.2c04298

42. Paulo, A., C. Castillo, and S. Neidle, *Targeting Promoter Quadruplex Nucleic Acids for Cancer Therapy*. 2017. DOI: 10.1021/acs.jmedchem.5b01835

43. Yang, C., et al., *Analysis of hypoxia-induced metabolic reprogramming*. Methods Enzymol., 2014. 542: p. 425-455. DOI: 10.1016/B978-0-12-416618-9.00022-4

44. Seagroves, T.N., et al., *Transcription factor HIF-1 is a necessary mediator of the pasteur effect in mammalian cells*. Mol Cell Biol, 2001. 21(10): p. 3436-3444. DOI: 10.1128/MCB.21.10.3436-3444.2001

45. Semenza, G.L., et al., *Transcriptional regulation of genes encoding glycolytic enzymes by hypoxia-inducible factor 1*. J. Biol. Chem., 1994. 269(38): p. 23757-23763.DOI: https://doi.org/10.1016/S0021-9258(17)31580-6

46. Burgess, K., *Ion Chromatography Coupled with Mass Spectrometry for Metabolomics*.

47. Zeng, Z., et al., *The pyruvate dehydrogenase complex in sepsis: metabolic regulation and targeted therapy*. Front. Nutr., 2021. 8: p. 783164. DOI: 10.3389/fnut.2021.783164

48. Kierans, S. and C. Taylor, *Regulation of glycolysis by the hypoxia-inducible factor (HIF): implications for cellular physiology*. The Journal of physiology, 2021. 599(1): p. 23-37. DOI: 10.1113/JP280572

49. Semenza, G.L., et al., *Hypoxia response elements in the aldolase A, enolase 1, and lactate dehydrogenase A gene promoters contain essential binding sites for hypoxia-inducible factor 1*. J. Biol. Chem., 1996. 271(51): p. 32529-32537. DOI: 10.1074/jbc.271.51.32529

50. Alfarouk, K.O., et al., *Glycolysis, tumor metabolism, cancer growth and dissemination. A new pH-based etiopathogenic perspective and therapeutic approach to an old cancer question*. Oncoscience, 2014. 1(12): p. 777. DOI: 10.18632/oncoscience.109

51. Taegtmeyer, H., *Metabolic responses to cardiac hypoxia. Increased production of succinate by rabbit papillary muscles*. Circ. Res., 1978. 43(5): p. 808-815. DOI: 10.1161/01.res.43.5.808

52. Kim, J.-w., et al., *HIF-1-mediated expression of pyruvate dehydrogenase kinase: a metabolic switch required for cellular adaptation to hypoxia*. Cell metabolism, 2006. 3(3): p. 177-185. DOI: 10.1016/j.cmet.2006.02.002

53. Papandreou, I., et al., *HIF-1 mediates adaptation to hypoxia by actively downregulating mitochondrial oxygen consumption*. Cell metabolism, 2006. 3(3): p. 187-197. DOI: 10.1016/j.cmet.2006.01.012

54. Samanta, D., et al., *Hypoxia-inducible factors are required for chemotherapy resistance of breast cancer stem cells*. PNAS, 2014. 111(50): p. E5429-E5438. DOI: 10.1073/pnas.1421438111

55. Byersdorfer, C. and P. Reddy, *Intracellular Sensors and Cellular Metabolism in Allogeneic Hematopoietic Stem Cell Transplantation*, in Immune Biology of Allogeneic Hematopoietic Stem Cell Transplantation. 2019, Elsevier. p. 349-374. DOI: 10.1146/annurev.immunol.25.022106.141606

56. Iommarini, L., et al., *Non-canonical mechanisms regulating hypoxia-inducible factor 1 alpha in cancer*. Front. oncol., 2017. 7: p. 286. DOI: 10.3389/fonc.2017.00286

57. Ebert, B.L., J.D. Firth, and P.J. Ratcliffe, *Hypoxia and mitochondrial inhibitors regulate expression of glucose transporter-1 via distinct Cis-acting sequences*. J. Biol. Chem., 1995. 270(49): p. 29083-29089. DOI: 10.1074/jbc.270.49.29083

58. Iyer, N.V., et al., *Cellular and developmental control of O2 homeostasis by hypoxia-inducible factor 1α*. Genes & development, 1998. 12(2): p. 149-162. DOI: 10.1101/gad.12.2.149

59. Simon, M.C., *Coming up for air: HIF-1 and mitochondrial oxygen consumption*. Cell Metab., 2006. 3(3): p. 150-151. DOI: 10.1016/j.cmet.2006.02.007

60. Taylor, C.T. and C.C. Scholz, *The effect of HIF on metabolism and immunity*. Nat. Rev. Nephrol., 2022. 18(9): p. 573-587. DOI: 10.1038/s41581-022-00587-8

61. Goda, N. and M. Kanai, *Hypoxia-inducible factors and their roles in energy metabolism*. Int. J. Hematol., 2012. 95: p. 457-463. DOI: 10.1007/s12185-012-1069-y

62. Mole, D.R., et al., *2-oxoglutarate analogue inhibitors of HIF prolyl hydroxylase*. Bioorg Med Chem Lett., 2003. 13(16): p. 2677-2680. DOI: 10.1016/s0960-894x(03)00539-0

63. Rabinowitz, M.H., et al., *Inhibitors of HIF prolyl hydroxylases*, in Annual Reports in Medicinal Chemistry. 2010, Elsevier. p. 123-139. DOI: 10.1021/jm400386j

64. Tojo, K., et al., *Enhancement of glycolysis by inhibition of oxygen-sensing prolyl hydroxylases protects alveolar epithelial cells from acute lung injury*. The FASEB Journal, 2018. 32(4): p. 2258-2268. DOI: 10.1096/fj.201700888R

65. Ito, M., et al., *Prolyl hydroxylase inhibition protects the kidneys from ischemia via upregulation of glycogen storage*. Kidney Int., 2020. 97(4): p. 687-701. DOI 10.1016/j.kint.2019.10.020

66. Summer, L., et al., *Proposed minimum reporting standards for chemical analysis*. Metabolomics, 2007. 3(3): p. 211-221. DOI: 10.1007/s11306-007-0082-2

67. Pang, Z., et al., *MetaboAnalyst 5.0: narrowing the gap between raw spectra and functional insights*. Nuc. Acids Res., 2021. 49(W1): p. W388-W396.DOI: https://doi.org/10.1093/nar/gkab382

68. Kierans, S.J., et al., *Hypoxia induces a glycolytic complex in intestinal epithelial cells independent of HIF-1-driven glycolytic gene expression*.PNAS., 2023. 120(35): p. e2208117120.DOI: https://doi.org/10.1073/pnas.2208117120

69. Pascale, A., et al., *Microbiota and metabolic diseases*. Endocrine, 2018. 61: p. 357-371. DOI: 10.1007/s12020-018-1605-5

70. Gao, J., et al., *Metabolomic analysis of human plasma sample after exposed to high altitude and return to sea level*. Plos one, 2023. 18(3): p. e0282301. DOI: 10.1371/journal.pone.0282301

71. Valdés, A., et al., *Comprehensive metabolomic study of the response of HK-2 cells to hyperglycemic hypoxic diabetic-like milieu*. Scientific Reports, 2021. 11(1): p. 5058. DOI: 10.1038/s41598-021-84590-2

72. Cohen, E.B., R.C. Geck, and A. Toker, *Metabolic pathway alterations in microvascular endothelial cells in response to hypoxia*. PloS One, 2020. 15(7): p. e0232072. DOI: 10.1371/journal.pone.0232072

73. d'Alessandro, A., et al., *AltitudeOmics: red blood cell metabolic adaptation to high altitude hypoxia*. J. Proteome Res., 2016. 15(10): p. 3883-3895. DOI: 10.1021/acs.jproteome.6b00733

74. Kind, T. and O. Fiehn, *Seven Golden Rules for heuristic filtering of molecular formulas obtained by accurate mass spectrometry*. BMC bioinformatics, 2007. 8: p. 1-20. DOI: 10.1186/1471-2105-8-105

75. Mahmod, I.F., et al., *Comparative Metabolomics Analysis of Weedy Rice (Oryza spp.) across Peninsular Malaysia*. Agriculture, 2023. 13(6): p. 1230. DOI: **https://doi.org/10.3390/agriculture13061230**

76. Farrés, M., et al., *Comparison of the variable importance in projection (VIP) and of the selectivity ratio (SR) methods for variable selection and interpretation*. J. Chemom., 2015. 29(10): p. 528-536.DOI: **https://doi.org/10.1002/cem.2736**

77. Mehmood, T., et al., A review of variable selection methods in partial least squares regression. Chemometrics and intelligent laboratory systems, 2012. 118: p. 62-69.DOI: https://doi.org/10.1016/j.chemolab.2012.07.010

78. Ikeda, K., et al., *Mitochondrial supercomplex assembly promotes breast and endometrial tumorigenesis by metabolic alterations and enhanced hypoxia tolerance*. Nat Commun, 2019. 10(1): p. 4108. DOI: 10.1038/s41467-019-12124-6

79. Zhiqiang Pang, J.C., Jeff Xia. Statistical Analysis. 2023-07-24.

80. Gehlenborg, N. and B. Wong, *Heat maps*. Nature Methods, 2012. 9(3): p. 213. DOI: 10.1038/nmeth.1902

81. Chong, J., D.S. Wishart, and J. Xia, *Using MetaboAnalyst 4.0 for comprehensive and integrative metabolomics data analysis*. Curr. Protoc. Bioinform., 2019. 68(1): p. e86. DOI: 10.1002/cpbi.86

82. Hasan, M.M., et al., *Desorption ionization using through-hole alumina membrane offers higher reproducibility than 2, 5-dihydroxybenzoic acid, a widely used matrix in Fourier transform ion cyclotron resonance mass spectrometry imaging analysis*. Rapid Communications in Mass Spectrometry, 2021. 35(10): p. e9076. DOI: 10.1002/rcm.9076

83. Korfmacher, W.A., *Using mass spectrometry for drug metabolism studies*. 2009: CRC Press.

84. Tsouka, S. and M. Masoodi, *Metabolic pathway analysis: advantages and pitfalls for the functional interpretation of metabolomics and lipidomics data*. Biomolecules, 2023. 13(2): p. 244. DOI: 10.3390/biom13020244

85. Booth, S.C., A.M. Weljie, and R.J. Turner, *Computational tools for the secondary analysis of metabolomics experiments*. CSBJ, 2013. 4(5): p. e201301003. DOI: 10.5936/csbj.201301003

86. Khatri, P., M. Sirota, and A.J. Butte, *Ten years of pathway analysis: current approaches and outstanding challenges*. PLoS computational biology, 2012. 8(2): p. e1002375. DOI: 10.1371/journal.pcbi.1002375

87. Lu, Y., Z. Pang, and J. Xia, *Comprehensive investigation of pathway enrichment methods for functional interpretation of LC–MS global metabolomics data*. Briefings in Bioinformatics, 2023. 24(1): p. bbac553. DOI: 10.1093/bib/bbac553

88. Wang, W., et al., T*argeting pyrimidine metabolism in the era of precision cancer medicine*. Front. oncol., 2021. 11: p. 684961. DOI: 10.3389/fonc.2021.684961

89. Bajzikova, M., et al., *Reactivation of dihydroorotate dehydrogenase-driven pyrimidine biosynthesis restores tumor growth of respiration-deficient cancer cells*. Cell metabolism, 2019. 29(2): p. 399-416. e10. DOI: 10.1016/j.cmet.2018.10.014

90. Okesli, A., C. Khosla, and M.C. Bassik, *Human pyrimidine nucleotide biosynthesis as a target for antiviral chemotherapy*. Curr Opin Biotechnol., 2017. 48: p. 127-134. DOI: 10.1016/j.copbio.2017.03.010

91. Brown, K.K., et al., *Adaptive reprogramming of de novo pyrimidine synthesis is a metabolic vulnerability in triple-negative breast cancer*. Cancer discovery, 2017. 7(4): p. 391-399. DOI: 10.1158/2159-8290.CD-16-0611

92. Mathur, D., et al., *PTEN regulates glutamine flux to pyrimidine synthesis and sensitivity to dihydroorotate dehydrogenase inhibition*. Cancer discovery, 2017. 7(4): p. 380-390. DOI: 10.1158/2159-8290.CD-16-0612

93. Cunningham, J.T., et al., Protein and nucleotide biosynthesis are coupled by a single rate-limiting enzyme, PRPS2, to drive cancer. Cell, 2014. 157(5): p. 1088-1103. DOI: 10.1016/j.cell.2014.03.052

94. Ma S, Yeom J, Lim YH. *Specific activation of hypoxia-inducible factor-2α by propionate metabolism via a β-oxidation-like pathway stimulates MUC2 production in intestinal goblet cells*. Biomed. Pharmacother. 2022 Nov 1;155:113672. DOI: 10.1016/j.biopha.2022.113672

95. Dodd MS, Sousa Fialho MD, Montes Aparicio CN, Kerr M, Timm KN, Griffin JL, Luiken JJ, Glatz JF, Tyler DJ, Heather LC. *Fatty acids prevent hypoxia-inducible factor-1α signaling through decreased succinate in diabetes*. J Am Coll Cardiol Basic Trans Science. 2018 Aug;3(4):485-98. DOI: 10.1016/j.jacbts.2018.04.005

96. Badawi, Y., P. Ramamoorthy, and g. Shi, *Hypoxia-inducible factor 1 protects hypoxic astrocytes against glutamate toxicity*. ASN neuro, 2012. 4(4): p. AN20120006. DOI: 10.1042/AN20120006

97. Watanabe, Y., et al., Glutathione adducts induced by ischemia and deletion of glutaredoxin-1 stabilize HIF-1α and improve limb revascularization. PNAS, 2016. 113(21): p.

6011-6016. DOI: https://doi.org/10.1073/pnas.1524198113

98. Wieder, C., et al., Avoiding the misuse of pathway analysis tools in environmental metabolomics. Environ Sci Technol., 2022. 56(20): p. 14219-14222. DOI: 10.1021/acs.est.2c05588

99. Wieder, C., et al., *Pathway analysis in metabolomics: Recommendations for the use of over-representation analysis*. PLoS computational biology, 2021. 17(9): p. e1009105. DOI: 10.1371/journal.pcbi.1009105

100. Koblitz, J., D. Schomburg, and M. Neumann-Schaal, *MetaboMAPS: pathway sharing and multi-omics data visualization in metabolic context*. F1000Research, 2020. 9. DOI: 10.12688/f1000research.23427.2

101. Chan MC, Ilott NE, Schödel J, Sims D, Tumber A, Lippl K, Mole DR, Pugh CW, Ratcliffe PJ, Ponting CP, Schofield CJ. *Tuning the transcriptional response to hypoxia by inhibiting hypoxia-inducible factor (HIF) prolyl and asparaginyl hydroxylases.* J. Biol. Chem., 2016 Sep 1;291(39):20661-73. doi: 10.1074/jbc.M116.749291

102. Szablewski, L., *Distribution of glucose transporters in renal diseases*. J. Biomed. Sci., 2017. 24: p. 1-12. DOI: https://doi.org/10.1186/s12929-017-0371-7

103. Sędzikowska, A. and L. Szablewski, *Human glucose transporters in renal glucose homeostasis*. Int. J. Mol. Sci., 2021. 22(24): p. 13522. DOI: 10.3390/ijms222413522

104. Wei, X., et al., *Molecular mechanisms underlying the role of hypoxia-inducible factor-1 α in metabolic reprogramming in renal fibrosis*. Front. Endocrinol., 2022. 13: p. 927329. DOI: 10.3389/fendo.2022.927329

105. Nowak, N., A. Kulma, and J. Gutowicz, *Up-regulation of key glycolysis proteins in cancer development*. Open life sciences, 2018. 13(1): p. 569-581. DOI: 10.1515/biol-2018-0068

106. Didiasova, M., L. Schaefer, and M. Wygrecka, *When place matters: shuttling of enolase-1 across cellular compartments*. Front. cell dev. biol., 2019. 7: p. 61. DOI: 10.3389/fcell.2019.00061

107. Shim, H., et al., *c-Myc transactivation of LDH-A: implications for tumor metabolism and growth*. PNAS, 1997. 94(13): p. 6658-6663. DOI: 10.1073/pnas.94.13.6658

108. Gomes, M.T.R., et al., *STING regulates metabolic reprogramming in macrophages via HIF-1α during Brucella infection*. PLoS pathogens, 2021. 17(5): p. e1009597. DOI: 10.1371/journal.ppat.1009597

109. Cumming, B.M., et al., *Mycobacterium tuberculosis induces decelerated bioenergetic metabolism in human macrophages*. Elife, 2018. 7: p. e39169. DOI: 10.7554/eLife.39169

110. Luo W, Hu H, Chang R, Zhong J, Knabel M, O'Meally R, Cole RN, Pandey A, Semenza GL. Pyruvate kinase M2 is a PHD3-stimulated coactivator for hypoxia-inducible factor 1. Cell. 2011 May 27;145(5):732-44.

111. Semenza GL. Hypoxia-inducible factors in physiology and medicine. Cell. 2012 Feb 3;148(3):399-408.

112. Karlstaedt A, Zhang X, Vitrac H, Harmancey R, Vasquez H, Wang JH, Goodell MA, Taegtmeyer H. Oncometabolite d-2-hydroxyglutarate impairs α-ketoglutarate dehydrogenase and contractile function in rodent heart. Proceedings of the National Academy of Sciences. 2016 Sep 13;113(37):10436-41.

113. Yuan Y, Hilliard G, Ferguson T, Millhorn DE. Cobalt inhibits the interaction between hypoxia-inducible factor-α and von Hippel-Lindau protein by direct binding to hypoxia-inducible factor-α. Journal of Biological Chemistry. 2003 May 2;278(18):15911-6.

114. Tripathi VK, Subramaniyan SA, Hwang I. Molecular and Cellular Response of Co-cultured Cells toward Cobalt Chloride ($CoCl_2$)-Induced Hypoxia. ACS Omega. 2019 Dec 2;4(25):20882-20893. doi: 10.1021/acsomega.9b01474. PMID: 31867478; PMCID: PMC6921254.

115. Zhu X, Jiang L, Wei X, Long M, Du Y. Roxadustat: Not just for anemia. Front Pharmacol. 2022 Aug 29;13:971795. doi: 10.3389/fphar.2022.971795. PMID: 36105189; PMCID: PMC9465375.

116. Mäkinen, S., Sree, S., Ala-Nisula, T. *et al.* Activation of the hypoxia-inducible factor pathway by roxadustat improves glucose metabolism in human primary myotubes from men. *Diabetologia* **67**, 1943–1954 (2024). https://doi.org/10.1007/s00125-024-06185-6

117. Sousa Fialho MDL, Purnama U, Dennis KMJH, Montes Aparicio CN, Castro-Guarda M, Massourides E, Tyler DJ, Carr CA, Heather LC. Activation of HIF1α Rescues the Hypoxic Response and Reverses Metabolic Dysfunction in the Diabetic Heart. Diabetes. 2021 Nov;70(11):2518-2531. doi: 10.2337/db21-0398. Epub 2021 Sep 15. PMID: 34526367; PMCID: PMC8564414.

118. Kathagen-Buhmann A, Schulte A, Weller J, Holz M, Herold-Mende C, Glass R, Lamszus K. Glycolysis and the pentose phosphate pathway are differentially associated with the dichotomous regulation of glioblastoma cell migration versus proliferation. Neuro Oncol.

2016 Sep;18(9):1219-29. doi: 10.1093/neuonc/now024. Epub 2016 Feb 24. PMID: 26917237; PMCID: PMC4998991.

119. Walsby-Tickle, J., et al., *Anion-exchange chromatography mass spectrometry provides extensive coverage of primary metabolic pathways revealing altered metabolism in IDH1 mutant cells*. Commun Biol , 2020. 3(1): p. 247. DOI: https://doi.org/10.1038/s42003-020-0957-6

120. Walsby-Tickle, J., *Investigating isocitrate dehydrogenase mutations in cancer using new metabolomics methods,* in Depart of Chemistry. 2020, University of Oxford.

121. Xia, J., et al., *MetaboAnalyst 2.0—a comprehensive server for metabolomic data analysis*. Nuc. Acids Res., 2012. 40(W1): p. W127-W133. DOI: 10.1093/nar/gks374

122. Xia J, Psychogios N, Young N, Wishart DS. *MetaboAnalyst: a web server for metabolomic data analysis and interpretation.* Nuc. Acids Res.. 2009 Jul 1;37(suppl_2):W652-60. DOI: 10.1093/nar/gkp356

123. Chen X, Robinson DG, Storey JD. T*he functional false discovery rate with applications to genomics*. Biostatistics. 2021 Jan 1;22(1):68-81. DOI: 10.1093/biostatistics/kxz010

Chapter 6

Conclusions and further work

6.1. Conclusions

Clinically available PHD inhibitors have demonstrated therapeutic efficacy for the treatment of anaemia [1], but there is considerable further scope to explore new methods for PHD modulation through synthetic and naturally originated compounds, both with respect to the inhibition and enhancement of PHD activity.

The work described in this thesis principally concerned cellular studies to the extent to which PHD selective and non-selective small-molecules and $CoCl_2$ mimic the natural response to hypoxia. In addition to the clinically used PHD inhibitors (Roxadustat and Molidustat), studies were also carried out on $CoCl_2$, a novel PHD inhibitor (IOX5), a prodrug form of IOX5, an approach intended to enhance cell permeability, and a PHD2 activity enhancing molecule.

Studies were also carried out on a natural cobalt ion source from a diet component (*Spinacia Oleracea* leaf extracts) and proline analogues[2,3]. One aim was to compare the abilities of seemingly selective modulation (e.g. PHD inhibitor drugs) with likely broader mimics of hypoxia, in particular by using a metabolomic MS based approach, something that has not previously been explored in detail with respect to comparing different mimics of the natural hypoxic response. A comprehensive semi targeted metabolomics protocol was developed and used to investigate the impacts of hypoxia (1% O_2), $CoCl_2$ and the clinical PHD inhibitors Roxadustat and Molidustat on mammalian cell metabolism. This was expanded by using IC-MS–based semitargeted metabolomics in HEK 293T cells to profile the metabolic consequences of PHD inhibitors (Roxadustat, Molidustat), hypoxia, and $CoCl_2$ and impact of these treatments on glycolytic flux.

As described in **Chapter 2,** cellular studies on IOX5 demonstrated that the extent of HIF-α stabilisation observed was dependent both on the dose and the duration of treatment. Thus, after 6 hours of treatment, 100µM of IOX5 resulted in clear stabilisation of HIF-1α, but 50µM of IOX5 did not do so. However, IOX5 showed an ability to stabilize HIF-1α when a concentration of only 0.5µM was used for 18 hours of treatment. The overall results reveal that the novel PHD inhibitor IOX5 is remarkably potent at inducing HIF-1α accumulation compared to the tested clinical PHD inhibitors (Roxadustat, Daprodustat and Molidustat).

Cytotoxicity assay results indicate that even at relatively high concentrations treatment of cells with IOX5 is non-toxic. Two different cell lines, HEK 293T and HEPG2 were used to evaluate the cytotoxicity of IOX5; ~70% and ˜80% of cells, respectively, were viable after treatment with high doses (up to 500 µM) of IOX5 compared to the control. The cytotoxicity of IOX5 was compared with that of Roxadustat. Both the tested cell lines showed the same impact on cell viability upon IOX5 treatment. However, in the case of HEK 293T cells, IOX5 was less cytotoxic than compared to Roxadustat but at higher concentrations (300 & 500 µM) both IOX5 and Roxadustat treatment groups showed very similar effects.

Consistent with its positive effect on HIF-α stabilisation, IOX5 also showed an influence on hypoxia-responsive gene expression in HEK 293T cells. Amongst all the genes examined, the *HIF1α,* and *VEGF* genes were substantially upregulated in HEK 293T cells compared to the control group. IOX5 did not seem to have any significant influence on *EPO* and *CA9* gene expression compared to the control group. At least in the case of the *CA9* gene, this may reflect a need for FIH inhibition for optimal HIF mediated expression of certain HIF target

genes [9]. The results for IOX5 were compared with those for Roxadustat. Interestingly, like IOX5, Roxadustat also showed a similar effect on hypoxia-related gene expression, i.e. the *HIF1α,* and *VEGF* genes were substantially upregulated whereas the *EPO* and *CA9* genes were not altered by Roxadustat when compared with the controls.

In-vivo experiments on mice revealed that IOX5 significantly increases the RBC, HGB and HCT levels compared to the pre-treatment state. 8 days of treatment of IOX5 (15mg/kg) increased the RBC count in experimental mice, but did not increase the HGB and HCT levels compared to the preclinical state. However, after 4- and 8-days treatment 30mg/kg of IOX5 significantly increased the RBC, HGB and HCT levels (except day 4 RBC count) when compared with the treated state. On the other hand, the clinically used PHD inhibitor Daprodustat, was not observed to substantially increase the RBC, HGB and HCT levels compared to the pre-treatment state. Further In-vivo animal experiments with IOX5 are ongoing.

This thesis also describes work on a prodrug form of IOX5, which was prepared to explore the possibilities of improving IOX5 by being activated in a specific intracellular system. Treatment of cells with 20, 50 & 100μM of the IOX5 prodrug was observed to stabilize HIF-1α when incubated for 6 hours. These observations indicate that cell permeability may be an issue with IOX5. However, the prodrug showed its ability to stabilize HIF-1α even at the lower concentration of 1 μM when incubated for 18 hours. Considering the overall results, the prodrug of IOX5 is remarkably potent at causing HIF-1α accumulation compared to the available clinical PHD inhibitors. More, detailed cellular investigations of prodrug (**6**) are required to assay its capacity to stabilize HIF-1α in vivo.

The work described in this thesis **(Chapter 3)** examined $CoCl_2$, a hypoxia mimic which has been used to treat anaemia and likely works, at least in part, via PHD inhibition[10-13]. However, $CoCl_2$ treatment has side effects[14,15], though it is used (illegally) by some athletes[13]. There is a possibility that a natural cobalt containing human diet could act as a PHD inhibitor. After initial literature analysis, spinach was selected to carry out an extraction procedure to provide material for and run cellular investigations because spinach is enriched with cobalt ions, is readily available, and is consumed by many people. More cellular investigations especially with different cell lines are required to establish the HIF-1α accumulation capacity of optimal spinach extracts. Different types of natural extraction such as commercial spinach powder or another cobalt-rich diet could be evaluated in further studies. Spinach leaf extractions were prepared, and ICP-MS was used to demonstrate the presence of cobalt and to approximately determine the amount of cobalt present in the extracts. The application of extracts from *Spinacia Oleracea* leaves (750 μg/ml) to HEK 293T cells initially did not show any signs of HIF-1α upregulation when incubated for 6 hours. However, when the HEK 293T cell incubation time was increased to 24 hours following treatment *Spinacia Oleracea* leaves extraction (750 μg/ml) the extracts were observed to stabilize the HIF-1α signal. Although compared to the natural spinach extraction, the application of pure $CoCl_2$ produces a ratio of stronger HIF-1α signal, the results highlight the future potential of natural products to treat anaemia, without any possible side effects that come along with synthetic drugs. Further N-oxalylglycine is a broad spectrum plant metabolite that is a 2OG oxygenase, including PHD inhibitor[16]. Thus, in future work studying the effect of plant extracts containing NOG, if possible, in combination with cobalt containing extracts is of interest.

Previously when proline analogues were incorporated into synthesized peptides, they have been shown to inhibit the PHDs[17-22]. **Chapter 3** describes work done to evaluate the possibility that treatment of HEK 293T cells with L-proline and proline-derived amino acids such as L-4-thiazolidine carboxylic acid, L-proline methyl ester hydrochloride, L-azetidine-2-carboxylic acid, 4-hydroxy proline may cause stabilisation HIF-1α protein. Deuterated proline was also evaluated in terms of its HIF-1α stabilising capacity. Among them, 100 μM of L-4-thiazolidine carboxylic acid and L-proline methyl ester hydrochloride were most effective at stabilising HIF-1α protein compared to controls. Although Roxadustat, produces a stronger HIF-1α signal compared to the proline analogues, treatment of cells with 100 μM of L-azetidine-2-carboxylic acid or D_7-deuterated proline also manifested HIF-1α upregulation. By contrast, 4-hydroxy proline, was not effective at stabilising HIF-1α protein. **Chapter 3** describes studies evaluating the possibility that a natural diet may upregulate HIF-α.

Cytotoxicity assays were carried out on L-4-thiazolidine carboxylic acid and L-proline. The assay results indicate that even relatively high concentrations of L-4-thiazolidine carboxylic acid and L-proline treatment are non-toxic. Thus ˜51% and ˜64%, respectively, of cells, were viable after 48 hours of treatment with a relatively high dose (500 μM) of L-4-thiazolidine carboxylic acid or L-proline compared to the control respectively.

Of the tested proline analogues, L-4-thiazolidine carboxylic acid caused relatively strong and continuous accumulation of HIF-1α; further cellular investigations were thus carried out on L-4-carboxylic thiazolidine acid. L-4-Thiazolidine carboxylic acid showed an influence on hypoxia-responsive gene expression in HEK 293T cells. Among all the genes examined

the *HIF1α* and *VEGF* genes were significantly upregulated in HEK 293T cells compared to the control group. However, L-4-thiazolidine carboxylic acid did not seem to have any substantial influence on *EPO* and *CA9* expression compared to the control.

The mechanism by which the proline analogues and the proline ethyl ester hydrochloride itself cause HIF1α upregulation is not clear. It was originally thought that they might be incorporated into proteins via the translation machinery and result in impaired PHD catalysis. This appears to be less likely as proline itself has an effect. Nonetheless, it cannot be ruled out that this occurs at least to some extent. An alternative possibility is that tested proline/proline analogues affect metabolism (in a presently undefined manner) in a way that causes upregulation of HIF1α, or it is possible that proline availability in cells, at least for HIF-α biosynthesis is limited. One study on the effect of proline analogues on collagen biosynthesis apparently supports this possibility [23,24]. The observation that L-4-thiazolidine carboxylate upregulates HIF1α are of interest, as it is formed, likely including in cells, by the reaction of L-cysteine with formaldehyde, as shown in recent work to which I contributed[25]. It is possible that in cells L-4-thiazolidine carboxylate releases formaldehyde that results in HIF1α upregulation.

Chapter 4 describes studies on a compound that apparently enhances PHD activity and so reduces HIF-α levels. The effects of the enhancer on PHD activity were evaluated in two different conditions: hypoxia (1% O_2) and normoxia. Studies have shown under extreme hypoxia (0.5% O_2) treatment with **7** (100μM) reduced HIF1α levels in Hep3B and 206p0 cells compared to the control and under 3% O_2 (compared to the controls), treatment with **7** (50

or 100μM) reduced HIF1α levels in Hep3B cells; in the case of 206p0 and 143B cells, treatment with **7** (100μM) reduced HIF-α levels [26,27]. The hypoxia experiments (1% O_2) were conducted **(Chapter 4)** using the HEK 293T cell line. In HEK 293T cells under 1% O_2 the PHD enhancer reduced HIF1α levels at 20, 50 & 100 μM treatments. With normoxia experiments, 100μM of the PHD enhancer was tested in combination with two different concentrations of the PHD inhibitor Roxadustat (10 & 20μM). In the presence of Roxadustat the PHD enhancer showed an ability to inhibit HIF1α accumulation. The PHD enhancer was also tested on glioma cell lines (LN18), (mentioned in **chapter 4**) in the presence of Roxadustat (10 & 20μM) and demonstrated its ability to prevent HIF1α accumulation when treated for 24 hours compared to the control.

Studies have shown that chemotherapeutic treatment can induce HIF1α stability in the TNBC cell line [28,29]. An experiment conducted **(Chapter 4)** on the MDA-MB-231 cell line showed that cells treated with a chemotherapeutic agent, paclitaxel (10nM) for 48 hours, induced HIF1α accumulation but co-administration with the 100μM of the PHD enhancer with paclitaxel reduced the HIF1α level compared to controls. More experiments on the application of a combination of PHD enhancer and chemotherapeutic agents on TNBC cells are of interest.

Protein levels of PHD2 were also analysed during all the immunoblotting experiments. PHD2 protein levels were observed to substantially increase in the presence of **7** (100 μM) in comparison to the control. **7** (100 μM) in combination with **1** (10 or 20 μM) showed similar or

increased PHD2 protein levels in comparison to **1** (10 or 20 µM). Although work was carried out, to investigate the mechanism of action of the PHD enhancer, this is still unclear.

Comprehensive semi-targeted metabolomics studies were conducted to investigate the metabolomic consequences of treatment with hypoxia (1%), $CoCl_2$ (150µM), and PHD inhibitors: Roxadustat (20 & 100µM) and Molidustat (100µM) on HEK 293T cells **(Chapter 5).** A workflow for these semi targeted metabolomics studies was developed. All the five experimental conditions studied (hypoxia (1% O_2), $CoCl_2$, PHD inhibitors (Roxadustat and Molidustat)) were competent in inducing HIF-1α accumulation in HEK 293T cells. Therefore, all the semi targeted metabolomics analyses were compared to search for common features. Interestingly, univariant analyses (Volcano plot) identified the presence of some common metabolites and compound features which were significantly altered (either up or down regulated) in at least two of the experimental groups.

During all these five metabolomics studies, a univariate statistical analysis was conducted in order to: 1. to provide an overview or assessment of initial data quality (and identify potential outliers), 2. To identify potential individual metabolites at the early stage which may have an impact on creating differences between groups or any probable biomarkers, 3. to identify and prioritize metabolites (metabolites with large changes in concentration between groups) for further multivariate analysis. After univariate analysis, multivariate analyses were performed to investigate metabolic phenotypes associated with the treatments. Multivariate analyses were performed to identify similar patterns of altered metabolites using multivariate models (PLS-DA and HCA). In all the semi targeted metabolomics experiments (except with

Roxadustat at 100µM), some VIP metabolites were predicted during univariate analysis (volcano plot). A similar pattern of altered metabolites was observed in multivariate analysis (HCA map) as observed by the univariate analysis (volcano plot).

$CoCl_2$ has not been widely assessed from a metabolomic viewpoint; the results demonstrate that it induces a metabolic shift supporting glycolysis and interrupts mitochondrial function, consistent with HIF stabilization [5]. Overall, the semi targeted metabolomics analysis showed that hypoxia, hypoxia mimics, and Roxadustat at lower concentrations (20 µM) tend to upregulate and downregulate certain metabolites compared to the controls. Importantly, on the other hand, Roxadustat and Molidustat at higher concentrations (100 µM) appeared to have less impact on metabolite and/ or compound features abundances compared to the control.

Untargeted pathway analysis gave similar outcomes. Pathway analysis showed that hypoxia and hypoxic mimicking agents significantly altered several metabolomic pathways. On the other hand, the selective PHD inhibitors significantly altered only a few metabolomic pathways. Hence, a key conclusion that can be drawn is that hypoxia and hypoxic mimic agents exert more extensive impacts compared to the PHD inhibitors on mammalian cell HEK 293T cells. Perhaps due to the PHD inhibitor selectivity, there are other factors relevant to the hypoxia sensing and response processes.

The work measured the impacts of hypoxia, hypoxia mimic agents, and selective PHD inhibitors on the glycolysis pathway/changes in glycolytic metabolites (glucose, glyceraldehyde 3-phosphate, fructose 6-phosphate, fructose 1,6-phosphate, pyruvate, lactic

acid) during metabolomics studies. Most, but not all, of the glycolytic metabolites were significantly upregulated when measured. In all the experimental groups, lactic acid was significantly upregulated. hypoxic mammalian cells or inhibiting PHD enzyme or HIF stabilization can exert impact on the glycolysis pathway.

Glycolysis gene expression (*GLUT1, HK 2, PDK1, ENO 1, and LDHA*) levels were measured using the RT-qPCR technique. Hypoxia significantly upregulates all the tested gene expressions, whereas other experimental groups at their lower concentrations (100 & 150 µM of $CoCl_2$, 20 & 100 µM of Roxadustat, and Molidustat) did not upregulate gene expression levels. Interestingly, with an increased dose the other treatment group (300 µM of $CoCl_2$, 200 µM of Roxadustat, and Molidustat) showed significant upregulation of glycolysis gene expression level. Therefore, it can be proposed that selective PHD inhibitors have a more limited impact on HEK293t cells metabolomics compared to natural hypoxia or hypoxia mimic agent (at least under the tested conditions).

The impact of PHD inhibitors (100 µM of Roxadustat and Molidustat) and hypoxia mimicking agents (150 µM $CoCl_2$) on glycolytic rate was measured using the Seahorse glycolytic rate assay technique. During the Sea Horse experiment, all the treatment groups showed increased glycolytic proton efflux compared to the control, indicating a high rate of conversion of glucose to pyruvate or lactate. These results were expected, because a similar outcome was seen during metabolomics analysis as lactic acid was high in abundance in all the treatment groups. However, among the experimental groups, Roxadustat showed the

highest increment in glycoPER rate, followed by Molidustat and $CoCl_2$ group. Overall, the results show inhibition of PHDs influences the glycolysis rate.

Hence, one conclusion that can be drawn from these results (by interpretation of IC-MS data, data processing through progenesis, data analysis and interpretation through metaboanalyst software, Mummichog pathway analysis and glycolysis gene expression analysis) that hypoxia/hypoxia mimics have more extensive impacts than the selective PHD inhibitors. At a simple level, this implies that there is more to the hypoxic response than PHD inhibition/HIF-α upregulation. One additional factor is FIH, one role of which seems to regulate the set of genes upregulated by HIF, though it likely has other roles [30-32].

This work described here did not measure the influence of hypoxia on the glycolytic rate – it would be useful to do this for comparison. Further, although all the described metabolomics studies involved n=10 (in some cases outliers were discarded) biological replicates to study metabolomic changes after each experimental treatment, however, for further studies more biological replicates may be considered.

6.2 References

1. Dhillon S. Roxadustat: first global approval. Drugs. 2019 Apr 1;79:563-72.
2. Papadopoulou A, Meyer F, Buller RM. Engineering Fe (II)/α-ketoglutarate-dependent halogenases and desaturases. Biochemistry. 2022 Apr 21;62(2):229-40.
3. Jaakkola, P., Mole, D. R., Tian, Y. M., Wilson, M. I., Gielbert, J., Gaskell, S. J., ... & Ratcliffe, P. J. (2001). Targeting of HIF-alpha to the von Hippel-Lindau ubiquitylation complex by O2-regulated prolyl hydroxylation. *Science*, 292(5516), 468–472. https://doi.org/10.1126/science.1059796
4. Li RL, He LY, Zhang Q, Liu J, Lu F, Duan HX, Fan LH, Peng W, Huang YL, Wu CJ. HIF-1α is a potential molecular target for herbal medicine to treat diseases. Drug design, development and therapy. 2020 Nov 16:4915-49.
5. Yuan Y, Hilliard G, Ferguson T, Millhorn DE. Cobalt inhibits the interaction between hypoxia-inducible factor-alpha and von Hippel-Lindau protein by direct binding to hypoxia-inducible factor-alpha. J Biol Chem. 2003 May 2;278(18):15911-6. doi: 10.1074/jbc.M300463200. Epub 2003 Feb 26. PMID: 12606543.
6. Masoud, G.N. and W. Li, *HIF-1α pathway: role, regulation and intervention for cancer therapy.* Acta Pharm. Sin. B., 2015. 5(5): p. 378-389. DOI: 10.1016/j.apsb.2015.05.007.
7. Zhao, Y., et al., *HIF-1α signaling: Essential roles in tumorigenesis and implications in targeted therapies.* Genes Dis. , 2024. 11(1): p. 234-251. DOI: 10.1016/j.gendis.2023.02.039
8. Ortmann, B.M., *Hypoxia-inducible factor in cancer: from pathway regulation to therapeutic opportunity.* BMJ Oncology, 2024. 3(1).

9. Chan, M.C., et al., *Tuning the transcriptional response to hypoxia by inhibiting hypoxia-inducible factor (HIF) prolyl and asparaginyl hydroxylases.* J. Biol. Chem., 2016. 291(39): p. 20661-20673. DOI: 10.1074/jbc.M116.749291
10. Fraisl, P., J. Aragonés, and P. Carmeliet, *Inhibition of oxygen sensors as a therapeutic strategy for ischaemic and inflammatory disease.* Nat. Rev. Drug Discov. , 2009. 8(2): p. 139-152. DOI: 10.1038/nrd2761
11. Yuan, Y., et al., *Cobalt inhibits the interaction between hypoxia-inducible factor-α and von Hippel-Lindau protein by direct binding to hypoxia-inducible factor-α.* J. Biol. Chem., 2003. 278(18): p. 15911-15916. DOI: 10.1074/jbc.M300463200
12. Matsuura, H., et al., *Inhibition of prolyl hydroxylase domain-containing protein downregulates vascular angiotensin II type 1 receptor.* Hypertension, 2011. 58(3): p. 386-393. DOI: 10.1161/HYPERTENSIONAHA.110.167106
13. Skalny, A.V., et al., *Cobalt in athletes: hypoxia and doping-new crossroads.* J. Appl. Biomed., 2019. 17(1): p. 28-28. DOI: 10.32725/jab.2018.003
14. Bowie, E. and P. Hurley, *Cobalt chloride in the treatment of refractory anaemia in patients undergoing long-term haemodialysis.* Aust N Zeal J Med., 1975. 5(4): p. 306-313. DOI: 10.1111/j.1445-5994.1975.tb03263.x
15. Manifold, I., M. Platts, and A. Kennedy, *Cobalt cardiomyopathy in a patient on maintenance haemodialysis.* Br. Med. J., 1978. 2(6152): p. 1609. DOI: 10.1136/bmj.2.6152.1609
16. Al-Qahtani, K., et al., *The broad spectrum 2-oxoglutarate oxygenase inhibitor N-oxalylglycine is present in rhubarb and spinach leaves.* Phytochemistry, 2015. 117: p.

456-461. DOI: 10.1016/j.phytochem.2015.06.028

17. Gorres, K.L., et al., *Conformational preferences of substrates for human prolyl 4-hydroxylase*. Biochemistry, 2008. 47(36): p. 9447-9455. DOI: 10.1021/bi8009373
18. Li, K., Y. Zheng, and X. Wang, *The potential relationship between HIF-1α and amino acid metabolism after hypoxic ischemia and dual effects on neurons*. Front. Neurosci., 2021. 15: p. 676553. DOI: 10.3389/fnins.2021.676553
19. Kwon, H.S., et al., *Inhibition of a prolyl hydroxylase domain (PHD) by substrate analog peptides.* Bioorg. Med. Chem. Lett., 2011. 21(14): p. 4325-4328. DOI: 10.1016/j.bmcl.2011.05.050
20. Ma, X., et al., *Effect of proline analogues on activity of human prolyl hydroxylase and the regulation of HIF signal transduction pathway.* PLoS One, 2014. 9(4): p. e95692. DOI: 10.1371/journal.pone.0095692
21. Ahn, D.-R., et al., *HIF-1α Peptide Derivatives with modifications at the hydroxyproline residue as activators of HIF-1α. Bioorg.* Med. Chem. Lett., 2009. 19(15): p. 4403-4405. DOI: 10.1016/j.bmcl.2009.05.083
22. Tegley, C.M., et al., *Discovery of novel hydroxy-thiazoles as HIF-α prolyl hydroxylase inhibitors: SAR, synthesis, and modeling evaluation*. Bioorg. Med. Chem. Lett., 2008. 18(14): p. 3925-3928. DOI: 10.1016/j.bmcl.2008.06.031
23. Tanner, J.J., S.-M. Fendt, and D.F. Becker, *The proline cycle as a potential cancer therapy target.* Biochemistry, 2018. 57(25): p. 3433-3444. DOI: 10.1021/acs.biochem.8b00215
24. Amgarten, B., et al., *Collagen labelling with an azide-proline chemical reporter in live*

cells. Chem. Commun., 2015. 51(25): p. 5250-5252. DOI: 10.1039/c4cc07974d

25. John, T., et al., *Aldehyde-mediated inhibition of asparagine biosynthesis has implications for diabetes and alcoholism*. Chem. Sci., 2024. 15(7): p. 2509-2517. DOI: 10.1039/d3sc06551k
26. Holt-Martyn, J., *Novel and selective small molecule inhibitors and activators for the prolyl hydroxylase domain enzyme*. 2018, D.Phil thesis, University of Oxford.
27. Yeh, T.-L., et al., *Molecular and cellular mechanisms of HIF prolyl hydroxylase inhibitors in clinical trials.* Chem. Sci., 2017. 8(11): p. 7651-7668. DOI: 10.1039/c7sc02103h
28. Samanta, D., et al., *Hypoxia-inducible factors are required for chemotherapy resistance of breast cancer stem cells.* Proc Natl Acad Sci., 2014. 111(50): p. E5429-E5438. DOI: 10.1073/pnas.1421438111
29. Bhola, N.E., et al., *TGF-β inhibition enhances chemotherapy action against triple-negative breast cancer.* J Clin Invest., 2013. 123(3): p. 1348-1358. DOI: 10.1172/JCI65416
30. Stolze, I.P., et al., *Genetic analysis of the role of the asparaginyl hydroxylase factor inhibiting hypoxia-inducible factor (HIF) in regulating HIF transcriptional target genes*. J. Biol. Chem., 2004. 279(41): p. 42719-42725. DOI: 10.1074/jbc.M406713200
31. Wang, E., et al., *The role of factor inhibiting HIF (FIH-1) in inhibiting HIF-1 transcriptional activity in glioblastoma multiforme*. PLoS One, 2014. 9(1): p. e86102. DOI: 10.1371/journal.pone.0086102
32. Sim, J., et al., *The factor inhibiting HIF asparaginyl hydroxylase regulates oxidative metabolism and accelerates metabolic adaptation to hypoxia.* Cell metabolism, 2018.

27(4): p. 898-913. DOI: 10.1016/j.cmet.2018.02.020

7. Appendix

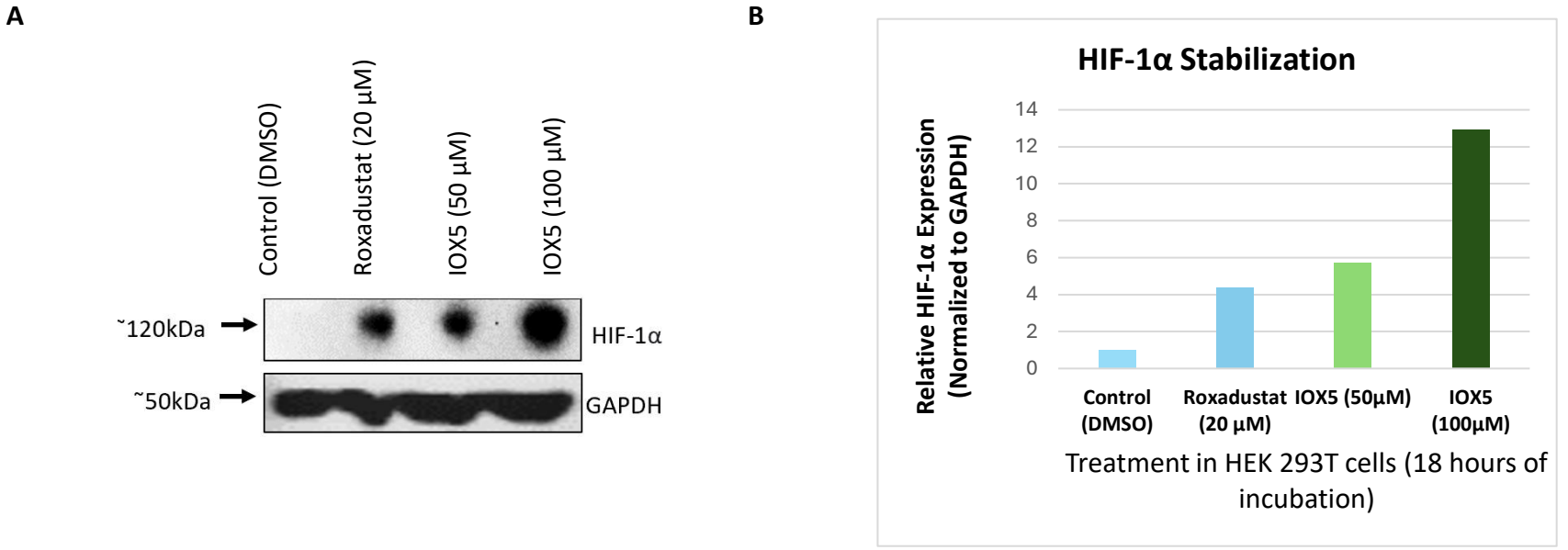


Figure A.7.1: Stabilization of HIF-1α through cellular inhibition of HIF prolyl hydroxylation by 5. **(A)** Immunoblot analysis of the protein expression of HIF-1α in HEK 293T cells treated with **5** (100 & 50 µM) and **1** (20 µM) for 18 hours in normoxia. **(B)** Quantification of HIF-1α after treatment for 18 hours in normoxia.

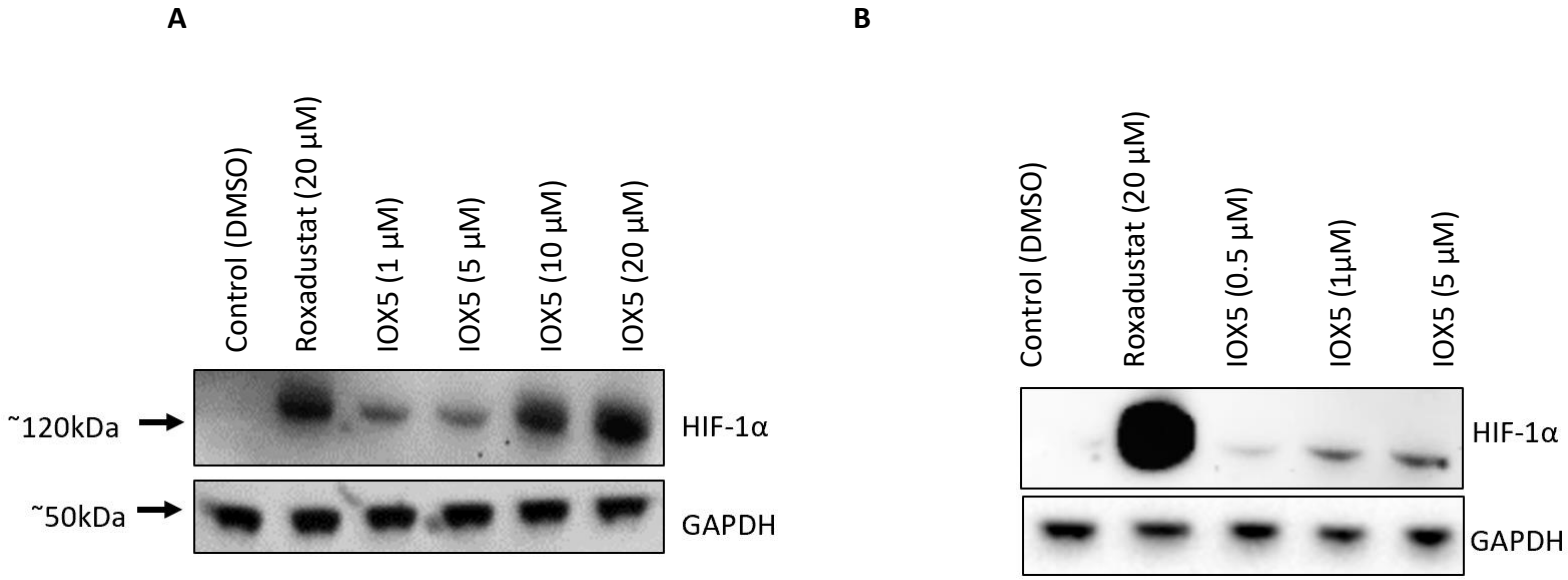


Figure A. 7.2: Stabilization of HIF-1α through cellular inhibition of HIF prolyl hydroxylation by different concentrations of 5**.** (A & B) Immunoblot analysis of the protein expression of HIF-1α in HEK 293T cells treated with **5** (20,10,5,1&0.5 µM) and **1** (20 µM) for 18 hours in normoxia.

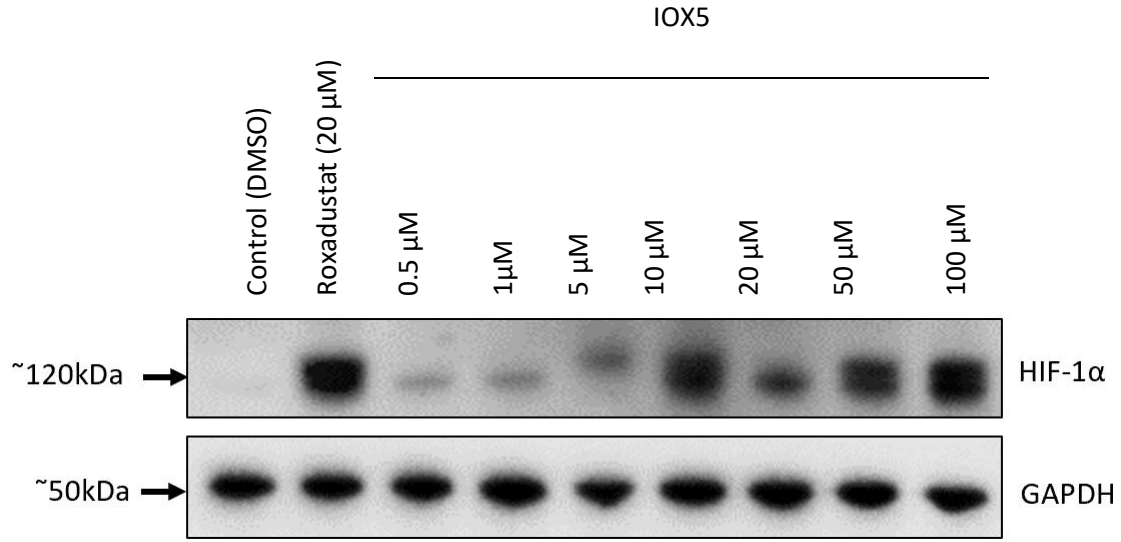
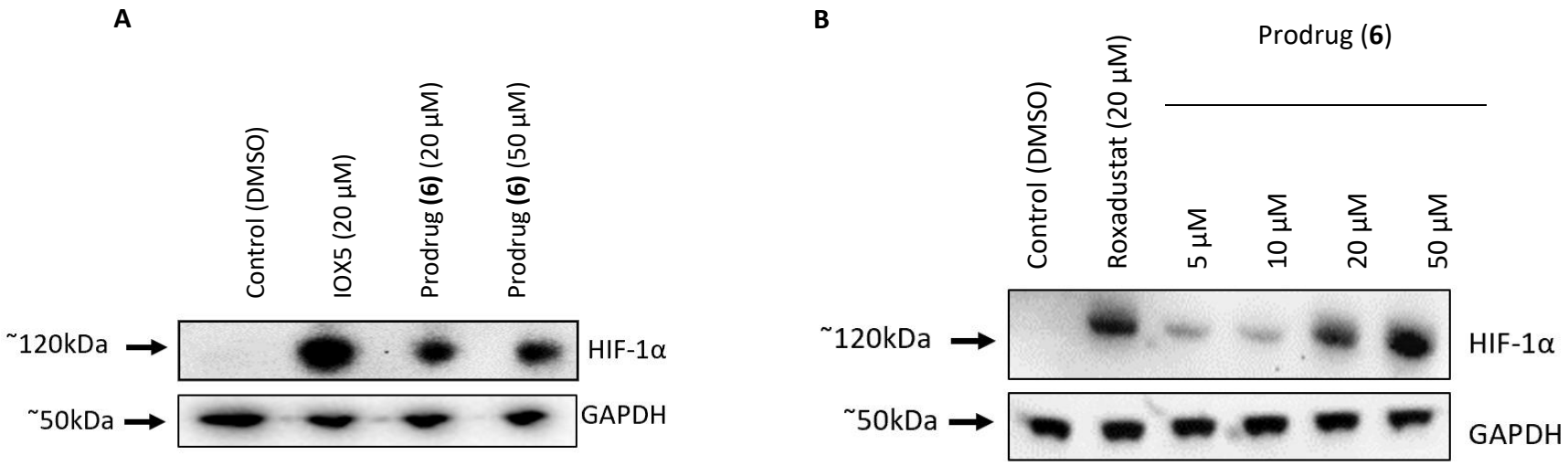


Figure A.7.3 : Stabilization of HIF-1 α through cellular inhibition of HIF prolyl hydroxylation by different concentrations of 5. Immunoblot analysis of the protein expression of HIF-1α in HEK 293T cells treated with **5** (100, 50, 20, 10, 5, 1 & 0.5 µM) and **1** (20 µM) for 18 hours in normoxia.


A
Control (DMSO)
IOX5 (20 µM)
Prodrug (6) (20 µM)
Prodrug (6) (50 µM)
~120kDa
HIF-1α
~50kDa
GAPDH
B
Prodrug (6)
Control (DMSO)
Roxadustat (20 µM)
5 µM
10 µM
20 µM
50 µM
~120kDa
HIF-1α
~50kDa
GAPDH

C

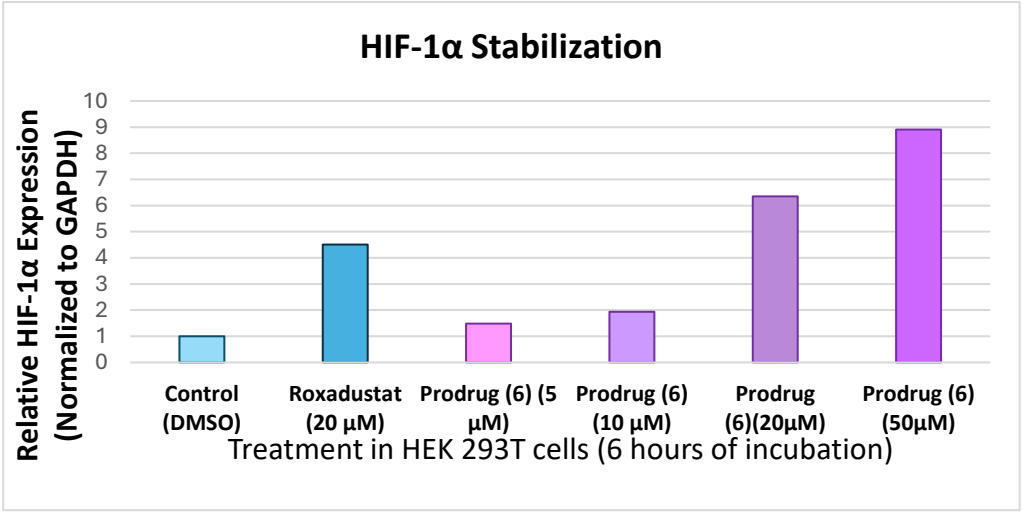
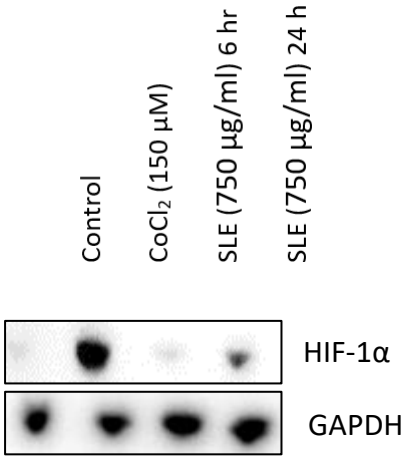
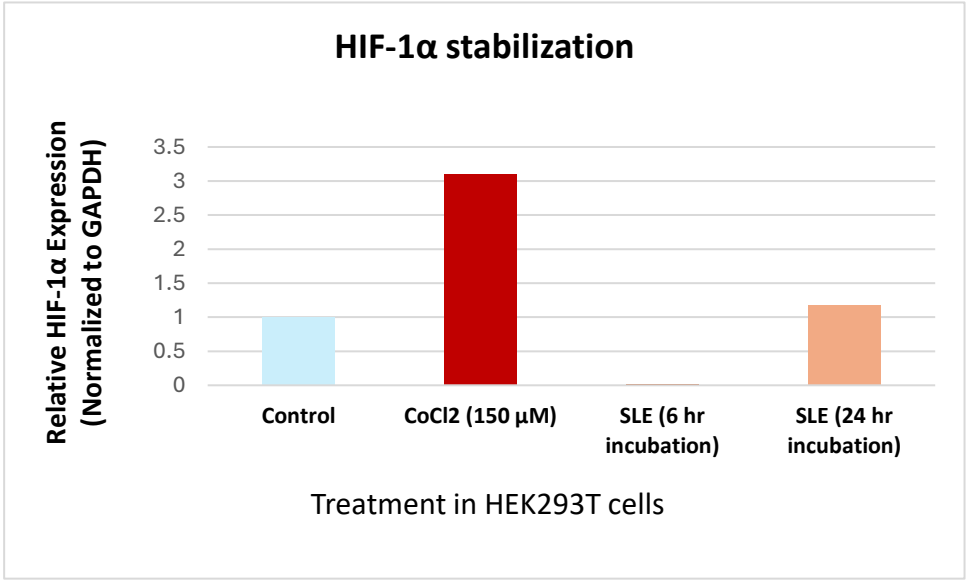

HIF-1α Stabilization
Relative HIF-1α Expression (Normalized to GAPDH)
10
9
8
7
6
5
4
3
2
1
0
Control (DMSO)
Roxadustat (20 µM)
Prodrug (6) (5 µM)
Prodrug (6) (10 µM)
Prodrug (6)(20µM)
Prodrug (6) (50µM)
Treatment in HEK 293T cells (6 hours of incubation)

Figure A.7.4 : Stabilization of HIF-1α through cellular inhibition of HIF prolyl hydroxylation by 6. (A) Immunoblot analysis of the protein expression of HIF-1α in HEK 293T cells treated with **6** (50 & 20 µM) and **5** (20 µM) for 6 hours in normoxia. (B)Immunoblot analysis of the protein expression of HIF-1α in HEK 293T cells treated with **6** (50, 20, 10 & 5 µM) and **1** (20 µM) for 6 hours in normoxia. (C) Quantification of HIF-1α after treatment for 6 hours of treatment. Comparing the results with 20µM of **1**, **6** was able to stabilize HIF-1α at 50 and 20 µM; at 10 and 5 µM there was weak evidence for HIF-1α accumulation (**Figure A. 7.4 B).**





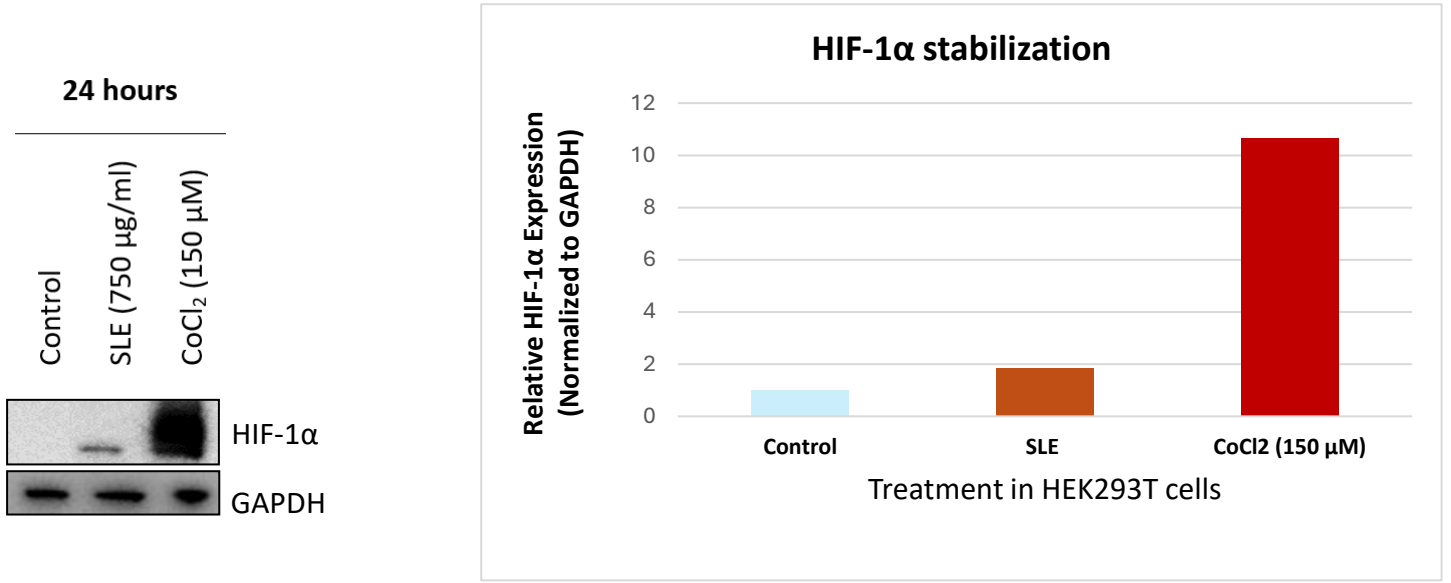
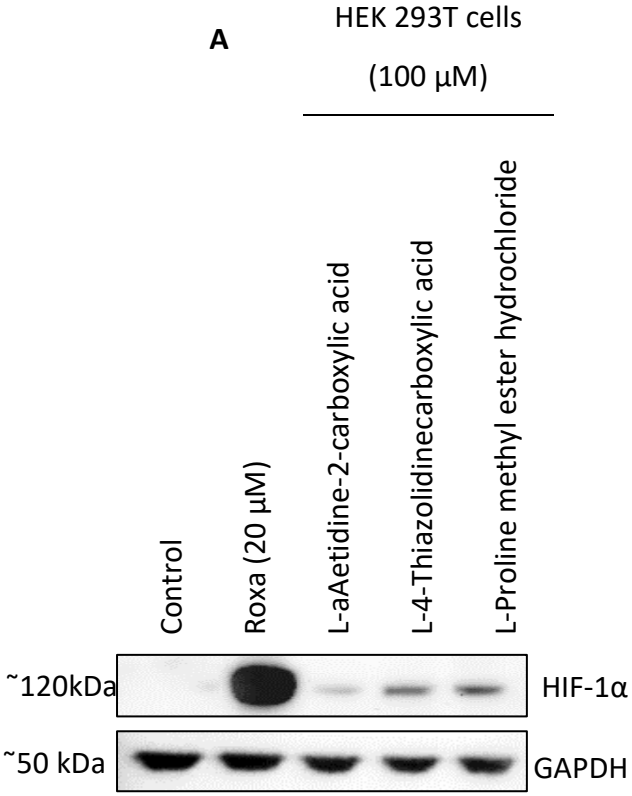
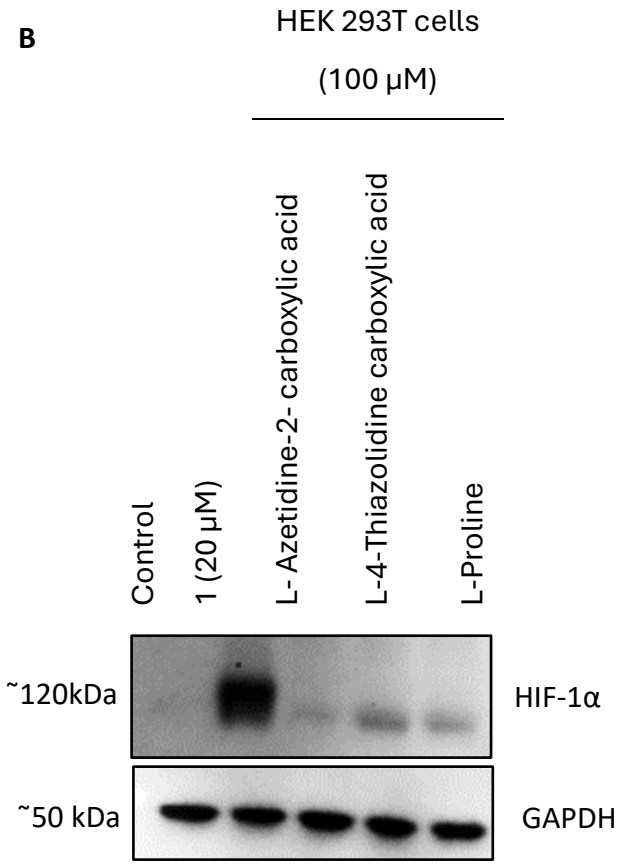
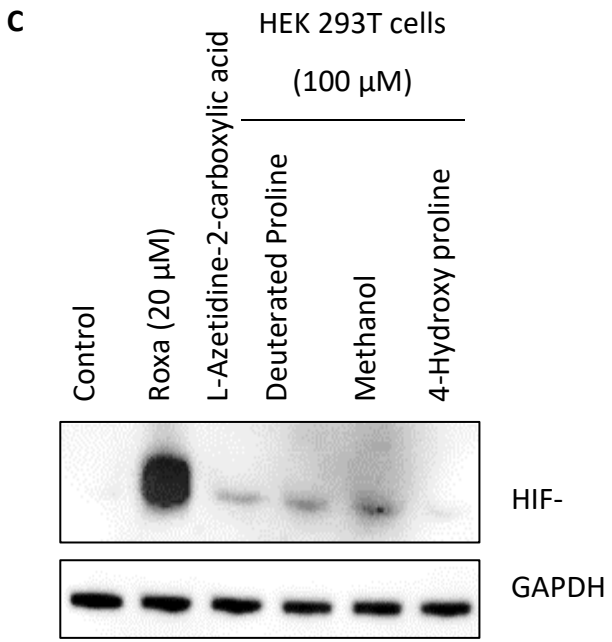


Figure A.7.5: Stabilization of HIF-1α through cellular inhibition of HIF prolyl hydroxylation by spinach (Spinacia Oleracea) leaf extracts (SLE). (A) Immunoblot analysis of HIF-1α in HEK 293T cells treated with spinach (*Spinacia Oleracea*) leaf extracts (SLE) (750 µg/ml)) or $CoCl_2$ (150 µM) for 6 or 24 hours in normoxia. (C) Immunoblot analysis of HIF-1α in HEK 293T cells treated with spinach (*Spinacia Oleracea*) leaf extraction (SLE) (750 µg/ml)) and $CoCl_2$ (150 µM) for 24 hours in normoxia. SLE = spinach (*Spinacia Oleracea*) leaf extracts.


A
HEK 293T cells
(100 µM)
Control
Roxa (20 µM)
L-aAetidine-2-carboxylic acid
L-4-Thiazolidinecarboxylic acid
L-Proline methyl ester hydrochloride
~120kDa
HIF-1α
~50 kDa
GAPDH


B
HEK 293T cells
(100 µM)
Control
1 (20 µM)
L- Azetidine-2- carboxylic acid
L-4-Thiazolidine carboxylic acid
L-Proline
~120kDa
HIF-1α
~50 kDa
GAPDH


C
HEK 293T cells
(100 µM)
Control
Roxa (20 µM)
L-Azetidine-2-carboxylic acid
Deuterated Proline
Methanol
4-Hydroxy proline
HIF-
GAPDH

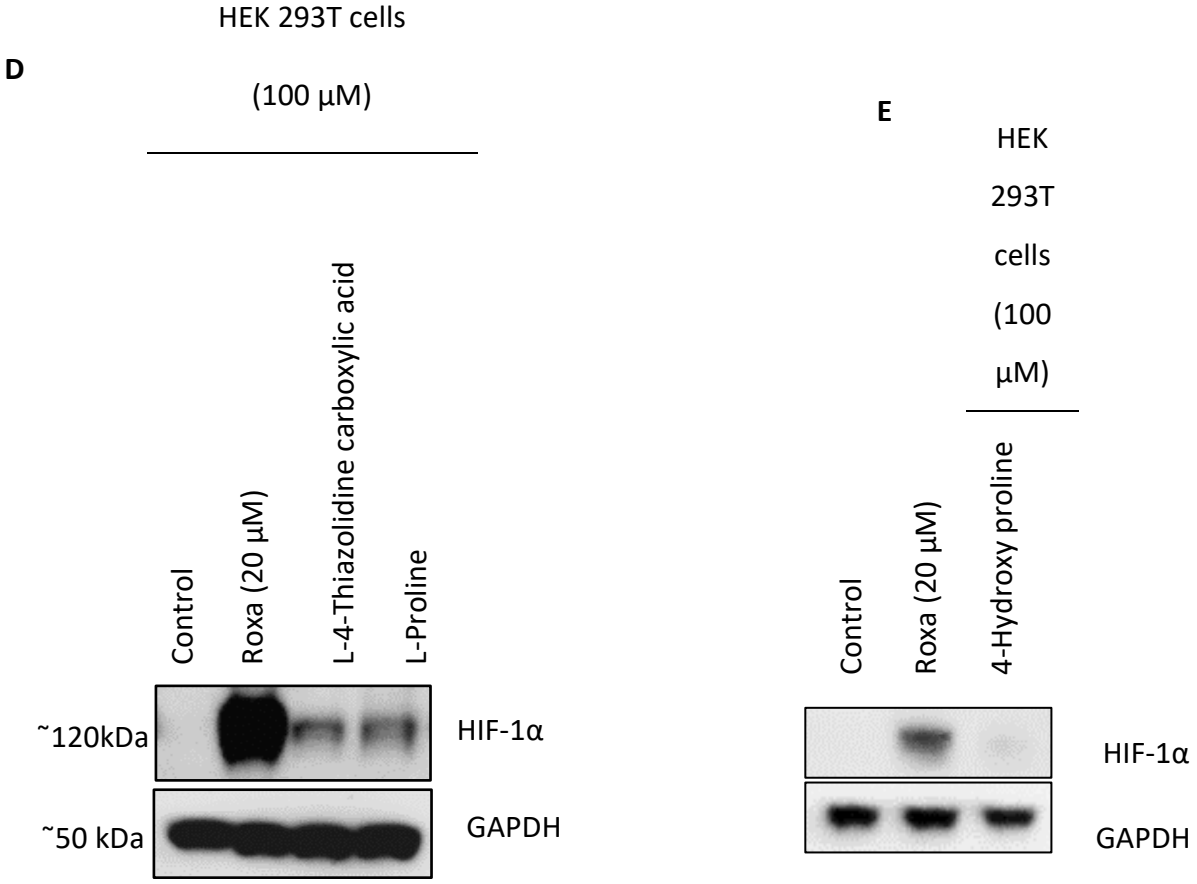


Figure A.7.6: Stabilization of HIF-1α through cellular inhibition of HIF prolyl hydroxylation by different proline-derived amino acids. (A) Immunoblot analysis of HIF-1α in HEK 293T cells treated with L-proline methyl ester hydrochloride, L-azetidine-2-carboxylic acid or L-4-thiazolidine carboxylic acid (100 µM) for 24 hours in normoxia. (B) Immunoblot analysis of HIF-1α in HEK 293T cells treated with L-proline, L-

azetidine-2-carboxylic acid or L-4-thiazolidine carboxylic acid (100 µM) for 24 hours in normoxia. (C) Immunoblot analysis of HIF-1α in HEK 293T cells treated with L-azetidine-2-carboxylic acid, methanol or deuterated proline (100 µM) for 24 hours in normoxia. The deuterated proline is labelled "D_7" which means all the C-H bonds were replaced with C-^{2}H bonds. (D) Immunoblot analysis of HIF-1α in HEK 293T cells treated with L-4-thiazolidine carboxylic acid, or L-proline (100 µM) for 24 hours in normoxia. (E) Immunoblot analysis of HIF-1α in HEK 293T cells treated with 4-hydroxyproline (100 µM) for 24 hours in normoxia.

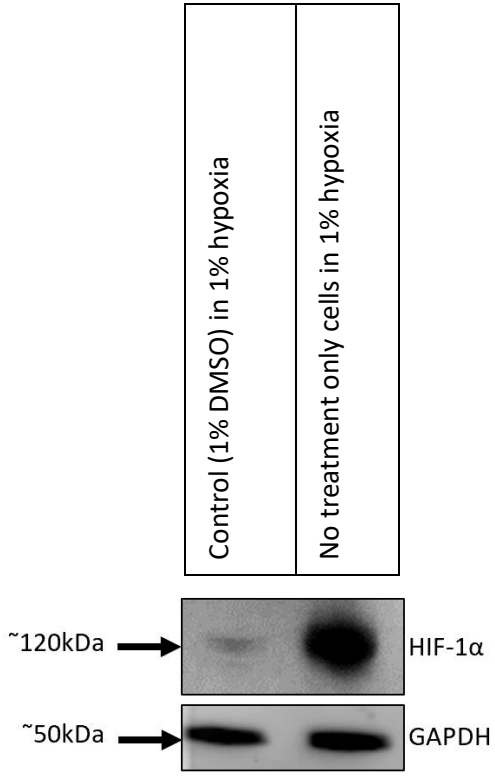


Figure A. 7.7: Hypoxia (1% O2) leads to stabilization of HIF-1α protein in HEK 293T. Immunoblot image showing that under hypoxia (1% O_2) for 24 hours, HEK 293T cells accumulate HIF-1α' not the DMSO also shows increases in HIF-1α.

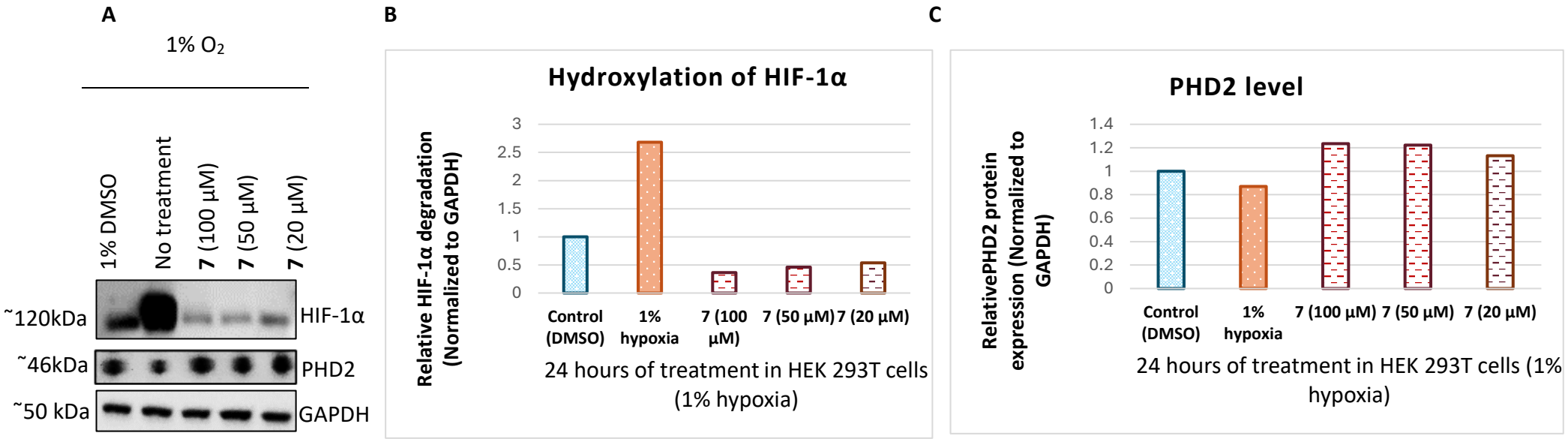
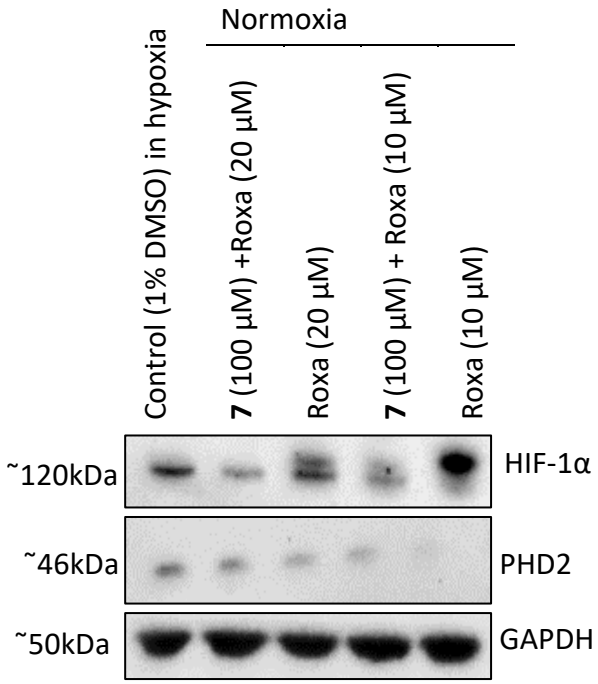
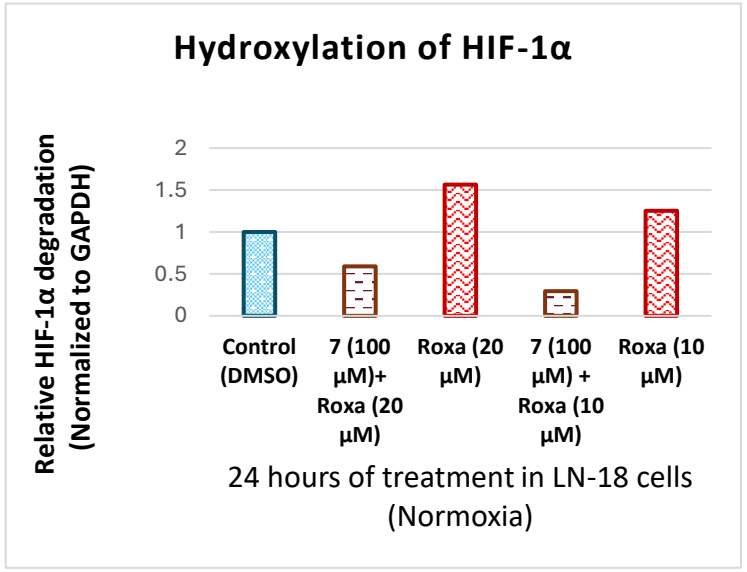


Figure A.7.8: Effects of 7 on HIF-1α in 1% O2. (A) Immunoblotting image showing evidence for degradation of HIF-1α in HEK 293T treated with 100, 50 and 20 µM of **7** for 24 hours at 1% O_2. Control (1% DMSO) and cells with no treatment showed high HIF-1α levels. (B) Quantification of HIF-1α degradation after 24 hours treatment of **7** using 'Image J software'. (C) Quantification of PHD2 enzyme expression after 24-hour treatment with **7** using 'Image J software'.





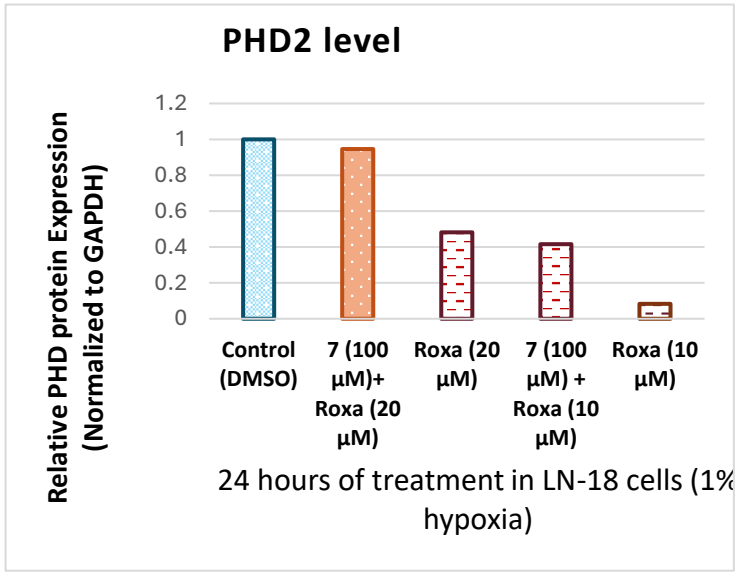


Figure A.7.9: Effects of HIF-1α by 7 in the presence of PHD inhibitor, 1**.** (**A**) Immunoblots showing HIF-1α levels in LN-18 cells when incubated for 24 hours with **7** (100µM) in the presence of **1** at 10 µM and 20 µM in normoxia. (**B**) Quantification of HIF-1α degradation after 24 hours treatment of **7** 100µM in a presence of **1** at 10 µM and 20 µM in normoxic condition using 'Image J software'.

Table A. 7.1: Data base of metabolites measured by IC-MS. (Database used during Progenesis QI for metabolite identification. The databases were developed by McCullagh group.)

Compound ID	Description	Neutral Mass	Adduct	Retention time (min)
HMDB0000001	1-Methylhistidine	169.08513	M-H	0.00
HMDB0001301	1-Pyrroline-5-carboxylic acid	113.04768	M-H	0.00
HMDB0002006	2,3-Diaminopropionic acid	104.05913	M-H	0.00
N/A	2-amino-5-hydroxybenzoic acid	153.04314	M-H	0.00
HMDB0001123	2-Aminobenzoic acid/Anthranilic acid	137.04768	M-H	0.00
HMDB0001906	2-Aminoisobutyric acid	103.06333	M-H	0.00
HMDB0032059	2-Bromophenol	171.95293	M-H	0.00
HMDB0002039	2-Pyrrolidinone	85.05331	M-H	0.00
HMDB0012153	3,4,Dihydroxybenzylamine	139.06388	M-H	0.00
HMDB0001376	3-deoxy-2-keto-6-phosphogluconic acid	258.01407	M-H	0.00
HMDB0001476	3-Hydroxyanthranilic acid	153.04314	M-H	0.00

HMDB0059969	3-methoxyphenylacetic acid	166.06299	M-H	0.00
HMDB0001904	3-Nitrotyrosine	226.05897	M-H	0.00
HMDB0000725	4-Hydroxyproline	131.05824	M-H	0.00
HMDB0036619	5,7-Dihydroxyflavone (Chrysin)	254.05846	M-H	0.00
HMDB0001149	5-Aminolevulinic acid	131.05879	M-H	0.00
HMDB0001206	Acetyl-CoA	809.12577	M-H	0.00
HMDB0001494	Acetylphosphate	139.98801	M-H	0.00
HMDB0000034	Adenine	135.05450	M-H	0.00
HMDB0000650	Alpha-aminobutyrate	103.06333	M-H	0.00
HMDB0002166	Alpha-aminoisobutyrate	103.06333	M-H	0.00
N/A	Benzoyl-L-citrulline methyl ester	293.13810	M-H	0.00
HMDB0000056	Beta-Alanine	89.04768	M-H	0.00
HMDB0000033	Carnosine	225.09931	M-H	0.00
HMDB0000904	Citrulline	175.09569	M-H	0.00
HMDB0000574	Cysteine	121.01975	M-H	0.00
HMDB0000089	Cytidine	243.08607	M-H	0.00
HMDB0001176	Cytidine monophosphate N-acetylneuraminic acid	614.14727	M-H	0.00
HMDB0000630	Cytosine	111.04326	M-H	0.00
HMDB0000101	Deoxyadenosine	251.10184	M-H	0.00
HMDB0001532	Deoxyadenosine triphosphate	491.00083	M-H	0.00
HMDB0000014	Deoxycytidine	227.09115	M-H	0.00
HMDB0000085	deoxyguanosine	267.09675	M-H	0.00
HMDB0246094	Deoxythymidine	225.08808	M-H	0.00
HMDB0000181	Dihydroxyphenylalanine (L-DOPA)	197.06881	M-H	0.00
HMDB0000073	Dopamine	153.07898	M-H	0.00

HMDB0000900	Ergocalciferol	396.33867	M-H	0.00
HMDB0000878	Ergosterol	396.33867	M-H	0.00
HMDB0001321	Erythrose 4-phosphate	200.00859	M-H	0.00
N/A	Ethionine	163.06725	M-H	0.00
HMDB0001514	Glucosamine	179.07937	M-H	0.00
HMDB0000148	Glutamic acid	147.05316	M-H	0.00
HMDB0000641	Glutamine	146.06914	M-H	0.00
HMDB0000133	Guanosine	283.09167	M-H	0.00
HMDB0030311	Harmine	212.09551	M-H	0.00
HMDB0000870	Histamine	111.08020	M-H	0.00
N/A	Homarine	137.04768	M-H	0.00
HMDB0000732	Hydroxykynurenine	224.08026	M-H	0.00
HMDB0000157	Hypoxanthine	136.03851	M-H	0.00
HMDB0001190	Indole-3-acetaldehyde	159.06841	M-H	0.00
HMDB0000684	Kynurenine	208.08479	M-H	0.00
HMDB0060486	Mandelonitrile	133.05276	M-H	0.00
HMDB0001892	Menadione	172.05298	M-H	0.00
HMDB0032617	Methyl phenylacetate	150.06863	M-H	0.00
N/A	Mildronate	146.10498	M-H	0.00
HMDB0003502	Myo-inositol hexakisphosphate/Phytic Acid	659.86192	M-H	0.00
N/A	N-Acetyl cytosine	153.05437	M-H	0.00
HMDB0003357	N-Acetyl ornithine	174.10044	M-H	0.00
HMDB0001406	Nicotinamide	122.04801	M-H	0.00
HMDB0013716	Norvaline	117.07953	M-H	0.00
HMDB0062802	Parabanic Acid/Oxalylyurea	114.00599	M-H	0.00

HMDB0000821	Phenylacetylglycine/Phenaceturic acid	193.07444	M-H	0.00
HMDB0000774	Pregnenolone sulfate	396.19759	M-H	0.00
HMDB0015169	Procainamide	235.16846	M-H	0.00
HMDB0001275	Propionyl-CoA	823.14197	M-H	0.00
HMDB0001431	Pyridoxamine	168.08988	M-H	0.00
HMDB0001852	Retinoic acid	300.20948	M-H	0.00
HMDB0000244	Riboflavin	376.13828	M-H	0.00
HMDB0000279	Saccharopine	276.13214	M-H	0.00
HMDB0001185	S-adenosyl methionine	399.14506	M-H	0.00
HMDB0001895	Salicylic acid	138.03224	M-H	0.00
HMDB0000234	Testosterone	288.20948	M-H	0.00
HMDB0029178	Thialysine	164.06250	M-H	0.00
HMDB0002666	Thiamine monophosphate	344.07026	M-H	0.00
HMDB0001372	Thiamine pyrophosphate	424.03715	M-H	0.00
HMDB0062562	Trans-urocanate	137.03565	M-H	0.00
HMDB0000303	Tryptamine	160.10060	M-H	0.00
HMDB0014724	Diclofenac	295.01614	M-H	1.22
HMDB0033816	Mytilitol	194.07959	M-H	2.58
HMDB0003418	tagatose	180.06339	M-H	2.85
HMDB0000131	Glycerol	92.04734	M-H	2.86
HMDB0029942	Arabinose	150.05282	M-H	3.06
HMDB0029965	Methyl beta-D-glucopyranoside	194.07904	M-H	3.15
HMDB0002928	Maltitol	344.13186	M-H	3.16
HMDB0000211	Myoinositol	180.06339	M-H	3.19
HMDB0000163	Maltose	342.11621	M-H	3.22
HMDB0000765	Mannitol	182.07904	M-H	3.22

HMDB0006088	Scyllitol	180.06339	M-H	3.23
HMDB0002917	Xylitol	152.06847	M-H	3.23
HMDB0004136	Threitol	122.05791	M-H	3.24
HMDB0000508	Adonitol (ribitol)	152.06847	M-H	3.25
HMDB0003213	Raffinose	504.16904	M-H	3.26
HMDB0000568	Arabitol	152.06847	M-H	3.31
HMDB0000247	Sorbitol	182.07904	M-H	3.32
N/A	4-Hydroxypyrrolidinone	101.04768	M-H	3.39
HMDB0000186	Lactose	342.11676	M-H	3.42
HMDB0000215	N-Acetyl-D-glucosamine	221.08994	M-H	3.43
HMDB0033442	Mytilin B	346.13816	M-H	3.50
HMDB0000621	Ribulose	150.05282	M-H	3.51
HMDB0000143	Galactose	180.06339	M-H	3.53
HMDB0012326	Gulose	180.06339	M-H	3.54
HMDB0001151	Allose	180.06339	M-H	3.56
HMDB0000122	Glucose	180.06339	M-H	3.58
HMDB0001266	Sorbose	180.06339	M-H	3.60
HMDB0000169	Mannose	180.06339	M-H	3.63
HMDB0001129	N-Acetylmannosamine (ManNac)	221.08994	M-H	3.63
HMDB0001644	Xylulose	150.05282	M-H	3.64
HMDB0039002	Mytilin A	332.12251	M-H	3.67
HMDB0000283	Ribose	150.05282	M-H	3.67
HMDB0000660	Fructose	180.06339	M-H	3.68
HMDB0013287	Ne,Ne dimethyllysine	174.13683	M-H	3.79
HMDB0002005	Methionine sulfoxide	165.04596	M-H	3.84
HMDB0000042	Acetic acid	60.02113	M-H	3.85

HMDB0001413	Citicoline	488.10787	M-H	4.09
HMDB0000783	Propionyl-glycine	131.05824	M-H	4.27
HMDB0094701	N-Acetyl proline	157.07444	M-H	4.41
HMDB0001369	1-Pyrroline hydroxycarboxylic acid	129.04259	M-H	4.48
HMDB0003011	O-Acetylserine	147.05316	M-H	4.54
HMDB0000766	N-Acetyl-L-alanine	131.05824	M-H	4.56
HMDB0000532	Acetylglycine	117.04259	M-H	4.63
HMDB0000026	Ureidopropionic acid	132.05404	M-H	4.70
HMDB0000267	Pyroglutamic acid	129.04314	M-H	4.73
HMDB0003072	Quinic acid	192.06339	M-H	4.74
HMDB0000076	Dihydrouracil	114.04238	M-H	4.77
HMDB0003466	Gulono-1,4-lactone	178.04770	M-H	4.79
HMDB0000150	Gluconolactone	178.04774	M-H	4.84
HMDB0000710	4-Hydroxybutyric acid	104.04734	M-H	4.85
HMDB0000625	Gluconate	196.05830	M-H	4.87
HMDB0001167	Methyl glyoxal/Pyruvaldehyde	72.02168	M-H	4.89
HMDB0000539	Arabinonic acid	166.04774	M-H	4.9
HMDB0035030	Amygdalin	457.15840	M-H	4.93
HMDB0000023	3-Hydroxyisobutyric acid	104.04734	M-H	4.95
HMDB0000230	N-acetylneuraminic acid	309.10600	M-H	4.96
HMDB0000139	Glyceric acid	106.02661	M-H	5.00
HMDB0000023	Hydroxy-isobutyric acid	104.04734	M-H	5.01
HMDB0000190	Lactic acid	90.03169	M-H	5.02
HMDB0001882	Dihydroxyacetone	90.03169	M-H	5.03
HMDB0011757	N-Acetylvaline	159.08954	M-H	5.03
HMDB0000210	Pantothenic acid	219.11067	M-H	5.10

HMDB0000525	5-Hydroxyhexanoic acid	132.07919	M-H	5.12
HMDB0061881	4-Acetylbutyrate	130.06354	M-H	5.13
HMDB0000239	Pyridoxine	169.07389	M-H	5.22
HMDB0003070	Shikimic acid	174.05282	M-H	5.30
HMDB0012141	(R)-2,3-Dihydroxy-3-methylbutanoate	134.05790	M-H	5.31
HMDB0000251	Taurine	125.01466	M-H	5.32
HMDB0000011	3-Hydroxybutyric acid	104.04734	M-H	5.36
HMDB0000115	Glycolic acid (new)	76.01600	M-H	5.36
HMDB0001873	Isobutyric acid	88.05243	M-H	5.39
HMDB0000754	3-Hydroxyisovaleric acid	118.06354	M-H	5.41
HMDB0000008	2-Hydroxybutyric acid	104.04734	M-H	5.47
HMDB0012710	3-Dehydroquinate	190.04774	M-H	5.63
HMDB0341363	Nicotinic Acid N-Oxide	139.02694	M-H	5.66
HMDB0254310	Maleamate	115.02690	M-H	5.73
HMDB0000237	Propionic acid	74.03733	M-H	5.93
HMDB0240389	Pantoic acid	148.07360	M-H	5.95
HMDB0000462	Allantoin	158.04454	M-H	6.13
HMDB0011745	N-Acetyl-L-methionine	191.06161	M-H	6.16
HMDB0000678	Isovalerylglycine	159.08954	M-H	6.20
HMDB0001259	Succinic semialdehyde	102.03169	M-H	6.22
N/A	4-Methyl-2-ureido-pentanoic acid/Carbamoyl isoleucine	174.10099	M-H	6.36
HMDB0246808	5-Hydroxymethyl-2'-deoxyuridine	258.08500	M-H	6.48
HMDB0000039	Butyric acid	88.05243	M-H	6.51
HMDB0000243	Pyruvic acid	88.01604	M-H	6.76
HMDB0001015	N-Formyl-methionine	177.04596	M-H	6.79

HMDB0000718	Isovaleric Acid	102.06863	M-H	6.91
HMDB0062180	Lactoyl-isoleucine	203.11631	M-H	7.02
HMDB0003344	Glycoaldehyde	60.02113	M-H	7.52
N/A	5-formyl-2'-deoxyuridine	256.06954	M-H	7.53
N/A	N-Formyl-DL-ethionine	191.06216	M-H	7.53
HMDB0000012	Deoxyuridine	228.07462	M-H	7.60
HMDB0000624	Leucic acid	132.07919	M-H	7.60
HMDB0002545	Galacturonic acid (new)	194.04270	M-H	7.61
HMDB0000317	2-hydroxy-3-methylvaleric acid	132.07860	M-H	7.66
HMDB0000892	Valeric Acid	102.06863	M-H	7.76
HMDB0000005	2-Ketobutyric acid	102.03169	M-H	7.79
HMDB0002207	Hydroxyisoheptanoic acid	146.09484	M-H	7.87
HMDB0001624	2-hydroxyhexanoic acid	132.07860	M-H	8.02
HMDB0003193	Testosterone glucuronide	464.24047	M-H	8.06
HMDB0000119	Glyoxylic acid	74.00039	M-H	8.26
HMDB0000127	Glucuronic acid	194.04265	M-H	8.39
HMDB0000019	alpha-Ketoisovaleric acid	116.04734	M-H	8.48
HMDB0001511	Phosphocreatine	211.03636	M-H	8.72
HMDB0000300	Uracil	112.02728	M-H	8.77
HMDB0000512	N-Acetyl-L-phenylalanine	207.08954	M-H	8.95
N/A	maltose-1-phosphate	422.2764	M-H	8.97
HMDB0000296	Uridine	244.06954	M-H	9.09
HMDB0001367	N-acetyl-glucosamine-1-phosphate	301.05627	M-H	9.11
HMDB0005831	Sorbitol-6-phosphate	262.04537	M-H	9.23
HMDB0032923	Kojic acid	142.02661	M-H	9.29
HMDB0001865	Oxovaleric Acid	116.04789	M-H	9.30

HMDB0011616	Adenosine 2',3'-cyclic phosphate	329.05197	M-H	9.41
HMDB0011140	Hypusine	233.17449	M-H	9.42
N/A	sucrose-6'-phosphate	422.27640	M-H	9.45
HMDB0000645	Galactose 1-phosphate	260.02972	M-H	9.56
HMDB0001124	trehalose-6-phosphate	422.08255	M-H	9.59
HMDB0005765	Ophthalmic Acid	289.12793	M-H	9.66
HMDB0000218	Orotidylic acid/OMP	368.02624	M-H	9.67
HMDB0000617	2-Furoate	112.01600	M-H	9.73
HMDB0000126	Glycerol 3-phosphate	172.01367	M-H	9.75
HMDB0001586	Glucose 1-phosphate	260.02972	M-H	9.77
HMDB0255868	Succinyl-Homoserine	219.07400	M-H	9.85
HMDB0060150	Cysteamine	77.02992	M-H	9.87
HMDB0304061	2-C-Methylerythritol 4-phosphate	214.02424	M-H	9.88
HMDB0001138	N-Acetylglutamate	189.06427	M-H	9.94
HMDB0000535	Caproic acid/Hexanoic acid	116.08428	M-H	9.99
HMDB0000902	NAD+	663.10912	M-H	10.04
HMDB0000262	Thymine	126.04293	M-H	10.06
HMDB0000812	N-Acetyl-aspartate	175.04807	M-H	10.09
HMDB0000092	Dimethylglycine	103.06333	M-H	10.23
HMDB0001213	1-Deoxy-D-xylulose 5-phosphate	214.02424	M-H	10.32
HMDB0001564	CDP-ethanolamine	446.06038	M-H	10.36
HMDB0001202	dCMP	307.05694	M-H	10.39
HMDB0062590	Tropic acid	166.06300	M-H	10.41
N/A	DL-Threo-beta-Hydroxyaspartic acid	148.02515	M-H	10.50
N/A	Diaminocyclohexane tetra acetic acid (DCTA)	345.13034	M-H	10.60

N/A	Butyl ureidosuccinic acid	232.10647	M-H	10.61
HMDB0013233	Gamma-delta-Dioxovaleric acid	130.02661	M-H	10.65
HMDB0000491	3-Methyl-2-oxovaleric acid	130.06299	M-H	10.67
HMDB0000355	3-Hydroxymethylglutarate	162.05282	M-H	10.68
HMDB0000828	Ureidosuccinic acid (N-carbamoyl-L-aspartic acid)	176.04332	M-H	10.69
HMDB0060509	Sedoheptulose 1-phosphate	290.04028	M-H	10.74
HMDB0000752	Methylglutaric acid	146.05791	M-H	10.75
HMDB0015109	EDTA	292.09067	M-H	10.83
N/A	3-Ethylmalate	162.05280	M-H	10.85
HMDB0062739	D-erythro-3-Methylmalate	148.03720	M-H	10.87
HMDB0002393	N-Methyl-D-aspartic acid	147.05316	M-H	10.87
HMDB0000426	Citramalic acid	148.03717	M-H	10.89
HMDB0000639	Galactaric acid (mucic acid)	210.03757	M-H	10.91
HMDB0000661	Glutaric acid	132.04226	M-H	10.95
HMDB0000695	4-methyl-2-oxovaleric acid (ketoleucine)	130.06299	M-H	10.96
HMDB0059655	2-Hydroxyglutarate	148.03717	M-H	10.98
HMDB0000956	Tartaric acid	150.01640	M-H	11.04
HMDB0000254	Succinic acid	118.02661	M-H	11.06
HMDB0000095	Cytidine monophosphate	323.05185	M-H	11.12
HMDB0000744	Malic acid (new)	134.02150	M-H	11.14
HMDB0001031	Deoxyribose 5-phosphate	214.02424	M-H	11.24
HMDB0012882	Adipate semialdehyde	130.06299	M-H	11.34
HMDB0000714	Hippuric acid	179.05824	M-H	11.42
HMDB0000528	Hydroorotic acid	158.03276	M-H	11.44

HMDB0002441	3,3 Dimethyl glutarate	160.07356	M-H	11.46
HMDB0013701	3-Oxoglutarate	174.05280	M-H	11.48
HMDB0012283	Prephenic Acid	226.04774	M-H	11.51
HMDB0001127	6-phosphonoglucono-lactone	258.01462	M-H	11.52
HMDB0003349	Dihydroorotic acid	158.03276	M-H	11.52
HMDB0000622	Ethylmalonic acid	132.04226	M-H	11.54
HMDB0001890	Acetylcysteine	163.03031	M-H	11.57
HMDB0001352	Hydroxypyruvic acid	104.01096	M-H	11.61
HMDB0000691	Malonic acid (new)	104.01100	M-H	11.62
HMDB0000191	Aspartate	133.03751	M-H	11.78
HMDB0001112	Glyceraldehyde 3-phosphate	169.99802	M-H	11.86
HMDB0006797	Sorbose 1-phosphate	260.02917	M-H	11.89
HMDB0000634	Citraconic acid	130.02661	M-H	11.92
HMDB0001212	Hydantoin-5-propionic acid	172.04786	M-H	11.93
N/A	Galactose-6-phosphate	260.02917	M-H	11.94
N/A	2-butyl-3-ureido-succinate	232.10592	M-H	11.98
HMDB0002757	Cysteic acid	169.00449	M-H	11.99
HMDB0000663	Saccharic acid	210.03757	M-H	12.05
HMDB0002092	Itaconic acid	130.02661	M-H	12.10
HMDB0000176	Maleic acid	116.01096	M-H	12.19
HMDB0001062	N-Acetyl-D-Glucosamine 6-Phosphate	301.05627	M-H	12.20
HMDB0012156	3-isopropylmalic acid	176.06850	M-H	12.22
HMDB0032797	Jasmonic acid	210.12559	M-H	12.22
HMDB0000402	2-Isopropylmalic acid	176.06847	M-H	12.27
HMDB0000044	Ascorbate	176.03209	M-H	12.31
HMDB0001401	Glucose 6-phosphate	260.02972	M-H	12.35

HMDB0000749	Mesaconic acid	130.02661	M-H	12.39
HMDB0001121	N-Acetyl-D-mannosamine 6-phosphate (ManNac-6-P)	301.05627	M-H	12.39
HMDB0000223	Oxalacetic acid	132.00587	M-H	12.39
HMDB0000620	Glutaconic acid	130.02661	M-H	12.50
HMDB0255221	N-Oxalylglycine	147.01680	M-H	12.53
N/A	trans-2,3-epoxysuccinic acid	132.00590	M-H	12.53
HMDB0001517	AICA-Ribonucleotide	338.06275	M-H	12.55
HMDB0060466	4-Hydroxy-2-oxoglutarate	162.01644	M-H	12.60
HMDB0000124	Fructose 6-phosphate	260.02972	M-H	12.60
HMDB0000225	Oxoadipic acid	160.03717	M-H	12.60
HMDB0003559	Gibberellin A3	346.14164	M-H	12.68
HMDB0000208	2-Oxoglutaric acid	146.02152	M-H	12.72
HMDB0001078	Mannose 6-phosphate	260.02972	M-H	12.75
HMDB0000202	Methyl malonic acid	118.02661	M-H	12.84
HMDB0000905	dAMP	331.06817	M-H	12.91
HMDB0001254	Glucosamine 6-phosphate	259.04570	M-H	13.06
HMDB0040733	Phenylacetic Acid	136.05298	M-H	13.07
HMDB0000868	Xylulose 5-phosphate	230.01915	M-H	13.08
HMDB0000618	Ribulose 5-phosphate	230.01915	M-H	13.11
HMDB0001548	Ribose 5-phosphate	230.01915	M-H	13.16
HMDB0002329	Oxalic acid	89.99531	M-H	13.25
HMDB0014684	Fluorouracil	130.01786	M-H	13.27
HMDB0036093	Abscisic acid	264.13620	M-H	13.28
HMDB0001068	Sedoheptulose 7-phosphate	290.04028	M-H	13.29
HMDB0000393	cis,cis-Muconate	142.02660	M-H	13.31

HMDB0000232	Quinolinic acid	167.02186	M-H	13.34
N/A	5-formyluracil	140.02219	M-H	13.36
HMDB0000134	Fumarate	116.01096	M-H	13.42
HMDB0011717	Nonate	188.10541	M-H	13.85
HMDB0000045	Adenosine monophosphate (AMP)	347.06308	M-H	13.87
HMDB0246430	4-formylbenzoic acid	150.03169	M-H	13.97
HMDB0006488	N-Acetyl-L-glutamate 5-semialdehyde	173.06881	M-H	13.97
HMDB0006268	N-Acetylneuraminate 9-phosphate	389.07231	M-H	13.98
HMDB0015050	Phenformin	241.10997	M-H	14.07
HMDB0003540	3'-AMP	347.06254	M-H	14.14
HMDB0006557	ADP Glucose	589.08224	M-H	14.17
HMDB0001067	N-Acetylaspartylglutamic acid	304.09067	M-H	14.29
N/A	Quisqualic acid	189.03912	M-H	14.33
N/A	2-Hydroxy-4-phenylbutanoic acid	180.07919	M-H	14.39
HMDB0003911	3-Aminoisobutanoic acid	103.06333	M-H	14.40
HMDB0000370	Glyphosate/2-Amino-3-phosphonopropionic acid	169.01456	M-H	14.52
N/A	3-[(2,4-dioxo-1H-pyrimidine-6-carbonyl)amino]propanoic acid (DB28)	227.04690	M-H	14.68
HMDB0013593	1,4 dihydrotheritol	154.01222	M-H	14.69
HMDB0000711	Hydroxyoctanoic acid	160.11049	M-H	14.70
HMDB0001343	Mevalonic acid-5P	228.03989	M-H	14.73
HMDB0001316	6-Phosphogluconic acid	276.02463	M-H	14.76
HMDB0001721	O-Phosphoserine (new)	185.00892	M-H	14.84
HMDB0005784	3-Hydroxytyrosol	154.06299	M-H	14.94
HMDB0000058	Cyclic AMP	329.05252	M-H	14.94

HMDB0001096	Carbamoyl phosphate	140.98271	M-H	15.06
HMDB0015256	Tolbutamide	270.10436	M-H	15.08
HMDB0000227	Mevalonic acid	148.07356	M-H	15.14
HMDB0304060	2-C-Methyl-D-erythritol-2,4-cyclopyrophosphate	277.99620	M-H	15.28
HMDB0000788	Orotidine	288.05882	M-H	15.30
HMDB0000125	Glutathione (GSH)	307.08381	M-H	15.33
HMDB0001473	Dihydroxyacetone phosphate (new)	169.99800	M-H	15.43
HMDB0000291	4-Hydroxy-3-methoxymandelic acid	198.05282	M-H	15.45
HMDB0001245	dCDP	387.02327	M-H	15.46
N/A	Acetyl-6-formylpterin	231.05490	M-H	15.67
HMDB0000807	3-Phosphoglyceric acid	185.99294	M-H	15.73
HMDB0006471	Methylisocitric acid	206.04265	M-H	15.82
HMDB0000226	Orotic acid	156.01711	M-H	16.04
HMDB0000379	2-Methylcitric acid	206.04320	M-H	16.09
HMDB0000764	Hydrocinnamic acid	150.06863	M-H	16.17
HMDB0015020	Clomifene	405.18594	M-H	16.22
HMDB0001049	Glutamylcysteine	250.06289	M-H	16.25
HMDB0000816	Phosphoglycolic acid	155.98237	M-H	16.26
HMDB0000362	2-Phosphoglyceric acid	185.99294	M-H	16.34
N/A	Dehydrocholic acid	402.24063	M-H	16.40
HMDB0002107	Phthalate	166.02660	M-H	16.51
HMDB0001546	Cytidine diphosphate	403.01763	M-H	16.54
HMDB0001870	benzoic acid	122.03678	M-H	16.58
N/A	1-Hydroxy-2-methyl-2-butenyl 4-pyrophosphate	262.00074	M-H	16.68

HMDB0000094	Citric acid	192.02700	M-H	16.72
HMDB0002085	Syringic acid	198.05282	M-H	16.82
HMDB0001409	dUMP	308.04095	M-H	16.88
HMDB0001227	Thymidine 5'-phosphate (TMP)	322.05660	M-H	16.89
HMDB0000130	Homogentisic acid	168.04226	M-H	16.90
HMDB0000020	p-Hydroxyphenylacetic acid	152.04789	M-H	16.97
HMDB0000217	NADP+	743.07545	M-H	17.00
HMDB0000118	Homovanillic acid	182.05791	M-H	17.02
HMDB0001328	dTDP-D-glucose	564.07576	M-H	17.06
HMDB0060320	(Z)-But-1-ene-1,2,4-tricarboxylate	188.03210	M-H	17.07
HMDB0000290	Uridine diphosphate-N-acetylglucosamine	607.08157	M-H	17.18
HMDB0000193	Isocitrate *	192.02700	M-H	17.30
N/A	4-Hydroxyphenylbutyric acid	179.07137	M-H	17.51
HMDB0001047	Fructose 2,6 diphosphate	339.99605	M-H	17.52
HMDB0004284	Tyrosol	138.06808	M-H	17.77
HMDB0000263	Phosphoenolpyruvic acid	167.98237	M-H	17.81
HMDB0000072	cis-Aconitic acid	174.01644	M-H	17.86
HMDB0013713	N-Acetyltryptophan	246.10044	M-H	17.86
HMDB0001487	NADH	665.12477	M-2H	17.88
HMDB0032572	Methylparaben	152.04734	M-H	17.89
HMDB0000302	UDP-galactose	566.05502	M-H	17.96
HMDB0000792	Sebacic acid	202.12051	M-H	18.03
HMDB0002833	Testosterone sulfate	368.16629	M-H	18.09
HMDB0244973	4-hydroxyphenyl glycine/Oxfenicine	167.05824	M-H	18.12
HMDB0001101	4-Methoxybenzoic acid	152.04730	M-H	18.16

HMDB0001347	Isopentenyl pyrophosphate	246.00583	M-H	18.18
HMDB0013188	3-Hydroxypicolinic acid	139.02694	M-H	18.21
HMDB0001508	dADP	411.03450	M-H	18.27
HMDB0000500	4-Hydroxybenzoic acid	138.03169	M-H	18.33
HMDB0000288	Uridine 5'-monophosphate	324.03587	M-H	18.37
HMDB0001120	Dimethylallyl pyrophosphate	246.00583	M-H	18.45
HMDB0000286	UDP-glucose	566.05502	M-H	18.48
HMDB0000965	Hypotaurine	109.01975	M-H	18.60
HMDB0000289	Uric acid	168.02834	M-H	18.92
HMDB0006555	dIMP	332.05219	M-H	18.99
HMDB0003333	8-Hydroxy-deoxyguanosine	283.09167	M-H	19.00
HMDB0002825	Theobromine	180.06418	M-H	19.00
HMDB0060274	Sedoheptulose 1,7-bisphosphate	370.00661	M-H	19.08
HMDB0247933	Acetylenedicarboxylic acid	113.99530	M-H	19.17
N/A	5-Hydroxy-methyl-dCTP	497.00016	M-H	19.40
N/A	5-formylsalicylic acid	166.02661	M-H	19.73
N/A	5-Methyl-dCTP	481.00525	M-H	19.78
HMDB0011615	8-Oxo-dGTP	522.99011	M-H	19.78
HMDB0011688	Ribulose 1,5,diphosphate	309.98603	M-H	19.79
HMDB0001339	Glutaryl CoA	881.14690	M-H	19.81
HMDB0001341	Adenosine diphosphate	427.02941	M-H	19.90
HMDB0000998	dCTP	466.98960	M-H	20.05
HMDB0000482	Octanoic acid	144.11503	M-H	20.06
HMDB0001044	dGMP	347.06308	M-H	20.15
HMDB0001058	Fructose 1,6-bisphosphate	339.99605	M-H	20.30
N/A	5-Formyl-dCTP	494.98505	M-H	20.45

N/A	Hydroxy-methyl-dUTP	497.98418	M-H	20.48
HMDB0062484	2,4-dihydroxybenzaldehyde	138.02440	M-H	20.55
HMDB0029635	Toluate	136.05240	M-H	20.64
HMDB0001554	Xanthylic acid/XMP	364.04256	M-H	20.70
HMDB0011621	Cinnamoylglycine	205.07334	M-H	20.81
HMDB0014897	Tetracycline	444.15272	M-H	20.98
HMDB0000082	Cytidine triphosphate	482.98451	M-H	20.99
HMDB0003518	Homocitric acid	206.04265	M-H	21.27
HMDB0001491	Pyridoxal 5'-phosphate	247.02457	M-H	21.42
HMDB0013220	Beta-Citryl-L-glutamic acid	321.06960	M-H	21.49
HMDB0014615	Fluoxetine	309.13460	M-H	21.52
HMDB0000175	Inosine monophosphate	348.04710	M-H	21.57
HMDB0001336	3,4-dihydroxyphenyl acetic acid	168.04226	M-H	21.64
HMDB0002466	3-Hydroxybenzoic acid	138.03224	M-H	21.92
HMDB0001397	Guanosine monophosphate	363.05800	M-H	21.97
HMDB0001294	2,3-Diphosphoglyceric acid	265.95927	M-H	22.07
HMDB0001000	dUDP	388.00728	M-H	22.07
HMDB0001274	TDP	402.02293	M-H	22.17
HMDB0000280	Phosphoribosyl pyrophosphate (PRPP)	389.95181	M-H	22.18
HMDB0012308	Vanillin	152.04789	M-H	22.20
HMDB0001200	N-Formylkynurenine	236.08026	M-H	22.44
HMDB0000957	1,2-Dihydroxybenzene	110.03678	M-H	22.64
HMDB0001332	Adenylsuccinate	463.07404	M-H	23.07
HMDB0000295	Uridine 5'-diphosphate	404.00220	M-H	23.34
HMDB0001314	Cyclic GMP	345.04743	M-H	23.36
HMDB0032616	Sinapic acid	224.06847	M-H	23.75

HMDB0001856	Protocatechuic acid	154.02661	M-H	24.01
HMDB0013674	1,2,3-Trihydroxybenzene/Pyrogallol	126.03224	M-H	24.16
HMDB0000935	UDP-glucoronate	580.03428	M-H	24.22
HMDB0000538	Adenosine triphosphate (ATP)	506.99575	M-H	24.53
HMDB0000960	dGDP	427.02941	M-H	24.67
HMDB0125090	2,4,6-trihydroxybenzaldehyde	154.01930	M-H	24.82
HMDB0001423	Coenzyme A	767.11521	M-H	24.88
HMDB0001520	Flavin Mononucleotide (unconfirmed)	456.10461	M-H	25.26
HMDB0000954	Ferulic acid	194.05791	M-H	25.36
HMDB0001191	dUTP	467.97361	M-H	25.45
HMDB0000958	trans-aconitate	174.01644	M-H	25.49
HMDB0001342	Thymidine triphosphate	481.98926	M-H	25.82
HMDB0001143	Inositol 1,3,4-trisphosphate	419.96238	M-H	25.85
HMDB0000763	5-Hydroxyindoleacetic acid	191.05824	M-H	25.98
HMDB0000671	Indole-3-lactic acid	205.07389	M-H	26.03
HMDB0015464	Yohimbine	354.19489	M-H	26.07
HMDB0003335	IDP	428.01343	M-H	26.47
HMDB0000707	4-Hydroxyphenylpyruvic acid	180.04226	M-H	26.57
HMDB0001855	5-Hydroxytryptophol	177.07898	M-H	26.62
HMDB0001248	FAD	785.15713	M-H	26.72
HMDB0000285	Uridine triphosphate	483.96853	M-H	26.76
HMDB0001201	Guanosine diphosphate (GDP)	443.02378	M-H	26.81
HMDB0002035	p-Coumaric acid	164.04734	M-H	27.20
N/A	Methyl 3-hydroxybenzoate	152.04789	M-H	27.40
HMDB0000930	trans-cinnamic acid	148.05243	M-H	27.46
HMDB0000197	Indoleacetic acid	175.06333	M-H	27.49

HMDB0000873	4-Methylcatechol	124.05298	M-H	27.62
HMDB0243941	1-Methyl indole	131.07405	M-H	28.33
HMDB0004096	5-Methoxyindoleacetate	205.07389	M-H	28.43
HMDB0005782	Hesperitin	302.07849	M-H	28.50
HMDB0005794	Quercetin	302.04210	M-H	28.65
HMDB0038804	6-hydroxy-2,5,7,8-tetramethylchromane-2-carboxylic acid (Trolox)	250.12051	M-H	28.68
HMDB0000205	Phenylpyruvic acid	164.04734	M-H	28.83
HMDB0001440	dGTP	506.99520	M-H	28.94
HMDB0000189	Inosine triphosphate	507.97976	M-H	29.54
HMDB0014733	Oxytetracylcine	460.14818	M-H	29.58
HMDB0005807	Gallic acid	170.02150	M-H	29.59
HMDB0001273	Guanosine triphosphate	522.99066	M-H	29.88
HMDB0000397	2-Pyrocatechuic acid	154.02661	M-H	30.45
HMDB0004823	Lanthionine ketimine	189.01013	M-H	30.82
HMDB0000152	2,5-Dihydroxybenzoic acid	154.02661	M-H	30.88
HMDB0001484	Acetoacetyl-CoA	851.13634	M-H	31.46
HMDB0004815	Methyl-4-hydroxybenzoic acid	152.04789	M-H	32.63
HMDB0001879	aspirin	180.04226	M_H	32.85
HMDB0001964	Caffeic acid	180.04230	M-H	32.92
HMDB0240656	Lanthionine	208.05233	M-H	33.00
HMDB0029416	Targinine	188.12787	M-H	33.55
N/A	1-Methyl-1H-indole-3-carboxamide	174.07986	M-H	33.86
HMDB0001498	Myo-inositol-1,4,5-phosphate	419.96238	M-2H	36.06
HMDB0000060	Acetoacetate	102.03169	M-H	N/A

HMDB0031257	Dimethyl fumarate	144.04226	M-H	N/A
HMDB0000700	Hydroxypropionic acid	90.03224	M-H	N/A
HMDB0006112	Malondialdehyde	72.02113	M-H	N/A
HMDB0000221	NADPH	745.09110	M-2H	N/A
HMDB0000715	Kynurenic acid	189.04259	M-H	N/A
HMDB0000195	Inosine	268.08077	M-H	N/A
HMDB0001847	Caffeine	194.08092	M-H	N/A
HMDB0003164	Chlorogenic acid	354.09563	M-H	N/A
HMDB0006456	N-Acetyl-L-glutamyl 5-phosphate	269.03005	M-H	N/A
HMDB0002670	Naringenin	272.06902	M-H	N/A
HMDB0013112	UDP-N-acetyl-D-mannosamine (unconfirmed)	607.08157	M-H	N/A

Table A.7.2: Table showing parameters used during metabolite annotation from the IC-MS data for all the experiments. The following criteria's (RTE > 0.5 min, ME > 3 ppm, IS < 90%) was followed when annotated compound as putative or confident. RTE=Retention Time Error, MS=Mass Error and ISS=Isotope similarity.

Accepted Description	Mass Error (ppm)	Isotope Similarity	Retention Time Error (mins)	Max Abundance	Mini CV%	Confident or putative	Comment
1,2,3-Trihydroxybenzene/Pyrogallol	-1.16253	95.5836	-0.52965	16.19413	55.78	c	
1-Methyl indole	-1.63271	90.5809	-1.92342	0	---	c	
1-Pyrroline-5-carboxylic acid	4.41956	98.3833	2.919867	1869.11	4.9	p	ME and RTE
2,3-Diphosphoglyceric acid	0.02318	94.4964	0.768083	386.3329	10.86	c	
2,5-Dihydroxybenzoic acid	0.97143	97.7832	1.8211	56.25218	32.63	p	RTE
2-C-Methylerythritol 4-phosphate	0.81319	71.9857	-2.17077	155.3691	13.49	p	ISS
2-Hydroxy-4-phenylbutanoic acid	-3.91891	99.2413	0.051817	4.908364	160.04	c	
2-Hydroxyglutarate	3.02253	99.4391	0.9011	204.8464	27.87	c	
2-Isopropylmalic acid	-0.86964	99.5007	0.1716	16.11378	201.53	c	
2-Methylcitric acid	-2.8114	99.3001	-1.09617	1584.574	21.24	c	
2-Oxoglutaric acid	1.91936		0.19595	65.93946	21.33	p	No ISS
2-Phosphoglyceric acid	-0.51226	99.7287	-1.89818	316626.9	22.55	c	
3-(2,5-Dioxoimidazolidin-4-yl)propanoic acid	0.81163	92.1416		11.19902	22.43	p	No RTE

3,3 Dimethyl glutarate	0.19014	99.5949	-1.55893	303.1772	43.84	c	
3,4-dihydroxyphenyl acetic acid	0.67569	93.1437	-2.53878	87.76403	21.42	c	
3-Dehydroquinate	-0.80963	94.5606	2.829517	0	---	p	RTE
3-deoxy-2-keto-6-phosphogluconic acid	2.19235	99.0938	-1.41307	21.88496	32.2	c	
3-Hydroxyisovaleric acid	-0.00877	95.6961	1.880067	38.07187	13.83	p	RTE
3-Hydroxymethylglutarate	0.38524	95.4956	2.564983	0	---	p	RTE
3-methoxyphenylacetic acid	-0.54279	98.5076	2.6372	47.4235	172.93	p	RTE
4-Acetylbutyrate	-0.9398	89.1543	-1.41512	530.7264	14.56	p	ISS
4-Hydroxy-2-oxoglutarate	0.22474	93.3952		0	---	p	No RTE
4-Hydroxy-3-methoxymandelic acid	-0.84007	89.5791	-1.57583	0	---	p	ISS
4-Hydroxybenzoic acid	1.99307	98.481	-2.82733	364.7273	38.97	c	
4-hydroxyphenyl glycine/Oxfenicine	1.58237	90.7184	2.362017	0.03149	266.3	p	RTE
4-Hydroxyproline	2.51276	98.8244	-0.42862	8756.939	20.3	c	
4-Methyl-2-ureido-pentanoic acid/Carbamoyl isoleucine	-4.21921	91.8404	-1.4389	26.38825	189.05	c	
5-Hydroxyhexanoic acid	-0.41868	92.9797	-2.37442	133.3467	18.06	c	
5-Hydroxyindoleacetic acid	-0.02243	97.953	-2.27937	3.130399	86.33	c	
5-Hydroxymethyl-2'-deoxyuridine	0.57791	76.9031	2.378367	345.7421	21.9	p	ISS and RTE
5-Methoxyindoleacetate	-0.00027	87.7668	1.149917	0	---	p	ISS
6-hydroxy-2,5,7,8-tetramethylchromane-2-carboxylic acid (Trolox)	-0.40528	98.0514	-1.97347	0	---	c	
6-Phosphogluconic acid	-0.21498	99.0054	-1.66335	16823.54	7.57	c	

6-phosphonoglucono-lactone	-0.33379	91.6198	-0.71507	487.6731	11.63	c	
8-Hydroxy-deoxyguanosine	0.51796	90.6458	-1.97462	0	---	c	
8-Oxo-dGTP	1.02964	93.4793	2.520233	4915.641	23.25	p	RTE
Abscisic acid	-0.0009	84.0919	0.61205	0.961749	218.37	p	ISS
Acetoacetate	4.8795	97.2622	-1.46512	162.3738	19.48	p	ME
Acetylcysteine	0.56663	89.1081	-0.95492	359.2845	35.76	p	ISS
Adenine	2.04064	97.6291	-2.46782	2.961148	100.33	c	
Adenosine 2',3'-cyclic phosphate	2.64887	96.1083	-0.55163	0	---	c	
Adenosine diphosphate	0.85981	98.2953	2.510233	7094745	19.24	c	
Adenosine monophosphate (AMP)	0.40516	92.1962	1.335467	0	---	c	
Adenosine triphosphate (ATP)	-0.45579	95.6253	2.084567	1080.215	17.15	p	RTE
Adenylsuccinate	-0.08354	82.1079	-1.9068	498.5128	13.05	p	ISS
Adipate semialdehyde	3.44197	98.9931	-1.79948	11396.65	6.16	C	
Adonitol (ribitol)	2.43451	95.6656	1.266283	2195.233	12	c	
ADP Glucose	0.98981	79.4841	-1.44782	81.45699	142.2	p	ISS
Allantoin	-3.22481	94.2561	-0.75398	1593.246	6.13	c	
Alpha-aminobutyrate	1.57447	98.681	0.285083	1.004799	138.67	c	
Arabinonic acid	0.171	96.7832	-0.77372	6167.934	12.91	c	
Arabitol	0.91555	99.7338	-0.04745	741.2372	14.43	c	
Ascorbate	-0.99745	92.3875	2.081817	17.32208	39.22	p	RTE
Aspartate	3.20918	97.4737	-2.52862	1065.65	21.28	c	
Beta-Alanine	2.98172	98.9189	-0.86052	226.3787	16.48	c	
Beta-Citryl-L-glutamic acid	1.00913	98.5287	-0.7143	171980.3	11.84	c	

Butyl ureidosuccinic acid	-2.72169		1.293567	0	---	p	No ISS
Butyric acid	-1.7492	96.0551	0.510817	0	---	c	
Caffeic acid	-3.87655	99.3225		1.059124	316.23	p	No RTE
Caproic acid/Hexanoic acid	-1.03334	97.8548	2.616217	176.2953	15.15	p	RTE
cis-Aconitic acid	1.84943	92.4085	-1.03485	15.53755	60.63	c	
Citric acid	-1.2064	99.4341	0.662217	209.3593	55.11	c	
Cysteic acid	-0.02236	91.793	-1.28725	5415.756	10.27	c	
Cytidine	4.52673	92.0641	-2.81118	2253.265	6.75	p	ME
Cytidine diphosphate	2.2915	98.2424	2.9759	369577	12.68	p	RTE
Cytidine monophosphate	0.77041	94.6754	-2.82487	1145.285	21.86	c	
Cytidine monophosphate N-acetylneuraminic acid	3.22187	95.1501	-0.83487	8038.143	19.57	p	ME
Cytidine triphosphate	0.20273	98.1959	-1.7441	132795.4	11.68	c	
Cytosine	3.42605	94.4731	-1.48367	12.27756	52.62	p	ME
dCTP	0.41058	94.6949	-1.01927	1680.063	10.06	c	
Deoxyadenosine triphosphate	-0.07252	95.8748	-2.30993	4334.343	12.43	c	
Deoxyribose 5-phosphate	-0.86356		2.738733	0.489209	316.23	p	No ISS and RTE
Deoxyuridine	-2.4399	88.9084	0.822933	29.63161	41.97	p	ISS
dGMP	1.05236	95.0065	2.802817	0	---	p	RTE
Dihydroorotic acid	1.79122	78.9772	1.88665	26.9174	13.88	p	ISS and RTE
Dihydroxyacetone	2.9649	99.9509	-0.43323	2179843	7.06	c	
Dihydroxyacetone phosphate	-0.01539	95.3904	-0.38507	173.5445	12.11	c	

Dimethyl fumarate	2.66089	97.8881	1.833833	24.87315	30.31	p	RTE
Dimethylallyl pyrophosphate	-0.85785	97.4915	-2.31293	0	---	c	
DL-Threo-beta-Hydroxyaspartic acid	-0.36203	94.2604	2.330767	0	---	p	RTE
dTDP-D-glucose	1.9875	95.8478	-1.41705	10900.64	15.3	c	
dUMP	0.28435	96.7027	-1.6447	483.086	13.4	c	
EDTA	0.50392	96.5681	-1.18543	7259.946	3.41	c	
Erythrose 4-phosphate	0.7273	94.1427	0.60665	227.037	15.87	c	
Flavin Mononucleotide (unconfirmed)	0.82272	91.8074		250.6984	59.92	p	No RTE
Fluorouracil	3.36956	95.6537	-1.47023	465.3393	111.66	p	ME
Fructose	-0.69568	97.9761	1.246767	39931.24	7.97	c	
Fructose 1,6-bisphosphate	1.06502		1.580067	1491.305	8.98	p	No ISS and RTE
Fructose 2,6 diphosphate	1.0461	99.4947	1.112517	132273.2	12.76	c	
Fructose 6-phosphate	-0.37426	98.6142	1.066467	96.72432	21.22	c	
Fumarate	3.86909	99.8002	-1.72643	11031.42	12.08	p	ME
Galactaric acid (mucic acid)	0.11452	91.8501	-0.99605	542.4397	25.67	c	
Gluconate	-0.54322		-1.25927	1801.431	64.15	p	No ISS
Gluconolactone	0.84034	92.3665	-0.67367	4.29719	178.3	c	
Glucose	0.37383	96.4113	-0.01927	1837.578	16.41	c	
Glucose 1-phosphate	-0.3123	99.3048	-0.90772	34250.52	16.75	c	
Glucuronic acid	-0.38214	99.4968	-0.9542	884.5414	13.08	c	
Glutaconic acid	3.73369	99.7098	2.580917	4920.117	15.36	p	ME
Glutamic acid	1.7127	93.7642	-1.08383	260377.7	38.55	c	

Glutamine	2.72972	97.0111	1.0072	283.0636	9.7	c	
Glutamylcysteine	-2.43867	93.7866	2.316333	7.171446	92.18	p	RTE
Glutaric acid	2.51472	98.0977	-1.01893	888.0538	20.19	c	
Glutathione (GSH)	0.40336	76.289	0.671183	80.95089	27.61	p	ISS
Glyceraldehyde 3-phosphate	0.10624	97.8892	0.464167	3406.362	22.56	c	
Glyceric acid	4.36345		-1.01348	59411.47	6.14	p	No ISS
Glycerol	3.6412	99.6027	-0.02617	152960	7.45	p	ME
Glycerol	-0.87481	98.2588	1.970567	1328.022	10.35	c	
Glycerol 3-phosphate	-0.05327		2.970767	0	---	p	No ISS and RTE
Glycolic acid	-0.64903	98.9963	-1.65313	6314.399	15.63	c	
Glyphosate/2-Amino-3-phosphonopropionic acid	-3.2699	95.7969	-1.1385	5.484982	128.81	c	
Guanosine diphosphate (GDP)	1.93864	98.0952	-0.05873	537943.1	17.07	c	
Guanosine monophosphate	0.7794	94.2294	-2.15878	1854.367	10.22	c	
Hippuric acid	-0.756	89.7564	1.608683	0	---	p	ISS and RTE
Homogentisic acid	-0.30304	93.4537	-2.69965	14.94985	96.11	c	
Homovanillic acid	-0.55474	98.1628	-2.51083	1154.745	8.79	c	
Hydroxy-indole acetic acid	0.25841	94.4951	-1.72942	0.777917	213.68	c	
Hydroxy-isobutyric acid	1.89675	98.3816	2.276133	1585.335	4.44	p	RTE
IDP	0.23443	96.931	0.559317	144.4204	44.68	c	
Indole-3-lactic acid	-0.1544	97.9696	0.186533	0	---	c	
Indoleacetic acid	-0.81335	89.1993	-2.02342	90.36636	41.28	p	ISS

Inosine	-4.87016	92.652	-1.81945	436.6964	54.02	c	
Inosine monophosphate	0.59667	97.3931	2.2825	3.598477	155.68	p	RTE
Inositol 1,3,4-trisphosphate	0.96815	90.2788	-1.29937	1506.87	34.77	c	
Isovalerylglycine	0.36691	91.9551	-1.61442	777.8365	72.09	c	
Jasmonic acid	0.05878	93.3699	1.018683	696.6945	25.97	c	
Kojic acid	2.32379	98.2111	1.493033	43.7024	33.55	c	
Kynurenic acid	-0.69415	97.7657	-1.36263	479.1914	77.83	c	
Lactose	-0.61694	92.7456	-0.28158	929.6098	21.98	c	
Lactoyl-isoleucine	-2.82248	97.7057	-1.92343	432.2097	212.24	c	
Leucic acid	-0.2078	96.1545	1.348367	3.992311	114.54	c	
Malic acid	2.58403	99.9437	-1.01262	78891.55	16.46	c	
Malitol	0.73249	85.3674	-0.41745	21.69541	89.76	p	ISS
Methionine sulfoxide	1.77724	88.9157		102.8861	8.4	p	no RTE
Methyl beta-D-glucopyranoside	-0.14454	96.4256	0.670733	57.75502	44.47	c	
Methyl phenylacetate	-1.59688	97.182	0.331817	0	---	c	
Methylglutaric acid	3.1935	97.5496	0.893217	0.684198	188.4	p	ME
Methylparaben	2.37204	97.1234	2.291217	0	---	p	RTE
Mytilitol	-3.18399	98.4939	0.08255	2.49626	189.82	c	
N-Acetyl proline	-3.36849	99.361	-0.63917	49.22408	110	c	
N-Acetyl-aspartate	-0.83874	92.5193	-0.77862	202613.3	21.98	c	
N-Acetylaspartylglutamic acid	0.86281	98.4353	-1.16132	36919.43	9.4	c	
N-Acetyl-D-glucosamine	-0.45776	96.6555	-0.0837	0	---	c	
N-acetyl-glucosamine-1-phosphate	0.43882	95.5457	-2.6036	849.3232	38.09	c	

N-Acetylglutamate	-3.71434	94.199	2.550417	10.53874	196.14	p	RTE
N-Acetyl-L-alanine	2.04748	94.5908	-0.36052	4128.364	14.43	c	
N-Acetyl-L-methionine	-0.29625	94.1555	-0.52488	4678.054	20.44	c	
N-Acetyl-L-phenylalanine	-0.05539	95.6608	0.754567	0	---	c	
N-Acetylneuraminic acid (Sialic acid)	0.81576	97.5827	-0.61348	19369.31	21.49	c	
N-Acetyltryptophan	-0.49246	97.9886	-1.7097	167.9002	85.56	c	
N-Acetylvaline	0.21418	91.8669	0.746783	156.4377	49.91	c	
NADH	1.93194	94.6524	-0.77503	7693.26	14.75	c	
NADPH	3.59343	85.1171	-1.30878	46.40106	152.91	p	ME
Naringenin	-4.77447	90.0987		1250.473	14.22	p	No RTE
N-Formyl-methionine	-0.76126	94.5358	-0.66698	580.8068	39.14	c	
Nicotinic Acid N-Oxide	2.25557	93.0375	-1.98888	48.50376	83.23	c	
Nonate	-3.2235	96.6424	-0.4285	1978.177	4.87	c	
N-Oxalylglycine	1.47468	99.0413	0.0872	0.622036	243.02	c	
O-Acetylserine	1.56318	93.711	-0.49052	40437.95	7.89	c	
Octanoic acid	1.48532	98.8244	-0.81803	5893.413	10.92	c	
O-Phosphoserine	0.0261	95.0366	1.272167	4.100244	143.38	c	
Orotic acid	1.21044	93.1714	-2.23883	3535.533	11.6	c	
Orotidine	2.39351	94.9858	-2.31127	964.9273	12.11	c	
Oxalic acid	3.13688	99.8055	0.22065	902.9373	12.26	p	ME
Oxoadipic acid	0.34439	99.4931	-0.13353	4.464555	134.38	c	
Oxovaleric Acid	-0.72225	95.7383	0.149233	4341.867	4.88	c	
Pantothenic acid	-0.06507	95.4942	1.440067	144.9206	7.36	c	

Phenylacetylglycine/Phenaceturic acid	-2.99848	94.7036	0.71395	93.80926	8.85	c	
Phenylpyruvic acid	0.85206	95.8193	-1.24485	257.0811	13.3	c	
Phosphocreatine	-2.80317	95.2409	-0.5018	341836.9	10.28	c	
Phosphoenolpyruvic acid	-0.30945	99.7409	-1.63733	34691.9	10.38	c	
Phosphoglycolic acid	1.25188	96.4316	0.002667	384.4629	11.68	c	
Phosphoribosyl pyrophosphate (PRPP)	1.11867	91.4912	0.030233	4112.259	24.87	c	
Protocatechuic acid	1.20926	97.1002	-2.41308	493.5099	25.19	c	
Pyridoxal 5'-phosphate	-0.19843	94.366	-2.11877	534.5203	7.52	c	
Pyruvic acid	2.95524	99.2752	-1.8789	16860.91	16.3	c	
Quinolinic acid	-0.05394	99.3215	-1.64023	115.0746	23.64	c	
Raffinose	-0.81169	88.2551	0.3248	420.6206	20.59	p	ISS
Ribose 5-phosphate	0.10586	96.1445	-1.28643	3151.028	4.86	c	
Ribose 5-phosphate	-0.06357	98.1891	0.43065	1186.043	111.74	c	
Ribulose 1,5,diphosphate	-0.73794	92.1575	-2.98708	396.3507	14.34	c	
Ribulose 5-phosphate	0.12122	94.275	-0.61737	2066.048	10.83	c	
Salicylic acid	-1.77167	99.3928	1.8111	7262.998	32.78	c	
Sedoheptulose 1,7-bisphosphate	0.86239	98.7768	0.341883	10456.97	7.3	c	
Sedoheptulose 1-phosphate	0.34451	97.8632	-0.70055	2004.461	6.81	c	
Shikimic acid	1.05347	91.5976	-0.29943	2.914038	141.27	c	
Sorbitol	-0.59066	98.6602	-0.01158	11849.98	21.09	c	
Sorbitol-6-phosphate	-0.41177	98.6789	0.2228	13968.82	15.76	c	

Succinic acid semialdehyde	4.70521	98.6247	-2.7499	168.6224	8.17	c	
Succinyl-Homoserine	0.91556	93.4072	-0.55163	26.41394	186.24	c	
Taurine	2.91296	92.9563	-0.68442	146268.4	11.73	c	
TDP	0.90225	97.8713	2.040267	15105.28	10.69	p	RTE
Thiamine monophosphate	3.59535	93.8116		0	---	p	ME and no RTE
Threitol	3.86636	94.7888	-0.02158	379.2156	18.71	p	ME
Thymidine 5'-phosphate (TMP)	0.52461	98.6176	-1.3147	2745.75	14.86	c	
Thymidine triphosphate	0.11092	98.0603	-1.65973	7131.264	19.72	c	
Thymine	2.8554	97.8553	-1.3505	0.274342	316.23	c	
UDP-galactose	1.51197	97.3922	-1.19708	10809.63	10.59	c	
UDP-glucoronate	1.46952	90.484	-2.18408	2132.854	28.16	c	
UDP-glucose	0.46568	80.8432	1.308	58.13495	111.76	p	ISS
UDP-N-acetyl-D-mannosamine (unconfirmed)	0.65113	98.574		155072	11.14	p	No RTE
Uracil	4.4755	96.8004	-1.21077	274.6336	7.14	p	ME
Ureidosuccinic acid (N-carbamoyl-L-aspartic acid)	0.05905	98.8997	1.239767	3.770883	118.58	c	
Uric acid	-0.23092	93.6496	-2.46132	3242.213	2.43	c	
Uridine	-0.19989	97.0882	-2.5018	619.5384	7.84	c	
Uridine 5'-diphosphate	0.94666	98.7714	0.78425	1519970	20.63	c	
Uridine 5'-monophosphate	0.9486	93.7311	-2.9542	2019.73	17.43	c	
Uridine triphosphate	0.16894	98.7194	-2.68575	272927.2	16.33	c	
Valeric Acid	-0.50063	98.9177	-2.62018	728.0995	15.47	c	

Vanillin	-1.56729	91.0573		0	---	p	No RTE
Xanthylic acid	-1.12621	94.3195	-1.17818	316.5752	7.03	c	
Xylulose	2.29645	93.5675	0.034883	309.7348	28.11	c	

.

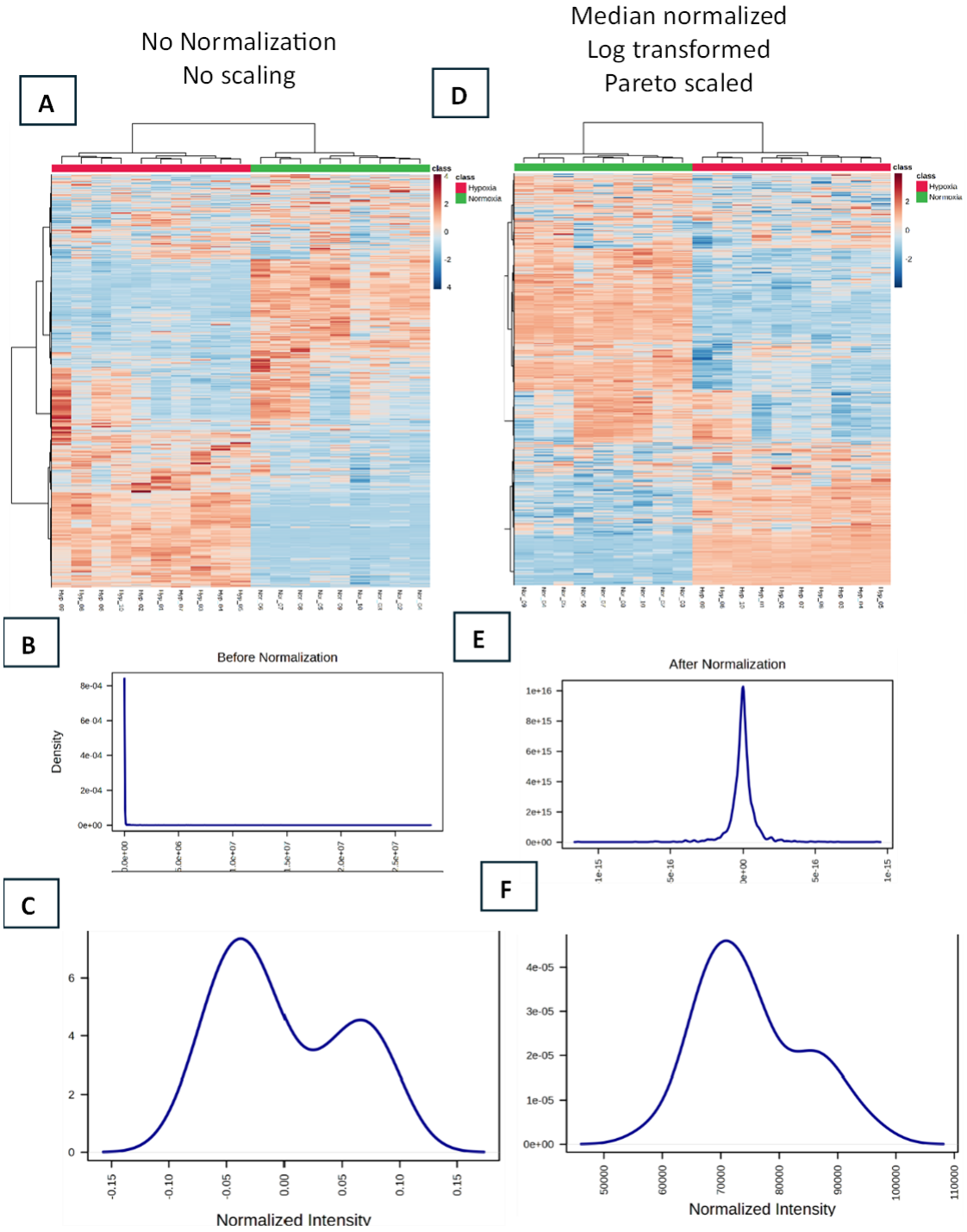
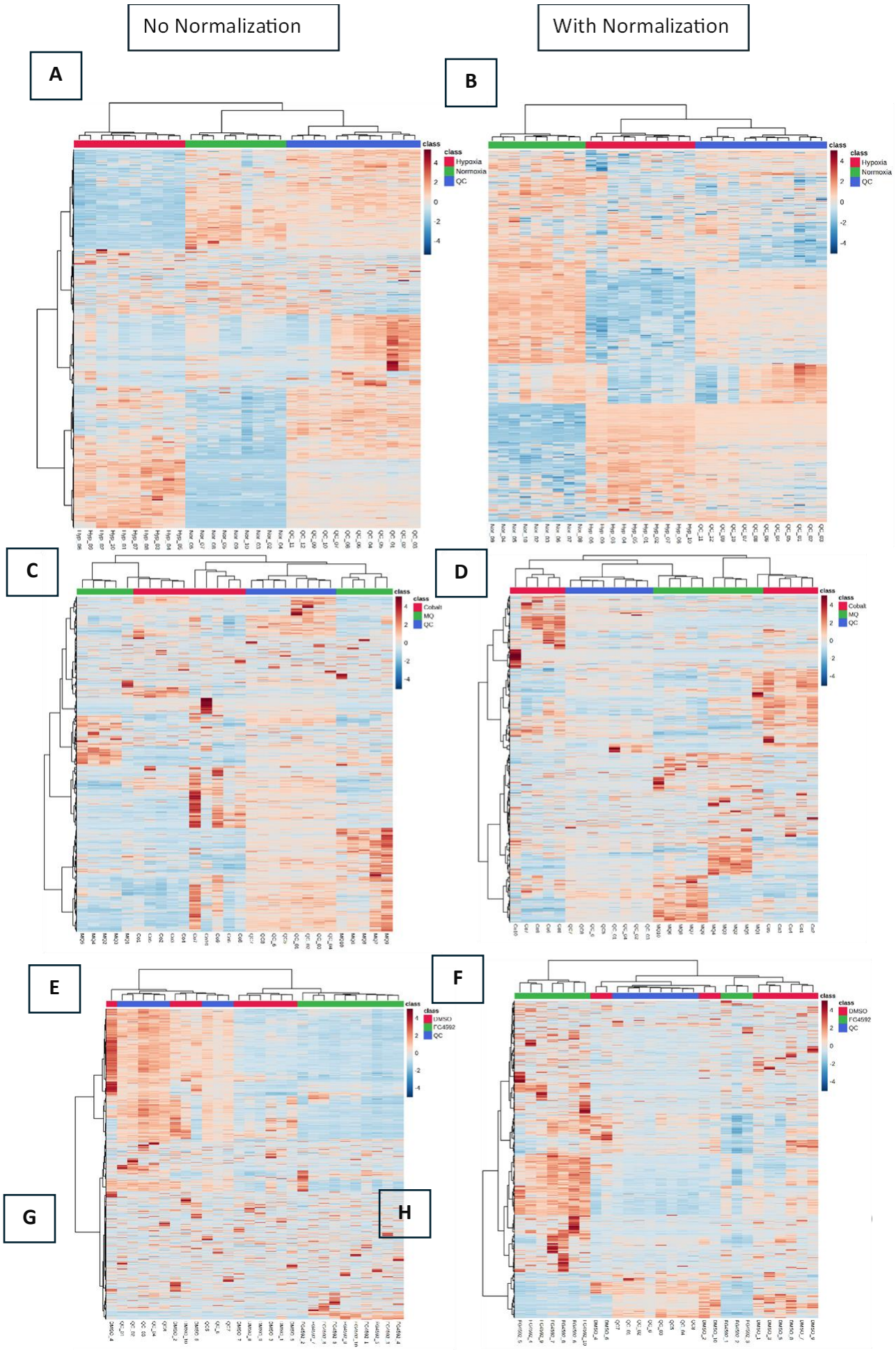


Figure A.7.10: Before and after normalization and heatmap results of IC-MS data from the hypoxia and normoxia metabolomics experiment. (a) Heatmap, (b) feature view and (c) sample view plots of IC-MS data before normalisation and scaling. (d) Heatmap, (e) feature view and (f) sample view plots of IC-MS data after median normalisation, log transformed and pareto-scaling.


No Normalization
With Normalization
A
B
C
D
E
F
G
H
class
Hypoxia
Normoxia
QC
Cobalt
MQ
DMSO
FG4592

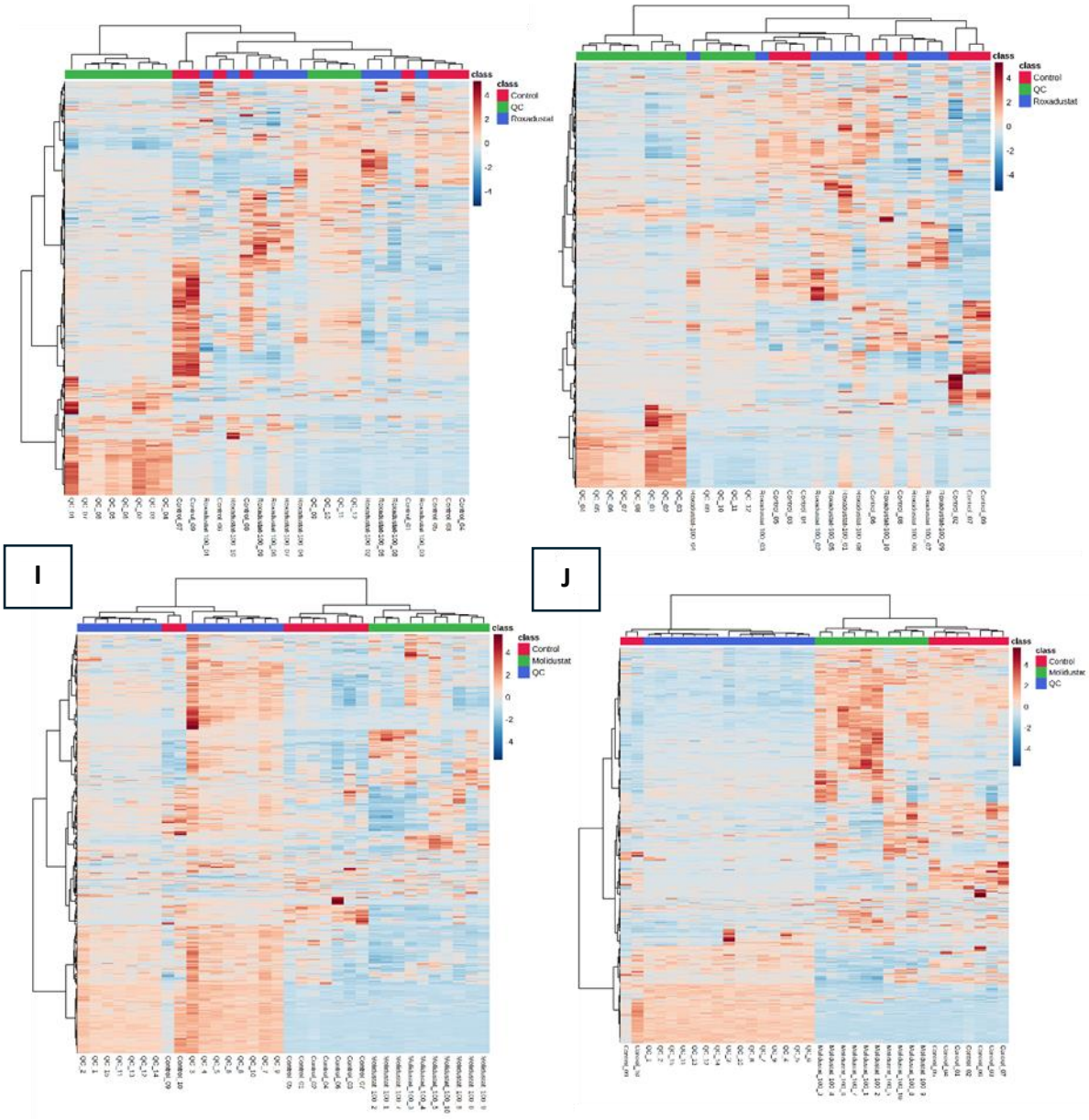


Figure A.7.11: Before and after normalization of heatmap with QC samples. **(A & B)** 1% O_2 ,**(C & D)** $CoCl_2$ (150 µM), **(E & F)** Roxadustat (20 µM), **(G & H)** Roxadustat (100 µM), and **(I &J)** Molidustat (100 µM).

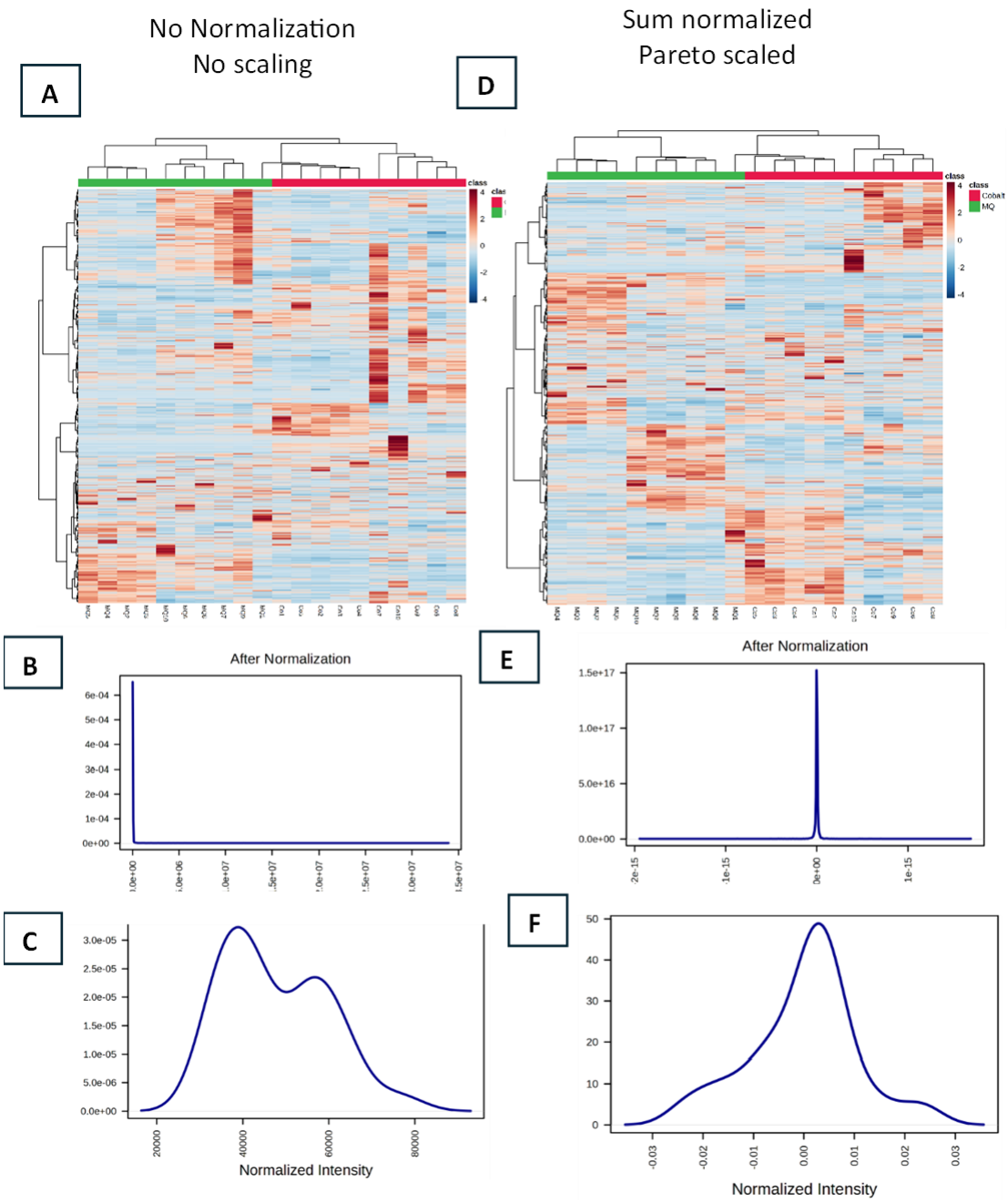


Figure A.7.12: Before and after normalization and heatmap results of IC-MS data from the CoCl2 and control metabolomics experiment**.** (a) Heatmap, (b) feature view and (c) sample view plots of IC-MS data before normalisation and scaling. (d) Heatmap, (e) feature view and (f) sample view plots of IC-MS data after sum normalisation and pareto-scaling.

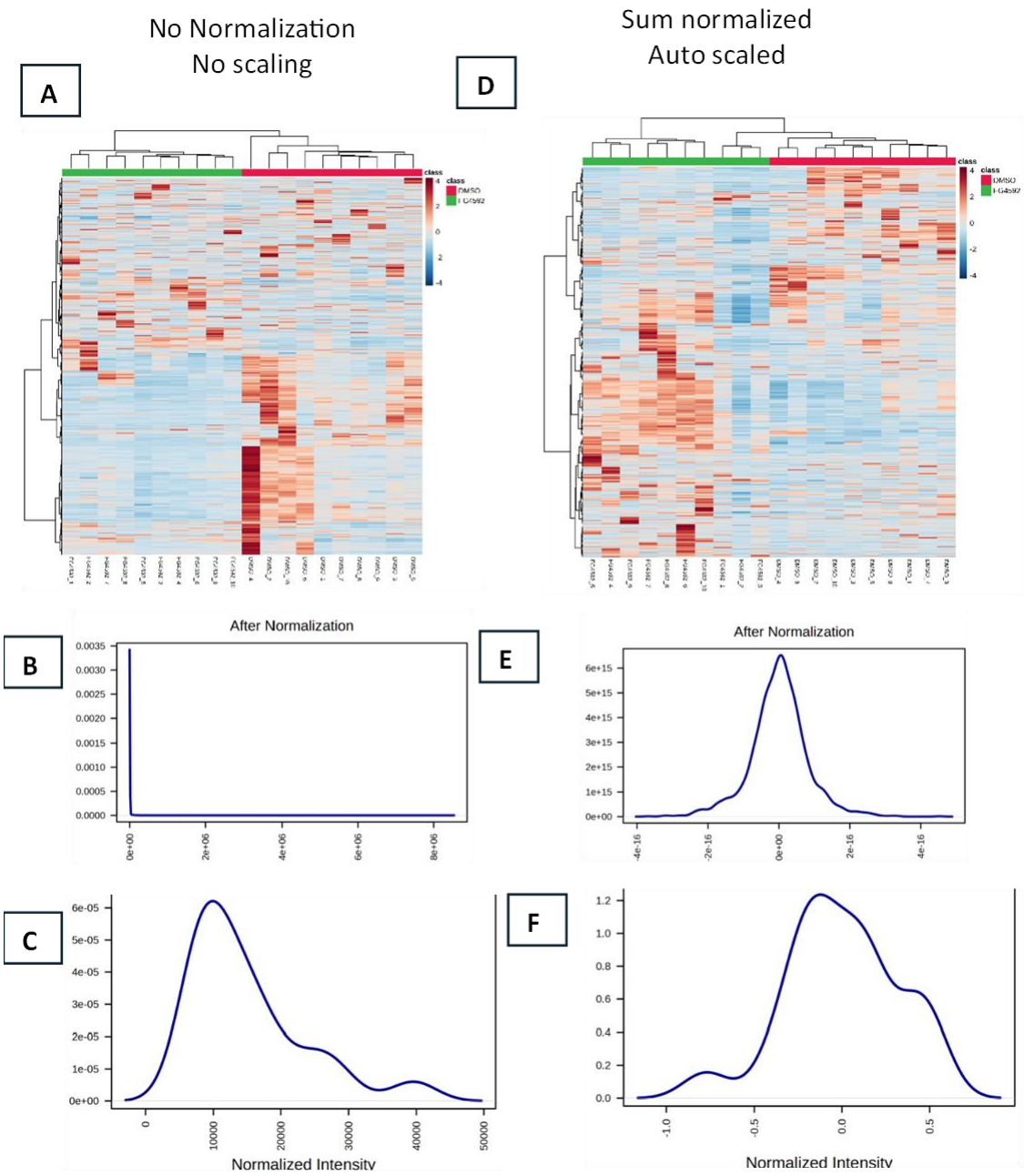


Figure A.7.13: Before and after normalization and heatmap results of IC-MS data from the Roxadustat (20 µM) and control metabolomics experiment. (a) Heatmap, (b) feature view and (c) sample view plots of IC-MS data before normalisation and scaling. (d) Heatmap, (e) feature view and (f) sample view plots of IC-MS data after sum normalisation and auto-scaling.

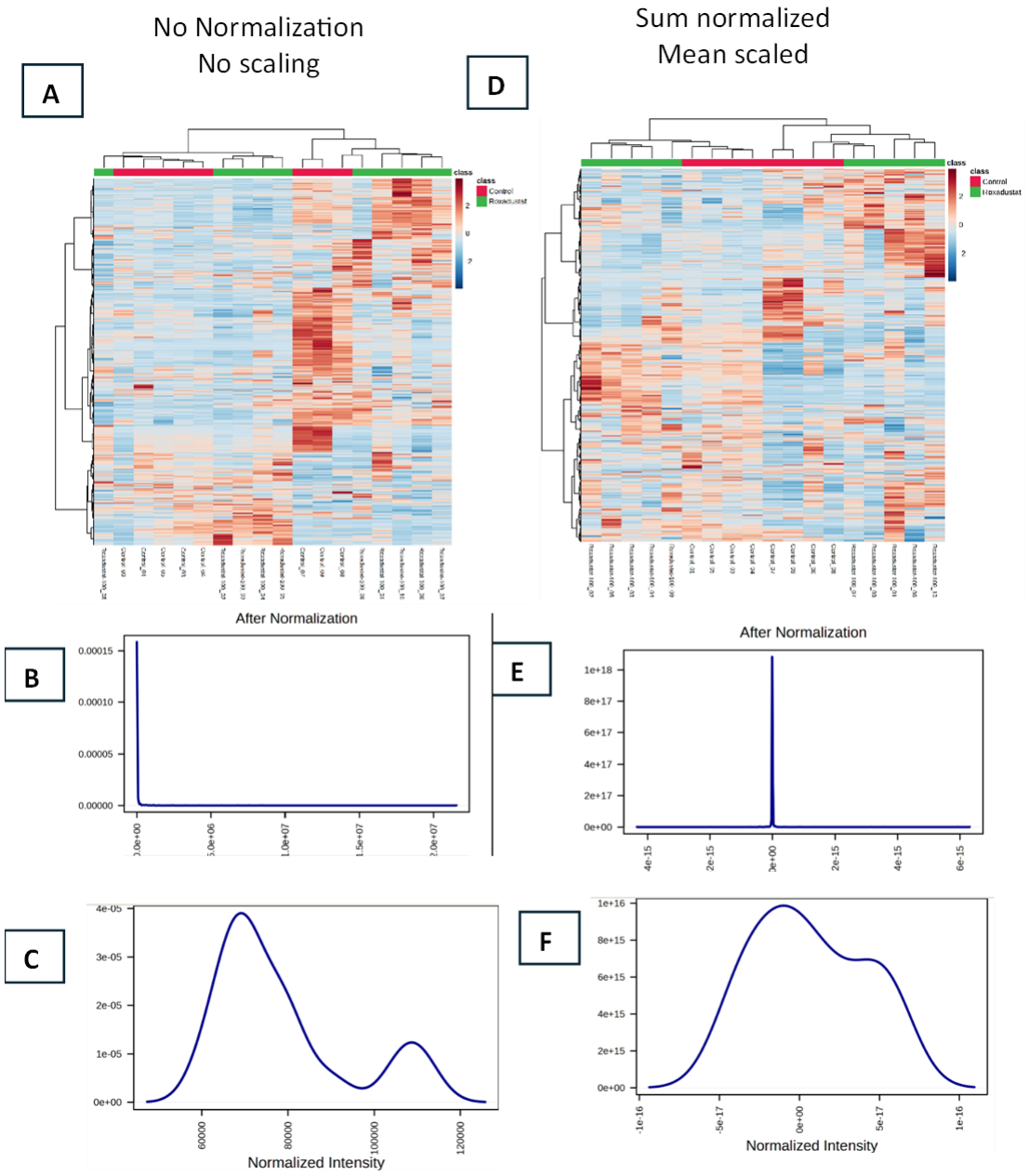


Figure A.7.14: Before and after normalization and heatmap results of IC-MS data from the Roxadustat (100 µM) and control metabolomics experiment. (a) Heatmap, (b) feature view and (c) sample view plots of IC-MS data before normalisation and scaling. (d) Heatmap, (e) feature view and (f) sample view plots of IC-MS data after sum normalisation and mean-scaling.

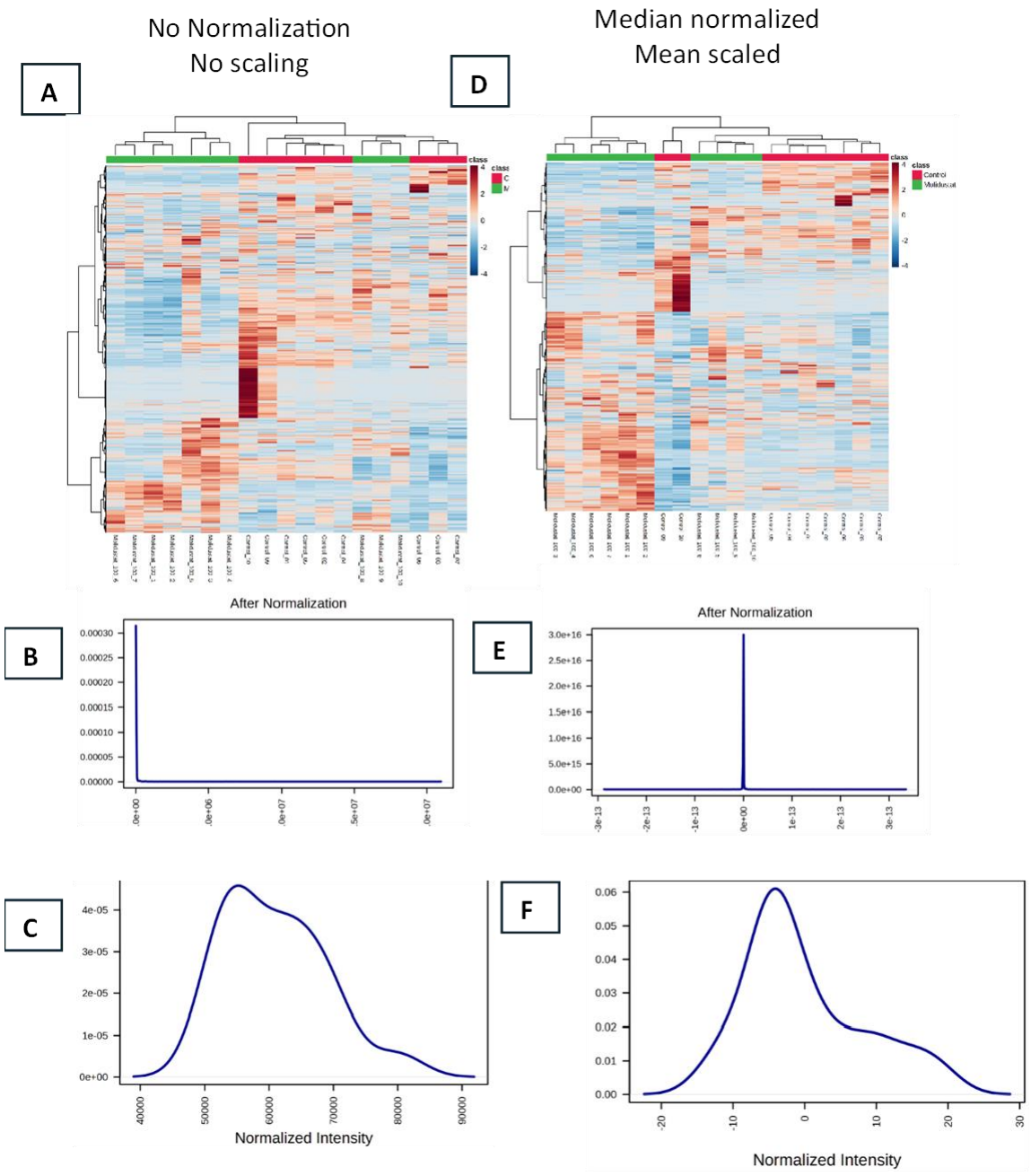


Figure A.7.15: Before and after normalization and heatmap results of IC-MS data from the Molidustat (100 µM) and control metabolomics experiment. (a) Heatmap, (b) feature view and (c) sample view plots of IC-MS data before normalisation and scaling. (d) Heatmap, (e) feature view and (f) sample view plots of IC-MS data after median normalisation and mean-scaling.

Table A.7.3: Identified metabolites from the IC-MS data of hypoxia and normoxia treated HEK293T cells.

Accepted Description	Fragmentation Score	Mass Error (ppm)	Isotope Similarity	Retention Time Error (mins)	Maximum Abundance	Minimum CV%
Ureidosuccinic acid (N-carbamoyl-L-aspartic acid)	0	0.87277	94.589	-0.48012	136882.1	8.63
Inosine	2.75	-4.38171	93.27131	-1.6156	11202.12	8.89
Aspartate	83.3	1.525275	94.76685	-1.89702	635841.1	10.27
Ureidopropionic acid	0	-2.79618	95.75618	-0.5489	2197.662	15.56
Sedoheptulose 1-phosphate	0	1.675067	98.93362	1.220283	115135.2	8.49
NADH	94.8	3.797349	97.75702	-0.83905	326308.3	7.01
Succinic acid semialdehyde	0	1.009448	99.39999	-1.14007	27476.31	8.51
Dihydroorotic acid	0	0.902277	93.15018	1.621383	120.7971	53.64
O-Acetylserine	0	1.439712	93.68969	-0.37532	303165.8	7.64
Acetylglycine	92	1.486522	97.60378	-0.08532	14075.73	6.64
Cytidine triphosphate	6.09	1.365386	98.43664	-1.72787	1883012	7.87
dCTP	92.7	1.623733	96.84581	-1.04432	34203.02	9.08
Citric acid	86.9	1.078367	99.54738	-1.62655	2137719	6.69
N-Acetylneuraminic acid (Sialic acid)	93.5	1.883993	91.62794	-0.50283	158065.3	4.59
2-Phosphoglyceric acid	96.7	1.178558	99.53137	-1.8497	641483.8	9.56
UDP-glucose	0	3.145432	98.4019	-1.5793	378370.4	7.04

5-Hydroxymethyl-2'-deoxyuridine	0	1.472632	87.7272	-0.3337	273.1249	19.48
Xylitol	0	1.428122	95.95925	1.466567	3263.73	24.42
Uridine 5'-monophosphate	45.5	2.135979	98.53757	-1.9102	1889937	8.62
Phosphocreatine	4.79	-1.26462	95.25139	-0.31992	601233.5	12.27
Fumarate	36.2	1.539656	98.99567	-1.53418	64670.37	6.8
2,3-Diphosphoglyceric acid	0	0.971151	99.05267	-1.78362	45231.47	13.18
2-Hydroxybutyric acid	41.3	1.466119	97.42015	-0.61508	17003.6	16.47
Galactose 1-phosphate	0	0.94603	96.98606	-0.31992	363112.5	2.97
dIMP	0	-1.90586	91.58009	-1.3649	3033.256	14.74
N-Acetylglutamate	72.7	-1.88271	91.64238	-0.57935	190372.3	5.16
Methylisocitric acid	0	1.391677	97.27884	-1.08283	17379.84	16.13
Beta-Citryl-L-glutamic acid	0	1.992624	98.57095	-0.76837	1752682	11.69
Glucose 1-phosphate	46.5	0.744529	99.18273	1.09035	300358.2	6.87
UDP-N-acetyl-D-mannosamine (unconfirmed)	0	1.971507	98.73592		5646721	5.85
DL-Threo-beta-Hydroxyaspartic acid	0	4.018011	94.26037	-1.10553	180.6736	32.56
Phenylacetic Acid	0	-2.24651	93.14587	1.367417	2169.123	5.67
cis-Aconitic acid	0	0.66588	96.75453	1.732933	6430.327	11.31
3-Hydroxyisovaleric acid	0	-3.33875	93.99974	-0.67322	1454.489	9.37
Dihydroxyacetone phosphate	0	1.257219	95.39042	-0.43965	788.7099	10.09
Methyl beta-D-glucopyranoside	0	0.738069	95.06942	0.183317	2930.616	7.59
Cytidine monophosphate	45.1	1.927533	93.28162	-1.40012	19406.35	6.54
Dimethyl fumarate	0	1.491392	96.5667	1.57305	731.3319	13.47
Thymidine 5'-phosphate (TMP)	93.7	1.14606	94.27234	-1.23598	43573.13	19.75

Deoxyribose 5-phosphate	2.95	1.89752		-0.74973	14062.7	8.84
Hippuric acid	59.5	0.930771	98.68949	-1.18493	10540.49	22.87
N-Acetyl-aspartate	78.4	0.730005	98.27096	-0.62738	1142406	6.71
IDP	0	2.24828	92.698	0.451517	4354.816	6.04
3-(2,5-Dioxoimidazolidin-4-yl)propanoic acid	0	1.289071	92.65409		417.9038	16.49
8-Hydroxy-deoxyguanosine	0	1.071245	86.99241	0.138633	1257.651	23.87
Threitol	65.1	1.553908	97.64471	0.209467	8019.181	8.96
N-Acetylaspartylglutamic acid	0	1.961661	98.11087	-1.06347	380517.7	10.82
Cytidine monophosphate N-acetylneuraminic acid	0	4.965656	97.88145	-0.65085	235436	9.97
Arabinonic acid	53	0.871797	96.26983	-0.64343	19636	9.47
Cysteic acid	68	0.909027	95.62163	-1.20088	11947.37	12.5
Glycerol	51.2	1.030342	99.73732	0.1992	705429.5	3.28
dTDP-D-glucose	0	3.114144	97.83503	-1.4512	682527	7.81
Oxovaleric Acid	0	-3.21701	95.3317	0.144817	33121.16	7.9
Gluconolactone	0	0.636438	92.36654	-1.84037	1400.747	12.68
N-Acetyl-L-alanine	86.9	1.123162	97.5887	-0.24532	37568.78	17.35
Glucose	0	1.229667	92.34558	1.434133	1858.426	9.28
Phenylacetylglycine/Phenaceturic acid	0	-1.27653	94.00958	0.722233	1078.395	29.36
Galacturonic acid	57.2	1.170406	97.59176	-0.03843	6429.391	8.66
1-Deoxy-D-xylulose 5-phosphate	0	2.719362	93.47887	-1.24992	2194.393	16.5
dUMP	0	0.64486	93.31609	-1.65068	9143.554	14.03
Erythrose 4-phosphate	0	4.533118	94.14265	0.647917	1145.864	28.06
Pantothenic acid	58.9	1.027881	97.77578	-0.54893	325199.8	6.31

Dihydroxyacetone	0	-0.3119	98.94894	-1.54093	42507.48	4.6
Glutaric acid	43.6	1.453123	96.23716	-0.86947	7103.134	9.45
Beta-Alanine	51.3	1.196883	96.08783	-1.6708	3575.283	20.08
Allantoin	0	-2.61255	93.68598	0.36555	336.9177	21.15
Guanosine diphosphate (GDP)	96.4	3.218789	98.06139	-0.25915	6893500	12.87
2-Ketobutyric acid	57.2	1.242037	95.1951	-0.86208	3006.567	7.02
Caffeic acid	0	-1.46667	85.45298		92.08212	19.5
Ribose 5-phosphate	55.2	1.528615	98.36415	-1.17797	74627.98	6.28
Adenosine monophosphate (AMP)	52.2	2.080349	94.81783	-1.09222	48143.26	7.21
Syringic acid	0	2.017721	89.57914	-0.50633	968.3724	10.45
Flavin Mononucleotide	0	1.559097	92.14478		8866.587	6.83
Ribulose 5-phosphate	33.1	2.104674	95.77503	-0.48628	18644.23	9.23
Hydroxy-isobutyric acid	0	0.731857	96.71301	-1.26093	1799.703	7.47
2-Hydroxyglutarate	0	2.33554	97.54878	-0.89947	5926.393	8.82
Ascorbate	0	1.120389	92.97145	-1.28585	1807.88	9.74
N-acetyl-glucosamine-1-phosphate	0	2.056344	89.295	1.522283	786.766	18.37
4-Hydroxyproline	88	1.471355	94.02821	-0.27738	44341.94	8.37
Xanthylic acid	0	-0.19317	93.46079	-1.8134	892.4729	15.44
Glutathione (GSH)	0	1.531385	91.92701	0.810783	2031.517	11.23
3-Methyl-2-oxovaleric acid	0	1.964956	99.17519	-1.19867	173736.8	9.24
Sorbitol-6-phosphate	0	1.321076	97.64766	-0.71365	12345.22	13.71
3-Dehydroquinate	0	1.370689	91.30568	-0.116	2209.699	6.5
2-C-Methylerythritol 4-phosphate	0	0.849331	86.93961	-0.61935	451.7704	22.63

3,4-dihydroxyphenyl acetic acid	0	1.536493	66.11707	-1.41198	866.526	22.52
Fructose 2,6 diphosphate	0	2.134109	98.95828	-0.5961	262558.8	5.49
3-methoxyphenylacetic acid	0	0.752023	94.45977	1.1002	16837.2	22.83
Acetylphosphate	0	-1.6385	96.6595	-0.64797	242.1285	23.33
Ribulose 1,5,diphosphate	0	-0.05916	92.15746	1.473933	1028.462	20.28
Uridine 5'-diphosphate	11.6	1.598485	96.04801	-1.75615	37489.56	11.04
Glycolic acid	48.1	0.583373	97.9766	-0.73903	5086.928	22.29
Glycerol 3-phosphate	0	1.315196		-1.88023	482.2769	10.22
Uridine triphosphate	5.69	1.466423	93.53759	-0.76962	6131.635	14.87
Thymidine triphosphate	5.78	1.547025	98.27151	-1.73518	92287.23	8.36
Glyceric acid	2.97	0.94571		-0.90283	17486.19	13.73
N-Acetyl-L-methionine	81.9	1.34274	96.91648	-0.35622	52243.96	16.76
Raffinose	5.3	0.809959	90.48064	0.504133	6330.377	16.73
Cysteine	0	1.146589	91.09965	-0.63958	94.7349	32.63
Taurine	92.8	1.288925	93.00997	-0.47322	745881.2	3.11
Fructose 1,6-bisphosphate	40.5	2.322332		1.5227	3347.546	10.16
Sedoheptulose 1,7-bisphosphate	0	1.963106	98.76594	0.354917	143408.7	7.18
Hypotaurine	0	1.574993	92.08373	-1.18998	3441.416	10.5
Lactose	67.3	0.653502	96.74033	-0.05053	89566.39	14.63
6-Phosphogluconic acid	0	0.947286	99.02552	-1.62208	129803	11.93
Adonitol (ribitol)	61.6	1.265562	97.94954	0.063317	15234.74	7.22
Adenine	0	1.678859	93.45269	1.3698	6793.331	10.85
Succinyl-Homoserine	0	3.083401	56.7536	-0.33992	583.6776	29.09
Sorbitol	53.6	0.740092	99.0442	0.153317	149972.4	9.15
Glucuronic acid	0	1.130821	92.07082	0.733933	14.85198	116.82
3-Hydroxymethylglutarate	77.2	1.270044	96.51571	-0.87702	9858.266	17.93

4-Hydroxy-3-methoxymandelic acid	0	2.09798	96.77529	-0.65463	1042.414	13.89
4-Hydroxy-2-oxoglutarate	0	1.751015	67.47919		154.6107	37.69
Quinolinic acid	0	1.666472	91.52616	-1.56688	687.1282	36.46
Cytidine diphosphate	0	3.206906	94.1897	-1.12755	19180.08	8.54
Adenosine triphosphate (ATP)	5.22	1.096896	95.7075	0.37105	44536.56	8.97
Acetylcysteine	23.2	1.386	95.9365	-0.86645	22838.75	28.64
Octanoic acid	6.97	1.460796	94.66823	-1.6038	18699.52	14.38
Glutamylcysteine	0	-0.16072	92.12945	-1.58958	10968.55	43.92
Leucic acid	0	-2.27086	96.26514	1.008967	246.2668	35.65
Valeric Acid	0	-4.36793	95.37967	0.350533	1470.881	9
Glyphosate/2-Amino-3-phosphonopropionic acid	0	-2.57732	77.11897	-1.05985	311.9594	37.99
Malondialdehyde	0	-0.503	97.84227	1.374067	3028.259	7.2
Malic acid	55.9	1.560468	99.66805	-0.90593	565968.9	9.29
Galactaric acid (mucic acid)	48.2	1.745612	91.85014	-0.93947	11028.1	36.54
TDP	97.5	2.148006	98.13791	1.964817	326181.6	11.49
dGTP	0	1.594782	85.32064	-0.13188	1597.3	11.34
5-Hydroxyhexanoic acid	0	-1.41658	92.9797	-1.74425	375.6972	17.51
Succinic acid	86.5	1.753089	98.84517	-0.87593	62005.89	9.48
Acetoacetate	0	0.948141	95.05312	-0.97182	404.5025	20.59
4-Hydroxybenzoic acid	0	1.520064	96.23601	0.807583	7459.18	23.57
2-Oxoglutaric acid	0	1.539779		0.707917	382.2235	14.97
Naringenin	0	-3.42822	90.46808		9508.252	7.66
Adipate semialdehyde	0	2.115796	99.38047	-1.38928	136340	9.29
Salicylic acid	0	-2.36955	97.45568	0.791967	38337.14	33.44

Gamma-delta-Dioxovaleric acid	0	1.368396	98.16457	-1.73013	319.7716	12.92
N-Formyl-methionine	0	0.97029	96.31115	-0.5837	8120.316	36.07
Glutaconic acid	0	1.562213	93.82588	0.264283	310.9035	10.22
dUTP	0	1.575531	86.99033	-1.76518	1131.144	10.72
Homovanillic acid	0	1.083039	89.87067	-1.23922	303.4906	14.22
Oxoadipic acid	58.2	1.305594	96.41035	-1.666	6408.659	33.88
Isocitrate	0	0.588884	96.75767	-0.01757	4018.726	37.72
Methylglutaric acid	0	1.164297	92.78851	0.779217	669.5016	17.07
Caproic acid/Hexanoic acid	0	-3.20644	95.7966	0.744467	10165.35	11.67
Gluconate	64	1.006735		-0.50182	210803.6	8.24
O-Phosphoserine	43.7	1.401289	97.30796	-1.15998	3700.386	29.06
Phosphoglycolic acid	57.5	1.765182	98.62187	-1.39235	2549.191	45.34
Ferulic acid	0	1.22063	88.83505	-0.01848	1023.029	10.11
Quinic acid	20.7	1.069362	96.6551	-0.75532	4263.252	16.94
Guanosine monophosphate	0	1.613721	86.3602	1.141967	1132.102	16.22
dGMP	33.9	1.36633	86.56675	1.666317	5335.674	38.16
N-Acetyl-L-phenylalanine	26.2	1.306651	96.8417	-0.50823	4459.265	51.14
Lactoyl-isoleucine	0	-1.33759	98.12205	0.0658	25888	10.74
Fluorouracil	0	2.03224	97.24643	-1.94563	13546.86	48.84
N-Acetyltryptophan	90.9	0.882737	95.74024	-1.89622	11126.9	52.63
N-Acetyl proline	0	-2.20525	94.49371	-0.43532	1833.702	63.8
N-Acetylvaline	93	1.407052	94.18173	-0.32903	7309.768	44.5
Hydroxypyruvic acid	0	1.521575	97.7579	-1.0234	7479.609	11.08
Glucosamine 6-phosphate	0	1.177921	91.47412	1.3927	301.7433	15.87
Butyl ureidosuccinic acid	0	-0.9382		0.594417	950.1028	54.31
Isovalerylglycine	35.6	1.130108	96.57799	-0.43827	2796.952	49.17

Abscisic acid	0	1.778692	91.72172	-1.46688	832.8684	70.9
3,3 Dimethyl glutarate	83.7	1.378856	96.51768	-1.45777	6756.231	38.91
N-Acetyl-L-glutamyl 5-phosphate	0	-3.58389	90.51724		25.32853	109.95
Alpha-aminoisobutyrate	0	1.255769	94.89747	0.015933	77.81754	76.44
Serine	0	0.664162	95.71624	0.130417	52.71437	29.3
2-Isopropylmalic acid	5.88	0.951669	95.73063	-1.0391	6078.379	59.86
Pyroglutamic acid	19.3	-2.6331	93.94457	-0.32182	555532.2	9.58
Phosphoribosyl pyrophosphate (PRPP)	0	1.329967	91.49121	-0.03368	10796.09	36.05
Itaconic acid	0	1.636893	93.82588	0.127533	320.4438	13.71
Nonate	0	-1.73686	97.9863	-0.51347	43883.07	21.79
4-Hydroxybutyric acid	0	1.006733	96.60199	0.4936	892.0876	24.45
Guanosine triphosphate	0	0.904446		-1.46857	3410.513	24.61
Uracil	72.2	1.522584	98.44277	-1.34697	565.1981	12.11
Nicotinic Acid N-Oxide	73.2	1.507918	94.12622	-1.07587	2054.799	60.53
Pyruvic acid	66.4	1.059812	99.53044	-0.78497	109380	10.91
1,2,3-Trihydroxybenzene/Pyrogallol	0	-2.34133	93.0434	0.61235	837.363	5.87
4-Methyl-2-ureido-pentanoic acid/Carbamoyl isoleucine	0	-2.29474	91.30838	-0.67622	759.9012	123.31
Kojic acid	0	1.433919	97.02598	1.8066	569.9274	12.66
Hydroxyoctanoic acid	0	-2.1198	95.78401	0.053033	980.034	10.4
2-Hydroxy-4-phenylbutanoic acid	0	-1.6021	91.70224	0.89345	2911.523	65.68
N-Acetyl ornithine	0	0.977443	94.52792	-1.02518	591.7336	118.33

Table A.7.4: The significantly altered identified metabolites when treated with hypoxia and Normoxia identified by volcano plot.

Identified metabolites	FC	log2(FC)	p.adjusted	-log10(p)
Xylitol	2.3324	1.2218	0.00073	3.1396
Uridine diphosphate-N-acetylglucosamine	0.66348	-0.59187	5.25E-08	7.2802
Uridine 5'-monophosphate	1.5467	0.62916	0.00018	3.7486
Ureidopropionic acid	17.52	4.1309	3.75E-09	8.4263
UDP-glucose	1.6399	0.71365	5.27E-05	4.2786
Thymidine 5'-phosphate (TMP)	0.49729	-1.0078	9.41E-06	5.0264
Taurine	0.58807	-0.76594	0.00332	2.4787
Succinic acid semialdehyde	3.7531	1.9081	1.54E-07	6.8125
Sorbitol-6-phosphate	0.54223	-0.88304	3.69E-05	4.4326
Sorbitol	0.58866	-0.76449	0.00185	2.7328
Sedoheptulose 1-phosphate	3.2191	1.6866	8.88E-12	11.052
Ribulose 5-phosphate	0.55256	-0.85579	4.29E-05	4.367
Ribulose 1,5,diphosphate	0.38795	-1.3661	4.14E-05	4.3828
Quinolinic acid	0.53854	-0.89288	0.00979	2.0093
Phosphocreatine	0.19	-2.3959	2.32E-06	5.6336
Phenylacetylglycine/Phenaceturic acid	0.35359	-1.4999	6.30E-05	4.2009
Phenylacetic Acid	0.56834	-0.81517	7.70E-07	6.1133
Oxovaleric Acid	0.3383	-1.5636	0.00028	3.5535
O-Phosphoserine	0.65906	-0.60152	0.01789	1.7473

O-Acetylserine	0.31961	-1.6456	1.24E-07	6.9072
N-carbamoyl-L-aspartic acid	145.21	7.182	7.46E-15	14.127
NADH	0.06728	-3.8938	3.96E-08	7.4024
N-Acetylneuraminic acid (Sialic acid)	0.62311	-0.68243	1.14E-09	8.9447
N-Acetyl-L-alanine	0.62885	-0.66922	0.00084	3.074
N-Acetylglutamate	1.5115	0.596	0.00089	3.0515
Methylisocitric acid	0.29617	-1.7555	1.15E-06	5.9381
Methyl beta-D-glucopyranoside	15.227	3.9285	1.76E-06	5.7537
Leucic acid	0.35508	-1.4938	2.48E-05	4.6062
isocitrate	0.23787	-2.0717	1.77E-07	6.752
Inosine	0.35405	-1.498	1.12E-07	6.9499
IDP	0.05723	-4.1271	3.56E-06	5.4487
Hypotaurine	0.63716	-0.65027	0.0026	2.5851
Hydroxy-isobutyric acid	0.65296	-0.61494	5.79E-05	4.237
Hippuric acid	0.4452	-1.1675	8.23E-06	5.0848
Guanosine diphosphate (GDP)	0.58046	-0.78472	0.00029	3.5378
Glycerol	1.5822	0.6619	0.00492	2.3076
Glucose 1-phosphate	2.1078	1.0757	3.74E-05	4.4268
Gluconolactone	0.41273	-1.2767	5.91E-05	4.2287
Gluconate	0.6651	-0.58835	0.02074	1.6833
Galactaric acid (mucic acid)	0.64168	-0.64007	0.03336	1.4768
Fructose 1,6-bisphosphate	126.74	6.9857	4.88E-11	10.312
Flavin Mononucleotide	0.56801	-0.816	0.00455	2.3422
dUMP	0.35609	-1.4897	0.00039	3.4102

dTDP-D-glucose	0.62752	-0.67226	3.09E-06	5.5102
DL-Threo-beta-Hydroxyaspartic acid	0.06231	-4.0044	1.04E-05	4.9847
dIMP	1.8798	0.91057	8.86E-05	4.0525
Dihydroxyacetone phosphate	0.3732	-1.422	1.30E-05	4.8871
Dihydroorotic acid	19.767	4.305	6.93E-11	10.159
dGMP	0.52928	-0.91789	0.03148	1.5019
Deoxyribose 5-phosphate	0.5709	-0.80868	7.77E-06	5.1097
dCTP	2.2801	1.1891	2.82E-06	5.5501
Cytidine triphosphate	1.5403	0.62318	2.19E-05	4.6587
Cytidine monophosphate N-acetylneuraminic acid	0.59719	-0.74374	2.47E-07	6.6077
Cytidine monophosphate	0.48879	-1.0327	2.65E-06	5.5773
Cytidine diphosphate	0.47778	-1.0656	0.0057	2.244
Cysteic acid	2.1849	1.1276	0.00131	2.8817
Citric acid	0.23782	-2.0721	1.77E-07	6.7509
Beta-Citryl-L-glutamic acid	0.38379	-1.3816	6.22E-06	5.2061
Beta-Alanine	1.5313	0.61475	0.00801	2.0964
Aspartate	26.72	4.7399	7.29E-13	12.137
Arabinonic acid	0.598	-0.74177	1.38E-06	5.861
Allantoin	0.51111	-0.96829	2.25E-06	5.6482
Acetylphosphate	0.25949	-1.9462	1.77E-07	6.7509
Acetylglycine	0.31973	-1.6451	3.50E-07	6.4554

Table A.7.5: All pathways found by the untargeted pathway analysis during hypoxia vs normoxia experiment on HEK 293T cells. PW = pathway, Fisher's Exact Test, EASE = Expression Analysis Systematic Explorer. Emp = empirical, p = p-value, adj = adjusted, cpd= compound.

Pathway Name	PW total	Hits. total	Hits. sig	Expected	P(Fisher)	P(EASE)	Emp.Hits	Empirical	Adj P.Fisher	cpd. hits
Pentose phosphate pathway	37	37	31	5.6345	1.59E-05	7.30E-05	41	0.41	0.001635	C00121;C00281;C01801;C00442;C01101;C00508;C00020;C02076;C00620;C00259;C00199;C00198;C00231;C00092;C00661;C00117;C00111;C00119;C00118;C00084;C05345;C00279;C00447;C00085;C06222;C00221;C01172;C00309;C01218;C00673;C05382
Glycolysis and Gluconeogenesis	49	39	32	7.4618	2.70E-05	0.000112	0	0	0.002754	C00027;C00149;C00035;C00036;C00900;C05378;C00103;C00668;C00092;C00020;C00236;C00010;C00111;C00031;C00354;C00118;C00197;C00085;C01136;C00665;C05345;C00227;C01231;C00084;C00631;C00221;C01159;C01172;C00267;C00661;C00186;C05993

Ascorbate (Vitamin C) and Aldarate Metabolism	29	20	18	4.4162	0.000185	0.001179	0	0	0.018724	C00027;C00127;C01040;C01041;C00725;C00051;C00601;C02147;CE5985;C05412;C05411;C00072;C04575;C00818;C00425;C01620;C02045
Aspartate and asparagine metabolism	114	54	39	17.36	0.000584	0.001485	0	0	0.058361	C00025;C00027;C00026;C00020;C00148;C03440;C00232;C00010;C00152;C02238;CE1944;C03740;C05572;C02356;C00402;C05938;C05931;C05932;C05936;C00062;C00109;C00986;CE1059;C00989;C01879;C02630;C01157;CE4788;C00127;C01165;C02946;C05947;C00051;C00036;C00037;C00334;C04281;C04282;C00049
Fructose and mannose metabolism	33	29	23	5.0253	0.001048	0.003653	13	0.13	0.103742	C05378;C00577;C00275;C01019;C00665;C00095;C00661;C00159;C00035;C00111;C00031;CE3075;C00085;CE1787;C00354;C05345;C00636;C00267;C02976;C02985;C01094;C03693;CE2847
Histidine metabolism	33	20	17	5.0253	0.001218	0.005547	0	0	0.119335	C00025;C00027;C00026;C00020;C00101;CE7220;C05665;C00439;C00785;C00986;C00099;C00051;C00010;C05828;C05827;CE2065;C00388

Pyrimidine metabolism	70	54	37	10.66	0.003858	0.008363	7	0.07	0.374265	C00106;C01801;C00029;C00364;C00365;C00104;C00020;C00025;C00055;C00906;C00438;C00361;C05145;C00041;C00458;C00705;C00349;C00105;C01346;C00214;C00881;C00119;C00337;C00075;C00131;C00442;C00429;C00526;C00286;C00035;C00672;C00103;C00239;C02642;C00049;C00099;C00460
Phosphatidylinositol phosphate metabolism	59	27	20	8.9847	0.009139	0.024737	0	0	0.877315	C00124;C01225;C04299;C01220;C00055;C01245;C01243;C03546;C00092;C00010;C00116;C05981;C03862;C00137;C04006;C04063;C04062;C01177;C00043;C15658
Butanoate metabolism	34	22	16	5.1776	0.02576	0.065208	0	0	1	C00025;C00026;C00020;C00109;C06144;C03087;C01089;C00232;C06006;C00010;C05984;C00334;C00246;C00164;C00042;C06010

Purine metabolism	80	56	35	12.183	0.038113	0.065343	7	0.07	1	C00366;C00025;C00027;C00362;C00020;C00360;C00361;C00144;C00942;C04677;C00104;C01041;C00121;C00101;C00559;C00131;C01344;C00499;C05512;C00037;C00294;C00035;C01551;C00119;C00130;C06196;C01762;C04734;C00442;C00286;C00672;C00655;C00385;C00049;C00072
Alanine and Aspartate Metabolism	30	21	15	4.5685	0.038738	0.092896	0	0	1	C00025;C00027;C00026;C00020;C00062;C00940;C00099;C00010;C00036;C00037;C00152;C00133;C00402;C00041;C00049
Glycine, serine, alanine and threonine metabolism	88	50	31	13.401	0.057062	0.096359	0	0	1	C00025;C00027;C00026;C00020;C01026;C00010;C00062;CE2026;C00256;C00258;C03508;C00300;C00430;C00084;C01888;C00160;C00168;C00101;C00065;C00109;C01146;C05519;C00188;C00051;C00197;C02305;C00213;C00037;C00133;C00937;C00041
Glycosphingolipid metabolism	67	23	16	10.203	0.046039	0.10307	0	0	1	C00124;C00128;C00029;C00270;C00054;C00055;C00962;C00052;C00010;C00035;C00031;C00065;C00059;C00043;C01582;C00203

Lysine metabolism	52	23	16	7.9187	0.046039	0.10307	5	0.05	1	C00025;C00027;C00026;C00020;C00322;C04092;C04076;C03239;C00450;C00010;C00037;C01181;C00956;C00408;C00449;C00042
Propanoate metabolism	31	18	13	4.7208	0.047883	0.11752	0	0	1	C00020;C00109;C00804;C00036;C02225;C06002;C00010;C05984;C01013;C00164;C04593;C00163;C00207
Beta-Alanine metabolism	20	13	10	3.0457	0.046138	0.13255	0	0	1	C00025;C00010;C00027;C05665;C00334;C00986;C00099;C00026;C01013;C00049
Sialic acid metabolism	107	26	17	16.294	0.083856	0.16134	0	0	1	C05401;C01582;C00221;C04257;C04006;C00065;C00270;C05394;C00116;C00267;C01177;C00124;C00128;C00055;C03546;C00137;C04776
Carbon fixation	10	10	8	1.5228	0.054879	0.17142	66	0.66	1	C00036;C00085;C00111;C00279;C00354;C00118;C00231;C00049
Arginine and Proline Metabolism	45	32	20	6.8527	0.10704	0.18594	5	0.05	1	C00025;C00148;C00026;C00062;C03912;C00036;C02946;C05947;C03564;C00170;C00763;C00010;C00027;C04281;C01157;C01165;C05938;C00042;C00049;C05936

Urea cycle/amino group metabolism	85	34	21	12.944	0.11406	0.19301	4	0.04	1	C00025;C00148;C01586;C00101;C00062;C03912;C02946;C00300;C00213;C00010;C00037;C00334;C05198;C00170;C00026;C01165;C01449;C01250;C00547;C00049;C05936
Glutamate metabolism	15	12	9	2.2842	0.073261	0.19331	1	0.01	1	C00025;C00026;C00127;C00041;C00334;C00042;C03912;C00051;C00232
Aminosugars metabolism	69	31	19	10.507	0.14048	0.23461	0	0	1	C00025;C00104;C00329;C00128;C00275;C04501;C04256;C04257;C00270;C00055;C00010;C00357;C00075;C00085;C01170;C00043;C03557;C03410;C00203
Glycosphingolipid biosynthesis - ganglioseries	62	11	8	9.4415	0.11399	0.27441	6	0.06	1	C00124;C00128;C00035;C01582;C00054;C00055;C00052;C00203
Glutathione Metabolism	19	11	8	2.8934	0.11399	0.27441	0	0	1	C01879;C00027;C00025;C00127;C03740;C00041;C00051;C00037

Galactose metabolism	41	38	22	6.2436	0.20979	0.31228	9	0.09	1	C00104;C00124;C00103;C00029;C05401;C00577;C05394;C00052;C05399;C03785;C00159;C00116;C00111;C00031;C00075;C00795;C02336;C00446;C00221;C00267;C00095;C01097
Fatty acid oxidation, peroxisome	28	4	4	4.2639	0.062913	0.31291	0	0	1	C00027;C00026;C00010;C00042
Ubiquinone Biosynthesis	10	4	4	1.5228	0.062913	0.31291	0	0	1	C00010;C00020;C00156;C00811
Vitamin A (retinol) metabolism	67	17	11	10.203	0.16729	0.31452	0	0	1	C00027;C16681;CE5575;CE5014;C15493;retinal-11-cis;C00020;C00010;CE5589;C00376;CE5757;retinal-cis-9;C02110;C00777
Hexose phosphorylation	20	19	12	3.0457	0.18091	0.32379	15	0.15	1	C00159;C00104;C00329;C00031;C02965;C00275;C00085;C00131;C00095;C05838;C00092;C00738
O-Glycan biosynthesis	16	6	5	2.4365	0.11015	0.34427	0	0	1	C00128;C00043;C00055;C00052;C00203
Phytanic acid peroxisoma	34	6	5	5.1776	0.11015	0.34427	0	0	1	C00027;C00026;C00020;C00010;C00042

l oxidation										
Glycosphingolipid biosynthesis - globoseries	16	8	6	2.4365	0.14562	0.36388	0	0	1	C00035;C00055;C00052;C00128;C00984;C00203
Blood Group Biosynthesis	44	8	6	6.7004	0.14562	0.36388	0	0	1	C00128;C00055;C00035;C00052;C00043;C00203
Glycosphingolipid biosynthesis - neolactoseries	16	8	6	2.4365	0.14562	0.36388	0	0	1	C00035;C00128;C00043;C00055;C00052;C00203
Selenoamino acid metabolism	35	8	6	5.3299	0.14562	0.36388	3	0.03	1	C00020;C00101;C00065;C00109;C00018;C00041
Glyoxylate and Dicarboxylate Metabolism	12	10	7	1.8274	0.17323	0.37763	0	0	1	C00027;C00111;C00631;C00258;C00310;C00160;C00168
N-Glycan biosynthesis	48	16	10	7.3096	0.22927	0.40268	12	0.12	1	C00105;C00128;C00055;C00052;C00159;C00035;C03862;C00029;C00031;C00043

Valine, leucine and isoleucine degradation	65	26	15	9.8984	0.28147	0.42362	46	0.46	1	C00025;C00027;C00026;C00020;C00349;C00141;C00164;C00042;C01188;C06001;C00010;CE5068;C06002;C03284;C02170
Omega-6 fatty acid metabolism	55	3	3	8.3755	0.12583	0.50082	0	0	1	C00027;C00020;C00010
Alkaloid biosynthesis II	10	5	4	1.5228	0.18888	0.50103	0	0	1	C00010;C00027;C00020
CoA Catabolism	7	5	4	1.066	0.18888	0.50103	0	0	1	C00010;C00020;C00864;C01134
Nitrogen metabolism	6	5	4	0.9137	0.18888	0.50103	0	0	1	C00025;C00152;C01353;C00049
Glycosphingolipid biosynthesis - lactoseries	14	7	5	2.132	0.22837	0.5012	0	0	1	C00035;C00128;C00055;C00052;C00203
Keratan sulfate biosynthesis	66	7	5	10.051	0.22837	0.5012	17	0.17	1	C00128;C00055;C00054;C00052;C00043
Squalene and cholesterol biosynthesi	55	11	7	8.3755	0.27691	0.50149	0	0	1	C00027;C01107;C00418;C01143;C00010;C00164;CE5956

s										
Pentose and Glucuronate Interconversions	15	15	9	2.2842	0.30666	0.50174	68	0.68	1	C00105;C00532;C00259;C00379;C00312;C00310;C00199;C00231;C05385;C00309
Vitamin B3 (nicotinate and nicotinamide) metabolism	28	17	10	4.2639	0.31781	0.50185	27	0.27	1	C00025;C00027;C00020;C00062;C01185;C00455;C00119;C00442;C00049;C03246
TCA cycle	31	17	10	4.7208	0.31781	0.50185	25	0.25	1	C00149;C00026;C00104;C00311;C00010;C00036;C00158;C00035;C00042;C00417
Glycerophospholipid metabolism	156	33	18	23.756	0.36901	0.50258	11	0.11	1	C05401;C01225;C01996;C00010;CE0520;C00258;C00670;C00065;C01582;C00577;C00116;C00111;C01177;C03557;C00184;C00513;C00055;C00137
Pyruvate Metabolism	20	18	10	3.0457	0.41189	0.59551	0	0	1	C00010;C00149;C00256;C00424;C00036;C00937;C00186;C05235;C00051;C00111;C00207;C00661
Keratan	68	8	5	10.355	0.3663	0.63853	5	0.05	1	C00124;C00270;C00059;C01019

sulfate degradation										;C00203
Vitamin B1 (thiamin) metabolism	20	8	5	3.0457	0.3663	0.63853	4	0.04	1	C00010;C00020;C00322;C00026;C16255
C5-Branched dibasic acid metabolism	10	6	4	1.5228	0.34633	0.6578	7	0.07	1	C00010;C00035;C00490;C01732
N-Glycan Degradation	16	6	4	2.4365	0.34633	0.6578	7	0.07	1	C00159;C00124;C00270;C01019
Vitamin B5 - CoA biosynthesis from pantothenate	12	11	6	1.8274	0.50448	0.72807	0	0	1	C00010;C00020;C04079;C03492;C00864;C01134
Leukotriene metabolism	92	11	6	14.01	0.50448	0.72807	0	0	1	C00027;C00020;C00010;C00302;C00051;C00037
3-oxo-10R-octadecatrienoate beta-oxidation	27	2	2	4.1116	0.25137	0.75082	0	0	1	C00027;C00010
Glycosylphosphatidylin	6	2	2	0.9137	0.25137	0.75082	0	0	1	C00010;C03862

ositol(GPI)-anchor biosynthesis										
Trihydroxycoprostanoyl-CoA beta-oxidation	9	2	2	1.3705	0.25137	0.75082	0	0	1	C00010;C00027
Vitamin E metabolism	54	7	4	8.2233	0.50361	0.77524	0	0	1	C00027;C00020;C00601;C00010
Heparan sulfate degradation	34	7	4	5.1776	0.50361	0.77524	17	0.17	1	C00124;C00059;C00010;C00181
Chondroitin sulfate degradation	37	5	3	5.6345	0.50309	0.81387	82	0.82	1	C00124;C00059;C00181
Prostaglandin formation from arachidonate	78	17	8	11.878	0.69202	0.83729	0	0	1	C00425;C01041;CE4878;C00051;C00020;C00010;C00072;C00027
Caffeine metabolism	11	8	4	1.6751	0.64093	0.85727	4	0.04	1	C13747;C16365;C16361;C16358;C07480;C16353

Tryptophan metabolism	94	53	24	14.315	0.80885	0.87306	10	0.1	1	C00025;C00027;C00026;C00020;C00010;C05651;C05660;C00643;C02220;CE2122;C00479;C00632;CE3087;CE3086;C00322;C04409;C00051;C00936;C03824;C05636;C05638;C00637;C03227;C00041
Fatty acid oxidation	35	3	2	5.3299	0.50247	0.87582	0	0	1	C00027;C00010
Mono-unsaturated fatty acid beta-oxidation	19	3	2	2.8934	0.50247	0.87582	0	0	1	C00010;C00020
Omega-3 fatty acid metabolism	39	6	3	5.939	0.65986	0.89191	10	0.1	1	C00027;C00020;C00010
Vitamin B6 (pyridoxine) metabolism	11	6	3	1.6751	0.65986	0.89191	5	0.05	1	C00018;C00027;C00314
De novo fatty acid biosynthesis	106	9	4	16.142	0.75042	0.91178	47	0.47	1	C00020;C00010;C03242;C00054
Proteoglycan biosynthesi	27	9	4	4.1116	0.75042	0.91178	67	0.67	1	C00043;C00054;C00052;C00203

s										
Drug metabolism - other enzymes	31	19	8	4.7208	0.82669	0.91942	1	0.01	1	C16622;C16633;C07585;C11173;C07648;C11736;C12739;C07054
Tyrosine metabolism	160	73	32	24.365	0.8944	0.93	7	0.07	1	C00027;C00026;C00020;CE1957;C00025;C00822;C00010;C00425;C03758;C01036;C02505;C00059;C00547;CE6316;C00072;C03765;C00084;C00166;C01061;C05604;C00355;C07086;C09642;C00127;CE5536;C05580;C00054;C00051;C00601;C02763;C00164;C00041
Vitamin B9 (folate) metabolism	33	17	7	5.0253	0.83955	0.93075	0	0	1	C00025;C00065;C00101;C05928;C00037;C00504;C00921
Di-unsaturated fatty acid beta-oxidation	26	4	2	3.9593	0.69038	0.93818	0	0	1	C00020;C00010
Methionine and cysteine metabolism	94	45	19	14.315	0.89377	0.93821	36	0.36	1	C00025;C00027;C00026;C00020;CE1401;C01180;C00010;C00109;C00302;C00491;C00094;C00101;C00065;C00170;C00127;C00054;C00051;C00059;C00037

Fatty Acid Metabolism	63	7	3	9.5938	0.77704	0.93858	0	0	1	C00027;C00116;C00010
Starch and Sucrose Metabolism	33	18	7	5.0253	0.88617	0.95396	28	0.28	1	C00105;C00103;C00029;C00760;C00031;C00221;C00267
Vitamin B2 (riboflavin) metabolism	8	5	2	1.2183	0.81524	0.96926	14	0.14	1	C00020;C00255
Nucleotide Sugar Metabolism	7	5	2	1.066	0.81524	0.96926	46	0.46	1	C00103;C00842
Porphyrin metabolism	43	14	5	6.5482	0.91388	0.97251	78	0.78	1	C00430;C00010;C00037;C00072;C00425
Bile acid biosynthesis	82	15	5	12.487	0.94375	0.98333	0	0	1	C00027;C00037;C00020;C00010;C00163
Androgen and estrogen biosynthesis and metabolism	95	15	5	14.467	0.94375	0.98333	31	0.31	1	C00027;C00468;C00054;C00051;C00059
Arachidonic acid metabolism	95	23	8	14.467	0.95697	0.98398	19	0.19	1	C00025;C00027;C00020;C00010;C00116;C00127;C00051;C00037
Putative	27	6	2	4.1116	0.89293	0.98473	81	0.81	1	C00025;C00051

anti-Inflammatory metabolites formation from EPA										
Fatty acid activation	74	13	4	11.269	0.95613	0.98934	45	0.45	1	C00020;C00010;C00246;C03242
C21-steroid hormone biosynthesis and metabolism	112	21	6	17.056	0.98802	0.99676	0	0	1	C00410;C00468;C00084;C00054;C00059
Linoleate metabolism	46	19	4	7.005	0.99807	0.99968	86	0.86	1	C00127;C01041;C00051;C00072
D4&E4-neuroprostanes formation	37	19	3	5.6345	0.99969	0.99997	5	0.05	1	C01041;C00072;C00425
Xenobiotics metabolism	110	42	9	16.751	0.99998	1	89	0.89	1	C00054;C00051;C06755;C14789;C14854;C14862;C14864;C14865;C14874
Vitamin D3 (cholecalciferol) metabolism	16	7	1	2.4365	0.99254	1	29	0.29	1	C00027
Hyaluronan	8	6	1	1.2183	0.98493	1	95	0.95	1	C00043

Metabolism										
Carnitine shuttle	72	3	1	10.964	0.87664	1	0	0	1	C00010
Parathio degradation	6	2	1	0.9137	0.75192	1	25	0.25	1	C06608
Vitamin H (biotin) metabolism	5	1	1	0.76141	0.50165	1	0	0	1	C00020
Biopterin metabolism	22	13	1	3.3502	0.99989	1	54	0.54	1	C03684
Lipoate metabolism	8	2	1	1.2183	0.75192	1	73	0.73	1	C00725
Drug metabolism - cytochrome P450	53	17	1	8.071	0.99999	1	52	0.52	1	C16601;C16602;C07496
Saturated fatty acids beta-oxidation	36	3	1	5.4822	0.87664	1	0	0	1	C00010
Polyunsaturated fatty acid biosynthesis	21	2	1	3.1979	0.75192	1	0	0	1	C00010

Limonene and pinene degradation	10	2	1	1.5228	0.75192	1	9	0.09	1	C06306;C06078
Benzoate degradation via CoA ligation	4	1	1	0.60913	0.50165	1	0	0	1	C00146
Dimethyl-branched-chain fatty acid mitochondrial beta-oxidation	19	2	1	2.8934	0.75192	1	0	0	1	C00010

Table A.7.6: Identified metabolites from the IC-MS data of 150 µM of $CoCl_2$ vs control treated HEK293T cells.

Accepted Description	Fragmentation Score	Mass Error (ppm)	Isotope Similarity	Retention Time Error (mins)	Maximum Abundance	Minimum CV%
Glutathione (GSH)	44.1	0.503609	95.80599	-0.31447	7319023.5	3.55
dUTP	0	0.255209	92.47343	-1.59797	2660.5022	60.32
N-Acetylglutamate	68.4	-2.95097	98.82265	-0.59633	249755.94	8.83
Guanosine diphosphate (GDP)	0	1.633008	89.22495	-1.62205	2250.9	11.69
Uric acid	79.5	-0.43672	93.09026	-2.45788	10132.469	9.2
2-Ketobutyric acid	73.2	0.163405	98.61244	-0.7991	5507.3867	5.5
Fructose 6-phosphate	33.2	-0.1457	98.59214	-2.99912	167940.46	6.11
Inosine	1.55	-4.76851	94.72171	-0.63865	13682.82	7.73
Fructose 1,6-bisphosphate	32.2	0.075359		1.71555	3272.3938	9.36
Acetylcysteine	0	1.312855	88.93613	2.398733	65.9761	67.19
5-Hydroxymethyl-2'-deoxyuridine	0	1.066339	96.41862	-2.32537	64633.478	7.92
O-Acetylserine	0	0.319662	93.71699	-0.20537	1671129.7	6.29
Cysteic acid	77.3	-0.14913	91.77887	-1.11995	54938.479	9.95
N-Acetylneuraminate 9-phosphate	0	4.131351	91.88287	-2.67242	9269.3934	9.49
Ophthalmic Acid	0	3.977033	86.42486	-2.85755	187.69443	19.2
dUMP	0	0.007347	94.46277	-1.56068	8916.7105	17.87
Glycerol 3-phosphate	72.1	0.003654		-0.73075	163724.1	4.18
Pyruvic acid	22.8	0.211411	92.25465	-0.83028	8467.7497	21.23
Uridine	0	0.722289	88.93613	0.835817	182.64586	27.23
Methionine sulfoxide	46.7	0.0154	99.64196	-0.8168	178226.96	4.9
Lactoyl-isoleucine	25.3	-0.26183	91.78448	-2.43213	2586.1067	7.97
Deoxyribose 5-phosphate	0	2.075643	87.66374		1212.9226	9.4
4-Hydroxyproline	0	0.303062	88.91573		14717.522	26.4
Lanthionine ketimine	97	1.771018	97.98275	0.000333	5604744.7	11.06
Dihydroxyacetone phosphate	0	-2.50654	89.47604	-1.71402	117.92668	42.52
Threitol	6.06	0.555581		-0.70932	15590.574	8.87
Xanthylic acid	0	0.496179	93.73547	2.715817	18462.064	3.81
Caffeic acid	0	-2.72084	87.80273	-1.936	478.12328	11.36

Glutamine	0	0.314311	78.69618	2.0878	491.06462	13.93
N-Acetylaspartylglutamic acid	0	0.135996	98.72554	0.225167	825.95008	5.37
Succinic acid	0	-0.79454	92.69862	-1.60715	2420.7632	14.5
3-(2,5-Dioxoimidazolidin-4-yl)propanoic acid	0	-2.41899	89.8911		337.02849	36.99
Glutaric acid	0	0.296278	97.35672	1.2193	1582.6152	4.37
3,3 Dimethyl glutarate	0	0.449557	98.70949	-1.02192	512739.74	9.4
2-Phosphoglyceric acid	91.2	0.542348	99.51015	-0.82717	59511.699	8.65
2-Oxoglutaric acid	0	4.745213	92.14161		240.44073	24.64
Malic acid	65.5	0.136544	97.75179	-0.85208	4435.9906	5.58
Succinic acid semialdehyde	0	0.320716	91.78403	-2.62388	183.07353	33.54
Aspartate	97.3	-0.28563	99.75713	-1.73102	1749364.5	13.23
Glyceric acid	37.5	0.240857		-1.2397	166972.81	10.75
Xylulose	0	0.51393	91.39008	-0.77763	2788.5251	10.87
Raffinose	65.8	0.651007	98.74588	-2.90157	6944.8398	14.43
Oxoadipic acid	0	-0.08892	99.26631	-1.08355	25273.649	11.86
NADH	78.2	0.324542	94.73054	-0.70995	195121.28	1.99
Fructose 2,6 diphosphate	3.24	-0.09225		-0.99515	160738.25	4.82
2-Hydroxyglutarate	97.4	1.722255	93.33794	-2.83062	77659.822	7.77
Deoxyuridine	9.27	-0.50546	96.04167	0.35695	5538.0171	10.31
Guanosine monophosphate	0	0.180546	92.14161		68.233846	20.05
4-Acetylbutyrate	4.75	0.578285	91.25162	0.4527	3191.9479	10.23
Cinnamoylglycine	77.7	-0.13414	96.11702	-1.54475	2084.4984	37.51
2-Hydroxybutyric acid	94.4	0.706569	96.7529	-0.69392	60456.56	32.81
N-Acetyl-L-methionine	0	0.035589	99.06824	-0.1093	264889.71	10.69
Taurine	69	0.539238	96.80611	-2.66157	2575.0668	16.03
Uridine 5'-diphosphate	0	-3.14962	93.31162	1.060467	313.71562	35.04
2,3-Diphosphoglyceric acid	36	0.435674	93.10726	2.509383	40355.314	12.2
3-Dehydroquinate	0	-3.66332	93.09751	1.245517	1529.8456	5.54
1-Methyl-1H-indole-3-carboxamide	0	2.982902	90.82344	2.950367	735.69517	7.47
Glycolic acid	0	0.270806	97.33048	1.455867	1916.7637	6.87
Guanosine	36.4	0.518777	95.89845	-2.12557	16933.887	24.47
Hippuric acid	85.2	0.14834	93.66253	-0.44602	35835.879	5.05

6-phosphonoglucono-lactone	92.4	-0.10584	92.96352	-0.60578	736877.56	3.58
Dihydroxyacetone	11.2	-0.17629	94.87044	-1.54238	42080.229	9.2
Phenylacetylglycine/Phenaceturic acid	0	0.261732	99.36508	-1.67463	58320.756	12.84
Salicylic acid	0	-0.33295	95.39042	-0.38597	843.25032	11.28
UDP-glucoronate	13.4	0.020667	94.16701	-0.10708	1887.0768	7.88
Dimethyl fumarate	0	-2.69685	88.86555	1.3883	236.0161	14.88
Inositol 1,3,4-trisphosphate	27.6	-0.37863	99.00237	-2.23483	22516.285	4.77
Galactaric acid (mucic acid)	0	4.684006	86.99241	-1.23392	157.3521	59.46
Homovanillic acid	62.1	-0.18298	98.8885	-1.00327	5491.5948	7.32
Sedoheptulose 1,7-bisphosphate	0	-1.50175	93.95746	-0.71597	2102.205	9.08
Pantothenic acid	0	0.339078	96.74799	-2.90157	1790.717	16.41
Adenosine diphosphate	54.2	0.226492	99.93633	-0.3401	6296187.7	3.7
Thymidine 5'-phosphate (TMP)	0	-2.96316	96.13126	-1.34817	1416.3862	33.66
3-methoxyphenylacetic acid	0	-3.68781	95.66212	1.71545	11495.941	23.85
Adenosine triphosphate (ATP)	0	0.707558	88.95261	0.8908	1201.0554	14.62
Citric acid	0	0.279035	94.15971	-2.00238	49805.813	11.34
Ribulose 5-phosphate	0	0.582531	95.90396	-1.1975	313.16037	45.59
Phosphoenolpyruvic acid	0	1.039565	93.73171	-1.12062	9474.9361	10.81
Kojic acid	0	0.445343	91.85014	-2.80188	1645.3282	16.46
Sorbose	1.8	0.223527	97.80699	-2.42838	16271.561	8.28
Hydroxypyruvic acid	0	0.161511	99.53049	1.302183	571075.72	12.66
Glutamic acid	0	-0.04234	98.17305	-1.24742	31841.554	9.93
Arabitol	58.8	-0.0537	97.93025	-0.54455	591195.44	7.3
Phosphocreatine	14.4	0.948419	98.06624	2.6093	42549318	7.13
3-Hydroxytyrosol	93.5	-0.10636	96.16518	-1.16792	52431.407	14.58
Phosphoglycolic acid	0	0.051262	94.40597	1.267583	1351.4778	49.36
Naringenin	4.93	-0.02679	98.08936	-2.1307	14667772	4.82
Beta-Citryl-L-glutamic acid	0	-0.65241	98.25314	-0.4496	17486.184	12.8
Protocatechuic acid	0	-0.15113	83.36701	-1.89318	44.895297	19.67
Pyridoxal 5'-phosphate	44.2	0.605627	93.95771	-1.20127	421478.04	7.68

Hydroorotic acid	21.8	-0.24061	99.69819	-1.5822	201738.82	10.32
Inosine monophosphate	0	0.754637	92.83081	1.7314	50.929729	48.07
Acetylglycine	28.3	-0.06487	97.1028	1.3399	78084.78	6.5
Glyceraldehyde 3-phosphate	0	0.480988	97.85026	-0.91028	1133.69	8
N-Acetyl-L-alanine	0	0.555886	95.99693	0.081567	365.22428	11.5
N-Acetylneuraminic acid (Sialic acid)	91.2	0.239244	93.74078	-0.9904	1424647.5	3.9
Galacturonic acid	78.2	-0.35292	99.1296	-1.07597	444450.35	5.89
EDTA	65.3	-0.00708	96.62484	0.21145	2849.8847	4.13
TDP	0	-2.13304	93.55075	1.3762	455.68569	13.08
2-Isopropylmalic acid	0	0.305208	91.03655	-0.97838	428.07348	9.48
Lactose	53.3	0.281411	96.4316	0.0578	2937.8329	16.75
Oxalic acid	0	-4.00884	89.51116		15022.688	10.98
O-Phosphoserine	0	0.402771	98.76773	-0.65975	2221667.4	11.23
Thymidine triphosphate	14.9	0.464875	96.58391	-2.4241	2978.0773	15.02
Sorbitol	74.4	-0.06295	97.18746	-2.05158	13909.391	7.38
Xylulose 5-phosphate	0	-0.98343	92.64078	-1.09008	4871.8036	15.58
Sedoheptulose 1-phosphate	0	-2.55129	88.86555	-0.17338	460.73884	10.53
Propionyl-glycine	0	0.39307	72.33964		572.71475	6
Ribulose 1,5,diphosphate	29.4	-0.11268	96.75644	0.09145	768.33543	7.43
Cytidine triphosphate	54	0.346398	96.27624	-2.28158	15942.339	7.61
Uracil	96.2	0.231814	97.75867	-0.07305	16660.307	8.25
Inosine triphosphate	31.3	-0.02985	98.28786	2.613767	43341.697	13.07
Theobromine	74.4	-0.39667	98.34021	-0.23305	28652.119	8.47
Arabinonic acid	0	0.264644	92.38808	2.950583	397.88363	13.88
Orotidine	69.8	-0.21399	97.70459	-0.01305	4720.0532	4.28
IDP	0	0.531697	68.81676	-0.81208	33.114349	141.39
2-Methylcitric acid	73.2	0.342701	69.06932	-1.32927	1126.2682	19.43
Isovalerylglycine	0	0.137503	93.67183	-0.36305	339445.71	6.08
Uridine 5'-monophosphate	97.7	0.293864	98.11438	2.195167	162414.7	11.24
Flavin Mononucleotide (unconfirmed)	0	-2.27427	97.40024	0.119633	5318.4003	10.7
Uridine triphosphate	0	-1.19246	91.57676	-1.69327	72.538668	25.64
dCTP	0	0.538975	93.67914	2.54325	487148.97	3.08
Gluconate	58.7	-1.5955	94.23294	-0.11855	7760.1103	5.35

dGTP	0	0.394075	94.93096	1.52485	8532.7473	7.49
Methylglutaric acid	51.1	0.450957	99.10653	-1.36615	12067.313	4.63
Glucose	0	0.570429	87.41376	-0.08963	879.1875	12.05
Caproic acid/Hexanoic acid	0	-0.00668	98.72404	0.529917	29960.301	14.91
Adenosine monophosphate (AMP)	61	0.3103	97.41615	-1.0604	3576.3341	18.16
3-Hydroxyisovaleric acid	0	1.051187	98.6517	-0.88208	6967.551	6.73
6-Phosphogluconic acid	5.67	0.461404	98.35557	-1.50483	93165.353	10.87
N-Acetyl-aspartate	64	-0.06809	98.8779	0.15145	49958.673	3.11
Isocitrate	33.4	0.111572	92.91584	1.110417	17098.184	14.32
N-Formyl-methionine	0	0.501095	98.12758	-0.62957	24643.28	7.55
dTDP-D-glucose	0	0.604001	95.70634	1.38245	236.21658	54.67
Cytidine monophosphate	0	-0.86735	95.17065	-0.60387	1985.9773	18.21
Hydroxyoctanoic acid	6	0.55841	98.47018	-1.6252	1661413.2	16.23
Uridine diphosphate-N-acetylglucosamine	38.8	0.490569	96.66311	-1.13942	484.42294	4.66
Malonic acid	4.12	-0.54789	97.0657	-2.83625	3415.7459	64.8
3,4-dihydroxyphenyl acetic acid	0	-4.17824	70.67463	2.452333	130.74427	23.43
Sebacic acid	68.9	-0.49242	95.31472	-0.66515	19324.051	8.61
Phosphoribosyl pyrophosphate (PRPP)	0	2.497952	95.89887	-2.24122	10560.302	7.03
Coenzyme A	0	0.942303	96.30136	2.105517	337.69249	56.31
Adenylsuccinate	20.2	-0.17228	92.32194	0.65125	3524.9516	13.34
Sorbitol-6-phosphate	0	-2.80291	97.26119	-1.30838	17667.803	6.06
3-Hydroxymethylglutarate	32.3	-0.30404	94.75198	0.3599	657.50852	7.31
UDP-galactose	0	-1.23688	98.62813	-1.66032	10417.525	3.63
Glutaconic acid	45.4	0.264125	95.18747	-2.86283	38507.911	5.76
Octanoic acid	0	-0.11152	89.79353		2218.343	18.61
Saccharic acid	6.02	0.402302	98.7852	-2.59062	2385125	9.68
Erythrose 4-phosphate	0	-1.08807	99.02859	1.027967	49036.731	10.82
N-Oxalylglycine	90	0.641257	97.76701	-2.87157	4984.2244	12.69
Deoxyadenosine triphosphate	0	-2.69953	94.31417	0.787917	505.43277	9.27
Ferulic acid	87.6	0.03921	96.57094	-0.88367	19034.107	8.53
Succinyl-Homoserine	56.7	-0.15962	95.16805	2.75285	712.71673	15.33

Allantoin	46.4	-0.21334		-1.66483	3425.1314	12.55
N-Acetyl proline	51.4	-0.34152	98.71216	-0.02393	19270.825	5.14
Cytidine monophosphate N-acetylneuraminic acid	0	0.976919	89.60904	0.531517	2334.6302	15.47
Nonate	91.2	0.240462	93.75118	2.362083	6182124	3.18
cis-Aconitic acid	0	0.49529	92.78851	-2.32002	657.40362	18.49
Orotic acid	18	-0.05918	99.08454	-0.59168	181660.94	3.43
Maleic acid	0	-0.70396	92.72076	2.517617	21830.529	17.61
dADP	0	-4.55148	93.93548	0.906117	1388.9341	9.3
Hydroxy-isobutyric acid	0	-2.45222	88.86555	-2.71383	259.76965	11.71
Nicotinic Acid N-Oxide	52.2	-0.16625	94.08191	-1.01455	27523.4	3.27
8-Oxo-dGTP	0	0.252543	59.43393	-0.13597	715.64319	16.87
5-Hydroxyhexanoic acid	3.13	-0.01359		-2.22483	31409.347	8.61
dGMP	0	1.29966	93.58875	1.573817	302.01193	18.68
Cytidine diphosphate	0	0.649959	87.91683	-0.84243	141.55562	18.42
Ascorbate	0	-4.09449	98.03378	0.40705	2726.1082	6.43
N-acetyl-glucosamine-1-phosphate	0	0.495608	91.38002	-0.6438	4544.1051	16.6
Glucuronic acid	25.8	0.173412	93.63256	1.60235	3991.0553	4.2
Hydroxyisoheptanoic acid	0	-0.41032	92.25436	2.00385	1263.9892	6.86
Oxovaleric Acid	0	-0.00112	91.57676	-1.24995	26.155648	83.93
1,2,3-Trihydroxybenzene/Pyrogallol	10.8	0.334509	98.85642	0.879383	10084971	9.74
Glycerol	0	0.284019	93.33504	2.9264	5965.9106	7.03
3-Methyl-2-oxovaleric acid	43	-0.04671	95.27779	-0.52405	13550.028	13.04
Cytidine	0	-0.44713	96.09165	2.41155	6961.3307	17.45
Malondialdehyde	0	-0.37816	94.33811	-0.54992	1008.4651	7.07

Table A.7.7: The significantly altered identified metabolites when treated with 150µM of $CoCl_2$ and control identified by volcano plot.

Identified metabolites	FC	log2(FC)	p.adjusted	-log10(p)
Uric acid	0.25206	-1.9882	0.008852	2.053
Taurine	0.62414	-0.68007	0.046133	1.336
Salicylic acid	2.3505	1.233	0.008049	2.0942
Pyruvic acid	2.4946	1.3188	0.006461	2.1897
Protocatechuic acid	1.7417	0.80053	0.018333	1.7368
Phenylacetylglycine/Phenaceturic acid	2.8225	1.497	0.013505	1.8695
O-Acetylserine	0.40529	-1.303	0.001963	2.707
N-Acetylneuraminate 9-phosphate	2.1131	1.0793	0.028237	1.5492
N-Acetylglutamate	1.8809	0.91144	0.003543	2.4506
N-Acetylaspartylglutamic acid	0.52115	-0.94022	0.016585	1.7803
Methionine sulfoxide	2.799	1.4849	0.005208	2.2833
Inosine	2.0658	1.0467	0.000353	3.4516
Glycerol 3-phosphate	2.7348	1.4514	0.012062	1.9186
Glutathione (GSH)	1.8806	0.91118	8.84E-05	4.0537
Glutamine	0.55589	-0.84713	0.035511	1.4496
Galactaric acid (mucic acid)	1.5766	0.65684	0.005208	2.2833
dUTP	0.030908	-5.0159	0.003068	2.5131
dUMP	2.6604	1.4116	0.011092	1.955
Deoxyribose 5-phosphate	1.5986	0.67678	0.006349	2.1973
Aspartate	0.37132	-1.4293	0.011199	1.9508
Acetylcysteine	2.864	1.518	0.004454	2.3513
4-Acetylbutyrate	1.6625	0.73339	0.016669	1.7781
2-Ketobutyric acid	2.593	1.3746	0.003485	2.4578

Table A.7.8: All pathways found by the untargeted pathway analysis during 150µM of $CoCl_2$ vs control experiment on HEK 293T cells. PW = pathway, Fisher's Exact Test, EASE = Expression Analysis Systematic Explorer. Emp = empirical, p = p-value, adj = adjusted, cpd= compound.

Pathway Name	**PW total**	**Hits. total**	**Hits. sig**	**Expected**	**P(Fisher)**	**P(EASE)**	**Emp.Hits**	**Empirical**	**Adj P.Fisher**	**cpd. hits**
Aspartate and asparagine metabolism	114	54	28	9.041	2.47E-05	7.53E-05	0	0	0.00215	C00025;C00026;C00020; C03440;C00232;C00016; C0129 ;C02238;C03740;C00097; C052 ;C00402;C05938;C05932; C059; C00109;C00669;C00989; C01879
Butanoate metabolism	34	24	15	2.6964	0.00015	0.00065	0	0	0.01244	C00025;C00026;C00020; C00022;C05125;C01089; C00232;C05984;C00016; C00246;C00164

										C00073;C00430;C01888; C00109; C00579;C02218;C00051; C00213; C00133;C00041
Histidine metabolism	33	20	12	2.6171	0.0012	0.00479	0	0	0.10157	C00025;C00026;C00020; C03680; C00664;C05828;C02835; C00222
Arginine and Proline Metabolism	45	33	16	3.5688	0.00388	0.01041	0	0	0.31418	C00025;C00026;C00022; C03912;C00016;C00147; C04281;C01157;C01165; C05938;C00049;C05936
Lysine metabolism	52	22	12	4.124	0.00365	0.01207	0	0	0.29928	C00025; C00026; C00020; C04092; C00450; C00956; C00408; C00449
Propanoate metabolism	31	17	10	2.4585	0.00388	0.01475	0	0	0.31418	C00020;C00109; C00804;C00036; C00222; C00164
Glutamate	15	12	8	1.1896	0.00341	0.01664	0	0	0.283	C00025;C00026;C00041;

metabolism										C00022;
Alanine and Aspartate Metabolism	30	23	12	2.3792	0.00589	0.01793	0	0	0.46536	C00025;C00026;C00020; C00022; C00133;C00402;C00041; C00049
Pyruvate Metabolism	20	18	10	1.5861	0.00676	0.02296	0	0	0.527	C02912;C00149;C00256; C00022; C00546;C02917
Valine, leucine and isoleucine degradation	65	24	12	5.1549	0.0091	0.02567	0	0	0.69983	C00025;C00026;C00020; C00349; C01188;C06001;C06002; C05119
Glutathione Metabolism	19	11	7	1.5068	0.00909	0.03932	0	0	0.69983	C01879;C00025;C03740; C00041;
Beta-Alanine metabolism	20	12	7	1.5861	0.01704	0.06201	0	0	1	C00025;C05665;C00099; C00026;

Purine metabolism	80	58	21	6.3446	0.04967	0.0845	0	0	1	C00366;C00025;C00362; C00147;C05512;C00294; C03090; C00700;C04376;C00081; C00286; C00672;C00655;C00385; C00022; C00049;C00072
Vitamin B3 (nicotinate and nicotinamide) metabolism	28	16	8	2.2206	0.0326	0.09116	0	0	1	C00025;C00020;C00455; C05841;
Ascorbate (Vitamin C) and Aldarate Metabolism	29	21	9	2.2999	0.06743	0.14888	0	0	1	C01040;C00051;C00191; C02147; C02045
Pyrimidine metabolism	70	55	19	5.5515	0.09326	0.14972	0	0	1	C01801;C00022;C00364; C00365; C00349;C01346;C00178; C00881; C00475;C00081;C00286; C00672; C00049;C00099;C00460

Urea cycle/amino group metabolism	85	33	12	6.7411	0.12014	0.2103	0	0	1	C00025;C03912;C02946; C00624; C01165;C01250;C00049; C05936
Vitamin B9 (folate) metabolism	33	16	7	2.6171	0.09294	0.21166	0	0	1	C00025;C04376;C01045; C00664;
Xenobiotics metabolism	110	43	14	8.7238	0.20123	0.3052	0	0	1	C00051;C00053;C00870; C14856; C14802;C14803;C14800; C14806; C14804;C14805
Vitamin B5 - CoA biosynthesis from pantothenate	12	12	5	0.95168	0.1772	0.37814	0	0	1	C00020;C04079;C01134; C00831;

Methionine and cysteine metabolism	94	49	15	7.4548	0.27183	0.383	0	0	1	C00025;C00026;C00020; C00022; C00097;C05823;C00073; C02218; C00506;C00051;C02712
Nitrogen metabolism	6	5	3	0.47584	0.11356	0.38564	0	0	1	C00025;C01353;C00049
Porphyrin metabolism	43	16	6	3.4102	0.21473	0.40119	0	0	1	C05520;C00430;C00191; C00016;
Vitamin B1 (thiamin) metabolism	20	9	4	1.5861	0.18356	0.4239	0	0	1	C00020;C05125;C00022; C00026
C5-Branched dibasic acid metabolism	10	6	3	0.79307	0.18465	0.48704	0	0	1	C00022;C00490;C01732
CoA Catabolism	7	6	3	0.55515	0.18465	0.48704	0	0	1	C00020;C00831;C01134

Tryptophan metabolism	94	54	15	7.4548	0.43164	0.55104	0	0	1	C00025;C00026;C00020; C05645; C05637;C00108;C02470; C01717; C00051;C05639;C00041
Heparan sulfate degradation	34	7	3	2.6964	0.26373	0.57729	12	0.12	1	C00140;C06472;C00191; C00181
Vitamin B2 (riboflavin) metabolism	8	3	2	0.63446	0.16714	0.59316	0	0	1	C00020;C00016
Mono-unsaturated fatty acid beta-oxidation	19	3	2	1.5068	0.16714	0.59316	0	0	1	C00016;C00020

Pentose phosphate pathway	37	36	10	2.9344	0.46592	0.61367	0	0	1	C00121;C00281;C01801; C00508; C12214;C06222;C00309; C00673; C05382
Arachidonic acid metabolism	95	12	4	7.5342	0.38158	0.63728	0	0	1	C00025;C00020;C00016; C00051
Prostaglandin formation from arachidonate	78	12	4	6.1859	0.38158	0.63728	0	0	1	CE0737;C00051;C00020; C00072
Di-unsaturated fatty acid beta-oxidation	26	4	2	2.062	0.2782	0.69877	0	0	1	C00020;C00016
Alkaloid biosynthesis II	10	4	2	0.79307	0.2782	0.69877	0	0	1	C00020;C00180

Vitamin H (biotin) metabolism	5	4	2	0.39653	0.2782	0.69877	0	0	1	C00020;C05921
Selenoamino acid metabolism	35	9	3	2.7757	0.42697	0.7215	0	0	1	C00020;C00109;C00041
TCA cycle	31	19	5	2.4585	0.57523	0.76694	0	0	1	C00149;C00026;C00016; C00579;
Carbon fixation	10	10	3	0.79307	0.50425	0.77663	47	0.47	1	C00036;C00022;C00049
Putative anti-Inflammatory metabolites formation from EPA	27	5	2	2.1413	0.38795	0.77705	2	0.02	1	C00025;C00051

Squalene and cholesterol biosynthesis	55	11	3	4.3619	0.5758	0.82199	0	0	1	C01107;C00016;C00164
Hyaluronan Metabolism	8	6	2	0.63446	0.4896	0.83505	1	0.01	1	C00140;C00191
Chondroitin sulfate degradation	37	6	2	2.9344	0.4896	0.83505	32	0.32	1	C06472;C00191;C00181
Ubiquinone Biosynthesis	10	6	2	0.79307	0.4896	0.83505	2	0.02	1	C00020;C00156
Tyrosine metabolism	160	72	16	12.689	0.81441	0.87807	0	0	1	C00026;C00020;C00025; C00022; C01036;C00097;C00072; C00082; C01061;C00355;C02218; C00051; C00053;C00164;C00041; CE2174

Leukotriene metabolism	92	13	3	7.2962	0.69804	0.88875	0	0	1	C00020;C00302;C00051
Fatty acid activation	74	13	3	5.8687	0.69804	0.88875	2	0.02	1	C00020;C00016;C00246
Phytanic acid peroxisomal oxidation	34	8	2	2.6964	0.65799	0.90982	7	0.07	1	C00026;C00020
Aminosugars metabolism	69	34	7	5.4722	0.82286	0.91062	0	0	1	C00025;C00022;C00140; C00645; C00352;C00081;C06241
Glycolysis and Gluconeogenesis	49	39	8	3.886	0.83702	0.91472	2	0.02	1	C00149;C00036;C05125; C00022; C00579;C00020;C00186; C05993

Sialic acid metabolism	107	25	5	8.4858	0.82055	0.92197	0	0	1	C06241;C00140;C00645; C05394; C05396
Vitamin A (retinol) metabolism	67	9	2	5.3136	0.724	0.93336	1	0.01	1	C00020;CE5653
Proteoglycan biosynthesis	27	9	2	2.1413	0.724	0.93336	2	0.02	1	C00053;C00190
Glycerophospholipid metabolism	156	36	7	12.372	0.86763	0.93663	2	0.02	1	C00222;C00307;CE0520; C00258; C00577;C00570;C00184; C00513
Glyoxylate and Dicarboxylate Metabolism	12	11	2	0.95168	0.82407	0.96365	39	0.39	1	C00258;C00310
De novo fatty acid biosynthesis	106	12	2	8.4065	0.86078	0.97317	7	0.07	1	C00020;C05921

Linoleate metabolism	46	15	2	3.6481	0.93287	0.98923	6	0.06	1	C00051;C00072
Androgen and estrogen biosynthesis and metabolism	95	15	2	7.5342	0.93287	0.98923	0	0	1	C00051;C00053
Pentose and Glucuronate Interconversions	15	15	2	1.1896	0.93287	0.98923	35	0.35	1	C00259;C00312;C00618; C00310;
Galactose metabolism	41	39	5	3.2516	0.98746	0.99638	5	0.05	1	C05396;C00140;C00577; C05394;
Hexose phosphorylation	20	20	2	1.5861	0.9814	0.99767	4	0.04	1	C00081;C00352
Bile acid biosynthesis	82	21	2	6.5032	0.98572	0.99829	0	0	1	C00020;C00016
Fructose and mannose metabolism	33	31	3	2.6171	0.99446	0.99904	18	0.18	1	C14830;C00577;C01222; CE2847

Glycosphingolipid metabolism	67	26	2	5.3136	0.99631	0.99963	5	0.05	1	C00016;C00053
Phosphatidylinositol phosphate metabolism	59	33	2	4.6791	0.99948	0.99996	31	0.31	1	C00191;C15658
Glycosphingolipid biosynthesis - ganglioseries	62	12	1	4.917	0.97364	1	37	0.37	1	C00053
R Group Synthesis	7	2	1	0.55515	0.45235	1	0	0	1	C00016
Keratan sulfate degradation	68	7	1	5.3929	0.87927	1	20	0.2	1	C00140
Parathio degradation	6	3	1	0.47584	0.59496	1	0	0	1	C00870

Biopterin metabolism	22	11	1	1.7448	0.96424	1	3	0.03	1	C00082
Vitamin E metabolism	54	5	1	4.2826	0.77869	1	15	0.15	1	C00020
Lipoate metabolism	8	2	1	0.63446	0.45235	1	2	0.02	1	C00579
Fatty acid oxidation	35	4	1	2.7757	0.70054	1	0	0	1	C00016
Saturated fatty acids beta-oxidation	36	5	1	2.855	0.77869	1	0	0	1	C00016
Omega-3 fatty acid metabolism	39	5	1	3.093	0.77869	1	1	0.01	1	C00020

D4&E4-neuroprostanes formation	37	26	1	2.9344	0.99965	1	0	0	1	C00072
Fatty acid oxidation, peroxisome	28	5	1	2.2206	0.77869	1	15	0.15	1	C00026
Keratan sulfate biosynthesis	66	7	1	5.2343	0.87927	1	16	0.16	1	C00053
Dimethyl-branched-chain fatty acid mitochondrial beta-oxidation	19	2	1	1.5068	0.45235	1	0	0	1	C00016
Vitamin B6 (pyridoxine) metabolism	11	7	1	0.87238	0.87927	1	0	0	1	C00534

N-Glycan Degradation	16	5	1	1.2689	0.77869	1	34	0.34	1	C00140
Nucleotide Sugar Metabolism	7	5	1	0.55515	0.77869	1	14	0.14	1	C00190
Drug metabolism - other enzymes	31	16	1	2.4585	0.99225	1	0	0	1	C16630
C21-steroid hormone biosynthesis and metabolism	112	17	1	8.8824	0.9943	1	6	0.06	1	C00053
Starch and Sucrose Metabolism	33	18	1	2.6171	0.99581	1	24	0.24	1	C00760
Omega-6 fatty acid metabolism	55	4	1	4.3619	0.70054	1	10	0.1	1	C00020

Table A.7.9: Identified metabolites from the IC-MS data of 20 µM of Roxadustat versus control treated HEK293T cells

Accepted Description	Fragmentation Score	Mass Error (ppm)	Isotope Similarity	Retention Time Error (mins)	Maximum Abundance	Minimum CV%
4-Acetylbutyrate	0	-0.9398	89.15434	-1.41512	530.7264	14.56
Acetylglycine	91.5	3.754776	97.9045	-0.20052	2041.567	4.02
N-Acetylneuraminic acid (Sialic acid)	47.3	0.815764	97.58273	-0.61348	19369.31	21.49
Glucuronic acid	85.2	-0.38214	99.49678	-0.9542	884.5414	13.08
Leucic acid	0	-1.42408	99.63192	0.006167	2712.805	13.11
N-Acetyl-aspartate	96.6	-0.83874	92.51934	-0.77862	202613.3	21.98
4-Hydroxyproline	25.9	-0.40616	92.07082	1.480783	270.0385	8.76
2-Isopropylmalic acid	88.4	2.512757	98.82442	-0.42862	8756.939	20.3
N-Acetylaspartylglutamic acid	8.5	-0.86964	99.50066	0.1716	16.11378	201.53
Homovanillic acid	0	0.86281	98.43527	-1.16132	36919.43	9.4
2-Methylcitric acid	20.3	-0.55474	98.16282	-2.51083	1154.745	8.79
Phosphoenolpyruvic acid	0	-2.8114	99.30011	-1.09617	1584.574	21.24
Beta-Citryl-L-glutamic acid	6.85	-0.30945	99.7409	-1.63733	34691.9	10.38
Indole-3-lactic acid	0	1.009129	98.52873	-0.7143	171980.3	11.84
Dimethyl fumarate	92.9	-0.38028	98.28578	-2.33942	0.066324	316.23

Phosphoglycolic acid	0	2.660891	97.88808	1.833833	24.87315	30.31
3-deoxy-2-keto-6-phosphogluconic acid	82.3	1.360562	99.82941	-1.42542	286.5335	14.42
2-Phosphoglyceric acid	88.8	2.192349	99.0938	-1.41307	21.88496	32.2
Glyphosate/2-Amino-3-phosphonopropionic acid	97.2	-0.51226	99.7287	-1.89818	316626.9	22.55
N-Acetylglutamate	0	-3.2699	95.79687	-1.1385	5.484982	128.81
Phosphocreatine	76.3	-3.25303	91.35485	-0.68788	25945.3	27.12
3-Dehydroquinate	4.24	-2.80317	95.24093	-0.5018	341836.9	10.28
Malitol	0	-1.44994	99.34549	-0.67918	12492.2	5.43
Threitol	73.4	-0.65625	98.79026	-0.77858	467.3055	10.1
Gluconolactone	47.5	0.73249	85.36738	-0.41745	21.69541	89.76
Sorbitol	0	3.866362	94.78875	-0.02158	379.2156	18.71
Lactose	0	0.123427	97.41455	-1.95158	78.81413	24.39
Dihydroxyacetone	76.2	-0.59066	98.66023	-0.01158	11849.98	21.09
Glycerol	14.8	-0.61694	92.74556	-0.28158	929.6098	21.98
3-Hydroxyisovaleric acid	0	-1.32613	98.94716	-1.90617	12543.19	9.1
Glyceric acid	54.5	3.641203	99.6027	-0.02617	152960	7.45
N-Acetyl-D-glucosamine	0	-0.59597	93.99974	-2.50617	8.637036	102.35
Glucose	0	2.348657		-2.2937	7756.049	18.65
N-Acetyl proline	30.8	-0.45776	96.65555	-0.0837	0	---
N-Acetyl-L-alanine	0	0.373832	96.41126	-0.01927	1837.578	16.41
5-Hydroxymethyl-2'-deoxyuridine	50.3	-3.36849	99.361	-0.63917	49.22408	110
Adonitol (ribitol)	27.7	2.047476	94.59077	-0.36052	4128.364	14.43
Fructose	0	0.84034	92.36654	-0.67367	4.29719	178.3
5-Hydroxyhexanoic acid	0	0.407384	96.20254	-2.44367	10484.1	10.17

Taurine	0	2.434506	95.66563	1.266283	2195.233	12
Isovalerylglycine	3.48	4.363447		-1.01348	59411.47	6.14
Shikimic acid	43.1	2.964905	99.95088	-0.43323	2179843	7.06
Methyl beta-D-glucopyranoside	59.5	-0.69568	97.97614	1.246767	39931.24	7.97
Lactoyl-isoleucine	0	-0.45687	95.9146	-0.71143	36.17675	46.94
Allantoin	0	-0.41868	92.9797	-2.37442	133.3467	18.06
N-Acetylvaline	94	2.912964	92.95628	-0.68442	146268.4	11.73
N-Formyl-methionine	73.6	0.366914	91.9551	-1.61442	777.8365	72.09
N-Acetyl-L-phenylalanine	0	3.788602	94.69858	0.567267	5.719336	70.37
Caproic acid/Hexanoic acid	0	1.053471	91.59758	-0.29943	2.914038	141.27
3-(2,5-Dioxoimidazolidin-4-yl)propanoic acid	0	-0.78152	91.26372	2.090567	46.7688	23.46
Uridine	0	0.349035	63.56749	1.8611	42.04912	33.48
Hydroxy-isobutyric acid	0	-2.82248	97.70566	-1.92343	432.2097	212.24
Butyric acid	0	-3.22481	94.2561	-0.75398	1593.246	6.13
Valeric Acid	32	0.214176	91.86685	0.746783	156.4377	49.91
Uracil	0	-0.66414	97.27491	0.328817	223.0712	7
Glucose 1-phosphate	0	4.534829	98.09192	1.993017	252.9477	5.9
Alpha-aminobutyrate	0	-0.76126	94.53579	-0.66698	580.8068	39.14
Butyl ureidosuccinic acid	0	0.163748	98.34885	-2.64043	0	---
Deoxyribose 5-phosphate	0	-0.64162	78.10382	-2.0418	0	---
Naringenin	0	0.811634	92.14161		11.19902	22.43
Adenosine 2',3'-cyclic phosphate	27.6	-0.19989	97.0882	-2.5018	619.5384	7.84
Sorbitol-6-phosphate	0	1.896751	98.3816	2.276133	1585.335	4.44
3-Hydroxymethylglutarate	0	-1.7492	96.05507	0.510817	0	---
3,3 Dimethyl glutarate	0	-0.50063	98.91765	-2.62018	728.0995	15.47

Succinic acid semialdehyde	0	-3.16647	95.22819	0.009817	381.9524	12.5
2-Hydroxyglutarate	0	-0.53437	93.99974	1.7824	18.42544	40.52
Sedoheptulose 1-phosphate	0	-0.00877	95.69605	1.880067	38.07187	13.83
Oxovaleric Acid	3.66	4.475499	96.80045	-1.21077	274.6336	7.14
Kojic acid	0	-0.04923	96.87084	-1.95077	25826.08	7.88
Acetylcysteine	0	1.697729	94.89747	-2.17218	0	---
Thiamine monophosphate	52.5	-0.80963	94.56058	2.829517	0	---
Dihydroxyacetone phosphate	0	-2.28107		-1.9562	0	---
6-phosphonoglucono-lactone	46.1	-0.3123	99.30479	-0.90772	34250.52	16.75
Cysteic acid	1.58	1.123171		-2.20163	489.3393	32.93
Erythrose 4-phosphate	0	-4.77447	90.09865		1250.473	14.22
Glutaconic acid	0	2.445004	92.88432	-0.05417	0	---
Ascorbate	0	-0.41177	98.67887	0.2228	13968.82	15.76
Galactaric acid (mucic acid)	0	-0.2879		-1.51797	0.657052	282.84
N-acetyl-glucosamine-1-phosphate	24.9	-0.05539	95.66084	0.754567	0	---
N-Oxalylglycine	7.96	0.619919	98.30176	-1.00922	1516.381	13.61
Adenosine monophosphate (AMP)	98.3	0.190136	99.59487	-1.55893	303.1772	43.84
Aspartate	0	4.705206	98.62468	-2.7499	168.6224	8.17
4-Hydroxybutyric acid	0	3.204433	99.24622	-0.95605	886.8338	16.55
Fumarate	0	0.344511	97.86318	-0.70055	2004.461	6.81
Ureidosuccinic acid (N-carbamoyl-L-aspartic acid)	4.83	0.356096		-0.849	1281.639	8.59
Quinolinic acid	0	-0.34209	98.49934	2.743033	0	---
Abscisic acid	7.45	2.323792	98.2111	1.493033	43.7024	33.55

Glutamine	0	1.574475	98.68101	0.285083	1.004799	138.67
DL-Threo-beta-Hydroxyaspartic acid	31.5	0.566629	89.10812	-0.95492	359.2845	35.76
Glycerol 3-phosphate	0	3.595346	93.81158		0	---
Fructose 6-phosphate	0	-0.01539	95.39042	-0.38507	173.5445	12.11
2-Oxoglutaric acid	0	-0.33379	91.61985	-0.71507	487.6731	11.63
2-Hydroxy-4-phenylbutanoic acid	77.8	-0.02236	91.79301	-1.28725	5415.756	10.27
Hippuric acid	0	-2.54996	86.11474	1.159483	10.83762	31.34
Jasmonic acid	0	-0.73562	94.14265	-1.91052	11.42163	121.62
Dihydroorotic acid	0	3.677267	99.21715	-1.59285	31.45797	22.57
Oxalic acid	0	1.466584	98.85035	0.33715	56.71363	35.43
O-Phosphoserine	5.26	-1.10597	94.52571	-1.26285	143.1648	11.54
4-Hydroxy-2-oxoglutarate	0	-1.03334	97.85484	2.616217	176.2953	15.15
Orotidine	7.8	-0.68434	95.3363	-1.12378	543.7527	52.72
Orotic acid	55	-0.30106	91.85014	0.256217	0	---
Cytidine diphosphate	0	0.815717	95.94596	-0.46378	2596.546	11.49
Thymidine 5'-phosphate (TMP)	29.8	1.801189	94.28182	-1.29928	453.6936	29.79
dTDP-D-glucose	0	-0.90241	92.25436	1.404083	15.03502	37.47
Glutathione (GSH)	0	0.017059	90.38279	0.694083	58.76385	26.15
4-Hydroxybenzoic acid	0	-0.14821	86.56675	-2.40592	0	---
Citric acid	0	-4.0786	63.41722	1.973217	0	---
Dimethylallyl pyrophosphate	83.4	2.691847	94.68892	-0.06065	36158.44	4.23
Ribulose 1,5,diphosphate	0	1.807939	98.66138	1.1545	129.2254	23.37
UDP-galactose	0	3.022525	99.43912	0.9011	204.8464	27.87
cis-Aconitic acid	21.6	3.869087	99.80024	-1.72643	11031.42	12.08
Fructose 2,6 diphosphate	0	-2.72169		1.293567	0	---

Sedoheptulose 1,7-bisphosphate	0	0.059049	98.89974	1.239767	3.770883	118.58
8-Hydroxy-deoxyguanosine	0	-0.05394	99.32151	-1.64023	115.0746	23.64
dCTP	0	0.31849	98.94977	1.359767	4178.133	7.57
Glutamylcysteine	17.8	2.441726	96.72864	-1.45523	63.24838	21.84
Cytidine triphosphate	0	1.322779	88.93613	0.729867	7.770332	45.08
Xanthylic acid	0	-3.71434	94.19898	2.550417	10.53874	196.14
Adenosine diphosphate	0	-2.27341	97.32286	1.058683	0	---
dGMP	0	1.538912	97.29809	1.838683	52.88392	32.19
Uridine 5'-monophosphate	0	2.729722	97.01113	1.0072	283.0636	9.7
2,3-Diphosphoglyceric acid	0	0.388309	86.56675	-1.1628	0	---
Phosphoribosyl pyrophosphate (PRPP)	0	-0.36203	94.26037	2.330767	0	---
4-hydroxyphenyl glycine/Oxfenicine	0	-0.05327		2.970767	0	---
Adenylsuccinate	37	0.59421	96.38597	-1.07923	1077.208	9.31
Uridine 5'-diphosphate	25.7	-0.37426	98.61423	1.066467	96.72432	21.22
Fructose 1,6-bisphosphate	0	4.787122	99.25971	0.3521	222.1903	22.47
Deoxyadenosine triphosphate	74.8	1.919361		0.19595	65.93946	21.33
UDP-glucoronate	0	-3.82733	94.78836	-1.34405	0	---
Flavin Mononucleotide (unconfirmed)	0	1.645016	98.46762	2.478683	0.958453	235.25
8-Oxo-dGTP	49	-0.756	89.7564	1.608683	0	---
1,2,3-Trihydroxybenzene/Pyrogallol	15.3	0.058781	93.36991	1.018683	696.6945	25.97
Protocatechuic acid	0	0.385242	95.4956	2.564983	0	---
Inositol 1,3,4-trisphosphate	0	2.635561	96.14421	0.2615	11.7814	81.83

dUTP	0	1.79122	78.97723	1.88665	26.9174	13.88
Inosine monophosphate	88.8	3.136885	99.8055	0.22065	902.9373	12.26
Guanosine diphosphate (GDP)	92.1	-0.12972	95.28511	-1.23935	1612.506	12.53
Adenosine triphosphate (ATP)	0	0.224737	93.39519		0	---
6-hydroxy-2,5,7,8-tetramethylchromane-2-carboxylic acid (Trolox)	0	2.39351	94.98576	-2.31127	964.9273	12.11
Phenylpyruvic acid	0	-2.92271	98.2093	-1.83795	0	---
5-Methoxyindoleacetate	0	-0.0009	84.09186	0.61205	0.961749	218.37
Salicylic acid	53.8	1.210439	93.17141	-2.23883	3535.533	11.6
2,5-Dihydroxybenzoic acid	0	-3.91891	99.24131	0.051817	4.908364	160.04
Hydroxy-indole acetic acid	0	0.405163	92.19625	1.335467	0	---
IDP	0	2.137448	95.20802	-1.16453	2423.472	19.23
Indoleacetic acid	0	3.733693	99.7098	2.580917	4920.117	15.36
1-Methyl indole	90.4	0.524609	98.61756	-1.3147	2745.75	14.86
Kynurenic acid	0	1.987499	95.84783	-1.41705	10900.64	15.3
Uridine triphosphate	0	0.403355	76.28898	0.671183	80.95089	27.61
Guanosine monophosphate	0	1.993066	98.48097	-2.82733	364.7273	38.97
5-Hydroxyindoleacetic acid	0	-1.16023	99.40695	-0.58733	1685.685	20.62
Vanillin	7.96	-0.85785	97.49147	-2.31293	0	---
Caffeic acid	0	-0.73794	92.15746	-2.98708	396.3507	14.34
Thymidine triphosphate	0	1.511975	97.39225	-1.19708	10809.63	10.59
TDP	0	1.849431	92.40848	-1.03485	15.53755	60.63
NADPH	0	1.127734	98.51034	-0.23373	16991.77	11.41
3,4-dihydroxyphenyl acetic acid	0	-1.2064	99.43409	0.662217	209.3593	55.11
Methylparaben	0	0.91343	97.10416	-1.32163	1859.285	11.95

UDP-glucose	0	0.517963	90.64583	-1.97462	0	---
Pyridoxal 5'-phosphate	85.4	0.410584	94.69493	-1.01927	1680.063	10.06
Octanoic acid	0	1.0461	99.49474	1.112517	132273.2	12.76
Uric acid	0	-2.43867	93.78659	2.316333	7.171446	92.18
N-Acetyltryptophan	0	1.078362	76.55041	-1.69497	129.2189	22.26
NADH	6.48	0.202735	98.19588	-1.7441	132795.4	11.68
UDP-N-acetyl-D-mannosamine (unconfirmed)	0	-1.42427	96.72539	-0.26818	259.5663	32.91
dUMP	0	-1.12621	94.31954	-1.17818	316.5752	7.03
Nonate	18.9	0.631953	85.93981	-0.26818	428.4033	18.96
Homogentisic acid	0	0.595183	90.22476	-0.50878	0	---
Methyl phenylacetate	0	0.661936	88.05046	1.566833	190.0879	17.99
4-Hydroxy-3-methoxymandelic acid	0	-0.05992	99.48732	-1.75867	44289.46	12.03
Glyceraldehyde 3-phosphate	0	-1.17336	97.10504	0.870983	1108.823	13.6
Glutamic acid	0	0.829119	96.91402	-1.60902	1598.223	14.19
Ribose 5-phosphate	0	1.582368	90.71841	2.362017	0.03149	266.3
6-Phosphogluconic acid	0	-0.08354	82.10788	-1.9068	498.5128	13.05
Oxoadipic acid	49.3	0.854604	96.29554	2.85495	3863.371	12.67
ADP Glucose	12	0.829798	97.70219	-2.39505	8554.516	14.41
Adenine	42.5	1.065023		1.580067	1491.305	8.98
3-methoxyphenylacetic acid	91.2	-0.07252	95.87481	-2.30993	4334.343	12.43
1-Pyrroline-5-carboxylic acid	0	1.469523	90.48399	-2.18408	2132.854	28.16
Methionine sulfoxide	10.8	0.37757	91.17796	-1.62495	1851.115	17.74
Fluorouracil	0	0.82272	91.80745		250.6984	59.92
Methylglutaric acid	0	-1.27833	95.4251	2.510233	15522.34	14.98

Cytidine monophosphate	0	1.118675	91.49121	0.030233	4112.259	24.87
Malic acid	15.6	0.859814	98.29532	2.510233	7094745	19.24
Succinyl-Homoserine	0	1.029639	93.4793	2.520233	4915.641	23.25
Phenylacetylglycine/Phenaceturic acid	0	-1.16253	95.58356	-0.52965	16.19413	55.78
Glutaric acid	35.4	1.209263	97.10016	-2.41308	493.5099	25.19
EDTA	0	1.052364	95.00654	2.802817	0	---
Adipate semialdehyde	0	1.019637	90.27875	-2.08973	124.5757	50.76
Ribulose 5-phosphate	0	-0.44564	86.99033	-1.68973	315.4559	17.96
Cytidine monophosphate N-acetylneuraminic acid	53.5	0.596666	97.39306	2.2825	3.598477	155.68
Thymine	12.3	0.946662	98.77141	0.78425	1519970	20.63
Deoxyuridine	91.2	1.875416	89.75096	-2.92575	5156.258	20.64
2-C-Methylerythritol 4-phosphate	5.39	-0.45579	95.62531	2.084567	1080.215	17.15
Pantothenic acid	0	-0.40528	98.05145	-1.97347	0	---
Cytidine	26.9	0.852064	95.81934	-1.24485	257.0811	13.3
N-Acetyl-L-methionine	0	-0.00027	87.76678	1.149917	0	---
4-Methyl-2-ureido-pentanoic acid/Carbamoyl isoleucine	0	-1.77167	99.39282	1.8111	7262.998	32.78
Pyruvic acid	85.6	0.971434	97.78316	1.8211	56.25218	32.63
Arabinonic acid	96.1	1.938643	98.09521	-0.05873	537943.1	17.07
O-Acetylserine	7.96	-0.1544	97.9696	0.186533	0	---
Cytosine	0	-0.75853	88.98101	0.796533	0	---
Nicotinic Acid N-Oxide	21.2	0.234426	96.93098	0.559317	144.4204	44.68
Beta-Alanine	76.9	-0.81335	89.1993	-2.02342	90.36636	41.28
Inosine	0	-1.63271	90.58092	-1.92342	0	---

Xylulose	0	-0.69415	97.76568	-1.36263	479.1914	77.83
Acetoacetate	6.16	-0.29489	92.97272	0.464633	2308.321	12.75
Glycolic acid	0	0.258413	94.49507	-1.72942	0.777917	213.68
Gluconate	6.54	0.168939	98.71937	-2.68575	272927.2	16.33
Raffinose	34.4	0.638594	92.88304	2.41425	4882.832	28.89
Mytilitol	0	0.96815	90.27875	-1.29937	1506.87	34.77
Arabitol	38.9	-0.02243	97.95297	-2.27937	3.130399	86.33

Table A.7.10: The significantly altered identified metabolites when treated with 20µM of Roxadustat and control identified by volcano plot.

Identified metabolites	FC	log2(FC)	p.adjusted	-log10(p)
Uridine triphosphate	0.37057	-1.4322	0.000411	3.3867
Phosphocreatine	0.51017	-0.97096	0.009853	2.0064
Phenylpyruvic acid	0.4716	-1.0844	0.007786	2.1087
N-Acetylglutamate	0.38569	-1.3745	0.000931	3.0312
Inositol 1,3,4-trisphosphate	0.29943	-1.7397	0.000301	3.5221
4-Acetylbutyrate	0.28998	-1.786	0.010711	1.9702
3,3 Dimethyl glutarate	1.839	0.87895	0.032086	1.4937
2,3-Diphosphoglyceric acid	0.39368	-1.3449	0.00276	2.5591

Table A.7.11: All pathways found by the untargeted pathway analysis during 20µM of Roxadusta vs control experiment on HEK 293T cells. PW = pathway, Fisher's Exact Test, EASE = Expression Analysis Systematic Explorer. Emp = empirical, p = p-value, adj = adjusted, cpd= compound.

Pathway Name	Pathway total	Hits. total	Hits. sig	Expected	P(Fisher)	P(EASE)	Emp .Hits	Empirical	Adj P.Fisher	Adj P.EASE	cpd.hits
Glutamate metabolism	15	12	5	0.78474	0.039305	0.13128	0	0	1	1	C00025;C00064;C03912;C00051;C00232
Arginine and Proline Metabolism	45	34	8	2.3542	0.21239	0.3539	0	0	1	1	C00025;C03912;C03564;C04582;C00073;C04188;C00147;C04281;C05938;C00064
Nitrogen metabolism	6	4	2	0.3139	0.13793	0.52633	1	0.01	1	1	C00025;C00064
Carbon fixation	10	10	3	0.52316	0.23684	0.52846	2	0.02	1	1	C00279;C00354;C00231
Butanoate metabolism	34	22	5	1.7787	0.31956	0.53069	0	0	1	1	C00025;C00109;C05548;C00232;C00164;C06010

Glutathione Metabolism	19	11	3	0.994	0.28732	0.58283	2	0.02	1	1	C01879;C00025;C00051
Pyrimidine metabolism	70	54	10	3.6621	0.44798	0.5875	0	0	1	1	C00106;C00064;C05100;C00025;C00906;C00349;C01346;C00214;C00178;C00442
N-Glycan Degradation	16	5	2	0.83705	0.20472	0.60726	0	0	1	1	C00159;C00124;C00140
Methionine and cysteine metabolism	94	45	8	4.9177	0.51679	0.6688	0	0	1	1	C00025;C04582;C00109;C00302;C00073;C00051;C15606;C00606
Histidine metabolism	33	21	4	1.7264	0.49682	0.72163	1	0.01	1	1	C00025;C00051;C05828;C02835
Ascorbate (Vitamin C) and Aldarate Metabolism	29	21	4	1.5172	0.49682	0.72163	0	0	1	1	C00051;C05411;C00072;C04575;C00425
Keratan sulfate degradation	68	7	2	3.5575	0.34303	0.73019	1	0.01	1	1	C00124;C00140
Heparan sulfate	34	7	2	1.7787	0.34303	0.73019	3	0.03	1	1	C00140;C00124

degradation											
Lysine metabolism	52	22	4	2.7204	0.53621	0.75178	2	0.02	1	1	C00025;C04092;C05543;C00450
Vitamin B3 (nicotinate and nicotinamide) metabolism	28	15	3	1.4648	0.4879	0.75389	0	0	1	1	C00025;C00064;C00442
Phosphatidylinositol phosphate metabolism	59	31	5	3.0866	0.63553	0.80216	0	0	1	1	C00124;C01288;C01225;C01220;C01245;C01243;C00137;C04063;C04062
Linoleate metabolism	46	24	4	2.4065	0.61007	0.80423	0	0	1	1	C08261;C00051;CE5898;C00072
Propanoate metabolism	31	17	3	1.6218	0.57807	0.8143	0	0	1	1	C00109;C00804;C06002;C01013;C00164;C00163

Tryptophan metabolism	94	53	8	4.9177	0.71436	0.82765	0	0	1	1	C00025;C05647;C05651;C02220;C00272;C00632;C00328;C00051;C00936;C03227
Aspartate and asparagine metabolism	114	54	8	5.964	0.73495	0.84251	0	0	1	1	C00025;C00232;C05572;C05938;C05932;C00064;C00109;C01879;C02630;C00051;C04281;C04282
Tyrosine metabolism	160	68	10	8.3705	0.75829	0.8491	0	0	1	1	C00025;C00425;C00072;C03765;C00064;C00272;C00355;C07086;CE5536;C05581;C05583;C05582;C00051;C00164
Urea cycle/amino group metabolism	85	34	5	4.4469	0.71934	0.85832	1	0.01	1	1	C00025;C01586;C03912;C00073;C01250

Androgen and estrogen biosynthesis and metabolism	95	19	3	4.97	0.6577	0.86117	0	0	1	1	C05290;CE2186;CE2183;CE2182;CE5248;C05140;C05302;CE5247;C00051;C05284
Putative anti-Inflammatory metabolites formation from EPA	27	11	2	1.4125	0.58664	0.87301	0	0	1	1	C00025;C00051
Alanine and Aspartate Metabolism	30	20	3	1.5695	0.69327	0.88033	0	0	1	1	C00025;C00940;C00064
Prostaglandin formation from arachidonate	78	20	3	4.0806	0.69327	0.88033	0	0	1	1	C00425;C00051;C00072
Beta-Alanine metabolism	20	13	2	1.0463	0.68113	0.91299	1	0.01	1	1	C00025;C01013
Aminosugars metabolism	69	31	4	3.6098	0.80652	0.92057	0	0	1	1	C00025;C00140;C00064;C00645
Pentose and Glucuronate Interconversi	15	15	2	0.78474	0.75732	0.94045	3	0.03	1	1	C00199;C00231;C05385

ons											
Arachidonic acid metabolism	95	16	2	4.97	0.78919	0.95075	0	0	1	1	C00025;C00051
Porphyrin metabolism	43	16	2	2.2496	0.78919	0.95075	3	0.03	1	1	C00072;C00425
Leukotriene metabolism	92	16	2	4.8131	0.78919	0.95075	0	0	1	1	C00302;C00051
Valine, leucine and isoleucine degradation	65	26	3	3.4005	0.85044	0.95259	1	0.01	1	1	C00025;C00349;C00164;C06002
Drug metabolism - other enzymes	31	17	2	1.6218	0.81735	0.95927	0	0	1	1	C16622;C04646
Fructose and mannose metabolism	33	27	3	1.7264	0.86844	0.95958	2	0.02	1	1	C05378;C00577;C00665;C00095;C00159;C00031;C00354;C00267;C02985;C03693
Pentose phosphate pathway	37	36	4	1.9357	0.89092	0.96049	2	0.02	1	1	C00281;C00442;C01101;C00620;C00199;C00231;C00117;C00279;C00447;C06222;

											C00221;C05382
Glycine, serine, alanine and threonine metabolism	88	53	6	4.6038	0.91644	0.96385	0	0	1	1	C00025;C00256;C00073;C00109;C00051;C00937
Pyruvate Metabolism	20	18	2	1.0463	0.8421	0.96633	3	0.03	1	1	C00256;C00424;C00937;C00186;C05235;C00051
Glycolysis and Gluconeogenesis	49	38	4	2.5635	0.91446	0.97042	2	0.02	1	1	C00900;C05378;C00031;C00354;C00665;C01231;C00221;C00267;C00186
Purine metabolism	80	55	6	4.1853	0.93289	0.97191	0	0	1	1	C00366;C00025;C00147;C00442;C00064;C00385;C00072
Glycerophospholipid metabolism	156	31	3	8.1613	0.92279	0.97887	4	0.04	1	1	C01225;C01582;C00577;C00570;C00184;C00137

Galactose metabolism	41	33	3	2.145	0.94148	0.98482	1	0.01	1	1	C00124;C00140;C00577;C03785;C00159;C00031;C00795;C02336;C00221;C00267;C00095
Sialic acid metabolism	107	23	2	5.5978	0.92598	0.98705	1	0.01	1	1	C00140;C01582;C00221;C00645;C00267;C00124;C00137
D4&E4-neuroprostanes formation	37	26	2	1.9357	0.95391	0.99272	0	0	1	1	C00072;C00425
Xenobiotics metabolism	110	37	2	5.7547	0.99258	0.99914	1	0.01	1	1	C00051;CN0016
Hyaluronan Metabolism	8	5	1	0.41853	0.60984	1	2	0.02	1	1	C00140
N-Glycan biosynthesis	48	15	1	2.5112	0.94162	1	11	0.11	1	1	C00159;C00031
Glycosphingolipid biosynthesis - ganglioseries	62	10	1	3.2436	0.84864	1	12	0.12	1	1	C00124;C01582
C5-Branched dibasic acid metabolism	10	6	1	0.52316	0.67701	1	15	0.15	1	1	C00490;C01732
Chondroitin sulfate	37	5	1	1.9357	0.60984	1	13	0.13	1	1	C00124

degradation											
Hexose phosphorylation	20	17	1	1.0463	0.96018	1	9	0.09	1	1	C00159;C00031;C00095;C00738
Squalene and cholesterol biosynthesis	55	15	1	2.8774	0.94162	1	3	0.03	1	1	C00164
3-oxo-10R-octadecatrienoate beta-oxidation	27	8	1	1.4125	0.77879	1	0	0	1	1	CE5326;CE5314
Alkaloid biosynthesis II	10	6	1	0.52316	0.67701	1	1	0.01	1	1	C00180
Vitamin B1 (thiamin) metabolism	20	8	1	1.0463	0.77879	1	6	0.06	1	1	C01081
Glycosphingolipid biosynthesis - globoseries	16	8	1	0.83705	0.77879	1	7	0.07	1	1	C00984
Vitamin B5 - CoA biosynthesis from pantothenat	12	11	1	0.62779	0.87484	1	5	0.05	1	1	C00864

e											
Bile acid biosynthesis	82	10	1	4.2899	0.84864	1	0	0	1	1	C00163
Biopterin metabolism	22	14	1	1.1509	0.92933	1	1	0.01	1	1	C00272
Vitamin B9 (folate) metabolism	33	16	1	1.7264	0.95178	1	4	0.04	1	1	C00025
Vitamin A (retinol) metabolism	67	10	1	3.5052	0.84864	1	0	0	1	1	CE5757
CoA Catabolism	7	5	1	0.36621	0.60984	1	1	0.01	1	1	C00864
TCA cycle	31	17	1	1.6218	0.96018	1	23	0.23	1	1	C00311;C00158;C00417
Glycosphingolipid metabolism	67	21	1	3.5052	0.98153	1	15	0.15	1	1	C00124;C00962;C00031;C01582
Vitamin B6 (pyridoxine) metabolism	11	7	1	0.57547	0.73267	1	1	0.01	1	1	C00847
Ubiquinone Biosynthesis	10	5	1	0.52316	0.60984	1	1	0.01	1	1	C00156
C21-steroid hormone	112	28	1	5.8594	0.99523	1	3	0.03	1	1	C05284

biosynthesis and metabolism											
Starch and Sucrose Metabolism	33	14	1	1.7264	0.92933	1	9	0.09	1	1	C00031;C00221;C00267
Selenoamino acid metabolism	35	10	1	1.8311	0.84864	1	5	0.05	1	1	C00109

Table A.7.12: Identified metabolites from the IC-MS data of 100 µM of Roxadustat vs control treated HEK293T cells.

Accepted Description	Fragmentation Score	Mass Error (ppm)	Isotope Similarity	Retention Time Error (mins)	Max Abundance	Minimum CV%
Malic acid	77.7	1.211793	99.38925	-1.00373	664351.8	7.65
N-Acetylaspartylglutamic acid	0	1.465363	97.73149	-1.18018	173555	10.73
Acetylglycine	85.5	1.06475	95.68874	-0.11427	9656.535	14.64
Ribulose 1,5,diphosphate	0	-0.37354	98.43032	0.760467	167315	12.78
N-Acetylglutamate	66.3	-2.32549	98.20167	-0.6299	158972.9	11.77
Phosphocreatine	4.49	-1.53398	95.28623	-0.36848	397348	18.08
Glucose	26.8	0.580234	99.11022	-0.53935	745675.3	10.98
Beta-Citryl-L-glutamic acid	0	1.582246	98.03009	-0.91998	1313283	7.36
3-Phosphoglyceric acid	28.8	0.834174	99.33708	-1.4125	808798.2	6.07
N-Acetyl-aspartate	87.7	0.267329	92.48322	-0.69065	668025.6	14.32
Isocitrate	71.2	0.687081	99.51841	-2.30298	2115264	8.74
Phosphoenolpyruvic acid	2.28	0.828812	99.32062	-1.7786	108127.7	6.08
Pyridoxal 5'-phosphate	47.8	0.559115	90.00116	-2.30847	4412.209	11.34
Sedoheptulose 1,7-bisphosphate	0	1.518523	97.20318	0.250633	63396.67	11.12
Glutamylcysteine	0	-1.90168	89.4483	2.38095	603.5189	73.96
Xanthylic acid	0	-0.34096	91.84502	-1.98102	1387.467	21.78
Inosine monophosphate	0	-0.28555	90.69213	-1.42272	2485.896	19.23
Cytidine diphosphate	51.4	1.726267	94.67501	-2.63937	13844.97	20.71
Cytidine triphosphate	0	2.850927	97.52244	2.822217	2367872	8.81
Flavin Mononucleotide	6.03	0.988186	97.8639	-1.89778	906109.6	9.57

(unconfirmed)						
Deoxyadenosine triphosphate	0	1.477786	89.26462		3098.321	15.08
NADPH	0	-0.75629	96.18032	1.37825	14931.17	21.95
UDP-glucoronate	96.5	0.892414	95.25436	-2.55648	17209.3	16.4
Fructose 1,6-bisphosphate	0	3.614856	95.48478	0.633	2700.169	37.24
Octanoic acid	0	2.072215	92.46602	-2.37622	10810.19	20.96
Adenylsuccinate	0	1.830316		1.41165	2173.759	27.34
dTDP-D-glucose	0	0.476412	91.17918	-0.05302	222.0404	55.39
Uridine diphosphate-N-acetylglucosamine	0	1.075357	92.19108	-2.14892	2453.7	35
Thymidine 5'-phosphate (TMP)	0	2.589451	95.92515	-1.51238	220168.9	6.5
NADH	3.39	1.674535	98.37391	-2.21953	2546160	8
Sebacic acid	93	0.702545	91.79594	-1.32968	17697.93	10.52
Citric acid	94.1	3.225164	96.96944	-0.91848	297121.8	14.34
Homovanillic acid	0	1.239789	88.75344	-2.31133	844.726	22.54
Methylisocitric acid	0	0.136019	97.33072	-0.66345	23802.58	9.47
2-Hydroxy-4-phenylbutanoic acid	0	-1.71822	92.0838	-1.86177	11777.16	58.27
Adenine	3.77	1.033294	97.685	-2.70833	13307.18	9.43
dGMP	0	1.049082	95.51773	-1.18985	7049.729	25.23
dCTP	0	-2.49209	89.09598	0.857017	4153.445	49.34
Uric acid	0	1.377017	93.89646	2.811033	13723.4	26.29
dIMP	0	-0.77144	97.92562	-1.65897	43473.87	21.58
dADP	47.8	1.504848	95.83503	-2.43897	261814.6	21.95
dGDP	0	1.503521	96.87016	-1.4884	21569.47	11.2
Ferulic acid	33.3	1.630636		-1.87743	1601633	5.78
Guanosine diphosphate (GDP)	0	1.16778	92.73898	-1.11423	6608.651	24.16

TDP	0	1.476741	95.19117	1.903833	2985.185	12.8
Thymidine triphosphate	74.3	0.20061	95.68354	-2.73592	11261.29	11.56
Adenosine triphosphate (ATP)	0	1.856518	89.10457	2.842067	4475.181	14.08
Protocatechuic acid	0	-1.83861	86.8924	-1.5324	1174.108	17.81
Inositol 1,3,4-trisphosphate	0	1.415778	92.64715	-0.81623	3138.919	24.5
Uridine triphosphate	0	-1.81742	85.3623	0.784733	1225.093	40.46
3-Hydroxyisovaleric acid	0	1.472544	97.84341	-2.52725	22460673	5.23
Glyceric acid	0	0.780182	88.83505	2.4402	48.33321	77.46
N-Formyl-methionine	95.4	2.689059	96.83927	-0.38642	3430309	9.13
N-Acetyl-L-methionine	95.6	1.699436	95.6192	1.8547	156233.1	10.35
Lactoyl-isoleucine	5.66	1.171737	95.20317	-1.8453	27525.35	12.54
Galacturonic acid	4.97	0.626287	97.94539	-2.38725	8903014	9.73
Leucic acid	0	0.623729	92.11982	-1.92283	5036.641	16.67
3-(2,5-Dioxoimidazolidin-4-yl)propanoic acid	21.7	1.138372	95.05953	-2.81873	6340.643	9.4
Allantoin	0	1.72214	96.97118	-1.47043	3371.64	153.36
Deoxyuridine	6	0.963578	98.24483	-2.94043	1529187	5.52
Taurine	0	-3.37711	98.08872	0.353617	4824.151	6.95
Arabinonic acid	0	0.598852		0.7094	88430.55	7.77
N-Acetylneuraminic acid (Sialic acid)	0	0.60162	83.9216	-0.65127	1005.739	10.82
Lactic acid	73.6	1.021786	95.26071	-0.43307	24331.35	11.91
Pantothenic acid	0	-2.03858	96.74217	0.022667	5776.429	15.86
Inosine	43.9	0.80887	96.52945	-0.17445	3407.384	11.4
Caffeic acid	0	-2.94716	97.38478	-0.5662	3095.172	36.86
Oxovaleric Acid	0	0.814622	92.14161		95.96101	23.32

3-Dehydroquinate	0	-2.76169	93.68598	0.52345	360.842	20.84
2-C-Methylerythritol 4-phosphate	0	0.556535	88.90844	-0.9762	58.75445	80.26
Uracil	0	-2.84438	93.77684	-0.71858	6627.904	11.4
Threitol	93.4	0.871442	92.97099	-0.64013	737236.5	7.64
Lactose	57.1	0.263976	96.00795	-0.6901	12203.53	6.87
Hydroxy-isobutyric acid	2.78	0.477996		-0.97155	24330.88	9.62
Xylulose	0	0.599702	90.51802	-0.57155	5865.515	10.3
Adonitol (ribitol)	30.6	0.566148	99.9143	-0.71867	4958837	8.06
Sorbitol	59.1	0.575499	97.94369	-0.6062	335886.3	8.95
N-Acetylvaline	8.2	-4.7065	94.00318	-0.7385	13763.49	10.25
Methyl beta-D-glucopyranoside	0	-1.34098	89.8911		148.2682	28.55
Quinic acid	0	-3.64393	96.25694	0.110867	25578.58	6.21
Pyroglutamic acid	0	-1.24885	92.10407	-2.16913	178.1991	21.32
Gluconate	0	0.693728	91.30568	2.160867	1907.333	9.14
5-Hydroxymethyl-2'-deoxyuridine	0	1.445242	63.22229	-2.20913	322.2789	21.52
N-Acetyl-L-alanine	0	1.323393	94.60782	-1.38442	414.4252	13
O-Acetylserine	0	0.748933	89.18166	2.751617	261.5009	16.41
Raffinose	69.8	1.127034	97.84906	0.182217	6928.626	10.2
Fumarate	73.5	0.092879	95.71361	-0.07778	31364.66	10.95
4-Hydroxyproline	0	-0.67199	98.96799	-1.90725	45848.71	14.55
Ribulose 5-phosphate	0	0.539175	96.97263	-1.31725	1831.166	9.82
Succinyl-Homoserine	40.7	0.755599	96.0134	-0.49725	2562.543	15.43
Sedoheptulose 7-phosphate	69.8	1.008756	97.75092	0.03065	13647.18	10.34
Prephenic Acid	56	0.373925	99.03706	0.12065	117693	12
Adenosine monophosphate (AMP)	0	0.497272	91.64962	-1.01147	15.58627	125.33

Oxoadipic acid	0	0.357443	95.55278	1.13695	571.9545	33.05
Cysteic acid	22.8	0.627072	95.56892	-0.86305	1441.524	14.76
4-Hydroxybutyric acid	16.1	-2.98698	93.85954	-0.37632	350899.5	7.97
Glyceraldehyde 3-phosphate	61.4	0.635179		-0.55632	199451.2	4.18
Succinic acid semialdehyde	0	1.326139	93.3547	-2.36632	912.6286	23.86
2-Oxoglutaric acid	92	0.852455	95.89066	-0.27427	25093.28	10.2
Fluorouracil	0	1.039827	93.64771	-0.40427	248353.4	12.7
2-Isopropylmalic acid	0	0.728012	90.00901	0.46505	4093.236	12.54
Acetylphosphate	39.1	1.133333	97.87709	-1.59928	46118.61	8.08
Orotic acid	0	1.0378	95.46664	2.571567	2317.236	15.92
Nonate	52.5	1.730051	97.54482	2.267817	66347.92	4.86
Succinic acid	0	2.124683	61.55637	2.460683	2278.088	11.81
4-Hydroxy-2-oxoglutarate	80.7	0.991105		-1.33932	36982.84	5.08
O-Phosphoserine	0	2.328603	88.40906	0.471583	211.0011	21.64
Orotidine	56	1.535235	96.55359	-1.21927	195629.3	20.68
6-Phosphogluconic acid	50.7	0.658507	95.84727	-1.43292	6270.289	11.06
Glycerol 3-phosphate	56.2	0.444732	90.7937	-1.25783	3330.342	20.42
3-methoxyphenylacetic acid	0	0.533214	96.29895	0.433417	786.8769	18.68
3-Hydroxymethylglutarate	0	1.395913	78.92382	-1.01468	681.6659	20.91
Ureidosuccinic acid (N-carbamoyl-L-aspartic acid)	0	0.485922	99.17549	-1.19618	40968.38	7.94
Isovaleric Acid	34.7	0.739098		-1.35233	214895.5	7.95
2-Hydroxyglutarate	0	1.409067	70.80603	-1.92292	295.4309	31.45
Phenylacetylglycine/Phenaceturic acid	5.93	0.347224	96.01407	-1.09983	3208.807	42.9
Galactaric acid (mucic acid)	0	-2.50388	88.08424	1.68005	2050.709	30.05

Methylglutaric acid	29.5	0.790009	97.20902	2.401167	25502.31	7.56
Sedoheptulose 1-phosphate	55.5	1.134375	93.17141	-2.3549	11314.37	10.84
Glutaric acid	0	-2.07494	96.81036	-0.55668	15400.92	19.17
Malondialdehyde	0	0.635413	96.51505	2.269917	1244.116	13.87
Hippuric acid	0	1.561492	93.39519		101.82	55.51
Cytidine monophosphate	55.5	0.717036	96.91408	-1.19055	4220.22	15.85
Cytidine monophosphate N-acetylneuraminic acid	0	2.843657	94.856	-2.44055	7608.76	8.11
Glucose 1-phosphate	0	1.395871		0.6681	405.7336	16.65
3-Methyl-2-oxovaleric acid	0	0.462681	98.23753	-1.6619	133909.4	8.67
Sorbitol-6-phosphate	0	0.824322	88.90844	0.983	32.22492	74.14
Naringenin	81.3	0.895268		-0.79593	906239.8	9.53
1-Pyrroline-5-carboxylic acid	0	1.072869	87.7272	2.514067	510.6991	35.84
Aspartate	0	1.478456	90.07092	-0.18498	25.85909	271.24

Table A.7.13: Identified metabolites from the IC-MS data of 100 µM of Molidustat vs control treated HEK293T cells.

Accepted Description	Fragmentation Score	Mass Error (ppm)	Isotope Similarity	Retention Time Error (mins)	Maximum Abundance	Mini CV%
3-isopropylmalic acid	0	-1.96603	91.57676	-1.75185	915.444	17.57
3-Hydroxytyrosol	0	-1.6298	91.03655	-1.08555	371.256	18.45
4-Hydroxy-2-oxoglutarate	0	-0.55004	93.39519		32.80212	70.05
2,5 Dihydroxybenzoic Acid	0	21.24102	91.84675	4.208783	15.55673	55.36
Dimethoxy-4-Hydroxycinnamic Acid	0	-19.3585	91.90015	3.63815	111.4225	77.38
EDTA	0	-0.8933	87.28823	-1.5988	56633.94	4.88
Cytidine monophosphate N-acetylneuraminic acid	0	2.026272	95.9721	-0.71448	72871.41	11.83
O-Phosphoserine (new)	64.4	-1.5268	99.14655	0.0081	7653.613	8.04
Succinyl-Homoserine *	0	-0.04135	92.60355	-0.1788	5007.501	6.13
Octanoic acid	6.5	-1.17789	97.3293	-1.26887	53769.82	9.45
Dihydrouracil	0	3.638987	94.58617	1.318083	325.0619	17.99
Toluate (new)	0	-0.85685	93.17596	-1.79857	3559.934	7.12
Cytidine	0	3.810275	88.575	1.215683	1011.888	14.73
2-Isopropylmalic acid	0	-1.40702	91.57676	1.3041	466.6616	25.96
Beta-Citryl-L-glutamic acid	0	-0.47402	98.68458	-0.81882	1301222	10.8
Cytidine triphosphate	6.01	-1.15822	98.14355	-1.74742	924771.4	11.94
2-C-Methyl-D-Erythritol 4-	0	-0.3489		2.341833	30794.83	12.81

phosphate						
Phosphoserine	0	19.87329	96.55825	2.141833	480.0958	61.43
Indomethacin	0	-5.44693	60.84175	1.717717	83.16371	92.28
CDP-ethanolamine (new)	0	-0.92407	94.8623	0.0477	16482.27	6.55
N-Oxalylglycine *	0	-0.53	93.39519		147.7463	23.77
Hydroxypropionic acid	0	4.908574	56.20822	0.9517	554.8336	14.72
Octanoic Acid	0	-26.594	96.07469	2.211833	1.145134	213.02
2,3-Diphosphoglyceric acid	0	-1.17899	95.87469	3.6597	776.8213	6.96
Isovitexin	0	-1.61064	99.37793	-1.84623	78347.22	15.16
2-Amino-3-phosphonopropionic acid/Glyphosate	0	12.80956	86.13501	-3.4439	7283.992	11.31
Glycerol	0	27.17269	95.25849	2.2861	726.0033	24.36
Threitol	58.2	-1.81509	99.96142	0.118567	491474.1	7.69
Nonate	0	10.43511	97.76265	-1.0139	310.0927	15.93
Glucosamine 6-phosphate	60.2	-1.337	97.32749	0.198567	4361.45	7.66
N-Acetyl-aspartate	0	-4.38979	97.90125	-0.5203	32319.65	5.72
3,3 Dimethyl glutarate	0	-28.2582	95.25849	2.208567	185.3095	42.04
DL-threo-beta-Hydroxyaspartic acid *	0	-1.82489	85.03985	1.343883	256.3535	36.27
N-Acetyl-L-phenylalanine	96.3	-2.06611	92.53205	-0.69552	937790.9	11.13
Raffinose	0	-0.81744	91.78403	-1.64185	65.85785	47.05
Phosphoribosyl pyrophosphate (PRPP)	0	1.212888	94.26037	-1.14977	93.85259	66.92
Tetracycline	0	-1.23142	93.72755	-0.43663	656.0782	12.26
Ribulose 1,5,diphosphate	6.22	-1.67035	93.15714	0.481433	7397.267	11.71
trans-Ferulic acid	0	-0.56094	98.83852	-1.58887	51713.55	13.16

3-nitrotyrosine	0	-13.0671	92.40177	-1.97857	486.0459	28.87
Xanthylic acid	0	-2.25387	99.0943	0.891133	118604.3	11.69
cis-Aconitic acid	0	21.08505	96.52289	2.734483	71448.68	11.3
4-Hydroxyproline	0	-2.8173	95.82528	-0.8639	2063.77	10.49
6-Phosphogluconic acid	0	-1.13996	88.92887	0.261433	359.9171	62.84
Naringenin	0	-2.62113	91.24568	-1.34598	3420.57	12.56
Erythrose 4-phosphate	0	-1.94865	96.42451	1.681183	6478.07	13.14
Ophthalmic Acid	90.7	-1.3835	94.04727	-0.34552	40406.34	12.1
2-Aminocaprylic acid	0	-1.64479	99.08217	-1.6383	204066.1	11.9
Oxoadipic acid	0	-0.76536	93.39519		156.7168	40.28
Pantoic acid (new)	0	20.62809	90.62689	0.440417	575.143	13.87
Glutamylcysteine	0	-0.8525	91.82625	-1.17972	1869.887	9.83
Glycerol 3-phosphate	0	-0.01477	96.01987	0.6317	3150.5	15.26
Gluconate	0	-3.09865	86.42486	1.185683	309.0727	24.04
Aspartate	0	-0.91542	39.70393	1.783633	43.19444	67.19
Clofibrate	0	-1.68314	36.02118	1.979983	295.0805	26.33
Hydrocinnamic acid	0	14.07762	88.92887	0.5677	39.55801	74.1
Riboflavin 5-monophosphate	0	-1.59004	96.59839	-0.36053	1854.596	7.28
Phosphorylcholine Chloride	0	-4.25475	87.85569	-0.75165	2193.331	60.96
3-Dehydroquinate	0	-0.45759		-1.94513	206.4589	21.01
Galacturonic acid (new)	0	-1.90989		0.595283	807.8803	17.77
N-Acetyl-L-methionine	88	-1.05481	98.40852	0.08065	119718.7	4.41
dGMP	0	9.191622	66.02096	1.036983	115.4598	61.28
Thymidine triphosphate	0	-24.3182	90.27205	-2.6159	894.2353	68.77
Aspirin	0	-19.533	85.93861	2.298783	865.3167	10.75
Quinolinic acid	0	-1.24612	93.41284	0.0641	318.5921	33.97

Uridine 5'-diphosphate	0	-16.4123	70.1579	2.471533	2306.298	13.08
Tricine	36.8	-1.34206	94.47903	-0.1759	1756.777	8.49
dUMP	0	-1.97912	92.07082	-1.09575	433.4344	12.95
dIMP	0	13.47034	91.72084	-0.71575	712.9874	13.02
2,2-Diphenyl-1-picrylhydrazyl	79.8	-1.40512	95.28705	-0.41625	26401.1	9.15
Thymidine 5'-phosphate (TMP)	38.2	-1.98095	86.56675	1.717833	1063.033	50.07
3,4-Dehydro-L-proline	0	-0.87273	86.04251	-0.56102	953.3094	19.26
N-Acetylproline	0	-4.11772	70.80769	4.52185	1424.153	15.25
Phosphocreatine	57.4	-1.4788	95.71001	-0.91815	5297.599	5.23
Acetylphosphate	0	-1.26324	91.52616	-1.57007	813.2925	6.36
Fructose 2,6 diphosphate	11.6	-0.97605	96.33406	-1.80667	26995.43	9.53
dTDP-D-glucose	0	-1.46933	96.32376	3.892233	6317.136	7.87
UDP-N-acetyl-D-mannosamine (unconfirmed)	0	-1.5126	93.60161	-1.65088	2542.423	21.01
Cytidine monophosphate	0	-4.16834	91.0895	-1.42555	1389.93	15.73
Hippuric acid	0	0.977688	79.65258	3.809117	8286.66	28.42
Taurine	96.7	-1.46827	94.16812	-1.27312	16028.33	12.69
Butyric acid	0	-6.25882	93.90838	4.08995	9.731486	301.92
dUTP	0	-5.25757	95.9839	1.86995	442.3037	14.54
TDP	50	-3.87498	95.23893	-0.38075	780662.2	13.53
4-Hydroxybutyric acid	0	-4.4176	98.90354	-0.64582	119.3893	24.96
Adenine	0	-0.33578	98.94867	-0.15567	243464.4	6.87
Ascorbate	0	0.495669	96.91214	-1.50428	605352.5	9.69
Gibberellin A3	0	-0.21635	98.59831		3833862	13.08
Methyl 4-hydroxybenzoate	0	-0.68607	92.25317	-1.37985	5936.492	7.55
Salicylic Acid	56	-1.70455	98.92213	-1.13815	6181.427	10.42

Flavin Mononucleotide (unconfirmed)	92.4	-1.47133	93.0186	-0.61397	928822.1	5.91
Cysteic acid	0	-0.86335	77.98337	-0.7681	202.3411	15.37
2-hydroxy-3-methylvaleric acid (new)	87	-1.617	96.05532	-0.69055	2167.972	6.78
Lactoyl-isoleucine	5.7	-0.96755	97.51968	-1.77313	57728.49	10.25
N-Acetyl ornithine	0	-0.83647	91.68427	-1.80313	1604.272	16.51
N-Formyl-methionine	99.1	-0.47856	97.88199	1.926867	254190.2	8.71
Myristic Acid	0	-1.27437	95.8582	0.243167	1055.632	9.65
Menadione	0	-1.07943	93.07049	1.310483	5305.157	6.67
alpha-Ketoisovaleric acid (new)	8.51	-0.5068	94.09196	-0.27673	5407.982	10.05
2-Oxoglutaric acid	0	-2.09771	95.07378	-1.26697	1469.572	15.23
NADH	0	3.587285	80.15634	-1.78683	566.9579	19.16
2-Amino-3-methoxybenzoic acid/3-methoxyanthranilic acid	0	25.64244	96.26408	4.683033	1509.295	12.36
Phosphoenolpyruvic acid	0	23.18518	92.0552	0.384	65.05992	30.21
Aminoheptanoic acid	0	-0.52471	80.14981		691.3488	27.2
Uracil	72.1	-1.74257	91.71541	-1.2516	6887.06	15.01
Homogentisic acid	0	-0.84861	97.91403	-0.2357	4062.892	15.94
Hydroxyoctanoic acid	0	-4.06668	97.27412	0.053633	6558.649	12.33
Phenyl acetate	0	-2.14349	91.30838	-1.65637	1166.195	54.32
Malic acid (new)	0	-0.45185	94.14265	-1.66197	604.9005	51.33
dADP	0	-0.58195	93.25663	1.863617	1757.882	11.67
N-acetyltryptophan	0	-1.43154	92.40848	-1.28917	1831.094	14.99
Maleamate (new)	0	-1.67542	88.42213	-0.57068	832.4019	11.95
Acetylglycine	0	-5.06819	91.67052	2.66945	303.022	15.8

O-Acetylserine	0	-1.85087	85.33083	2.413867	592.3484	23.63
Glycolic acid (new)	0	-18.5173	88.38606	-0.17122	57.85648	40.34
Aspartame	0	-1.20111	98.06678	0.038783	24089.24	6.31
N-Acetyl-DL-Valine	47.1	-1.39546		-1.29987	80021.55	8.32
Uridine 5'-monophosphate	0	-2.05239	92.54141	-1.07053	710.4808	72.06
Phenylacetylglycine/Phenaceturic acid	93.6	1.044298	96.90976	-0.78613	128273.7	8.74
AICAR (new)	0	1.809156	90.71841	3.779717	25.17758	69.01
3,4-Dihydroxyphenylacetic acid	48.8	-1.51734	99.57983	-1.69175	92155.3	8.88
Galactaric acid (mucic acid)	0	-1.0821	91.83632	2.4046	11.76798	64.27
Quinic acid	0	-1.71451	94.13197	-1.58142	1835.463	40.16
Malathion	0	-1.17225	96.6484	-1.33643	801.3759	10.02
dCTP	0	-1.35365	94.9556	-1.17413	752.3696	7.91
Glucuronic acid	0	-4.76144	96.2552	-0.02205	938.4811	8.7
Citicoline (new)	0	8.818808	96.77895	1.42795	3062.573	14.12
Myricetin	76.3	-0.99768	99.55644	0.187433	598103	7.82
Methyl beta-D-glucopyranoside	0	-0.26375	86.14463	-0.78138	205.6927	118.96
N-Acetyl-L-glutamate 5-semialdehyde	0	3.631157	94.6687	1.4536	977.1564	31.52
Glutamine	0	-2.73315	96.05373	-1.59752	4768.001	12.73
Phosphoglycolic acid	0	-1.45287	94.72022	-1.66403	32.69548	56.64
Glutathione (GSH)	90.3	-1.32348	97.70246	-0.12403	18690.58	8.4
Gallic acid (new)	0	-1.35635	93.64077	-0.41403	247185.6	8.84
dGTP	34.1	-1.65232	97.81089	-0.27545	13902.14	8.18
Guanosine diphosphate (GDP)	0	-2.9152	92.76737	-1.61403	1050.808	17.15
IDP	0	-1.44215	93.483	2.5136	1085.739	9.25

N-acetylneuraminic acid (new)	0	-2.25569	89.46363	-0.32403	212.8299	22.17
Cytidine diphosphate	45.5	-0.47044	98.39857	-1.9185	756175.9	9.29
Glyceric acid	0	-4.13841	97.17941	0.75075	5067.49	8.42
Fructose 1,6-bisphosphate	0	-4.29574	96.4145	-0.15948	100953.5	6.52
Succinic acid	0	13.25334	62.34126	0.439133	676.0126	14.03
Glucosamine	47.5	-1.34589	91.85014	-0.95925	1621.749	22.94
Sedoheptulose 1,7-bisphosphate	19.8	-1.50294	95.31287	-0.79403	1269.664	9.81
Malondialdehyde	0	-0.21987	97.84556	0.57075	17419.75	9.01
Syringic acid	0	-1.74378	80.38759	-0.4607	1058.617	13.09
Citric acid *	0	-8.40328	87.61285	1.1936	332.0564	13.92
Arabinonic acid	0	0.056958	93.41284	-1.6033	226.9612	53.92
Sedoheptulose 1-phosphate	90	-0.80806	94.98921	-1.06693	12932.72	17.4
Pantothenic acid	0	-1.60796	94.67404	1.582033	4008.889	4.85
Methylglutaric acid	0	-3.19716	82.33121	-0.0433	1257.546	46.77
Prephenic Acid	0	7.351876	83.38865	0.55035	2401.184	18.58
Glyceraldehyde 3-phosphate	0	-2.17459	94.66924	0.9812	1196.004	8.94
Urocanic acid	0	-1.08024	91.46367	-1.3507	226.2343	26.89
Adenosine monophosphate (AMP)	0	-1.01712	97.03159	1.0914	405.3023	17.28
Isovalerylglycine	0	-1.27828	93.25061	-1.41435	739.9587	10.06
3-Hydroxymethylglutarate	0	-0.47773	84.44102	-0.25435	1402.175	17.5
UDP-galactose	0	1.145058	83.5142	-1.37077	117.1639	37.88
3-methoxyphenylacetic acid	44.5	-0.78754	94.78659	-0.25435	2367752	2.82
Fumarate	0	-21.7323	88.49638	0.4836	15482.02	7.35
Citramalic acid	0	-0.63348	85.32064	-1.13447	872.9566	35.93
Glucose 1-phosphate	97.6	0.481515	97.92846	-0.28292	4706840	10.74

Hydroxy-isobutyric acid	10.9	-0.5059	98.91415	0.5798	9453847	11.85
Mannitol	21.8	-0.69209	94.86307	0.4034	16888.76	7.82
Sorbitol	80	-0.83171	92.26856	-0.35698	63496.18	9.21
Glutaric acid	0	0.793805	95.18301	-1.14685	10425.22	23.18
Oxfenicine/4-hydroxyphenylglycine	2.86	-1.82951		-0.95698	26970.51	12.58
Ribose 5-phosphate	36.7	-0.41376		1.524183	2993.359	13.36
Methylisocitric acid	86.7	-1.08751	98.95936	-0.92257	141446	7.72
3-Phosphoglyceric acid	0	-1.89276	95.97288	-1.4596	1099.468	11.72
Pyruvic acid	21.7	-1.79798	91.38841	0.124317	3919.387	19.21
2-Phosphoglyceric acid	0	-0.51762	97.72283	-1.35032	14389.92	8.71
2-Hydroxybutyric acid	0	-3.11071	97.84743	1.327433	4676.568	6.83
Lactic acid	0	-1.1412	91.06823	0.301817	3007.303	10.41
Butyl ureidosuccinic acid	87.1	-1.45908	99.6607	-1.67408	14222511	8.74
Deoxyribose 5-phosphate	60.9	-2.24228	96.46771	-0.75672	14518.16	8.38
Adonitol (ribitol)	0	-0.96508	97.61595	-0.67957	31115.69	9.18
2-Hydroxyglutarate	59.6	-1.61014	97.94263	-0.60182	369217.2	11.44
3-Methyl-2-oxovaleric acid	61.2	-1.66793		-0.56555	180863.3	7.88
N-Acetyl-D-Glucosamine 6-Phosphate	57.9	-1.17177	98.70275	-0.66957	33977.74	7.77
N-Acetyl-L-alanine	0	-0.98717	89.43836		3554.737	13.49
Isocitrate *	0	-0.30855	88.40906	0.7644	705.5039	15.54
p-Hydroxyphenylacetic acid	0	-1.7883	91.57676	-0.21155	133.3812	129.83
Gluconolactone	0	-0.97677	95.39042	-0.93645	531.49	11.12
Ureidosuccinic acid (N-carbamoyl-L-aspartic acid)	0	-16.4007	92.5831	2.63565	21.29865	93.49

N-acetyl-glucosamine-1-phosphate	0	-0.46888	92.78744	-0.91567	15030.36	2.67
4-methyl-2-oxovaleric acid (ketoleucine) (new)	50.8	-1.67121	97.39474	0.268567	5697.115	8.85
(R)-2,3-Dihydroxy-3-methylbutanoate (new)	0	-0.33469	91.84826	0.779517	4291.197	9.22
Propionyl-glycine	0	-1.36503	93.86911	0.133167	1605.567	5.68
Ribulose	0	0.445207	97.45995	-1.25362	135980.5	7.54
Xylulose	0	-1.04002	93.71106	-0.25555	793184.6	6.57
Dimethylglycine	52.6	-1.68946	97.19854	0.894133	2500.734	11.69
Fructose 6-phosphate	0	-1.9345	94.28857	1.125167	1914.462	18.89
Glucose	0	-1.5596	17.67395	0.4414	1119.186	9.07

TableA.7.14: The significantly altered identified metabolites when treated with 100 µM of Molidustat and control identified by volcano plot.

Identified metabolites	FC	log2(FC)	p. adjusted	-log10(p)
Xylulose	0.53583	-0.90014	0.0271	1.567
UDP-N-acetyl-D-mannosamine	0.38322	-1.3837	0.014596	1.8358
Trans-Ferulic acid	0.56657	-0.81967	0.015217	1.8177
Thymidine triphosphate	0.51238	-0.96472	0.006772	2.1693
TDP	0.52005	-0.94328	0.007742	2.1111
Sorbitol	0.4766	-1.0692	0.003621	2.4412
Phosphoenolpyruvic acid	0.50078	-0.99775	0.024793	1.6057
N-Acetyl-L-methionine	1.5595	0.6411	0.015679	1.8047
N-Acetyl-aspartate	0.57382	-0.80134	0.015845	1.8001
Methyl isocitric acid	2.0716	1.0507	0.013411	1.8725
Isocitrate	0.13049	-2.938	0.007359	2.1332
Glyceric acid	2.0323	1.0231	0.004869	2.3126
Glutathione (GSH)	0.64539	-0.63176	0.002728	2.5642
Fructose 6-phosphate	0.38888	-1.3626	0.013276	1.8769
Fructose 2,6 diphosphate	0.53432	-0.90423	0.001433	2.8437
Erythrose 4-phosphate	0.31365	-1.6728	0.015144	1.8198
EDTA	0.47952	-1.0603	0.011681	1.9325
dTDP-D-glucose	0.37218	-1.4259	0.011583	1.9362
Citric acid	0.10808	-3.2098	0.006827	2.1657
CDP-ethanolamine	0.58174	-0.78156	0.013455	1.8711
AICAR	0.19977	-2.3236	0.007359	2.1332
6-Phosphogluconic acid	0.37773	-1.4046	0.018024	1.7441

4-Hydroxyproline	0.59871	-0.74008	0.015144	1.8198
(R)-2,3-Dihydroxy-3-methylbutanoate	0.34509	-1.5349	0.007742	2.1111

Table A 7.18.15: All pathways found by the untargeted pathway analysis during 100µM of Molidustat vs control experiment on HEK 293T cells. PW = pathway, Fisher's Exact Test, EASE = Expression Analysis Systematic Explorer. Emp = empirical, p = p-value, adj = adjusted, cpd= compound.

Pathway Name	Pathway total	Hits. Total	Hits. sig	Expected	P (Fisher)	P(EASE)	Em. Hits	Empirical	Adj P. Fisher	Adj P.EASE	Cpd
Pentose phosphate pathway	37	36	33	4.2782	2.35E-09	2.43E-08	0	0	2.24E-07	2.31E-06	C00121;C00281;C0034; C00442;C01101;C0050; C00020;C02076;C0062; C00257;C00259;C0019; C00231;C00092;C1221; C12214;C00661;C0011; C00111;C00118;C0534; C00279;C00447;C0008; C06222;C01236;C0022; C01172;C00309;C0121; C00673;C00301;C05382

Glycolysis and Gluconeogenesis	49	35	26	5.6658	0.000337	0.001123	0	0	0.031682	0.105524	C00149;C00035;C00900;C05378;C00103;C00022;C00579;C00668;C00092;C00020;C00111;C00033;C00031;C00354;C00118;C00197;C00085;C00665;C05345;C00227;C01231;C00631;C00221;C00248;C01172;C00267;C00661;C00186;C05993
Fructose and mannose metabolism	33	29	21	3.8157	0.0023	0.006976	0	0	0.213872	0.648768	C00325;C05378;C00577;C00275;C01019;C00665;C00095;C00661;C00159;C00035;C00111;C00031;CE3074;CE3075;C00085;C00354;C05345;C00636;C00267;C02976;C00096;C02985;C01094;C03693;CE2846
Butanoate metabolism	34	20	15	3.9314	0.006057	0.020046	0	0	0.551205	1	C00025;C00026;C00020;C00022;C00109;C05548;C03087;C01089;C00232;C06006;C05984;C00033;C00164;C00042;C06010

Glyoxylate and Dicarboxylate Metabolism	12	10	9	1.3875	0.004391	0.026587	0	0	0.403972	1	C00111;C00631;C00258;C00266;C00310;C00160;C00048;C00168;C00988
Hexose phosphorylation	20	18	13	2.3126	0.017666	0.051595	0	0	1	1	C00159;C00104;C00329;C00031;C02965;C00275;C00085;C00131;C00095;C00092;C00206;C00738;C00352
Sialic acid metabolism	107	22	15	12.372	0.023351	0.058913	0	0	1	1	C06241;C00140;C01582;C00221;C04257;C00645;C04006;C00065;C05396;C00267;C01177;C00124;C00055;C03546;C00137
Valine, leucine and isoleucine degradation	65	22	15	7.5158	0.023351	0.058913	0	0	1	1	C00025;C00026;C00020;C00349;C00141;C00164;C00042;C03465;C06001;C00233;CE2028;C06002;C00248;C00671;C02170

Pentose and Glucuronate Interconversions	15	13	10	1.7344	0.01994	0.068105	11	0.11	1	1	C00105;C00167;C00259;C00312;C00310;C00199;C00800;C00231;C05385;C00309
Arginine and Proline Metabolism	45	32	20	5.2033	0.033339	0.06858	0	0	1	1	C00025;C00148;C00026;C00022;C03912;C03564;C04582;C00073;C00763;C04188;C00147;C01137;C00048;C00058;C04281;C01157;C01165;C05938;C00042;C00049
Amino sugars metabolism	69	32	20	7.9783	0.033339	0.06858	0	0	1	1	C00025;C00104;C00329;C00022;C00140;C00275;C04501;C04256;C04257;C00033;C00645;C00055;C00357;C00352;C00085;C06241;C01170;C00043;C03557;C00203

Carbon fixation	10	10	8	1.1563	0.027111	0.10044	10	0.1	1	1	C00085;C00111; C00279;C00022; C00354;C00118; C00231;C00049
Phosphatidylinositol phosphate metabolism	59	24	15	6.8221	0.063299	0.13022	1	0.01	1	1	C00124;C00033; C01225;C04299; C01220;C00055; C03546;C00092; C03862;C00137; C04006;C04063; C04062;C01177; C00043
Glycosphingolipid biosynthesis – ganglion series	62	11	8	7.1689	0.060636	0.17196	0	0	1	1	C00124;C00035; C01582;C00054; C00055;C00053; C00325;C00203
Glycerophospholipid metabolism	156	31	18	18.038	0.09814	0.17339	0	0	1	1	C01225;C00222; C01233;C00258; C00093;C00670; C00065;C01582; C00577;C06893; C00111;C01177; C03557;C00184; C00513;C00055; C00033;C00137

Pyrimidine metabolism	70	53	28	8.094	0.15261	0.22345	1	0.01	1	1	C00106;C00022;C00364;C00206;C00104;C00020;C00025;C00055;C00906;C00361;C00459;C00705;C00349;C00105;C00214;C00881;C00295;C00112;C00299;C00131;C00442;C00429;C00035;C00672;C00103;C00239;C02642;C00049
Pyruvate Metabolism	20	18	11	2.3126	0.1274	0.25007	0	0	1	1	C02912;C00149;C00256;C00022;C00186;C00051;C00546;C00111;C02917;C00661;C00033
TCA cycle	31	18	11	3.5845	0.1274	0.25007	4	0.04	1	1	C00149;C00026;C00104;C00579;C00311;C00158;C00033;C00248;C00035;C00042;C00417

N-Glycan biosynthesis	48	16	10	5.5501	0.1237	0.25355	0	0	1	1	C00105;C00325; C00112;C00055; C00096;C00159; C00035;C03862; C00031;C00043
Glutamate metabolism	15	10	7	1.7344	0.10195	0.2601	0	0	1	1	C00025;C00026; C00022;C00042; C03912;C00051; C00232
Glycine, serine, alanine and threonine metabolism	88	48	25	10.175	0.19717	0.28345	0	0	1	1	C00025;C00026; C00020;C00022; CE1554;C00546; C00256;C00258; C03508;C00073; C00430;C00248; C00160;C00168; C00065;C00109; C01146;C00579; C00988;C00051; C00197;C02305; C00033;C00048

Glycosphingolipid metabolism	67	21	12	7.7471	0.18391	0.31856	0	0	1	1	C00124;C00325;C00054;C00055;C00962;C00035;C00031;C00065;C00053;C00043;C01582;C00203
Proteoglycan biosynthesis	27	9	6	3.122	0.16632	0.3778	0	0	1	1	C00033;C00043;C00054;C00167;C00053;C00203
N-Glycan Degradation	16	5	4	1.85	0.13168	0.40651	4	0.04	1	1	C00159;C00124;C00140;C01019
Nucleotide Sugar Metabolism	7	5	4	0.8094	0.13168	0.40651	0	0	1	1	C00103;C00459;C00167;C00842
Vitamin H (biotin) metabolism	5	3	3	0.57814	0.091441	0.42506	0	0	1	1	C00120;C00020;C05921
Alanine and Aspartate Metabolism	30	21	11	3.4688	0.32297	0.48807	0	0	1	1	C00025;C00026;C00020;C00022;C00940;C01042;C00033;C00152;C00402;C00049;C00048

Glycosphingolipid biosynthesis - Globo series	16	8	5	1.85	0.26169	0.52312	3	0.03	1	1	C00035;C00055; C00325; C00984;C00203
Blood Group Biosynthesis	44	8	5	5.0876	0.26169	0.52312	0	0	1	1	C00325;C00055; C00035;C00043; C00203
Glycosphingolipid biosynthesis - lacto and neolacto series	16	8	5	1.85	0.26169	0.52312	0	0	1	1	C00035;C00325; C00043;C00055; C00203
C5-Branched dibasic acid metabolism	10	6	4	1.1563	0.2565	0.55868	19	0.19	1	1	C00035;C00022; C00490;C01732
Vitamin B1 (thiamin) metabolism	20	6	4	2.3126	0.2565	0.55868	0	0	1	1	C00020;C00322; C00022;C00026
Phytanic acid peroxisomal oxidation	34	6	4	3.9314	0.2565	0.55868	0	0	1	1	C00026;C00020; C00058;C00042

Ascorbate (Vitamin C) and Aldarate Metabolism	29	20	10	3.3532	0.41201	0.58675	12	0.12	1	1	C00800;C00051; C05412;C05411; C00072;glac;C04575; C00818;C00425; C01620
Propanoate metabolism	31	18	9	3.5845	0.4256	0.60973	0	0	1	1	C00020;C00109; C02225;C06002; C05984;C01013; C00222;C00164; C04593
Prostaglandin formation from arachidonate	78	9	5	9.019	0.3809	0.63937	1	0.01	1	1	C00425;CE0737; C00051;C00020; C00072

Methionine and cysteine metabolism	94	46	21	10.869	0.52948	0.6411	0	0	1	1	C00025;C00026; C00020;C00022; C01137;C04582; C01180;C00053; C00109;C00302; C00094;C00073; C00245;C00065; C00519;C00054; C00051;C02712; C00606;C00033; C00048
Aspartate and asparagine metabolism	114	53	24	13.182	0.54566	0.64851	0	0	1	1	C00025; C00026; C00020;C00148; C03440;C00232; C00152; C01239;C02238; C05572;C00402; C05938;C05931; C00109;C04540; C00989;C01879; C02630;C01157; CE4788;C01165; C00051;C00058; C00033;C04281; C04282;C00049

Galactose metabolism	41	35	16	4.7408	0.53847	0.66595	1	0.01	1	1	C00104;C05396; C00124;C00103; C00140;tag1p-D; C00577;C00112; C03785;C00159; C00111;C00031; C00795;C02336; C00446;C00221; C00267;C00095; C01097
Keratan sulfate degradation	68	7	4	7.8627	0.39393	0.68432	13	0.13	1	1	C00124;C00140; C01019;C00203
Glycosphingolipid biosynthesis – lacto series	14	7	4	1.6188	0.39393	0.68432	3	0.03	1	1	C00035;C00325; C00055;C00203
Keratan sulfate biosynthesis	66	7	4	7.6315	0.39393	0.68432	10	0.1	1	1	C00055;C00054; C00053;C00043

Putative anti-Inflammatory metabolites formation from EPA	27	2	2	3.122	0.20329	0.69775	0	0	1	1	C00025;C00051
Beta-Alanine metabolism	20	10	5	2.3126	0.49891	0.73528	0	0	1	1	C00025;C00026;C01013;C00049;C00222
Hyaluronan Metabolism	8	5	3	0.92502	0.40891	0.74447	16	0.16	1	1	C00140;C00043;C00167
CoA Catabolism	7	5	3	0.8094	0.40891	0.74447	0	0	1	1	C00020;C01134;C00882
Limonene and pinene degradation	10	5	3	1.1563	0.40891	0.74447	0	0	1	1	C06306;C02452;C06078;C00964;C02759
Nitrogen metabolism	6	5	3	0.69377	0.40891	0.74447	0	0	1	1	C00025;C00152;C00049
Porphyrin metabolism	43	13	6	4.972	0.57755	0.77394	11	0.11	1	1	co;C00430;C00237;C00072;C00425;C00167
Squalene and cholesterol biosynthesis	55	8	4	6.3595	0.52617	0.78105	0	0	1	1	C01107;C01143;C00058;C00164

Leukotriene metabolism	92	8	4	10.638	0.52617	0.78105	0	0	1	1	C00020;CE5968; C00302;C00051
Vitamin B3 (nicotinate and nicotinamide) metabolism	28	16	7	3.2376	0.63929	0.80484	21	0.21	1	1	C00025;C00020; C00455;C00442; C00301;C00049; C03246
Lysine metabolism	52	24	10	6.0127	0.70823	0.83075	60	0.6	1	1	C00025;C00026; C00020;C00322; C04092;C00579; C00450;C00956; C00248;C00042
D4&E4-neuroprostanes formation	37	3	2	4.2782	0.42699	0.8341	37	0.37	1	1	C00072;C00425
Starch and Sucrose Metabolism	33	14	6	3.8157	0.66769	0.83498	7	0.07	1	1	C00105;C00103; C00031;C00221; C00267;C00167
O-Glycan biosynthesis	16	6	3	1.85	0.56132	0.83736	4	0.04	1	1	C00043;C00055; C00203
De novo fatty acid	106	7	3	12.257	0.68686	0.89857	3	0.03	1	1	C00020;C05921; C00054

biosynthesis											
Heparan sulfate degradation	34	7	3	3.9314	0.68686	0.89857	57	0.57	1	1	C00140;C00124; C00181
Seleno amino acid metabolism	35	7	3	4.047	0.68686	0.89857	11	0.11	1	1	C00020;C00065; C00109
Purine metabolism	80	56	22	9.2502	0.85353	0.90561	2	0.02	1	1	C00025;C00362; C00020;C00360; C00361;C00942; C00104;C00121; C00147;C04640; C00131;C05512; C00035;C06196; C00442;C03373; C00672;C00022; C00049;C00206; C03794;C00072
Fatty acid oxidation, peroxisome	28	4	2	3.2376	0.61141	0.90904	0	0	1	1	C00026;C00042
Vitamin B5 - CoA biosynthesis from	12	11	4	1.3875	0.81293	0.93609	3	0.03	1	1	C00020;C00112; C01134;C00882

pantothenate											
Histidine metabolism	33	17	6	3.8157	0.85803	0.94239	28	0.28	1	1	C00025;C00026;C00020;C00051;C05827;C00222
Chondroitin sulfate degradation	37	5	2	4.2782	0.74641	0.95018	84	0.84	1	1	C00124;C00181
Drug metabolism - other enzymes	31	15	5	3.5845	0.88386	0.95902	1	0.01	1	1	C16635;C07585;C11173;C07648;C04646
C21-steroid hormone biosynthesis and metabolism	112	15	5	12.95	0.88386	0.95902	1	0.01	1	1	C00167;C00054;C00053;C00058;C00033
Linoleate metabolism	46	18	6	5.3189	0.89696	0.96064	1	0.01	1	1	C00051;C00072;C14825;C14826;C14762;C00167
Arachidonic acid metabolism	95	9	3	10.985	0.85371	0.96228	0	0	1	1	C00025;C00020;C00051

Vitamin B9 (folate) metabolism	33	16	5	3.8157	0.91845	0.97308	1	0.01	1	1	C00025;C00065; C01045;C00058; C00445
Glutathione Metabolism	19	10	3	2.1969	0.90328	0.97739	23	0.23	1	1	C01879;C00025; C00051
Urea cycle/amino group metabolism	85	28	9	9.8284	0.947	0.97772	23	0.23	1	1	C00025;C00148; C03912;C00073; C00033;C01137; C00026;C01165; C00049
Xenobiotics metabolism	110	40	13	12.719	0.96641	0.98438	1	0.01	1	1	C00054;C00051; C00053;C14792; C14793;C14791; C06755;C14856; C00167;C14855; C14854;C14876; C13645
Androgen and estrogen biosynthesis and metabolism	95	15	4	10.985	0.9599	0.98992	3	0.03	1	1	C00167;C00054; C00051;C00053

Tyrosine metabolism	160	64	21	18.5	0.98687	0.99329	1	0.01	1	1	C00026;C00020; CE1957;C00025; C00022;C00425; C00544;CE6316; C00072;C05577; C00167;C0027; C05576;C1369; C01161;C0005; C00051;C0005; C00058;C00164
Bile acid biosynthesis	82	10	2	9.4815	0.97782	0.99758	5	0.05	1	1	C00020;C00245
Biopterin metabolism	22	12	2	2.5438	0.99227	0.99929	3	0.03	1	1	C00272;C00058
Tryptophan metabolism	94	44	11	10.869	0.99864	0.99955	29	0.29	1	1	C00025; C0002; C00020; C0027; CE2949; CE308; C00322; C0005; C00058; C0093; C03824
Vitamin A (retinol) metabolism	67	15	2	7.7471	0.99849	0.99989	21	0.21	1	1	C00167; C00020

Di-unsaturated fatty acid beta-oxidation	26	4	1	3.0063	0.9099	1	30	0.3	1	1	C00020
Vitamin B2 (riboflavin) metabolism	8	4	1	0.92502	0.9099	1	14	0.14	1	1	C00020
3-oxo-10R-octadecatrienoate beta-oxidation	27	6	1	3.122	0.97313	1	0	0	1	1	CE5326; CE5314
Alkaloid biosynthesis II	10	5	1	1.1563	0.95077	1	79	0.79	1	1	C00020
Glycosylphosphatidylinositol (GPI)-anchor biosynthesis	6	2	1	0.69377	0.69918	1	0	0	1	1	C03862
Parathion degradation	6	1	1	0.69377	0.45124	1	0	0	1	1	C06608
Vitamin E metabolism	54	4	1	6.2439	0.9099	1	53	0.53	1	1	C00020

Caffeine metabolism	11	5	1	1.2719	0.95077	1	36	0.36	1	1	C16358; C16353
Lipoate metabolism	8	3	1	0.92502	0.83527	1	19	0.19	1	1	C00579
Drug metabolism - cytochrome P450	53	9	1	6.1283	0.99566	1	12	0.12	1	1	C16608
Fatty Acid Metabolism	63	8	1	7.2846	0.99202	1	3	0.03	1	1	C00058
Omega-3 fatty acid metabolism	39	5	1	4.5095	0.95077	1	16	0.16	1	1	C00020
Mono-unsaturated fatty acid beta-oxidation	19	3	1	2.1969	0.83527	1	14	0.14	1	1	C00020
Vitamin K metabolism	3	1	1	0.34688	0.45124	1	0	0	1	1	C05850
Fatty acid activation	74	8	1	8.5565	0.99202	1	62	0.62	1	1	C00020
Ubiquinone Biosynthesis	10	5	1	1.1563	0.95077	1	85	0.85	1	1	C00020

Omega-6 fatty acid metabolism	55	3	1	6.3595	0.83527	1	0	0	1	1	C00020